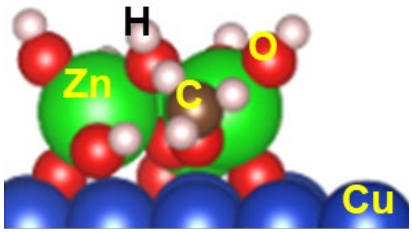

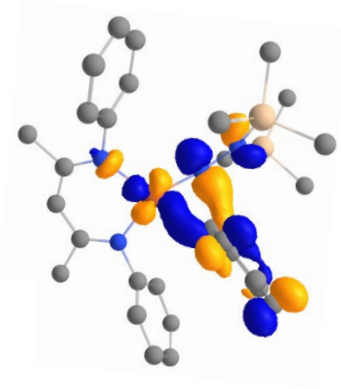

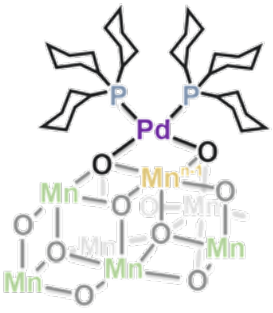

U.S. DEPARTMENT OF ENERGY | Office of Science

2023 Catalysis Science PI Meeting

Roadmap for Catalysis Science Solutions of the Future

Hilton Rockville Hotel & Executive Meeting Center
Rockville, MD
September 26 – 28, 2023

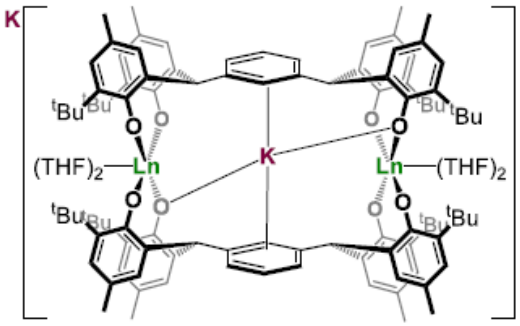

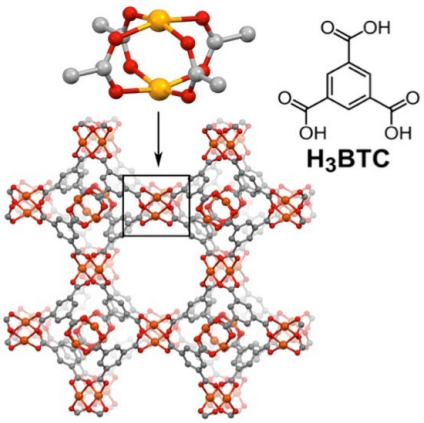

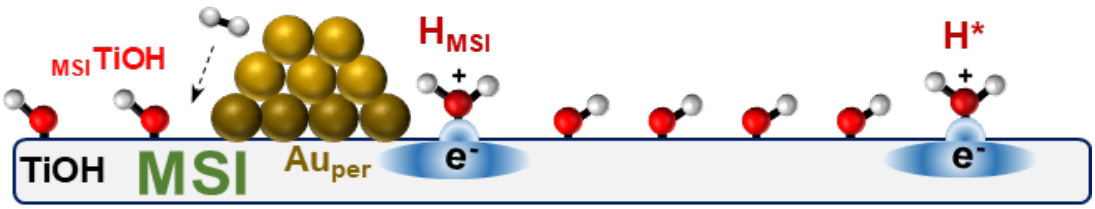

Program and Abstracts for the

2023 BES Catalysis Science Research PI Meeting: "Roadmap for Catalysis Science Solutions of the Future"

Hilton Rockville Hotel & Executive Meeting Center
Rockville, MD
September 26 - 28, 2023

The research grants and contracts described in this document are supported by the U.S. Department of Energy, Office of Science/Basic Energy Sciences, as part of the Catalysis Science Program within the Chemical Sciences, Geosciences and Biosciences Division

FOREWORD

The 2023 Catalysis Science Research PI Meeting is sponsored by the Division of Chemical Sciences, Geosciences and Biosciences, Office of Basic Energy Sciences (BES), U.S. Department of Energy. It is held on September 26-28, 2023, at the Hilton Rockeville Hotel in Rockeville, Maryland. The purposes of this meeting are to discuss the recent advances in the chemical, physical, and biological bases of catalysis science, to foster exchange of ideas and cooperation among BES/Catalysis Science Program PIs, and to discuss the new science challenges and opportunities recently emerging in catalytic technologies for energy production and use.

Catalysis research activities within BES emphasize fundamental research aimed at understanding reaction mechanisms and, ultimately, controlling the chemical conversion of natural and artificial feedstocks to useful energy carriers. The long-term goals of this research are to discover fundamental scientific principles, and to produce insightful approaches for the prediction of catalyst structure-reactivity behavior. Such knowledge, integrated with advances in chemical and materials synthesis, *in-situ* and *operando* analytical instrumentation, chemical kinetics and dynamics measurements, and computational chemistry methods, will allow the control of chemical reactions along desired pathways. This new knowledge will impact the efficiency of conversion of natural resources into fuels, chemicals, materials, or other forms of energy, while minimizing the impact to the environment.

The purpose of this meeting is to highlight the fundamental advances in catalysis science of relevance to the energy, economic and environmental future of the U.S. This year's meeting "*Roadmap for Catalysis Science Solutions of the Future*" is aimed at looking forward to emerging challenges and new opportunities in catalysis science. We formulated several sub themes for the meeting to address 'Emerging driving forces in Catalysis and Industry for Energy Applications' and 'Diversity, Equity, Accessibility & Energy Justice in Chemical Science Research' as a segue to discuss key foundational science research underpinning technologies of the future. This year's program includes two plenary sessions featuring 7 talks, as well as 20 oral and 66 poster presentations by BES/Catalysis Science PIs.

Special thanks to the program investigators and their students, postdocs, and collaborators for their dedication to the continuous success and visibility of the BES/Catalysis Science Program. We also thank the Oak Ridge Institute for Science and Education staff for the logistical and web support of the meeting. Finally, very special thanks go to Raul Miranda[3] for his longstanding and continuing contributions to the BES/Catalysis Science Program, now from his role as Team Lead for Chemical Transformations in the BES/Chemical Sciences, Geosciences and Biosciences Division.

Christine Thomas[1], Sanjaya Senanayake[2], Viviane Schwartz[3], Chris Bradley[3], Carrie Farberow[3], and Eric Wiedner[3]
[1]The Ohio State University
[2]Brookhaven National Laboratory
[3]Catalysis Science Program, Office of Basic Energy Sciences, US Department of Energy

2023 Catalysis Science PI Meeting

'Roadmap for Catalysis Science Solutions of the Future'

September 26th – 28th, 2023

Program Chairs: Christine Thomas and Sanjaya Senanayake

Tuesday, September 26

OPENING SESSION

8:30-9:00 am Welcoming Remarks and Program Updates
Viviane Schwartz and Chris Bradley, DOE/BES/Catalysis Science Program

9:00-9:20 am BES Update
Gail McLean, Acting Division Director, DOE/BES/Chemical Science, Geosciences and Biosciences Division

9:20-9:30 am Welcome from Meeting Chairs
Christine Thomas, Ohio State University and **Sanjaya Senanayake**, Brookhaven National Laboratory

PI SESSION I

Session Chair: **Eugene Chen**, Colorado State Univesity

9:30 – 10:05 am *Metal Encapsulation Strategies to Optimize and Minimize PGE Use in Heterogeneous Catalysts*
Matteo Cargnello, Stanford University

10:05 – 10:20 am Break

10:20 – 10:55 am *Fundamentals of Catalysis and Chemical Transformations*
Zili Wu, Oakridge National Laboratory

10:55 – 11:30 am *Carbonylation Catalysis as a Tool for Precision Polymer Synthesis*
Ian Tonks, University of Minnesota

11:30 am – 12:05 pm *Catalyst-free Upcycling of PMMA via a Doping Strategy*
Tianning Diao, New York University

12:05 – 1:30 pm **Working Lunch**

PLENARY SESSION I – Emerging Forces in Catalysis and Industry

Session Chairs: **Viviane Schwartz and Chris Bradley**, DOE/BES/Catalysis Science Program

1:30 – 2:25 pm *Developing our Energy Future*
Javier Guzman, Energy and Technology Advisor, ExxonMobil

2:25 – 3:25 pm Panel – *Emerging Forces in Catalysis and Industry for Energy Applications*
Panelists: **Javier Guzman**, ExxonMobil; **Francesca Toma**, Helmholtz-Zentrum Hereon; **Paul Chirik**, Princeton University; **Sheima Khatib**, Virginia Tech; **Jeff Greeley**, Purdue University; **Elizabeth Biddinger**, The City College of New York
Moderator: **Karl Mueller**, Pacific Northwest National Laboratory

3:35 – 3:50 pm Break

PI SESSION II

Session Chair: **Rachel Getman**, Ohio State University

3:50 – 4:25 pm *Metallacyclic Lanthanide Catalysts for the Selective Conversion of Atmospheric N_2 to Secondary Silylamines*
Polly Arnold, Lawrence Berkeley National Laboratory

4:25 – 5:00 pm *Improving the Accuracy of ML-models for Metal Oxide Surface Catalysis with Bulk Electronic Structure Descriptors*
Kirsten Winther, SLAC National Accelerator Laboratory

5:00 – 7:00 pm **Dinner (on your own)**

POSTER SESSION I

7:00 – 9:00 pm

<u>Wednesday, September 27</u>

PI SESSION III

Session Chair: **Robert Rioux**, Pennsylvania State University

8:30 – 9:05 am *Rates and Reversibility of CO_2 Hydrogenation on Cu-based Catalysts*
Aditya Bhan, University of Minnesota

9:05 – 9:40 am *Molecular Co-electrocatalytic CO_2 Reduction with Redox Mediators*
Charles Machan, University of Virginia

9:40 – 10:15 am *Well-defined Cu/MOx/ZnO Ternary Catalysts for CO_2 Hydrogenation*
Michael White, Brookhaven National Laboratory

10:15 – 10:30 am Break

PI SESSION IV

Session Chair: **Smaranda Marinescu**, University of Southern California

10:30 – 11:05 am *Electrocatalytic Oxygen Atom Transfer Reactions*
Karthish Manthiram, California Institute of Technology

11:05 – 11:40 am *Single-molecule Photoelectrocatalysis:2D Junction Effects on 3D Photocatalysts*
Peng Chen, Cornell University

10:40 – 12:15 am *Selective Electrochemical Upgrading of Biomass-Derived Molecules to Fuels and Chemicals*
Kyoung-Shin Choi, University of Wisconsin

12:15 – 1:30 pm **Working Lunch**

Plenary Session II – Diversity, Equity, Inclusion, Accessibility & Energy Justice

Session Chair: **Lisandro Cunci**, University of Puerto Rico, Rio Piedras

Speakers and Panelists: **Ping Ge**, DOE Office of Workforce Development for Teachers and Scientists; **Nastaran Ghazi**, DOE Office of Scientific Workforce Diversity, Equity, and Inclusion; **Natalie Melcer**, DOE Office of the Deputy Director for Science Programs; **Samuel Herbert**, DOE Energy Justice Policy Division; **Sederra Ross**, ACS Green Chemistry Institute; **Lynn Villafuerte**, DOE DEIA Workforce Engagement Division

1:30 – 2:50 pm Plenary Session Presentations

2:50 – 4:00 pm Panel – *Diversity, Equity, Inclusion, Accessibility & Energy Justice in Chemical Science Research*

4:00 – 4:15 pm Break

Early Career Awardee Session
Session Chair: **Alison Fout**, Texas A&M University

4:15 – 4:30 pm *Selective Degradation of Polymer Waste to Commodity Chemicals*
Erin Stache, Princeton University

4:30 – 4:45 pm *Functionalization of Methane and Carbon Dioxide Using Earth Abundant Metal Frustrated Lewis Pair Catalysts*
Kensha Clarke, University of Mississippi

4:45 – 5:00 pm *Interpretable Deep Learning for Advancing Field-enhanced Catalysis*
Fanglin Chen, University of Massachusetts Lowell

5:00 – 7:00 pm **Dinner (on your own)**

POSTER SESSION II

7:00 – 9:00 pm

Thursday, September 28

PLENARY SESSION III
Session Chairs: **Viviane Schwartz** and **Chris Bradley**, DOE/BES/Catalysis Science Program

8:00 – 8:55 am *Catalysis Research at the Institute of Functional Materials for Sustainability*
Francesca Toma, Head of Institute of Functional Materials for Sustainability, Helmholtz - Zentrum Hereon

PI SESSION V
Session Chair: **Umit Ozkan**, Ohio State University

8:55 – 9:30 am *Olefin Metathesis by Supported Molybdena Catalysts*
Israel Wachs, Lehigh University

9:30 – 10:05 am *Intermetallic Catalysts for Probing and Designing Hydrogenation Active Sites*
Michael Janik, Pennsylvania State University

10:05 – 10:20 am Break

PI SESSION VI

Session Chair: **Alan Goldman**, Rutgers University

10:20 – 10:55 am *Antimony-based Strategies for Small-molecule Activation and Catalysis*
Francois Gabbai, Texas A&M University

10:55 – 11:30 am *Supported Electrophilic d^0 Metal Hydrides for Hydrogenolysis Reactions*
Matthew Conley, University of California, Riverside

11:30 – 12:05 pm *Mechanistic and Reactivity Studies of Dimeric and Monomeric Copper Hydrides*
Ba Tran, Pacific Northwest National Laboratory

CLOSING SESSION

12:05 – 12:15 pm Final Remarks
Christine Thomas, Sanjaya Senanayake, Viviane Schwartz, and Chris Bradley

12:15 pm Adjourn

POSTER SESSION I

Tuesday, September 26

1. **Physics-based design principles for complex chemical reactions**
   Frank Abild-Pedersen, Shyama Charan Mandal
   SUNCAT Center for Interface Science and Catalysis, SLAC National Accelerator Laboratory

2. **Gold Catalyzed Polymerization Reactions of Unsaturated Substrates: Towards New Functional, Recyclable, and Upcycled Aromatic Polymers**
   Jason D. Azoulay, Eric King, and Naresh Eedugurala
   Georgia Institute of Technology

3. **Co-ACCESS at SSRL: Developing Synchrotron Operando Characterization Capabilities for the Catalysis Community**
   Simon R Bare[1], Adam S. Hoffman[1], Jiyun Hong[1], Jorge Perez-Aguilar[1], Rachita Rana[2], Fernando Vila[3]
   [1]SSRL, SLAC National Accelerator Laboratory
   [2]Department of Chemical Engineering, University of California at Davis
   [3]Department of Physics, University of Washington

4. **Rotating Ring-Disk Electrodes Show that Chloride-Mediated Electrochemical Ethanol Oxidation Occurs in Discrete One-Electron Steps**
   Bart M. Bartlett, Siqi Li, Ryan D. Van Daele, Katherine Morrissey
   Department of Chemistry, University of Michigan

5. **Speciation and Sources of Copper Electrocatalyst Fouling During Electrochemical Hydrogenation and Hydrogenolysis of Furfural in Acid**
   Elizabeth Biddinger and Andrew S. May
   Department of Chemical Engineering, The City College of New York, CUNY, New York

6. **Quantifying the activity of alloy catalysts under working conditions**
   Jesse Q. Bond, Robson Schuarca, and Yaqin Tang
   Biomedical and Chemical Engineering, Syracuse University

7. **Gas-Phase Hydrogenation and Hydroformylation with Metal-Organic Framework Catalysts**
   Donna A. Chen,[1] Juan D. Jimenez,[2] Sanjaya D. Senanayake,[2] Natalia B. Shustova,[1] Deependra M. Shakya,[1] Musbau Gbadamosi,[1] Konstantinos D. Vogiatzis,[3] and Gavin McCarver[3]
   [1]University of South Carolina, Department of Chemistry and Biochemistry
   [2]Brookhaven National Laboratory, Chemistry Division
   [3]University of Tennessee at Knoxville, Department of Chemistry

25. Catalyst design strategies for multifunctional metal-promoted zeolites in methane dehydroaromatization

Sheima J. Khatib[1], Md Sifat Hossain[1], Gagandeep Singh Dhillon[2,3], Liping Liu[1], Hongliang Xin[1], Apoorva Sridhar[2,4], Emanuele J. Hiennadi[1], Jiyun Hong[5], Simon R. Bare[5]

[1] Department of Chemical Engineering, Virginia Tech, Blacksburg, VA 24061, USA

[2] Department of Chemical Engineering, Texas Tech University, Lubbock, TX 79409, USA

[3] Lydian Labs Inc., Cambridge, MA-02139, USA

[4] Intel Co, Hillsboro, OR 97124, USA

[5] SSRL, SLAC National Accelerator Laboratory, Menlo Park, CA 94025, USA

26. Mechanistic Investigations of Gas-Phase and Surface-Mediated Oxidative Coupling Reactions

Coleman X. Kronawitter, Ambarish R. Kulkarni

University of California, Davis

27. Low-Temperature Electrocatalytic Manufacturing of Essential Chemical Building Blocks

Brian M. Tackett, B. W. Boudouris, R. Gounder, Jeffrey P. Greeley, Jeffrey T. Miller

Purdue University, Chemical Engineering

28. Converting Carbon and Nitrogen Waste Products to Valuable C-N Compounds

V. Sara Thoi

Department of Chemistry, Johns Hopkins University

29. Towards a polyolefin-based refinery: Understanding and controlling the critical reaction steps

Huamin Wang, Johannes A. Lercher

Institute for Integrated Catalysis, Pacific Northwest National Laboratory

30. Linking operando spectroscopy with microkinetic modeling to unravel the catalytic mechanism for CH_4 oxidation on IrO_2(110)

Jason F. Weaver[1], Jovenal Jamir[1], Minkyu Kim[2], Connor Pope[1], Aravind Asthagiri[3]

[1] Department of Chemical Engineering, University of Florida

[2] School of Chemical Engineering, Yeungnam University

[3] William G. Lowrie Chemical & Biomolecular Engineering, The Ohio State University

31. Non-Orthogonal Tandem Catalysis in Compartmentalized Nanoreactors

Marcus Weck,[1] Eman Ahmed,[1] Jinwon Cho,[2] Seung Soon Jang,[2] Christopher W. Jones,[2] Fangbei Liu,[1] Joshua Polster,[1] Jules Zambito,[1] Wenyang Zhao[2]

[1] Department of Chemistry and Molecular Design Institute, New York University

[2] School of Chemical & Biomolecular Engineering and School of Materials Science & Engineering, Georgia Institute of Technology

POSTER SESSION II

Wednesday, September 27

32. Theoretical studies on BES Catalysis Core Program
Líney Árnadóttir,[a,b] Greg Collinge,[a] Jack Fuller,[a] Bojana Ginovska,[a] Mal-Soon Lee,[a] Simone Raugei, [a] Greg Schenter[a]
[a] Physical and Computational Sciences Directorate and Institute for Integrated Catalysis, Pacific Northwest National Laboratory
[b] School of Chemical, Biological, and Environmental Engineering, Oregon State University

33. The Role of Surface Hydroxyls and Entropy in Hydrogen Spillover
Bert D. Chandler,[1,5] Akbar Mahdavi-Shakib,[1] Todd N. Whittaker,[2,3] Tae Yong Yun,[1] K. B. Sravan Kumar,[4] Lauren C. Rich,[2] Shengguang Wang,[4] Robert M. Rioux,[1,5] Lars C. Grabow[4]
[1]Department of Chemical Engineering, The Pennsylvania State University
[2]Department of Chemistry, Trinity University
[3]Department of Chemical and Biological Engineering, The University of Colorado, Boulder
[4]Department of Chemical and Biomolecular Engineering, University of Houston
[5]Department of Chemistry, The Pennsylvania State University

34. Redesigning Polymers to Leverage A Circular Economy (RePLACE)
Eugene Y.-X. Chen,[1] Garret M. Miyake,[1] Linda J. Broadbelt,[2] Tobin J. Marks,[2] Yuriy Román-Leshkov[3]
[1] Colorado State University
[2] Northwestern University
[3] Massachusetts Institute of Technology

35. Metal Carbides/Nitrides and Bimetallic Alloys as Low-cost Electrocatalysts
Jingguang Chen,[1,2] Neal Biswas,[1] Hansen Mou,[1] Kevin Turaczy,[1] Samay Garg,[1] Qiaowan Chang,[1] Shyam Kattel,[3] Feng Jiao[4]
[1] Department of Chemical Engineering, Columbia University
[2] Chemistry Division, Brookhaven National Laboratory
[3] Florida A&M University
[4] University of Deleware

36. Theory-guided Innovation of High-performance Electrocatalysts for CO2 Reduction
Zhongfang Chen,[1] William E. Mustain[2]
[1] Department of Chemistry, University of Puerto Rico at Rio Piedras
[2] Department of Chemical Engineering, University of South Carolina

37. Catalytic production of hydrogen and solid carbon from methane over MgO supported catalysts

Steven Crossley,[1] Daniel Resasco,[1] Bin Wang,[1] Anibal Boscoboinik[2]
[1] University of Oklahoma, Department of Sustainable Chemical, Biological and Materials Engineering
[2] Brookhaven National Laboratory, Center for Functional Nanomaterials

38. Catalysts Research in Oxygen Reduction and Oxidation Reactions to Increase Representation in Energy Science in Puerto Rico

Lisandro Cunci
Department of Chemistry, University of Puerto Rico – Rio Piedras Campus

39. Designing, Developing, And Understanding Electrocatalysts and Interfaces for Energy Conversion Reactions

Thomas F. Jaramillo
Department of Chemical Engineering, Stanford University
Department of Energy Science Engineering, Stanford Doerr School of Sustainability
Photon Science, SLAC National Accelerator Laboratory

40. Following Ultrafast Reaction Dynamics and Capturing Rare Intermediates in Heterogeneous Catalysis

Tony F. Heinz, Frank Abild-Pedersen, Alan Luntz, Anders Nilsson, Hirohito Ogasawara, Johannes Voss
SLAC National Accelerator Laboratory

41. Dithiolene-Based Coordination Complexes and Polymers For H_2 Evolution and CO_2 Reduction

Smaranda C. Marinescu
Chemistry Department, University of Southern California

42. Bimetallic Catalysts for Bio-oil Upgrading: A Multi-Scale Modeling Approach

Jean-Sabin McEwen[a,c], Naseeha Cardwell[a], Isaac Onyango[a], Neeru Chaudhary[a], Alyssa J. R. Hensley[a,b], Xianghui Zhang[a], Sten Lambeets[c], Megan Rose Hawkins[a], Greg Collinge[c], Cody B. Cockreham[a], Junnan Shangguan[d], Reinhard Denecke[e], Yong Wang[a,c], Cathy Chin[d], Di Wu[a], Pierre Gaspard[f], Thierry Visart de Bocarmé[f], Daniel Perea[c]
[a] Washington State University (WSU), Pullman, WA 99164, USA
[b] Stevens Institute of Technology, Hoboken, New Jersey 07030 USA
[c] Pacific Northwest National Laboratory, Richland, WA 99352, USA
[d] University of Toronto, ON M5P 2G8, Canada
[e] University of Leipzig, Leipzig, D-04103, Germany
[f] Université Libre de Bruxelles, Brussels, B-1050, Belgium

43. Tailoring the near-surface environment of Rh single-atom catalysts for selective CO_2 hydrogenation

Will Medlin, Alex Jenkins, Erin Dunphy, Charles Musgrave, Michael Toney
Dept. of Chemical and Biological Engineering, University of Colorado

44. Homocoupling of CE_2 (E = O, S) by polynuclear metal complexes
Leslie J. Murray, William R. Buratto, Maria Victoria Lorenzo Ocampo, Bradley W. Musselman
University of Florida

45. Tuning Cationic Sites in Nonstoichiometric Mixed Metal Oxides for Oxygen Electrocatalysis at Solid/Liquid Interfaces
Eranda Nikolla
Department of Chemical Engineering, University of Michigan

46. Highly Reactive Main Group Cations and C-F Activation
Oleg V. Ozerov, Derek W. Leong, S. Olivia Gunther, Nattamai Bhuvanesh
Department of Chemistry, Texas A&M University

47. Fundamental studies of multifunctional electrocatalysis on heteroatom-doped carbon nanostructures (CNx)
Umit S. Ozkan, Dishari Basu, Niharika Vennala, Aravind Asthagiri, Anne Co[1]
Department of Chemical and Biomolecular Engineering, The Ohio State University
[1] Department of Chemistry and Biochemistry, The Ohio State University

48. Reactivity of Terminal Magnesium Hydride and Methyl Complexes towards Carbonyl Compounds: Access to Terminal Alkoxide and Enolate Complexes and Catalytic Activity
Gerard Parkin, David Vaccaro
Department of Chemistry, Columbia University

49. PCET Mediators for Reductive Electrocatalysis
Jonas C. Peters, Pablo Garrido-Barros, Matthew J. Chalkley, Joseph Derosa, Mengdi Li, Enric Adillon, John Ovian, Alexander I. Alabugin, Jonas Baumgärtner
Division of Chemistry and Chemical Engineering, California Institute of Technology

50. Development of an integrated multiscale methodology for simulating electrocatalysis at the metal oxide – electrolyte interface
Craig Plaisance
Cain Department of Chemical Engineering, Louisiana State University

51. Anchoring Active Sites for Enhanced Catalyst Performance in Dry Reforming of Methane
Felipe Polo-Garzon[1], Junyan Zhang[1], Meijia Li[1], Yuanyuan Li[1], Zili Wu[1,2], Zhenzhen Yang[1], Sheng Dai[1,3]
[1] Chemical Sciences Division, Oak Ridge National Laboratory
[2] Center for Nanophase Materials Sciences, Oak Ridge National Laboratory
[3] Department of Chemistry, University of Tennessee, Knoxville, TN 37996

52. Catalytic Reactions at Solid-Liquid Interfaces: Solvent Effects on Activity, Selectivity and Reaction Mechanisms
Robert M Rioux[1,2], Yanyu Mu[1], Tianze Xie[1], Jeonghwan Lee[1], Kathryn MacIntosh[1]
[1] Department of Chemical Engineering, The Pennsylvania State University
[2] Department of Chemistry, The Pennsylvania State University

53. Towards electrostatic modulation of the thermochemistry of a Ru hydrogenation catalyst
Caroline T. Saouma, Abhijit Bera
Department of Chemistry, University of Utah

54. Fluxional Nature of Heterogeneous Catalysts
Philippe Sautet, Geng Sun, Simran Kumari, Anastassia N. Alexandrova
Department of Chemical and Biomolecular Engineering, University of California Los Angeles
Department of Chemistry and Biochemistry, University of California Los Angeles

55. Biocatalytic Nanoparticles that Enable Supra-biological Cascade Reactions
Daniel K. Schwartz, Joel L. Kaar
University of Colorado Boulder

56. Mechanocatalytic Oxidative Cracking of Poly(ethylene) via a Heterogeneous Fenton Process
Carsten Sievers, Van Son Nguyen, Yuchen Chang, Erin V. Phillips, Jacob A. DeWitt
School of Chemical & Biomolecular Engineering, Georgia Institute of Technology

57. Nucleophilic Imido Ligand Enables New Catalytic Transformations of an Iron Complex
Jeremy Smith, Yafei Gao, Maren Pink, Veronica Carta
Department of Chemistry, Indiana University

58. Sustained Low-Temperature Electrochemical Methane Reforming Reaction on Commercial Pt/C and PtRu/C Electrocatalysts
YuYe J. Tong, Dejun Chen, Rachel A. Aterrado, Tianyu Ma, Thomas C. Allison
Georgetown University

59. Ni and Fe photocatalysis revisited with transient XANES spectroscopy
Josh Vura-Weis
Department of Chemistry, University of Illinois at Urbana-Champaign,

60. Electrocatalytic Ammonia Oxidation by Earth-Abundant Metal Complexes
Timothy H. Warren, Md Estak Ahmed, Pokhraj Ghosh, Danushka Ekanayake, Fatimah Alsultan
Department of Chemistry, Michigan State University

61. Multi-State Mechanocatalysis
Ross A. Widenhoefer, Stephen L. Craig, Xujun Zheng, Daniel Duan, Jack Malek, Yichen Yu, Rosemary Buhrman
Department of Chemistry, Duke University

62. Infusing Theory into Deep Learning for Advancing Catalysis Science
Hongliang Xin
Virginia Tech

63. Engineering nanostructured interfaces of hexagonal boron nitride-based materials towards enhanced catalysis
Zhenzhen Yang,[1] Meijia Li,[1] Zili Wu,[1] Miaofang Chi,[1] De-en Jiang,[2] Sheng Dai[1]
[1] Chemical Sciences Division, Oak Ridge National Laboratory
[2] Department of Chemical and Biomolecular Engineering, Vanderbilt University

64. Selective Oxidation of Oxygenates with Well-Defined Gold-Based Surface Catalytic Sites
Francisco Zaera
Department of Chemistry and UCR Center for Catalysis, University of California, Riverside

65. Heterostructure Interfaces for Electrocatalytic Oxygen and Hydrogen Evolution Reactions
Sen Zhang
Department of Chemistry, University of Virginia

66. C-H Amination/Aza-Cope Depolymerization of Diene Polymers
Aleksandr V. Zhukhovitskiy, Maxim Ratushnyy, and Sydney E. Towell
Department of Chemistry, University of North Carolina at Chapel Hill

TABLE OF CONTENTS

ABSTRACTS

ORAL PRESENTATION ABSTRACTS

Matteo Cargnello

Metal Encapsulation Strategies to Optimize and Minimize PGE Use in Heterogeneous Catalysts

Frank Abild-Pedersen, Simon Bare, Stacey Bent, Matteo Cargnello, Melissa Cendejas, Miaofang Chi, Abinash Kumar, Gennaro Liccardo, Shyama Mandal, Bang Nhan, Sydney Richardson, Jacob Smith, Mickey Stone

SUNCAT Center for Interface Science and Catalysis, SLAC National Accelerator Laboratory
Stanford University and SUNCAT Center for Interface Science and Catalysis
Oak Ridge National Laboratory

Presentation Abstract

Platinum-group elements (PGEs) are critical materials used in heterogeneous catalysts, and there is a critical need for reducing their usage through increasing the catalytic efficiency or by replacing them with more abundant elements. Catalytic converters account for 33% of the world's Pt use, 85% of Pd, and 90% of Rh, and improving their efficiency is crucial to decrease our dependency on these rare and expensive metals. Current usage of larger amounts of Pt, Pd and Rh than necessary is due to catalyst deactivation at high temperatures in the exhaust gas mixture, which leads to sintering and loss of activity. Our work demonstrates an approach where Pt/Pd-based catalysts are active and stable under air and steam conditions above 1,000 °C. These results prompted us to investigate and understand the reasons for such stability, as well as how to further improve these catalysts through a theory-driven approach supported by detailed *operando* characterization and precise synthesis. Overall, the project vision is to understand the catalytic activity and stability of PGE-containing materials and significantly improve their efficiency and reduce their usage by more than 50%.

In this talk, I will discuss our recent work related to the fundamental understanding of catalyst stability, as well as the development of methods to further improve their activity and performance for emission control reactions. Using a combination of colloidal and atomic layer deposition synthesis, advanced characterization using synchrotron and microscopy techniques, as well as density functional theory calculations, we unveiled that oxide overcoats reduce the sintering tendency of Pt-based catalysts and that this method can be extended to several combinations of metal and oxide supported catalysts, including Pd- and Rh-based catalysts. Overall, our results improve our knowledge of sinter-resistant materials to improve the efficiency of PGE usage that can be extended to other areas of heterogeneous catalysis.

New Tools for Degradable Polyester Synthesis Incorporating CO and CO_2 Comonomers

Ian Tonks
University of Minnesota

Presentation Abstract

Polyesters are versatile plastics that are attractive platforms for the development of potentially degradable or recyclable materials. Our research group is interested in the design and implementation of new polymerization strategies that incorporate biorenewable monomers into degradable polyesters, with a focus on carbonylation and carboxylation strategies that use CO or CO_2 to build the ester subunit during polymerization. In this talk, two main strategies will be discussed: first, the head-to-tail carbonylation of bioderived a,w-enols to generate branched polyesters; and second, the telomerization of butadiene with CO_2 and subsequent ring-opening polymerization to generate vinyl-sidechain functionalized polyesters containing 30% CO_2 by weight. Fundamental organometallic studies into reaction mechanism, as well as ligand effects on catalysis, feature prominently in our continued reaction development.

Catalyst-Free Upcycling of PMMA to MMA via a Doping Strategy

Mason Chin and Tianning Diao*
Chemistry Department, New York University

Presentation Abstract

The upcycling of polymers to monomers has emerged as an appealing strategy to mitigate the accumulation of plastic waste by fostering a circular economy. Poly(methyl methacrylate) (PMMA) is a widely used commodity polymer that offers a cheap, light-weight, and shatter-resistant alternative to glass. Currently, approximately 90% of PMMA waste ends up in landfills. While PMMA can be commercially recycled back into monomers via pyrolysis, the high reaction temperature of 400 ºC often leads to impure monomer recovery and diminished energy efficiency. We have developed a doping strategy that facilitates chemical upcycling at a reduced temperature of 150 °C, enabling the reversion to MMA suitable for repolymerization. Central to this method is the incorporation of a nominal amount of an α-substituted styrene co-monomer, which forms a weak head-to-head linkage between α-substituted styrene dyads within the backbone of the polymer.

Polly L. Arnold

Metallacyclic lanthanide catalysts for the selective conversion of atmospheric N_2 to secondary silylamines

Anthony Wong,[1] Matthew Hernandez,[1] Jaden Lara,[1] Francis Y. T. Lam,[1] T. Michael Trinh,[1] Leonardo dos Anjos Cunha,[1] Devin Hernandez,[1] Martin Head-Gordon,[1] Guodong Rao,[2] R. David Britt,[2] Yang Ha,[1] Jinghua Guo,[1] Nikolas Kaltsoyannis,[3] Polly L. Arnold[1]
1. University of California, Berkeley, and Lawrence Berkeley National Laboratory; Berkeley, California CA 94720, US. 2. University of California, Davis; Davis, California CA 95616, US. 3. University of Manchester, Oxford Road, Manchester, UK.

Presentation Abstract

Dinitrogen is a challenging molecule to activate and reduce to useful products. The range of d-block metal complexes that can catalyze dinitrogen reduction to ammonia or tris(silyl)amines under ambient conditions has increased in recent years, and now includes more electropositive metal complexes, rather than the traditional electron-rich middle and late cations used by nature and industry. Conventional f-block metal complexes do not have filled d-orbitals that would enable binding of N_2. We have used arene-bridged tetraphenolates to form metallacyclic structures by coordination to lanthanide or group 4 cations that can bind dinitrogen in the cavity and catalyze its conversion to bis(silyl)amines in ambient conditions. The unusual double-substitution product is attributed to the steric control afforded by the metalacycle's pocket. This is the first time that lanthanide complexes have been shown to catalyze nitrogen reduction. We will discuss the potential role of d- and f-orbitals by the f-block catalysts, by comparison of the series' most active member, samarium, with uranium and group 4 analogues. We will also consider the role of the π-systems in the ligand in retaining stabilizing group 1 metal cations in the catalyst coordination sphere and electron transfer. Electron paramagnetic resonance (EPR), NMR, Raman and IR spectroscopies, X-ray diffraction, X-ray spectroscopies, and computational studies provide insight into the mechanism of the reductive functionalization. These results suggest new catalytic applications for members of the lanthanide series that are almost as abundant as copper, and less toxic than iron.

Kirsten T. Winther

Improving the accuracy of ML-models for metal oxide surface catalysis with bulk electronic structure descriptors

Ben Comer, Neha Bothra, Ruchika Mahajan, Michaela Burke Stevens, Frank Abild-Pedersen, Johannes Voss, Michal Bajdich, Kirsten T. Winther

SUNCAT Center for Interface Science and Catalysis
SLAC National Accelerator Laboratory

Presentation Abstract

The advancement of clean hydrogen technologies relies on the discovery of high performing catalysts for the oxygen evolution reaction (OER) and oxygen reduction reaction (ORR). To achieve this goal, affordable and abundant alternatives to precious metal catalysts with sufficient stability and catalytic activity must be discovered. Ab initio simulations combined with machine learning (ML) methods can play an important role in screening a larger search space of potential catalysts materials of higher structural and compositional complexity. Here, transition metal oxides (TMOs) is a promising class of material where cation and/or anion mixing and doping can be applied to tune material properties.

In this talk I will show how electronic and structural descriptors derived from bulk DFT calculations can improve ML models for the OER and ORR on transition metal oxides. In previous work [1] we demonstrated that the electronic structure of the bulk TMO, obtained as the crystal orbital Hamiltonian populations (COHP) of the metal-oxygen bond, is an excellent descriptor for O and OH adsorption. Here, I will discuss our extended model for O and OH adsorption across crystal structures and oxidation states, utilizing a new dataset of adsorption on binary (AxOy) oxide surfaces spanning the entire transition metal series. Building on our recent work, we extend the COHP-based model to a ML-based prediction of adsorption across multiple oxidation states to obtain a MAE < 0.2 eV for the O-OH and OH adsorption energy descriptors. These results can enable a more efficient screening of catalysts on the bulk level of DFT computation to significantly reduce the computational cost.

Furthermore, I will discuss how the COHP analysis can be applied to oxide surfaces to understand the impact of metal valency, structural reorganization, and magnetization on adsorption energetics. Last, I will discuss recent progress on collecting and accessing computational and experimental data on catalysis-hub.org.

[1] Comer et al. JPCC 2022 126 (18)

Rates and reversibility of CO_2 hydrogenation on Cu-based catalysts

Ting C. Lin, Aditya Bhan
Department of Chemical Engineering and Materials Science
University of Minnesota Twin Cities

Presentation Abstract

Kinetics of reaction pathways involved in the conversion of CO_2 to methanol and to CO on $Cu/ZnO/Al_2O_3$ are resolved using in situ chemical titration, steady-state kinetic measurements, and mathematical formalisms for reversibility to assess salient species governing methanol selectivity and yield during CO_2 hydrogenation. Across a range of CO_2:H_2 = 1:1 to CO_2:H_2 = 1:80.5, active site density determined from in situ chlorine uptake remained invariant; hence, observed trends in rates can be interpreted as only arising from reaction kinetics and not from changing active site density. Kinetic and thermodynamic contributions to rates are decoupled to evaluate forward and reverse rates of methanol synthesis and reverse water-gas shift (RWGS) reactions. These kinetic analyses show that the forward rates of methanol synthesis exhibit persistent first order dependence on P_{H2} and are inhibited by H_2O more significantly than those of RWGS. In contrast, the reverse rates of methanol synthesis and RWGS are both inhibited by H_2. Consequently, without any modifications to the $Cu/ZnO/Al_2O_3$ catalyst formulation, methanol selectivity can be increased to >80% by increasing inlet H_2 partial pressure and methanol yield can be enhanced by ~20% by adding water adsorbents even under conditions far from equilibrium.

DE-SC00019028: Polyfunctional catalysis for upgrading C_1 feedstocks

Student(s): Brandon Foley, Neil Razdan, Xinyu Li, Ting Lin

Kinetic description of site ensembles on catalytic surfaces

The ubiquitously-used Langmuir-Hinshelwood (LH) formalism is an incomplete kinetic description as it relies on the implicit assumption that adsorbed species are uniformly distributed. Even in simple catalytic reactions such as A + A → A_2 (Table 1), the LH model results in miscounted site pairs and, consequently, miscalculated rates, coverages, reaction orders, and degrees of rate control. In Table 1, the general rate expression of the surface reaction in step 2 is given by $r = k_r(z/2)\theta_{AA}$ where z is the coordination of the surface lattice and θ_{AA} is the fraction of pairs of sites which contain two A^* species. By the LH formalism, the mean-field metric, $\mu_{ij} = \theta_{ij}(\theta_i\theta_j)^{-1}$, is assumed unity for all site pairs ij, giving the site-pair coverage of $\theta_{AA} = \theta_A^2$. The veracity of this approximation is contingent on a sufficiently randomizing process – namely,

Table 1: $2A_{(g)} \rightarrow A_{2(g)}$ with adsorbate surface diffusion.

#	Step	Rate constants
1	$A_{(g)} + * \leftrightarrow A^*$	$k_{ads} = 1$, $k_{des} = 1$
2	$A^* + A^* \rightarrow A_2 + **$	$k_r = 50$
n/a	$A^* + * \leftrightarrow * + A^*$	$k_{diff} = 1$

arbitrarily-fast surface diffusion – to ensure there are no spatial correlations between sites. If diffusion of each adsorbate is not infinitely-fast compared to catalysis, rigorous description of resultant congregation ($\mu_{ij} > 1$) and partitioning ($\mu_{ij} < 1$) of surface species requires derivation of elementary step rate expressions unique to each multi-site ensemble.

Explicit derivation of the surface reaction (step 2) rate equation for A^*–A^* pairs can be accomplished using a conditional-probability-based higher-order formalism to account for the loss of an A^*–A^* pair for each surface reaction event as well as the additional loss of an A^*–A^* pair if the reactive center is neighbored by another A^*-occupied site. This yields

$$\frac{d\theta_{AA}}{dt} = k_r\left(-\theta_{AA} - 2\theta_{AAA} - 4\theta_{\substack{A\\AA}}\right) = -k_r\theta_{AA}\left(1 + \frac{6\theta_{AA}}{\theta_A}\right)$$

where the second equality utilizes a truncation procedure to obtain an ensemble-specific rate equation in terms of one- and two-site coverages. Ensemble-specific rate equations such as these arise for each elementary step including surface diffusion, are critical to the improvements of higher-order kinetic descriptions, and capture clustering ($\mu_{ij} > 1$) and isolation ($\mu_{ij} < 1$) phenomena inaccessible to the LH formalism.

Figure 1 shows select mean-field metrics (μ), reaction orders (Ψ), and degrees of rate control (X_{RC}) for the reaction in Table 1 as a function of the partial pressure of $A_{(g)}$ (P_A) on a 2D square lattice. For $P_A < 10^{-2}$, μ_{AA} calculated by the higher-order formalism is far less than unity (i.e. $\mu_{AA} = 0.13 < 1$ in Fig. 1(A)), indicating an isolation of A^* species unnoticed by the LH model. The dearth of A^*–A^* pairs results from (i) rapidity of surface reaction which quickly annihilates neighboring A^* species (i.e. $k_r >> k_{des}$) and (ii) surface diffusion rates which are insufficient to ally separated A^* (i.e. $k_{diff} \sim k_{des} << k_r$). The LH formalism assumes infinitely-fast surface diffusion and miscalculates $X_{RC,diff} = 0$. In actuality, as the higher-order formalism shows, the diffusive conveyance of A^* species is the most kinetically-relevant step (i.e. $X_{RC,diff} \sim 0.7$ in Fig. 1(C)) and is responsible for redressing the scarcity of A^*–A^* pairs necessary for $A_{2(g)}$ formation. The isolation of A^* also places a kinetic burden on $A_{(g)}$ adsorption to generate A^*–A^* pairs to which the LH formalism is ignorant – resulting in the LH model underestimating Ψ_A by as much as ~0.4 for $P_A = 10^{-4} - 10^{0}$ (Fig. 1(B)). The presented higher-order formalism is general to site ensembles of any size, quantitatively accounts for surface diffusion, and can readily be modified to include energetic adsorbate interactions.

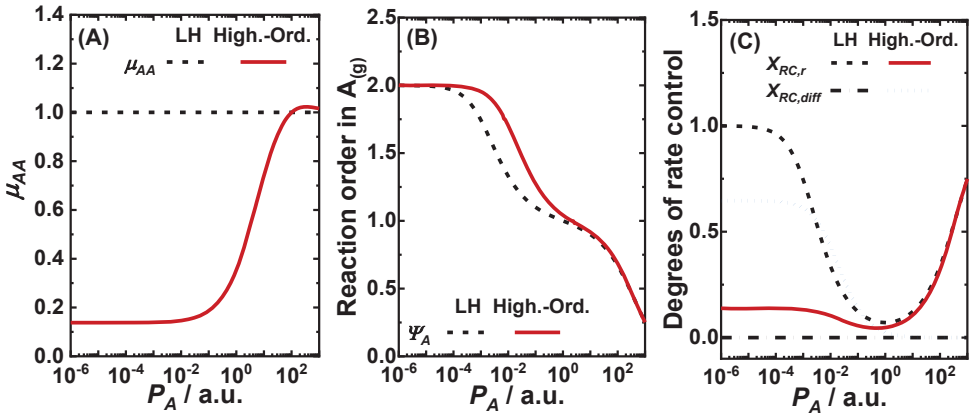

Figure 1. Kinetic descriptors of the reaction system in Table 1 calculated by the Langmuir-Hinshelwood (LH) and higher-order (High.-Ord.) formalisms.

Rates and reversibility of CO_2 hydrogenation on Cu-based catalysts

CO_2 hydrogenation, in contrast with CO hydrogenation, can form both methanol and CO via the methanol synthesis reaction ($CO_2 + 3H_2 \rightleftarrows CH_3OH + H_2O$) and the reverse water-gas shift (RWGS) reaction ($CO_2 + H_2 \rightleftarrows CO + H_2O$). The presence of two reaction pathways adds ambiguity to the reaction network, the relevant active site(s), and the surface intermediate(s) involved during catalysis. Regarding the active site for the conventional $Cu/ZnO/Al_2O_3$ catalyst formulation, the extent of Cu-Zn interaction has been postulated to vary with the reduction potential experienced by the catalyst. These dynamic changes, if prevalent, hinder kinetic analyses of rates and selectivity as rate measurements necessarily reflect a convolution of changing active site density and changing chemical activity of the species present. The elucidation of the intrinsic kinetic behaviors is further hampered by thermodynamics, which imposes severe equilibrium limitation and results in observed net reaction rates of methanol synthesis that include both kinetic and thermodynamic contributions. The assessment of methanol selectivity and yield of CO_2 hydrogenation from a kinetic standpoint must therefore address both the catalyst active site density and disambiguate kinetic and thermodynamic driving forces.

Based on a constant Cl uptake measured during in situ methylene chloride titration across different H_2:CO_2 ratios, the active site density of $Cu/ZnO/Al_2O_3$ under working conditions was first demonstrated to remain invariant with changing H_2:CO_2 ratio. This observation does not preclude complex Cu-Zn interactions but simply demonstrates that measured trends in reaction rate and selectivity are derived solely from the underlying reaction kinetics. Accordingly, measured first order dependence of methanol synthesis on H_2 partial pressure, which persists up to H_2:CO_2 = 100:1, indicates a dearth of H* species during catalysis. While the evaluation of apparent reaction orders is undoubtedly a fruitful and perhaps predominant approach to evince possible reaction mechanisms, validation of purported reaction pathways often requires derivation of rate expressions, which, in turn, requires assumptions regarding the reaction network connectivity. Instead, the reversible nature of CO_2 hydrogenation can be leveraged to invoke formalisms grounded in thermodynamics and reversibility. These relations not only provide stringent requirements on network connectivity between methanol synthesis and RWGS but also enable the deconvolution of net rates of CO_2 hydrogenation into their constitutive unidirectional forward and reverse components for intrinsic kinetic analyses.

To discern whether methanol is formed directly from CO_2 or from a sequential RWGS and CO hydrogenation ($CO + 2H_2 \rightleftarrows CH_3OH$) pathway, we utilize two thermodynamic constraints for reversible reactions: (i) the effective reversibility of an overall reaction is the product of the reversibility of its constituent elementary steps regardless of the network connectivity, and (ii) the reversibility of each constitutive elementary step in a closed catalytic cycle must be less than unity for the reaction to proceed in the forward direction per de Donder's inequality. Consequently, a sequential RWGS and CO hydrogenation pathway for methanol synthesis requires the effective reversibility of methanol synthesis to be smaller than that of RWGS.

$$Z_{\text{eff},CO_2\rightarrow CH_3OH} = Z_{\text{eff},CO_2\rightarrow CO} Z_{\text{eff},CO\rightarrow CH_3OH} \Rightarrow Z_{\text{eff},\text{CO}_2\rightarrow CH_3OH} \leq Z_{\text{eff},CO_2\rightarrow CO}$$

Under the conditions studied, however, the measured overall reversibility for methanol synthesis is *higher* than that of RWGS (Fig. 2), contradicting the requirement for any postulated sequential RWGS and CO hydrogenation pathway for the generation of methanol. The CO_2-to-CO-to-CH_3OH sequential pathway is therefore thermodynamically

forbidden under the conditions studied; the reaction network of CO_2 hydrogenation should instead be branched, with CO and CH_3OH stemming from distinct pathways (Scheme 1).

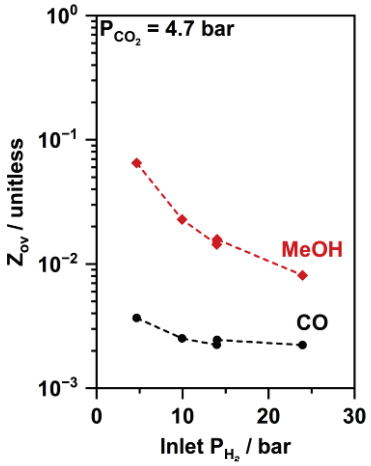

Figure 2. Methanol synthesis (red) and RWGS (black) overall reversibility as a function of P_{H2} on $Cu/ZnO/Al_2O_3$ at P_{CO2} = 4.7 bar.

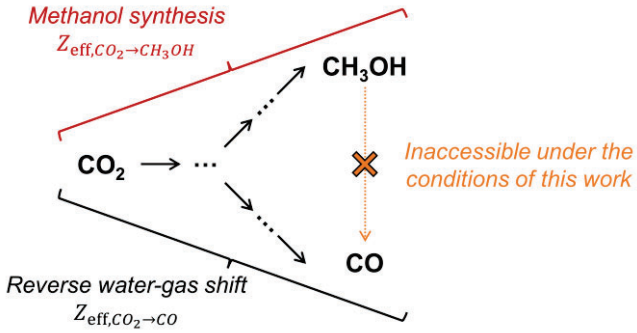

Scheme 1. Postulated branching reaction network for CO_2 hydrogenation. Stoichiometric amount of H_2 and H_2O are omitted for simplicity.

A branching pathway as shown in Scheme 1 enables the determination of rates specific to the methanol synthesis and RWGS pathways. By leveraging the characteristic equation of a plug flow reactor and by utilizing the definition of effective reversibility, unidirectional forward and reverse turnover frequency (TOF) can be determined based on measured net rates and reversibility values at different CO_2 chemical conversions. This analysis showed that H_2O preferentially inhibits the forward rate of methanol synthesis over the forward rate of RWGS, and that H_2 inhibits the reverse rates of both methanol synthesis and RWGS despite H_2 enhancing methanol synthesis forward rate (Fig. 3). Together, these results prescribe and demonstrate practical approaches to enhance methanol yield and selectivity from a kinetic standpoint – increasing P_{H2} by changing feed composition and decreasing P_{H2O} by adding water adsorbents – all without changing the conventional $Cu/ZnO/Al_2O_3$ formulation.

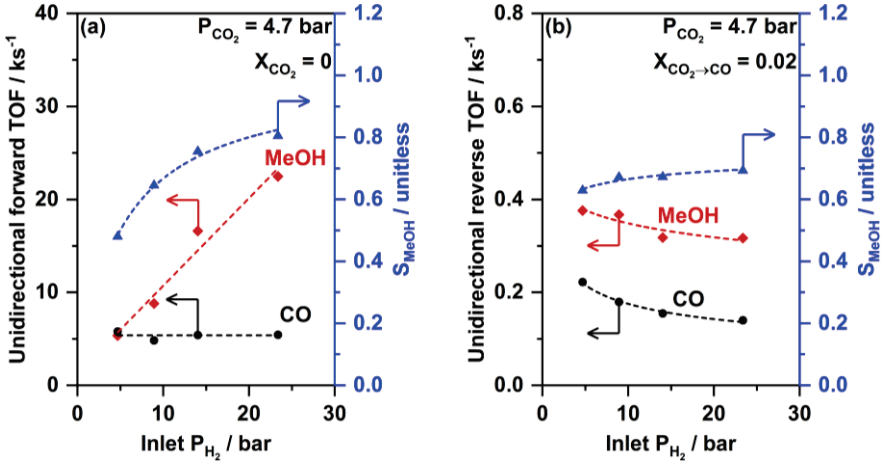

Figure 3. Instantaneous unidirectional (a) forward and (b) reverse rates of methanol synthesis (red) and RWGS (black) at 523 K on $Cu/ZnO/Al_2O_3$ as a function of P_{H2} at P_{CO2} = 4.7 bar.

Publications Acknowledging this Grant in 2019-2023

(I) Intellectually led by this grant

1. Razdan, N. K.; Kumar, A.; Bhan, A. Controlling kinetic and diffusive length-scales during absorptive hydrogen removal in methane dehydroaromatization on MoC_x/H-ZSM-5 catalysts. *J. Catal.* **2019**, *372*, 370-381.
2. Foley, B. L.; Bhan, A. Degrees of rate control at non(pseudo)steady-state conditions. *ACS Catal.* **2019**, *10*, 2556-2564.
3. Foley, B. L.; Bhan, A. Degree of rate control and De Donder relations – An interpretation based on transition state theory. *J. Catal.* **2020**, *384*, 231-251.
4. Razdan, N. K.; Kumar, A.; Bhan, A. Influence of ethylene and acetylene on the rate and reversibility of methane dehydroaromatization on Mo/H-ZSM-5. *J. Catal.* **2020**, *384*, 261-271.
5. Razdan, N. K.; Kumar, A.; Foley, B. F.; Bhan, A. Carbidic Mo is the sole kinetically-relevant active site for catalytic methane dehydaromatization on Mo/H-ZSM-5. *J. Catal.* **2020**, *389*, 667-676.
6. Foley, B. L.; Bhan, A. Thermodynamically consistent forward and reverse degrees of rate control in reversible reactions. *J. Catal.* **2020**, *389*, 566-577.
7. Razdan, N. K.; Bhan, A. Kinetic description of site ensembles on catalytic surfaces. *Proc. Nat. Acad. Sci.* **2021**, *118*, e2019055118.
8. Razdan, N. K.; Bhan, A. Kinetic description of site ensembles on catalytic surfaces. *J. Catal.* **2021**, *404*, 726-744.
9. Lin, T. C.; Razdan, N. K.; Bhan, A. Rates and reversibilities in interconnected reaction networks. *ACS Catal.* **2022**, *12*, 3100-3110.
10. Bhan, A.; Delgass W. N. Best practices in catalysis. *J. Catal.* **2022**, *405*, 419-429.
11. Razdan, N. K.; Lin, T. C., Bhan, A. Concepts relevant for the kinetic analysis of reversible reaction systems. *Chem. Rev.* **2023**, *123*, 2950-3006.

(II) Jointly funded by this grant and other grants with intellectual leadership by other funding sources

12. Li, X.; Han, H.; Xu, W.; Hwang, S-J.; Lu, P.; Bhan, A.; Tsapatsis, M. Enhanced reactivity of accessible protons in sodalite cages of faujasite zeolites. *Angew. Chem. Int. Ed.* **2022**, *61*, e202111180.
13. Li, X.; Han, H.; Xu, W.; Hwang, S-J.; Shi, Z.; Lu, P.; Bhan, A.; Tsapatsis, M. Acid catalysis over low-silica faujasite zeolites. *J. Am. Chem. Soc.* **2022**, *144*, 9324-9329.
14. Li, X.; Han, H.; Evangelou, N.; Wichrowski, N.; Lu, P.; Xu, W.; Hwang, S-J.; Zhao, W.; Song, C.; Guo, X.; Bhan, A.; Kevrikidis, I.; Tsapatsis, M. Machine Learning-Assisted Crystal Engineering of a Zeolite. *Nat. Comm.* **2023**, *14*, 3152-3163.

Charles W. Machan

Molecular Co-Electrocatalytic CO_2 Reduction with Redox Mediators

Charles W. Machan,* Amelia G. Reid, Connor A. Koellner,
Megan E. Moberg, and Shelby L. Hooe
Department of Chemistry, University of Virginia
Charlottesville, VA 22901; machan@virginia.edu

Presentation Abstract

Anthropogenic carbon dioxide (CO_2) emissions continue to be the primary contributor to climate change. The development of catalytic processes for the efficient conversion of CO_2 to useful chemical precursors or fuels could result in a 'closed loop' for carbon, if emissions from combustion are converted back into reduced and high-energy small molecules using renewable sources. The use of redox mediators (RMs), which transfer electrons and sometimes protons during a reaction of interest, is a possible solution to improving the activity and scalability of molecular electrocatalysts for CO_2 reduction. However, fundamental advancements in our understanding of co-catalytic activation strategies are still required to realize this strategy.

We are investigating the use of sulfone- and phosphole-based RMs with molecular Cr complexes for electrocatalytic CO_2 reduction to carbon monoxide (CO). Our preliminary results show that sulfone- and phosphole-based RMs with aromatic components can interact with electrocatalysts that have redox-active aromatic ligand fragments after CO_2 binding and reduction. In these systems, association is driven by weak axial coordination, the interaction of the aromatic anion(s), and dispersion effects. We find that the strength of the interaction can be tuned to improve the activity of catalysis at lower overpotentials by modifying redox potential and aromatic character of the RM and the catalyst. Interestingly, proper design can lead to inverse potential scaling for the observed activity, suggesting that the redox potential of the catalyst and RM are good proxies for energy of the aromatic components involved in co-catalyst speciation.

Michael G. White

Well-Defined $Cu/MO_x/ZnO$ Ternary Catalysts for CO_2 Hydrogenation

Luolin Shi,[1] and Jason Wang[1] and Michael G. White[1,2]
[1]Department of Chemistry, Stony Brook University, Stony Brook, NY 11794
[2]Chemistry Division, Brookhaven National Laboratory, Upton, NY 11973

Presentation Abstract

The chemical conversion of carbon dioxide has gained widespread interest as an alternative route for producing commodity chemicals such as methanol while also mitigating greenhouse gas emissions through capture and reutilization. The commercial $Cu/ZnO/Al_2O_2$ catalyst for methanol synthesis suffers from limited conversion and selectivity for CO_2 hydrogenation to methanol and alternative catalysts employing ZrO_2 or other metal oxides as promoters exhibit improved performance. Mechanistically, the activation and binding of CO_2 is thought to occur on the oxide components, while Cu provides H-atoms for hydrogenation steps via H_2 dissociation and spillover to intermediates at the Cu-oxide interface. The active phases at the Cu-oxide interface, however, are still largely uncertain including the size-dependence of the Cu nanoparticles and presence of Cu^+ sites. In this project, we are investigating the roles of Cu, ZnO and ZrO_2 and their synergy in promoting CO_2 hydrogenation using planar model catalysts composed of size-selected Cu_n clusters deposited onto ZnO, ZrO_2 and ZrO_2/ZnO supports (single crystal, powders and thin films). The formation and evolution of surface intermediates (e.g., formate and methoxy) are probed by XPS and infrared reflectance absorption spectroscopy (IRRAS) under near ambient pressures of $CO_2 + H_2$ and elevated temperatures. These results provide insight into the mechanism of CO_2 hydrogenation reaction on $Cu/ZrO_2/ZnO$ catalysts, the influence of Cu particle size, and the relative importance of Cu-oxide and $ZnO\text{-}ZrO_2$ interfaces which can aid the development of optimal catalysts for CO_2 conversion to methanol.

FWP-BNL-CO040: Catalysis for Advanced Fuel Synthesis

Electrocatalytic epoxidation via water activation

Karthish Manthiram
California Institute of Technology, Division of Chemistry and Chemical Engineering

Presentation Abstract

Oxygen-atom functionalization of chemical intermediates to generate epoxides is critical for the production of diverse textiles, plastics, and pharmaceuticals. The wet chemical and thermochemical routes used today suffer from large carbon dioxide footprints, stoichiometric waste products, and hazardous reagents. In this presentation, we will discuss methods by which water can be used as the oxygen source in functionalization reactions, such as epoxidation, with tailored metal and metal oxide nanoparticle anodic electrocatalysts. At the cathode, hydrogen is selectively generated, reflecting that this reaction can be thought of as a derivative of water splitting, in which the oxidizing equivalents go towards generating a valuable product rather than generating molecular oxygen. Doping the surface with single atoms can provide tunability over oxygen electrophilicity, a critical parameter in controlling epoxidation rates. We have developed mechanistic understanding of how water is activated, providing means by which the selectivity for oxygen-atom functionalization can be rationally improved.

Single-molecule photoelectrocatalysis: 2D junction effects on 3D photocatalysts

Peng Chen
Cornell University, Department of Chemistry and Chemical Biology

Presentation Abstract

This presentation will describe our efforts in developing and applying single-molecule imaging approaches to study (photo)(electro)catalysis on nano- and micro-scale particles. I will first give some background on single-molecule, super-resolution fluorescence imaging of catalytic reactions on single catalyst particles, with some examples. I will then focus on a recent study of photoelectrocatalytic properties of particulate semiconductor photocatalysts, which are paramount for many solar energy conversion technologies. In anisotropically shaped photocatalyst particles, the different constituent facets may form inter-facet junctions at their adjoining edges, analogous to lateral two-dimensional (2D) heterojunctions or pseudo-2D junctions made of few-layer 2D materials. Using subfacet-level multimodal functional imaging, we uncover inter-facet junction effects on anisotropically shaped bismuth vanadate ($BiVO_4$) particles and identify the characteristics of near-edge transition zones on the particle surface, which underpin the whole-particle photoelectrochemistry. We further show that chemical doping modulates the widths of such near-edge surface transition zones, consequently altering particles' performance. Decoupled facet-size scaling laws further translate inter-facet junction effects into quantitative particle-size engineering principles, revealing surprising multiphasic size dependences of whole-particle photoelectrode performance. The imaging tools, the analytical framework and the inter-facet junction concept pave new avenues towards understanding, predicting and engineering (opto)electronic and photoelectrochemical properties of faceted semiconducting materials, with broad implications in energy science and semiconductor technology.

Electrochemical Hydrogenation, Hydrogenolysis, and Dehydrogenation for Reductive and Oxidative Biomass Upgrading

Kyoung-Shin Choi and J. R. Schmidt
University of Wisconsin-Madison

Presentation Abstract

Due to growing energy demands as well as environmental concerns, the production of fuels and building block chemicals from renewable sources has become an important area of research. In particular, the use of biomass as feedstock for the production of fuels and building block chemicals holds great promise due to its abundance, accessibility, and worldwide distribution. Owing to the considerable and continuing decrease in the cost of electricity provided by renewable energy sources, electrochemical processes have become viable and appealing routes for reductive and oxidative biomass conversion. The use of electrochemical potential to drive oxidation and reduction reactions has the advantage of performing the reactions at ambient temperature and pressure without requiring the continuous consumption of reductants and oxidants.

Most biomass intermediates contain multiple functional groups. Therefore, achieving reduction and oxidation of only the desired functional groups is critical for efficient and selective upgrading of biomass intermediates. For reductive biomass upgrading, many intermediates containing oxygenated moieties such as carbonyl and alcohol groups must be selectively reduced to form desired fuels and chemicals. Thus, controlling the selectivity between hydrogenation and hydrogenolysis is of great importance for these transformations. For oxidative upgrading, partial oxidation of biomass intermediates to molecules that have greater value than the starting molecules while avoiding their complete oxidation to CO_2 is needed. Since most biomass intermediates contain multiple alcohol and aldehyde groups, the ability to selectively dehydrogenate only the desired functional group (alcohol vs aldehyde, primary alcohol vs secondary alcohol) will be vitally important for efficient and selective chemical production via biomass conversion.

In this presentation, we will discuss electrochemical hydrogenation, hydrogenolysis, and dehydrogenation processes and mechanisms that our group has been investigating for the conversion of biomass-derived molecules (e.g., 5-hydroxymethylfurfural, glycerol) to various valuable fuels and chemicals. Through this discussion, we hope to provide new insights to build general mechanistic frameworks for electrochemical hydrogenation, hydrogenolysis, and dehydrogenation reactions based on which more efficient and selective electrocatalysts and optimal reactions conditions to produce desired fuels and chemicals can be identified.

Selective Degradation of Polymer Waste to Commodity Chemicals

Erin E. Stache*, Sewon Oh, Hanning Jiang
Department of Chemistry, Princeton University

Presentation Abstract

While plastics have enabled our modern society, the scale of commercial polymer production, dismal recycling levels, and the absence of environmental degradation pathways have led to the vast accumulation of plastics in the environment. This talk will discuss our work towards leveraging fundamental principles of organic chemistry to convert polymer waste into valuable commodity chemicals. Using polymer waste as a commodity chemical feedstock lessens dependence on fossil fuels and remediates plastic buildup in the environment. We are developing selective strategies for valorizing polymer waste using the fundamental kinetics and thermodynamics of C–H bonds and abstraction agents. We convert commercial polymers into divergent commodity chemical streams through selective C–H abstraction and modulation of reaction conditions. We also demonstrate selective valorization in mixed polymer waste based on kinetic and thermodynamic selectivity principles. Successful demonstration of these approaches will motivate new recycling approaches and research into the chemical upcycling of commercial polymer waste.

Kensha M. Clark

Non-Oxidative Methane Activation by Metal-Based Frustrated Lewis Pairs

Kensha Marie Clark
Department of Chemistry and Biochemistry, University of Mississippi

Presentation Abstract

Activation of the thermodynamically strong, kinetically inert C–H bonds of methane remains a major barrier to its broader use as a major chemical feedstock. To address this challenge, earth abundant metal-based frustrated Lewis pairs (FLPs) that facilely and selectively activate C–H bonds have been designed. The metal complexes, which serve as the acidic FLP component, are supported by the flexible tripodal ligand, tris(2-(benzylidene)aminoethyl)amine (TRIM). It was found that these FLPs readily and reversibly activate methane at room temperature, whereby the formation of isotopomers of methane and of the reaction solvents suggests that this reactivity is also selective for sp^2 and sp^3 C–H bonds (*i.e.*, weaker C-heteroatom bonds are unaffected). In addition to this process, steps towards coupling this reactivity with known transformations facilitated by zinc-alkyl complexes for catalytic methane functionalization will be discussed.

Interpretable Deep Learning for Advancing Field-Enhanced Catalysis

Fanglin Che
Department of Chemical Engineering, University of Massachusetts Lowell

Presentation Abstract

Electric fields can modify the adsorption of polarized species and enhance the reaction rates and selectivity by a few orders of magnitude. These field-enhanced chemical processes provide a sustainable, energy-efficient, modular setup to store renewable electricity chemically. However, the high-cost of computations for field-dipole interactions on energetics has resulted in a trial-and-error approach for field-driven experimental processes. It is important to develop an interpretable deep learning approach to advance an in-depth understanding of field-dipole effects and promote electrostatic catalysis.

In this research, we focus on a case study of carbon-neutral hydrogen production and utilization, e.g., ammonia cracking and synthesis, over earth-abundant metal catalysts. In particular, we will (1) probe the local fields of nanoparticles under working conditions, (2) predict field-driven adsorption energetics with an interpretable deep learning approach, and (3) discover the optimal field-dipole effects on catalysis.

Interpretable deep learning of field-dipole interaction represents a new paradigm for designing high performance catalysis where large local field exists for renewable-energy related technologies, such as electrostatic catalysis, electrocatalysis, and fuel cells. The fundamental science of how field-dipole interactions has the potential to alter the energetics of ammonia cracking. In addition, synthesis of earth-abundant-based nanoparticle catalysts with low-coordinated sites will improve the energy efficiency of carbon-free hydrogen production, utilization, and storage.

Israel E. Wachs

Olefin Metathesis by Supported Molybdena Catalysts

Israel E. Wachs, Srinivas Ranagarajan, Bin Zhang, Eli M. Ream
Department of Chemical & Biomolecular Engineering, Lehigh University

Presentation Abstract

A global shortage of propylene, a major commodity chemical intermediate, has resulted in recent years because of the milder petroleum cracking conditions currently employed in refineries to produce heavier fuels and the domestic shift to lighter natural gas from fracking (mostly CH_4, minor C_2H_6 and traces of C_3H_8/C_4H_{10}). This has created a growing gap between propylene supply and demand. Olefin metathesis (C_2H_4 + $CH_3CH_2{=}CH_2CH_3 \rightarrow 2\ CH_2{=}CHCH_3$) by supported metal oxide catalysts has emerged as the fastest growing process for on-purpose propylene. In spite of the importance of the olefin metathesis reaction, much confusion still exists about this reaction by supported metal oxide catalysts.

The objectives of these studies are to determine the fundamentals of olefin metathesis by supported metal oxide catalysts and apply the new insights to molecularly design more efficient catalysts. The supported MoO_x catalysts were selected for the current studies because of their importance for industrial olefin metathesis. The oxide support and its anchoring sites for MoO_x were found to be critical in controlling the performance of the supported MoO_x active sites ($Al_2O_3 >> SiO_2 >> ZrO_2 \sim TiO_2 \sim CeO_2$). The surface MoO_x sites are easily activated on Al_2O_3 and only activated at high temperatures on SiO_2 by propylene because of the weak redox characteristic of the Al and Si ligands with Al > Si. In contrast, the surface MoO_x sites on the more redox supports (ZrO_2, TiO_2, and CeO_2) become occupied by stable surface acetate groups that poison the activated MoO_x sites by blocking them for olefin metathesis. These fundamental insights suggest a catalyst synthesis approach to enhance the performance of the model supported MoO_x/SiO_2 catalyst for olefin metathesis by controlling the support ligands and anchoring sites for MoO_x.

The supported MoO_x/SiO_2 catalyst is considered a model system because it exclusively consists of isolated dioxo $(O{=})_2Mo(\text{-}O\text{-}Si)_2$ sites, but ~40% of the MoO_x sites volatilize at the required high temperatures during propylene activation for olefin metathesis. Designing supported MoO_x/SiO_2 catalysts that could be activated at lower temperatures would circumvent this technical problem. It was hypothesized that this may be achieved by surface modifying the SiO_2 support with surface AlO_x sites that are more efficient in activating surface MoO_x sites than SiO_x ligands. Subsequent to completely dispersing the alumina AlO_x sites on the SiO_2 support, surface MoO_x sites were selectively anchored at the surface AlO_x sites because of the greater affinity of AlO_x than SiO_x for MoO_x (driven by their differences in surface free energy of Al_2O_3 and SiO_2). The molecularly engineered supported $MoO_4/AlO_x/SiO_2$ catalyst was indeed found to activate at mild temperatures (~100°C) and avoid volatilization of the surface MoO_4 sites. This resulted in dramatically increasing the number of activates surface MoO_x sites and their TOF for olefin metathesis.

Michael J. Janik

Intermetallic catalysts for probing and designing hydrogenation active sites

Michael J. Janik, Robert M. Rioux, Angela Nguyen, Jin Li, Haoran He, Griffin Canning, Ahmed Hamed
Department of Chemical Engineering, Pennsylvania State University

Presentation Abstract

Catalysis research seeks to connect the composition and structure of active sites to the catalytic activity and selectivity to desired products. Intermetallics – multi-metal systems with a well-defined arrangement of the metal atom – offer a platform to control active site structure and composition. We combined high throughput density functional theory (DFT) calculations, machine learning approaches, and microkinetic modeling (MKM) together with experimental synthesis, characterization, and catalytic testing to define active site requirements for selective hydrogenation catalysis. The combination of DFT, MKM, and experimental studies is used to demonstrate catalytic differences between isolated Pd monomer, Pd3 trimer, and Pd-M-Pd (M=Cu, Ag, Au) sites exposed in gamma-brass intermetallic systems. The development of a computational workflow to predictively design sites selective for a range of hydrogenation reactions will be discussed. This computational workflow uses high throughput, automated DFT calculations, scaling relationships, and ML prediction of adsorption energies to mine libraries of intermetallic structures for surfaces that may offer selective hydrogenation of target unsaturated moieties. The use of this workflow to recommend intermetallics for semi-hydrogenation of acetylene will be presented.

François P. Gabbaï

Antimony-based strategies for small-molecule activation and catalysis

François P. Gabbaï
Department of Chemistry, Texas A&M University

Presentation Abstract

Antimony compounds are known for their remarkable Lewis acidity, particularly in their pentavalent forms. Additionally, their redox-active nature, with facile transitions between trivalent and pentavalent states, presents unique opportunities for small molecule activation and catalysis. This presentation explores these aspects, focusing on two key areas. We will begin by detailing the synthesis of two novel distibines based on the 9,9-dimethylxanthene and 9,9-dimethyldihydroacridine scaffolds and their interactions with molecular oxygen. While no reaction occurs with oxygen alone, the reductive properties of these distibines is potentiated in the presence of electron-rich *ortho*-quinone such as phenanthraquinone. Indeed, in the presence of such an *ortho*-quinone, the reaction proceeds by oxidation of the two antimony atoms to the + V state in concert with reductive cleavage of the O_2 molecule. As confirmed by ^{18}O labeling experiments, the two resulting oxo units combine with the ortho-quinone to form an α,α,β,β-tetraolate ligand that bridges the two antimony(V) centers. The reaction mechanism, supported by NMR spectroscopy and computational modeling, suggests a pathway where one stibine is converted into a semiquinone/peroxoantimony intermediate before reacting with the second stibine. The resulting α,α,β,β-tetrolate distiborane derivative can be triggered to release two equivalents of water as O_2 reduction product by acidolysis and reduction. These last steps also regenerate the original bis-antimony(III) derivative, offering prospects for catalytic applications. In the second segment, we will demonstrate how redox modulation at the antimony center of phosphinostibine platforms can fine-tune the reactivity of late transition metals coordinated to the phosphine ligand. We will illustrate this concept using a phosphine gold complex featuring a triaryl stibine at the upper rim of a 9,9-dimethylxanthene scaffold. Structural, computational, and experimental data show that oxidizing the stibine moiety into a stiborane using an *ortho*-quinone activates the carbophilic reactivity of the gold center. Computational modeling further suggests that this reactivity enhancement stems from the Lewis acidity of the stiborane, which engages the gold-bound chloride anion via a pnictogen bond. Altogether, our study showcases organoantimony derivatives' versatile and promising role in small molecule activation and catalysis, offering new avenues for chemical transformations and applications.

Matthew P. Conley

Supported Electrophilic d^0 Metal Hydrides for Hydrogenolysis Reactions

Matthew P. Conley*, Jiaxin Gao, Kavyasripriya Samudrala
University of California, Riverside
Department of Chemistry

Presentation Abstract

This talk will describe synthesis and characterization of well-defined organometallics on surfaces that behave similarly to weakly coordinating anions.[1] We apply these reactive species to the hydrogenolysis of alkanes and/or alkane metathesis reactions depending on the active site generated in the grafting reaction. For example, we showed that sulfated aluminum oxide (**SAO**) reacts with Ta(=CH^{t}Bu)(CH$_2$^{t}Bu)$_3$ to form organotantalum species that react with H_2 to form electrophilic tantalum hydride (Ta–H$^+$) sites that are active in hydrogenolysis and alkane metathesis reactions.[2] In both reactions Ta–H$^+$ is more active than related neutral Ta–H sites supported on silica. This reaction chemistry extends to melts of high-density polyethylene (HDPE), where Ta–H$^+$ converts 30 % of a HDPE (M_n = 2.5 kg mol^{-1}; $Đ$ = 3.6) to low molecular weight paraffins under hydrogenolysis conditions. Subsequent studies showed that the Ta–H$^+$ sites react with isotactic polypropylene (iPP, M_n = 13.3 kDa; $Đ$ = 2.4; mmmm = 94 %) to form atactic oils in good yield.[3] Experiments with D_2, and complementary trapping experiments with HBPin, show that Ta-H$^+$ sites react with iPP at both -CH$_3$ and -CH$_2$- groups in iPP, but not with -CH- groups.

We also investigated reactions of Cp$_2$Hf(CH$_3$)$_2$ and silica containing strong aluminum Lewis acid sites[4] to form Cp$_2$Hf–CH$_3$$^+$ paired to aluminate anions.[5] Solid-state NMR characterization shows that this reaction also forms neutral organohafnium and hafnium sites lacking methyl groups. Cp$_2$Hf–CH$_3$$^+$ reacts with iPP in the presence of H_2 to form oils with moderate molecular weights (M_n = 290 - 1200 Da) in good yields. The aliphatic oils show characteristic $^{13}C\{^1H\}$ NMR properties consistent with complete loss of diastereoselectivity and formation of regioirregular errors under 1 atm H_2. This latter set of results suggests that a typical Ziegler-Natta type active site is compatible in a common reaction used to digest waste plastic into smaller aliphatic fragments.

References:

[1] Samudrala, K. K.; Conley, M. P. *Chem. Commun.* **2023**, *59*, 4115-4127.
[2] Gao, J.; Zhu, L.; Conley, M. P. *J. Am. Chem. Soc.* **2023**, *145*, 4964-4968. Related work: Lai, Q.; Mason, A. H.; Agarwal, A.; Edenfiled, W. C.; Zhang, X.; Kobayashi, T.; Kratish, Y.; Marks, T. J. *Chemrxiv*, DOI: 10.26434/chemrxiv-2023-24gfx.
[3] Gao, J.; Zhu, L.; Conley, M. P. *ACS Catal.* **2023**, *13*, 10765–10769.
[4] Samudrala, K. K.; Huynh, W.; Dorn, R. W.; Rossini, A. J. *Angew. Chem., Int. Ed.* **2022**, *61*, e202205745.
[5] Samudrala, K. K.; Conley, M. P. *Submitted*

Ba L. Tran

Mechanistic and Reactivity Studies of Dimeric and Monomeric Copper Hydrides

Amy L. Speelman, Evan A. Patrick, David E. Ryan, Jeremy D. Erickson, R. Morris Bullock, Ba L. Tran
Pacific Northwest National Laboratory
Physical & Computational Sciences Directorate

Presentation Abstract

Controlling the nuclearity of metal sites to enhance reactivity is central to homogeneous and heterogenous catalysis. Among transition metal hydride complexes, copper hydride (CuH) monomers are highly unstable and generally exist as multinuclear aggregates. Kinetic and structural studies on the insertion reactions of aldehyde, ketone, ester, amide, and unsaturated hydrocarbons with a series of [(NHC) $CuH]_2$ dimers have enabled the design of *N*-heterocyclic carbene ligands that promote cooperativity of proximal *and* distal sites to destabilize the ground-state structure of the dimer in favor of monomer formation. Access to isolable CuH monomers has exhibited new insertion chemistry with internal alkenes and has facilitated mechanistic analysis of the aggregation process and the disaggregation of clusters back to the reactive monomer. Mechanistic observations in the insertion reactions of the dimer series also prompted the application of solid-gas reactions of single crystal to single crystal transformations, allowing for the identification of a rare pathway of direct CO_2 insertion into the $[Cu_2H_2]$ core without requiring formation of transient (NHC)CuH monomers by complete dimer dissociation.

NATIONAL LABORATORIES ABSTRACTS

Aaron D. Sadow

Uniform catalytic environments at the interface: characterization of sites and distributions, catalytic activity and reaction mechanisms

Takeshi Kobayashi, Frédéric A. Perras, Long Qi, Damien Culver, Aaron D. Sadow
Ames National Laboratory, U.S. DOE, Iowa State University, Ames, IA 50011-3111

Presentation Abstract

The mission of the Ames Lab collaborative Program in Catalysis Science is to enable efficient and selective transformations by developing new catalytic principles for uniting the best features of homogeneous and heterogeneous catalysis in 3D environments. The overarching goal of this fundamental research is to synthesize and study highly uniform solid catalysts that mediate the difficult carbon-oxygen and carbon-hydrogen bond cleavage reactions, which are needed to utilize bioderived feedstocks and abundant hydrocarbons for chemical synthesis. To this end our research team combines expertise in mesoporous and nanostructured catalyst synthesis, organometallic chemistry, kinetics and mechanisms of catalytic reactions, and solid-state (SS)NMR, including the ultrasensitive dynamic nuclear polarization (DNP) technique. Uniform materials are essential because their spectroscopic features characterize the most important and most pertinent species and functionality for affecting the overall catalytic properties, thus facilitating the rational improvement of catalysts. Unfortunately, catalytic species operating at the solid-liquid interface rarely approach the ideal homogeneity (sometimes) epitomized by chemistry in a single phase. To address this gap, our team combines advanced materials synthesis and surface organometallic chemistry with cutting-edge NMR spectroscopic methods to construct uniform organometallic catalytic sites, distributed evenly in the uniform environments created by pores of hierarchical functionalized mesoporous materials. These species represent several classes of catalysts commonly applied in hydrogenations and hydrodeoxygenations of oxygenates or in C-H bond activations, which are nonetheless currently limited. Using the uniform materials and operando spectroscopy, we elucidate molecular-level mechanisms, including those involved in complex reaction networks, and then ameliorate the features that constrain catalytic performance.

AL-03-380-011: Homogeneous and Interfacial Catalysis in 3D Controlled Environments
Postdoc(s): Mita Halder, Praveen Kumar, Yuting Li, Marco Mais, Scott Southern,
Student(s): Puranjan Chatterjee, Austin Thompson

RECENT PROGRESS

Publications Acknowledging this Grant in 2019-2023
Source of support for the work published

(I) ***Intellectually led by this grant*** 2020 [1-7] 2021 [8-14] 2022[15-25] 2023[26, 27]

(II) ***Jointly funded by this grant and other grants with intellectual leadership by other funding sources*** 2020 [28-38] 2021 [39-45] 2022[46-52] 2023[53-58]

Single-site Catalysts for C–O hydrogenolysis. Single-site first-row transition metals show promising performance in selective catalytic hydrogenation, but they are less well-studied for more complex reaction pathways such as C–O hydrogenolysis. Their ability to perform selective C–O hydrogenolysis of oxygenated hydrocarbons depends on both the ligands directly bound to the metal ion as well as longer-range contributions from the non-innocent support. We discovered that a single-site Fe catalyst with a well-defined local structure supported on non-innocent nitrogen-doped carbons (N-Cs) can catalyze C–O bond hydrogenolysis of aryl alcohols and ethers. Mechanistic investigation revealed that the reactivity is enabled by the chemical and redox non-innocence of the N-C support. According to spectroscopic analyses, the as-synthesized catalyst contains mostly penta-coordinated Fe^{III} sites with four in-plane nitrogen donor ligands and one axial hydroxyl ligand. In the presence of 20 bar H_2 at 170-230 °C, the hydroxyl ligand is lost when $N_4Fe^{III}OH$ is reduced to N_4Fe^{II}. Alcohol binding to the tetra-coordinated Fe^{II} sites leads to homolytic cleavage of the O-H bond accompanied by re-oxidation to Fe^{III}. Subsequent formation of a new C-H bond involving a carbon atom in the N-C support is promoted by electron stabilization due to the presence of adjacent additional graphitic nitrogen atoms. The support also promotes H_2 splitting. The direct involvement of the N-C support is analogous to the behavior of chemically- and redox-non-innocent ligands in molecular catalysts based on first-row transition metal ions. The participation of the N-C support in the hydrogenolysis mechanism enhances the ability of M-N-Cs based on first-row transition metals to achieve the types of strong bond activation needed to upgrade renewable feedstocks. The non-innocence of the support can be also found to play role in the electrocatalytic reduction of CO_2,[25] opening broad opportunities for rational design of novel catalysts for challenging chemical reactions to meet the challenges for a carbon-neutral future.

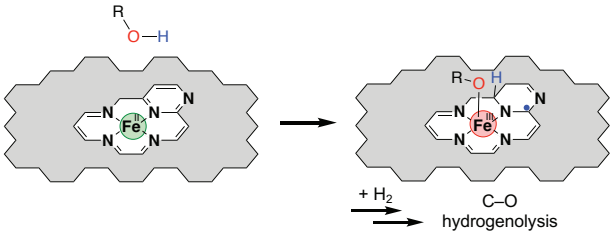

Figure 1. Proposed chemical and redox non-innocence of an extended N-doped carbon support, which promotes homolytic O-H bond cleavage of alcohols at atomically-dispersed Fe^{II} sites. One-electron oxidation of Fe^{II} to Fe^{III} is accompanied by free radical generation at carbon, stabilized by adjacent N.

CH Bond Functionalization by Supported Early Metal Catalysts. Surface supported, high oxidation state early transition metal hydrides, such as $(\equiv SiO)_3ZrH$ catalyze H/D exchange of CH bonds, which is proposed to involve dehydrometalation via a σ-bond metathesis step and deutereolysis of the Zr–C bond through the microscopic reverse, thus also σ-bond metathesis (Figure 1, top). Our team has been investigating new reactions that that desymmetrize this process by introducing an organocarbyl group acceptor (E–H in Figure 2). This approach has a potential advantage over oxidative chemistry, in the organometallic products (boranes, silane, alanes, etc.) and reactants can be more

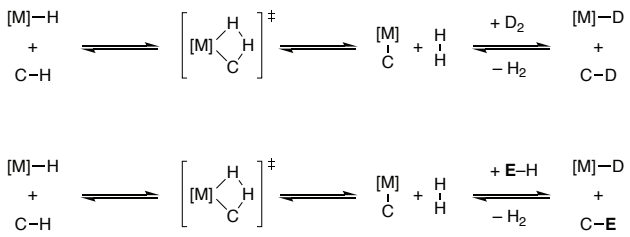

Figure 2. Strategy for CH functionalization by group transfer to a main group element

closed matched in energy. As a result, the kinetic selectivity of the reaction may not be undermined by competitive formation of thermodynamically driven reaction products.

First, we have shown that lanthanum borohydride, grafted into the pores of the faujasite zeolite HY_{30}, catalyzes the C–H borylation of benzene to form phenyl pinacolborane (PhBpin) and eliminate H_2.[15] The active sites are derived from lanthanum species that are bonded to former Brønsted acid sites (BAS) generated from bridging ≡SiO(H)Al≡ surface functionality. The formation of PhBpin is linear, suggesting that CH borylation is zero-order in HBpin. The residual BAS catalyze HBpin decomposition, however, the HBpin concentration dependence appears to be first order. Therefore, to minimize HBpin decomposition and increase PhBpin yield, CH borylation reactions are performed under conditions with dilute HBpin. The active species may be an adduct of hydridolanthanum with HBpin (i.e., dihydropinacolborate), or a lanthanum hydride itself.

We considered that other adducts of early metals and Lewis acids containing reactive groups could also lead to CH functionalization. Specifically, early metal tetraorgano aluminates (AlR_4, R = alkyl, hydrido) generated from the combination of alkyl or hydridometal species and trialkyl aluminum. Early metal tetraalkylaluminates or the free transition metal organometallic may then be reactive for bond activation. Organoaluminum are appealing as reactants for CH functionalization because many are made on commodity scale, aluminum is readily available in the earth's crust, and organoaluminum reagents are useful for functionalization via oxidation or transmetalation. Alkylaluminums, such as triethylaluminum, are prepared from aluminum, ethylene, and hydrogen in an atom economical hydrogen activation and insertion process. In addition to serving as alkyl group acceptors after CH activation/metalation, alkylaluminum species may serve as activators of inert transition metal precatalysts and scavengers of oxidizing impurities. In the context of these ideas, we investigated ≡Si–O–Zr(O*t*Bu)$_3$ as a precatalyst for the CH alumination of hydrocarbons. n-Dodecane and triethylaluminum react in the presence of ≡Si–O–Zr(O*t*Bu)$_3$ to give 1-dodecanol in 40% yield after oxidative workup (Figure 3).[53] Some dodecane diol is formed, and the n-dodecane is isomerized but not shortened (e.g., decane or decanol are not detected in products). Reaction of cyclooctane and triethylaluminum in the presence of ≡Si–O–Zr(O*t*Bu)$_3$ as precatalyst gives only ring-opened products; because these are formally unsaturated, chain growth and carbaluminated products are observed as well. Thus, the activated catalysts readily catalyzes C–C bond cleavage, but chain shortening is not detected. We rationalize this observation based on two reactive valences on Zr participating in C–C cleavage, which always keeps the chain bonded to the active sites (Figure 4).

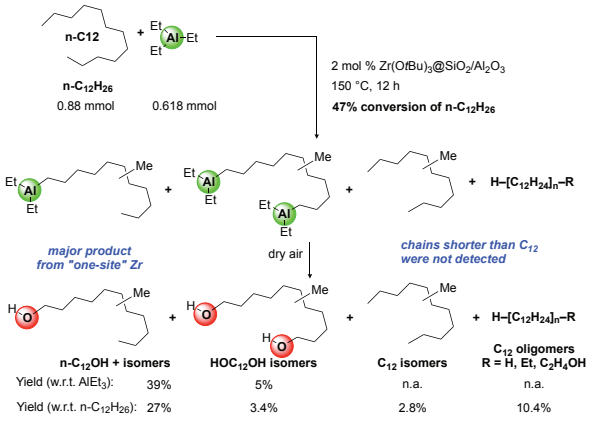

Figure 3. CH alumination of dodecane.

Interestingly, methane and triethylaluminum react in the presence of ≡Si–O–Zr(O*t*Bu)$_3$ as precatalyst to give methylaluminum species and ethane. Trimethylaluminum cannot be manufactured through the efficient, insertive process used to make triethylaluminum; instead, sodium reduction and redistribution of Me_xAl_{3-x} (synthesized from Al and MeCl) gives Me_3Al and $AlCl_3$ (and NaCl). Thus, the direct CH alumination of methane from $AlEt_3$ could be much more efficient.

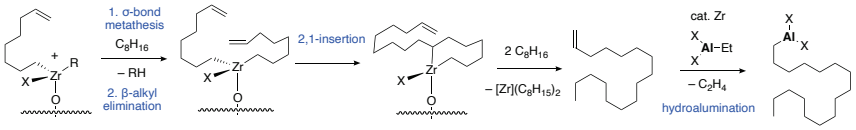

Figure 4. C-C cleavage without chain shortening, making use of dialkyl zirconium surface sites.

Solid-State NMR to Characterize Uniform Catalytic Materials. The development of catalysts that efficiently catalyze new reactions, including C-H alumination and borylation, requires a detailed understanding of the structure of the catalytic active site. This is a far from trivial task as most characterization tools that are available for surface characterization are either highly local (1D NMR, DRIFTS, XAS, XPS) or function in the super-molecular regime (electron microscopy). We have developed unique NMR methods that leverage sensitivity enhancements afforded by dynamic nuclear polarization (DNP) to reveal detailed three-dimensional structures of supported species, including their orientation on the surface, conformation, and configuration. Most recently, these methods have been generalized and made available to the scientific community through the publication of a free and open-source program called INTERFACES (Figure 5). The program enables the simultaneous fitting of interatomic distances and surface-to-atom distance data, obtained from dipolar recoupling approaches, to a single (or multiple) molecular species. We have applied NMR distance measurements to the study of the structure of borylation catalysts, including the measurement of ^{1}H-^{31}P distances to hydride sites in a catalytic intermediate. Most recently, approaches aimed at the structural determination of silica-supported catalysts were further generalized through the demonstration that surface ^{17}O labels could be used for probing the distance between nuclear sites on the catalyst and the support plane.

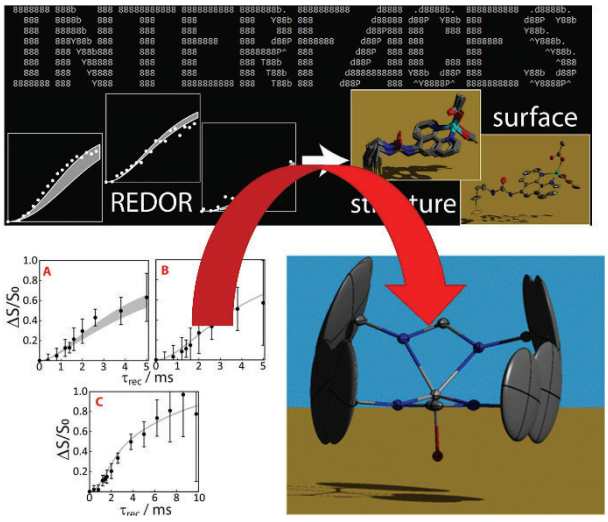

Figure 5. Depiction of the method developed for the solution of high-resolution structures of supported catalysts. Dipolar recoupling data is first acquired using sensitivity-enhanced NMR and this is then analyzed using the INTERFACES program to reveal a distribution of surface species.

It is important to not only consider molecular structure but also the impact of intersite proximities, which can lead to synergies between sites. We previously introduced dipole coupling measurements to measure intersite proximities, but such approaches can be complicated when the sites are identical given that the same nuclear pairs can be found both inter- and intramolecularly. We addressed this shortcoming by the measurement of high-quanta multiple-quantum correlation through a new multiplex experiment (Figure 6).

For example, since cyclopentadienyl ligands (Cp) have five equivalent ^{1}Hs, the presence of 6-quantum coherence arising from six Cp ^{1}Hs indicates that at least two Cp ligands are in close proximity. The proximity can further be quantified by measuring the magnitude of the dipolar coupling; however, because the dipolar interactions are partially averaged by molecular motions. As such, the internuclear distance determined by this method is often overestimated. To address this limitation, we coupled NMR with molecular dynamics simulations to estimate the degree of motional averaging felt by the nuclei.

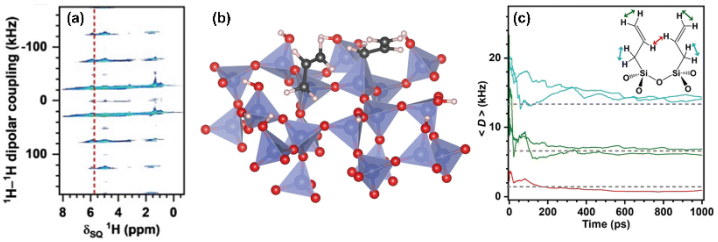

Figure 6. ^{1}H DQ/SQ spectrum for allyl/SiO_2 (a), MD model (b), and agreement between experimental dipolar couplings and MD (c).

Awards or leadership activities during 2019-2022 calendar years

Frédéric Perras: DOE Early Career Award (2020)
Long Qi: Great Plains Catalysis Society Meeting organizing committee (2020, 2022)
Aaron Sadow: Director of Institute for Cooperative Upcycling of Plastics (iCOUP) DOE-EFRC (2020)
Aaron Sadow: Great Plains Catalysis Society Meeting organizing committee (2022)
Aaron Sadow: Fulbright US Scholars Fellowship (2020-1)
Aaron Sadow: Trapp Innovation Award (2022)
Frédéric Perras: Recognized as an emerging researcher by the Journal of Physical Chemistry (2023)
Frédéric Perras: Awarded the Caldarelli Prize in Magnetic Resonance (2023)
Aaron Sadow: AAAS Fellow (2023)

Publications Acknowledging this Grant in 2020-2023 and addition References

1. Zhou, H.; Wang, H.; Sadow, A. D.; Slowing, I. I., Toward Hydrogen Economy: Selective Guaiacol Hydrogenolysis Under Ambient Hydrogen Pressure. *Appl. Catal. B* **2020,** *270*, 118890-118899. doi:10.1016/j.apcatb.2020.118890
2. Wang, Z.; Patnaik, S.; Eedugurala, N.; Manzano, J. S.; Slowing, I. I.; Kobayashi, T.; Sadow, A. D.; Pruski, M., Silica-Supported Organolanthanum Catalysts for C–O Bond Cleavage in Epoxides. *J. Am. Chem. Soc.* **2020,** *142*, 2935-2947. doi:10.1021/jacs.9b11606
3. Singappuli-Arachchige, D.; Slowing, I. I., Control of Interfacial pH in Mesoporous Silica Nanoparticles via Surface Functionalization. *J. Chem. Phys.* **2020,** *152*, 034703. doi:10.1063/1.5138912
4. Qi, L.; Chen, J.; Zhang, B.; Nie, R.; Qi, Z.; Kobayashi, T.; Bao, Z.; Yang, Q.; Ren, Q.; Sun, Q.; Zhang, Z.; Huang, W., Deciphering a Reaction Network for the Switchable Production of Tetrahydroquinoline or Quinoline with MOF-Supported Pd Tandem Catalysts. *ACS Catal.* **2020,** *10*, 5707-5714. doi:10.1021/acscatal.0c00899

5. Manzano, J. S.; Wang, H.; Kobayashi, T.; Naik, P.; Lai, K. C.; Evans, J. W.; Slowing, I. I., Kinetics of the Functionalization of Mesoporous Silica Nanoparticles: Implications on Surface Group Distributions, Adsorption and Catalysis. *Microporous Mesoporous Mater.* **2020,** *305*, 110276. doi:10.1016/j.micromeso.2020.110276
6. Luo, Z.; Nie, R.; Nguyen, V. T.; Biswas, A.; Behera, R. K.; Wu, X.; Kobayashi, T.; Sadow, A.; Wang, B.; Huang, W.; Qi, L., Transition Metal-like Carbocatalyst. *Nat. Commun.* **2020,** *11*, 4091. doi:10.1038/s41467-020-17909-8
7. Hafezisefat, P.; Lindstrom, J. K.; Brown, R. C.; Qi, L., Non-catalytic Oxidative Depolymerization of Lignin in Perfluorodecalin to Produce Phenolic Monomers. *Green Chem.* **2020,** *22*, 6567-6578. doi:10.1039/D0GC02505D
8. Patnaik, S.; Kanbur, U.; Ellern, A.; Sadow, A. D., Hydrosilane σ-Adduct Intermediates in an Adaptive Zinc-Catalyzed Cross-dehydrocoupling of Si−H and O−H Bonds. *Chem. Eur. J.* **2021,** *27*, 10428-10436. doi:10.1002/chem.202101146
9. Naik, P. J.; Chatterjee, P.; Chen, S.; Huang, W.; Slowing, I. I., Regulating the Catalytic Activity of Pd Nanoparticles by Confinement in Ordered Mesoporous Supports. *ChemCatChem* **2021,** *13*, 539-542. doi:10.1002/cctc.202001594
10. Eedugurala, N.; Wang, Z.; Kanbur, U.; Ellern, A.; Pruski, M.; Sadow, A. D., Synthesis and Characterization of Tris(oxazolinyl)borato Copper(II) and Copper(I) Complexes. *Helv. Chim. Acta* **2021,** *104*, e2000209. doi:10.1002/hlca.202000209
11. Boteju, K. C.; Venkatesh, A.; Chu, Y.-Y.; Wan, S.; Ellern, A.; Rossini, A. J.; Sadow, A. D., Ancillary Steric Effects on the Activation of SiH Bonds in Arylsilazido Rare-Earth Compounds. *Organometallics* **2021,** *40*, 1654-1669. doi:10.1021/acs.organomet.1c00162
12. Perras, F. A.; Paterson, A. L.; Syed, Z. H.; Kropf, A. J.; Kaphan, D. M.; Delferro, M.; Pruski, M., Revealing the Configuration and Conformation of Surface Organometallic Catalysts with DNP-Enhanced NMR. *J. Phys. Chem. C* **2021,** *125*, 13433-13442. doi:10.1021/acs.jpcc.1c03176
13. Chen, J.; Qi, L.; Zhang, B.; Chen, M.; Kobayashi, T.; Bao, Z.; Yang, Q.; Ren, Q.; Huang, W.; Zhang, Z., Tandem Synthesis of Tetrahydroquinolines and Identification of the Reaction Network by Operando NMR. *Catal. Sci. Technol.* **2021,** *11*, 4332-4341. doi:10.1039/D1CY00418B
14. Naik, P. J.; An, Y.; Sedinkin, S. L.; Masching, H.; Freppon, D.; Smith, E. A.; Venditti, V.; Slowing, I. I., Non-Innocent Role of the Ceria Support in Pd-Catalyzed Halophenol Hydrodehalogenation. *ACS Catal.* **2021**, 10553-10564. doi:10.1021/acscatal.1c02716
15. Li, Y.; Kanbur, U.; Cui, J.; Wang, G.; Kobayashi, T.; Sadow, A. D.; Qi, L., Supported Lanthanum Borohydride Catalyzes CH Borylation Inside Zeolite Micropores. *Angew. Chem. Int. Ed.* **2022,** *61*, e202117394. doi:10.1002/anie.202117394
16. Perras, F. A.; Kanbur, U.; Paterson, A. L.; Chatterjee, P.; Slowing, I. I.; Sadow, A. D., Determining the Three-Dimensional Structures of Silica-Supported Metal Complexes from the Ground Up. *Inorg. Chem.* **2022,** *61*, 1067-1078. doi:10.1021/acs.inorgchem.1c03200
17. Chatterjee, P.; Wang, H.; Manzano, J. S.; Kanbur, U.; Sadow, A. D.; Slowing, I. I., Surface Ligands Enhance the Catalytic Activity of Supported Au Nanoparticles

for the Aerobic α-Oxidation of Amines to Amides. *Catal. Sci. Technol.* **2022,** *12*, 1922-1933. doi:10.1039/D1CY02121D
18. Cui, J.; Chatterjee, P.; Slowing, I. I.; Kobayashi, T., In Situ ^{29}Si Solid-State NMR Study of Grafting of Organoalkoxysilanes to Mesoporous Silica Nanoparticles. *Microporous Mesoporous Mater.* **2022,** *339*, 112019. doi:10.1016/j.micromeso.2022.112019
19. Lin, Y.; Nie, R.; Li, Y.; Wu, X.; Yu, J.; Xie, S.; Shen, Y.; Mao, S.; Chen, Y.; Lu, D.; Bao, Z.; Yang, Q.; Ren, Q.; Yang, Y.; Liu, F.; Qi, L.; Huang, W.; Zhang, Z., Highly Efficient and Anti-poisoning Single-atom Cobalt Catalyst for Selective Hydrogenation of Nitroarenes. *Nano Research* **2022**. doi:10.1007/s12274-022-4294-6
20. Luo, Z.; Yin, Z.; Yu, J.; Yan, Y.; Hu, B.; Nie, R.; Kolln, A. F.; Wu, X.; Behera, R. K.; Chen, M.; Zhou, L.; Liu, F.; Wang, B.; Huang, W.; Zhang, S.; Qi, L., General Synthetic Strategy to Ordered Mesoporous Carbon Catalysts with Single-Atom Metal Sites for Electrochemical CO_2 Reduction. *Small* **2022,** *18*, 2107799. doi:10.1002/smll.202107799
21. Hu, H.; Nie, Y.; Tao, Y.; Huang, W.; Qi, L.; Nie, R., Metal-free Carbocatalyst for Room Temperature Acceptorless Dehydrogenation of N-Heterocycles. *Sci. Adv.* **2022,** *8*, eabl9478. doi:10.1126/sciadv.abl9478
22. Chu, Y.-Y.; Lolinco, A.; Eedugurala, N.; Ellern, A.; Windus, T. L.; Sadow, A. D., Reversible Ligand Protonation in Noninnocent Constrained-Geometry-Like Group 4 Complexes. *Organometallics* **2022,** *41*, 141-154. doi:10.1021/acs.organomet.1c00612
23. Cunningham, J.; Perras, F. A., INTERFACES. A Program for Determining the 3D Structures of Surfaces Sites Using NMR Data. *J. Magn. Reson. Open* **2022,** *12-13*, 100066. doi:10.1016/j.jmro.2022.100066
24. Kobayashi, T.; Liu, D.-J.; Perras, F. A., Spatial Arrangement of Dynamic Surface Species from Solid-state NMR and Machine Learning-Accelerated MD Simulations. *Chem. Commun.* **2022,** *58*, 13939-13942. doi:10.1039/D2CC05861H
25. Yin, Z.; Yu, J.; Xie, Z.; Yu, S.-W.; Zhang, L.; Akauola, T.; Chen, J. G.; Huang, W.; Qi, L.; Zhang, S., Hybrid Catalyst Coupling Single-Atom Ni and Nanoscale Cu for Efficient CO2 Electroreduction to Ethylene. *J. Am. Chem. Soc.* **2022,** *144*, 20931-20938. doi:10.1021/jacs.2c09773
26. Perras, F. A.; Arroyave, A.; Southern, S. A.; Lamb, J. V.; Li, Y.; LaPointe, A.; Delferro, M., Double-Resonance ^{17}O NMR Experiments Reveal Unique Configurational Information for Surface Organometallic Complexes. *Chem. Commun.* **2023,** *59*, 4604-4607. doi:10.1039/D3CC00899A
27. Shekar, S. C.; Perras, F. A., Multiplex Detection of Multiple-Quantum/Single-Quantum NMR Correlation Spectra. *J. Phys. Chem. C* **2023,** *127*, 7352-7359. doi:10.1021/acs.jpcc.3c00857
28. Zhou, H.; Wang, H.; Perras, F. A.; Naik, P.; Pruski, M.; Sadow, A. D.; Slowing, I. I., Two-step Conversion of Kraft Lignin to Nylon Precursors Under Mild Conditions. *Green Chem.* **2020,** *22*, 4676-4682. doi:10.1039/D0GC01220C
29. Zhang, W.; Xu, C.; Kobayashi, T.; Zhong, Y.; Guo, Z.; Zhan, H.; Pruski, M.; Huang, W., Hydrazone-Linked Heptazine Polymeric Carbon Nitrides for Synergistic

Visible-Light-Driven Catalysis. *Chem. Eur. J.* **2020,** *26*, 7358-7364. doi:10.1002/chem.202000934
30. Sedinkin, S. L.; An, Y.; Naik, P.; Slowing, I. I.; Venditti, V., An Organogel Library for Solution NMR Analysis of Nanoparticle Suspensions in Non-Aqueous Samples. *J. Magn. Reson.* **2020,** *321*, 106874. doi:10.1016/j.jmr.2020.106874
31. Schroer, G.; Deischter, J.; Zensen, T.; Kraus, J.; Pöppler, A.-C.; Qi, L.; Scott, S.; Delidovich, I., Structure-Performance Correlations of Cross-Linked Boronic Acid Polymers as Adsorbents for Fecovery of Fructose from Glucose–Fructose Mixtures. *Green Chem.* **2020,** *22*, 550-562. doi:10.1039/C9GC03151K
32. Manzano, J. S.; Wang, H.; Qi, L.; Slowing, I. I., Macroscale Control of Reactivity using 3D Printed Materials with Intrinsic Catalytic Properties. *Appl. Catal., A* **2020,** *605*, 117794. doi:10.1016/j.apcata.2020.117794
33. Han, Y.; Slowing, I. I.; Evans, J. W., Surface Structure of Linear Nanopores in Amorphous Silica: Comparison of Properties for Different Pore Generation Algorithms. *J. Chem. Phys.* **2020,** *153*, 124708. doi:10.1063/5.0021317
34. Egner, T. K.; Naik, P.; An, Y.; Venkatesh, A.; Rossini, A. J.; Slowing, I. I.; Venditti, V., 'Surface Contrast' NMR Reveals Non-innocent Role of Support in Pd/CeO_2 Catalyzed Phenol Hydrogenation. *ChemCatChem* **2020,** *12*, 4160-4166. doi:10.1002/cctc.202000608
35. Dong, B.; Mansour, N.; Pei, Y.; Wang, Z.; Huang, T.; Filbrun, S. L.; Chen, M.; Cheng, X.; Pruski, M.; Huang, W.; Fang, N., Single Molecule Investigation of Nanoconfinement Hydrophobicity in Heterogeneous Catalysis. *J. Am. Chem. Soc.* **2020**. doi:10.1021/jacs.0c05905
36. Chen, J.; Zhang, B.; Qi, L.; Pei, Y.; Nie, R.; Heintz, P.; Luan, X.; Bao, Z.; Yang, Q.; Ren, Q.; Zhang, Z.; Huang, W., Facile Fabrication of Hierarchical MOF–Metal Nanoparticle Tandem Catalysts for the Synthesis of Bioactive Molecules. *ACS Appl. Mater. Interfaces* **2020,** *12*, 23002-23009. doi:10.1021/acsami.0c05344
37. Chapovetsky, A.; Langeslay, R. R.; Celik, G.; Perras, F. A.; Pruski, M.; Ferrandon, M. S.; Wegener, E. C.; Kim, H.; Dogan, F.; Wen, J.; Khetrapal, N.; Sharma, P.; White, J.; Kropf, A. J.; Sattelberger, A. P.; Kaphan, D. M.; Delferro, M., Activation of Low-Valent, Multiply M–M Bonded Group VI Dimers toward Catalytic Olefin Metathesis via Surface Organometallic Chemistry. *Organometallics* **2020,** *39*, 1035-1045. doi:10.1021/acs.organomet.9b00787
38. An, Y.; Naik, P.; Slowing, I. I.; Venditti, V., Substrate–Support Interactions Mediate Hydrogenation of Phenolic Compounds by Pd/CeO_2 Nanorods. *ACS Appl. Nano Mater.* **2020,** *3*, 11282-11288. doi:10.1021/acsanm.0c02381
39. Perras, F. A.; Paterson, A. L., High Field Solid-State NMR of Challenging Nuclei in Inorganic Systems. In *Reference Module in Chemistry, Molecular Sciences and Chemical Engineering*, Elsevier: 2021.
40. Matsuki, Y.; Kobayashi, T.; Fukazawa, J.; Perras, F. A.; Pruski, M.; Fujiwara, T., Efficiency Analysis of Helium-cooled MAS DNP: Case Studies of Surface-modified Nanoparticles and Homogeneous Small-molecule Solutions. *Phys. Chem. Chem. Phys.* **2021,** *23*, 4919-4926. doi:10.1039/D0CP05658H
41. Sluiter, J. B.; Michel, K. P.; Addison, B.; Zeng, Y.; Michener, W.; Paterson, A. L.; Perras, F. A.; Wolfrum, E. J., Direct Determination of Cellulosic Glucan Content

in Starch-containing Samples. *Cellulose* **2021,** *28*, 1989-2002. doi:10.1007/s10570-020-03652-2
42. Paterson, A. L.; Liu, D.-J.; Kanbur, U.; Sadow, A. D.; Perras, F. A., Observing the Three-Dimensional Dynamics of Supported Metal Complexes. *Inorg. Chem. Front.* **2021,** *8*, 1416-1431. doi:10.1039/D0QI01241F
43. Zhang, J.; Mason, A. H.; Wang, Y.; Motta, A.; Kobayashi, T.; Pruski, M.; Gao, Y.; Marks, T. J., Beyond the Active Site. Cp*$ZrMe_3$/Sulfated Alumina-Catalyzed Olefin Polymerization Tacticity via Catalyst···Surface Ion-Pairing. *ChemCatChem* **2021,** *13*, 2564-2569. doi:10.1002/cctc.202100406
44. Chen, M.; Yan, Y.; Gebre, M.; Ordonez, C.; Liu, F.; Qi, L.; Lamkins, A.; Jing, D.; Dolge, K.; Zhang, B.; Heintz, P.; Shoemaker, D. P.; Wang, B.; Huang, W., Thermal Unequilibrium of PdSn Intermetallic Nanocatalysts: From In Situ Tailored Synthesis to Unexpected Hydrogenation Selectivity. *Angew. Chem. Int. Ed.* **2021,** *60*, 18309-18317. doi:10.1002/anie.202106515
45. Li, G.; Wang, B.; Kobayashi, T.; Pruski, M.; Resasco, D. E., Optimizing the Surface Distribution of Acid Sites for Cooperative Catalysis in Condensation Reactions Promoted by Water. *Chem Catalysis* **2021,** *in press*.
46. Gao, J.; Dorn, R. W.; Laurent, G. P.; Perras, F. A.; Rossini, A. J.; Conley, M. P., A Heterogeneous Palladium Catalyst for the Polymerization of Olefins Prepared by Halide Abstraction Using Surface R_3Si^+ Species. *Angew. Chem. Int. Ed.* **2022,** *61*, e202117279. doi:10.1002/anie.202117279
47. Fought, E. L.; Han, Y.; Windus, T. L.; Slowing, I. I.; Kobayashi, T.; Evans, J. W., Modeling of Linear Nanopores in a-SiO_2 Tuning Pore Surface Structure. *Microporous Mesoporous Mater.* **2022,** *341*, 112077. doi:10.1016/j.micromeso.2022.112077
48. Luo, S.; Wang, T.; Qi, L.; Tompsett, G. A.; Timko, M. T.; Auerbach, S. M.; Fan, W., Titrating Controlled Defects into Si-LTA Zeolite Crystals Using Multiple Organic Structure-Directing Agents. *Chem. Mater.* **2022,** *34*, 1789-1799. doi:10.1021/acs.chemmater.1c04036
49. Crandall, Z.; Basemann, K.; Qi, L.; Windus, T. L., Rxn Rover: Automation of Chemical Reactions with User-friendly, Modular Software. *React. Chem. Eng.* **2022,** *7*, 416-428. doi:10.1039/D1RE00265A
50. Fan, J.; Suo, X.; Wang, T.; Wang, Z.; Do-Thanh, C.-L.; Mahurin, S. M.; Kobayashi, T.; Yang, Z.; Dai, S., Mechanochemistry-driven Phase Transformation of Crystalline Covalent Triazine Frameworks Assisted by Alkaline Molten Salts. *J. Mater. Chem. A* **2022,** *10*, 14310-14315. doi:10.1039/D2TA02117J
51. Fan, J.; Wang, T.; Chen, H.; Wang, Z.; Thapaliya, B. P.; Kobayashi, T.; Yuan, Y.; Popovs, I.; Yang, Z.; Dai, S., Mechanochemistry-Driven Construction of Aza-fused π-Conjugated Networks Toward Enhanced Energy Storage. *Adv. Func. Mater.* **2022**, 2202669. doi:10.1002/adfm.202202669
52. Deshpande, N.; Chen, J.-Y.; Kobayashi, T.; Cho, E. H.; Pineault, H.; Lin, L.-C.; Brunelli, N. A., Investigating the Impact of Micropore Volume of Aminosilica Functionalized SBA-15 on Catalytic Activity for Amine-catalyzed Reactions. *J. Catal.* **2022,** *414*, 356-364. doi:10.1016/j.jcat.2022.09.016
53. Kanbur, U.; Paterson, A. L.; Rodriguez, J.; Kocen, A. L.; Yappert, R.; Hackler, R. A.; Wang, Y.-Y.; Peters, B.; Delferro, M.; LaPointe, A. M.; Coates, G. W.;

Perras, F. A.; Sadow, A. D., Zirconium-Catalyzed C–H Alumination of Polyolefins, Paraffins, and Methane. *J. Am. Chem. Soc.* **2023,** *145*, 2901-2910. doi:10.1021/jacs.2c11056

54. Zhao, T. Y.; Meirow, M.; Tennakoon, A.; Wu, X.; Paterson, A. L.; Qi, L.; LaPointe, A. M.; Lamb, J. V.; Kobayashi, T.; Delferro, M.; Sadow, A. D.; Huang, W.; Luijten, E.; Perras, F. A., Mechanistic Insights into Processive Polyethylene Hydrogenolysis through In Situ NMR. *Macromol.* **2023,** *56*, 4287-4295. doi:10.1021/acs.macromol.3c00474
55. Drabo, P.; Fischer, M.; Emondts, M.; Hamm, J.; Engelke, M.; Simonis, M.; Qi, L.; Scott, S. L.; Palkovits, R.; Delidovich, I., Solvent Effects on Catalytic Activity and Selectivity in Amine-catalyzed D-Fructose Isomerization. *J. Catal.* **2023,** *418*, 13-21. doi:10.1016/j.jcat.2022.12.029
56. Staples, O.; Ferrandon, M. S.; Laurent, G. P.; Kanbur, U.; Kropf, A. J.; Gau, M. R.; Carroll, P. J.; McCullough, K.; Sorsche, D.; Perras, F. A.; Delferro, M.; Kaphan, D. M.; Mindiola, D. J., Silica Supported Organometallic Ir^{I} Complexes Enable Efficient Catalytic Methane Borylation. *J. Am. Chem. Soc.* **2023,** *145*, 7992-8000. doi:10.1021/jacs.2c13612
57. Wei, X.; Johnson, G.; Ye, Y.; Cui, M.; Yu, S.-W.; Ran, Y.; Cai, J.; Liu, Z.; Chen, X.; Gao, W.; Bean, P. J. L.; Zhang, W.; Zhao, T. Y.; Perras, F. A.; Crumlin, E. J.; Zhang, X.; Davis, R. J.; Wu, Z.; Zhang, S., Surfactants Used in Colloidal Synthesis Modulate Ni Nanoparticle Surface Evolution for Selective CO_2 Hydrogenation. *J. Am. Chem. Soc.* **2023,** *145*, 14298-14306. doi:10.1021/jacs.3c02739
58. Chu, Y.-Y.; García Alejo, A.; Bud'ko, S. L.; Boteju, K.; Patnaik, S.; Ellern, A.; Pérez García, M.; Sadow, A. D., Structure and Magnetic Properties of Homoleptic Trivalent Tris(alkyl)lanthanides. *Inorg. Chem.* **2023,** *62*, 11751-11760. doi:10.1021/acs.inorgchem.3c00435

Massimiliano Delferro

Non-Traditional Catalyst Supports in Surface Organometallic Chemistry

Uddhav Kanbur, Joshua DeMuth, Jackie Hall, Yu Lim Kim, Magali Ferrandon, A. Jeremy Kropf, Cong Liu, David M. Kaphan, and Max Delferro

Chemical Sciences and Engineering Division, Argonne National Laboratory, Lemont, IL 60439 USA

Chemisorption of organometallic complexes on inorganic supports is a powerful strategy for developing heterogeneous, single-site, homogeneous-in-function catalysts. Typical support materials, most commonly silica (SiO_2) and alumina (Al_2O_3), play a crucial role in stabilizing reaction intermediates and site-isolating reactive species throughout the catalytic cycle but the inert nature of these catalyst supports precludes direct modulation or augmentation of catalytic processes by manipulation of the support akin to electronic ligand design and "redox non-innocence" in homogeneous catalysis. In this regard, the development of heterogeneous catalysts for selective ethylene oligomerization operating via the oxidative cyclization mechanism is challenging. Several prominent homogeneous systems for ethylene involving metallacycles have been developed (eg. Phillips systems) and are mainly comprised of a redox-active transition metal complex (eg. chromium) and an alkylating agent (AlR_3). Typically, the activation of these complexes leads to the formation of lower valent species capable of coordinating and oxidatively adding two ethylene molecules to form a metallacyclopentane. Our group have developed an activator-free system by leveraging the electronic properties of traditional inorganic supports. Chromium on lithium titanium oxide (Cr@LTO) mediates the formation of hexenes from ethylene with selectivity up to80%, sustained over long reaction times (~72 h). The reduced

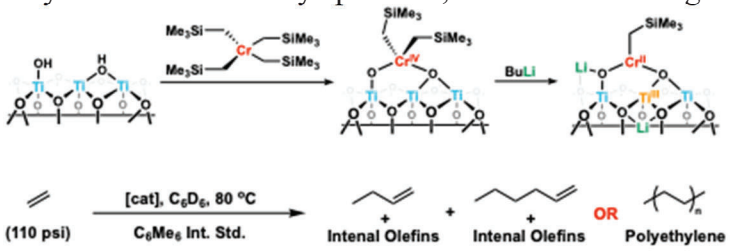

Catalyst	Polymer	Oligomer (C4/C6)	Initial rate (mol / mol Cr s^{-1} x 10^{-3})	Tunovers (17h)
Cr/TiO_2	✓	N/A	1221	3358
$Cr/Li_{0.005}TiO_2$	✓	N/A	105	1703
$Cr/Li_{0.01}TiO_2$	✓	N/A	98.2	822
$Cr/Li_{0.1}TiO_2$	N/A	✓ (48/52)	5.45	153
$Cr/Li_{0.6}TiO_2$	N/A	✓ (20/80)	5.85	321

chromium catalyst is obtained either by lithiation of a titania-supported chromium complex using n-butyllithium, or directly by a reductive grafting step involving the immobilization of a chromium complex onto lithium-intercalated titanium oxide. Extensive spectroscopic characterization of the chromium materials has been conducted, including XPS, XAS, EPR and DRIFTs, all of which suggest reduced chromium species. Kinetic studies on the Cr@LTO/ethylene system revealed a first order dependence on chromium and second order dependence on ethylene, consistent with the oxidative cyclization mechanism. Lithium incorporation in the anatase titania support has also been varied to provide a range of materials $Cr@Li_xTiO_2$ ($0.05 < x < 0.6$) and their reactivity toward ethylene oligomerization has been studied. At low lithium intercalation levels ($x < 0.1$) exclusive polymerization was observed while a crossover to oligomerization occurs at higher lithium loadings ($x>0.1$). This trend confirms that chemical reactivity can be leveraged by changing the electronic properties of the support.

FWP59066: Selective Upgrading of Alkenes via Organometallic-Support Electronic Interactions

Principal Investigators: Massimiliano Delferro (Lead PI), David M. Kaphan, Cong Liu, A. Jeremy Kropf
Additional Argonne Staff: Magali Ferrandon
Postdocs: Jackie Hall, Yu Lim Kim, Uddhav Kanbur, Joshua DeMuth
Affiliations: Chemical Sciences and Engineering Division, Argonne National Laboratory, Lemont, IL 60439

RECENT PROGRESS

Goals. The overarching goal of the Catalysis Science Program at Argonne is to understand how catalytic processes can be controlled through modulation of the electronic interactions between supported organometallic catalysts and non-traditional or non-innocent surfaces. Our group has achieved success in each of our three cross-cutting core scientific areas—experimentation, computation, and X-ray characterization. Our experimental efforts have focused on two sub-thrusts, the understanding of complex, multi-component active sites and the investigation of Li-ion battery cathodes as tunable, "redox non-innocent" catalyst supports. For the first task, we synthesized a well-defined, organoiridium catalyst on high-surface area silica for selective hydroboration of methane. In this work, we have demonstrated that grafting of methane borylation catalyst on surfaces is an effective strategy to disfavor multinuclear deactivation pathways, increasing catalyst activity and selectivity toward desired monoborylated product. Furthermore, we have shown that Isolated Pd atoms supported on high surface area MnO_2, prepared by the oxidative grafting of (bis(tricyclohexylphosphine-palladium(0)), catalyze the low temperature (≤325 K) oxidation of CO with results of *in situ*/*operando* and *ex situ* spectroscopic characterization signifying a synergistic role of Pd and MnO_2 in facilitating redox turnovers. In addition, we are advancing computational methods for the prediction of X-ray absorption near-edge spectroscopy (XANES) features for supported and unsupported chromium, iron, and nickel catalysts.

Methane Upgrading: Deactivation-Resistant Supported Organometallic Catalyst. Catalytic C-H borylation is an attractive method for the conversion of the most abundant hydrocarbon, methane (CH_4), to a mild nucleophilic building block. However, existing CH_4 borylation catalysts often suffer from low turnover numbers and conversions, which is hypothesized to result from inactive metal hydride agglomerates. Herein we report that the heterogenization of a bisphosphine molecular precatalyst, [(dmpe)Ir(cod)CH_3] **1-**CH_3 (dmpe = ,2-bis(dimethylphosphino)-ethane; cod = 1,5-cyclooctadiene), onto amorphous silica (SiO_2) dramatically enhances its performance, yielding a catalyst that is 12-times more efficient than the current standard for CH_4 borylation (Figure 1). The catalyst affords over 2000 turnovers at 150 °C in 16 hours with a selectivity of 91.5 % for mono- vs. di-borylation. Higher catalyst loadings improve yield and selectivity for the monoborylated product (H_3CBpin) with 82.8 % yield and > 99 % selectivity being achieved for 1255 TON. X-ray absorption spectroscopy (XAS) and dynamic nuclear polarization (DNP)-enhanced

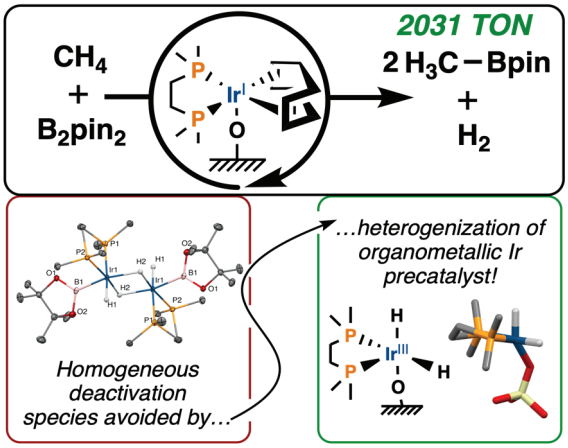

Figure 1. Supported organoiridium (1+) bisphospine complex catalyzed the selective borylation of methane.

solid-state NMR spectroscopic studies identify the supported precatalyst as an Ir^{I} species, and indicate that upon completion of catalysis, multinuclear Ir polyhydrides are not formed, consistent with the hypothesis that immobilization of the organometallic Ir species on a surface prevents bimolecular decomposition pathways. Immobilization of the homogeneous Ir^{I} fragment onto amorphous silica represents a unique, and simple, strategy to improve the activity and longevity of a methane borylation catalyst.

Atomically-Dispersed Pd on MnO_2 Catalyzes the Low-Temperature (≤ 50 °C) Oxidation of CO to CO_2. Oxidative grafting is applied to introduce atomically-dispersed Pd on MnO_2 and the resulting material (Pd/MnO_2) is catalytically active (> 50 turnovers, 17 h, 50 °C) for the low temperature (≤ 50 °C) oxidation of CO (7.7 kPa O_2, 2.6 kPa CO). *Ex situ* XAFS measurements indicate that the isolated Pd is reluctant to sintering (< 20% converted to metallic particles) over 7 hours of reaction (Figure 2). Transient structural changes to the catalyst are investigated by *operando* X-ray absorption and infrared spectroscopy measurements. Results indicate a correspondence between short-term (< 2 h) catalyst deactivation and saturation of MnO_2 with carbonates, suggesting a synergistic role of Pd and MnO_2 in facilitating redox turnovers. Specifically, in situ infrared spectroscopy and transient kinetic measurements point toward irreversible carbonate formation at 50 °C leading to short-term catalyst deactivation, although this influence can be mitigated through competitive adsorption with oxygen at high O_2:CO concentrations. Additional XAS and XPS measurements were conducted to evaluate transient structural changes to the catalyst over multiple cycles of reaction and regeneration (O_2 treatment at 300 °C), with preliminary XAS results indicating a near complete change in the oxide phase to Mn_3O_4 following regeneration at 300 °C. The impact of MnO_x phase on the catalyst reactivity (and propensity for carbonate poisoning) were further investigated by *in situ* infrared spectroscopy measurements. Participation of lattice oxygen and oxygen adatoms in CO_2 formation during initial reaction times were also considered by isotopic tracer experiments with $^{18}O_2$ during flow reaction experiments to probe the formation of mixed CO_2 isotopologues or oxygen exchange with the surface.

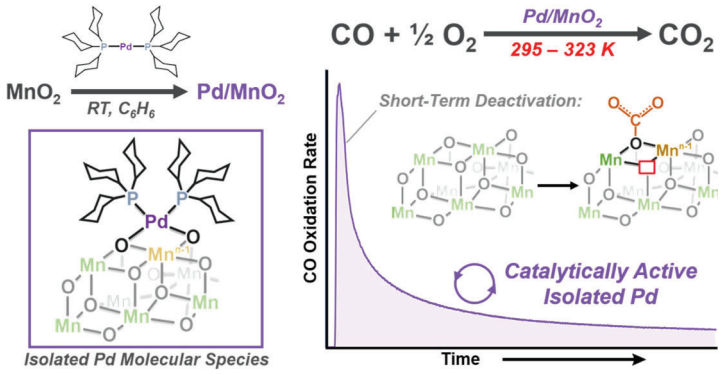

Figure 2. Supported Single-atom palladium on MnO_2 catalyzed the low temperature oxidation of CO to CO_2.

Additionally, preliminary results of modulating the Pd loading on MnO_2 reveal turnover rates (per mol Pd) increase systematically with decreasing Pd concentration despite low surface occupation of Pd atoms (0.23 atoms / nm^2). Conversely, bulky PCy_3 ligands retained on the catalyst may occlude 80 – 90 % of the surface and inhibit the catalytic performance. Pd modulation and influence of added phosphine ligands on the catalyst surface are considered in the overall context of the CO oxidation mechanism over Pd/MnO_2 in this follow-up study.

Lithium-Ion Battery Materials as Tunable, "Redox Non-Innocent" Catalyst Supports. Building off results for the well-defined doping of Ni on $Li_xMn_2O_4$ through oxidative grafting of an organonickel(0) complex, we demonstrate the general exploration of oxidative grafting for supporting an array of organometallic and well-defined molecular complexes (M = V, Fe, Ni, Cu, Zr, Pd, Ag, and Au) onto manganese oxide supports ($LiMn_2O_4$ and MnO_2). Addition of each metal was completed in a solution of benzene at room temperature and byproducts monitored by ^1H NMR provide insight into the mechanism of grafting. The structure of the supported metals was evaluated by XAFS analysis, with results suggesting the formation of isolated surface atoms and molecular fragments for several of the metallic precursors. Moreover, the catalytic propensity of the MnO_2-supported metals was evaluated for both the oxidation of cyclohexane (^tBuOOH, 70 °C, CH_3CN) and carbon monoxide (O_2, 25 - 50 °C), with results providing insight into the metal-dependent performance of the catalysts. In addition, the influence of support lithiation on the electronic properties of Cu species supported on $Li_xMn_2O_4$ was investigated to further understand this capability for tuning catalytic proficiency. $Li_xMn_2O_4$ with various degrees of lithiation (x = 0, 0.1, 0.3, 0.7, 1.0, 2.0) was prepared by reaction of MnO_2 with n-BuLi at room temperature in benzene. Cu was then added by addition of copper mesityl (Mes_xCu_x, x = 4, 5) to a suspension of $Li_xMn_2O_4$ benzene at room temperature (Figure 3a) and the resultant materials were evaluated as catalyst for the oxidative homocoupling of alkynes. Results of reaction of phenylacetylene (23 °C, benzene, in air) revealed that Cu/MnO_2 and $Cu/LiMn_2O_4$ were both competent as catalysts for the coupling reaction whereas bare MnO_2 and Mes_xCu_x supported on SiO_2 provided no measurable activity, signifying the vital interaction of Cu with the $Li_xMn_2O_4$ support. Additionally, $Cu/Li_xMn_2O_4$, although showing initially lower activity than Cu/MnO_2, displayed stable reaction rates until complete substrate conversion unlike Cu/MnO_2 which exhibited rates that decelerated quickly during reaction, indicating a role of the surface redox state on the catalytic properties of the supported Cu. Characterization of Cu oxidation

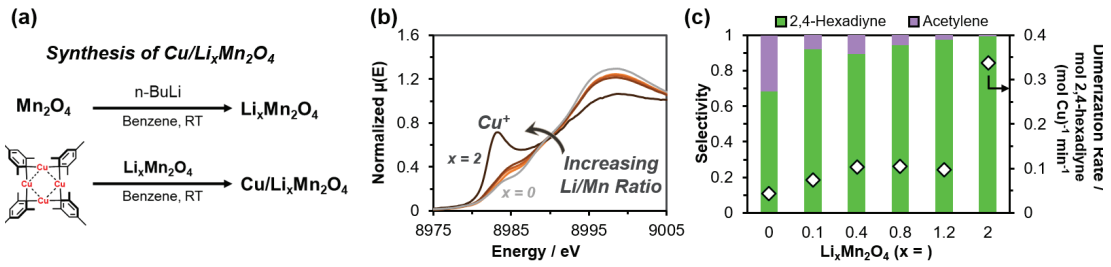

Figure 3. (a) Schematic representing the synthesis procedure for $Cu/Li_xMn_2O_4$. (b) Cu K-edge X-ray absorption near edge structure (XANES) of $Cu/Li_xMn_2O_4$ with increasing Li (x = #) content. (c) Results of the oxidative coupling of propyne over $Cu/Li_xMn_2O_4$ with various Li (x = #) concentrations indicating the rate of dimerization and product selectivity.

state by X-ray absorption spectroscopy (XAS) revealed a systematic decrease in Cu oxidation state with increasing lithiation, with Cu/MnO_2 being close to completely Cu^{2+} and Cu/$Li_2Mn_2O_4$ appearing to be fully Cu^+ (Figure 3b), providing the speciation of grafted Cu is strongly influenced by the redox state of the support. Additional flow reaction experiments of the oxidative coupling of propyne (200 °C, C_3:O_2 = 1, 24 h) revealed that increasing lithium reduction not only increases the turnover rate of dimerization to 2,4-hexadiyne, but also leads to improved selectivity over acetylene formation (Figure 3c). Future investigations of the reaction mechanism and influence of surface and Cu redox state on the activity for aerobic alkyne dimerization will be completed to gain further insight into impacts on individual elementary steps of oxidation and C-C coupling.

Furthermore, to understand the redox non-innocent properties of lithium manganese oxide as catalyst support, DFT calculations were carried out for transition metal (Fe, Co, Ni, and Cu) single atom catalysts supported on $LiMn_2O_4$ and $Li_2Mn_2O_4$. Based on Bader charge analysis, the metal centers on $Li_2Mn_2O_4$ carries are more reduced than those over $LiMn_2O_4$. This means the further lithiation into the catalyst support can increase the charge densities at the active center to further tune the active site electronic properties and catalytic activity. To further approve this concept, the mechanistic study of hydrogenation of cyclohexene forming cyclohexane has been studied over these materials (Figure 4). DFT calculations show that the H_2 activation happens at the single-atom metal sites via hetero-lytic cleavage route involving a lattice oxygen and a surface oxygen vacancy. In addition, the first step hydrogenation of cyclohexene forming C_6H_{11}* binds over single atom catalyst sites are the most endothermic steps in all cases, which makes it a potential rate limiting step. And the formation of cyclohexane from C_6H_{11}* is another thermodynamically favored step. More interestingly, the first hydrogenation step is much more endothermic over $LiMn_2O_4$ than $Li_2Mn_2O_4$ supports, which makes the reaction over $LiMn_2O_4$ less favorable, consistent with Bader charge analysis.

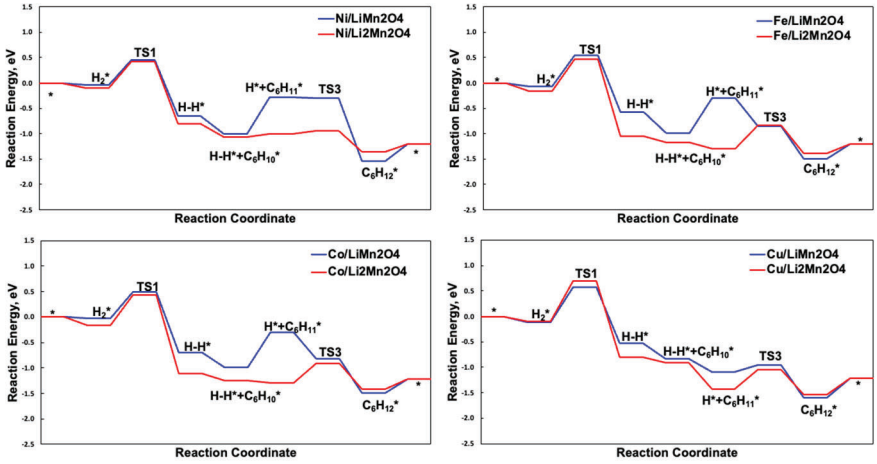

Figure 4. Free-energy diagrams for the hydrogenation of cyclohexene catalyzed by Ni, Fe, Cu, Co on $LiMn_2O_4$ (blue) and $Li_2Mn_2O_4$ (red).

Supported Single-Site Metals on Silicon Nitride Catalyze Non-Oxidative Dehydrogenation of Light Alkanes. In addition to understanding metal-surface electronic communication for organometallic sites on redox-tunable oxides, we are further probing the effect of the local surface environment by exploring nitride support materials. We have developed a method for synthesis of well-defined, high surface area silicon nitrides with

finely tuned surface chemistry (i.e. $SiNH_2$ and Si(NH)Si) that is suitable for grafting organometallic precursors ($ZrBn_4$, Fe_2Mes_4, $VMes_3THF$, $Cr(Me_3SiMe)_4$). The nitride coordination environment offers several potential catalytic benefits, including increased basicity for heterolytic bond activation and improved stabilization of low-valent reactive species due to increased orbital overlap and covalency. The synthesis of silicon nitride was performed through dehalogenation of silicon tetrachloride followed by high temperature (1000 °C) ammoniolysis. Further treatment of the silicon nitride in vacuo at 200 °C results in a high surface area material (>450 m^2/g) abundant in Bronsted acid sites (>5 H^+/nm^2), namely $SiNH_2$ and Si(NH)Si, that is suitable for grafting organometallic precursors. Currently, we have developed a supported alkyl zirconium complex by grafting tetrabenzyl zirconium onto silicon nitride via deprotonation of the alkyl ligands. NMR spectroscopic analysis suggests that the resultant supported material is comprised of bisalkylated zirconium. Corresponding analysis by DRIFTS suggests selective grafting of the organozirconium precursor at $SiNH_2$ sites over competing Si(NH)Si acid sites. Further analysis by solid state ^{15}N NMR reveals the formation of Zr-N bonds consistent with grafting by alkyl deprotonation. The catalytic performance of this silicon nitride supported alkyl zirconium complex was assessed in the dehydrogenation reaction of propane into propene. Initial catalytic experiments employed 50 mg of organozirconium on silicon nitride in a flow reactor with a 5 mL/min flow rate of 2.3% propane in argon at 450 °C (Figure 5). Analysis of product gases by GC-FID/TCD reveals propane conversion rates reaching over 30% and achieving excellent selectivity towards dehydrogenation to propene (>95%). A comparative experiment with the same alkyl zirconium precursor grafted on silica reveals that this silica supported analogue does not dehydrogenate propene under these conditions. Raman spectroscopic analysis of the recovered silica supported complex reveals the characteristic D and G bands of coking products, which may be causing the stifled catalytic performance. Overall, these results indicate that silicon nitride may be a favorable support material in heterogeneous catalysis with increased resistance to coking, improved product yields and selectivity.

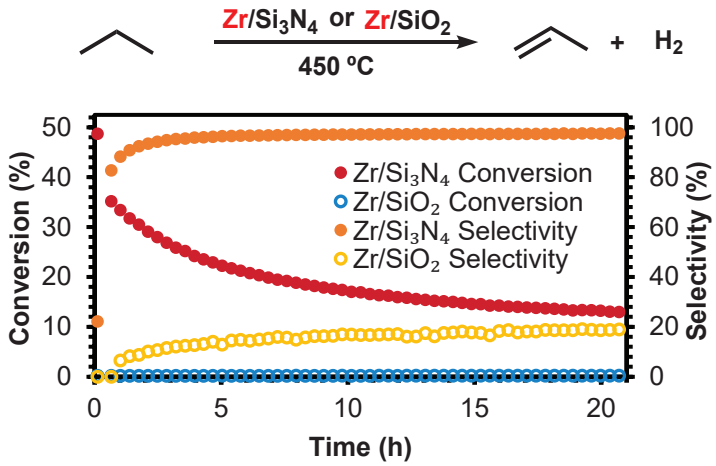

Figure 5. Dehydrogenation of propane in a plug flow reactor catalyzed by single-atom Zr on high-surface area Si_3N_4 and SiO_2.

Publications Acknowledging this Grant in 2020-2022

Work at Argonne funded solely by this FWP with Argonne as the lead institution:

1) Hall, J. N.; Kropf, A. J.; Kanbur, U.; Dogan, F.; Byron, C.; Wen, J.; Delferro, M.; Kahan, D. M. Structural and reactive evolution of oxidatively grafted Pd catalysts on

MnO_2 for the low-temperature oxidation of CO. *Chem. Commun.* **2023**, *59* (45), 6861-6864. DOI: 10.1039/D3CC01094E.

2) Staples, O.; Ferrandon, M. S.; Laurent, G. P.; Kanbur, U.; Kropf, A. J.; Gau, M. R.; Carroll, P. J.; McCullough, K.; Sorsche, D.; Perras, F. A.; Delferro, M.; Kaphan, D. M.; Mindiola, D. J. Silica Supported Organometallic Ir^{I} Complexes Enable Efficient Catalytic Methane Borylation. *J. Am. Chem. Soc.* **2023**, *145* (14), 7992-8000. DOI: 10.1021/jacs.2c13612.

3) Chapovetsky, A.; Kennedy, R. M.; Witzke, R.; Wegener, E. C.; Dogan, F.; Patel, P.; Ferrandon, M.; Niklas, J.; Poluektov, O. G.; Rui, N.; Senanayake, S. D.; Rodriguez, J. A.; Zaluzec, N. J.; Yu, L.; Wen, J.; Johnson, C.; Jenks, C. J.; Kropf, A. J.; Liu, C.; Delferro, M.; Kaphan, D. M. Lithium-Ion Battery Materials as Tunable, "Redox Non-Innocent" Catalyst Supports. *ACS Catal.* **2022**, *12*, 7233-7242 (DOI: 10.1021/acscatal.2c00935).

4) Ferrandon, M. S.; Byron, C.; Celik, G.; Zhang, Y.; Ni, C.; Sloppy, J.; McCormick, R. A.; Booksh, K.; Teplyakov, A. V.; Delferro, M. Grafted Nickel-Promoter Catalysts for Dry Reforming of Methane Identified through High-Throughput Experimentation. *Appl. Catal., A* **2022**, *629*, 118379 (DOI: 10.1016/j.apcata.2021.118379).

5) Patel, P.; Lu, Z.; Jafari, M. G.; Hernandez-Prieto, C.; Zatsepin, P.; Mindiola, D. J.; Kaphan, D. M.; Delferro, M.; Kropf, A. J.; Liu, C. Integrated Experimental and Computational K-Edge X-ray Absorption Near-Edge Structure Analysis of Vanadium Catalysts. *J. Phys. Chem. C* **2022**, *126*, 11949-11962 (DOI: 10.1021/acs.jpcc.2c02049).

6) Patel, P.; Wells, R. H.; Kaphan, D. M.; Delferro, M.; Skodje, R. T.; Liu, C., Computational Investigation of the Role of Active Site Heterogeneity for a Supported Organovanadium(III) Hydrogenation Catalyst. *ACS Catal.* **2021**, 11, 1-16 (DOI: 10.1021/acscatal.1c00688).

7) Mindiola, D. J.; Delferro, M.; Humphrey, S. M., Organometallic Chemistry at Various Length Scales: More Than Just Metal–Carbon Bonds Bring Chemists Together. *Organometallics* **2020**, *39*, 881-882 (DOI: 10.1021/acs.organomet.0c00198).

8) Witzke, R. J.; Chapovetsky, A.; Conley, M. P.; Kaphan, D. M.; Delferro, M., Nontraditional Catalyst Supports in Surface Organometallic Chemistry. *ACS Catal.* **2020**, *10*, 11822-11840 (DOI: 10.1021/acscatal.0c03350).

9) Chapovetsky, A.; Patel, P.; Liu, C.; Sattelberger, A. P.; Kaphan, D. M.; Delferro, M., Electrochemical Investigation of Low-Valent Multiply M≡M Bonded Group VI Dimers: A Standard Chemical Reduction Leads to an Unexpected Product. *Organometallics* **2020**, *39*, 4430-4436 (DOI: 10.1021/acs.organomet.0c00533).

10) Chapovetsky, A.; Langeslay, R. R.; Celik, G.; Perras, F. A.; Pruski, M.; Ferrandon, M. S.; Wegener, E. C.; Kim, H.; Dogan, F.; Wen, J.; Khetrapal, N.; Sharma, P.; White, J.; Kropf, A. J.; Sattelberger, A. P.; Kaphan, D. M.; Delferro, M., Activation of Low-Valent, Multiply M–M Bonded Group VI Dimers toward Catalytic Olefin Metathesis

via Surface Organometallic Chemistry. *Organometallics* **2020**, *39*, 1035–1045 (DOI: 10.1021/acs.organomet.9b00787).

Patents

9) Ferrandon, M.; Celik, G.; Delferro, M.; Multimetallic catalysts for methanation of carbon dioxide and dry reforming of methane. US20220040677A1.

10) Kaphan, D.; Delferro, M.; Chapovetsky, A.; Jenks, C. J.; Johnson, C. S.; Lithium-ion battery cathode and anode materials as tunable and dynamically responsive support materials for single site heterogeneous catalysis. US20220126277A1.

Work at Argonne funded by this FWP with Argonne not the lead institution

11) Xu, J.; Patel, P.; Liu, D.-J.; Xu, T.; Liu, C. Understanding the Dynamic Evolution of Atomically Dispersed Cu Catalyst for Co2 Electrochemical Conversion Using Integrated XANES Analysis and Mechanistic Studies. *J. Catal.* **2023**, *425*, 296-305. (DOI: 10.1016/j.jcat.2023.06.020).
12) Barrios-Vargas, L. J.; Abeynayake, N. S.; Secrist, C.; Le, N.; Webster, C. E.; Donnadieu, B.; Kaphan, D. M.; Roy, A.; Ibarra, I. A.; Montiel-Palma, V. Homogeneous versus MOF-supported catalysis: A direct comparison of catalytic hydroboration at Ni tripodal P_3E (E = Si, Ge) complexes. *Dalton Trans.* **2023**, *52*, 8883-8892 (DOI: 10.1039/D3DT01328F).
13) Hall, J. N.; Kropf, A. J.; Delferro, M.; Bollini, P. Kinetic and X-ray Absorption Spectroscopic Analysis of Catalytic Redox Cycles over Highly Uniform Polymetal Oxo Clusters. *ACS Catal.* **2023**, *13* (8), 5406-5427 (DOI: 10.1021/acscatal.2c06023).
14) Bukowski, B. C.; Purdy, S. C.; Wegener, E. C.; Wu, Z.; Kropf, A. J.; Zhang, G.; Miller, J. T.; Greeley, J. Intermetallic alloy structure–activity descriptors derived from inelastic X-ray scattering. *Phys. Chem. Chem. Phys.* **2023**, *25* (16), 11216-11226 (DOI: 10.1039/D3CP00330B).
15) Perras, F. A.; Arroyave, A.; Southern, S. A.; Lamb, J. V.; Li, Y.; LaPointe, A.; Delferro, M. Double-resonance ^{17}O NMR experiments reveal unique configurational information for surface organometallic complexes. *Chem. Commun.* **2023**, *59* (31), 4604-4607 (DOI: 10.1039/D3CC00899A).
16) Zhu, Y.; Mukherjee, D.; Helgert, T. R.; Nguyen, S. T. (Catecholate)Cu^{I}_2-Displayed Porous Organic Polymers as Efficient Heterogeneous Catalysts for the Mild and Selective Aerobic Oxidation of Alcohols. *CCS Chemistry* **2023**, *5* (2), 445-454 (DOI: doi:10.31635/ccschem.022.202101765).

17) Jafari, M.G.; Fehn, D.; Reinholdt, A.; Hernandez-Prieto, C.; Patel, P.; Gau, M. R.; Carroll, P. J.; Krzystek, J.; Liu, C.; Ozarowski, A.; Telser, J.; Delferro, M.; Meyer, K.; Mindiola, D. J. Tale of Three Molecular Nitrides: Mononuclear Vanadium (V) and (IV) Nitrides As Well As a Mixed-Valence Trivanadium Nitride Having a V_3N_4 Double-Diamond Core. *J. Am. Chem. Soc.* **2022**, *144*, 10201-102019 (DOI: 10.1021/jacs.2c00276).

18) An, S.; Patel, P.; Liu, C.; Skodje, R. T. Computational Aspects of Single-Molecule Kinetics for Coupled Catalytic Cycles: A Spectral Analysis. *J. Phys. Chem. A* **2022**, *126*, 23, 3783-3796 (DOI: 10.1021/acs.jpca.2c02153).

19) Wells, R.; An, S.; Patel, P.; Liu, C.; Skodje, R. T. Single Molecule Kinetics of Styrene Hydrogenation on Silica Supported Vanadium: The Role of Disorder for One-Atom Catalysts. *J. Phys. Chem. C* **2021**, *125*, 37, 20286–20300 (DOI: 10.1021/acs.jpcc.1c04759).

20) Jafari, M. G.; Park, Y.; Pudasaini, B.; Kurogi, T.; Carroll, P. J.; Kaphan, D. M.; Kropf, J.; Delferro, M.; Baik, M.-H.; Mindiola, D. J. Phosphorus-Atom Transfer from Phosphaethynolate to an Alkylidyne. *Angew. Chem., Int. Ed.* **2021**, *60*, 24411-24417 (DOI: 10.1002/anie.202107475).

21) Kou, J.; Zhu Chen, J.; Gao, J.; Zhang, X.; Zhu, J.; Ghosh, A.; Liu, W.; Kropf, A. J.; Zemlyanov, D.; Ma, R.; Guo, X.; Datye, A. K.; Zhang, G.; Guo, L.; Miller, J. T. Structural and Catalytic Properties of Isolated Pt^{2+} Sites in Platinum Phosphide (PtP_2). *ACS Catal.* **2021**, *11*, 13496- 13509 (DOI: 10.1021/acscatal.1c03970).

22) Kaphan, D. M.; Brereton, K. R.; Klet, R. C.; Witzke, R. J.; Miller, A. J. M.; Mulfort, K. L.; Delferro, M.; Tiede, D. M., Photocatalytic Transfer Hydrogenation in Water: Insight into Mechanism and Catalyst Speciation. *Organometallics* **2021**, *40*, 1482-1491 (DOI: 10.1021/acs.organomet.1c00133).

23) Liu, P.; Zhang, Y.; Liu, C.; Emery, J. D.; Das, A.; Bedzyk, M. J.; Hock, A. S.; Martinson, A. B. F. Thermal Atomic Layer Deposition of Gold: Mechanistic Insights, Nucleation, and Epitaxy. *ACS Appl. Mater. Interfaces* **2021**, *13*(7), 9091–9100 (DOI: 10.1021/acsami.0c17943).

24) Perras, F. A.; Paterson, A. L.; Syed, Z. H.; Kropf, A. J.; Kaphan, D. M.; Delferro, M.; Pruski, M., Revealing the Configuration and Conformation of Surface Organometallic Catalysts with DNP-Enhanced NMR. *J. Phys. Chem. C* **2021**, *125*, 13433-13442 (DOI: 10.1021/acs.jpcc.1c03176).

25) Wang, J.; Lu, Y.; Liu, L.; Yu, L.; Yang, C.; Delferro, M.; Hoffman, A. S.; Bare, S. R.; Karim, A. M.; Xin, H., Catalytic CO Oxidation on MgAl2O4-Supported Iridium Single Atoms: Ligand Configuration and Site Geometry. *J. Phys. Chem. C* **2021**, *125*, 11380-11390. (DOI: 10.1021/acs.jpcc.1c02287),

26) Robison, L.; Gong, X.; Evans, A. M.; Son, F. A.; Wang, X.; Redfern, L. R.; Wasson, M. C.; Syed, Z. H.; Chen, Z.; Idrees, K. B.; Islamoglu, T.; Delferro, M.; Dichtel, W. R.; Coudert, F.-X.; Gianneschi, N. C.; Farha, O. K., Transient Catenation in a Zirconium-Based Metal-Organic Framework and Its Effect on Mechanical Stability and Sorption Properties. *J. Am. Chem. Soc.* **2021**, *143*, 1503-1512 (DOI: 10.1021/jacs.0c11266).

27) Fagiolari, L.; Bini, M.; Costantino, F.; Gatto, G.; Kropf, A. J.; Marmottini, F.; Nocchetti, M.; Wegener, E. C.; Zaccaria, F.; Delferro, M.; Vivani, R.; Macchioni, A.,

Iridium-Doped Nanosized Zn–Al Layered Double Hydroxides as Efficient Water Oxidation Catalysts. *ACS Appl. Mater. Interfaces* **2020**, *12*, 32736–32745 (DOI: 10.1021/acsami.0c07925).

28) Wegener, E. C.; Bukowski, B. C.; Yang, D.; Wu, Z.; Kropf, A. J.; Delgass, W. N.; Greeley, J.; Zhang, G.; Miller, J. T., Intermetallic Compounds as an Alternative to Single-atom Alloy Catalysts: Geometric and Electronic Structures from Advanced X-ray Spectroscopies and Computational Studies. *ChemCatChem* **2020**, *12*, 1325-1333 (DOI: 10.1002/cctc.201901869).

29) Purdy, S. C.; Ghanekar, P.; Mitchell, G.; Kropf, A. J.; Zemlyanov, D. Y.; Ren, Y.; Ribeiro, F.; Delgass, W. N.; Greeley, J.; Miller, J. T., Origin of Electronic Modification of Platinum in a Pt_3V Alloy and Its Consequences for Propane Dehydrogenation Catalysis. *ACS Appl. Energy Mater.* **2020**, *3*, 1410-1422 (DOI: 10.1021/acsaem.9b01373).

30) ZhuChen, J.; Gao, J.; Probus, P. R.; Liu, W.; Wu, X.; Wegener, E. C.; Kropf, A. J.; Zemlyanov, D.; Zhang, G.; Yang, X.; Miller, J., The Effect of Strong Metal-Support Interaction (SMSI) on Pt-Ti/SiO_2 and Pt-Nb/SiO_2 Catalysts for Propane Dehydrogenation. *Catal. Sci. Technol.* **2020**, 5973-5982 (DOI: 10.1039/D0CY00897D).

31) Choudhury, D.; Mandia, D. J.; Langeslay, R. R.; Yanguas-Gil, A.; Letourneau, S.; Sattelberger, A. P.; Balasubramanium, M.; Mane, A. U.; Delferro, M.; Elam, J. W., Atomic Layer Deposition of HfO_2 Films Using Carbon-Free Tetrakis(tetrahydroborato)hafnium and Water. *J. Vac. Sci. Technol. A* **2020,** *38*, 042407 (DOI: 10.1116/6.0000053).

32) Pei, Y.; Chen, M.; Zhong, X.; Zhao, T. Y.; Ferrer, M.-J.; Maligal-Ganesh, R. V.; Ma, T.; Zhang, B.; Qi, Z.; Zhou, L.; Bowers, C. R.; Liu, C.; Huang, W., Pairwise Semi-Hydrogenation of Alkyne to cis-Alkene on Platinum-Tin Intermetallic Compounds. *Nanoscale* **2020**, *12*, 8519-8524 (DOI: 10.1039/D0NR00920B).

33) H. Xu, D. Rebollar, H. He, L. Chong, Y. Liu, C. Liu, C.-J. Sun, T. Li, J. V. Muntean, R. E. Winans, D.-J. Liu, T. Xu. Highly Selective Electrocatalytic CO_2 Reduction to Ethanol by Metallic Clusters Dynamically Formed from Atomically Dispersed Copper. *Nat. Energy* **2020**, *5*, 623–632 (DOI: 10.1038/s41560-020-0666-x).

José A Rodriguez

Catalysis for Advanced Fuel Synthesis and High Value Chemicals

José A. Rodriguez, Ping Liu, Sanjaya D. Senanayake, Jingguang Chen
and Michael G. White
Brookhaven National Laboratory, Chemistry Department

Presentation Abstract

This research program pursues understanding of the behavior and performance of catalysts that use C1 chemistry for the synthesis of fuels and high-value chemical by elucidating catalytically important properties of well-defined surfaces, films, powders and nanostructures. It addresses the conversion and manipulation of C-O and C-H bonds in small molecules. A main focus is on the activation and conversion of CO_2 and CH_4 to oxygenates, olefins or syngas. Emphasis is placed on understanding basic principles of surface reactivity, full characterization of active phases, and on mechanistic studies as a function of surface strucuture and composition. There are three thrusts. Thrust 1, Catalysis for C1 Chemistry, focuses on the transformation of methane to valuable chemicals and the production of alcohols through hydrogenation of CO_2. Thrust 2, Multi-carbon Products via Tandem Reactions of CO_2 and Alkanes, investigates catalytic processes using light alkanes, such as ethane, to activate CO_2, to produce either synthesis gas via the dry reforming pathway ($C_2H_6 + 2CO_2 \rightarrow 4CO + 3H_2$) or valuable olefins through the oxidative dehydrogenation pathway ($C_2H_6 + CO_2 \rightarrow C_2H_4 + CO + H_2O$). And Thrust 3, Nanostructured Interfaces for Catalysis, uses novel approaches to prepare and characterize metal and metal compound nanostructures (oxides, carbides, nitrides, sulfides), including cluster deposition and imaging to advance understanding of supported nanocatalysts used in Thrusts 1 and 2 for the conversion of CO_2, CH_4 and light alkanes. The research makes use of the unique tools available at BNL for *in-situ* materials characterization and computational modeling.

FWP-BNL-CO040: Catalysis for Advanced Fuel Synthesis and Energy, Conversion of C-O and C-H bonds

Co-PIs: Ping Liu, Sanjaya Senanayake, Jingguang Chen, and Michael G. White
Postdoc(s): Jorge Moncada, Irene Barba-Nieto, Vikram Mehar, Erwei Huang, Juan Jimenez, Arephin Islam, Prabhakar Kasala
Student(s): Erwei Huang, Yi Tian, Hong Zhang, Kaixi Deng, Wenjie Liao, Luolin Shi, Jason Wang, Yuxi Wang
Affiliations(s): All the students are from SUNY Stony Brook, most of them from the Department of Chemistry

RECENT PROGRESS

C1 chemistry involves the conversion of molecules that contain one carbon atom into valuable products. C1 chemistry is expected to become a major area of interest for the transportation fuel and chemical industries in the relatively near future. In general, the feedstocks for C1 chemistry include natural gas (mostly methane), carbon monoxide, carbon dioxide, methanol and synthesis gas (a mixture of carbon monoxide and hydrogen). Thus, a fundamental understanding of the conversion of C-O and C-H bonds is essential for controlling C1 chemistry. The Catalysis Group at BNL has been quite active in this area. The systems under investigation involved pure metal catalysts or catalysts that contained compounds of metals with light elements (C, N, O, S). We have developed and applied synchrotron-based techniques for *in-situ* characterization (AP-XPS, XRD, PDF, XAS) to understand catalyst function in operating environments. Theoretical methods for catalytic science have also been advanced (optimized KMC, reaction network analysis). In the last three and a half years (2020-2023 time period), this program has led research published in 64 articles[1-64] and collaborated on 25 additional articles led by external collaborators.[65-89] In the last three years, major research achievements are:

- Identification of general pathways for the bonding and activation of CO_2 and CH_4 on metal-oxide, metal-nitride and metal-carbide interfaces.[1,10,11,15,21,23,24,35,43,67,70]
- Development of novel metal-indium oxide interfaces for the selective conversion of CO_2 to methanol.[8,9,32,64]
- Identification and study of the active sites in inverse oxide/metal systems (ZnO/Cu, ZrO_2/Cu, SnO_x/Cu) and their role in CO_2 and CH_4 conversion.[8,13,14,16.22,32,58]
- Unraveling the active role that water can play in the synthesis of alcohols through the partial oxidation of methane or the hydrogenation of CO_2.[22,66,]
- Studies identifying the effects of alkali promoters and water on the selectivity of CO_2 hydrogenation towards methanol and ethanol synthesis.
- Fundamental studies on the wet reforming of CH_4 at low temperatures.[58,59.]
- Combining CO_2 reduction with propane oxidative dehydrogenation over bimetallic catalysts.[4,5,88]
- Using CO_2 and ethane in the production of C3 oxygenates.[3,4,26,60]
- CO_2-assisted propane aromatization.[2,26]
- Studies showing a correlation between the structural properties, chemical state, and catalytic properties of alkali oxide islands dispersed on metals.[7,44.56]
- Detailed proof via *operando* studies that metal/oxide and metal/nitride catalysts are dynamic entities that change as a function of reaction conditions during CO_2 hydrogenation and CH_4 conversion reactions.[43,55]
- Participation in the design and implementation of instrumentation to carry out *in-situ* quick XAFS/IR and XRD/IR studies at the NSLS-II and APS. Active participants in the Synchrotron Catalysis Consortium and the design of the end stations for three beam lines (IOS, XPD, QAS) at the NSLS-II.[67.74.75]

- Development of theoretical tools for the study of catalysis science using machine learning, reaction network analysis, and advanced Kinetic Monte Carlo. Identification of fundamental descriptors for C1 catalysis. [77,86.,44,53]

These are examples of the research done during the 2020-2023 period:

A. Inverse oxide/metal systems (ZnO/Cu, ZrO_2/Cu, SnO_x/Cu) as active catalysts for CO_2 and CH_4 conversion

Mixtures of CuO-ZnO are frequently used as catalysts for the WGS and the synthesis of methanol.[25,34,44,57] A recent transmission electron microscopy (TEM) study by Lunkenbein, et al. has revealed that strong metal-support interactions between Cu and ZnO

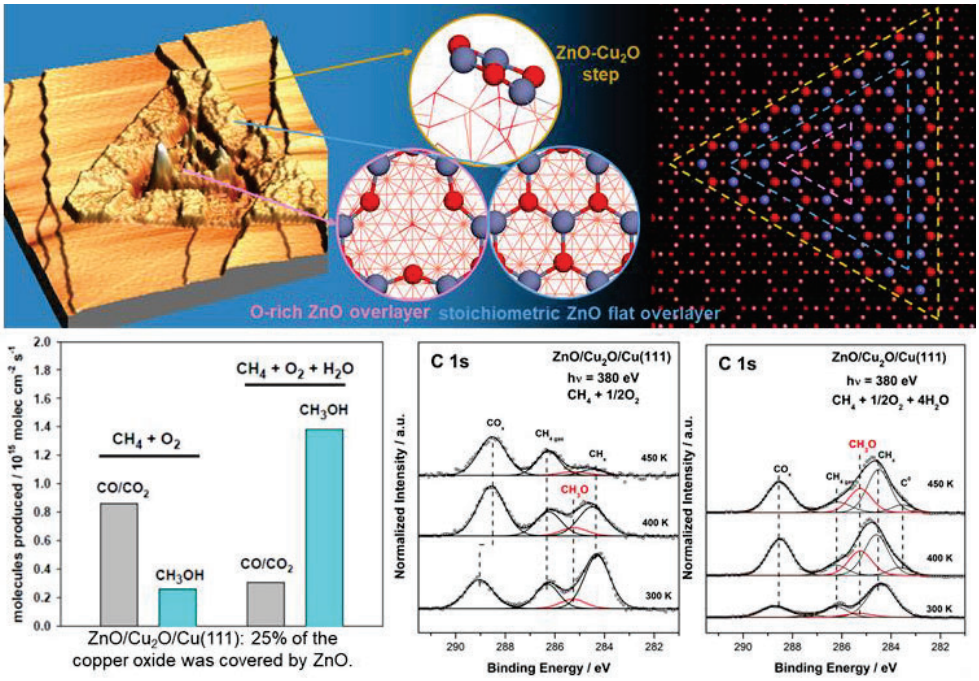

Figure 1. Multiple sites on $ZnO/Cu_2O/Cu(111)$ catalysts observed by STM (top left) and simulated by DFT (top middle) and KMC (top right) during methane oxidation. Different methanol selectivity (reactor testing, bottom left) and intermediates (XPS, bottom middle and right) upon exposure to different gas mixtures.[44]

lead to the formation of a ZnO overlayer on top of the Cu particles in an industrial $Cu/ZnO/Al_2O_3$ catalyst under reaction conditions. Such formation of an oxide overlayer on Cu could create a catalytically active metal-oxide interface. We have performed a systematic study using scanning tunneling microscopy (STM) to investigate the growth modes of ZnO on Cu(111) under different preparation conditions.[34,44] Zn was deposited on Cu(111) or CuO_x/Cu(111) surfaces under various conditions. When Zn was deposited at 300 K with subsequent exposure to O_2 at higher temperatures (400-550 K), small particles of ZnO (< 20 nm in size) were produced on the surface. For Zn deposition onto CuO_x/Cu(111) at elevated temperatures (450-600 K) in an oxygen ambient, large ZnO islands (300-650 nm in size) were produced which were very rough and spread over several terraces of Cu(111), see top of Figure 1.[34,44] XPS/Auger spectra showed that all the preparation conditions led to the formation of $ZnO/CuO_x/Cu(111)$ surfaces where the oxidation state of zinc was uniform.[34,44]

We studied the catalytic activity of the ZnO/CuO_x/Cu(111) systems and found they were active for the oxidation of CO, the water-gas shift and the hydrogenation of CO_2, see Figure 1.[34,44] In our studies, we did not see graphite-like structures as seen for the powder catalyst under reaction conditions by Lunkenbein et al. However, in catalytic tests, we found that our ZnO/ CuO_x/Cu(111) systems were very active for the synthesis of methanol from CO_2 hydrogenation or the partial oxidation of methane.[34,44] Figure 1 compares the catalytic activity of a Cu_2O/Cu(111) system where ~ 30% of the copper oxide substrate was covered with ZnO. The addition of water to the reaction feed modified the surface reaction paths enhancing the generation of adsorbed CH_3O (XPS data) and the evolution of CH_3OH into gas phase (catalytic test). ZnO to the copper substrate enhanced the catalytic activity by two to three orders of magnitude.[44] These experimental results are consistent with the predictions of DFT and KMC calculations which show that water has a triple role in the CH4 → CH_3OH, favoring the partial dissociation of the alkane and the desorption of the formed methanol.[44]

B. Model Cu-Oxide Ternary Catalysts

Some of the most active and selective catalysts for CO_2 hydrogenation to CH_3OH involve a combination of Cu, ZrO_2 and ZnO, each of which appears to play a different and symbiotic role in the reaction.[66] Mechanistically, the activation and binding of CO_2 and its hydrogenated intermediates is thought to occur on the oxide components, while Cu provides H-atoms for hydrogenation steps via H_2 dissociation and spillover to CO_2 bound at the Cu-oxide interface. Surfaces of Cu nanoparticles can also promote the reverse water-gas-shift (RWGS) and methanation reactions that limit selectivity to CH_3OH. The active phases at the Cu-oxide interface, however, are still largely uncertain including the size-dependence of the Cu nanoparticles and presence of Cu^+ sites. Our most recent work focused on Cu size-effects and uncovering multicomponent Cu_2O/ Cu(111), which previously demonstrated its potential application as an excellent support in various catalytic processes, such as, water-gas shift reaction (WGS), CO oxidation, CH_4 conversions, CO_2 hydrogenations, etc., was used as a prototypical model surface to mimic the sites in active enzymes and zeolites for CH_4 reforming.[16,44,45,66] Using CH_3OH as a probe molecule, one of desired products for C1 catalysis, DFT studies showed a facile dissociation on Cu_2O/Cu(111).[35] Next, we investigated methanol surface interactions using model ternary catalysts prepared by size-

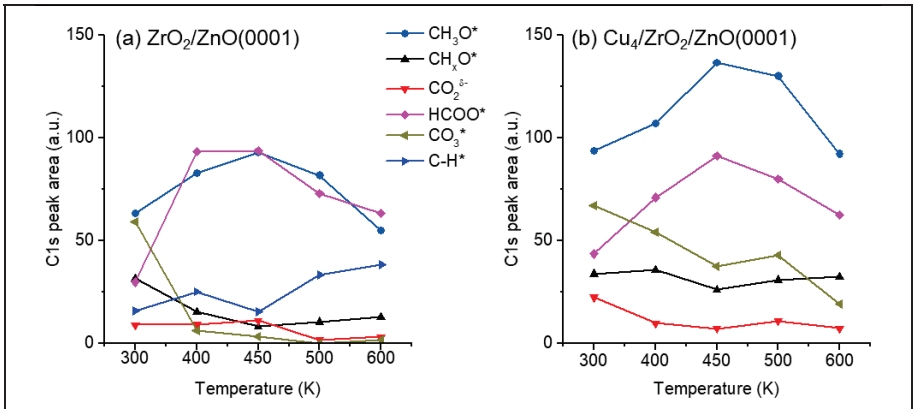

Figure 2: Temperature dependence of surface concentrations of reaction intermediates formed under CO_2 hydrogenation conditions at 450 K on (a) ZrO_2/ZnO(0001) and (b) Cu_4/ZrO_2/ZnO(0001). The data were extracted from peak areas in C1s core level spectra taken by NAP-XPS.

selected cluster deposition. Specifically, ZnO(0001) single crystals, ALD-prepared ZnO thin films or ZnO powders were used as a supports for the deposition of size-selected Cu_n (n = 2, 4) clusters and ZrO_2 nanoclusters.[16]

Reactivity under CO_2 hydrogenation conditions was probed using NAP-XPS (Figure 2). The presence of Cu_2 and Cu_4 clusters strongly enhances the formation of hydrogenation intermediates on the $Cu_n/ZrO_2/ZnO$ ternary system compared to the ZrO_2/ZnO oxide-only system indicating high activity for H_2 dissociation and spillover for ultra-small Cu clusters. Both carbonate and formate intermediates are present on the $Cu_n/ZrO_2/ZnO$ ternary and ZrO_2/ZnO binary catalysts with the relative concentrations reflecting the coverage of ZrO_2 (see Figure 38). The latter implies that the two oxides act independently, with both the "carbonate" and formate reaction pathways occurring simultaneously with H-atoms provided by the Cu_n clusters. Future experiments will explore the use of ZrO_2 thin films as supports for Cu_n clusters with and without ZnO overlayers.

C. Alkali-promoted selective CO_2 conversion to methanol and ethanol.

Experimental and theoretical studies indicate that cesium promotes the rates of methanol and ethanol formation on Cu/ZnO(000$\bar{1}$) catalysts.[31] A combination of XPS and calculations based on density functional theory and Kinetic Monte Carlo was used to study this phenomenon, see Figure 3. The results pinpointed the effects of doped alkali on the binding of reaction intermediates and transition states, and the operating reaction pathways, being able to promote the CO_2 conversion and more importantly the selectivity to methanol and ethanol. Descriptors were identified, which well described the catalytic behaviors and therefore were useful for the rational design of better Cu-based catalysts for CO_2 hydrogenation. [31] This work provided a better understanding of C-C bond formation and developed a descriptor-based method for rational screening of complex catalysts at a theoretical level.[31]

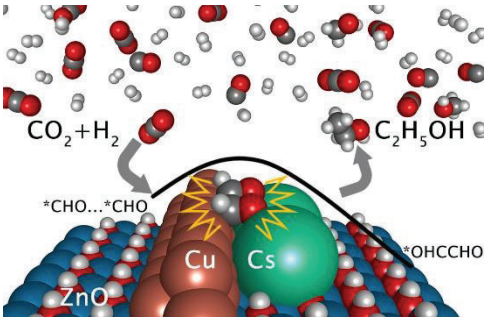

Figure 3 The path for the formation of ethanol through Cs-mediated CHO to CHO coupling on Cu/ZnO(000$\bar{1}$).

D. CO_2-assisted dry reforming and oxidative dehydrogenation of light alkanes

One of our objectives is to identify novel catalytic materials and approaches that can be used to control the reaction of CO_2 with alkanes, with dry reforming and oxidative dehydrogenation as major targets.[5,28,30] In tandem reaction schemes, the produced C_2H_4 can be subsequently reacted with CO and H_2 to yield CH_3CH_2CHO plus $CH_3CH_3CH_2OH$ (hydroformylation process).[49-52] During this funding cycle, we identified descriptors and predicted several classes of bimetallic catalysts supported on CeO_2 with high selectivity toward either reforming or dehydrogenation.[5,28,30.49-52]

As shown in Figure 4, a combination of experimental and theoretical efforts allowed us to create a descriptor-based map for predicting selectivity toward ethylene (dehydrogenation – red region) and syngas (dry reforming – blue region).[45,61] In general,

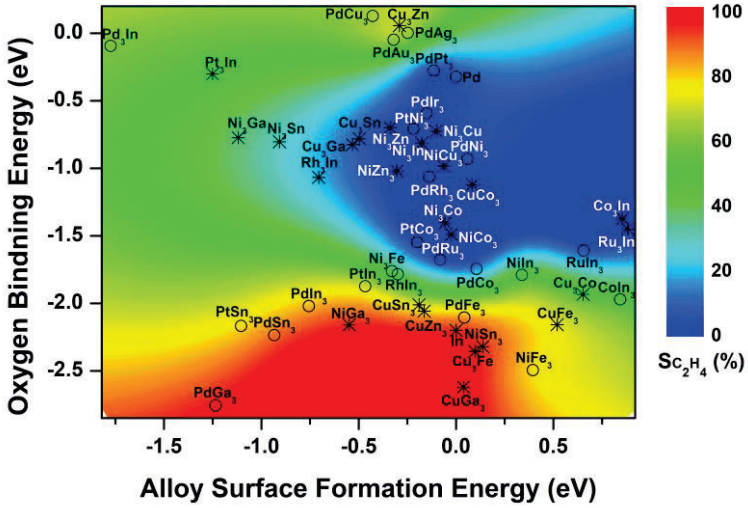

Figure 4. Descriptor-based contour map (circles: bimetallic systems where C_2H_4 selectivity have been measured experimentally; asterisks: bimetallic systems that have not been explored yet).

bimetallic-derived catalysts undergo reaction-induced surface phase transformation, and the resulting surface structure controls the selective C─H bond scission via the oxidative dehydrogenation of ethane (ODHE) and C─C bond scission via the dry reforming of ethane (DRE). To achieve high C_2H_4 selectivity, one of bimetallic components should be highly oxyphilic, to enable the formation of the oxide/metal interface, which favor ODHE rather than DRE by binding the $*C_2H_x$ species more strongly than $*C_2H_xO$, but moderately to allow facile removal of $*C_2H_4$. This descriptor-based correlation will be utilized as a guide for selecting catalysts that produce desired ratios of $CO/H_2/C_2H_4$ for hydroformylation and CO/H_2 for carbon-neutral H_2 production.

E. Metal/carbide catalysts for methane conversion

Methane is an extremely stable molecule which interacts poorly with surfaces of late transition metals such as Ni(111) or Pt(111). At room temperature, the sticking coefficient of methane on these surfaces is negligible ($< 10^{-8}$). Combining experiments with X-ray photoemission and accurate DFT based calculations, we have shown that small Ni clusters dispersed on TiC(001) are able to capture and dissociate methane at room temperature.[10,54] In DFT calculations, a small energy barrier of < 0.5 eV is predicted for CH_4 dissociation into adsorbed methyl and atomic hydrogen species (Figure 5).[10] In addition, the calculated reaction free energy profile at 300 K and 1 atm of CH_4 shows no effective energy barriers in the system.[10] We found a similar trend for the deposition of small Pt clusters on the carbide surface. A comparison to other reported systems that activate methane at room temperature, including oxide and zeolite-based materials, indicates that the metal/carbide systems activate with distinct chemistry.

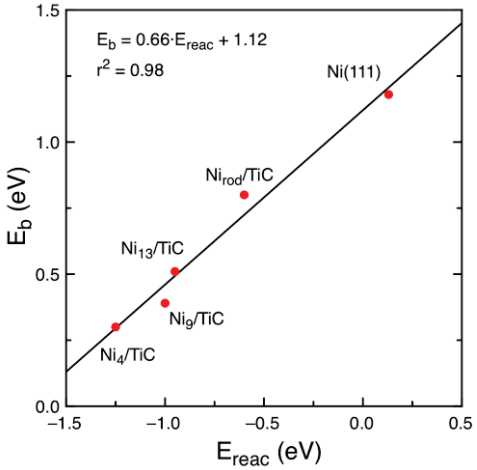

Figure 5: Energy barrier (E_b) for CH_4 to CH_3+H dissociation on the Ni/TiC systems and on Ni(111) versus the reaction energy (E_{reac}).

Publications for this grant (2020-2023)

In the 2020-2023 period, 69 articles have been published with this FWP as the main driver or the main provider of ideas, with nearly half of them published in high impact journals including *Science* (1), *Nature Communication* (2), *Angewandte Chemie International Edition* (1), *Journal of the American Chemical Society* (3), *ACS Catalysis* (14), *Chem* (1), *Matter* (1), *Joule* (1), *Chemical Engineering Journal* (1), *Applied Catalysis B: Environmental* (2) and *ACS Central Science* (1). In addition, there are 26 articles which this FWP has made a minor contribution. Graduate Students, postdoctoral fellows and PIs funded under this FWP are highlighted.

Exclusively funded by this grant and/or jointly funded by this grant and other grants with leading intellectual contribution from this grant:

1. Computational and Experimental Identification of Strong Synergy of Fe/ZnO Catalyst in Promoting Acetic Acid Synthesis from CH_4 and CO_2, Nie, X.; Ren, X.; Tu, C.; Song, C.; Guo, X.; Chen, J.G. *Chem. Commun.* **2020**, 56, 3983-3986. https://doi.org/10.1039/C9CC10055E

2. CO_2-assisted propane aromatization over phosphorous-modified Ga/ZSM-5 catalysts, Niu, X.; Nie, X.; Yang C.; Chen, J.G. *Catal. Sci. Tech.* 2020, 10, 1881-1888. https://doi.org/10.1039/C9CY02589H .

3. "Interfacial Active Sites for CO_2-Assisted Selective Cleavage of C-C/C-H Bonds in Ethane, Xie, Z.; Tian, D.; Xie, M.; Yang, S.; Xu, Y.; Rui, N.; Lee, J.H.; Senanayake, S.D.; Li, K.; Wang, H.; Kattel, S.; Chen, J.G., *Chem,* **2020**, 6, 2703-2716. https://doi.org/10.1016/j.chempr.2020.07.011

4. Reactions of CO_2 and Ethane Enable CO Bond Insertion for Production of C3 Oxygenates, Xie, Z.; Xu, Y.; Xie, M.; Chen, X.; Lee, J.H.; Stavitski, E.; Kattel S.; Chen, J.G. *Nature Commun.*, **2020**, 11, 1887. https://doi.org/10.1038/s41467-020-15849-x

5. Effect of oxide support on catalytic performance of FeNi-based catalysts for CO_2-assisted oxidative dehydrogenation of ethane, Yan, B.; Yao, S.; Chen, J.G., *ChemCatChem*, **2020**, 12, 494-503. https://doi.org/10.1002/cctc.201901585

6. Recent Advances in Carbon Dioxide Hydrogenation to Methanol via Heterogeneous Catalysis, Jiang, X.; Nie, X.; Guo, X.; Song, C.; Chen, J.G., *Chem. Rev.*, **2020**, 120, 7984-8034. https://doi.org/10.1021/acs.chemrev.9b00723.

7. Potassium-Promoted Methanol Synthesis from CO_2 Hydrogenation over Cu_xO/Cu(111) ($x \leq 2$) Model Surface: Rationalizing the Potential of Potassium in Catalysis, Liao, W.; Liu, P., *ACS Catal.* **2020**, 10, 5383-5958. https://doi.org/10.1021/acscatal.9b05226

8. Growth and structural studies of In/Au(111) alloys and InO_x/Au(111) inverse oxide/metal model catalysts, Kang, J.; Mahapatra, M.; Rui, N.; Orozco, I.; Shi, R.; Senanayake, S.D.; Rodriguez, J.A. *J. Chem. Phys.* **2020,** 152, 054702. https://doi.org/10.1063/1.5139237

9. Hydrogenation of CO_2 to Methanol on a Au^+-In_2O_{3-x} Catalyst, Rui, N.; Zhang, F.; Sun, K.; Liu, Z.; Xu, W.; Stavitski, E.; Senanayake, S. D.; Rodriguez, J. A.; Liu, C.-J. *ACS Catal.* **2020**, 10, 11307-11317. https://doi.org/10.1021/acscatal.0c02120

10. Boosting the Activity of Transition Metal Carbides towards Methane Activation by Nanostructuring, Figueras, M.; Gutierrez, R.A.; Prats, H.; Viñes, F.; Ramirez, P.J.; Illas F.; Rodriguez, J.A. *Phys. Chem. Chem. Phys.* 2020, 22, 7110-7118. https://doi.org/10.1039/D0CP00228C

11. Promoting Effect of Tungsten Carbide on Catalytic Activity of Cu for CO_2 Reduction, Koverga, A.A.; Florez, E.; Dorkis L.; Rodriguez, J.A. *Phys. Chem. Chem. Phys.* **2020**, 22, 13666-13679. https://doi.org/10.1039/D0CP00358A

12. Preparation and Structural Characterization of $ZrO_2/CuO_x/Cu(111)$ Inverse Model Catalysts, Shi, R.; Mahapatra, M.; Kang, J.; Orozco, I.; Senanayake S.D.; Rodriguez, J. A. *J. Phys. Chem. C*, **2020**, *124*, 10502-10508. https://doi.org/10.1021/acs.jpcc.0c00852

13. Studies of CO_2 Hydrogenation over Cobalt/Ceria Catalysts with *In-situ* Characterization: The Effect of Cobalt Loading and Metal-Support Interactions on the Catalytic Activity, Deng, K.; Lin, L.; Rui, N.; Vovchok, D.; Zhang, F.; Zhang, S.; Senanayake, S.D.; Kim, T.; Rodriguez, J. A. *Catal. Sci. Technol.* **2020**, 10, 6468-6482. https://doi.org/10.1039/D0CY00962H

14. In Situ Characterization of Metal/Oxide Catalysts for CO_2 Conversion: From Fundamental Aspects to Real Catalyst Design, Mahapatra, M.; Betancourt, L.E.; Liu, Z.; Vovchok, D.; Simonovis, J.P.; Rodriguez, J. A.; Senanayake, S.D. In: Heterogeneous Catalysis for Energy Applications (Edited by Tomas R. Reina and Jose A. Odriozola), chapter 13, pages 431-458, Royal Society of Chemistry (**2020**).

15. Activation of Gold on Metal Carbides: Novel Catalysts for C1 Chemistry, Rodriguez J.A. Front. Chem. **2020**, 7, 1-12. https://doi.org/10.3389/fchem.2019.00875

16. Reactivity of a Zirconia-Copper Inverse catalyst for CO_2 Hydrogenation, Ma, Y.; Wang, J.; Goodman, K. R.; Head, A. R.; Tong, X.; Stacchiola D. J.; White, M. G. *J. Phys. Chem. B.* **2020.** *124*, 22158–22172. https://doi.org/10.1021/acs.jpcc.0c06624

17. In Situ Structural Study of Manganese and Iron Oxide Promoted Rhodium Catalysts for Oxygenate Synthesis, Carrillo, P.; Shi, R.; Senanayake S. D.; White, M. G. *Appl. Catal. A*, **2020**, *608*, 117845. https://doi.org/10.1016/j.apcata.2020.117845

18. Morphology and Chemical Behavior of Model $CsO_x/Cu_2O/Cu(111)$ Nanocatalysts for Methanol Synthesis: Reaction with CO_2 and H_2, Hamlyn, R. C. E.; Mahapatra, M.; Orozco, I.; Hunt, A.; Waluyo, I.; White, M. G.; Senanayake, S.D.; Rodríguez, J. A. *J. Chem. Phys.,* **2020***, 152*, 044701. https://doi.org/10.1063/1.5129152

19. Structure and Chemical State of Cesium on Well-Defined Cu(111) and $Cu_2O/Cu(111)$ Surfaces, Hamlyn, R. C. E.; Mahapatra, M.; Orozco, I.; Waluyo, I.; Hunt, A.; Rodriguez, J. A.; White, M. G.; Senanayake, S. D. *J. Phys. Chem. C*, **2020**, *124*, 3107-3121. https://doi.org/10.1021/acs.jpcc.9b10608

20. Morphology and Reactivity of Size-selected Titanium Oxide Nanoclusters on Au(111), Goodman, K. R.; Wang, J.; Ma, Y.; Tong, X.; Stacchiola, D. J.; White, M. G. *J. Chem. Phys*., **2020**, *152*, 054714. https://doi.org/10.1063/1.5134453

21. Effects of Zr Doping into Ceria for the Dry Reforming of Methane over $Ni/CeZrO_2$ Catalysts: In Situ Studies with XRD, XAFS, and AP-XPS, Zhang, F.; Liu, Z.; Chen, X.;

Rui, N.; Betancourt, L. E.; Lin, L.; Xu, W.; Sun, C. J.; Abeykoon, A. M. M.; Rodriguez, J. A.; Teržan, J.; Lorber, K.; Djinović, P.; Senanayake, S. D. *ACS Catal.* **2020**, *10*, 3274–3284. https://doi.org/10.1021/acscatal.9b04451

22. Deciphering Dynamic Structural and Mechanistic Complexity in $Cu/CeO_2/ZSM-5$ Catalysts for the Reverse Water-Gas Shift Reaction, Vovchok, D.; Zhang, C.; Hwang, S.; Jiao, L.; Zhang, F.; Liu, Z.; Senanayake, S. D.; Rodriguez, J. A. *ACS Catal.* **2020**, *10* (17), 10216–10228. https://doi.org/10.1021/acscatal.0c01584.

23. Supported Molybdenum Carbide Nanoparticles as Hot Hydrogen Reservoirs for Catalytic Applications, Figueras, M.; Gutierrez, R.A.; Viñes, F.; Ramirez, P.J.; Rodriguez J.A.; Illas, F. *J. Phys. Chem. Lett.* **2020**, 11, 8437-8441. https://doi.org/10.1021/acs.jpclett.0c02608

24. Low Temperature Activation of Methane on Metal-Oxides and Complex Interfaces: Insights from Surface Science, Senanayake, S. D.; Rodriguez, J. A.; Weaver, J. F. *Acc. Chem. Res.* **2020**, *53* (8), 1488–1497. https://dx.doi.org/10.1021/acs.accounts.0c00194

25. Inverse ZrO_2/Cu as a Highly Efficient Methanol Synthesis Catalyst from CO_2 Hydrogenation, Wu, C.; Lin, L.; Liu, J.; Zhang, J.; Zhang, F.; Zhou, T.; Rui, N.; Yao, S.; Deng, Y.; Yang, F.; Xu, W.; Luo, J.; Zhao, Y.; Yan, B.; Wen, X-D.; Rodriguez, J.A.; Ma. D. *Nature Commun.* **2020**, *11*, 5767. DOI: 10.1038/s41467-020-19634-8

26. Recent advances in carbon dioxide hydrogenation to produce olefins and aromatics, D. Wang, Xie, Z.; M.D. Porosoff and Chen, J.G., *Chem*, **2021**, 7, 2277-2311. https://doi.org/10.1016/j.chempr.2021.02.024

27. Comparison of Heterogeneous Hydroformylation of Ethylene and Propylene over $RhCo_3$/MCM-41 Catalysts, Mao, M.; Z. Xie and Chen, J.G., *ACS Catal.* **2021**, 11, 14575-14585. https://doi.org/10.1021/acscatal.1c04359

28. Simultaneously Upgrading CO_2 and Light Alkanes into Value-added Products, Xie, Z.; E. Gomez and Chen, J.G., *AIChE J.*, **2021**, 67, e17249. https://doi.org/10.1002/aic.17249

29. Insight into Acetic Acid Synthesis from the Reaction of CH_4 and CO_2, Tu, C.; Nie, X.; Chen, J.G. *ACS Catal.* **2021**, *11*, 3384-3401. https://doi.org/10.1021/acscatal.0c05492

30. Bimetallic-Derived Catalysts and Their Application in Simultaneous Upgrading of CO_2 and Ethane Xie, Z.; Winter L.R.; Chen, J.G. *Matter*, **2021**, 3 408-440. https://doi.org/10.1016/j.matt.2020.11.013

31. Cesium-Induced Active Sites for C–C Coupling and Ethanol Synthesis from CO_2 Hydrogenation on $Cu/ZnO(000\bar{1})$ Surfaces, Wang, X.; Ramírez, P. J.; Liao, W.; Rodriguez, J. A.; Liu, P., *J. Am. Chem. Soc.* **2021**, 143, 13103-13112. https://doi.org/10.1021/jacs.1c03940.

32. Surface structure of mass-selected niobium oxide nanoclusters on Au(111), Wang, J.; Ma, Y.; Mahapatra, M.; Kang, J.; Senanayake, S. D.; Tong, X.; Stacchiola, D. J.; White, M. G. **N***anotechnology* **2021**, 32, 475601. https://doi.org/10.1088/1361-6528/ac1cc0

33. Surface characterization and methane activation on $SnO_x/Cu_2O/Cu(111)$ inverse oxide/metal catalysts, Kang, J.; Rui, N.; Huang, E.; Tian, Y.; Mahapatra, M.; Rosales,

R.; Orozco, I.; Shi, R.; Senanayake, S. D.; Liu, P.; Rodriguez, J. A., *Phys. Chem. Chem. Phys.* **2021**, http://dx.doi.org/10.1039/D1CP02829D.

34. Understanding Methanol Synthesis on Inverse ZnO/CuO_x/Cu Catalysts: Stability of CH_3O Species and Dynamic Nature of the Surface, Orozco, I.; Huang, E.; Mahapatra, M.; Kang, J.; Shi, R.; Nemšák, S.; Tong, X.; Senanayake, S. D.; Liu, P.; Rodríguez, J. A., *J. Phys. Chem. C* **2021**, *125*, 6673-6683. https://doi.org/10.1021/acs.jpcc.1c00392

35. In Situ Studies of Methanol Decomposition Over Cu(111) and Cu_2O/Cu(111): Effects of Reactant Pressure, Surface Morphology, and Hot Spots of Active Sites, Orozco, I.; Huang, E.; Mahapatra, M.; Shi, R.; Kang, J.; Nemšák, S.; Senanayake, S. D.; Liu, P.; Rodriguez, J. A., *J. Phys. Chem. C* **2021**, *125*, 558-571. https://doi.org/10.1021/acs.jpcc.0c09572

36. Methanol Synthesis from CO_2 Hydrogenation over a Potassium-Promoted Cu_xO/Cu(111) ($x \leq 2$) Model Surface: Rationalizing the Potential of Potassium in Catalysis, Liao, W.; Liu, P., *ACS Catal.* **2020**, *10*, 5723-5733. https://doi.org/10.1021/acscatal.9b05226

37. Metal-Support Interactions and C1 Chemistry: Transforming Pt-CeO_2 into a Highly Active and Stable Catalyst for the Conversion of Carbon Dioxide and Methane, Zhang, F.; Gutiérrez, R. A.; Lustemberg, P. G.; Liu, Z.; Rui, N.; Wu, T.; Ramírez, P. J.; Xu, W.; Idriss, H.; Ganduglia-Pirovano, M. V.; Senanayake, S. D.; Rodriguez, J. A. *ACS Catal.* **2021**, *11*, 1613–1623. https://doi.org/10.1021/acscatal.0c04694.

38. Adsorption and Activation of CO_2 on Pt/CeO_x/TiO_2(110): Role of the Pt-CeO_x Interface, Grinter, D. C.; Graciani, J.; Palomino, R. M.; Xu, F.; Waluyo, I.; Sanz, J. F.; Senanayake, S. D.; Rodriguez, J. A. *Surf. Sci.* **2021**, *710*, 121852. DOI: 10.1016/j.susc.2021.121852

39. Reaction Pathway for Coke-Free Methane Steam Reforming on a Ni/CeO_2 Catalyst: Active Sites and the Role of Metal–Support Interactions, Salcedo, A.; Lustemberg, P. G.; Rui, N.; Palomino, R. M.; Liu, Z.; Nemsak, S.; Senanayake, S. D.; Rodriguez, J. A.; Ganduglia-Pirovano, M. V.; Irigoyen, B. *ACS Catal.* **2021**, *11*, 8327–8337. https://doi.org/10.1021/acscatal.1c01604

40. CO_2 Hydrogenation over Heterogeneous Catalysts at Atmospheric Pressure: From Electronic Properties to Product Selectivity, Wang, Y.; Winter, L.R.; Chen J.G.; Yan, B. *Green Chem.*, **2021**, *23*, 249. https://doi.org/10.1039/D0GC03506H

41. Effect of Ni Particle Size on the Production of Renewable Methane from CO_2 over Ni/CeO_2 Catalyst, Lin, L.; Gerlak, C. A.; Liu, C.; Llorca, J.; Yao, S.; Rui, N.; Zhang, F.; Liu, Z.; Zhang, S.; Deng, K.; Rodriguez, J.A.; Senanayake, S.D. *J. Energy Chem.* **2021**, *61*, 602–611. https://doi.org/10.1016/ j.jechem.2021.02.021

42. Highly Active Ni/CeO_2 Catalyst for CO_2 Methanation: Preparation and Characterization, Rui, N.; Zhang, X.; Zhang, F.; Liu, Z.; Cao, X.; Xie, Z.; Zou, R.; Senanayake, S.D.; Yang, Y.; Rodriguez, J. A.; Liu, C.-J. *Appl. Catal. B Environ.* **2021**, 282, 119581. https://doi.org/10.1016/j.apcatb.2020.119581

43. Reversing Sintering Effect of Ni Particles on γ-Mo_2N via Strong Metal Support Interaction. Lin, L.; Liu, J.; Liu, X.; Gao, Z.; Rui, N.; Yao, S.; Zhang, F.; Wang, M.; Liu, C.; Han, L.; Yang, F.; Zhang, S.; Wen, X. D.; Senanayake, S. D.; Wu, Y.; Li, X.; Rodriguez, J. A.; Ma, D. *Nat. Commun*. **2021**, *12*, 6978. https://doi.org/10.1038/s41467-021-27116-8

44. Selective Methane Oxidation to Methanol on ZnO/Cu_2O/Cu(111) Catalysts: Unique Site-dependent Behaviours, Huang, E.; Orozco, I.; Ramírez, P.J.; Liu, Z.; Zhang, F.; Mahapatra, M.; Nemšák, S.; Senanayake, S. D.; Rodriguez, J. A.; Liu, P. *J. Am. Chem. Soc.* **2021**, *143*, 19018–19032. https://doi.org/10.1021/jacs.1c08063

45. CO_2 Hydrogenation on ZrO_2/Cu(111) Surfaces: Production of Methane and Methanol. Rui, N.; Shi, R.; Gutiérrez, R. A.; Rosales, R.; Kang, J.; Mahapatra, M.; Ramírez, P. J.; Senanayake, S. D.; Rodriguez, J. A. *Ind. Eng. Chem. Res.* **2021**, *60*, 18900–18906. https://doi.org/10.1021/acs.iecr.1c03229

46. General Descriptors for CO_2-Assisted Selective C─H/C─C Bond Scission in Ethane, Xie, Z.; Wang, X; Chen, X.; Liu P.; Chen, J.G. *J. Am. Chem. Soc.*, **2022**, 114, 4186-4195. https://doi.org/10.1021/jacs.1c13415

47. Can CO_2-assisted alkane dehydrogenation lead to negative CO_2 emissions? Biswas, A.N.; Xie, Z.; and Chen, J.G. *Joule*, **2022**, 6, 269-273. https://doi.org/10.1016/j.joule.2021.12.008

48. Oxygenate Production from Plasma-Activated Reaction of CO_2 and Ethane, Biswas, A.N.; Winter, L.R.; Loenders, B.; Xie, Z.; Bogaerts, A.; Chen, J.G. *ACS Energy Lett.*, **2022**, **7**, 236-241. https://doi.org/10.1021/acsenergylett.1c02355

49. Catalytic Tandem CO_2-Ethane Reactions and Hydroformylation for C3 Oxygenate Production, Xie, Z.; Guo, H.; Huang, E.; Mao, Z.; Chen, X.; Liu, P.; Chen, J.G., *ACS Catal.*, **2022**, 12, 8279-8290. https://doi.org/10.1021/acscatal.2c01700

50. CO_2-assisted ethane aromatization over zinc and phosphorous modified ZSM-5 catalysts, Tu, C.; Fan, H.; Wang, D.; Rui, N.; Du, Y.; Senanayake, S.D.; Xie, Z.; Nie, X.; Chen, J.G., *Appl. Catal. B: Environ.*, **2022**, 304, 120956. https://doi.org/10.1016/j.apcatb.2021.120956

51. Trends and Descriptors of Heterogeneous Hydroformylation Activity and Selectivity of RhM_3 (M = Fe, Co Ni, Cu and Zn) Catalysts", Z. Mao, Guo, H.; Xie, Z.; P. Liu and Chen, J.G., *Catalysis Science & Technology*, **2022**, 12, 4988-4992. https://doi.org/10.1039/D2CY00821A

52. Coupling CO_2 reduction with ethane aromatization for enhancing catalytic stability of iron-modified ZSM-5, Xie, Z.; E. Gomez, D. Wang, J.H. Lee, T. Wang and Chen, J.G. *J. Energy Chem.* **2022**, 66, 210-217. https://doi.org/10.1016/j.jechem.2021.08.005

53. Enhanced Descriptor Identification and Mechanism Understanding for Catalytic Activity using Data-Driven Framework: Revealing the Importance of Interactions between Elementary Steps, Liao, W.; Liu, P. *Catal. Sci. Tech.* **2022**, *12*, 3836–3845. https://doi.org/10.1039/D2CY00284A

54. In Situ Studies of Methane Activation Using Synchrotron-Based Techniques: Guiding the Conversion of C-H Bonds. Rodriguez, J. A.; Rui, N.; Zhang, F.; Senanayake, S. D. *ACS Catal*. **2022**, *12*, 5470–5488. https://doi.org/10.1021/acscatal.2c00941

55. Understanding the Surface Structure and Catalytic Activity of SnO_x/Au(111) Inverse Catalysts for CO_2 and H_2 Activation. Kang, J.; Rui, N.; Rosales, R.; Tian, Y.; Senanayake, S. D.; Rodriguez, J. A. *J. Phys. Chem. C* **2022**, *126*, 4862–4870. https://doi.org/10.1021/acs.jpcc.2c00138

56. The Interaction of K and O_2 on Au(111): Multiple Growth Modes of Potassium Oxide and Their Catalytic Activity for CO Oxidation, Shi, R.; Liao, W.; Ramirez, P. J.; Orozco, I.; Mahapatra, M.; Kang, J.; Hunt, A.; Waluyo, I.; Senanayake, S.; Liu, P.; Rodriguez, J. *Angew. Chem. Int. Ed.*, **2022**, *61*, e202208666. https://doi.org/10.1002/anie.202208666

57. CO_2 Hydrogenation to Methanol over Inverse ZrO_2/Cu(111) Catalysts: The Fate of Methoxy under Dry and Wet Conditions, Rui, N.; Huang, E.; Kim, J.; Mehar, V.; Shi, R.; Rosales, R.; Tian, Y.; Hunt, A.; Waluyo, I.; Senanayake, S.; Liu, P.; Rodriguez, J. *J. Phys. Chem. C.* **2022**, *126*, 4479–14486 (2022). https://doi.org/10.1021/acs.jpcc.2c03723

58. Highly Selective Methane to Methanol Conversion on SnO_2/Cu_2O/Cu(111) Catalysts: Unique Properties of SnO_2 Nanostructures and the Inhibition of the Direct Oxidative Combustion of Methane, Huang, E.; Rui, N.; Rosales, R.; Kang, J.; Nemšák, S.; Senanayake, S. D.; Rodriguez, J.; Liu, P. *ACS Catal.* **2022**, 12, 11253–11262. https://doi.org/10.1021/acscatal.2c03060.

59. Identification of Highly Selective Surface Pathways for Methane Dry Reforming using Mechano-Chemical Synthesis of Pd-CeO_2, Jiménez, J. D.; Betancourt, L. E.; Danielis, M.; Zhang, H.; Zhang, F.; Orozco, I.; Xu, W.; Llorca, J.; Liu, P.; Trovarelli, A. Rodríguez, J. A.; Colussi, S. Senanayake, S. D., *ACS Catal.* **2022**, 12, 12809–12822. https://doi.org/10.1021/acscatal.2c01120

60. Utilizing CO_2 as a Reactant for C3 Oxygenate Production via Tandem Reactions, Biswas, A.N.; Winter, L.R.; Xie Z.; Chen, J.G. *JACS Au*, **2023**, 3, 293-305. https://doi.org/10.1021/jacsau.2c00533

61. Descriptor-based Identification of Bimetallic-derived Catalysts for Selective Activation of Ethane with CO_2", Guo, H.; Xie, Z.; Wang, X.; Chen, J.G.; Liu, P., *EES Catal.*, **2023**, *1*, 17-25. https://doi.org/10.1039/D2EY00051B

62. The role of copper crystallization and segregation toward enhanced methanol synthesis via CO_2 hydrogenation over $CuZrO_2$ catalysts: A combined experimental and computational study, Marcos, F.C.F.; Alvim, R.S.; Lin, L.; Betancourt, L.E.; Petrolini, D.D.; Senanayake, S.D.; Alves, R.M.B.; Assaf, J.M.; Rodriguez, J.A.; Giudici, R.; Assaf, E.M. *Chem. Eng. J.* **2023**, *452*, 139519. https://doi.org/10.1016/j.cej.2022.139519

63. Tailoring and Identifying Brønsted Acid Sites on Metal Oxo-cluster of Metal-Organic Framework for Catalytic Transformation", Liang, W.; Wang, X.; Yang, W.; Zhao, S.; Wiley, D.; Haynes, B. S.; Jiang, Y.; Liu, P.; Huang, J. "*ACS Central Sci.* **2023**, *9*, 27-35. https://doi.org/10.1021/acscentsci.2c01140

64. Atomic structural origin of the high methanol selectivity over In_2O_3-metal interfaces: Metal-support interactions and the formation of a InOx overlayer in Ru/In_2O_3 catalyst during CO_2 hydrogenation, Rui, N.; Wang, X.; Deng, K.; Moncada, J.; Rosales, R.; Zhang, F.; Xu, W.; Waluyo, I.; Hunt, A.; Stavitski, E.; Senanayake, S. D.; Liu, P.; Rodriguez, J. A., *ACS Catal.* **2023**, *13*, 3187-3200. https://doi.org/10.1021/acscatal.2c06029

65. The α-WC(0001) surface as a hydrogen sponge: A first principle study of H_2 dissociation and formation of low and high coverages, Jimenez-Orozco, C.; Florez, E.; Rodriguez, J. A., *ChemCatChem* **2023**, *15*, https://doi.org/10.1002/ cctc.202300165

66. Microscopic investigation of H_2 reduced CuO_x/Cu(111) and ZnO/CuO_x/Cu(111) inverse catalysts: STM, AP-XPS and DFT studies, Mehar, V; Huang, E.; Shi, R.; Rui, N.; Rosales, R.; Waluyo, I.; Hunt, A.; Liu, P.; Rodriguez, J. A., *ACS Catal*. **2023**, *13*, 9857-9870. https://doi.org/10.1021/acscatal.3c02514

67. Activation and Conversion of Methane to Syngas over ZrO_2/Cu(111) Catalysts near Room Temperature, Huang, E.; Rui, N.; Rosales, R.; Liu, P.; Rodriguez, J. A., *J. Am. Chem. Soc.* 2023, 145, 15, 8326-8331; http://dx.doi.org/10.1021/jacs.3c01980

68. Theoretical Perspective of Promoting Direct Methane-to-Methanol Conversion at Complex Metal Oxide–Metal Interfaces. Huang, E.; Liu, P. *J. Phys. Chem. Lett.,* **2023**, *14* , 6556-6563. https://doi.org/10.1021/acs.jpclett. 3c01525

69. C_1 Chemistry on Metal Carbide Nanoparticles: Boosting the Conversion of CO_2 and CH_4. Rodriguez, J. A.; Jimenez-Orozco, C.; Florez, E.; Viñes, F; Illas, F.; *J. Phys. Chem. C*, **2023**, in press, https://doi.org/10.1021/acs.jpcc.3c04541

Jointly funded by this grant and other grants with relatively minor intellectual contribution from this grant:

70. Nucleation and Initial Stages of Growth During the Atomic Layer Deposition (ALD) of Titanium Oxide on Mesoporous Silica, Ke, W.; Liu, Y.; Wang, X.; Qin, X.; Chen, L.; Palomino, R.; Simonovis, J. P.; Lee, I.; Rodriguez, J. A.; Frenkel, A. I.; Liu, P.; Zaera, F. *Nano Letters* **2020**, 20, 6884-6890. https://doi.org/10.1021/acs.nanolett.0c02990

71. Insights into the Methanol Synthesis Mechanism via CO_2 Hydrogenation over Cu-ZnO-ZrO_2 Catalysts: Effects of Surfactant/Cu-Zn-Zr Molar Ratio, Marcos, F. C. F.; Linb, L.; Betancourt, L. E.; Senanayake, S. D.; Rodriguez, J. A.; Assaf, J. M.; Giudici, R. E.; Assaf, M. *J. CO_2 Util.*, **2020**, 41, 101215. https://doi.org/10.1016/j.jcou.2020.101215

72. Structural, Electronic and Magnetic Properties of Ni Nanoparticles Supported on the TiC(001) Surface, Lozano-Reis, P.; Sayos, R.; Rodriguez, J.A.; Illas, F. *Phys. Chem. Chem. Phys.* **2020**, 22, 26145-16154. https://doi.org/10.1039/D0CP04884D

73. Optimized Microwave-based Synthesis of Thermally-Stable Inverse Catalytic Core-Shell Motifs for CO2 Hydrogenation, Salvatore, K.L.; Deng, K.; Yue, S.; McGuire, S.; Rodriguez, J.A.; Wong, S.W. *ACS Appl. Mater. Interfaces*, **2020**, 12, 32591-32603. https://doi.org/10.1021/acsami.0c06430

74. Critical Hydrogen Coverage Effect on the Hydrogenation of Ethylene Catalyzed by δ-MoC (001): An *Ab Initio* Thermodynamic and Kinetic Study, Jimenez-Orozco, C.; Florez, E.; Viñes, F.; Rodriguez, J.A.; Illas, F. *ACS Catal*. **2020**, 10, 6213-6222. https://doi.org/10.1021/acscatal.0c00144

75. N_2 Fixation by Plasma-Activated Processes, Winter L.R.; Chen, J.G., *Joule*, **2021**, 5 300-315. https://doi.org/10.1016/j.joule.2020.11.009

76. CO_2 Hydrogenation over Heterogeneous Catalysts at Atmospheric Pressure: From Electronic Properties to Product Selectivity, Wang, Y.; Winter, L.R.; Chen, J.G.; Yan, B. *Green Chem.* **2021**, 23, 249-267. https://doi.org/10.1039/D0GC03506H

77. Methane Oxidation Activity and Nanoscale Characterization of Pd/CeO_2 Catalysts Prepared by Dry Milling Pd Acetate and Ceria, Danielis, M.; Betancourt, L.E.; Orozco, I.; Divins, N.J.; Llorca, J.; Rodríguez, J.A.; Senanayake, S.D.; Colussi, S.; Trovarelli, A.; *Appl. Catal. B Environ.* **2021**, 282, 119567. https://doi.org/10.1016/j.apcatb.2020.119567

78. Dynamic Structure of Active Sites in Ceria-Supported Pt Catalysts for the Water Gas Shift Reaction, Li, Y.; Kottwitz, M.; Vincent, J. L.; Enright, M. J.; Liu, Z.; Zhang, L.; Huang, J.; Senanayake, S. D.; Yang, W.-C. D.; Crozier, P. A.; Nuzzo, P. G.; Frenkel, A. I. *Nat. Commun.*, **2021**, 12, 914. https://doi.org/10.1038/s41467-021-21132-4

79. Growth, Sintering, and Chemical States of Co Supported on Reducible CeO_2(111) Thin Films: The Effects of the Metal Coverage and the Nature of the Support, Zhou, J.; Du, L.; Braedt, D. L.; Miao, J.; Senanayake, S. D. *J. Chem. Phys.* **2021**, 154, 044704. https://doi.org/10.1063/5.0036952

80. Rationalization of promoted reverse water gas shift reaction by Pt_3Ni alloy: Essential contribution from ensemble effect., Zhang, H.; Wang, X.; Frenkel, A. I.; Liu, P., *J. Chem. Phys.* **2021**, *154*, 014702. https://aip.scitation.org/doi/abs/10.1063/5.0037886

81. Aliovalent Doping of CeO_2 Improves the Stability of Atomically Dispersed Pt. Wang, H.; Kottwitz, M.; Rui, N.; Senanayake, S.; Marinković, N.; Li, Y.; Nuzzo, R.; Frenkel, A. *ACS Appl. Mater. Interfaces* **2021**, *13*, 52736–52742. https://doi.org/10.1021/acsami.1c18330

82. Heterogeneous Hydroformylation of Alkenes by Rh-based Catalysts, Liu, B.; Wang, Y.; Huang, N.; Lan, X.; Xie, Z.; Chen, J.G.; Wang, T. *Chem*, **2022**, 8, 2630-2658. https://doi.org/10.1016/j.chempr.2022.07.020

83. Utilizing bimetallic catalysts to mitigate coke formation in dry reforming of methane, Bitters J. S.; He, T.; Nestler, E.; Senanayake, S.D.; Chen, J.G.; Zhang, C. *J. Energy Chem.* **2022**, 68, 124-142. https://doi.org/10.1016/j.jechem.2021.11.041

84. Investigating the Elusive Nature of Atomic O from CO_2 Dissociation on Pd(111): The Role of Surface Hydrogen, Simonovis, J. ; Zhang, H.; Rui, N.; Hunt, A.; Orozco, I.; Liu, P.; Senanayake, S. D.; Rodriguez, J. A.; Waluyo, I. *J. Phys. Chem. C.* **2022**, *126*, 7870–7879. https://doi.org/10.1021/acs.jpcc.2c00976

85. Tuning Selectivity in the Direct Conversion of Methane to Methanol: Bimetallic Synergistic Effects on the Cleavage of C–H and O–H Bonds over NiCu/CeO_2 Catalysts. Lustemberg, P.; Senanayake, S.; Rodriguez, J.; Ganduglia-Pirovano, M. V. *J. Phys. Chem. Lett.* **2022**, *13*, 5589–5596. https://doi.org/10.1021/acs.jpclett.2c00885

86. Carbon Nanosphere-Encapsulated Fe Core − Shell Structures for Catalytic CO_2 Hydrogenation. Weber, D.; Rui, N.; Zhang, F.; Zhang, H.; Vovchok, D.; Wildy, M.; Arizapana, K.; Saporita, A.; Zhang, J. Z.; Senanayake, S. D.; Lu, P.; Zhang, C. *ACS Appl. Nano Mater.* **2022**, *5*, 11605-11616 https://doi.org/10.1021/acsanm.2c02602

87. Reaction-Driven Selective CO_2 Hydrogenation to Formic Acid on Pd(111), Zhang, H.; Wang, X.; Liu, P. *Phys. Chem. Chem. Phys.* **2022**, *24*, 16997-17003. https://doi.org/10.1039/D2CP01971J

88. Infrared Reflection Absorption Spectroscopy and Temperature-Programmed Desorption Studies of CO Adsorption on Ni/CeO_2 (111) Thin Films: The Role of the Ceria Support . Peterson, E. W.; Wang, H.; Liu, Z.; Ara, T.; Senanayake, S. D.; Rodriguez, J. A. *J. Vac. Sci. Technol. A* **2022**, *40*, 013209. https://doi.org/10.1116/6.0001409

89. Effect of Operating Parameters on H_2/CO_2 Conversion to Methanol over Cu-Zn Oxide Supported on ZrO_2 Polymorph Catalysts: Characterization and Kinetics. Marcos, F. C. F.; Cavalcanti, F. M.; Petrolini, D. D.; Lin, L.; Betancourt, L. E.; Senanayake, S. D.; Rodriguez, J. A.; Assaf, J. M.; Giudici, R.; Assaf, E. M. *Chem. Eng. J.* **2022**, *427*, 130947. doi.org/10.1016/j.cej.2021.130947

90. Au and Pt Remain Unoxidized on a CeO_2-Based Catalyst during the Water–Gas Shift Reaction, Reina, TR; Gonzalez-Castaño, M.; Lopez-Flores, V.; Martinez, L.M.; Zitolo, T.A.; Ivanova, S.; Xu, W.; Centeno, M.A.; Rodriguez, J.A.; Odriozola, J.A. *J. Am. Chem. Soc.* **2022**, *144*, 446-453. https://doi.org/10.1021/jacs.1c10481

91. Effect of nanostructuring on the interaction of CO_2 with molybdenum carbide nanoparticles. Jimenez-Orozco, C.; Figueras, M.; Florez, E.; Viñes, F.; Rodriguez, J.A.; Illas, F. *Phys. Chem. Chem. Phys.*, **2022**, *24*, 16556-16565. https://doi.org/10.1039/D2CP01143C

92. Enhanced Oxide Reduction by Hydrogen at Cuprous Oxide-Copper Interfaces near Ascending Step Edges, Xu, F.; An, W.; Baber, A. E.; Grinter, D.; White, M. G.; Liu, P.; Stacchiola, D. J. *J. Phys. Chem. C* **2022,** 126, 18645-18651. https://doi=10.1021/acs.jpcc.2c03719

93. Opportunities for CO_2 upgrading using tandem electrocatalytic-thermocatalytic processes, Garg, S.; Biswas, A.N.; Xie Z.; Chen, J.G., *Carbon Future*, **2023**, accepted.

94. Amino-tethering Synthesis Strategy toward Highly Accessible Sub-3 nm L10-PtM Catalysts for High-Power Fuel Cells, Gong, Q.; Zhang, H.; Cullen, D. A.; Jeon, S.; Yu, H.; Ren, Y.; Yang, Z.; Sun, C.; Stach, E. A.; Yu, Y.; Foucher, A. C.; Smart, M.; Filippelli, G. M.; Liu, P.; Xie, J., *Matter*, **2023**, *6*, 963-982. https://doi.org/10.1016/j.matt.2022.12.011

95. Ethylene Hydrogenation Molecular Mechanism on MoC_y Nanoparticles. Jimenez-Orozco, C.; Florez, E.; Viñes, F.; Rodriguez, J. A.; Illas, F. *J. Phys. Chem. C*., **2023**, *127,* 7666=7673 http://dx.doi.org/10.1021/acs.jpcc.3c00435

Catalysis Program at Lawrence Berkeley National Laboratory:
Harnessing Complexity for Catalytic Efficiency

John F. Hartwig-Program Leader, Polly L. Arnold, Alexis T. Bell, Robert G. Bergman (affiliate), Christopher J. Chang, Michelle C. Chang, Kenneth N. Raymond (affiliate), Miquel B. Salmeron, Gabor A. Somorjai (affiliate), T. Don Tilley, F. Dean Toste, Peidong Yang
Chemical Sciences Division, Lawrence Berkeley National Laboratory

Presentation Abstract

The LBNL Catalysis Program seeks to reveal foundational principles for the creation of new catalysts, realization of new processes, and creation of new approaches to learn how catalysts operate. The overarching theme of the current research is to reveal and exploit complexity inherent in, or designed to be a part of, catalytic systems that operate with high rates and selectivity. The types of catalysts and catalytic reactions studied in the current Catalysis Program, and the classes of mechanisms by which the catalysts react, are broad in scope, but converge on several themes that constitute the three subtasks. These three subtasks are organized by layers of complexity. The first subtask reveals and creates multiple functionality in a single active site; the second reveals and creates new catalytic systems that involve multiple catalytic sites that work cooperatively or that convert from one to another; the third subtask focuses on catalytic systems in which two components, one the active site and one the supramolecular confines of that site, work cooperatively to change the course of the catalytic transformation. Each of these subtasks directly addresses PROs in workshop reports on catalysis and cross-cutting themes of the BES CSGB division.

FWP Number: CH030201
FWP Title: Program in Catalysis and Chemical Transformations – Harnessing Complexity for Catalytic Efficiency

Postdoc(s): Chae, Sudong; Jaugstetter, Maximillian; Lee, Chin Ho; Narouz, Mina Raafat Ryad; Treacy, Sean

Student(s): Brown, Gretchen Mary; Carter, Robert Allan; Chen, Rei Chi; Conk, Richard James; Craescu, Cristina-Valentina; DeHovitz, Jacob; Elissiry, Luke Jacques; Feijoo, Julian; Fonseca Guzman, Maria Victoria; Heafner, Elizabeth Dawn; Hernandez, Matthew Rice; Herrera, Gabriel; Huffman, Calvin; Joyner, Isaac A; Kayrouz, Colby Scott; Kissman, Elijah N; Kynman, Amy E; Lara, Jaden Kentaro; Lefton, Natalie Grace; Leonhardt, Branden; Ma, Senjie; Maddi, Vincent John Pershing; Rothweiler, Aila Veena; Rutkauskaite, Ryte; See, Matthew S; Shan, Yu; Wheeler, Thomas A; Xia, Kelly Tianlu

RECENT PROGRESS

Subtask 1. Multifunctional Catalyst Systems for Selective Transformations

Subtask 1 focuses on the creation of multi-functional catalysts in which multiple interactions in the secondary coordination sphere or multiple metal centers within the coordination sphere impart a major influence on the activity and selectivity of the system. Such control includes the influence of secondary, non-covalent interactions on catalyst activity and selectivity, the effect of a second (or more) metal center on the electronic properties of the active site, or multimetallic interactions that enable transformations that would be difficult or impossible to achieve with a simple active site. These catalysts are being applied to transformations such as isomerization of and additions to alkenes, reductions of carbon dioxide and dinitrogen, and functionalization of hydrocarbons, which are crucial to efficient use of multiple feedstocks. Novel spectroscopic methods and reactor systems are being applied to monitor these processes as they are occurring, and modern theoretical methods are being used to interpret spectral data, to help elucidate reaction mechanisms, and to understand data on rates and selectivities. A selection of projects and recent results are described in the next sections.

1.1 Cooperative Lanthanide-Ligand Structures for Catalytic Reduction of Dinitrogen to Silylamines and Selective sp3 Carbon Fluorine Bond Functionalization (Arnold)

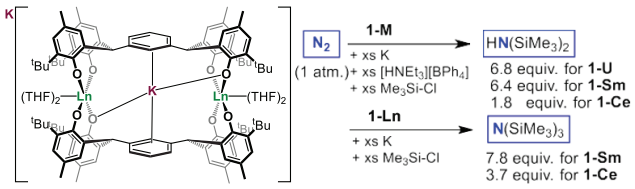

Figure 1.1. N2RR (nitrogen reduction reaction) by homogeneous lanthanide catalysts, with electron transfer controlled by the secondary metallacyclic environment.

The binding of dinitrogen to any f-block metal cation was considered impossible until the turn of the millennium, but a small yet growing number of weakly-bound N_2 complexes are now being reported. Chemists have spent more than a century trying to make low-energy catalysts for the N2RR reaction; reduction of atmospheric dinitrogen (N_2) to ammonia (NH_3), or directly to amines (NR_3). Hundreds of complexes based on metals from the d-block are now known to bind N_2, and a few catalysts for N_2 conversion to ammonia or tris(silyl)amine have been developed. We recently reported the first homogeneous, f-block catalysts that convert N_2 to silylamines under ambient conditions. Complexes of U(IV) and Th(IV) with defined ligand reactivity are shown to selectively form a secondary silylamine for the first time. Now we have shown that Ce and Sm analogues are the first non-radioactive f-block N_2RR catalysts that can be tuned to make secondary or tertiary amines from N_2 (Fig. 1.1). The rigid tetraphenol-arene ligands (mTP) form a metallacycle $Ln_2(mTP)_2$ containing a reactive C-H bond, the hydrogen of which is transferred to the first N-H bond, enabling selectivity for secondary amines. New data from the ALS infrared BL1.4, suggest that the M^0 reductant sequentially delivers electrons to an increasingly unsymmetrically bound, end-on Ln-N_2 unit within the cage near the Ln center, likely through the reducible ligand framework. The strongly reduced Ln-bound N_2 deprotonates a benzylic hydrogen on the ligand. Resonant Inelastic X-ray Scattering (RIXS) measurements at the N- and Ln- edges (ALS BL8) and theory by Prendergast at the Molecular Foundry are helping to clarify the Ln orbitals involved in this N_2 reduction.

Lanthanide complexes can also exhibit strong and tunable Lewis acidity, more highly ligand-dependent redox potentials than d-block analogues, and the capacity for rapid ligand exchange reactions. Indeed, selective mono-defluorination and alkylation of CF_3 groups have been achieved by simple, non-toxic, base metal catalysts for the first time. We hav developed a cerium photocatalyst (L)Ce(Cp^{Me4})$_2$ (2-Ce, Cp^{Me4} = C_5Me_4H, L= aryloxy NHC [2-O-3,5-^{t}Bu$_2$-C_6H_2(1-

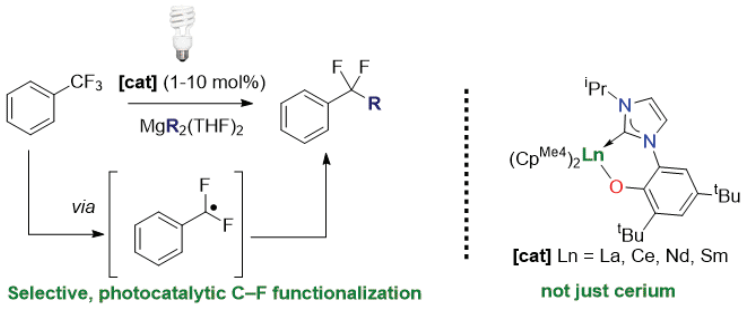

Figure 1.2. photocatalytic combination of base metal lanthanides and redox active ligands for manipulation of inert C-F bonds.

C{N(CH)$_2$N(^{i}Pr)})]) that combines the photoexcitable Ce(III) with multi-functional, tunable ligands to cleave and functionalize the strong and inert sp^3 C-F bond of PhCF$_3$ by an inner sphere mechanism. (Fig. 1.2) The NHC ligand (L) is essential for the cleavage of the strong C-F bond; it allows for additional light absorption and photoexcitation. Further, the oxidation of ligand L enables catalysis to occur with Ln metals that lack a metal-based redox event. Thus, tuning of the ligand redox properties by Ln Lewis acidity becomes possible. We have also shown that simple lanthanide cyclopentadienyl (Cp) complexes can photochemically cleave the sp^3 carbon-chlorine bond of unactivated chlorinated hydrocarbons, including those in polyvinyl chloride (PVC). Because light absorption by the Cp ligand is efficient, photocatalytic reactivity is enhanced for cerium and made possible for normally photoinactive lanthanide neighbors on the periodic table. Work is in progress within the LBNL program to develop new spectroscopic methodologies to detect and develop the halophilic interaction that is essential to the inner-sphere electron transfer in the mechanism.

Lam, F. Y. T.; Wong, A. R.; Trinh, M. T.; Kelly, R. P.; Rao, G.; Britt, R. D.; Arnold, P. L., Catalytic Reduction of Dinitrogen to Silylamines by Earth-Abundant Lanthanide Complexes. *submitted*.

Kynman, A. E.; Christodoulou, S.; Ouellette, E. T.; Peterson, A.; Kelly, S.; Maron, L.; Arnold, P. L. Photocatalytic Dechlorination of Unactivated Chlorocarbons Including PVC Using Organolanthanide Complexes. *Chem. Commun.* **2023**, Advance Article, DOI 10.1039/D3CC02906A

1.2 Electrocatalytic Carbon and Nitrogen Cycling by Molecular-Materials Platforms (C. Chang)

We have discovered porous cage catalysts that enhance the photochemical reduction of CO_2 (Fig. 1.3). The porous structure provides a confined space for CO_2 activation, while the cationic pendants facilitate electron transfer from the catalyst to CO_2. The cage catalyst featuring both porosity and charge effects exhibited 41-, 4-, and 6-fold higher activity than the parent iron porphyrin, neutral porous cage, or cationic iron porphyrin, respectively, with 97% selectivity for the formation of CO, achieving turnover numbers (TON) exceeding 7000 and initial TOF_{max} reaching 23 s^{-1}. Results from this program now show that embedding a cobalt porphyrin (CoTPP) catalyst into a supramolecular porous cage structure leads to efficient reduction of nitrate (NO_3^-) to ammonia (NH_3) in water, achieving total TON

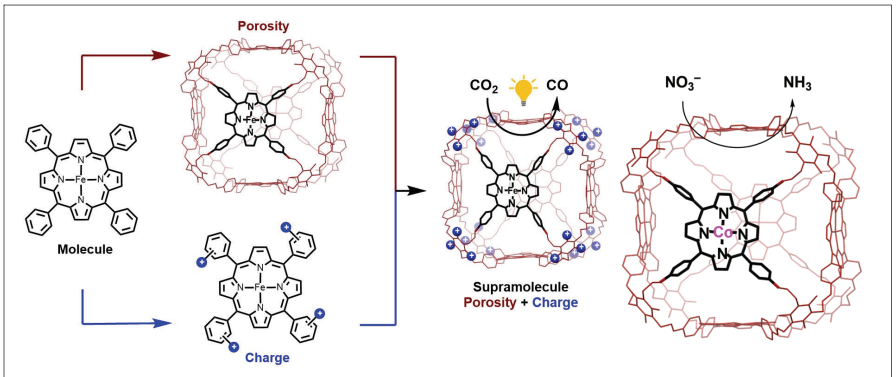

Figure 1.3. Combined supramolecular effects of porosity and charge.

exceeding 200,000 and TOF values exceeding 56 s^{-1}. The reactivity of the cobalt cage for NO_3^- reduction to NH_3 is much higher than its molecular analogue CoTPP, and the catalyst is stable over a longer period. These results highlight the benefits of this supramolecular design strategy. Host-guest interactions between NO_3^- and CoPB-C8 facilitate substrate capture and transport into the cage, increasing its local concentration and promoting reduction to NH_3.

An, L.; De La Torre, P.; Smith, P. T.; Narouz, M. R.; Chang, C. J., Synergistic Porosity and Charge Effects in a Supramolecular Porphyrin Cage Promote Efficient Photocatalytic CO_2 Reduction. *Angew. Chem. Int. Ed.* **2023**, *62* (5), e202209396. DOI 10.1002/anie.202209396.

1.3 Remote Hydroamination of Disubstituted Alkenes by a Combination of Isomerization and Regioselective N–H Addition (Hartwig)

The catalytic hydroamination of alkenes forms amines from hydrocarbons with full atom economy, but development of this transformation with unactivated aliphatic alkenes, particularly those with two or more substituents on the C=C bond, has been a long-standing challenge. In recent years, we have reported in *Nature* a catalyst for the hydroamination of unactivated internal alkenes with minimal alkene isomerization ("local functionalization") and in *Chem* the hydroamination of a broad scope of terminal alkenes. We have since reported that changing the amine and catalyst judiciously to promote alkene isomerization led to the combination of olefin isomerization and selective hydroamination of the small population of terminal alkene ("remote functionalization") within the equilibrating isomers. This process, wherein functional groups are incorporated distal to existing carbon–carbon double bonds, occurs by the isomerization of secondary and tertiary alkyl-metal intermediates into primary alkyl-metal intermediates before the reductive elimination to form the functionalized product. In this system, the relative rates for insertion of the olefin into the C-N bond and insertion into the M-H bond control the rate of olefin hydroamination vs isomerization, and these relative rates are strongly affected by the substituents at the periphery of the ligand and the counterion for the cationic catalysts (Fig. 1.4A). The catalyst activities vary as a function of the anion: BAr^F (tetrakis(3,5-bis(trifluoromethyl)phenyl)borate) > bistriflimide > triflate >> BF_4^- and PF_6^-. Although less active, the selectivity of the catalyst containing the bistriflimide counterion for hydroamination over isomerization is higher than that of the complex containing BAr^F. We have proposed that interaction of the anion with the amide and hydride influence selectivity. Future work seeks to further understand the origins of the differences in activity of the catalysts, particularly how the non-covalent interactions of the catalyst components change activity and chemoselectivity.

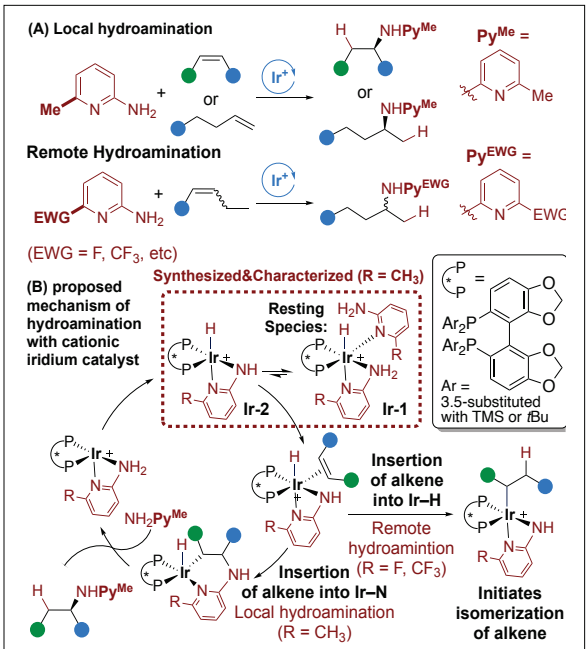

Figure 1.4. (A) local and remote hydroamination of unactivated alkenes with 2-aminopyridines and (B) proposed mechanism and related ongoing mechanistic studies.

Ma, S.; Fan, H.; Day, C.S.; Xi, Y.; Hartwig, J.H., Remote Hydroamination of Disubstituted Alkenes by a Combination of Isomerization and Regioselective N–H Addition. *J. Am. Chem. Soc.* **2023**, *145* (7), 3875–3881. DOI 10.1021/jacs.2c13054.

1.4 Investigations of Metal-Metal Cooperativity for Small Molecule Transformations and Catalysis (Tilley)

High concentrations of nitrogen oxides (NO_x) in the environment have adverse effects on human health. Catalysts that can reduce these toxic NO_x species to more benign small molecules, such as nitrogen or ammonia, are highly sought. While it is known that denitrifying bacteria contain enzymes with bimetallic active sites to catalyze NO_x reduction, their mechanisms are not fully understood. Modeling such enzymes, such as the Dicopper Nitrite Reductases (CuNIRs) and the Fe-Cu based Cytochrome c Oxidase (CcO), not only aids in the elucidation of their biological reductive pathways but also advances the pursuit of potent NO_x-reduction catalysts. To this end, we have isolated and characterized a dicopper nitrite complex, $[Cu_2(\kappa^2\text{-}O_2N)(DPFN)][NTf_2]$, that reductively cleaves a nitrite N–O bond by reaction with a Brønsted acid (such as $HNTf_2$) or a Lewis acid (such as $B(C_6F_5)_3$) to yield $[Cu_2(\mu\text{-}NO)(\mu\text{-}OH)(DPFN)][NTf_2]_2$. Remarkably, $[Cu_2(\kappa^2\text{-}O_2N)(DPFN)][NTf_2]$ also reacts with a variety of nitriles to form the corresponding dicopper(I) carboxylate complexes (Fig. 1.5). Current efforts are aimed at understanding the mechanism of these reactions and to studying O-atom transfer reactivity by the activation of other small molecules, such as carbon monoxide, isocyanides, and hydrogen. There is literature precedent for the metal-mediated catalytic reduction of nitrite by CO. Extending this reactivity to dicopper systems is of particular interest, considering their role in enzymatic nitrite reduction.

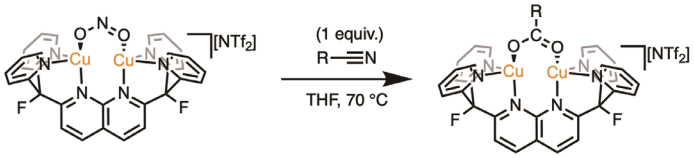

Figure 1.5. The reaction of a dicopper nitrite complex with nitriles yields the corresponding dicopper carboxylate complex.

Subtask 2. Cooperative and Evolving Multi-Catalytic Systems

Subtask 2 focuses on catalytic systems that comprise multiple catalysts. It encompasses systems in which multiple catalysts work together and systems in which multiple structures and compositions dynamically interconvert under operating conditions. Examples include multiple soluble metal complexes that operate synergistically in the same system to enable mild conditions for traditionally high temperature and pressure processes, multiple catalysts cooperatively disassembling long hydrocarbons by cleavage of C-C bonds or catenating components of biomass to form longer carbon chains, and nano-scale electrocatalysts that reduce CO_2 by changing shape, composition, and oxidation state during catalysis to generate environments that are highly active to form products containing C-C bonds. Again, new methods for *in situ* and *operando* spectroscopic and structural characterization are being developed to reveal these catalyst dynamics under operating conditions. This theme of catalysis with multiple and evolving catalysts has gained increased prominence during the past three years to become a dedicated subtask in the current review document.

2.1 Catalyst Restructuring Driven by Adsorbate Catalysis (Salmeron, Somorjai)

In collaboration with the Mavrikakis group at UW Madison, we have developed a theoretical framework for adsorbate-induced metal-metal bond breaking of catalyst solid surfaces that leads to the formation of catalyst metal clusters (Fig. 2.1). This study, using density functional theory calculations, kinetic Monte Carlo simulations, and scanning tunneling microscopy of CO on a nickel surface, elucidated the nature of active sites, which are not intrinsic to the isolated catalyst but arise from interaction with the

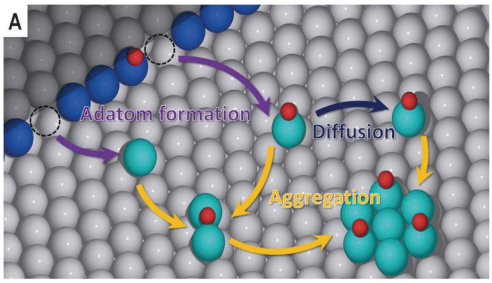

Figure 2.1. Adsorbate-induced metal cluster formation due to ejection of step-edge atoms.

reactants. The results serve as a starting point for screening a variety of catalytic systems that could exhibit adsorbate-induced clustering behavior (e.g., CO oxidation, ammonia oxidation on Ag and Cu, water-gas shift reaction, methanol synthesis on Cu, NO reduction by H_2 on Pt, methane oxidation on Pd, and methane steam reforming on Ni). This work underscores the importance of studying dynamic restructuring of nanocatalysts under reaction conditions, as the metal-metal bond breaking involved in catalyst structural evolution likely occurs more broadly than previous acknowledged.

Xu, L.; Lechner, B.A.J.; Je, L.; Somorjai, G.A.; Salmeron, M.; Mavrikakis, M., Formation of Active Sites on Transition-Metal Surfaces under Catalytic Reactive Conditions. *Science* **2023,** 380, 70–76. DOI 10.1126/science.add0089.

2.2 Liquid Multi-Element Alloys Catalyst for Highly Efficient Clean Hydrogen Production from Methane Pyrolysis (Su, Salmeron, Somorjai)

In recent years, multi-element alloys have been studied intensively for their distinct mechanical, physical, and chemical properties. Inspired by the tailoring of the electronic structure by metal-metal interactions in soluble, molecular, transition-metal catalysts, we introduced molybdenum to a nickel-bismuth system to reduce the negative charge on nickel and enable methane pyrolysis (MP) to form dihydrogen at lower temperatures. Indeed, we found that the interactions of Ni and Mo create a nickel with less negative charge and a molybdenum with positive charge that, together (NiMo-Bi, Ni 2.3 wt %, Mo 1.3 wt%, and Bi 96.4 wt%) catalyze MP with the highest known activity and with a high H_2 generation efficiency (4.05 mL_{H2} g_{Ni}^{-1} min^{-1}) at 800 °C (Fig. 2.2). This efficiency is 37 times greater than that of Ni-Bi catalysts. The E_a for MP catalyzed by NiMo-Bi is 81.2 kJ mol^{-1}. The MP process is widely recognized as a promising approach to clean dihydrogen production, but prior catalysts suffered from insufficient selectivity and activity at acceptable reaction temperatures.

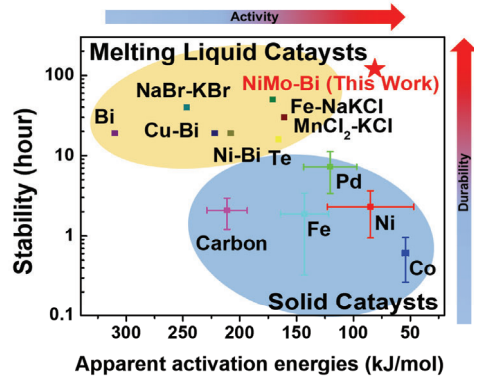

Figure 2.2. Stability and activity of various solid and melting liquid catalysts for production of H_2 from methane pyrolysis.

Chen, L.; Song, Z.; Zhang, S.; Chang, C.-K.; Chuang, Y.-C.; Peng, X.; Dun, C.; Urban, J.J.; Guo, J.; Chen, J.-L.; Prendergast, D.; Salmeron, M.; Somorjai, G.A.; Su, J., Ternary NiMo-Bi Liquid Alloy Catalyst for Efficient Hydrogen Production from Methane Pyrolysis, *Science*, **2023**, 381 6660 867-861, DOI 10.1126/science.adh8872.

2.3 Direct Observation of Cu Electrocatalyst Evolution using *Operando* 4D-STEM (Yang)

Copper is the sole element known to catalyze selective CO_2 electroreduction to multicarbon products. However, the structures of its active sites under reaction conditions have been poorly defined, particularly for high-performance Cu nanocatalysts, due, in part, to the lack of nanoscale, time-resolved *operando* and *in situ* methods. We provided the first definitive picture of copper active sites, metallic Cu nanograins, through a comprehensive *operando* study of the dynamic structural evolution of a family of Cu nanocatalysts, starting from (i) their initial nanoparticle (NP) ensemble, progressing through (ii) their catalytically active structure under the conditions of the CO_2 reduction reaction (CO_2RR), and ending with (iii) their post-electrolysis structure after exposure to air (Fig. 2.3). *Operando* electrochemical liquid cell scanning transmission electron microscopy (EC-STEM) enables quantitative electrochemistry with simultaneous quantitative

STEM imaging, diffraction, and spectroscopy. Correlative EC-STEM and high-energy-resolution X-ray spectroscopy have been used to probe the dynamic evolution of Cu NP ensembles under CO_2RR conditions. The rich nanograin boundaries bear undercoordinated Cu sites, the probable active sites for selective CO_2RR. *Operando* 4D-STEM revealed the structural evolution of the NP ensemble, with a spatial resolution close to 1 nm, as it transitions from the initial stage of loosely connected nanograins to the steady-state of closely packed nanograins as applied potentials approached their optimum for CO_2RR. The strategies reported may serve as a general platform to resolve electrocatalytic interfaces under real-time operating conditions across multiple spatiotemporal scales.

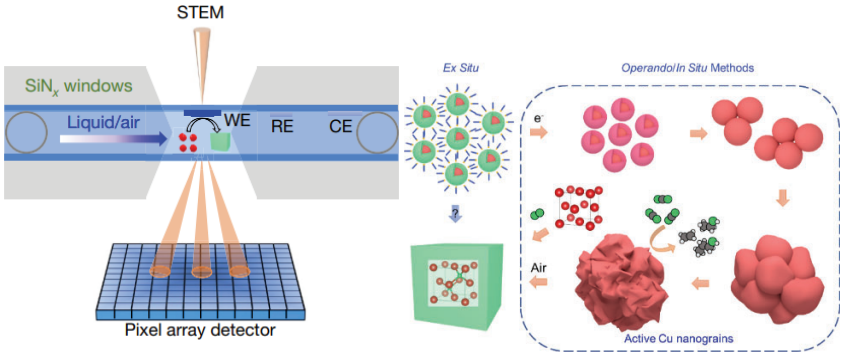

Figure 2.3. Multimodal *operando* methods reveal the complete lifecycle of Cu nanocatalysts during CO_2 electroreduction.

Yang, Y.; Louisia, S.; Yu, S.; Jin, J.; Roh, I.; Chen, C.; Guzman, M. V. F.; Feijoo, J.; Chen, P.; Pollock, C. J.; Huang, X.; Wang, H.; Shao, Y.; Wang, C.; Muller, D. A.; Abruña, H. D.; Yang, P., *Operando* Studies Reveal Active Cu Nanograins for CO_2 Electroreduction. *Nature* **2023,** 614, 262. DOI 10.1038/s41586-022-05540-0.

Subtask 3. Catalysis in Confined Spaces

The third subtask focuses on conducting catalysis in confined environments. This theme was initiated by work on catalysis within a supramolecular nanovessel and has been a long-standing component of this Catalysis Program. Now, this work on confined environments has motivated research on catalysis in a broader range of confined spaces, including new supramolecular cages, the pores of metal-organic frameworks (MOFs), boxes with metal-porphyrins as sides, and active sites of artificial and natural metalloenzymes. Recent highlights of these new directions that illustrate the broadened scope include the use of supramolecular hosts to achieve enzyme-like regioselectivity from reactions of polyunsaturated molecules, the use of new types of cages to reveal the role of charge on the rates of reactions promoted by these anionic assemblies, the use of a porous, 3-dimensional coordination network to stabilize an active form of the Co_4O_4 oxo cubane for prolonged electrocatalytic water splitting, regioselective C-H bond functionalizations by evolved artificial metalloenzymes, monomeric metal hydrides as new classes of abiotic enzyme intermediates, and new non-heme iron enzymes that catalyze halogenation reactions by control over the trajectory of the rebound step by the protein surroundings.

3.1 Mechanism of Carbene Transfer by the Artificial Metalloenzyme Ir(Me)-CYP119 (Hartwig)

Artificial metalloenzymes (ArMs), enzymes that contain non-native, typically synthetic, metal cofactors, constitute a flourishing class of biocatalysts for unnatural reactions. We report a structural and mechanistic study of an abiotic cyclopropanation reaction catalyzed by the ArM Ir(Me)-P450, containing the organometallic Ir(Me) unit in place of Fe in the hemin cofactor. The ArM contains a glycine in the position of the axial cysteine residue that typically binds to a natural heme cofactor. Thus, the artificial cofactor is bound non-covalently to the active site. Nevertheless,

the Ir-porphyrin complex sits in the position of the natural heme, but the Ir(Me) moiety points into the substrate channel (Fig. 3.1) and the open reaction site faces away. Mass spectrometry shows that the Ir(Me) unit remains intact throughout catalysis, and molecular dynamics simulations indicate that the two conformations of the cofactor ("methyl-up" vs. "methyl-down") are similar in energy. Combined, these results imply that the iridium-porphyrin must bind reversibly or, less likely, flip within the active site to orient the vacant face on the iridium-porphyrin toward the substrate channel. Kinetic studies showed that the cyclopropanation of carvone by ethyl diazoacetate (EDA) catalyzed by the Ir(Me)-CYP119, as measured by dinitrogen evolution, occurs after a pronounced induction period, while the reaction catalyzed by the free cofactor proceeds without an induction period. These results and crystallographic data, suggest that the enzyme must undergo a transformation to become an active catalyst, with a rate constant of $k_{induction} = 0.014\ s^{-1}$ from kinetic simulation. The cofactor dissociation equilibrium constant, K_d, and the association rate constant, k_{on}, were determined by fluorescence quenching experiments. From these data, the dissociation rate constant, k_{off}, ($k_{off} = k_{on}K_d = 0.27\ s^{-1}$) was shown to be kinetically competent to occur during the induction period and may proceed multiple times to allow proper orientation of the catalyst within the active site. These observations suggest that the Ir(Me)-CYP119 mutant adopts an inactive resting state in which the Ir(Me) unit of the cofactor is positioned towards the substrate channel, but the cofactor in the enzyme reorients by "flipping" to become the active catalyst, as shown in Fig. 3.1

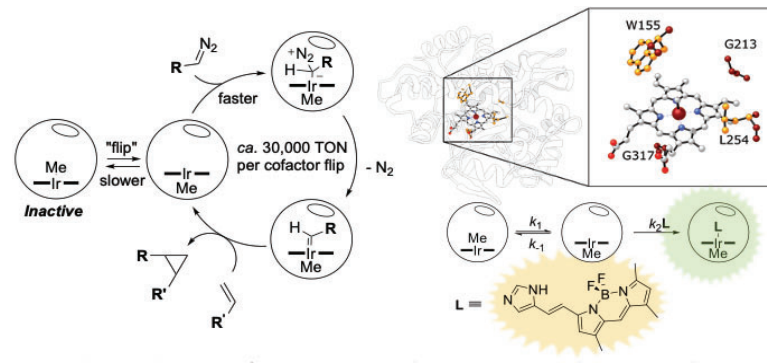

Figure 3.1. Ir(Me)-CYP119 active site from X-ray diffraction and summary of the mechanism of the cyclopropanation by Ir(Me)-CYP119.

Bloomer, B.J.; Natoli, S.N.; Garcia-Borràs, M.; Pereira, J.H.; Hu, D.B.; Adams, P.D.; Houk, K.N.; Clark, D.S.; Hartwig, J.F., Mechanistic and Structural Characterization of an Iridium-Containing Cytochrome Reveals Kinetically Relevant Cofactor Dynamics. *Nat. Cat.* **2023**, *6*, 39–51. DOI 10.1038/s41929-022-00899-9.

3.2 Mechanistic Studies of Engineered Fe Radical Halogenases (M. Chang)

Enzymes are prized for their ability to catalyze challenging reactions with exquisite selectivity, even when multiple reaction outcomes are possible. One of the most striking examples of this type are found in C-H activation reactions where metalloenzymes can abstract a H atom with high regio- and stereoselectivity in a structure with many similarly reactive bonds followed by stereoselective functionalization. We have been studying how Fe/α-ketoglutarate-dependent radical hydroxylases and halogenases can control reaction selectivity along two separate reaction

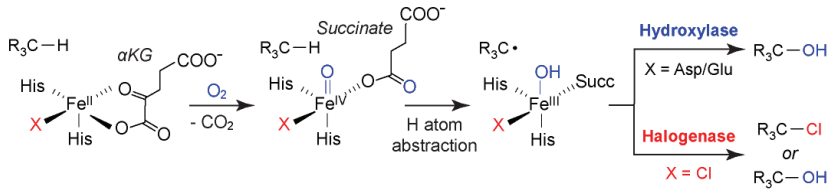

Figure 3.2. C-H activation by Feradical halogenases takes place via an Fe(IV)=O intermediate. Radical halogenases subsequently transfer X = Cl, Br rather than the hydroxyl group along a different reaction axis.

trajectories, first for C-H abstraction and then by halide transfer to catalyze halogenation of unactivated C(sp^3) positions (Fig. 3.2). One major question is what factors in the active site cause rebound of chloride over hydroxide given the Fe(III)-OH should be favorably placed subsequent to H atom abstraction by the Fe(IV)=O intermediate. For hydroxylases, only one reaction pathway is possible; for halogenases rebound with Cl and OH are both available. Although computational studies have probed the factors that control this chemoselectivity for the rebound step, it remained unclear what primary-sphere and secondary-sphere interactions within the active site of the halogenase control how rebound with the halide atom is favored.

We have used a combination of bioinformatics and protein engineering, in conjunction with a high throughput screen, to identify the minimal sequence changes that convert a hydroxylase enzyme (Hydrox) into a halogenase (Hal) enzyme. The sequences of hydroxylases and halogenases typically diverge by 60-70%, making it difficult to mechanistically and structurally compare these enzymes to identify the molecular factors that control the difference in reaction outcome. However, using a protein engineering approach, we have identified a 7% sequence divergence that allow the switch of Hydrox into a Hal with wild-type catalytic behavior. New studies show these mutations can be grouped into two types: those that control the switch from rebound at Fe-OH to rebound at Fe-Cl and those that enforce chloride binding in the active site. Indeed, studies of these different variants by stopped-flow kinetics show that the rate of formation and decay of the Fe(IV)=O unit is substantially different for Hydrox vs Hal. Interestingly the introduction of only two secondary sphere mutations into Hydrox, in addition to the mutation that allows the halide ion to bind Fe, is sufficient to switch the pre-steady state behavior of the hydroxylase to a profile that is equivalent to that of the halogenase. As such, these two residues and their function are now under investigation as a minimal model system to understand the molecular details of this selectivity switch that controls Fe-OH vs Fe-Cl rebound.

3.3 Mechanistic Investigations of Supramolecular Host Dynamics and its Impact on Selectivity (Toste, Raymond, Bergman)

Over the last decade, the importance of flexibility and conformational dynamics in catalysis has gained recognition. Noncovalent interactions have been found to stabilize favorable transition states, leading to the development of more selective small-molecule catalysts. Despite achieving high selectivity with the confined cavity of supramolecular host-catalyzed reactions, the impact of flexibility and conformational dynamics on rate and selectivity clearly remains an outstanding question. We recently discovered a positive correlation between the enantioselectivity in an aza-Darzens reaction and the flexibility of a supramolecular anionic tetrahedral host based on *tris*-bidentate coordination of the catecholate amides at cationic metal vertices. This connection was revealed by modulating the distal chiral amide appendage and varying the metal at the host vertices. To investigate if this correlation holds for different reactions, the effects of the host structure were studied on a host-catalyzed aza-Cope reaction. Initial results indicate a reversed selectivity trend for the aza-Cope reaction across a series of ene-ammonium substrates, with higher enantio-selectivities observed for bulkier substrates (Fig. 3.3a). However, variations in the host's distal chiral amide did not significantly affect enantioselectivity (Fig. 3.3b).

The differing selectivity observed in the aza-Cope and aza-Darzens condensation reactions across the catalyst series suggests that factors other than aperture deformation influence catalysis. In the aza-Cope rearrangement, for which cyclization within the host is the rate-limiting step, it is thought that the microenvironment of the cavity, specifically the breathability of the cage after substrate encapsulation, influences selectivity. We hypothesized that the bond rotation rates of an encapsulated bulky guest would serve as a probe for host cavity flexibility. Slower bond rotation rates would indicate more rigid cavities, indirectly measuring host flexibility and the ability to accommodate guest motion after encapsulation. We have shown a correlation between these bond

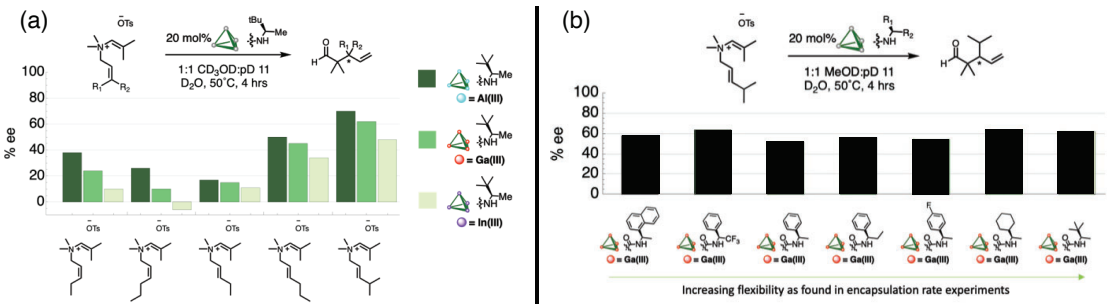

Figure 3.3. a) Differential enantioselectivity found for the aza-Cope rearrangement across the Al-, Ga-, and In-based hosts. b) No significant different in enantioselectivity found between hosts with different chiral amides.

rotation rates and enantioselectivity in the aza-Cope reaction for hosts based on Al, Ga, and In. We propose that further diversification at the metal vertices to adjust the strength of the metal-oxygen bonds will lead to varying scaffold rigidity, corresponding to the conformational freedom of encapsulated guests and thus the selectivity.

Program Publications List (2020-2023)

A. Publications that were solely supported by this FWP, and those in collaboration with others that are based on research that is intellectually led by the FWP and advances one or more of the FWP's objectives.

2020

Amit, E.; Dery, S.; Kim, S.; Roy, A.; Hu, Q.; Toste, F. D.; Gross, E., Electrochemical Deposition of N-heterocyclic Carbene Monolayers on Metal Surfaces. *Nat. Commun.* **2020**, *11* (1), 5714. DOI 10.1038/s41467-020-19500-7.

Amtawong, J.; Skjelstad, B. B.; Balcells, D.; Tilley, T. D., Concerted Proton-Electron Transfer Reactivity of an Oxidized Co_4O_4 Cubane. *Inorg. Chem.* **2020**, *59* (20), 15553–15560. DOI 10.1021/acs.inorgchem.0c02625.

Arnold, P. L.; Ochiai, T.; Lam, F. Y. T.; Kelly, R. P.; Seymour, M. L.; Maron, L., Metallacyclic Actinide Catalysts for Dinitrogen Conversion to Ammonia and Secondary Amines. *Nat. Chem.* **2020**, *12* (7), 654–659. DOI 10.1038/s41557-020-0457-9.

Chen, C.; Li, Y.; Yu, S.; Louisia, S.; Jin, J.; Li, M.; Ross, M. B.; Yang, P., Cu-Ag Tandem Catalysts for High-Rate CO_2 Electrolysis toward Multicarbons. *Joule* **2020**, *4* (8), 1688–1699. DOI 10.1016/j.joule.2020.07.009.

Derrick, J. S.; Loipersberger, M.; Chatterjee, R.; Iovan, D. A.; Smith, P. T.; Chakarawet, K.; Yano, J.; Long, J. R.; Head-Gordon, M.; Chang, C. J., Metal–Ligand Cooperativity via Exchange Coupling Promotes Iron- Catalyzed Electrochemical CO_2 Reduction at Low Overpotentials. *J. Am. Chem. Soc.* **2020**, *142* (48), 20489–20501. DOI 10.1021/jacs.0c10664.

Desnoyer, A. N.; Nicolay, A.; Rios, P.; Ziegler, M. S.; Tilley, T. D., Bimetallics in a Nutshell: Complexes Supported by Chelating Naphthyridine-Based Ligands. *Acc. Chem. Res.* **2020**, *53* (9), 1944–1956. DOI 10.1021/acs.accounts.0c00382.

Kim, D.; Yu, S.; Zheng, F.; Roh, I.; Li, Y.; Louisia, S.; Qi, Z.; Somorjai, G. A.; Frei, H.; Wang, L.-W.; Yang, P., Selective CO_2 Electrocatalysis at the Pseudocapacitive Nanoparticle/Ordered-Ligand Interlayer. *Nat. Energy* **2020**, *5* (12), 1032–1042. DOI 10.1038/s41560-020-00730-4.

Koshy, D. M.; Johnson, G. R.; Bustillo, K. C.; Bell, A. T., Scanning Nanobeam Diffraction and Energy Dispersive Spectroscopy Characterization of Characterization of a Model Mn-Promoted Co/Al2O3 Nanosphere Catalyst for Fischer–Tropsch Synthesis. *ACS Catal.* **2020**, *10*, 12071–12079. DOI 10.1021/acscatal.0c02546.

Nicolay, A.; Ziegler M. S.; Rochlitz, L.; Tilley, T. D., Low-Valent Iron and Cobalt Complexes Supported by a Rigid Xanthene-Based Disilylamido Ligand. *Polyhedron* **2020**, *180*, 114420. DOI 10.1016/j.poly.2020.114420.

Qi, L; Zhang, Y.; Conrad, M. A.; Russell, C. K.; Miller, J: Bell, A. T., Ethanol Conversion to Butadiene over Isolated Zinc and Yttrium Sites Grafted onto Dealuminated Beta Zeolite. *J. Am. Chem. Soc.* **2020** *142*, 14674–14687. DOI 10.1021/jacs.0c06906.

Qi, Z.; Chen, L.; Zhang, S.; Su, J.; Somorjai, G. A., A Mini Review of Cobalt-Based Nanocatalyst in Fischer-Tropsch Synthesis. *Appl. Catal. A-Gen.* **2020**, *602*, 117701. DOI 10.1016/j.apcata.2020.117701.

Qiu, Y.; Hartwig, J. F., Mechanism of Ni-Catalyzed Oxidations of Unactivated $C(sp^3)$–H Bonds. *J. Am. Chem. Soc.* **2020**, *142* (45), 19239–19248. DOI 10.1021/jacs.0c09157.

Xi, Y.; Su, B.; Qi, X.; Pedram, S.; Liu, P.; Hartwig, J. F., Application of Trimethylgermanyl-Substituted Bisphosphine Ligands with Enhanced Dispersion Interactions to Copper-Catalyzed Hydroboration of Disubstituted Alkenes. *J. Am. Chem. Soc.* **2020**, *142*, 18213–18222. DOI 10.1021/jacs.0c08746.

Morimoto, M.; Bierschenk, S. M., Xia, K. T.; Bergman, R. G.; Raymond, K. N.; Toste, F. D. Advances in Supramolecular Host-Mediated Reactivity *Nat. Catal.* **2020**, *3*, 969-984. DOI 10.1038/s41929-020-00528-3.

Zee, D. Z.; Nippe, M.; King, A. E.; Chang, C. J.; Long, J. R., Tuning Second Coordination Sphere Interactions in Polypyridyl–Iron Complexes to Achieve Selective Electrocatalytic Reduction of Carbon Dioxide to Carbon Monoxide. *Inorg. Chem.* **2020**, *59* (7), 5206–5217. DOI 10.1021/acs.inorgchem.0c00455.

Zhang, B.; Chen, C.; Chuang, W.; Chen, S.; Yang, P. Size Transformation of $Au_{22}(SG)_{18}$ Nanocluster and its Surface Sensitive Dynamics, *J. Am. Chem. Soc.* **2020**, *142*, 11514–11520. DOI: 10.1021/jacs.0c03919.

2021

Amtawong, J.; Skjelstad, B. B.; Handford, R. C.; Suslick, B. A.; Balcells, D.; Tilley, T. D., C–H Activation by $RuCo_3O_4$ Oxo Cubanes: Effects of Oxyl Radical Character and Metal–Metal Cooperativity. *J. Am. Chem. Soc.* **2021**, *143* (31), 12108–12119. DOI 10.1021/jacs.1c04069.

Chen, C.; Li, Y.; Yang, P., Address the "Alkalinity Problem" in CO_2 Electrolysis with Catalyst Design and Translation. *Joule* **2021**, *5* (4), 737–742. DOI 10.1016/j.joule.2021.02.008.

Chen, L.; Malollari, K. G.; Uliana, A.; Sanchez, D.; Messersmith, P. B.; Hartwig, J. F., Selective, Catalytic Oxidations of C-H Bonds in Polyethylenes Produce Functional Materials with Enhanced Adhesion. *Chem.* **2021**, *7* (1), 137–145. DOI 10.1016/j.chempr.2020.11.020.

Chen, L.; Qi, Z.; Peng, X.; Chen, J.-L.; Pao, C.-W.; Zhang, X.; Dun, C.; Young, M.; Prendergast, D.; Urban, J. J.; Guo, J.; Somorjai, G. A.; Su, J., Insights into the Mechanism of Methanol Steam Reforming Tandem Reaction over CeO_2 Supported Single-Site Catalysts. *J. Am. Chem. Soc.* **2021**, *143* (31), 12074–12081. DOI 10.1021/jacs.1c03895.

Chen, S.; Li, M.; Yu, S.; Louisia, S.; Chuang, W.; Gao, M.; Chen, C.; Jin, J.; Salmeron, M. B.; Yang, P., Ligand Removal of Au25 Nanoclusters by Thermal and Electrochemical Treatments for Selective CO_2 Electroreduction to CO. *J. Chem. Phys.* **2021**, *155* (5), 051101. DOI 10.1063/5.0059363.

Dery, S.; Mehlman, H.; Hale, L.; Carmiel-Kostan, M.; Yemini, R.; Ben-Tzvi, T.; Noked, M.; Toste, F. D.; Gross, E., Site-Independent Hydrogenation Reactions on Oxide-Supported Au Nanoparticles Facilitated by Intraparticle Hydrogen Atom Diffusion. *ACS Catal.* **2021**, *11* (15), 9875–9884. DOI 10.1021/acscatal.1c01987.

Desnoyer, A. N.; Nicolay, A.; Ziegler, M. S.; Lakshmi, K. V.; Cundari, T. R.; Tilley, T. D., A Dicopper Nitrenoid by Oxidation of a CuICuI Core: Synthesis, Electronic Structure, and Reactivity. *J. Am. Chem. Soc.* **2021**, *143* (18), 7135–7143. DOI 10.1021/jacs.1c02235.

Dombrowski, J. P.; Ziegler, M. S.; Phadke, N.; Mansoor, E.; Levine, D. S.; Head-Gordon, M.; Bell, A. T.; Tilley, T. D., Siloxyaluminate and Siloxygallate Complexes as Models for Framework and Partially-Hydrolyzed Framework Sites in Zeolites and Zeotypes. *Chem. Eur. J.* **2021**, *27* (1), 307–315. DOI 10.1002/chem.202002926.

Fuentes, M. A.; Gava, R.; Saper, N. I.; Romero, E.; Caballero, A.; Hartwig, J. F.; Pérez, P. J., Copper-Catalyzed Dehydrogenative Amidation of Light Alkanes. *Angew. Chem. Int. Ed.* **2021**, *60* (34), 18467–18471. DOI 10.1002/anie.202104737.

Ji, P.; Park, J.; Gu, Y.; Clark, D. S.; Hartwig, J. F., Abiotic Reduction of Ketones with Silanes Catalysed by Carbonic Anhydrase Through an Enzymatic Zinc Hydride. *Nat. Chem.* **2021**, *13* (4), 312–318. DOI 10.1038/s41557-020-00633-7.

Li, M.; Zhang, B.; Cheng, T.; Yu, S.; Louisia, S.; Chen, C.; Chen, S.; Cestellos-Blanco, S.; Goddard, W. A.; Yang, P., Sulfur-Doped Graphene Anchoring of Ultrafine Au25 Nanoclusters for Electrocatalysis. *Nano Res.* **2021**. DOI 10.1007/s12274-021-3561-2.

Liu, G.; Lee, M.; Kwon, S.; Zeng, G.; Eichhorn, J.; Buckley, A. K.; Toste, F. D.; Goddard, W. A.; Toma, F. M., CO_2 Reduction on Pure Cu Produces only H_2 after Subsurface O is Depleted: Theory and Experiment. *Proc. Natl. Acad. Sci. U.S.A.* **2021**, *118* (23), e2012649118. DOI 10.1073/pnas.2012649118.

Nicolay, A.; Héron, J.; Shin, C.; Kuramarohit, S.; Ziegler, M. S.; Balcells, D.; Tilley, T. D., Unsymmetrical Naphthyridine-Based Dicopper(I) Complexes: Synthesis, Stability, and Carbon–Hydrogen Bond Activations. *Organometallics* **2021**, *40* (12), 1866–1873. DOI 10.1021/acs.organomet.1c00188.

Nozik, D.; Tinga, F. M. P.; Bell, A. T., Propane Dehydrogenation and Cracking over Zn/H-MFI Prepared by Solid-State Ion Exchange of ZnCl. *ACS Catal.* **2021**, *11*, 23, 14489–14506. DOI 1021/acscatal.1c03641.

Phadke, N. M.; Mansoor, E.; Head-Gordon, M.; Bell, A. T., Mechanism and Kinetics of Light Alkane Dehydrogenation and Cracking over Isolated Ga Species in Ga/H-MFI. *ACS Catal.* **2021**, 11, 2062–2075. DOI 10.1021/acscatal.0c04906.

Qi, L; Babucci, M.; Zhang, Y.; Lund, A.; Liu, L.; Li, J.; Chen, Y.; Hoffman, A. S.; Bare, S. R.; Han, Y.; Gates, B. C.; Bell, A. T., Propane Dehydrogenation Catalyzed by Isolated Pt Atoms in ≡SiOZn−OH Nests in Dealuminated Zeolite Beta. *J. Am. Chem. Soc.* **2021** *143*, 21364–21378. DOI 10.1021/jacs.1c10261.

Qi, Z.; Chen, L.; Zhang, S.; Su, J.; Somorjai, G. A., Mechanism of Methanol Decomposition over Single-Site Pt1/CeO_2 Catalyst: A DRIFTS Study. *J. Am. Chem. Soc.* **2021**, *143* (1), 60–64. DOI 10.1021/jacs.0c10728.

Salmeron, M.; Eren, B., High-Pressure Scanning Tunneling Spectroscopy. *Chem. Rev.* **2021**, *121* (2), 962–1006. DOI 10.1021/acs.chemrev.0c00429.

Smith, P. T.; Benke, B. P.; An, L.; Kim, Y.; Kim, K.; Chang, C., A Supramolecular Porous Organic Cage Platform Promotes Electrochemical Hydrogen Evolution from Water Catalyzed by Cobalt Porphyrins. *ChemElectroChem* **2021**, *8* (9), 1653–1657. DOI 10.1002/celc.202100331.

Suslick, B. A.; Tilley, T. D., Olefin Hydroarylation Catalyzed by a Single-Component Cobalt(-I) Complex. *Org. Lett.* **2021**, *23* (4), 1495–1499. DOI 10.1021/acs.orglett.1c00258.

Van der Mynsbrugge, J.; Bell, A. T., Challenges for the Theoretical Description of the Mechanism and Kinetics of Reactions Catalyzed by Zeolites. *J. Catal.* **2021**, *404*, 832–849. DOI 10.1016/j.jcat.2021.08.048.

Witzke, R. J.; Hait, D.; Head-Gordon, M.; Tilley, T. D., Two-Coordinate Iron(I) Complexes on the Edge of Stability: Influence of Dispersion and Steric Effects. *Organometallics* **2021**, *40* (11), 1758–1764. DOI 10.1021/acs.organomet.1c00218.

Wuttig, A.; Derrick, J. S.; Loipersberger, M.; Snider, A.; Head-Gordon, M.; Chang, C. J.; Toste, F. D., Controlled Single-Electron Transfer via Metal–Ligand Cooperativity Drives Divergent Nickel-Electrocatalyzed Radical Pathways. *J. Am. Chem. Soc.* **2021**, *143* (18), 6990–7001. DOI 10.1021/jacs.1c01487.

Yu, S.; Kim, D.; Qi, Z.; Louisia, S.; Li, Y.; Somorjai, G. A.; Yang, P., Nanoparticle Assembly Induced Ligand Interactions for Enhanced Electrocatalytic CO_2 Conversion. *J. Am. Chem. Soc.* **2021**, *143*, 19919–19927. DOI 10.1021/jacs.1c09777.

Zhang, Y.; Qi, L.; Lund, A.; Lu, P.; Bell, A. T., Mechanism and Kinetics of Acetone Conversion to Isobutene over Isolated Hf Sites Grafted to Silicalite-1 and SiO_2. *J. Am. Chem. Soc.* **2021**, *143* (22), 8352–8366. DOI 10.1021/jacs.1c01315.

Wuttig, A.; Toste, F. D. The Interface is a Tunable Dimension in Electricity-Driven Organic Synthesis. *Nat. Sci.* **2021**, e20210036. DOI 10.1001/ntls.20210036.

2022

Amtawong, J.; Nguyen, A.I.; Tilley, T. D., Mechanistic Aspects of Cobalt Oxo Cubane Clusters in Oxidation Chemistry. *J. Am. Chem. Soc.* **2022**, *144* (32), 1475–1492. DOI 10.1021/jacs.1c11445.

Bell, A. T., Insights into the Mechanism and Kinetics of Propene Oxidation and Ammoxidation over Bismuth Molybdate Catalysts Derived from Experiments and Theory. *J. Catal.* **2022**, *408*, 436–452. DOI 10.1016/j.jcat.2021.05.009.

Bierschenk, S. M.; Pan, J. Y.; Settineri, N. S.; Warzok, U.; Bergman, R. G.; Raymond, K. N.; Toste, F. D., Impact of Host Flexibility on Selectivity in a Supramolecular-Host-Catalyzed Enantioselective aza-Darzens Reacton. *J. Am. Chem. Soc.* **2022**, *144* (25), 11425–11433. DOI 10.1021/jacs.2c04182.

Chen, C., Yu, S., Yang, Y., Louisia, S., Roh, I., Jin, J., Chen, S., Chen, P.-C., Shan, Y.; Yang, P., Exploration of the Bio-Analogous Asymmetric C-C Coupling Mechanism in Tandem CO_2 Electroreduction. *Nature Catal.* **2022**, (5), 878–887. DOI 10.1038/s41929-022-00844-w.

Chen, L.; Hou, K.; Verma, P.; Qi, Z.; Zhang, S.; Liu, Y.; Guo, J.; Stavila, V.; Allendorf, M.; Zheng L.; Salmeron, M.; Prendergast, D.; Su, J.; Somorjai, G., Reversible Dehydrogenation and Rehydrogenation of Cyclohexane and Methyl-Cyclohexane by Single Site Platinum Catalyst. *Nat. Commun.* **2022**, 13, 1092. DOI 10.1038/s41467-022-28607-y.

Conk, R. J.; Hanna, S.; Shi, J. X.; Yang, J.; Ciccia, N. R.; Qi, L.; Bloomer, B. J.; Heuvel, S.; Wills, T.; Su, J.; Bell, A. T.; Hartwig, J. F., Catalytic Deconstruction of Waste Polyethylene with Ethylene to Form Propylene. *Science* **2022**, *377*, 1561–1566. DOI 10.1126/science.add1088.

De La Torre, P.; Derrick, J. S.; Snider, A.; Smith, P. T.; Loipersberger, M.; Head-Gordon, M.; Chang, C. J., Exchange Coupling Determines Metal-Dependent Efficiency for Iron- and Cobalt-Catalyzed Photochemical CO_2 Reduction. *ACS Catal.* **2022**, *12* (14), 8484–8493. DOI 10.1021/acscatal.2c02072.

Derrick, J. S.; Loipersberger, M.; Nistanaki, S. K.; Rothweiler, A. V.; Head-Gordon, M.; Nichols, E. M.; Chang, C. J., Templating Bicarbonate in the Second Coordination Sphere Enhances Electrochemical CO_2 Reduction Catalyzed by Iron Porphyrins. *J. Am. Chem. Soc.* **2022**, *144* (26), 11656–11663. DOI 10.1021/jacs.2c02972.

Hanna, S.; Bloomer, B.; Ciccia, N. R.; Butcher, T. W.; Conk, R. J.; Hartwig, J. F., Contra-Thermodynamic Olefin Isomerization by Chain-Walking Hydroboration and Dehydroboration. *Org. Lett.* **2022**, *24* (4), 1005–1010. DOI 10.1021/acs.orglett.1c03124.

Kynman, A. E.; Elghanayan, L. K.; Desnoyer, A. N.; Yang, Y.; Sévery, L.; Di Giuseppe, A.; Tilley, T. D.; Maron, L.; Arnold, P.L., Controlled Monodefluorination and Alkylation of C(sp^3)–F Bonds by Lanthanide Photocatalysts: Importance of Metal–Ligand Cooperativity. *Chem. Sci.* **2022**, *13*, 14090–14100. DOI 10.1039/D2SC04192H.

Loipersberger, M.; Derrick, J. S.; Chang, C. J.; Head-Gordon, M., Deciphering Distinct Overpotential-Dependent Pathways for Electrochemical CO_2 Reduction Catalyzed by an Iron–Terpyridine Complex. *Inorg. Chem.* **2022**, *61* (18), 6919–6933. DOI 10.1021/acs.inorgchem.2c00279.

Louisia, S.; Kim, D.; Li, Y.; Gao, M.; Yu, S.; Roh, I.; Yang, P., The Presence and Role of the Intermediary CO Reservoir in Heterogeneous Electroreduction of CO_2. *Proc. Natl. Acad. Sci. U.S.A.* **2022**, *119* (18), e2201922119. DOI 10.1073/pnas.2201922119.

Ma, S.; Xi, Y.; Fan, H.; Roediger, S.; Hartwig, J. F., Enantioselective Hydroamination of Unactivated Terminal Alkenes. *Chem* **2022**, *8* (2), 532–542. DOI 10.1016/j.chempr.2021.12.005.

Narouz, M. R.; De La Torre, P.; An, L.; Chang, C. J., Multifunctional Charge and Hydrogen-Bond Effects of Second-Sphere Imidazolium Pendants Promote Capture and Electrochemical

Reduction of CO_2 in Water Catalyzed by Iron Porphyrins. *Angew. Chem. Int. Ed.* **2022**, *61* (37), e202207666. DOI 10.1002/anie.202207666.

Neugebauer, M.E.; Kissman, E.N.; Marchand, J.A.; Pelton, J.G.; Sambold, N.A.; Millar, D.C.; Chang, M.C.Y., Conversion of a Radical Hydroxylase Into a Halogenase Through Reaction Pathway Engineering. *Nat. Chem. Biol.* **2022**, *18* (2), 1171–179. DOI 10.1038/s41589-021-00944-x.

Nguyen, Q. N. N.; Xia, K. T.; Zhang, Y.; Chen, N.; Morimoto, M.; Pei, X.; Ha, Y.; Guo, J.; Yang, W.; Wang, L.-P.; Bergman, R. G.; Raymond, K. N.; Toste, F. D.; Tantillo, D. J., The Source of Rate Acceleration for Carbocation Cyclization in Biomimetic Supramolecular Cages. *J. Am. Chem. Soc.* **2022**, *144* (25), 11413–11424. DOI 10.1021/jacs.2c04179.

Nozik, D.; Bell, A. T., Role of Ga^{3+} Sites in Ethene Oligomerization over Ga/H-MFI. *ACS Catal.* **2022**, 12, 14173–14184. DOI 10.1021/acscatal.2c03357.

Piesch, M.; Nicolay, A.; Haimerl, M.; Seidl, M.; Balázs, G.; Tilley, T. D.; Scheer, M., Binding, Release and Functionalization of Intact Pnictogen Tetrahedra Coordinated to Dicopper Complexes. *Chem. Eur. J.* **2022**, *28* (45), e202201144. DOI 10.1002/chem.20220114.

Qi, L; Zhang, Y.; Babucci, M.; Chen, C.; Lu, P.; Li, J.; Dun, C.; Hoffman, A. S.; Urban, J. J.; Tsapatsis, M.; Bare, S. R.; Han, Y.; Gates, B. C.; Bell, A. T., Dehydrogenation of Propane and n-Butane Catalyzed by Isolated $PtZn_4$ Sites Supported on Self-Pillared Zeolite Pentasil Nanosheets. *ACS Catal.* **2022**, *12*, 11177–11189. DOI 10.1021/acscatal.2c01631.

Ríos, P.; See, M. S.; Handford, R. C.; Teat, S. J.; Tilley, T. D., Robust dicopper(I) μ-boryl Complexes Supported by a Dinucleating Naphthyridine-Based Ligand. *Chem. Sci.* **2022**, *13* (22), 6619–6625. DOI 10.1039/D2SC00848C.

Yang, S.; Zhao, X.; Lu, Y.-H.; Barnard, E.; Yang, P.; Baskin, A.; Lawson, J. W.; Prendergast, D.; Salmeron, M., The Nature of the Electrical Double Layer on Suspended Graphene Electrodes. *J. Am. Chem. Soc.* **2022**, *144* (29), 13327–13333. DOI 10.1021/jacs.2c03344.

Yang, Y.; Roh, I.; Louisia, S.; Chen, C.; Jin, J.; Yu, S.; Salmeron, M.; Wang, C.; Yang, P., *Operando* Resonant Soft X-ray Scattering Studies of Chemical Environment and Interparticle Dynamics of Cu Nanocatalysts for CO_2 Electroreduction. *J. Am. Chem. Soc.* **2022**, *144* (20), 8927–8931. DOI 10.1021/jacs.2c03662.

Yu, S.; Louisia, S.; Yang, P., The Interactive Dynamics of Nanocatalyst Structure and Microenvironment during Electrochemical CO_2 Conversion. *J. Am. Chem. Soc. Au* **2022**, *2* (3), 562–572. DOI 10.1021/jacsau.1c00562.

Zhang, Y.; Qi, L.; Leonhardt, B.; Bell, A. T., Mechanism and Kinetics of n-Butane Dehydrogenation to 1,3-Butadiene Catalyzed by Isolated Pt Sites Grafted into SiOZn-OH Nests in Dealuminated Zeolite Beta. *ACS Catal.* **2022**, 12, 3333–3345. DOI 10.1021/acscatal.2c00059.

2023

An, L.; De La Torre, P.; Smith, P. T.; Narouz, M. R.; Chang, C. J., Synergistic Porosity and Charge Effects in a Supramolecular Porphyrin Cage Promote Efficient Photocatalytic CO_2 Reduction. *Angew. Chem. Int. Ed.* **2023**, *62* (5), e202209396. DOI 10.1002/anie.202209396.

Bloomer, B.J.; Natoli, S.N.; Garcia-Borràs, M.; Pereira, J.H.; Hu, D.B.; Adams, P.D.; Houk, K.N.; Clark, D.S.; Hartwig, J.F., Mechanistic and Structural Characterization of an Iridium-Containing Cytochrome Reveals Kinetically Relevant Cofactor Dynamics. *Nat. Cat.* **2023**, *6*, 39–51. DOI 10.1038/s41929-022-00899-9.

Chen, L.; Song, Z.; Zhang, S.; Chang, C.-K.; Chuang, Y.-C.; Peng, X.; Dun, C.; Urban, J.J.; Guo, J.; Chen, J.-L.; Prendergast, D.; Salmeron, M.; Somorjai, G.A.; Su, J., Ternary NiMo-Bi Liquid Alloy Catalyst for Efficient Hydrogen Production from Methane Pyrolysis, *Science*, **2023**, 381 6660 867-861, DOI 10.1126/science.adh8872.

Chen, P.; Chen, C.; Yang, Y.; Maulana, A. L.; Jin,J.; Feijóo, J.; Yang, P., The Chemical and Structural Evolution of AgCu Catalysts in Electrochemical CO_2 Reduction. *J. Am. Chem. Soc.* **2023,** 145, 10116–10125. DOI 10.1021/jacs.3c00467

Kynman, A. E.; Christodoulou, S.; Ouellette, E. T.; Peterson, A.; Kelly, S.; Maron, L.; Arnold, P. L. Photocatalytic Dechlorination of Unactivated Chlorocarbons Including PVC Using Organolanthanide Complexes. *Chem. Commun.* **2023**, Advance Article, DOI 10.1039/D3CC02906A

Ma, S.; Fan, H.; Day, C.S.; Xi, Y.; Hartwig, J.H., Remote Hydroamination of Disubstituted Alkenes by a Combination of Isomerization and Regioselective N–H Addition. *J. Am. Chem. Soc.* **2023**, *145* (7), 3875–3881. DOI 10.1021/jacs.2c13054.

Qi, L.; Das, S.; Zhang, Y.; Nozik, D.; Gates, B. C.; Bell, A. T., Ethene Hydroformylation Catalyzed by Rhodium Dispersed with Zinc or Cobalt in Silanol Nests of Dealuminated Zeolite Beta. *J. Am. Chem. Soc.* **2023**, 145, 2911–2929. DOI 10.1021/jacs.2c11075.

Xu, L.; Lechner, B.A.J.; Je, L.; Somorjai, G.A.; Salmeron, M.; Mavrikakis, M., Formation of Active Sites on Transition-Metal Surfaces under Catalytic Reactive Conditions. *Science* **2023,** 380, 70–76. DOI 10.1126/science.add0089.

Yang, Y.; Louisia, S.; Yu, S.; Jin, J.; Roh, I.; Chen, C.; Guzman, M. V. F.; Feijoo, J.; Chen, P.; Pollock, C. J.; Huang, X.; Wang, H.; Shao, Y.; Wang, C.; Muller, D. A.; Abruña, H. D.; Yang, P., *Operando* Studies Reveal Active Cu Nanograins for CO_2 Electroreduction. *Nature* **2023,** 614, 262. DOI 10.1038/s41586-022-05540-0.

Yang, Y.; Tsun, J.; Jin, J.; Feijóo, J.; Roh, I.; Louisia, S.; Yu, S.; Guzman, M.F.; Chen, C.; Muller, D.; Abruña, H.; Yang, P., *Operando* Electrochemical Liquid-Cell STEM (EC-STEM) Studies of Evolving Cu Nanocatalysts for CO_2 Electroreduction. *ACS Sustain. Chem. Eng.* **2023** 11, 4119–4124. DOI 10.1021/acssuschemeng.2c06542.

B. Other publications reporting research receiving support from this FWP.

2020

Cowie, B. E.; Douair, I.; Maron, L.; Love, J. B.; Arnold, P. L., Selective oxo Ligand Functionalisation and Substitution Reactivity in an oxo/Catecholate-Bridged U^{IV}/U^{IV} Pacman Complex. *Chem. Sci.* **2020**, *11* (27), 7144–7157. DOI 10.1039/d0sc02297g. *Additional discussion, analysis, and writing of this manuscript (P.L.A.) was supported by the U.S. Department of Energy (DOE).*

Dovera, C. M.; Grintera, D. C., Yima, C. M.; Muryn, C. A.; Bluhm, H.; Salmeron, M.; Thornton, G. Orientation of Acetic Acid Hydrogen Bonded to TiO_2(110). *Surface Sci.* **2020,** 699, 121628. DOI 10.1016/j.susc.2020.121628. *FWP supported Salmeron's contributions.*

Janvelyan, N; van Spronsen, M.A.; Wu, C.H.; Qi, Z.; Montemore, M. N.; Shan, J.; Zakharov, D.N.; Xu, F.; Boscoboinik, A.; Salmeron, M.B.; Stach, E.; Flyztani-Stephanopoulos, M.; Biener, J.; Friend, C. M., Stabilization of a Nanoporous NiCu Catalyst for Non-oxidative Ethanol Dehydrogenation. *Cat. Sci. & Tech*. **2020**. *Materials characterization and catalysis experiments.*

O'Connor, R.; van Spronsen, M.A.; Egle, T.; Xu, F.; Kersell, H. R.; Oliver-Meseguer, J.; Karatok, M.; Salmeron, M.; Madix, R. J.; Friend, C.M., Hydrogen Migration at Restructuring Palladium–Silver Oxide Boundaries Dramatically Enhances Reduction Rate of Silver Oxide. *Nat. Commun*. **2020**, 11, 1844. DOI 10.1038/s41467-020-15536-x. *Acknowledges DOE -BES Award No. DE-SC0012573, and ALS facilities.*

Xi, Y.; Ma, S.; Hartwig, J. F., Catalytic Asymmetric Addition of an Amine N-H bond Across Internal Alkenes. *Nature* **2020**, *588* (7837), 254–260. DOI 10.1038/s41586-020-2919-z. *The*

development of the catalytic system and reagent and the mechanistic studies were supported by DOE. The application to asymmetric hydroamination was supported by NIH.

Zhang, S.; Chen, L.; Qi, Z.; Zhuo, L.; Chen, J.-L.; Pao, C.-W.; Su, J.; Somorjai, G. A., Insights into the Mechanism of n-Hexane Reforming over a Single-Site Platinum Catalyst. *J. Am. Chem. Soc.* **2020**, *142* (39), 16533–16537. DOI 10.1021/jacs.0c07911. *Catalysis synthesis and characterization was fund in part by DOE (Bell).*

2021

Arnold, P. L.; Halliday, C. J. V.; Puig-Urrea, L.; Nichol, G. S., Instantaneous and Phosphine-Catalyzed Arene Binding and Reduction by U(III) Complexes. *Inorg. Chem.* **2021**, *60* (6), 4162–4170. DOI 10.1021/acs.inorgchem.1c00327. *Additional discussion, analysis, and writing of this manuscript (P.L.A.) was supported by the U.S. Department of Energy (DOE).*

Day, C. S.; Fawcett, A.; Chatterjee, R.; Hartwig, J. F., Mechanistic Investigation of the Iron-Catalyzed Azidation of Alkyl C(sp^3)−H Bonds with Zhdankin's λ^3 Azidoiodane. *J. Am. Chem. Soc.* **2021**, *143* (39), 16184–16196. DOI 10.1021/jacs.1c07330. *The Catalysis program supported the EPR work.*

Dejesus, J. F.; Kerr, R. W. F.; Penchoff, D. A.; Carroll, X. B.; Peterson, C. C.; Arnold, P. L.; Jenkins, D. M., Actinide Tetra-n-Heterocyclic Carbene 'Sandwiches'. *Chem. Sci.* **2021**, *12* (22), 7882–7887. DOI 10.1039/D1SC01007G. *Additional discussion, analysis, and writing of this manuscript (P.L.A.) was supported by the U.S. Department of Energy (DOE).*

Gray, S. J.; Brown, K.; Francis, L. Y. T.; Garden, J. A.; Arnold, P. L., Dinuclear Ce(IV) Aryloxides: Highly Active Catalysts for Anhydride/Epoxide Ring-Opening Copolymerization. *Organometallics* **2021**, *40* (7), 948–958. DOI 10.1021/acs.organomet.1c00055. *Additional discussion, analysis, and writing of this manuscript (P.L.A.) was supported by the U.S. Department of Energy (DOE).*

Kerr, R. W. F.; Ewing, P. M. D. A.; Raman, S. K.; Smith, A. D.; Williams, C.K.; Arnold, P. L., Ultrarapid Cerium(III)–NHC Catalysts for High Molar Mass Cyclic Polylactide. *ACS Catal.* **2021**, *11* (3), 1563–1569. DOI 10.1021/acscatal.0c04858. *Additional discussion, analysis, and writing of this manuscript (P.L.A.) was supported by the U.S. Department of Energy (DOE).*

Lu, P.; Ghosh, S.; Dorneles De Mello, M.; Kamaluddin, H. S.; Li, X.; Kumar, G.; Duan, X.; Abeykoon, M.; Boscoboinik, J. A.; Qi, L.; Dai, H.; Luo, T.; Al-Thabaiti, S.; Narasimharao, K.; Khan, Z.; Rimer, J. D.; Bell, A. T.; Dauenhauer, P.; Mkhoyan, K. A.; Tsapatsis, M., Few-Unit-Cell MFI Zeolite Synthesized Using a Simple Di-Quaternary Ammonium Structure-Directing Agent. *Angew. Chem. Int. Ed.* **2021**, *60* (35), 19214–19221. DOI 10.1002/anie.202104574. *The Catalysis program supported Q.L.'s efforts in conducting reactions using the materials synthesized at Johns Hopkins University and A.T.B.'s effort on supervising this phase of the research and editing the paper.*

Mao, Y.; Loipersberger, M.; Kron, K. J.; Derrick, J. S.; Chang, C. J.; Sharada, S. M.; Head-Gordon, M., Consistent Inclusion of Continuum Solvation in Energy Decomposition Analysis: Theory and Application to Molecular CO_2 Reduction Catalysts. *Chem. Sci.* **2021**, *12* (4), 1398–1414. DOI 10.1039/d0sc05327a. *Synthetic compounds were provided to the collaboration with support from the DOE.*

Sakamoto, S.; Butcher, T. W.; Yang, J. L.; Hartwig, J. F., gem-Difluoroallylation of Aryl Halides and Pseudo Halides with Difluoroallylboron Reagents in High Regioselectivity. *Angew. Chem. Int. Ed.* **2021**, *60* (49), 25746–25752. DOI 10.1002/anie.202111476. *The FWP supported the work performed in the Program's Catalysis Facility.*

Zhao, J.; Ji, S.; Guo, C.; Li, H.; Dong, J.; Dong, J.; Guo, P.; Wang, D.; Li, Y.; Toste, F. D., A Heterogeneous Iridium Single-Atom-Site Catalyst for Highly Regioselective Carbenoid O-H Bond Insertion. *Nat. Catal.* **2021**, *4* (6), 523–531. DOI 10.1038/s41929-021-00637-7.

Additional discussion, analysis, and writing of this manuscript (F.D.T.) was supported by the U.S. Department of Energy (DOE).

2022

Aljama, H.; Head-Gordon, M.; Bell, A., Assessing the Stability of Pd-Exchanged Sites in Zeolites with the Aid of a High Throughput Quantum Chemistry Workflow. *Nat. Commun.* **2022**, *13* (1), 2910. DOI 10.1038/s41467-022-29505-z. *The Catalysis program supported A.T.B.'s efforts in conceptualizing the project, developing the methodology, data analysis, supervising the research and editing the paper.*

Berg, I.; Einav, A.; Hale, L.; Toste, F. D.; Gross, E., N-Heterocyclic Carbene Nanolayer for Copper Film Oxidation Mitigation. *Angew. Chem. Int. Ed.* **2022**, *61* (25), e202201093. DOI 10.1002/anie.202201093. *Synthesis of ligands (L.H.) and discussion, analysis, and writing of this manuscript (L.H. & F.D.T.) was supported by the U.S. Department of Energy (DOE).*

Cestellos-Blanco, S.; Louisia, S.; Ross, M. B.; Li, Y.; Soland, N. E.; Detomasi, T. C.; Spradlin, J. N. C.; Nomura, D. K.; Yang, P., Toward Abiotic Sugar Synthesis from CO_2 Electrolysis. *Joule* **2022**, *6* (10), 2304–2323. DOI 10.1016/j.joule.2022.08.007. *The Catalysis program contributed to experimental design, CO_2 reduction experiments and manuscript development.*

2023

Kurandina, D.; Huang, B.; Xu, W.; Hanikel, A. D.; Storoscio, G. D.; Wang, K.; Gagliardi, L.; Toste, F. D.; Yaghi, O. M., Porous Crystalline Nitrone-Linked Covalent Organic Framework. *Angew. Chem. Int. Ed.* **2023**, e202307674. DOI 10.1002/anie.202307674. *Synthesis of ligands (B.H.) and discussion, analysis, and writing of this manuscript (B.H. & F.D.T.) was supported by the U.S. Department of Energy.*

Zili Wu

FWP ERKCC96: Fundamentals of Catalysis and Chemical Transformations

PIs: Miaofang Chi, Sheng Dai, Stephan Irle, De-en Jiang (Vanderbilt University), Yuanyuan Li, Felipe Polo-Garzon, Zili Wu (lead PI), Zhenzhen Yang

Postdoc(s): Yang He, Ming Lei (Vanderbilt University), Meijia Li, Pilsun Yoo, Junyan Zhang

Student(s): Kevin Siniard (UTK), Haohong Song (Vanderbilt University)

Affiliation (s): Oak Ridge National Laboratory

RECENT PROGRESS

The overarching goal of this program is to understand how to control the catalytic activity, selectivity and stability in the activation and conversion of C-H and C=O bonds by tuning the local environment around the active sites on the surface and at the metal-oxide interface of complex oxides. We hypothesize that complex oxides including perovskites and high entropy oxides (HEOs), with their inherent large tuning space in cations, anions, chemical and electronic structures, can provide diverse local environments that can be harnessed to control and tune the catalytic activity, selectivity and stability for reactions involving C-H and C=O bonds. Specifically, we study two types of reactions to probe local environment effects: selective hydrogenation of unsaturated oxygenates, including CO_2; methane activation and dry reforming of methane (DRM). These reactions are chosen not only because of their sensitivity to local environment of catalysts, they are also relevant to the efficient use of the abundant CO_2 and shale gas as alternate carbon feedstocks, and to the decarbonization of fossil fuels and close the carbon cycle.

In the following, we summarize our past research accomplishments into two sections: **Part 1**. tuning local environment of catalytic sites to impact hydrogenation reactions, and **Part 2**. tuning local environment of catalytic sites to impact C-H and C=O bond activation and conversion.

Part 1. Tuning local environment of catalytic sites to impact hydrogenation reactions

A. H_2 activation and hydrogenation assisted with strong metanl-support interacatons (SMSIs)

A significant contribution of this program was on improving H_2 activation and conversion via novel approaches to construct SMSI in supported metal catalysts. The key innovation of our approaches lies in the much lower temperatures down to room temperature for SMSI layer formation, thus preventing sintering of metal nanoparticles that can occur during traditional SMSI formation conditions (H_2 treatment at >300 °C). The first example comes from the use of alcohol as a reducing agent of the oxide support to promote SMSI formation due to the fact that alcohols can reduce oxides easier than H_2. We showed, via IR spectroscopy of CO adsorption and electron energy loss spectroscopy (EELS), that during 2-propanol conversion over Pd/TiO_2, coverage of Pd sites occurs due to SMSI at low reaction temperatures, as low as ~190 °C (**Fig 1A**).[33] Such SMSI overlayers generated during reaction fully reverses upon exposure to O_2 at room temperature for ~15 h, which may have made its identification elusive up to now. Inspired by this discovery of SMSI at low temperature upon 2-propanol treatment, our team developed a strategy to promote SMSI under ambient conditions via a photochemistry-driven methodology (**Fig 1B**).[29] Encapsulation of Pd nanoparticles in Pd/TiO_2 with a TiO_x overlayer, the presence of Ti^{3+} species, and suppression of CO adsorption were achieved upon UV irradiation. The key lied in the generation of separated photoinduced reductive electrons (e^-) and oxidative holes (h^+), which subsequently triggered the formation of Ti^{3+} species/oxygen vacancies (O_v) and then interfacial $Pd–O_v–Ti^{3+}$ sites, affording SMSI in Pd/TiO_2. UV-induced SMSI promoted full hydrogenation of the alkyne group in phenyl-acetylene, whereas the base

Pd/TiO_2 led to semi and full hydrogenation. Such a photo-induced SMSI formation is found general to other supported metal systems such as Pd/ZnO and Pt/TiO_2.

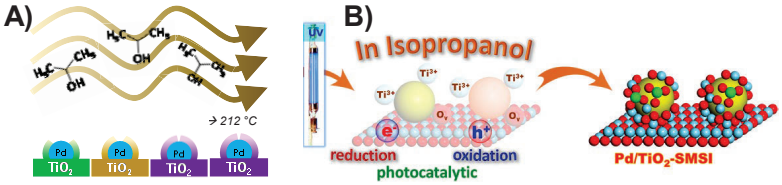

Fig 1. In situ blocking of Pd sites by TiOx SMSI layer during 2-propanol conversion at relative low temperatures over Pd/TiO_2. **B)** Photoinduced-SMSI on Pd/TiO_2 at ambient conditions in isopropanol.

Recently, we also devised several non-traditional approaches to synthesize artificial SMSI layers including mechanochemistry and ultrasonication routes with various supports such as boron nitride,[6] reducible oxides – TiO_2 and CeO_2.[57,63] A common theme in these studies is that with controlled SMSI encapsulation degree, metal catalysts (Pd, Pt etc.) showed much enhanced hydrogenation activity in alkyne and CO_2 conversion over the counterparts without SMSI layers. These research efforts provide insights into the role of encapsulation and suboxide defects on metal centers in H_2 activation and hydrogenation reactions.

B. H_2 activation and hydrogenation with heterogeneous Frustrated Lewis Pairs (FLPs)

Hydrogenation reactions promoted by earth-abundant non-metal catalysts under mild conditions is an attractive and challenging subject. In our recent work (Chen *et al.*),[43] sterically hindered Lewis acid ("B" center) and Lewis base ("N" center) sites were anchored within the rigid lattice of highly crystalline hexagonal boron nitride (h-BN) scaffolds to form the so-called FLPs (**Fig 2**). The active sites were created via precision defect regulation during the molten-salt-involved ($NaNH_2$ and $NaBH_4$) h-BN construction procedure. The as-afforded h-BN scaffolds achieved highly efficient H_2/D_2 activation and dissociation under ambient pressure via FLP-like behavior. Attractive catalytic efficiency in styrene hydrogenation reaction over the FLP BN catalyst far surpassed the current heterogeneous analogues such as bulk BN where little defects are present, underscoring the importance of precision regulation of the defect types in the h-BN skeleton. Extension of this concept was recently advanced by the construction of B- and N-enriched nanoporous π-conjugated networks (BN-NCNs) FLPs which also showed promising hydrogenation performances in both gas phase hydrogenation of acetylene and liquid phase styrene hydrogenation.[56] These results provide a promising approach to construct metal-free heterogeneous catalysts toward various hydrogenation reactions and potentially for the hydrogenation of CO_2.

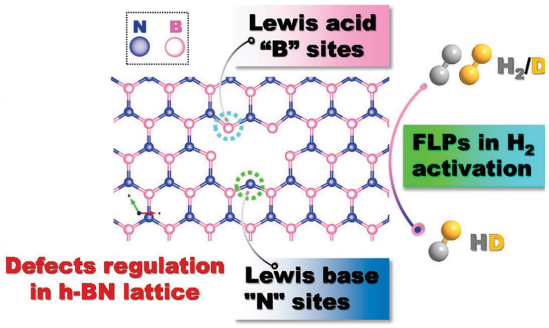

Fig 2. FLP sites created in BN with excellent capacity in activating H_2 and catalyzing hydrogenation reactions including CO_2.

C. Enhanced hydrogenation activity from anion sites tuning of perovskites

C1. acetylene semi-hydrogenation over $BaTiO_{2.5}H_{0.5}$ We used first-principles density functional theory (DFT), coupled with microkinetic modeling, to investigate acetylene semi-hydrogenation on a prototypical perovskite oxyhydride (POH), $BaTiO_{2.5}H_{0.5}$ (BTOH).[66] Two different mechanisms are examined on a representative surface of BTOH under the reaction conditions; although both are based on the Horiuti-Polanyi mechanism, the way that H_2 is activated is different. In mechanism a, a lattice hydride H atom and then a surface adsorbed H atom sequentially hydrogenate the adsorbed acetylene. In mechanism b, two lattice hydride H atoms from the BTOH sequentially hydrogenate the adsorbed acetylene. In both mechanisms, the H atoms are replenished from gas phase H_2 dissociation (**Fig 3**). A selectivity analysis for the temperature range of 373 – 673 K shows that the product observed is essentially only ethylene. This

work shows the potential of using lattice hydrides for selective hydrogenation, further demonstrated for CO_2 hydrogenation to methanol below.

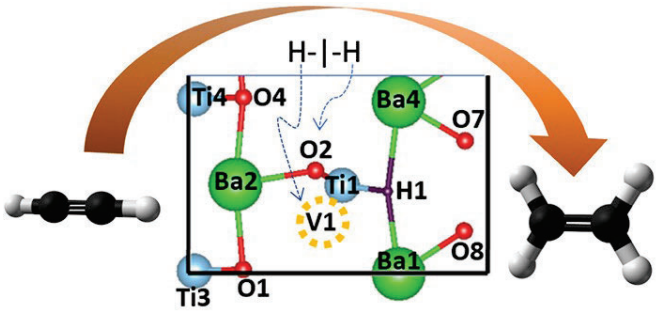

Fig 3. Mechanistic overview of acetylene hydrogenation over a BTOH surface.

C2. CO_2 hydrogenation to methanol promoted by lattice hydrides In an on-going work, we utilized POH as a support for Cu NPs in CO_2 hydrogenation. The yield to methanol on $Cu/BaTiO_{2.8}H_{0.2}$ is about 3 times over $Cu/BaTiO_3$ under the same reaction condition with similar selectivity to methanol. Combined state-of-the-art *operando* techniques were employed to confirm and understand the contribution of hydrides to the improved methanol production. Our study demonstrated that about half of the formate species bonded too strongly to the surface of $Cu/BaTiO_3$, which lowered the methanol formation rate. In comparison to $Cu/BaTiO_3$, the hydrides in the support could directly participate in the reaction, and the created surface vacancy sites were able to promote hydrogen dissociation (**Fig 4**). Furthermore, the hydrides in the oxyhydride support could reduce the surface reactivity of the Cu sites at the metal/support interface by transferring electrons to those Cu sites, which de-stabilizes the adsorbed formate intermediate and promotes methanol formation rate. The results from this work highlight a novel strategy in controlling the electronic metal – support interaction (EMSI) via anion site (hydride) tuning to enhance CO_2 hydrogenation to the desired alcohol product, which will be further explored for promoting CO_2 hydrogenation and C-C coupling reactions.

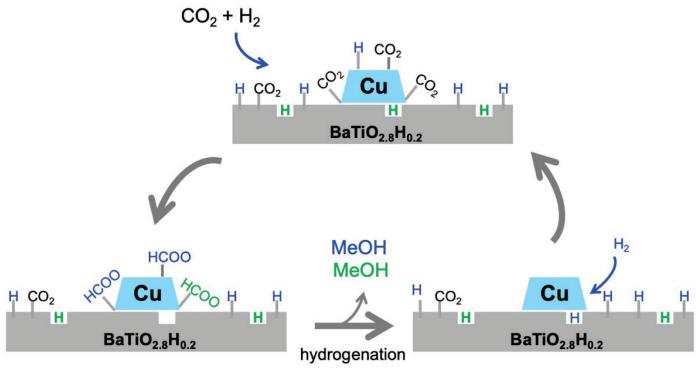

Fig 4. Proposed reaction mechanism of CO_2 hydrogenation to methanol over $Cu/BaTiO_{2.8}H_{0.2}$. (unpublished results)

D. Stable and selective CO_2 hydrogenation from cation sites tuning of high entropy oxides (HEOs)

configurational entropic (it refers to the number of ways that atoms or molecules pack together in the host matrix. More disorder of a system and higher randomness of a structure with a lower Gibbs free energy can contribute to the stability of host structure at high temperatures ($\Delta G = H - T\Delta S$)) stabilization effect in HEOs, we showed that exsoluted metal species (surface segregated out of the bulk of the HEO) are extremely stably under demanding hydrogenation conditions such as reverse water gas shift reaction (RWGS). Shown in **Fig 5**, CuFeCuNi alloy particles can be exsoluted from the HEO ($Zr_{0.5}(NiFeCuMnCo)_{0.5}O_x$) bulk structure upon 600°C H_2 treatment and dissolved back in the structure upon 550°C in air.[88] The entropic confinement effect from the HEO matrix endorses stable performance of the metal alloy for CO_2 hydrogenation selectively to CO at 400°C over 500hr, in sharp

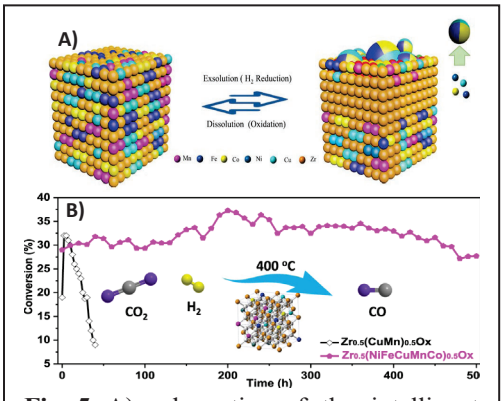

Fig 5 A) schematics of the intelligent behavior of HEOs; B) stable performance of HEO-derived catalyst in RWGS reaction.

contrast to the severe deactivation by the ternary doped $Zr_{0.5}(MnCu)_{0.5}O_x$ catalyst within 40hr. A similarly stabilization effect was also found in the RWGS reaction at 500°C over another HEO system ($Co_3MnNiCuZnOx$).[95] This unique entropic confinement effect will be capitalized to stabilize metal sites under harsh reaction conditions including C-C coupling reaction in CO_2 hydrogenation at elevated pressures, and in the high temperature DRM reaction.

E. Atomic level local geometric and electronic structures via advanced electron microscopy

A key enabling capability of this program is the ability to reveal the local geometric and electronic environment down to atomic scale by advanced electron microscopy and spectroscopy. On one hand, we develop and demonstrate an unsupervised machine learning method that allows us to reveal the presence and chemical information of the SMSI encapsulation layer that is otherwise hidden in STEM-EELS datasets.[26] This method not only provides a robust tool for the analysis of trace SMSI in catalysts, but is generally applicable to any materials and spectroscopy datasets of any material systems where revealing a trace signal is critical. On the other hand, we utilized four-dimensional scanning transmission electron microscopy (4D-STEM)-based differential phase contrast (DPC) imaging to directly probe the charge distribution at a metal – oxide support interface ($Au/SrTiO_3$) down to the atomic scale (**Fig 6**),[51] information that has previously been inaccessible by conventional microscopy and other experimental forms. By combining the experimental results with DFT calculations, the work reveals the atomic-scale mechanisms responsible for the highly active perimeter sites and demonstrates that the charge transfer behavior can be readily controlled using post-synthesis treatments. This work provides an effective method to elucidate the nature of EMSIs at the sub-nm scale, and presents new opportunities to better identify active sites and understand catalytic reaction mechanisms.

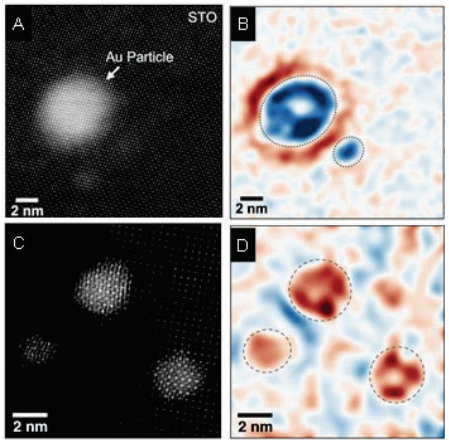

Fig 6. ADF-STEM (left) and corresponding charge density map (right) of Au nanoparticles on hydrogen treated $SrTO_3$ (STO, top row) and oxygen treated $SrTO_3$ (bottom row), respectively.

Part 2. Tuning local environment of catalytic sites to impact C-H and C=O activation

A. Boosting the C-H activation capability of single atoms by tailoring the local cooridnation environment

Although efforts have been made to improve the atomic efficiency of Pd-based catalysts in methane activation, there are intense and long-term debates on the active Pd species. The goal of this work is to reveal how the local electronic structure and atomic structure of Pd atoms can be tuned to enhance C-H bond activation and thus methane combustion. In a recent work,[68] we tuned the electronic structure of Pd single atoms by controlling the defects on the surface of ceria support and found that a simple thermal pretreatment to ceria prior to Pd deposition could create a unique anchoring site for Pd. According to XAS, XPS and IR results, the activated Pd single atom at this site had oxygen-deficient local structure and elongated interacting distance with ceria. These features facilitated the efficient conversion of methane compared to regular Pd SAs (**Fig. 7**). In addition to modifying the local electron density of Pd single atom sites, recently, we are

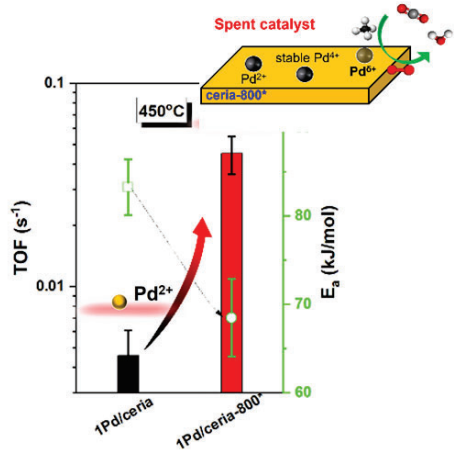

Fig 7. Comparison of TOF at 450 °C and activation energy (E_a) on 1Pd supported on two differently treated ceria.

tuning the Pd-Pd distances between single atom sites and find that paring Pd single atom sites and controlling their interatomic distances could help further improve the C-H bond activation capability. Currently, we are summarizing the results obtained from STEM, XAS, XPS, DRIFTS, and DFT calculations to reveal the reasons for the improved properties and associated working mechanisms. The concept of tuning metal size in the range of single atoms to clusters can be exploited in CO_2 hydrogenation to construct metal sites with different local environments to tune both activity and selectivity.

B. Controlling C-H bond activation via tuning the cation sites in complex oxides

Understanding how the change of cations in complex oxides impacts the ability in C-H bond activation can help to develop more efficient CH_4 conversion catalysts. However, the surface reconstruction of complex oxides made it complicated due to dynamic behavior in surface composition changes of the oxides under difference conditions. Our latest work[46] presents a detailed kinetic analysis of catalytic CH_4 combustion over a set of seven perovskites ($SrTiO_3$, $SrZrO_3$, $SrFeO_3$, $LaFeO_3$, $LaInO_3$, $LaCoO_3$, $LaMnO_3$) with various surface terminations (**Fig 8**). Steady-state isotopic transient kinetic analysis was employed to measure turnover frequency (TOF) and density of surface intermediates (*N*) under operando conditions. Top surface characterization elucidated performance-structure relationships between near-monolayer surface composition and intrinsic reactivity of the catalysts. In general, surface reconstruction is shown as a tool to tune TOF and *N* to improve reaction rates, a concept that could be utilized in our future studies of HEOs for DRM and CO_2 hydrogenation.

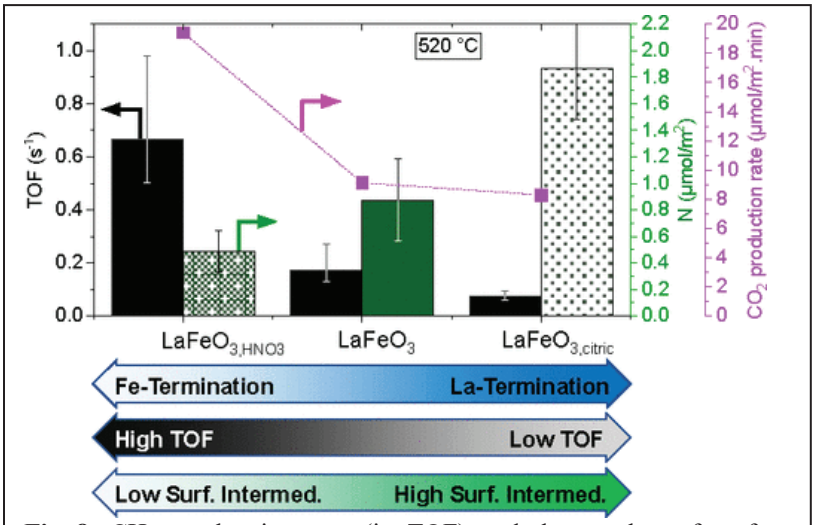

Fig 8. CH_4 combustion rate (in TOF) and the number of surface intermediates as well as CO_2 production rate vary several times over the same $LaFeO_3$ perovskite but with varying surface composition through different chemical treatments.

C. Achieving stable activity in dry reforming of methane (DRM) over high entropy oxides (HEOs)

Two major challenges in DRM are the coke formation and metal center sintering under harsh reach conditions. We postulate that both challenges can be addressed via the entropic factor offered by HOEs which can well stabilize single atoms or small clusters of active metal centers that are thermally stable and will not coke due to their isolated nature. To test the hypothesis, we studied DRM over an HEO catalyst ($NiMgCuCoZnO_x$) where 5 elements were included, including Ni and Mg (indispensable for DRM activity), along with Cu, Co, and Zn to provide structural stability due to similar atomic sizes. HEO synthesized using proper metal precursors exhibited superior stability during DRM at 650 °C. X-ray absorption spectroscopy (XAS) analysis of the spent samples showed mixed valence states of Ni species, indicating a high resistance to reduction of the Ni sites stabilized in HEO. This resistance could potentially decelerate the commonly observed sintering of Ni species during DRM. In addition, the HEO catalyst showed negligible carbon deposition, further contributing to the stable DRM performance. These observations support our above hypothesis.

To discern the role of each element in enabling the reaction mechanism for DRM, we synthesized 4-element oxide catalysts, where one metal from the HEO structure was removed at a time. As shown in **Fig 9**, When Ni or Mg was removed from the structure, the catalyst was inactive for DRM. When only Cu was removed

from the structure (NiMgCoZnOx), the catalyst exhibited superior reactivity in comparison to the HEO, even surpassing the widely-studied NiMgOx sample with higher Ni loading. Notably, when only Co is removed from the structure (NiMgCuZnOx), the catalyst exhibited enhanced stability. XAS was used to track the oxidation state change of Ni, the presumed active sites. Overall, the outstanding resistance to coke of HEO, and varying performance upon modification of the structure, evidences the promise of harnessing HEO surfaces for stable DRM, which will be further understood and exploited in our research.

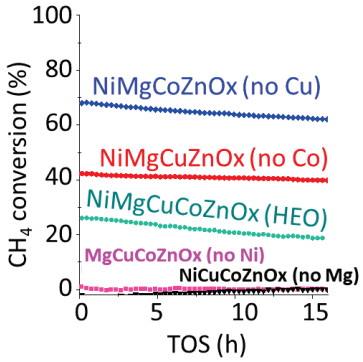

Fig 9. Promising stability of certain complex oxides and HEOs in DRM. (unpublished work).

D. Revealing surface composition/reconstruction of HEOs with advanced electron microscopy

It remains a challenge in understanding the surface composition and structure of HEOs. Taking advantage of the advanced STEM imaging and spectroscopy techniques in combination with DFT, we recently investigated the atomic-scale structural and chemical responses of a model HEO (CeYLaHfTiZrOx) to different high-temperature redox environments. The HEO particle bulk shows pseudorandom two-phase structure with a significant ability to accommodate oxygen vacancies, whereas the surface and subsurface layers exhibit dynamic elemental and structural reconstructions under different gas environments (shown in **Fig 10** as an example of the pristine HEO). The atomic arrangements and elemental distributions revealed in this study can serve as direct structural input for DFT calculations and guide the design of more efficient catalysts to take advantage of the dynamic surface structure of HEOs, which will be employed as a unique approach in our research in studying the structure of complex oxide-based catalysts.

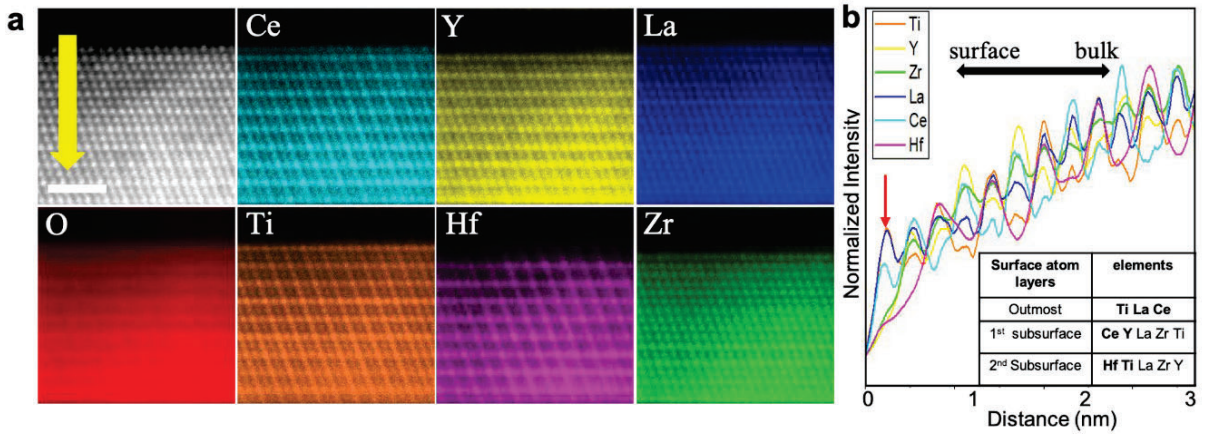

Fig 10. Atomic STEM analysis of the surface crystal structure and elemental distribution of a pristine HEO particle. a) HAADF-STEM analysis at the very edge of the particle in [110] zone axis and corresponding atomic STEM-EDX maps of Ce, Y, La, Hf, Ti and Zr. b) Line profiles of the EDX maps across the surface atom layers as indicated by the yellow arrow. Scale bar 2nm (unpublished work).

Publications Acknowledging this Grant (ERKCC96) in 2020 –2023 (total –110)

(I) Intellectually led by this grant (total – 69)

1. Bao, Z.; Fung, V.; Polo-Garzon, F.; Hood, Z. D.; Cao, S.; Chi, M.; Bai, L.; Jiang, D.-e.; Wu, Z., The interplay between surface facet and reconstruction on isopropanol conversion over SrTiO3 nanocrystals. *J. Catal.* **2020,** *384*, 49-60.
2. Chen, B.; Xiong, C.; Jiang, D.-e.; Savara, A., Ethanol Conversion over La0.7Sr0.3MnO3–x(100): Autocatalysis, Adjacent O-Vacancies, Disproportionation, and Dehydrogenation. *ACS Catal.* **2020,** *10* (21), 12920-12931.
3. Chen, H.; Jie, K.; Jafta, C. J.; Yang, Z.; Yao, S.; Liu, M.; Zhang, Z.; Liu, J.; Chi, M.; Fu, J.; Dai, S., An ultrastable heterostructured oxide catalyst based on high-entropy materials: A new strategy toward catalyst stabilization via synergistic interfacial interaction. *Appl. Catal. B: Environ.* **2020,** *276*, 119155.
4. Chen, H.; Lin, W.; Zhang, Z.; Yang, Z.; Jie, K.; Fu, J.; Yang, S.-z.; Dai, S., Facile benzene reduction promoted by a synergistically coupled Cu–Co–Ce ternary mixed oxide. *Chem. Sci.* **2020,** *11* (22), 5766-5771.
5. Chen, H.; Sun, Y.; Yang, S.; Wang, H.; Dmowski, W.; Egami, T.; Dai, S., Self-regenerative noble metal catalysts supported on high-entropy oxides. *Chem. Commun.* **2020,** *56* (95), 15056-15059.
6. Chen, H.; Yang, S.-Z.; Yang, Z.; Lin, W.; Xu, H.; Wan, Q.; Suo, X.; Wang, T.; Jiang, D.-e.; Fu, J.; Dai, S., Sinter-Resistant Nanoparticle Catalysts Achieved by 2D Boron Nitride-Based Strong Metal–Support Interactions: A New Twist on an Old Story. *ACS Cent. Sci.* **2020,** *6* (9), 1617-1627.
7. Dai, S., Across the Board: Sheng Dai on Catalyst Design by Entropic Factors. *ChemSusChem* **2020,** *13* (7), 1915-1917.
8. Doyle, P. J.; Savara, A.; Raiman, S. S., Extracting meaningful standard enthalpies and entropies of activation for surface reactions from kinetic rates. *React. Kinet. Mech. Catal.* **2020,** *129* (2), 551-581.
9. Fung, V.; Hu, G.; Wu, Z.; Jiang, D.-e., Descriptors for Hydrogen Evolution on Single Atom Catalysts in Nitrogen-Doped Graphene. *J. Phys. Chem. C* **2020,** *124* (36), 19571-19578.
10. Fung, V.; Hu, G.; Wu, Z.; Jiang, D.-e., Hydrogen in Nanocatalysis. *J. Phys. Chem. Lett.* **2020,** *11* (17), 7049-7057.
11. Huang, R.; Fung, V.; Wu, Z.; Jiang, D.-e., Understanding the conversion of ethanol to propene on In2O3 from first principles. *Catal. Today* **2020,** *350*, 19-24.
12. Kammert, J.; Moon, J.; Wu, Z., A review of the interactions between ceria and H₂ and the applications to selective hydrogenation of alkynes. *Chin. J. Catal.* **2020,** *41* (6), 901-914.
13. Liu, J.; Wang, L.; Okejiri, F.; Luo, J.; Zhao, J.; Zhang, P.; Liu, M.; Yang, S.; Zhang, Z.; Song, W.; Zhu, W.; Liu, J.; Zhao, Z.; Feng, G.; Xu, C.; Dai, S., Deep Understanding of Strong Metal Interface Confinement: A Journey of Pd/FeOx catalysts. *ACS Catal.* **2020,** *10*, 8950-8959.
14. Moon, J.; Cheng, Y.; Daemen, L. L.; Li, M.; Polo-Garzon, F.; Ramirez-Cuesta, A. J.; Wu, Z., Discriminating the Role of Surface Hydride and Hydroxyl for Acetylene Semi-Hydrogenation over Ceria Through in situ Neutron and Infrared Spectroscopy. *ACS Catal.* **2020,** *10* (9), 5278–5287.
15. Polo-Garzon, F.; Blum, T. F.; Fung, V.; Bao, Z.; Chen, H.; Huang, Z.; Mahurin, S. M.; Dai, S.; Chi, M.; Wu, Z., Alcohol-Induced Low-Temperature Blockage of Supported-Metal Catalysts for Enhanced Catalysis. *ACS Catal.* **2020,** *10*, 8515-8523.
16. Savara, A., Microkinetic simulation and fitting of the temperature programmed reaction of methanol on CeO2(111): H2 and H2O + V production. *React. Kinet. Mech. Catal.* **2020,** *129* (1), 181-203.
17. Savara, A.; Walker, E. A., CheKiPEUQ Intro 1: Bayesian Parameter Estimation Considering Uncertainty or Error from both Experiments and Theory. *ChemCatChem* **2020,** *12* (21), 5385-5400.
18. Tian, C.; Zhang, H.; Zhu, X.; Lin, B.; Liu, X.; Chen, H.; Zhang, Y.; Mullins, D. R.; Abney, C. W.; Shakouri, M.; Chernikov, R.; Hu, Y.; Polo-Garzon, F.; Wu, Z.; Fung, V.; Jiang, D.-e.; Liu, X.; Chi, M.; Liu Jimmy, J.; Dai, S., A new trick for an old support: Stabilizing gold single atoms on LaFeO3 perovskite. *Appl. Catal. B: Environ.* **2020,** *261*, 118178.
19. Wan, Q.; Fung, V.; Lin, S.; Wu, Z.; Jiang, D.-e., Perovskite-supported Pt single atoms for methane activation. *J. Mater. Chem. A* **2020,** *8* (8), 4362-4368.

20. Wang, F.; Wu, Z., Preface to Special Issue on Advances in Ceria Catalysis. *Chin. J. Catal.* **2020,** *41* (6), 899-900.
21. Wang, K.; Fung, V.; Wu, Z.; Jiang, D.-e., Stable Surface Terminations of a Perovskite Oxyhydride from First Principles. *J. Phys. Chem. C* **2020,** *124* (34), 18557-18563.
22. Wu, P.; Tan, S.; Moon, J.; Yan, Z.; Fung, V.; Li, N.; Yang, S.-Z.; Cheng, Y.; Abney, C. W.; Wu, Z.; Savara, A.; Momen, A. M.; Jiang, D.-e.; Su, D.; Li, H.; Zhu, W.; Dai, S.; Zhu, H., Harnessing strong metal–support interactions via a reverse route. *Nat. Commun.* **2020,** *11* (1), 3042.
23. Xu, H.; Zhang, Z.; Liu, J.; Do-Thanh, C.-L.; Chen, H.; Xu, S.; Lin, Q.; Jiao, Y.; Wang, J.; Wang, Y.; Chen, Y.; Dai, S., Entropy-stabilized single-atom Pd catalysts via high-entropy fluorite oxide supports. *Nat. Commun.* **2020,** *11* (1), 3908.
24. Zhang, X.; Savara, A.; Getman, R. B., A Method for Obtaining Liquid–Solid Adsorption Rates from Molecular Dynamics Simulations: Applied to Methanol on Pt(111) in H2O. *J. Chem. Theory Comput.* **2020,** *16* (4), 2680-2691.
25. Zhang, Y.; Mullins, D. R.; Savara, A., Surface Reactions and Catalytic Activities for Small Alcohols over LaMnO3(100) and La0.7Sr0.3MnO3(100): Dehydrogenation, Dehydration, and Oxidation. *J. Phys. Chem. C* **2020,** *124* (6), 3650-3663.
26. Blum, T.; Graves, J.; Zachman, M. J.; Polo-Garzon, F.; Wu, Z.; Kannan, R.; Pan, X.; Chi, M., Machine Learning Method Reveals Hidden Strong Metal-Support Interaction in Microscopy Datasets. *Small Methods* **2021,** *5* (n/a), 2100035.
27. Chen, H.; Wang, W.; Yang, Z.; Suo, X.; Lu, Z.; Xiao, W.; Dai, S., Alkaline salt-promoted construction of hydrophilic and nitrogen deficient graphitic carbon nitride with highly improved photocatalytic efficiency. *J. Mater. Chem. A* **2021,** *9* (8), 4700-4706.
28. Chen, H.; Yang, Z.; Peng, H.; Jie, K.; Li, P.; Ding, S.; Guo, W.; Suo, X.; Liu, J.; Yan, R.; Liu, W.; Do-Thanh, C.-L.; Wang, H.; Wang, Z.; Han, L.; Yang, W.; Dai, S., A bifunctional zeolitic porous liquid with incompatible Lewis pairs for antagonistic cascade catalysis. *Chem* **2021,** *7* (12), 3340-3358.
29. Chen, H.; Yang, Z.; Wang, X.; Polo-Garzon, F.; Halstenberg, P. W.; Wang, T.; Suo, X.; Yang, S.-Z.; Meyer, H. M.; Wu, Z.; Dai, S., Photoinduced Strong Metal–Support Interaction for Enhanced Catalysis. *J. Amer. Chem. Soc.* **2021,** *143* (23), 8521-8526.
30. Leng, Y.; Zhang, Z.; Chen, H.; Du, S.; Liu, J.; Nie, S.; Dong, Y.; Zhang, P.; Dai, S., Overcoming the phase separation within high-entropy metal carbide by poly(ionic liquid)s. *Chem. Commun.* **2021,** *57* (30), 3676-3679.
31. Liu, T.; Jiang, D.-e., Understanding the interaction between carboxylates and coinage metals from first principles. *The Journal of Chemical Physics* **2021,** *155* (3), 034301.
32. Okejiri, F.; Yang, Z.; Chen, H.; Do-Thanh, C.-L.; Wang, T.; Yang, S.; Dai, S., Ultrasound-driven fabrication of high-entropy alloy nanocatalysts promoted by alcoholic ionic liquids. *Nano Research* **2021**.
33. Polo-Garzon, F.; Blum, T. F.; Bao, Z.; Wang, K.; Fung, V.; Huang, Z.; Bickel, E. E.; Jiang, D.-e.; Chi, M.; Wu, Z., In Situ Strong Metal–Support Interaction (SMSI) Affects Catalytic Alcohol Conversion. *ACS Catal.* **2021,** *11* (4), 1938-1945.
34. Sun, Y.; Dai, S., High-entropy materials for catalysis: A new frontier. *Science Advances* **2021,** *7* (20), eabg1600.
35. Sun, Y.; Dai, S., High-entropy catalysts: Supremacy of diversity. *Chem Catalysis* **2021,** *1* (3), 490-492.
36. Wang, S.; Liu, T.; Jiang, D.-e., Locating Hydrides in Ligand-Protected Copper Nanoclusters by Deep Learning. *ACS Appl. Mater. Inter.* **2021,** *13* (45), 53468-53474.
37. Wang, S.; Wu, Z.; Dai, S.; Jiang, D.-e., Deep Learning Accelerated Determination of Hydride Locations in Metal Nanoclusters. *Angew. Chem. Int. Ed.* **2021,** *60* (22), 12289-12292.
38. Wang, X.; Li, M.; Wu, Z., In situ spectroscopic insights into the redox and acid-base properties of ceria catalysts. *Chin. J. Catal.* **2021,** *42* (12), 2122-2140.
39. Yang, W.; Gong, J.; Wang, X.; Bao, Z.; Guo, Y.; Wu, Z., A Review on the Impact of SO2 on the Oxidation of NO, Hydrocarbons, and CO in Diesel Emission Control Catalysis. *ACS Catal.* **2021,** *11* (20), 12446-12468.

40. Zhang, Z.; Yao, S.; Hu, X.; Okejiri, F.; He, K.; Liu, P.; Tian, Z.; Dravid, V. P.; Fu, J.; Zhu, X.; Dai, S., Sacrificial Synthesis of Supported Ru Single Atoms and Clusters on N-doped Carbon Derived from Covalent Triazine Frameworks: A Charge Modulation Approach. *Advanced Science* **2021,** *8* (3), 2001493.
41. Bao, Z.; Fung, V.; Moon, J.; Hood, Z.; Rochow, M.; Kammert, J.; Polo-Garzon, F.; Wu, Z., Revealing the interplay between "intelligent behavior" and surface reconstruction of non-precious metal doped SrTiO3 catalysts during methane combustion. *Catal. Today* **2022**.
42. Chen, B.; Xu, Y.; Xiong, C.; Rickard, S.; Boscoboinik, J. A.; Jiang, D.-e.; Kidder, M.; Savara, A., Mechanism for Acetone and Crotonaldehyde Production during Steam Reforming of Ethanol over La0.7Sr0.3MnO3–x Perovskite: Evidence for a Shared C4 Aldol Addition Intermediate. *ACS Catal.* **2022,** *12* (8), 4358-4374.
43. Chen, H.; Xiong, C.; Moon, J.; Ivanov, A. S.; Lin, W.; Wang, T.; Fu, J.; Jiang, D.-e.; Wu, Z.; Yang, Z.; Dai, S., Defect-Regulated Frustrated-Lewis-Pair Behavior of Boron Nitride in Ambient Pressure Hydrogen Activation. *J. Amer. Chem. Soc.* **2022,** *144* (24), 10688-10693.
44. Okejiri, F.; Fan, J.; Huang, Z.; Siniard, K. M.; Chi, M.; Polo-Garzon, F.; Yang, Z.; Dai, S., Ultrasound-mediated synthesis of nanoporous fluorite-structured high-entropy oxides toward noble metal stabilization. *iScience* **2022,** *25* (5), 104214.
45. Peng, H.; Dong, T.; Yang, S.; Chen, H.; Yang, Z.; Liu, W.; He, C.; Wu, P.; Tian, J.; Peng, Y.; Chu, X.; Wu, D.; An, T.; Wang, Y.; Dai, S., Intra-crystalline mesoporous zeolite encapsulation-derived thermally robust metal nanocatalyst in deep oxidation of light alkanes. *Nat. Commun.* **2022,** *13* (1), 295.
46. Polo-Garzon, F.; Fung, V.; Zhang, J.; Bao, Z.; Meyer, H. M.; Kidder, M.; Wu, Z., CH4 Activation over Perovskite Catalysts: True Density and Reactivity of Active Sites. *ACS Catal.* **2022**, 11845-11853.
47. Sun, Y.; Polo-Garzon, F.; Bao, Z.; Moon, J.; Huang, Z.; Chen, H.; Chen, Z.; Yang, Z.; Chi, M.; Wu, Z.; Liu, J.; Dai, S., Manipulating Copper Dispersion on Ceria for Enhanced Catalysis: A Nanocrystal-Based Atom-Trapping Strategy. *Advanced Science* **2022,** *9* (8), 2104749.
48. Sun, Y.; Wu, T.; Bao, Z.; Moon, J.; Huang, Z.; Chen, Z.; Chen, H.; Li, M.; Yang, Z.; Chi, M.; Toops, T. J.; Wu, Z.; Jiang, D.-e.; Liu, J.; Dai, S., Defect Engineering of Ceria Nanocrystals for Enhanced Catalysis via a High-Entropy Oxide Strategy. *ACS Centr. Sci.* **2022,** *8* (8), 1081-1090.
49. Wang, K.; Wu, Z.; Jiang, D.-e., Ammonia synthesis on BaTiO2.5H0.5: computational insights into the role of hydrides. *Physical Chemistry Chemical Physics* **2022,** *24* (3), 1496-1502.
50. Xiong, C.; Dai, S.; Wu, Z.; Jiang, D.-e., Single Atoms Anchored in Hexagonal Boron Nitride for Propane Dehydrogenation from First Principles. *ChemCatChem* **2022,** *14* (9), e202200133.
51. Zachman, M. J.; Fung, V.; Polo-Garzon, F.; Cao, S.; Moon, J.; Huang, Z.; Jiang, D.-e.; Wu, Z.; Chi, M., Measuring and directing charge transfer in heterogenous catalysts. *Nat. Commun.* **2022,** *13* (1), 3253.
52. Chen, B.; Rickard, S.; Bao, Z.; Wu, Z.; Kidder, M. K.; Savara, A., Evidence of redox cycling as a sub-mechanism in hydrogen production during ethanol steam reforming over La0.7Sr0.3MnO3-x perovskite oxide catalysts. *Applied Surface Science* **2023,** *617*, 156603.
53. Chen, H.; Jiang, D.-e.; Yang, Z.; Dai, S., Engineering Nanostructured Interfaces of Hexagonal Boron Nitride-Based Materials for Enhanced Catalysis. *Acc. Chem. Res.* **2023,** *56* (1), 52-65.
54. Fung, V.; Janik, M.; Crossley, S.; Chin, Y.-H. C.; Savara, A., Toward Understanding and Controlling Organic Reactions on Metal Oxide Catalysts. *J. Phys. Chem. C* **2023,** *127* (28), 13451-13465.
55. He, Y.; Zhang, J.; Polo-Garzon, F.; Wu, Z., Adsorbate-Induced Strong Metal–Support Interactions: Implications for Catalyst Design. *J. Phys. Chem. Lett.* **2023,** *14* (2), 524-534.
56. Li, M.; Qiu, L.; Popovs, I.; Yang, W.; Ivanov, A. S.; Kobayashi, T.; Thapaliya, B. P.; Moitra, D.; Yu, X.; Wu, Z.; Yang, Z.; Dai, S., Construction of Boron- and Nitrogen-Enriched Nanoporous π-Conjugated Networks Towards Enhanced Hydrogen Activation. *Angew. Chem. Int. Ed.* **2023,** *62* (28), e202302684.

57. Li, M.; Zhang, T.; Yang, S.-Z.; Sun, Y.; Zhang, J.; Polo-Garzon, F.; Siniard, K. M.; Yu, X.; Wu, Z.; Driscoll, D. M.; Ivanov, A. S.; Chen, H.; Yang, Z.; Dai, S., Mechanochemistry-Induced Strong Metal–Support Interactions Construction toward Enhanced Hydrogenation. *ACS Catal.* **2023**, 6114-6125.
58. Li, Y.; Wu, Z., A review of in situ/operando studies of heterogeneous catalytic hydrogenation of CO2 to methanol. *Catal. Today* **2023**, 114029.
59. Moon, J.; Cheng, Y.; Wu, Z.; Ramirez-Cuesta, A. J., Neutron Scattering (NS) Spectroscopy. In *Springer Handbook of Advanced Catalyst Characterization*, Wachs, I. E.; Bañares, M. A., Eds. Springer International Publishing: Cham, 2023; pp 493-516.
60. Moon, J.; Li, M.; Ramirez-Cuesta, A. J.; Wu, Z., Raman Spectroscopy. In *Springer Handbook of Advanced Catalyst Characterization*, Wachs, I. E.; Bañares, M. A., Eds. Springer International Publishing: Cham, 2023; pp 75-110.
61. Polo-Garzon, F., Case Study: Calorimetry. In *Springer Handbook of Advanced Catalyst Characterization*, Wachs, I. E.; Bañares, M. A., Eds. Springer International Publishing: Cham, 2023; pp 1061-1069.
62. Savara, A., Derivation of an Adsorption Isotherm, Chemical Potential, and Entropy for 2D Gas Adsorbates with Packing Exclusions and Attractive Interactions. *J. Phys. Chem. C* **2023,** *127* (28), 13573-13581.
63. Siniard, K. M.; Li, M.; Yang, S.-Z.; Zhang, J.; Polo-Garzon, F.; Wu, Z.; Yang, Z.; Dai, S., Ultrasonication-Induced Strong Metal-Support Interaction Construction in Water Towards Enhanced Catalysis. *Angew. Chem. Int. Ed.* **2023,** *62* (20), e202214322.
64. Sun, F.; Tang, Q.; Jiang, D.-e., Atomically Precise Metal Nanoclusters as Electrocatalysts. In *Atomically Precise Nanochemistry*, 2023; pp 195-225.
65. Sun, Y.; Yang, Z.; Dai, S., Nonclassical Strong Metal–Support Interactions for Enhanced Catalysis. *J. Phys. Chem. Lett.* **2023,** *14* (9), 2364-2377.
66. Wang Romero, K.; Polo-Garzon, F.; Wu, Z.; Savara, A.; Jiang, D.-e., Acetylene Semi-Hydrogenation on a Perovskite Oxyhydride Surface: Insights from First Principles and Microkinetic Modeling. *ACS Catal.* **2023,** *13*, 9213-9221.
67. Yang, W.; Kim, M.-Y.; Polo-Garzon, F.; Gong, J.; Jiang, X.; Huang, Z.; Chi, M.; Yu, X.; Wang, X.; Guo, Y.; Wu, Z., CH4 combustion over a commercial Pd/CeO2-ZrO2 three-way catalyst: Impact of thermal aging and sulfur exposure. *Chemical Engineering Journal* **2023,** *451*, 138930.
68. Yang, W.; Polo-Garzon, F.; Zhou, H.; Huang, Z.; Chi, M.; Meyer Iii, H.; Yu, X.; Li, Y.; Wu, Z., Boosting the Activity of Pd Single Atoms by Tuning Their Local Environment on Ceria for Methane Combustion. *Angew. Chem. Int. Ed.* **2023,** *62* (5), e202217323.
69. Yu, X.; Cheng, Y.; Li, Y.; Polo-Garzon, F.; Liu, J.; Mamontov, E.; Li, M.; Lennon, D.; Parker, S. F.; Ramirez-Cuesta, A. J.; Wu, Z., Neutron Scattering Studies of Heterogeneous Catalysis. *Chemical Reviews* **2023,** *123* (13), 8638-8700.

(II) Jointly funded by this grant and other grants with intellectual leadership by other funding sources (total - 41)

70. Cao, Y.; Fung, V.; Yao, Q.; Chen, T.; Zang, S.; Jiang, D.-e.; Xie, J., Control of single-ligand chemistry on thiolated Au25 nanoclusters. *Nat. Commun.* **2020,** *11* (1), 5498.
71. Chevrier, D. M.; Conn, B. E.; Li, B.; Jiang, D.-e.; Bigioni, T. P.; Chatt, A.; Zhang, P., Interactions between Ultrastable Na4Ag44(SR)30 Nanoclusters and Coordinating Solvents: Uncovering the Atomic-Scale Mechanism. *ACS Nano* **2020**.
72. Ding, Y.; Zhang, P.; Xiong, H.; Sun, X.; Klyushin, A.; Zhang, B.; Liu, Z.; Zhang, J.; Zhu, H.; Qiao, Z.-A.; Heumann, S.; Dai, S., Tuning regioselective oxidation toward phenol via atomically dispersed iron sites on carbon. *Green Chem.* **2020,** *22* (18), 6025-6032.
73. Feng, D.; Dong, Y.; Zhang, L.; Ge, X.; Zhang, W.; Dai, S.; Qiao, Z.-A., Holey Lamellar High Entropy Oxide as Ultra-Highly Active Heterogeneous Catalyst for Solvent-free Aerobic Oxidation of Benzyl Alcohol. *Angew. Chem. Int. Ed.* **2020,** *59* (44), 19503-19509.

74. Liu, K.-G.; Gao, X.-M.; Liu, T.; Hu, M.-L.; Jiang, D.-e., All-Carboxylate-Protected Superatomic Silver Nanocluster with an Unprecedented Rhombohedral Ag8 Core. *J. Amer. Chem. Soc.* **2020,** *142* (40), 16905-16909.
75. Shu, Y.; Chen, H.; Chen, N.; Duan, X.; Zhang, P.; Yang, S.; Bao, Z.; Wu, Z.; Dai, S., A Principle for Highly Active Metal Oxide Catalysts via NaCl-Based Solid Solution. *Chem* **2020,** *6* (7), 1723-1741.
76. Walker, E. A.; Ravisankar, K.; Savara, A., CheKiPEUQ Intro 2: Harnessing Uncertainties from Data Sets, Bayesian Design of Experiments in Chemical Kinetics. *ChemCatChem* **2020,** *12* (21), 5401-5410.
77. Wang, X.; Wang, Z.; García de Arquer, F. P.; Dinh, C.-T.; Ozden, A.; Li, Y. C.; Nam, D.-H.; Li, J.; Liu, Y.-S.; Wicks, J.; Chen, Z.; Chi, M.; Chen, B.; Wang, Y.; Tam, J.; Howe, J. Y.; Proppe, A.; Todorović, P.; Li, F.; Zhuang, T.-T.; Gabardo, C. M.; Kirmani, A. R.; McCallum, C.; Hung, S.-F.; Lum, Y.; Luo, M.; Min, Y.; Xu, A.; O'Brien, C. P.; Stephen, B.; Sun, B.; Ip, A. H.; Richter, L. J.; Kelley, S. O.; Sinton, D.; Sargent, E. H., Efficient electrically powered CO2-to-ethanol via suppression of deoxygenation. *Nat. Energy* **2020,** *5*, 478–486.
78. Yang, H.; Chen, X.; Hu, G.; Chen, W.-T.; Bradley, S. J.; Zhang, W.; Verma, G.; Nann, T.; Jiang, D.-e.; Kruger, P. E.; Wang, X.; Tian, H.; Waterhouse, G. I. N.; Telfer, S. G.; Ma, S., Highly efficient electrocatalytic hydrogen evolution promoted by O–Mo–C interfaces of ultrafine β-Mo2C nanostructures. *Chem. Sci.* **2020,** *11* (13), 3523-3530.
79. Yang, J.; Xiao, W.; Chi, X.; Lu, X.; Hu, S.; Wu, Z.; Tang, W.; Ren, Z.; Wang, S.; Yu, X.; Zhang, L.; Rusydi, A.; Ding, J.; Guo, Y.; Gao, P.-X., Solar-driven efficient methane catalytic oxidation over epitaxial ZnO/La0.8Sr0.2CoO3 heterojunctions. *Appl. Catal. B: Environ.* **2020,** *265*, 118469.
80. Yuk, S. F.; Lee, M.-S.; Collinge, G.; Zhang, J.; Padmaperuma, A. B.; Li, Z.; Polo-Garzon, F.; Wu, Z.; Glezakou, V.-A.; Rousseau, R., Mechanistic Understanding of Catalytic Conversion of Ethanol to 1-Butene over 2D-Pillared MFI Zeolite. *J. Phys. Chem. C* **2020,** *124* (52), 28437-28447.
81. Zhang, L.; Zhang, X.; Qian, K.; Li, Z.; Cheng, Y.; Daemen, L. L.; Wu, Z.; Huang, W., Activation and surface reactions of CO and H2 on ZnO powders and nanoplates under CO hydrogenation reaction conditions. *J. Energy Chem.* **2020,** *50*, 351-357.
82. Barboun, P. M.; Daemen, L. L.; Waitt, C.; Wu, Z.; Schneider, W. F.; Hicks, J. C., Inelastic Neutron Scattering Observation of Plasma-Promoted Nitrogen Reduction Intermediates on Ni/γ-Al2O3. *ACS Energy Letters* **2021,** *6* (6), 2048-2053.
83. Bhasker-Ranganath, S.; Rahman, M. S.; Zhao, C.; Calaza, F.; Wu, Z.; Xu, Y., Elucidating the Mechanism of Ambient-Temperature Aldol Condensation of Acetaldehyde on Ceria. *ACS Catal.* **2021**, 8621-8634.
84. Cao, Y.; Liu, T.; Chen, T.; Zhang, B.; Jiang, D.-e.; Xie, J., Revealing the etching process of water-soluble Au25 nanoclusters at the molecular level. *Nat. Commun.* **2021,** *12* (1), 3212.
85. Chen, Y.; Rana, R.; Sours, T.; Vila, F. D.; Cao, S.; Blum, T.; Hong, J.; Hoffman, A. S.; Fang, C.-Y.; Huang, Z.; Shang, C.; Wang, C.; Zeng, J.; Chi, M.; Kronawitter, C. X.; Bare, S. R.; Gates, B. C.; Kulkarni, A. R., A Theory-Guided X-ray Absorption Spectroscopy Approach for Identifying Active Sites in Atomically Dispersed Transition-Metal Catalysts. *J. Amer. Chem. Soc.* **2021,** *143* (48), 20144-20156.
86. Gao, W.; Elnabawy, A. O.; Hood, Z. D.; Shi, Y.; Wang, X.; Roling, L. T.; Pan, X.; Mavrikakis, M.; Xia, Y.; Chi, M., Atomistic insights into the nucleation and growth of platinum on palladium nanocrystals. *Nat. Commun.* **2021,** *12* (1), 3215.
87. He, X.; Walter, M.; Jiang, D.-e., Understanding Superatomic Ag Nanohydrides. *Small* **2021**, 2004808.
88. Hou, S.; Ma, X.; Shu, Y.; Bao, J.; Zhang, Q.; Chen, M.; Zhang, P.; Dai, S., Self-regeneration of supported transition metals by a high entropy-driven principle. *Nat. Commun.* **2021,** *12* (1), 5917.
89. Hutama, A. S.; Marlina, L. A.; Chou, C.-P.; Irle, S.; Hofer, T. S., Development of Density-Functional Tight-Binding Parameters for the Molecular Dynamics Simulation of Zirconia, Yttria, and Yttria-Stabilized Zirconia. *ACS Omega* **2021,** *6* (31), 20530-20548.
90. Lawson, S.; Farsad, A.; Adebayo, B.; Newport, K.; Schueddig, K.; Lowrey, E.; Polo-Garzon, F.; Rezaei, F.; Rownaghi, A. A., A Novel Method of 3D Printing High-Loaded Oxide/H-ZSM-5 Catalyst

Monoliths for Carbon Dioxide Reduction in Tandem with Propane Dehydrogenation. *Advanced Sustainable Systems* **2021,** *5* (3), 2000257.
91. Liu, X.; Li, B.; Han, G.; Liu, X.; Cao, Z.; Jiang, D.-e.; Sun, Y., Electrocatalytic synthesis of heterocycles from biomass-derived furfuryl alcohols. *Nat. Commun.* **2021,** *12* (1), 1868.
92. Moon, J.; Cheng, Y.; Daemen, L.; Novak, E.; Ramirez-Cuesta, A. J.; Wu, Z., On the Structural Transformation of Ni/BaH2 During a N2-H2 Chemical Looping Process for Ammonia Synthesis: A Joint In Situ Inelastic Neutron Scattering and First-Principles Simulation Study. *Topic Catal.* **2021,** *64*, 685-692.
93. Wang, Z.; Rong, J.; Lv, J.; Chong, R.; Zhang, L.; Wang, L.; Chang, Z.; Wang, X., Chelation-mediated in-situ formation of ultrathin cobalt (oxy)hydroxides on hematite photoanode towards enhanced photoelectrochemical water oxidation. *J. Energy Chem.* **2021,** *56*, 152-161.
94. Xu, X.; Wang, X.; Jiang, D.-e., Band Gap as a Novel Descriptor for the Reactivity of 2D Titanium Dioxide and its Supported Pt Single Atom for Methane Activation. *J. Phys. Chem. Lett.* **2021,** *12* (10), 2484-2488.
95. Zhao, J.; Bao, J.; Yang, S.; Niu, Q.; Xie, R.; Zhang, Q.; Chen, M.; Zhang, P.; Dai, S., Exsolution–Dissolution of Supported Metals on High-Entropy Co3MnNiCuZnOx: Toward Sintering-Resistant Catalysis. *ACS Catal.* **2021,** *11* (19), 12247-12257.
96. Zhu, M.; Tian, P.; Cao, X.; Chen, J.; Pu, T.; Shi, B.; Xu, J.; Moon, J.; Wu, Z.; Han, Y.-F., Vacancy engineering of the nickel-based catalysts for enhanced CO2 methanation. *Appl. Catal. B: Environ.* **2021,** *282*, 119561.
97. Zhu, X.; Gao, Y.; Wang, X.; Haribal, V.; Liu, J.; Neal, L. M.; Bao, Z.; Wu, Z.; Wang, H.; Li, F., A tailored multi-functional catalyst for ultra-efficient styrene production under a cyclic redox scheme. *Nat. Commun.* **2021,** *12* (1), 1329.
98. Chen, Y.; Rana, R.; Huang, Z.; Vila, F. D.; Sours, T.; Perez-Aguilar, J. E.; Zhao, X.; Hong, J.; Hoffman, A. S.; Li, X.; Shang, C.; Blum, T.; Zeng, J.; Chi, M.; Salmeron, M.; Kronawitter, C. X.; Bare, S. R.; Kulkarni, A. R.; Gates, B. C., Atomically Dispersed Platinum in Surface and Subsurface Sites on MgO Have Contrasting Catalytic Properties for CO Oxidation. *J. Phys. Chem. Lett.* **2022,** *13* (17), 3896-3903.
99. Fadaeerayeni, S.; Yu, X.; Sarnello, E.; Bao, Z.; Jiang, X.; Unocic, R. R.; Fang, L.; Wu, Z.; Li, T.; Xiang, Y., Ammonia-Assisted Light Alkane Anti-coke Reforming on Isolated ReOx Sites in Zeolite. *ACS Catal.* **2022,** *12* (5), 3165-3172.
100. Gao, Z.-H.; Wei, K.; Wu, T.; Dong, J.; Jiang, D.-e.; Sun, S.; Wang, L.-S., A Heteroleptic Gold Hydride Nanocluster for Efficient and Selective Electrocatalytic Reduction of CO2 to CO. *J. Amer. Chem. Soc.* **2022,** *144* (12), 5258-5262.
101. Iftikhar, S.; Martin, W.; Gao, Y.; Yu, X.; Wang, I.; Wu, Z.; Li, F., LaNixFe1−xO3 as flexible oxygen or carbon carriers for tunable syngas production and CO2 utilization. *Catal. Today* **2022**.
102. Li, W.; Nie, X.; Yang, H.; Wang, X.; Polo-Garzon, F.; Wu, Z.; Zhu, J.; Wang, J.; Liu, Y.; Shi, C.; Song, C.; Guo, X., Crystallographic dependence of CO2 hydrogenation pathways over HCP-Co and FCC-Co catalysts. *Appl. Catal. B: Environ.* **2022,** *315*, 121529.
103. Li, Y.; Song, Y.; Zhang, X.; Liu, T.; Xu, T.; Wang, H.; Jiang, D.-e.; Jin, R., Atomically Precise Au42 Nanorods with Longitudinal Excitons for an Intense Photothermal Effect. *J. Amer. Chem. Soc.* **2022,** *144* (27), 12381-12389.
104. Song, S.; Yang, K.; Zhang, P.; Wu, Z.; Li, J.; Su, H.; Dai, S.; Xu, C.; Li, Z.; Liu, J.; Song, W., Silicalite-1 Stabilizes Zn-Hydride Species for Efficient Propane Dehydrogenation. *ACS Catal.* **2022,** *12* (10), 5997-6006.
105. Wang, H.; Rui, N.; Senanayake, S. D.; Zhang, L.; Li, Y.; Frenkel, A. I., Tuning the Placement of Pt “Single Atoms” on a Mixed CeO2–TiO2 Support. *J. Phys. Chem. C* **2022,** *126* (38), 16187-16193.
106. Xie, H.; Xie, X.; Hu, G.; Prabhakaran, V.; Saha, S.; Gonzalez-Lopez, L.; Phakatkar, A. H.; Hong, M.; Wu, M.; Shahbazian-Yassar, R.; Ramani, V.; Al-Sheikhly, M. I.; Jiang, D.-e.; Shao, Y.; Hu, L., Ta–TiOx nanoparticles as radical scavengers to improve the durability of Fe–N–C oxygen reduction catalysts. *Nat. Energy* **2022,** *7* (3), 281-289.

107. Deng, Q.; Peng, H.; Yang, Z.; Wang, T.; Wang, J.; Zeng, Z.; Dai, S., A one-pot synthesis of high-density biofuels through bifunctional mesoporous zeolite-encapsulated Pd catalysts. *Appl. Catal. B: Environ.* **2023,** *337*, 122982.
108. He, X.; Ding, Y.; Huang, Z.; Liu, M.; Chi, M.; Wu, Z.; Segre, C. U.; Song, C.; Wang, X.; Guo, X., Engineering a Self-Grown TiO2/Ti-MOF Heterojunction with Selectively Anchored High-Density Pt Single-Atomic Cocatalysts for Efficient Visible-Light-Driven Hydrogen Evolution. *Angew. Chem. Int. Ed.* **2023,** *62* (25), e202217439.
109. Yu, X.; Moon, J.; Cheng, Y.; Daemen, L.; Liu, J.; Kim, S. W.; Kumar, A.; Chi, M.; Fung, V.; Ramirez-Cuesta, A. J.; Wu, Z., In Situ Neutron Scattering Study of the Structure Dynamics of the Ru/Ca2N:e– Catalyst in Ammonia Synthesis. *Chem. Mater.* **2023,** *35* (6), 2456-2462.
110. Zhao, X.; Wang, Y.; Chen, X.; Yu, X.; Li, W.; Zhang, S.; Meng, X.; Zhao, Z.-M.; Dong, T.; Anderson, A.; Aiyedun, A.; Li, Y.; Webb, E.; Wu, Z.; Kunc, V.; Ragauskas, A.; Ozcan, S.; Zhu, H., Sustainable bioplastics derived from renewable natural resources for food packaging. *Matter* **2023,** *6* (1), 97-127.

FWP 47319: Impact of catalytically active centers and their environment on rates and thermodynamic states along reaction paths

PI: Johannes A. Lercher

Subtask PIs: Liney Arnadottir, Zdenek Dohnálek, Oliver Gutiérrez-Tinoco, Johannes A. Lercher, Wendy J. Shaw, Ba Tran, Eric S. Wiedner

Co-PIs and Key Personnel: Aaron M. Appel, S. R. Morris Bullock, David A. Dixon, John L. Fulton, Feng Gao, Bojana Ginovska, Jian Zhi Hu, Enrique Iglesia, Andreas Jentys, Abhijeet Karkamkar, Bruce D. Kay, Greg A. Kimmel, Libor Kovarik, Mal-Soon Lee, John C. Linehan, Gregory K. Schenter, János Szanyi, Huamin Wang, Yong Wang.

The core objective of our Basic Energy Sciences (BES) Catalysis Sciences research program is to investigate three primary influences that minimize the difference between the excess chemical potentials of reacting substrates in their initial and transition states. These are (i) the structure and electronic attributes of the active centers, (ii) the steric configuration surrounding these centers, which encompasses the nature and orientation of functional groups, and (iii) the nature and interactions of co-adsorbates and solvents. While the structure and electronic properties of the catalytic center are critical in delineating the reaction trajectory, the steric arrangements around the active center facilitate directing molecules into specific orientations, bringing two molecules together, and stabilizing or destabilizing ground and transition states. Co-adsorbates and solvents can alter the active sites' specific chemical and electronic properties and influence the substrate's reactivity by attractive and repulsive interactions. Consequently, the program's structure addresses the three aspects that can control catalytic transformations: the active center, its adjacent environment, and the dynamic environment represented by interacting molecules nearby. Collectively, they define the catalytically active site and its characteristics. Our approach centers on critical C-C and C-H bond forming and C-O bond cleaving steps on acid-base and metal active sites to develop a predictive understanding and control of catalyzed processes. We combine kinetic measurements with spectroscopic characterization of the interacting reaction intermediates and the working catalysts.

RECENT PROGRESS

Operando mechanistic studies of reversible CO_2 hydrogenation by ruthenium complexes using high-pressure NMR spectroscopy. The ability to both reduce carbon dioxide with dihydrogen to formate and conduct the reverse reaction with the same catalyst is of interest for potential fuel generation and use. Ruthenium bis(diphosphine) complexes with and without pendant amines were reacted with mixtures of CO_2/H_2 gases in the presence of added base to catalytically yield formate. When the base was triethylamine, the reaction was found to be reversible, thereby catalytically regenerating H_2 and CO_2. The reactions were monitored using high-pressure, *operando* ^{1}H and $^{31}P\{^{1}H\}$ NMR spectroscopies at 18 °C in THF under 40 atm of a 1:1 mixture of H_2 and CO_2 (Figure 1). The rate

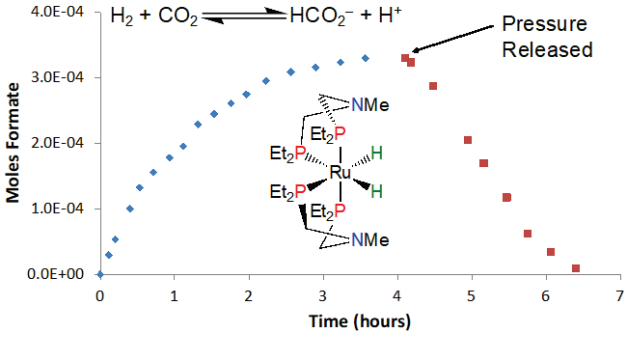

Figure 1. Through operando, high-pressure NMR spectroscopy, reversible hydrogenation of CO_2 was observed using a catalyst based on a ruthenium complex.

of production of formate was correlated with the observation of specific catalytic intermediates by NMR spectroscopy under catalytic conditions, including an observed hydrido-dihydrogen complex. From this *operando* study, a mechanism is proposed with two competing catalytic cycles, for which the predominant cycle is dependent on which base and catalyst are used. The role of the base is shown to be vital both for the observed catalytic rate and for the reversibility of the chemical transformation, indicating base selection should be carefully considered.

Mechanism-guided reaction discovery and ligand design by controlling the nuclearity of the Cu-H active site. Kinetic analysis for the insertion reactions of $[(NHC)CuH]_2$ dimers (NHC = *N*-heterocyclic carbene) with various substrates indicate two operating rate-limiting steps of formation of transient monomers from dimers or hydride transfer from a CuH-substrate complex (Figure 2). The rapid insertion of CO_2 into $[(NHC)CuH]_2$, which is proposed to proceed by the formation of the transient CuH monomer, contradicts the timescale for CuH monomerization from $[(NHC)CuH]_2$. An alternative mechanism is a direct CO_2 insertion into the $[Cu_2H_2]$ core without complete dimer dissociation to CuH monomers. To do so, we eliminated the plausibility of complete dimer dissociation by performing single-crystal to single-crystal (SC-SC) transformations of $[(NHC)CuH]_2$ and CO_2. The reaction proceeds by stepwise CO_2 insertion into $[(NHC)CuH]_2$ to produce a dicopper formate hydride complex followed by a dicopper bisformate complex. These dicopper complexes rupture in solution to produce corresponding monomeric formate complexes. SC-SC transformations of an organometallic complex and gaseous CO_2 provide a link between homogeneous and heterogeneous chemistry. The SC-SC approach provides a compelling opportunity to uncover new reactivity and unstable intermediates for other complexes with bridging hydrides for fundamental studies at the confluence of heterogeneous, homogeneous, and gas phase chemistry.

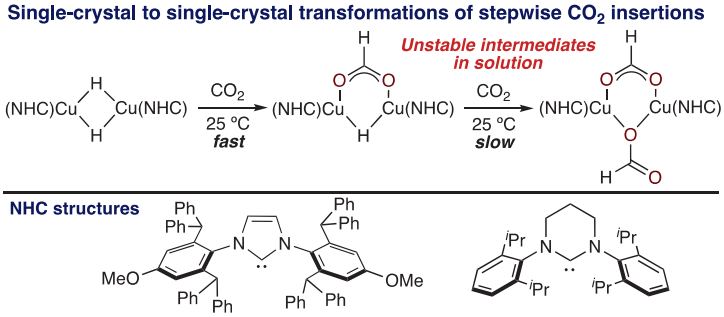

Figure 2. SC-SC reactions of $[(NHC)CuH]_2$ and CO_2 enabled the structural characterization of unusual dicopper formate intermediates by stepwise insertion of CO_2 into the $[Cu_2H_2]$ core.

Impact of outer coordination sphere functional groups on catalytic activity. The outer coordination sphere around the active site of an enzyme is demonstrated to be important, yet the design principles controlling that importance are not well established. In this work, we use a CO_2 reduction complex covalently attached to a well-structured protein to explore the mechanistic details of the outer coordination sphere, which showed activation of this complex for CO_2 reduction by placing it inside this protein scaffold, with the CO_2 + dihydride → formate being the rate-limiting step. Due to the covalent attachment of the complex in the scaffold, various isomers can be formed, orienting the Rh-H_2 active site and the interacting CO_2 differently. QM/MM free energy calculations (Figure 3) of the WT isomer where the guanidinium group of arginine 90 can hydrogen bond with CO_2 reduces the barrier, suggesting

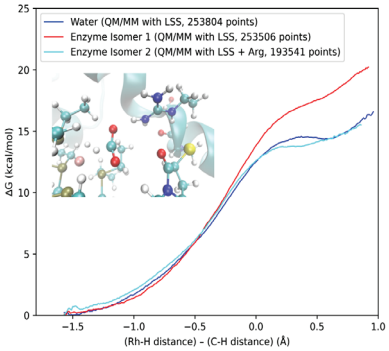

Figure 3. Arginine hydrogen-bonding interaction with CO_2; Arginine–CO_2 hydrogen bond reduces the barrier of hydride transfer (cian) in the proposed rate-determining step. Lack of H-bonding results in increased barrier in the protein (red).

that this interaction may be driving the activity in the enzyme, while the other isomers, that lack this interaction, do not. Previously, we had identified that the activity in variant D100R of the enzyme accelerates the rate 3-fold by positioning another arginine near the active site, possibly allowing for Arg-CO_2 hydrogen bonding in multiple isomers. Our current work is further exploring this hypothesis. We further probed the influence of the scaffold charge by introducing negative charges, expecting the opposite outcome, i.e., a reduction in rates. Our measurements show no statistically significant impact of the negative charge on catalysis, with the exception of the complex with four mutations in the outer coordination sphere, D100R/R98D/K191E/K111D, where the increase in rate is attributed to the positive charge added by replacing the aspartic acid (D) with arginine (R), rather than the negative charge.

The role of surface hydroxyls in the mobility of carboxylates on anatase TiO_2(101). The dynamics of reactive intermediates are important in catalysis for understanding transient species, which can drive reactivity and the transport of species to reaction centers. We investigated the dynamics of acetic acid on anatase TiO_2(101) using scanning tunneling microscopy experiments and density functional theory calculations. We demonstrate the concomitant diffusion of bidentate acetate and a bridging hydroxyl (Figure 4, top) and provide evidence for the transient formation of molecular, monodentate acetic acid. The diffusion rate is strongly dependent on the hydroxyl position and adjacent acetate(s). A facile three-step diffusion process (Figure 4, bottom) consisting of acetate and hydroxyl recombination, acetic acid rotation, and acetic acid dissociation is proposed. We further show that the location of an adjacent bridging hydroxyl relative to acetate is critically important. A significantly higher diffusion rate is demonstrated for bidentate acetate with a bridging hydroxyl on an adjacent O_{2c}–Ti_{5c} row relative to acetate (E_a = 0.36 eV) than a bridging hydroxyl on the same O_{2c}–Ti_{5c} row (E_a = 0.74 eV). Further, we show that the presence of adjacent bidentate acetate(s) decreases the diffusion rate of bidentate acetate, resulting in clustering that is a prerequisite for bimolecular reactions. This study demonstrates that bidentate acetate's dynamics could be important in forming monodentate species, which are proposed to drive selective ketonization.

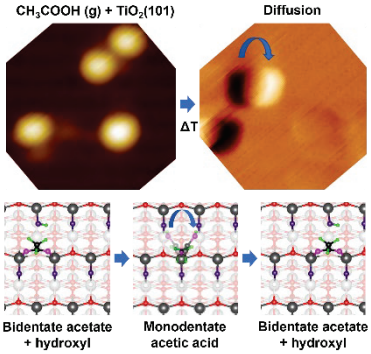

Figure 4. Top: Time-lapsed STM images allow for the determination of the concomitant diffusion of acetate and hydroxyl species. Bottom: Interconversion mechanism of bidentate acetate with a bridging hydroxyl on the same O_{2c}–Ti_{5c} row to a bridging hydroxyl on the adjacent O_{2c}–Ti_{5c} row.

Unraveling facet-dependent catalysis of anatase TiO_2 via blocking defect-bound hydroxyls with silanols. Model anatase nanoparticles with varying percentages of (001) and (101) faceted interfaces were synthesized to probe facet-dependent redox properties. From HAADF-STEM imaging, (001) planes were found to be composed of a significant curvature, with single and double atomic step edge sites separating segments of flat (001) terraces. To delineate their contribution in kinetic measurements, step edge sites were passivated by chemically grafting SiO_2. Probing with methanol oxidative dehydrogenation (ODH) revealed that incorporating only 0.1Si/nm^2 by atomic layer deposition led to a ~4-fold decrease in total redox areal rate, underscoring the notable catalytic influence of step edge sites. Further kinetic assessment before and after SiO_2 grafting revealed step edge sites did not change the rate-determining step for methanol ODH but only lowered the energy barrier for the ODH transition state. Methanol adsorption in DRIFTS and ^{13}C solid-state NMR revealed SiO_2 grafting suppressed methanol dissociative adsorption and further

conversion to a formate intermediate (**Error! Reference source not found.**), suggesting a minority of reactive lattice oxygen at step edge sites are responsible for the majority of surface redox functionality. Hydroxyl profiles in IR showed SiO_2 anchoring to the surface occurred via preferential consumption of terminal OH groups anchored to step edge sites. Further confirmation of SiO_2 placement at step edge sites was ascertained via ^{17}O NMR and iDPC-STEM imaging, affirming the hypothesis of selective passivation of O atoms at step edge sites, leaving exposed faceted terraces accessible for catalytic probing. This work outlines a versatile method to passivate anomalously reactive lattice sites on model oxide surfaces, thus enabling definitive kinetic assessment of site-specific catalytic functionality.

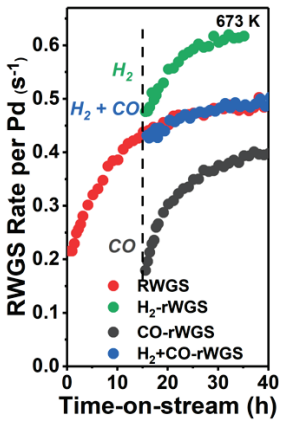

Figure 5. rWGS rate vs TOS at 400 °C on 0.0125 wt % Pd_1/TiO_2. In the first 15 h under the rWGS stream (red, 40% H_2, 10% CO_2), 40% H_2 (green), 5000 ppm CO (black), and 40% H_2 + 5000 ppm CO (blue) at 400 °C.

Dynamic evolution of Pd_1/TiO_2-A single atom catalysts during the reverse water gas shift reaction. In this work, we investigated the dynamic structural evolution of Pd/TiO_2-anatase single-atom catalysts (SACs) and their impacts on the reverse water−gas shift (rWGS) reaction. The atomic dispersion of Pd (at the low loadings of <0.05 wt%) was confirmed by high-angle annular dark-field scanning transmission electron microscopy (HAADF-STEM), X-ray absorption spectroscopy (XAS), and CO adsorption IR (CO-IR) measurements. These catalysts showed a slow, gradual increase in intrinsic activity with time-on-stream (Figure 5). The roles of individual gas components of the mixture the catalyst experiences during the rWGSR were studied in detail. Hydrogen greatly increased, while CO reduced the activity of the Pd_1/TiO_2 catalysts. *In situ/operando* XAS revealed that the bulk reduction of TiO_2 by H_2 or the reaction stream partially cleaves the Pd−O interface and modifies the electronic structure of Pd. The new coordination environment of Pd sites facilitates rWGS turnover through the carboxyl pathway, which overcomes the minor sintering of some Pd_1 into disordered, flattened particles. Such changes in the Pd coordination environment are reversed under air, which, at 400 °C, also redisperses Pd_n into Pd_1 and promote both the rWGS turnover and TiO_2 reduction by removing the auto-adsorbed carboxylate layers on TiO_2. On the other hand, the deactivation by CO is due to Pd_1 sintering into metallic nanoparticles. This work elucidated the complicated dynamics of Pd_1/TiO_2 under pretreatment and operando conditions and established structure−function relationships on these SACs.

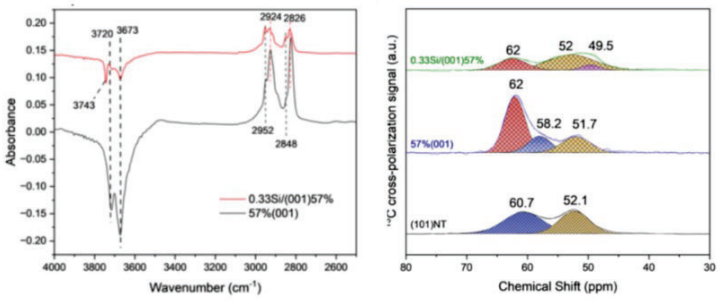

Figure 6. DRIFTS spectra (left) and ^{13}C cross-polarization MAS NMR (right) of methanol adsorption on 0.33Si/{001}57% compared to 57%{001}

Pt single-atoms and rafts supported on Fe_3O_4: Impact of nuclearity on reverse water-gas shift and acetone aldol condensation reactions. Here, we controlled the structure of Pt species supported on Fe_3O_4, ranging from single atoms to flat clusters of ≤20 atoms (rafts) and nanoparticles. We compared the activity of these structures for the reverse water-gas shift and aldol condensation reactions, aiming to uncover the ensemble effects across different catalytic reactions and to characterize the stability

of Pt species under dissimilar environments. We discovered that the rates of rWGS do not depend on the structure of Pt species at low temperatures (<290 °C), supporting a dual-site mechanism that H_2 and CO_2 adsorption occurred on Pt and iron oxide surfaces separately (**Error! Reference source not found.**). In the presence of H_2, high reaction temperatures (≥290 °C) trigger agglomeration of Pt single atoms and phase transition of the Fe_3O_4 into a mixture of reduced iron and iron carbides, consistent with reaction profiles and post-reaction characterizations. The instability of Pt single atoms under reductive environments at high temperatures is attributed to the interplay between the rates of hydrogen spillover towards the support and hydrogen addition to surface intermediates. Surprisingly, the flat Pt clusters are remarkably stable, maintaining the morphology of Pt and the phase of iron oxide support up to 350 °C in the rWGS. On the other hand, the rates of aldol condensation of acetone increase as the nuclearity of Pt species decreases, reaching a maximum with single Pt atoms. This arises from the ability of the single site to stabilize an enol intermediate form before the C-C coupling step. In summary, we provide valuable insight into how the properties of Pt species and their coordination with the support impact their catalytic properties and evolution under dissimilar reaction environments.

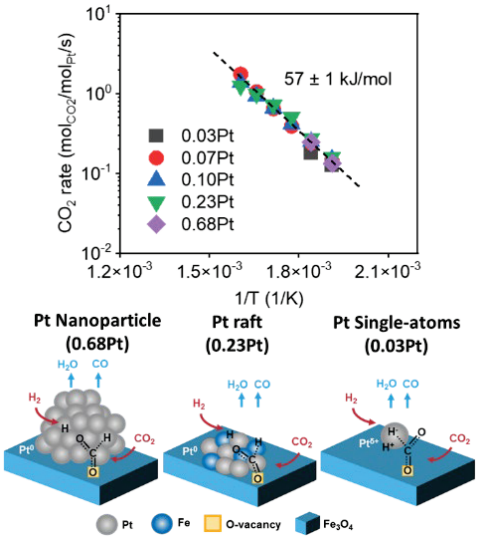

Figure 7. RWGS reaction on different Pt geometries: turn-over frequencies (TOFs) of the Pt catalysts (top) and scheme of rWGS mechanisms (bottom).

Proton-relay in heterogeneous electrocatalysis. Proton transfer is critically important to many electrocatalytic reactions, and directed proton delivery could open new avenues for the design of electrocatalysts. Here, we report that a metal oxide proton relay can be built within heterogeneous electrocatalyst architectures and improve the kinetics of proton-involved reactions. We develop proton transfer material on the solid/liquid interface (Pd/C interface with H_2O) and show how the rate of hydrogen evolution reaction (HER) can be controlled as a function of pH by varying the pK_a of the deposited metal oxides (such as MoO_3, CeO_2) on the solid-liquid interface. By combining experimental and computational simulation efforts, we show that rate enhancement of the HER reaction occurs when (i) the proton transfer energy barrier between the metal oxide surface and Pd nanoparticle is slower compared to that between water and Pd nanoparticle (Figure 8) and (ii) the pK_a of a proton relay matches the pH of the electrolyte solution. These findings demonstrate the possibility of controlling proton delivery and enhancing the rate by tuning the chemical properties and interfacial structure of metal/metal oxide junctions in heterogeneous electrocatalysts.

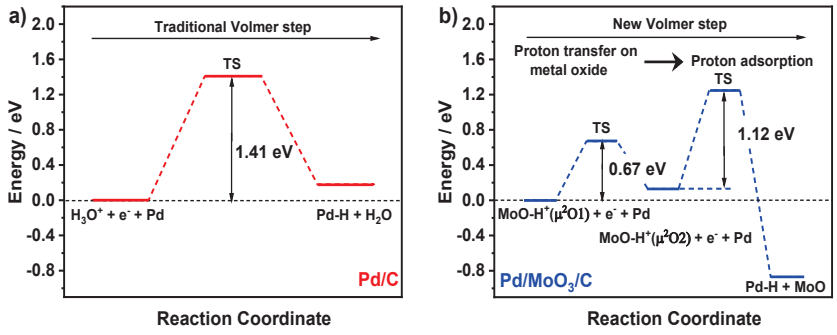

Figure 8. Computed electronic energy (eV) diagram of the Volmer reaction for (a) GO-PdH-acid and (b) GO-PdH-MoO_3 systems.

Impact of the environment of BEA-type zeolites for sorption of water and cyclohexanol. We have studied the interactions between water and cyclohexanol with the pore walls and functional groups of Brønsted acidic BEA-type zeolites (H-BEA). As water is adsorbed into the H-BEA micropore, it forms hydrated hydronium ions in conjunction with Brønsted acid sites, generating aqueous domains within the micropore (Figure 9). Meanwhile, organic molecules, like cyclohexanol, fill the remaining available space. The pore size of the zeolite H-BEA stabilizes hydrated hydronium ions ($H^+(H_2O)_{10}$) that are two H_2O molecules larger than those formed in the smaller pore zeolite H-ZSM-5 due to the lower entropy loss in the larger H-BEA pore. The "quasi-solid electrolyte" environment within the zeolite micropore, created by hydronium ions and the negatively charged framework, influences all adsorbed molecules. The higher the concentration of the hydronium ions (higher ionic strength), the higher the excess chemical potential of adsorbed molecules, leading to a lower equilibrium constant. This excess chemical potential destabilizes adsorbed cyclohexanol, and together with the better stabilization of the charged transition state, it may result in a lowered free energy barrier for dehydration.

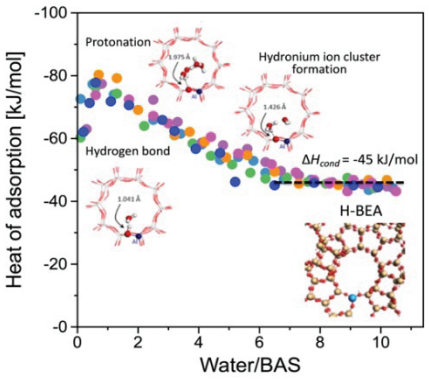

Figure 9. Adsorption isotherm and heat of water adsorption on H-BEA zeolites varying Si/Al ratio from 15 to 400.

Molecular understanding of the self-organization of short-chain alcohols in zeolites. Exploring how alcohols interact with zeolite pores offers profound insights into molecular dynamics at the nanoscale. We gravimetrically and calorimetrically studied the adsorption of C_1–C_4 alcohols in MFI (Silicalite-1 and H-ZSM-5) and Beta (siliceous Beta and H-Beta) framework zeolites. By examining the heat of adsorption for 1-alcohols in relation to their molecular weight on siliceous frameworks and frameworks containing BAS (Figure 10), we quantitatively assessed three distinct types of interactions between the alcohol molecule and the zeolite: (i) the interaction between the alkyl chain with the zeolite pore (approximately 10 kJ·mol^{-1} per carbon atom); (ii) the interaction between the alcohol-OH group and the zeolite pore (35 kJ·mol^{-1} in MFI framework and 30 kJ·mol^{-1} in BEA framework); and (iii) the additional interaction between the alcohol-OH group and the BAS (37 kJ·mol^{-1} in both MFI and Beta frameworks). This indicates that the alcohol OH groups interact with the silica walls of zeolites more strongly than the -CH_2- or -CH_3 groups. From this, we conclude that the primary constraint for water adsorption arises because its heat of condensation (45 kJ·mol^{-1}) surpasses its adsorption enthalpy (35 kJ·mol^{-1}). Though the size of protonated water clusters around Brønsted acid sites is constrained by entropy loss, their higher adsorption enthalpy allows otherwise similarly adsorbed alcohol molecules to fill the pores completely.

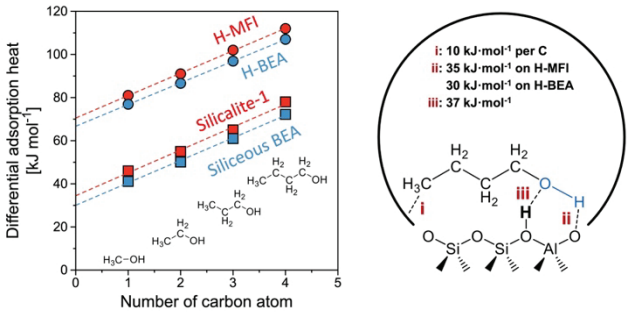

Figure 10. Differential heat of adsorption of C_1-C_4 primary alcohols as a function of carbon atom numbers on MFI- and BEA-type zeolites. Three different kinds of interaction between a primary alcohol molecule and BAS containing zeolite and their correlated contributions to the heat of adsorption are deconvoluted.

Publications Acknowledging this Grant in 2020-2023

Publications exclusively funded by this grant

2020

1. Collinge, G.; Yuk, S. F.; Nguyen, M.-T.; Lee, M.-S.; Glezakou, V.-A.; Rousseau, R., Effect of Collective Dynamics and Anharmonicity on Entropy in Heterogenous Catalysis: Building the Case for Advanced Molecular Simulations. *ACS Catal.* **2020**, *10*, 9236-9260. http://dx.doi.org/10.1021/acscatal.0c01501. (Solely funded)
2. Confer, M. P.; Outlaw, D. A.; Dixon, D. A., Potential Main Group Amine Borane-Based Chemical Hydrogen Storage Molecular Systems. *Comput. Theor. Chem.* **2020**, *1189*, 112953. http://dx.doi.org/10.1016/j.comptc.2020.112953. (Solely funded by this program)
3. Deshlahra, P.; Iglesia, E., Reactivity Descriptors in Acid Catalysis: Acid Strength, Proton Affinity and Host–Guest Interactions. *Chem. Commun.* **2020**, *56*, 7371-7398. http://dx.doi.org/10.1039/D0CC02593C. (Exclusively funded by this program)
4. Erickson, J. D.; Preston, A. Z.; Linehan, J. C.; Wiedner, E. S., Enhanced Hydrogenation of Carbon Dioxide to Methanol by a Ruthenium Complex with a Charged Outer-Coordination Sphere. *ACS Catal.* **2020**, *10*, 7419-7423. http://dx.doi.org/10.1021/acscatal.0c02268. (Sole Contribution.)
5. Jaegers, N. R.; Hu, W.; Wang, Y.; Hu, J. Z., High-Temperature and High-Pressure in Situ Magic Angle Spinning Nuclear Magnetic Resonance Spectroscopy. *JoVE* **2020**, e61794. http://dx.doi.org/doi:10.3791/61794. (Solely funded by this program)
6. Jaegers, N. R.; Wang, Y.; Hu, J. Z., Thermal Perturbation of Nmr Properties in Small Polar and Non-Polar Molecules. *Sci. Rep.* **2020**, *10*, 6097. http://dx.doi.org/10.1038/s41598-020-63174-6. (Solely funded)
7. Kovarik, L.; Bowden, M.; Andersen, A.; Jaegers, N. R.; Washton, N.; Szanyi, J., Quantification of High-Temperature Transition Al_2o_3 and Their Phase Transformations. *Angew. Chem. Int. Ed.* **2020**, 2-11. http://dx.doi.org/10.1002/anie.202009520. (Solely Funded)
8. Kwon, S.; Lin, T. C.; Iglesia, E., Elementary Steps and Site Requirements in Formic Acid Dehydration Reactions on Anatase and Rutile TiO_2 Surfaces. *J. Catal.* **2020**, *383*, 60-76. http://dx.doi.org/10.1016/j.jcat.2019.12.043. (Solely funded)
9. Kwon, S.; Lin, T. C.; Iglesia, E., Formic Acid Dehydration Rates and Elementary Steps on Lewis Acid–Base Site Pairs at Anatase and Rutile TiO_2 Surfaces. *J. Phys. Chem. C* **2020**, *124*, 20161-20174. http://dx.doi.org/10.1021/acs.jpcc.0c05721. (Solely funded)
10. Li, H.; Sun, J.; Li, G.; Wu, D.; Wang, Y., Real-Time Monitoring of Surface Acetone Enolization and Aldolization. *Catal. Sci. Technol.* **2020**, *10*, 935-939. http://dx.doi.org/10.1039/C9CY02339A. (HL, JS, GL, DW funded by this program)
11. Lin, F.; Chen, Y.; Zhang, L.; Mei, D.; Kovarik, L.; Sudduth, B.; Wang, H.; Gao, F.; Wang, Y., Single-Facet Dominant Anatase TiO_2 (101) and (001) Model Catalysts to Elucidate the Active Sites for Alkanol Dehydration. *ACS Catal.* **2020**, *10*, 4268-4279. http://dx.doi.org/10.1021/acscatal.9b04654. (Solely Funded)
12. McNeill, A. S.; Zhan, C.-G.; Appel, A. M.; Stanbury, D. M.; Dixon, D. A., The H•/H- Redox Couple and Absolute Hydration Energy of H. *J. Phys. Chem. A* **2020**, *124*, 6084-6095. http://dx.doi.org/10.1021/acs.jpca.0c03833. (Solely funded)

13. Milakovic, L.; Hintermeier, P. H.; Liu, Q.; Shi, H.; Liu, Y.; Barath, E.; Lercher, J. A., Towards Understanding and Predicting the Hydronium Ion Catalyzed Dehydration of Cyclic-Primary, Secondary and Tertiary Alcohols. *J. Catal.* **2020**, *390*, 237-243. http://dx.doi.org/10.1016/j.jcat.2020.08.009. (Solely funded by this program)
14. Nelson, N. C.; Chen, L.; Meira, D.; Kovarik, L.; Szanyi, J., In Situ Dispersion of Palladium on TiO_2 During Reverse Water–Gas Shift Reaction: Formation of Atomically Dispersed Palladium. *Angew. Chem. Int. Ed.* **2020**, *59*, 17657-17663. http://dx.doi.org/https://doi.org/10.1002/anie.202007576. (Solely Funded)
15. Nelson, N. C.; Szanyi, J., Heterolytic Hydrogen Activation: Understanding Support Effects in Water-Gas Shift, Hydrodeoxygenation, and CO Oxidation Catalysis. *ACS Catal.* **2020**, *10*, 5663-5671. http://dx.doi.org/10.1021/acscatal.0c01059. (N.C.N and J.S. were exclusively funded by this program for all the experiment work and manuscript writing.)
16. Persaud, R. R.; Chen, M.; Dixon, D. A., Prediction of Structures and Atomization Energies of Coinage Metals, $(M)_N$, $N < 20$: Extrapolation of Normalized Clustering Energies to Predict the Cohesive Energy. *J. Phys. Chem. A* **2020**, *124*, 1775-1786. http://dx.doi.org/10.1021/acs.jpca.9b11801. (Solely funded)
17. Stein, T. H.; Vasiliu, M.; Arduengo, A. J.; Dixon, D. A., Lewis Acidity and Basicity: Another Measure of Carbene Reactivity. *J. Phys. Chem. A* **2020**, *124*, 6096-6103. http://dx.doi.org/10.1021/acs.jpca.0c03877. (Solely funded)
18. Wang, M.; Zhao, Y.; Mei, D.; Bullock, R. M.; Gutiérrez, O. Y.; Camaioni, D. M.; Lercher, J. A., The Critical Role of Reductive Steps in the Nickel-Catalyzed Hydrogenolysis and Hydrolysis of Aryl Ether C−O Bonds. *Angew. Chem. Int. Ed.* **2020**, *59*, 1445-1449. http://dx.doi.org/10.1002/anie.201909551. (Solely funded)
19. Yuk, S. F.; Collinge, G.; Nguyen, M.-T.; Lee, M.-S.; Glezakou, V.-A.; Rousseau, R., Selective Acetylene Hydrogenation over Single Metal Atoms Supported on Fe_3o_4(001): A First-Principle Study. *J. Chem. Phys.* **2020**, *152*, 154703. http://dx.doi.org/10.1063/1.5142748. (Sole funding.)
20. Yuk, S. F.; Collinge, G.; Nguyen, M.-T.; Lee, M.-S.; Glezakou, V.-A.; Rousseau, R. *Single-Atom Catalysis: An Analogy between Heterogeneous and Homogeneous Catalysts* in *Advanced Heterogeneous Catalysts Volume 2: Applications at the Single-Atom Scale*; American Chemical Society, 2020; Vol. 1360; pp 1-15.
21. Zhang, J.; Sun, J.; Wang, Y., Recent Advances in the Selective Catalytic Hydrodeoxygenation of Lignin-Derived Oxygenates to Arenes. *Green Chem.* **2020**, *22*, 1072-1098. http://dx.doi.org/10.1039/C9GC02762A. (Solely funded)
22. Zhang, W.; Cheng, G.; Haller, G. L.; Liu, Y.; Lercher, J. A., Rate Enhancement of Acid-Catalyzed Alcohol Dehydration by Supramolecular Organic Capsules. *ACS Catal.* **2020**, *10*, 13371-13376. http://dx.doi.org/10.1021/acscatal.0c03625. (Solely funded)

2021

23. Allec, S. I.; Nguyen, M. T.; Rousseau, R.; Glezakou, V. A., The Role of Sub-Surface Hydrogen on Co_2 Reduction and Dynamics on Ni(110): An Ab Initio Molecular Dynamics Study. *J. Chem. Phys.* **2021**, *155*, 044702. http://dx.doi.org/10.1063/5.0048894. (Solely funded)
24. Chen, F.; Shetty, M.; Wang, M.; Shi, H.; Liu, Y. S.; Camaioni, D. M.; Gutierrez, O. Y.; Lercher, J. A., Differences in Mechanism and Rate of Zeolite-Catalyzed Cyclohexanol Dehydration in Apolar and Aqueous Phase. *ACS Catal.* **2021**, *11*, 2879-2888. http://dx.doi.org/10.1021/acscatal.0c05674. (Solely Funded)

25. Chen, L.; Kovarik, L.; Szanyi, J., Temperature-Dependent Communication between Pt/Al_2o_3 Catalysts and Anatase TiO_2 Dilutant: The Effects of Metal Migration and Carbon Transfer on the Reverse Water–Gas Shift Reaction. *ACS Catal.* **2021**, *11*, 12058-12067. http://dx.doi.org/10.1021/acscatal.1c03133. (Solely Funded)
26. Chen, L.; Smith, R. S.; Kay, B. D.; Dohnalek, Z., Formation of Gas-Phase Allyl Radicals from Glycerol on Rutile TiO_2(110). *J. Phys. Chem. C* **2021**, *125*, 7227-7239. http://dx.doi.org/10.1021/acs.jpcc.1c00991. (Solely funded)
27. Chen, L.; Unocic, R. R.; Hoffman, A. S.; Hong, J.; Braga, A. H.; Bao, Z.; Bare, S. R.; Szanyi, J., Unlocking the Catalytic Potential of TiO_2-Supported Pt Single Atoms for the Reverse Water–Gas Shift Reaction by Altering Their Chemical Environment. *JACS Au* **2021**. http://dx.doi.org/10.1021/jacsau.1c00111. (Solely funded)
28. Doudin, N.; Collinge, G.; Gurunathan, P. K.; Lee, M.-S.; Glezakou, V.-A.; Rousseau, R.; Dohnálek, Z., Creating Self-Assembled Arrays of Mono-Oxo $(Moo_3)_1$ Species on TiO_2(101) Via Deposition and Decomposition of $(Moo_3)_N$ Oligomers. *Proc. Natl. Acad. Sci. U.S.A.* **2021**, *118*, e2017703118. http://dx.doi.org/10.1073/pnas.2017703118. (Solely funded)
29. Doudin, N.; Collinge, G.; Persaud, R. R.; Gurunathan, P. K.; Lee, M.-S.; Glezakou, V. A.; Dixon, D. A.; Rousseau, R.; Dohnalek, Z., Binding and Stability of Mgo Monomers on Anatase TiO_2(101). *J. Chem. Phys.* **2021**, *154*, 204703. http://dx.doi.org/10.1063/5.0047521. (Solely funded)
30. Grifoni, E.; Piccini, G.; Lercher, J. A.; Glezakou, V.-A.; Rousseau, R.; Parrinello, M., Confinement Effects and Acid Strength in Zeolites. *Nat. Commun.* **2021**, *12*, 2630. http://dx.doi.org/10.1038/s41467-021-22936-0. (Solely funded)
31. Jaegers, N. R.; Wang, Y.; Hu, J. Z.; Wachs, I. E., Impact of Hydration on Supported V_2o_5/TiO_2 Catalysts as Explored by Magnetic Resonance Spectroscopy. *J. Phys. Chem. C* **2021**, *125*, 16766-16775. http://dx.doi.org/10.1021/acs.jpcc.1c04150. (Solely funded)
32. Khivantsev, K.; Jaegers, N. R.; Kwak, J.-H.; Szanyi, J.; Kovarik, L., Precise Identification and Characterization of Catalytically Active Sites on the Surface of Γ-Alumina. *Angew. Chem. Int. Ed.* **2021**. http://dx.doi.org/https://doi.org/10.1002/anie.202102106. (Solely funded)
33. Laureanti, J. A.; Su, Q.; Shaw, W. J., A Protein Scaffold Enables Hydrogen Evolution for a Ni-Bisdiphosphine Complex. *Dalton Trans.* **2021**, *50*, 15754-15759. http://dx.doi.org/10.1039/D1DT03295J. (Solely Funded)
34. Lee, I.; Lee, M.-S.; Tao, L.; Ikuno, T.; Khare, R.; Jentys, A.; Huthwelker, T.; Borca, C. N.; Kalinko, A.; Gutiérrez, O. Y.; Govind, N.; Fulton, J. L.; Hu, J. Z.; Glezakou, V.-A.; Rousseau, R.; Sanchez-Sanchez, M.; Lercher, J. A., Activity of Cu–Al–Oxo Extra-Framework Clusters for Selective Methane Oxidation on Cu-Exchanged Zeolites. *JACS Au* **2021**, *1*, 1412-1421. http://dx.doi.org/10.1021/jacsau.1c00196. (Solely Funded)
35. Lin, F.; Wang, H.; Zhao, Y.; Fu, J.; Mei, D.; Jaegers, N. R.; Gao, F.; Wang, Y., Elucidation of Active Sites in Aldol Condensation of Acetone over Single-Facet Dominant Anatase TiO_2 (101) and (001) Catalysts. *JACS Au* **2021**, *1*, 41-52. http://dx.doi.org/10.1021/jacsau.0c00028. (Solely Funded.)
36. Liu, Y.; Cheng, G.; Baráth, E.; Shi, H.; Lercher, J. A., Alkylation of Lignin-Derived Aromatic Oxygenates with Cyclic Alcohols on Acidic Zeolites. *Appl. Catal. B* **2021**, *281*, 119424. http://dx.doi.org/https://doi.org/10.1016/j.apcatb.2020.119424. (Solely funded)

37. Mayberry, D. D.; Linehan, J. C.; Appel, A. M., Designing Catalytic Systems Using Binary Solvent Mixtures: Impact of Mole Fraction of Water on Hydride Transfer. *Inorg. Chem.* **2021**, *60*, 17132-17140. http://dx.doi.org/10.1021/acs.inorgchem.1c02397. (Solely funded)
38. Milaković, L.; Hintermeier, P. H.; Liu, Y.; Baráth, E.; Lercher, J. A., Influence of Intracrystalline Ionic Strength in Mfi Zeolites on Aqueous Phase Dehydration of Methylcyclohexanols. *Angew. Chem. Int. Ed.* **2021**, *60*, 1-6. http://dx.doi.org/https://doi.org/10.1002/anie.202107947. (Solely Funded)
39. Peng, G.; Xu, L.; Glezakou, V.-A.; Mavrikakis, M., Mechanism of Methanol Synthesis on Ni(110). *Catal. Sci. Technol.* **2021**, *11*, 3279-3294. http://dx.doi.org/10.1039/D1CY00107H. (Soley funded)
40. Persaud, R. R.; Fang, Z.; Zall, C. M.; Appel, A. M.; Dixon, D. A., Computational Study of Triphosphine-Ligated Cu(I) Catalysts for Hydrogenation of Co2 to Formate. *J. Phys. Chem. A* **2021**, *125*, 6600-6610. http://dx.doi.org/10.1021/acs.jpca.1c04050. (Solely funded)
41. Speelman, A. L.; Tran, B. L.; Erickson, J. D.; Vasiliu, M.; Dixon, D. A.; Bullock, R. M., Accelerating the Insertion Reactions of (Nhc)Cu–H Via Remote Ligand Functionalization. *Chem. Sci. J.* **2021**, *12*, 11495-11505. http://dx.doi.org/10.1039/D1SC01911B. (Solely Funded)
42. Sudduth, B.; Yun, D. M.; Sun, J. M.; Wang, Y., Facet-Dependent Selectivity of Ceo_2 Nanoparticles in 2-Propanol Conversion. *J. Catal.* **2021**, *404*, 96-108. http://dx.doi.org/10.1016/j.jcat.2021.09.009. (Solely Funded)
43. Wiedner, E. S.; Preston, A. Z.; Helm, M. L.; Appel, A. M., Thermodynamic Trends for Reduction of CO by Molecular Complexes. *Organometallics* **2021**, *40*, 2039-2050. http://dx.doi.org/10.1021/acs.organomet.1c00178. (Solely Funded.)
44. Wu, Y.; Gao, F.; Wang, H.; Kovarik, L.; Sudduth, B.; Wang, Y., Probing Acid–Base Properties of Anatase TiO_2 Nanoparticles with Dominant {001} and {101} Facets Using Methanol Chemisorption and Surface Reactions. *J. Phys. Chem. C* **2021**, *125*, 3988-4000. http://dx.doi.org/10.1021/acs.jpcc.0c11107. (Solely funded.)
45. Xin, H.; Liu, Y.; Hu, C.; Lercher, J. A., Electronic Impact of Ni2p Nanoparticle Size on Hydrogenation Rates. *J. Catal.* **2021**, *401*, 129-136. http://dx.doi.org/https://doi.org/10.1016/j.jcat.2021.07.017. (Solely Funded)
46. Xu, S.; Jaegers, N. R.; Hu, W.; Kwak, J. H.; Bao, X.; Sun, J.; Wang, Y.; Hu, J. Z., High-Field One-Dimensional and Two-Dimensional ^{27}al Magic-Angle Spinning Nuclear Magnetic Resonance Study of Θ-, Δ-, and Γ-Al_2o_3 Dominated Aluminum Oxides: Toward Understanding the Al Sites in Γ-Al_2o_3. *ACS Omega* **2021**, *6*, 4090-4099. http://dx.doi.org/10.1021/acsomega.0c06163. (Solely funded)
47. Yang, G.; Maliekkal, V.; Chen, X.; Eckstein, S.; Shi, H.; Camaioni, D. M.; Baráth, E.; Haller, G. L.; Liu, Y.; Neurock, M.; Lercher, J. A., Rate Enhancement of Phenol Hydrogenation on Pt by Hydronium Ions in the Aqueous Phase. *J. Catal.* **2021**, *404*, 579-593. http://dx.doi.org/https://doi.org/10.1016/j.jcat.2021.11.003. (Solely Funded)
48. Yik, E.; Hibbitts, D.; Wang, H.; Iglesia, E., Hydrogenation and Cs Bond Activation Pathways in Thiophene and Tetrahydrothiophene Reactions on Sulfur-Passivated Surfaces of Ru, Pt, and Re Nanoparticles. *Appl. Catal. B: Environ.* **2021**, *291*, 119797. http://dx.doi.org/https://doi.org/10.1016/j.apcatb.2020.119797. (Solely funded)

49. Zhu, Y. F.; Yuk, S. F.; Zheng, J.; Nguyen, M. T.; Lee, M. S.; Szanyi, J.; Kovarik, L.; Zhu, Z. H.; Balasubramanian, M.; Glezakou, V. A.; Fulton, J. L.; Lercher, J. A.; Rousseau, R.; Gutierrez, O. Y., Environment of Metal-O-Fe Bonds Enabling High Activity in Co_2 Reduction on Single Metal Atoms and on Supported Nanoparticles. *J. Am. Chem. Soc.* **2021**, *143*, 5540-5549. http://dx.doi.org/10.1021/jacs.1c02276. (Solely Funded)

2022

50. Carroll, T. G.; Ryan, D. E.; Erickson, J. D.; Bullock, R. M.; Tran, B. L., Isolation of a Cu–H Monomer Enabled by Remote Steric Substitution of a N-Heterocyclic Carbene Ligand: Stoichiometric Insertion and Catalytic Hydroboration of Internal Alkenes. *J. Am. Chem. Soc.* **2022**, *144*, 13865-13873. http://dx.doi.org/10.1021/jacs.2c05376. (Solely funded)
51. Kadam, S. A.; Hwang, A.; Iglesia, E., Consequences of Intrapore Liquids on Reactivity, Selectivity, and Stability for Aldol Condensation Reactions on Anatase TiO_2 Catalysts. *ChemCatChem* **2022**, *14*, e202200059. http://dx.doi.org/https://doi.org/10.1002/cctc.202200059. (Solely Funded)
52. Khare, R.; Weindl, R.; Jentys, A.; Reuter, K.; Shi, H.; Lercher, J. A., Di- and Tetrameric Molybdenum Sulfide Clusters Activate and Stabilize Dihydrogen as Hydrides. *JACS Au* **2022**, *2*, 613-622. http://dx.doi.org/10.1021/jacsau.1c00507. (Solely Funded)
53. Li, H.; Hurlock, M. J.; Sudduth, B.; Li, J.; Sun, J.; Zhang, Q.; Wang, Y., Acetone to Isobutene Conversion on $Zn_xti_yo_z$: Effects of TiO_2 Facet. *J. Catal.* **2022**, *410*, 236-245. http://dx.doi.org/10.1016/j.jcat.2022.03.031. (Solely Funded)
54. Meyer, L. C.; Sanyal, U.; Stoerzinger, K. A.; Koh, K.; Fulton, J. L.; Camaioni, D. M.; Gutierrez, O. Y.; Lercher, J. A., Influence of the Molecular Structure on the Electrocatalytic Hydrogenation of Carbonyl Groups and H-2 Evolution on Pd. *ACS Catal.* **2022**, *12*, 11910-11917. http://dx.doi.org/10.1021/acscatal.2c03207. (Solely Funded)
55. Schmid, J.; Wang, M.; Gutiérrez, O. Y.; Bullock, R. M.; Camaioni, D. M.; Lercher, J. A., Controlling Reaction Routes in Noble-Metal-Catalyzed Conversion of Aryl Ethers. *Angew. Chem. Int. Ed.* **2022**, *n/a*, e202203172. http://dx.doi.org/https://doi.org/10.1002/anie.202203172. (Solely Funded)
56. Sharp, M. A.; Lee, C. J.; Mahapatra, M.; Smith, R. S.; Kay, B. D.; Dohnálek, Z., Preparation and Characterization of Model Homotopic Catalysts: Rh Adatoms, Nanoparticles, and Mixed Oxide Surfaces on Fe_3o_4(001). *The Journal of Physical Chemistry C* **2022**, *126*, 14448-14459. http://dx.doi.org/10.1021/acs.jpcc.2c03426. (Solely funded)
57. Sudduth, B.; Sun, J.; Wang, Y., Chemical Grafting of Highly Dispersed Vox/Ceo_2 for Increased Catalytic Activity in Methanol Oxidative Dehydrogenation. *Catal. Lett.* **2022**, *152*, 2980-2992. http://dx.doi.org/10.1007/s10562-021-03862-8. (Solely funded)

2023

58. Hu, Y.; Fang, Z.; Vasiliu, M.; Dixon, D. A., Computational Study of Dehydration and Dehydrogenation of Ethanol on $(TiO_2)_N$ (N = 2–4) Nanoclusters. *J. Phys. Chem. A* **2023**. http://dx.doi.org/10.1021/acs.jpca.3c00776. (Solely Funded)
59. Lin, F.; Hu, W.; Jaegers, N. R.; Gao, F.; Hu, J. Z.; Wang, H.; Wang, Y., Elucidation of the Roles of Water on the Reactivity of Surface Intermediates in Carboxylic Acid Ketonization on TiO_2. *J. Am. Chem. Soc.* **2023**, *145*, 99-109. http://dx.doi.org/10.1021/jacs.2c08511. (Solely Funded)
60. Ma, R. Z.; O'Connor, C. R.; Collinge, G.; Allec, S. I.; Lee, M. S.; Dohnalek, Z., The Role of Surface Hydroxyls in the Mobility of Carboxylates on Surfaces: Dynamics of Acetate

on Anatase TiO_2(101). *J. Phys. Chem. Lett.* **2023**, *14*, 2542-2550. http://dx.doi.org/10.1021/acs.jpclett.3c00175. (Solely Funded)
61. O'Connor, C. R.; Ma, R.; Collinge, G.; Lee, M.-S.; Kimmel, G. A.; Dohnálek, Z., Insights into Acetic Acid Binding and Ketene Formation on Anatase TiO_2(101). *Top. Catal.* **2023**. http://dx.doi.org/10.1007/s11244-023-01828-1. (Solely Funded)
62. Patrick, E. A.; Bowden, M. E.; Erickson, J. D.; Bullock, R. M.; Tran, B. L., Single-Crystal to Single-Crystal Transformations: Stepwise Co_2 Insertions into Bridging Hydrides of [(Nhc)Cuh]2 Complexes. *Angew. Chem. Int. Ed.* **2023**, *n/a*, e202304648. http://dx.doi.org/10.1002/anie.202304648. (Solely Funded)
63. Rupprechter, G.; Dohnalek, Z.; Volpe, A. F., Preface to "from Coadsorption and Catalysis at Solid Surfaces to Liquid-Solid Interfaces in Theory and Experiment, Published in Honor of Professor Robert K. Grasselli, Irsee Ix Symposium Kloster Irsee, Germany 16-19 June 2022 (Irsee Ix)". *Top. Catal.* **2023**. http://dx.doi.org/10.1007/s11244-023-01858-9. (Solely Funded)
64. Tran, B. L.; Erickson, J. D.; Speelman, A. L.; Bullock, R. M., Mechanistic Studies of Carbonyl Allylation Mediated by (Nhc)Cuh: Isoprene Insertion, Allylation, and B-Hydride Elimination. *Inorg. Chem.* **2023**, *62*, 342-352. http://dx.doi.org/10.1021/acs.inorgchem.2c03402. (Solely Funded)
65. Tian, J.; Collinge, G.; Yuk, S. F.; Lin, J.; Glezakou, V.-A.; Lee, M.-S.; Wang, Y.; Rousseau, R., Dynamically Formed Active Sites on Liquid Boron Oxide for Selective Oxidative Dehydrogenation of Propane. *ACS Catal.* **2023**, *13*, 8219-8236. http://dx.doi.org/10.1021/acscatal.3c01759. (Solely Funded)

Publications jointly funded by this grant and other grants with leading intellectual contributions from this grant.

2020

66. Barnett, K. L.; Vasiliu, M.; Stein, T. H.; Delahay, M. V.; Qu, F.; Gerlach, D. L.; Dixon, D. A.; Shaughnessy, K. H., Experimental and Computational Study of the Structure, Steric Properties, and Binding Equilibria of Neopentylphosphine Palladium Complexes. *Inorg. Chem.* **2020**, *59*, 5579-5592. http://dx.doi.org/10.1021/acs.inorgchem.0c00266. (DA Dixon, TH Stein, and M. Vasiliu were supported by this program for all the computational work and manuscript writing.)
67. Bowden, M. E.; Ginovska, B.; Jones, M. O.; Karkamkar, A. J.; Ramirez-Cuesta, A. J.; Daemen, L. L.; Schenter, G. K.; Miller, S. A.; Repo, T.; Chernichenko, K.; Leick, N.; Martinez, M. B.; Autrey, T., Heterolytic Scission of Hydrogen within a Crystalline Frustrated Lewis Pair. *Inorg. Chem.* **2020**, *59*, 15295-15301. http://dx.doi.org/10.1021/acs.inorgchem.0c02290. (Leading, M.E.B., B.G., A.J.K., G.K.S., and T.A. acknowledge support from this FWP.)
68. Bramley, G.; Nguyen, M.-T.; Glezakou, V.-A.; Rousseau, R.; Skylaris, C.-K., Reconciling Work Functions and Adsorption Enthalpies for Implicit Solvent Models: A Pt (111)/Water Interface Case Study. *J. Chem. Theory Comput.* **2020**, *16*, 2703-2715. http://dx.doi.org/10.1021/acs.jctc.0c00034. (Leading, V.-A.G., M.-T.N., and R.R. were supported by this program.)
69. Confer, M. P.; Allayarov, S. R.; Kim, I. P.; Markin, I. V.; Jackson, V. E.; Dixon, D. A., Direct Fluorination of Tetrafluoroethylene at Low Temperatures. *J. Fluorine Chem.*

2020, *232*, 109493. http://dx.doi.org/10.1016/j.jfluchem.2020.109493. (DA Dixon and M. P. Confer supported by this proposal for all of the computational work and writing the manuscript.)

70. Donaubauer, P. J.; Melzer, D. M.; Wanninger, K.; Mestl, G.; Sanchez-Sanchez, M.; Lercher, J. A.; Hinrichsen, O., Intrinsic Kinetic Model for Oxidative Dehydrogenation of Ethane over Movtenb Mixed Metal Oxides: A Mechanistic Approach. *Chem. Eng. J.* **2020**, *383*, 123195. http://dx.doi.org/https://doi.org/10.1016/j.cej.2019.123195. (J.A. Lercher was funded by this FWP for planning, interpretation of data, and writing of the manuscript.)
71. Ehrmaier, A.; Löbbert, L.; Sanchez-Sanchez, M.; Bermejo-Deval, R.; Lercher, J., Impact of Alkali and Alkali-Earth Cations on Ni-Catalyzed Dimerization of Butene. *ChemCatChem* **2020**, *12*, 3705-3711. http://dx.doi.org/10.1002/cctc.202000349. (J.A. Lercher was supported by this program for discussion of the results and leading the work.)
72. Jaegers, N. R.; Mueller, K. T.; Wang, Y.; Hu, J. Z., Variable Temperature and Pressure Operando Mas Nmr for Catalysis Science and Related Materials. *Acc. Chem. Res.* **2020**, *53*, 611-619. http://dx.doi.org/10.1021/acs.accounts.9b00557. (Major support by the BES program for the review of the catalyst applications.)
73. Laureanti, J. A.; Ginovska, B.; Buchko, G. W.; Schenter, G. K.; Hebert, M.; Zadvornyy, O. A.; Peters, J. W.; Shaw, W. J., A Positive Charge in the Outer Coordination Sphere of an Artificial Enzyme Increases Co_2 Hydrogenation. *Organometallics* **2020**, *39*, 1532-1544. http://dx.doi.org/10.1021/acs.organomet.9b00843. (Jointly funded lead contribution by this program. JWP was partially supported by the USDA National Institute of Food and Agriculture.)
74. Lu, Y. B.; Zhang, Z. H.; Lin, F.; Wang, H. M.; Wang, Y., Single-Atom Automobile Exhaust Catalysts. *ChemNanoMat* **2020**, 1659-1682. http://dx.doi.org/10.1002/cnma.202000407. (Leading, H.W. was supported by this FWP.)
75. Marcinkowski, M. D.; Adamsen, K. C.; Doudin, N.; Sharp, M. A.; Smith, R. S.; Wang, Y.; Wendt, S.; Lauritsen, J. V.; Parkinson, G. S.; Kay, B. D.; Dohnálek, Z., Adsorption and Reaction of Methanol on Fe_3o_4(001). *J. Chem. Phys.* **2020**, *152*, 064703. http://dx.doi.org/10.1063/1.5139418. (Leading, MDM, ND, MAS, RSS, YW, BDK, and ZD were funded by this program. MDM, ND, MAS, and YW acquired the data, carried out the analysis, and participated in preparing the manuscript. ZD, RSS, and BDK contributed to data analysis and manuscript preparation.)
76. Rousseau, R.; Glezakou, V.-A.; Selloni, A., Theoretical Insights into the Surface Physics and Chemistry of Redox-Active Oxides. *Nat. Rev. Mater.* **2020**, *5*, 460-475. http://dx.doi.org/10.1038/s41578-020-0198-9. (R.R. and V.A.G. partially supported by the program, R.R's major contribution to the writing, A.S. funded by the program at Princeton.)
77. Saal, T.; Blastik, Z. E.; Haiges, R.; Nirmalchandar, A.; Baxter, A. F.; Christe, K. O.; Vasiliu, M.; Dixon, D. A.; Beier, P.; Prakash, G. K. S., Protonation of Ch_3n_3 and Cf_3n_3 in Superacids: Isolation and Structural Characterization of Long-Lived Methyl- and Trifluoromethylamino Diazonium Ions. *Angew. Chem. Int. Ed.* **2020**, *59*. http://dx.doi.org/10.1002/anie.202002750. (DA Dixon and M. Vasiliu supported by this program for all the computational work and manuscript writing.)

78. Shreiber, S. T.; Kaplan, P. T.; Hughes, R. P.; Vasiliu, M.; Dixon, D. A.; Cramer, R. E.; Vicic, D. A., Syntheses, Solution Behavior, and Computational Bond Length Analyses of Trifluoromethyl and Perfluoroethyl Cuprate Salts. *J. Fluorine Chem.* **2020**, *234*, 109518. http://dx.doi.org/10.1016/j.jfluchem.2020.109518. (DA Dixon and M. Vasiliu supported by this proposal for all of the computational work and writing the manuscript.)
79. Singh, N.; Sanyal, U.; Ruehl, G.; Stoerzinger, K. A.; Gutiérrez, O. Y.; Camaioni, D. M.; Fulton, J. L.; Lercher, J. A.; Campbell, C. T., Aqueous Phase Catalytic and Electrocatalytic Hydrogenation of Phenol and Benzaldehyde over Platinum Group Metals. *J. Catal.* **2020**, *382*, 372-384. http://dx.doi.org/10.1016/j.jcat.2019.12.034. (D.M. Camaioni, J.L. Fulton, and J.A. Lercher were funded by this FWP. D. Camaioni and J.L. Fulton were supported by this program for supporting data analysis and interpretation of spectroscopic experiments. J.A. Lercher was supported by this program for planning and interpretation of data)
80. Tran, B. L.; Neisen, B. D.; Speelman, A. L.; Gunasekara, T.; Wiedner, E. S.; Bullock, R. M., Mechanistic Studies on the Insertion of Carbonyl Substrates into Cu-H: Different Rate-Limiting Steps as a Function of Electrophilicity. *Angew. Chem. Int. Ed.* **2020**, *59*, 8645-8653. http://dx.doi.org/10.1002/anie.201916406. (Lead contributions. B.L.T., B.D.N., A.L.S., E.S.W. support by DOE BES and R.M.B. T.G. was supported as part of the Center for Molecular Electrocatalysis, an Energy Frontier Research Center funded by the U.S. Department of Energy)
81. Wang, Y.; Wen, B.; Dahal, A.; Kimmel, G. A.; Rousseau, R.; Selloni, A.; Petrik, N. G.; Dohnalek, Z., Binding of Formic Acid on Anatase TiO_2(101). *J. Phys. Chem. C* **2020**, *124*, 20228-20239. http://dx.doi.org/10.1021/acs.jpcc.0c06031. (All experimental studies (YW, AD, GAK, NGP, and ZD) and theoretical contributions by RR were funded by this program.)
82. Zhang, S. G.; Li, H. X.; Appel, A. M.; Hall, M. B.; Bullock, R. M., Controlling P-C/C-H Bond Cleavage in Nickel Bis(Diphosphine) Complexes: Reactivity Scope, Mechanism, and Computations. *Organometallics* **2020**, *39*, 3306-3314. http://dx.doi.org/10.1021/acs.organomet.0c00388. (Leading, Zhang, Appel, and Bullock were supported by this project for experimental work, data analysis, and manuscript writing.)
83. Zheng, J.; Lee, I.; Khramenkova, E.; Wang, M.; Peng, B.; Gutierrez, O.; Fulton, J. L.; Camaioni, D.; Khare, R.; Jentys, A.; Haller, G.; Pidko, E.; Sanchez-Sanchez, M.; Lercher, J., Importance of Methane Chemical Potential for Its Conversion to Methanol on Cu-Exchanged Mordenite. *Chem. Eur. J.* **2020**, *26*, 7563-7567. http://dx.doi.org/10.1002/chem.202000772. (J. Zheng, M. Wang, B. Peng, O.Y. Gutierrez, J.L. Fulton, and D.M. Camaioni were funded by this FWP. J. Zheng, M. Wang, and B. Peng were supported by this program for the experimental work and writing of the first drafts. O.Y. Gutierrez, J.L. Fulton, and D. Camaioni were supported by this program for supporting data analysis and writing of the manuscript)
84. Zhu, Y.; Zheng, J.; Ye, J.; Cui, Y.; Koh, K.; Kovarik, L.; Camaioni, D. M.; Fulton, J. L.; Truhlar, D. G.; Neurock, M.; Cramer, C. J.; Gutiérrez, O. Y.; Lercher, J. A., Copper-Zirconia Interfaces in UiO-66 Enable Selective Catalytic Hydrogenation of Co_2 to Methanol. *Nat. Commun.* **2020**, *11*, 5849. http://dx.doi.org/10.1038/s41467-020-19438-w. (Jointly funded. Y.Z., L.K., D.M.C., J.F., and O. Y.G. acknowledge support from this project)

85. Zhu, Y. F.; Zhang, X.; Koh, K.; Kovarik, L.; Fulton, J. L.; Rosso, K. M.; Gutierrez, O. Y., Inverse Iron Oxide/Metal Catalysts from Galvanic Replacement. *Nat. Commun.* **2020**, *11*, 3269. http://dx.doi.org/10.1038/s41467-020-16830-4. (Y. Zhu, L. Kovarik, J.L. Fulton, and O.Y. Gutierrez were supported by this program for leading the work and performing kinetic and characterization experiments)

2021

86. Deng, F.; Huang, J.; Ember, E. E.; Achterhold, K.; Dierolf, M.; Jentys, A.; Liu, Y.; Pfeiffer, F.; Lercher, J. A., On the Mechanism of Catalytic Decarboxylation of Carboxylic Acids on Carbon-Supported Palladium Hydride. *ACS Catal.* **2021**, 14625-14634. http://dx.doi.org/10.1021/acscatal.1c03869. (Leading, J.A.L. was supported by this program)
87. Dey, A.; Houle, F. A.; Lubner, C. E.; Sevilla, M.; Shaw, W. J., Introduction to (Photo)Electrocatalysis for Renewable Energy. *Chem. Commun.* **2021**, *57*, 1540-1542. http://dx.doi.org/10.1039/D0CC90530E. (WJS acknowledges support by this FWP)
88. Giustra, Z. X.; Chen, G.; Vasiliu, M.; Karkamkar, A.; Autrey, T.; Dixon, D. A.; Liu, S.-Y., A Comparison of Hydrogen Release Kinetics from 5- and 6-Membered 1,2-Bn-Cycloalkanes. *RSC Adv.* **2021**, *11*, 34132-34136. http://dx.doi.org/10.1039/D1RA07477F. (Leading, Computational, DAD, Vasiliu funded by this FWP)
89. Kim, Y.; Collinge, G.; Lee, M.-S.; Khivantsev, K.; Cho, S. J.; Glezakou, V.-A.; Rousseau, R.; Szanyi, J.; Kwak, J. H., Surface Density Dependent Catalytic Activity of Single Palladium Atoms Supported on Ceria. *Angew. Chem. Int. Ed.* **2021**. http://dx.doi.org/https://doi.org/10.1002/anie.202105750. (Major contribution from the BES Catalysis Program; Multiple PIs from both theory and experiment)
90. Li, H.; Guo, D.; Ulumuddin, N.; Jaegers, N. R.; Sun, J.; Peng, B.; McEwen, J.-S.; Hu, J.; Wang, Y., Elucidating the Cooperative Roles of Water and Lewis Acid–Base Pairs in Cascade C–C Coupling and Self-Deoxygenation Reactions. *JACS Au* **2021**, *1*, 1471-1487. http://dx.doi.org/10.1021/jacsau.1c00218. (Leading)
91. Petrik, N. G.; Wang, Y.; Wen, B.; Wu, Y.; Ma, R.; Dahal, A.; Gao, F.; Rousseau, R.; Wang, Y.; Kimmel, G. A.; Selloni, A.; Dohnálek, Z., Conversion of Formic Acid on Single- and Nano-Crystalline Anatase TiO_2(101). *J. Phys. Chem. C* **2021**, *125*, 7686-7700. http://dx.doi.org/10.1021/acs.jpcc.1c00571. (N.G.P., Ya.W., Yi.W., R.M., A.D., F.G., R.R., Yo.W., G.A.K., and Z.D. were supported by this project)
92. Pfriem, N.; Liu, Y.; Zahn, F.; Shi, H.; Haller, G. L.; Lercher, J. A., Impact of the Local Concentration of Hydronium Ions at Tungstate Surfaces for Acid-Catalyzed Alcohol Dehydration. *J. Am. Chem. Soc.* **2021**, *143*, 20133-20143. http://dx.doi.org/10.1021/jacs.1c07203. (Leading, J.A.L. was supported by this FWP)
93. Yao, Y.; Wu, X.; Chen, B.; Tu, Z.; Gutiérrez, O. Y.; Cui, Y.; Wang, J.; Huang, J.; Xu, Y.; Sun, H.; Chen, H.; Yan, Z.; Mei, D.; Zhao, Y.; Lercher, J. A., Copper-Based Catalysts Confined in Carbon Nanocage Reactors for Condensed Ester Hydrogenation: Tuning Copper Species by Confined Sio2 and Methanol Resistance. *ACS Sustain. Chem. Eng.* **2021**, *9*, 16270-16280. http://dx.doi.org/10.1021/acssuschemeng.1c05526. (Leading, O.Y.G. and J.A.L. were supported by this FWP for contributing to the discussion of the results, planning, and writing of the manuscript.)

2022

94. Chalek, C. L.; Gole, J. L.; Dixon, D. A., Excited Electronic State Cross Sections for Group 3 Halide and Oxide Production: Evaluating Relative Excited-State Quantum

Yields. *J. Phys. Chem. A* **2022**, *126*, 3427-3432. http://dx.doi.org/10.1021/acs.jpca.2c01780. (Leading computational, DAD funded by this FWP)
95. Chen, L.; Kovarik, L.; Meira, D.; Szanyi, J., Differentiating and Understanding the Effects of Bulk and Surface Mo Doping on Co_2 Hydrogenation over Pd/Anatase-TiO_2. *ACS Catal.* **2022**, *12*, 13492-13500. http://dx.doi.org/10.1021/acscatal.2c03181. (Leading, J.S. and his team were supported by this FWP)
96. Chen, L.; Meyer, L. C.; Kovarik, L.; Meira, D.; Pereira-Hernandez, X. I.; Shi, H.; Khivantsev, K.; Gutiérrez, O. Y.; Szanyi, J., Disordered, Sub-Nanometer Ru Structures on Ceo2 Are Highly Efficient and Selective Catalysts in Polymer Upcycling by Hydrogenolysis. *ACS Catal.* **2022**, *12*, 4618-4627. http://dx.doi.org/10.1021/acscatal.2c00684. (Leading, J.S. and hid team were supported by this FWP)
97. Chen, L.; Zhu, Y.; Meyer, L. C.; Hale, L. V.; Le, T. T.; Karkamkar, A.; Lercher, J. A.; Gutiérrez, O. Y.; Szanyi, J., Effect of Reaction Conditions on the Hydrogenolysis of Polypropylene and Polyethylene into Gas and Liquid Alkanes. *React. Chem. Eng.* **2022**, *7*, 844-854. http://dx.doi.org/10.1039/D1RE00431J. (Leading, J.S. and hid team were supported by this FWP)
98. Cheng, G.; Zhang, W.; Jentys, A.; Ember, E. E.; Gutiérrez, O. Y.; Liu, Y.; Lercher, J. A., Importance of Interface Open Circuit Potential on Aqueous Hydrogenolytic Reduction of Benzyl Alcohol over Pd/C. *Nat. Commun.* **2022**, *13*, 7967. http://dx.doi.org/10.1038/s41467-022-35554-1. (Leading, J.A.L. was supported by this FWP)
99. Confer, M. P.; Qu, T.; Rupar, P. A.; Dixon, D. A., Composite Correlated Molecular Orbital Theory Calculations of Ring Strain for Use in Predicting Polymerization Reactions. *ChemPhysChem* **2022**, *23*, e202200133. http://dx.doi.org/https://doi.org/10.1002/cphc.202200133. (Leading computational, DAD, Confer funded by this FWP)
100. Devore, T. C.; Wang, H.; Winstead, C. B.; Gole, J. L.; Hu, Y.; Dixon, D. A., Electronically Excited Complex Formation in Magnesium Cluster–Halogen Atom Reactions. *J. Phys. Chem. A* **2022**, *126*, 1848-1860. http://dx.doi.org/10.1021/acs.jpca.2c00196. (Leading computational, DAD, Hu funded by this FWP)
101. Genc, A.; Kovarik, L.; Fraser, H. L., A Deep Learning Approach for Semantic Segmentation of Unbalanced Data in Electron Tomography of Catalytic Materials. *Sci. Rep.* **2022**, *12*, 16267. http://dx.doi.org/10.1038/s41598-022-16429-3. (Leading, L.K. conceived and led this work. Supported by this FWP)
102. Gole, J. L.; Chalek, C. L.; Mason, M. M.; de Melo, G. F.; Vasiliu, M.; Dixon, D. A., Observation of Selectively Populated Monohalide Excited States from the Reactions of Group 3 Metal (Sc, Y, and La) Monomers and Dimers with Halogen-Containing Molecules. *J. Phys. Chem. A* **2022**, *126*, 3403-3426. http://dx.doi.org/10.1021/acs.jpca.2c01779. (Leading computational, DAD, Mason, de Melo, Vasiliu funded by this FWP)
103. Grakovich, P. N.; Allayarov, S. R.; Confer, M. P.; Kalinin, L. A.; Frolov, I. A.; Rudneva, T. N.; Ivanov, L. F.; Dixon, D. A., Infrared Laser Ablation of Poly(Vinylidene Fluoride): The Loss of Hf. *J. Fluorine Chem.* **2022**, *255-256*, 109947. http://dx.doi.org/10.1016/j.jfluchem.2022.109947. (Leading computational, DAD, Confer funded by this FWP)

104. Hu, W.; Jaegers, N. R.; Winkelman, A. D.; Murali, S.; Mueller, K. T.; Wang, Y.; Hu, J. Z., Modelling Complex Molecular Interactions in Catalytic Materials for Energy Storage and Conversion in Nuclear Magnetic Resonance. *Front. Catal.* **2022**, *2*. http://dx.doi.org/10.3389/fctls.2022.935174. (Leading, the review on Catalysts was supported by this FWP)
105. Khivantsev, K.; Jaegers, N. R.; Kovarik, L.; Derewinski, M. A.; Kwak, J. H.; Szanyi, J., On the Nature of Extra-Framework Aluminum Species and Improved Catalytic Properties in Steamed Zeolites. *Molecules* **2022**, *27*, Art. No. 2352. http://dx.doi.org/10.3390/molecules27072352. (Leading)
106. Makoś, M. Z.; Gurunathan, P. K.; Raugei, S.; Kowalski, K.; Glezakou, V.-A.; Rousseau, R., Modeling Absolute Redox Potentials of Ferrocene in the Condensed Phase. *J. Phys. Chem. Lett.* **2022**, *13*, 10005-10010. http://dx.doi.org/10.1021/acs.jpclett.2c02447. (Leading, MZM, PKG, VAG, and RR were funded by this FWP.)
107. Milakovic, L.; Liu, Y.; Barath, E.; Lercher, J. A., Dehydration of Fatty Alcohols on Zirconia Supported Tungstate Catalysts. *Catal. Sci. Technol.* **2022**, *12*, 6084-6091. http://dx.doi.org/10.1039/d2cy00785a. (Leading, J.A.L. was supported by this FWP)
108. Ni, L.; Khare, R.; Bermejo-Deval, R.; Zhao, R.; Tao, L.; Liu, Y.; Lercher, J. A., Highly Active and Selective Sites for Propane Dehydrogenation in Zeolite Ga-Bea. *J. Am. Chem. Soc.* **2022**, *144*, 12347-12356. http://dx.doi.org/10.1021/jacs.2c03810. (Leading, J.A.L. was suported by this FWP)
109. Piccini, G. M.; Lee, M. S.; Yuk, S. F.; Zhang, D. F.; Collinge, G.; Kollias, L.; Nguyen, M. T.; Glezakou, V. A.; Rousseau, R., Ab Initio Molecular Dynamics with Enhanced Sampling in Heterogeneous Catalysis. *Catalysis Science & Technology* **2022**, *12*, 12-37. http://dx.doi.org/10.1039/d1cy01329g. (Leading, GMP, MSL, MTN, LK, and VAG acknowledge support from this FWP)
110. Vasiliu, M.; Edwards, K. C.; Tapu, D.; Castillo, C. E.; Stein, T. H.; Craciun, R.; Arduengo, A. J.; Dixon, D. A., Bond Dissociation Energies of Carbene–Carbene and Carbene–Main Group Adducts. *J. Phys. Chem. A* **2022**, *126*, 2658-2669. http://dx.doi.org/10.1021/acs.jpca.2c00921. (Leading, DAD, Edwards, Castillo, Stein, Craciun funded by this FWP)
111. Vij, A.; Wilson, W. W.; Haiges, R.; Edwards, K. C.; Dixon, D. A.; Christe, K. O., Fluoro-Nitrogen Cations. *Angew. Chem. Int. Ed.* **2022**, *61*, e202116565. http://dx.doi.org/https://doi.org/10.1002/anie.202116565. (Leading computational, DAD, Edwards supported by this FWP)
112. Yu, I. K. M.; Deng, F. L.; Chen, X.; Cheng, G. H.; Liu, Y.; Zhang, W.; Lercher, J. A., Impact of Hydronium Ions on the Pd-Catalyzed Furfural Hydrogenation. *Nat. Commun.* **2022**, *13*. http://dx.doi.org/10.1038/s41467-022-34608-8. (Leading, J.A.L. was supported by this FWP)
113. Zhao, R.; Haller, G. L.; Lercher, J. A., Alkene Adsorption and Cracking on Acidic Zeolites – a Gradual Process of Understanding. *Microporous Mesoporous Mater.* **2022**, 112390. http://dx.doi.org/10.1016/j.micromeso.2022.112390. (Leading, J.A.L. was supported by this FWP)

2023

114. Chen, L.; Allec, S. I.; Nguyen, M.-T.; Kovarik, L.; Hoffman, A. S.; Hong, J.; Meira, D.; Shi, H.; Bare, S. R.; Glezakou, V.-A.; Rousseau, R.; Szanyi, J., Dynamic Evolution of Palladium Single Atoms on Anatase Titania Support Determines the Reverse Water–Gas

Shift Activity. *J. Am. Chem. Soc.* **2023**, *145*, 10847-10860. http://dx.doi.org/10.1021/jacs.3c02326. (Leading, J.S. and hid team were supported by this FWP, conceptualization, review, editing, supervision)
115. Chen, L.; Moreira, J. B.; Meyer, L. C.; Szanyi, J., Efficient and Selective Dual-Pathway Polyolefin Hydro-Conversion over Unexpectedly Bifunctional M/TiO_2-Anatase Catalysts. *Appl. Catal. B: Environ.* **2023**, *335*, 122897. http://dx.doi.org/10.1016/j.apcatb.2023.122897. (Leading, J.S. and hid team were supported by this FWP, conceptualization, review, editing, supervision)
116. Jaegers, N.; Washton, N. M.; Wang, Y.; Hu, J. Z. *High-Field Nuclear Magnetic Resonance (Nmr) Spectroscopy* in *Springer Handbook of Advanced Catalyst Characterization*; Wachs, I. E., Bañares, M. A., Eds.; Springer International Publishing: Cham, 2023; pp 757-785.
117. Liu, Q.; Pfriem, N.; Cheng, G.; Baráth, E.; Liu, Y.; Lercher, J. A., Maximum Impact of Ionic Strength on Acid-Catalyzed Reaction Rates Induced by a Zeolite Microporous Environment. *Angew. Chem. Int. Ed.* **2023**, *62*, e202208693. http://dx.doi.org/10.1002/anie.202208693. (Leading, J.A.L. was supported by this FWP)
118. Tian, J.; Collinge, G.; Yuk, S. F.; Lin, J.; Glezakou, V.-A.; Lee, M.-S.; Wang, Y.; Rousseau, R., *ACS Catal.* **2023**, *13*, 8219-8236. http://dx.doi.org/10.1021/acscatal.3c01759. (Leading, J. T., G. C. were supported by this FWP)
119. Wang, Y.; Chen, X.; Shi, H.; Lercher, J. A., Catalytic Reforming of Methane with H_2s Via Dynamically Stabilized Sulfur on Transition Metal Oxides and Sulfides. *Nat. Catal.* **2023**, *6*, 204-214. http://dx.doi.org/10.1038/s41929-023-00922-7. (Leading, J.A.L. was supported by this FWP, supervised the project, analyzed results, and was involved in writing the manuscript.)
120. Zhao, R.; Khare, R.; Zhang, Y.; Sanchez-Sanchez, M.; Bermejo-Deval, R.; Liu, Y.; Lercher, J. A., Promotion of Adsorptive and Catalytic Properties of Zeolitic Brønsted Acid Sites by Proximal Extra-Framework Si(Oh)$_X$ Groups. *Nat. Catal.* **2023**, *6*, 68-79. http://dx.doi.org/10.1038/s41929-022-00906-z. (Leading, J.A.L. was supported by this FWP, supervised the work, and guided the project.)

Publications jointly funded by this grant and other grants with relatively minor intellectual contributions from this grant.

2020

121. Braga, A. H.; Costa, N. J. S.; Philippot, K.; Gonçalves, R. V.; Szanyi, J.; Rossi, L. M., Structure and Activity of Supported Bimetallic NiPd Nanoparticles: Influence of Preparation Method on Co_2 Reduction. *Chem. Eur. J.* **2020**, *12*, 2967-2976. http://dx.doi.org/10.1002/cctc.201902329. (Minor, J. Szanyi mentored/supervised visiting student AH Braga with the DRIFTS measurements; helped with data interpretation and MS preparation)
122. Fang, Z.; Wang, L.-C.; Wang, Y.; Sikorski, E.; Tan, S.; Li-Oakey, K. D.; Li, L.; Yablonsky, G.; Dixon, D. A.; Fushimi, R., Pt-Assisted Carbon Remediation of Mo_2c Materials for CO Disproportionation. *ACS Catal.* **2020**, *10*, 1894-1911. http://dx.doi.org/10.1021/acscatal.9b05225. (Minor, DA Dixon writing manuscript)
123. Hensley, A. J. R.; deJoode, I.; Wang, Y.; McEwen, J.-S., Identifying Trends in the Field Ionization of Diatomic Molecules over Adsorbate Covered Pd(331) Surfaces. *Top. Catal.*

2020, *63*, 1510-1521. http://dx.doi.org/10.1007/s11244-020-01392-y. (A.J.R.H., I.J., and J.-S.M. were primarily funded by this FWP)
124. Koh, K.; Sanyal, U.; Lee, M.-S.; Cheng, G.; Song, M.; Glezakou, V.-A.; Liu, Y.; Li, D.; Rousseau, R.; Gutiérrez, O. Y.; Karkamkar, A.; Derewinski, M.; Lercher, J. A., Electrochemically Tunable Proton-Coupled Electron Transfer in Pd-Catalyzed Benzaldehyde Hydrogenation. *Angew. Chem. Int. Ed.* **2020**, *59*, 1501-1505. http://dx.doi.org/10.1002/anie.201912241. (O. Gutierrez and M. Derewinski were supported by this program for kinetic analysis, material synthesis, and editing of the manuscript)
125. Laureanti, J.; Brandi, J.; Offor, E.; Engel, D.; Rallo, R.; Ginovska, B.; Martinez, X.; Baaden, M.; Baker, N. A., Visualizing Biomolecular Electrostatics in Virtual Reality with Unitymol-Apbs. *Protein Sci.* **2020**, *29*, 237-246. http://dx.doi.org/10.1002/pro.3773. (Minor contribution, BG supported by this program. MB acknowledges support from the "Initiative d'Excellence" program from the French State)
126. Lee, J.; Jang, E. J.; Oh, D. G.; Szanyi, J.; Kwak, J. H., Morphology and Size of Pt on Al_2o_3: The Role of Specific Metal-Support Interactions between Pt and Al_2o_3. *J. Catal.* **2020**, *385*, 204-212. http://dx.doi.org/10.1016/j.jcat.2020.03.019. (Minor contribution: J. Szanyi assisted with data analysis and contributed to MS preparation)
127. Lee, M.-S.; Saslow, S. A.; Um, W.; Kim, D.-S.; Kruger, A. A.; Rousseau, R.; Glezakou, V.-A., Impact of Cr and Co on ^{99}tc Retention in Magnetite: A Combined Study of Ab Initio Molecular Dynamics and Experiments. *J. Hazard. Mater.* **2020**, *387*, 121721. http://dx.doi.org/10.1016/j.jhazmat.2019.121721. (R.R. and V.-A.G. were partially supported by this program.)
128. Lopez-Ruiz, J. A.; Qiu, Y.; Andrews, E.; Gutierrez, O. Y.; Holladay, J. D., Electrocatalytic Valorization into H(2)and Hydrocarbons of an Aqueous Stream Derived from Hydrothermal Liquefaction. *J. Appl. Electrochem.* **2020**, 107-118. http://dx.doi.org/10.1007/s10800-020-01452-x. (M.D. was supported by this FWP)
129. Materna, K. L.; Lalaoui, N.; Laureanti, J. A.; Walsh, A. P.; Rimgard, B. P.; Lomoth, R.; Thapper, A.; Ott, S.; Shaw, W. J.; Tian, H.; Hammarström, L., Using Surface Amide Couplings to Assemble Photocathodes for Solar Fuel Production Applications. *ACS Appl. Mater. Interfaces* **2020**, *12*, 4501-4509. http://dx.doi.org/10.1021/acsami.9b19003. (Minor. W.J.S., A.P.W., and J.A.L. were supported by the U.S. Department of Energy)
130. Polino, D.; Grifoni, E.; Rousseau, R.; Parrinello, M.; Glezakou, V.-A., How Collective Phenomena Impact Co_2 Reactivity and Speciation in Different Media. *J. Phys. Chem. A* **2020**, *124*, 3963-3975. http://dx.doi.org/10.1021/acs.jpca.9b11744. (V.-A.G. scoped the research and together with R.R. performed some of the simulations. All authors contributed to the writing of the manuscript)
131. Vollmer, M. V.; Ye, J.; Linehan, J. C.; Graziano, B. J.; Preston, A.; Wiedner, E. S.; Lu, C. C., Cobalt-Group 13 Complexes Catalyze Co_2 Hydrogenation Via a Co(−I)/Co(I) Redox Cycle. *ACS Catal.* **2020**, *10*, 2459-2470. http://dx.doi.org/10.1021/acscatal.9b03534. (Minor contribution. JC Linehan and A Preston were supported by this project to help collect and interpret high-pressure NMR spectroscopy data. ES Wiedner was supported by this project to help collect and interpret high-pressure cyclic voltammetry data)
132. Wang, S.; Li, S.; Dixon, D. A., Mechanism of Selective and Complete Oxidation in La_2o_3-Catalyzed Oxidative Coupling of Methane. *Catal. Sci. Technol.* **2020**, *10*, 2602-

2614. http://dx.doi.org/10.1039/D0CY00141D. (Minor. DA Dixon was supported by this program and helped to interpret the computational results and write the paper)
133. Wang, X.; Liu, N.; Zhang, Q.; Liang, X.; Chen, B.; Mei, D., Thermodynamic and Kinetic Roles of H_2 in Structure Evolution of Urchin-Like Co: A Density Functional Theory Study. *Particuology* **2020**, *48*, 2-12. http://dx.doi.org/10.1016/j.partic.2018.08.007. (DM was funded by this program to perform computational studies.)
134. Yao, Y.; Wu, X.; Gutiérrez, O. Y.; Ji, J.; Jin, P.; Wang, S.; Xu, Y.; Zhao, Y.; Wang, S.; Ma, X.; Lercher, J. A., Roles of Cu^+ and Cu^0 Sites in Liquid-Phase Hydrogenation of Esters on Core-Shell $Cuzn_x$@C Catalysts. *Appl. Catal. B* **2020**, *267*, 118698. http://dx.doi.org/10.1016/j.apcatb.2020.118698. (O.Y. Gutierrez and J.A. Lercher were funded by this FWP. O.Y. Gutierrez was supported by this program for contributing to the discussion of the results and writing of the manuscript; J.A. Lercher was supported by this program for discussion of the results, planning, and writing of the manuscript)
135. Zhang, J. H.; Sudduth, B.; Sun, J. M.; Wang, Y., Hydrodeoxygenation of Lignin-Derived Aromatic Oxygenates over Pd-Fe Bimetallic Catalyst: A Mechanistic Study of Direct C-O Bond Cleavage and Direct Ring Hydrogenation. *Catal. Lett.* **2020**. http://dx.doi.org/10.1007/s10562-020-03352-3. (Y.W. was partially supported by this program.)
136. Zhao, Y.; Zhu, X.; Wang, H.; Han, J.; Mei, D.; Ge, Q., Aqueous Phase Aldol Condensation of Formaldehyde and Acetone on Anatase TiO_2(101) Surface: A Theoretical Investigation. *ChemCatChem* **2020**, *12*, 1220-1229. http://dx.doi.org/10.1002/cctc.201901736. (DM was funded by this program to perform computational studies.)

2021

137. Cheng, G. H.; Jentys, A.; Gutierrez, O. Y.; Liu, Y.; Chin, Y. H.; Lercher, J. A., Critical Role of Solvent-Modulated Hydrogen-Binding Strength in the Catalytic Hydrogenation of Benzaldehyde on Palladium. *Nat. Catal.* **2021**, *4*, 976-985. http://dx.doi.org/10.1038/s41929-021-00701-2. (Minor, O.Y.G, and J.A.L. acknowledge the support for their contribution to this project)
138. Chu, Y.; Sanyal, U.; Li, X. S.; Qiu, Y.; Song, M.; Engelhard, M. H.; Davidson, S. D.; Koh, K.; Meyer, L. C.; Zheng, J.; Xie, X.; Li, D.; Liu, J.; Gutiérrez, O. Y.; Wang, Y.; Shao, Y., Tuning Proton Transfer and Catalytic Properties in Triple Junction Nanostructured Catalysts. *Nano Energy* **2021**, *86*, 106046. http://dx.doi.org/https://doi.org/10.1016/j.nanoen.2021.106046. (O.Y. Gutierrez and Y. Wang were funded by this FWP for the coordination of experimental work, interpretation of data, and writing of the manuscript)
139. Hensley, A. J. R.; Collinge, G.; Wang, Y.; McEwen, J. S., Guiding the Design of Oxidation-Resistant Fe-Based Single Atom Alloy Catalysts with Insights from Configurational Space. *J. Chem. Phys.* **2021**, *154*, 174709. http://dx.doi.org/10.1063/5.0048698. (Minor, A.J.R.H., G.C., and J.-S.M. were primarily funded by this program)
140. Lai, J.-K.; Jaegers, N. R.; Lis, B. M.; Guo, M.; Ford, M. E.; Walter, E.; Wang, Y.; Hu, J. Z.; Wachs, I. E., Structure–Activity Relationships of Hydrothermally Aged Titania-Supported Vanadium–Tungsten Oxide Catalysts for SCR of No_x Emissions with Nh_3. *ACS Catal.* **2021**, *11*, 12096-12111. http://dx.doi.org/10.1021/acscatal.1c02130. (Minor, Wang, Y. was supported by this FWP)
141. Lee, C. J.; Sharp, M. A.; Smith, R. S.; Kay, B. D.; Dohnálek, Z., Adsorption of Ethane, Ethene, and Ethyne on Reconstructed Fe_3o_4(001). *Surf. Sci.* **2021**, *714*, 121932.

http://dx.doi.org/https://doi.org/10.1016/j.susc.2021.121932. (Minor, CJL and MAS carried out the experiments and the data analysis and were supported on this program)
142. Maluf, N. E. C.; Braga, A. H.; Gothe, M. L.; Borges, L. R.; Alves, G. A. S.; Goncalves, R. V.; Szanyi, J.; Vidinha, P.; Rossi, L. M., Zeolitic-Imidazolate Framework Derived Intermetallic Nickel Zinc Carbide Material as a Selective Catalyst for Co_2 to CO Reduction at High Pressure. *Eur. J. Inorg. Chem.* **2021**, *2021*, 4521-4529. http://dx.doi.org/10.1002/ejic.202100530. (minor, J. Szanyi acknowledges the support of his work by this FWP)
143. Pfriem, N.; Hintermeier, P. H.; Eckstein, S.; Kim, S.; Liu, Q.; Shi, H.; Milakovic, L.; Liu, Y.; Haller, G. L.; Baráth, E.; Liu, Y.; Lercher, J. A., Role of the Ionic Environment in Enhancing the Activity of Reacting Molecules in Zeolite Pores. *Science* **2021**, *372*, 952-957. http://dx.doi.org/10.1126/science.abh3418. (J.A.L. was funded by this program.)
144. Sanyal, U.; Yuk, S. F.; Koh, K.; Lee, M. S.; Stoerzinger, K.; Zhang, D.; Meyer, L. C.; Lopez-Ruiz, J. A.; Karkamkar, A.; Holladay, J. D.; Camaioni, D. M.; Nguyen, M. T.; Glezakou, V. A.; Rousseau, R.; Gutiérrez, O. Y.; Lercher, J. A., Hydrogen Bonding Enhances the Electrochemical Hydrogenation of Benzaldehyde in the Aqueous Phase. *Angew. Chem. Int. Ed.* **2021**, *60*, 290-296. http://dx.doi.org/10.1002/anie.202008178. (DM Camaioni was supported by this program for writing the manuscript and as a scientific advisor. JA Lercher was supported by this program as science lead and for writing the manuscript.)
145. Shaimukhametova, I. F.; Bogdanova, S. A.; Allayarov, S. R.; Dixon, D. A., Influence of Irradiation with Helium Ions on the Surface Properties of Kynar Polyvinylidene Fluoride. *High Energ. Chem.* **2021**, *55*, 502-506. http://dx.doi.org/10.1134/s0018143921060126. (Minor, D.A.D funded by this FWP for the reviewing and editing.)
146. Shetty, M.; Wang, H.; Chen, F.; Jaegers, N.; Liu, Y.; Camaioni, D. M.; Gutiérrez, O. Y.; Lercher, J. A., Directing the Rate-Enhancement for Hydronium Ion Catalyzed Dehydration Via Organization of Alkanols in Nanoscopic Confinements. *Angew. Chem. Int. Ed.* **2021**, *60*, 2304-2311. http://dx.doi.org/https://doi.org/10.1002/anie.202009835. (D.M.C. and J.A.L. were supported by the FWP for contributing to the discussion of the results, planning, and writing of the manuscript.)
147. Weindl, R.; Khare, R.; Kovarik, L.; Jentys, A.; Reuter, K.; Shi, H.; Lercher, J. A., Zeolite-Stabilized Di- and Tetranuclear Molybdenum Sulfide Clusters Form Stable Catalytic Hydrogenation Sites. *Angew. Chem. Int. Ed.* **2021**, *60*, 9301-9305. http://dx.doi.org/https://doi.org/10.1002/anie.202015769. (Minor, J.A.L. funded by this FWP, conceptual work and structural determinations)

2022

148. Akhade, S. A.; Lee, M.-S.; Meyer, L. C.; Yuk, S. F.; Nguyen, M.-T.; Sanyal, U.; Egbert, J. D.; Gutiérrez, O. Y.; Glezakou, V.-A.; Rousseau, R., Impact of Functional Groups on the Electrocatalytic Hydrogenation of Aromatic Carbonyls to Alcohols. *Catal. Today* **2022**, *397-399*, 63-68. http://dx.doi.org/https://doi.org/10.1016/j.cattod.2021.11.047. (Minor, L.C.M. and O.Y.G. would like to acknowledge support by this FWP)
149. Arpini, B. H.; Braga, A. H.; Borges, L. R.; Vidinha, P.; Gonçalves, R. V.; Szanyi, J.; Rossi, L. M., Tuning Co2 Hydrogenation Selectivity by N-Doped Carbon Coating over Nickel Nanoparticles Supported on Sio2. *ACS Sustain. Chem. Eng.* **2022**, *10*, 2331-2342. http://dx.doi.org/10.1021/acssuschemeng.1c05847. (Minor, J.S. acknowledges the support of his work through this FWP)

150. Barth, I.; Akinola, J.; Lee, J.; Gutiérrez, O. Y.; Sanyal, U.; Singh, N.; Goldsmith, B. R., Explaining the Structure Sensitivity of Pt and Rh for Aqueous-Phase Hydrogenation of Phenol. *J. Chem. Phys.* **2022**, *156*, 104703. http://dx.doi.org/10.1063/5.0085298. (Minor, O.Y.G would like to acknowledge support by this FWP)
151. García-Vargas, C. E.; Collinge, G.; Yun, D.; Lee, M.-S.; Muravev, V.; Su, Y.-Q.; Pereira-Hernández, X. I.; Jiang, D.; Glezakou, V.-A.; Hensen, E. J. M.; Rousseau, R.; Datye, A. K.; Wang, Y., Activation of Lattice and Adatom Oxygen by Highly Stable Ceria-Supported Cu Single Atoms. *ACS Catal.* **2022**, *12*, 13649-13662. http://dx.doi.org/10.1021/acscatal.2c04001. (Minor, C.E.G.-V and G.C contributed equally. Experiments performed by C.E.G.-V, D.Y., V.M., Y-Q.S., X.I.P.H., and D.J. with computations performed by G.C. and M.-S.L. All authors collaborated on the design of the research and prep of manuscript)
152. Li, X.; Pereira-Hernandez, X. I.; Chen, Y. Z.; Xu, J.; Zhao, J. K.; Pao, C. W.; Fang, C. Y.; Zeng, J.; Wang, Y.; Gates, B. C.; Liu, J. Y., Functional Ceox Nanoglues for Robust Atomically Dispersed Catalysts. *Nature* **2022**, *611*, 284-288. http://dx.doi.org/10.1038/s41586-022-05251-6. (Minor, J.L., X.L., designed studies and synthesis work, X.I.P.-H. and Y.W. carried out CO Drifts experiments in early stages. Y.C., C.-W.P., C.-Y.F., B.C.G., J.X., J.Z. performed other experiments, X.L. and J.L. wrote the manuscript, all authors discussed and commented on the manuscript.)
153. Lin, F.; Lu, Y.; Unocic, K. A.; Habas, S. E.; Griffin, M. B.; Schaidle, J. A.; Meyer, H. M.; Wang, Y.; Wang, H., Deactivation by Potassium Accumulation on a Pt/TiO2 Bifunctional Catalyst for Biomass Catalytic Fast Pyrolysis. *ACS Catal.* **2022**, *12*, 465-480. http://dx.doi.org/10.1021/acscatal.1c02368. (Minor, Y. Lu and Y. Wang would acknowledge the financial support of this FWP related to the measurement of CO oxidation kinetics)
154. Moore, C.; Zhang, D.; Rousseau, R.; Glezakou, V.-A.; McEwen, J.-S., Determining the Adsorption Energetics of 2,3-Butanediol on Ruo_2(110): Coupling First-Principles Calculations with Global Optimizers. *Front. Energy Res.* **2022**, *9*, Art. No. 781001. http://dx.doi.org/10.3389/fenrg.2021.781001. (Minor, V-AG, RR, and DZ acknowledge funding from this FWP.)
155. Qiu, Y.; Lopez-Ruiz, J. A.; Zhu, G. M.; Engelhard, M. H.; Gutierrez, O. Y.; Holladay, J. D., Electrocatalytic Decarboxylation of Carboxylic Acids over Ruo_2 and Pt Nanoparticles. *Appl. Catal. B: Environ* **2022**, *305*. http://dx.doi.org/10.1016/j.apcatb.2021.121060. (minor, O.Y.G would like to acknowledge support by this FWP)
156. Tao, L.; Lee, I.; Khare, R.; Jentys, A.; Fulton, J. L.; Sanchez-Sanchez, M.; Lercher, J. A., Speciation of Cu-Oxo Clusters in Ferrierite for Selective Oxidation of Methane to Methanol. *Chem. Mater.* **2022**, *34*, 4355-4363. http://dx.doi.org/10.1021/acs.chemmater.1c04249. (Minor, JLF was supported by this FWP)
157. Wiedner, E. S.; Appel, A. M.; Raugei, S.; Shaw, W. J.; Bullock, R. M., Molecular Catalysts with Diphosphine Ligands Containing Pendant Amines. *Chem. Rev.* **2022**. http://dx.doi.org/10.1021/acs.chemrev.1c01001. (Minor, W.J.S. was funded by this FWP)
158. Xia, G.-J.; Lee, M.-S.; Glezakou, V.-A.; Rousseau, R.; Wang, Y.-G., Diffusion and Surface Segregation of Interstitial Ti Defects Induced by Electronic Metal–Support Interactions on a Au/TiO_2 Nanocatalyst. *ACS Catal.* **2022**, *12*, 4455-4464. http://dx.doi.org/10.1021/acscatal.2c00159. (Minor, V-A.G and R.R. were supported by this FWP)

2023

159. Chaudhary, N.; Onyango, I.; Wang, Y.; McEwen, J.-S., Determining Catalytically Relevant Surfaces through Coverage-Dependent Lattice Gas Models: Carbon Adsorption on Fe(100). *J. Phys. Chem.* **2023**, *127*, 14163-14176. http://dx.doi.org/10.1021/acs.jpcc.3c01761. (Minor, Y.W. was funded under this FWP involved in the review and editing.)
160. Chen, F.; Kim, S.; Barpaga, D.; Fulton, J. L.; Motkuri, R. K.; Gutiérrez, O. Y.; Camaioni, D. M.; Lercher, J. A., Activity of Brønsted Acid Sites in UiO-66 for Cyclohexanol Dehydration. *Top. Catal.* **2023**. http://dx.doi.org/10.1007/s11244-023-01830-7. (Minor, F.C., S.K., J.L.F., and D.M.C were funded under this FWP for reviewing and editing.)
161. Evans, P. E., Wang, Yang, Sushko, Peter, Dohnalek, Zdenek, Understanding Pd-Te Cluster Formation on WTe_2: From a Kinetically Hindered Distribution to Thermodynamically Controlled Monodispersity. *PNAS Nexus* **2023**. http://dx.doi.org/10.1093/pnasnexus/pgad212. (Minor, Y.W. was funded under the BES Catalysis Program to carry out the initial proof of concept studies.)
162. Gajardo, J.; Colmenares-Zerpa, J.; Peixoto, A. F.; Silva, D. S. A.; Silva, J. A.; Gispert-Guirado, F.; Llorca, J.; Urquieta-Gonzalez, E. A.; Santos, J. B. O.; Szanyi, J.; Sepúlveda, C.; Álvarez, M. G.; Chimentão, R. J., Revealing the Effects of High Al Loading Incorporation in the SBA-15 Silica Mesoporous Material. *J. Porous Mater.* **2023**, *30*. http://dx.doi.org/10.1007/s10934-023-01453-z. (Minor, JS conducted the IR experiments, all other authors were involved in conceptualization, methodology, investigation, writing, review, and editing.)
163. Khivantsev, K.; Derewinski, M. A.; Szanyi, J., Novel and Emerging Concepts Related to Cationic Species in Zeolites: Characterization, Chemistry and Catalysis. *Microporous Mesoporous Mater.* **2023**, *358*, 112378. http://dx.doi.org/10.1016/j.micromeso.2022.112378. (Minor, Review article, J.S. assisted in the writing and editing.)
164. Oostrom, M.; Akers, S.; Garrett, N.; Hanson, E.; Shaw, W.; Laureanti, J. A., Classifying Metal-Binding Sites with Neural Networks. *Protein Sci.* **2023**, *32*, e4591. http://dx.doi.org/10.1002/pro.4591. (Minor, M.O. and J.A.L. performed analysis, investigation, methodology, review, and editing equally, with S.A., N.G., E.H., supporting. W.S. supervision, review, and editing lead.)
165. Zhou, J.; Yang, P.; Kots, P. A.; Cohen, M.; Chen, Y.; Quinn, C. M.; de Mello, M. D.; Anibal Boscoboinik, J.; Shaw, W. J.; Caratzoulas, S.; Zheng, W.; Vlachos, D. G., Tuning the Reactivity of Carbon Surfaces with Oxygen-Containing Functional Groups. *Nat. Commun.* **2023**, *14*, 2293. http://dx.doi.org/10.1038/s41467-023-37962-3. (Minor, Y.C. performed the liquid-phase absorbed ^{15}N ACN ssNMR, and W.S. guided the liquid-phase absorbed ^{15}N ACN ssNMR.)

Designing, Developing, And Understanding Electrocatalysts and Interfaces for Energy Conversion Reactions

Thomas F. Jaramillo, Professor
Department of Chemical Engineering, Stanford University, School of Engineering
Department of Energy Science Engineering, Stanford Doerr School of Sustainability
Photon Science, SLAC National Accelerator Laboratory

Presentation Abstract

Many emerging technologies require improved electrocatalysts in order to meet technological targets for performance - efficiency, durability, etc. - needed to enable widespread commercialization. Understanding electrocatalysts and their interfaces is paramount to designing and developing improved systems. This poster will describe efforts along these lines at the SUNCAT Center for Interface Science and Catalysis. Four particular areas will be discussed: (1) New catalyst design and development, (2) Operando spectroscopy to understand catalyst dynamics, (3) Understanding electrolyte/microenvironment effects in catalysis, and (4) Co-designing catalysis and separations processes. Examples will be provided for each of these four areas. This includes (1) a systematic study involving the design, synthesis, and characterization of metal-organic frameworks (MOFs) as catalysts for the oxygen reduction reaction (ORR). (2) an operando X-ray Absorption Spectroscopy (XAS) study of Mn on the surface of a Ag-MnOx catalyst for the ORR. (3) A study of anion effects in acid electrolytes on Pt catalysts for the oxygen evolution reaction, ORR and the hydrogen oxidation and reduction reactions (HOR, HER). And (4) An exploration of opportunities for reactive nitrogen management by combining electrocatalysis with separation processes. The overarching theme of the poster is the need to take a multi-disciplinary, multi-modal approach in order to solve some of the outstanding challenges in catalyst design and development for energy conversion reactions.

Grant or FWP Number: FWP10049
SUNCAT Center for Interface Science and Catalysis FWP10049

PI: Thomas F. Jaramillo
Co-PIs: Frank Abild-Pedersen, Kirsten Winther, Simon Bare, Zhenan Bao, Michal Bajdich, Matteo Cargnello, Johannes Voss, Stacey Bent, William Tarpeh, Michaela Burke Stevens, Adam Nielander, Adam Hoffman

RECENT PROGRESS

Task 1: Catalysis Data Science and Computational Infrastructure

The data science task focuses on integrating catalysis data on our platform catalysis-hub.org and on developing machine-learning models for catalytic performance from combined experimental and computational data.

We have extended our catalysis data platform catalysis-hub.org from computational heterogeneous catalysis data to experimental data. In an evolving data infrastructure, we have begun to integrate experimental data on water catalysis as first prototype examples. In this initial data integration phase, collected data currently consists of catalyst materials properties, such as composition, morphology, crystal structure and oxidation states, as well as XRD and XPS characterization spectra. In addition, catalytic performance metrics are stored together with testing conditions and the catalyst matrix, including CV curves and derived onset potentials. These experimental data are accessible through our Python Cathub API (https://github.com/SUNCAT-Center/CatHub). As a first use-case of this integrated computational and experimental data, we have devised human-interpretable machine learning models imposing physicality constraints (https://github.com/vossjo/gplearn) to predict realistic catalyst performance metrics for ORR catalysts. These data integration efforts serve as a starting point aiming at incorporation of more types of catalysis data within and beyond the SUNCAT FWP.

On the computational catalysis data science and method development side, we have developed a solver for microkinetic models with improved convergence and the ability to deal with complicated adsorbate-adsorbate interactions models (https://github.com/sudarshanv01/catmap-mirror/tree/update-numbers-solver). To extend the range of electronic descriptors that can be extracted from our catalysis data and to enable predictions on complex catalyst structures out of reach for DFT simulations, we have devised tight-binding parametrizations for alloys of all transition-metals.

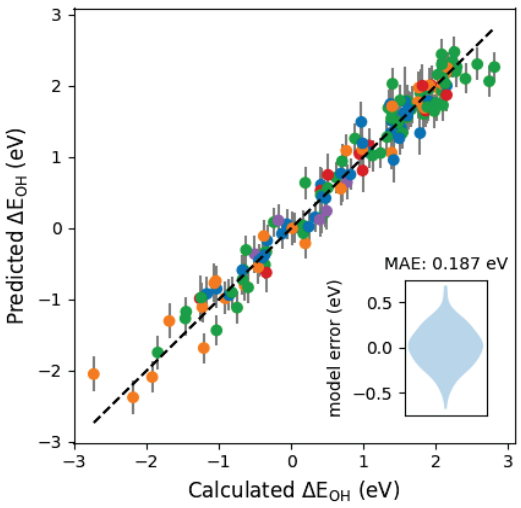

Figure 1. Performance of 5-descriptor Gaussian Process regression model for the prediction of OH adsorption energies across +2, +3, +4, +5 and +6 transition metal oxides. Descriptors include the bulk M(d)-O(20) ICOHP combined with non-DFT bulk and surface descriptors. The MAE is obtained from an average over leave-on-out cross validation across 140 training points.

We have developed a generalizable ML model for O and OH adsorption on (AxOy) transition metal oxides. Higher accuracy is achieved by utilizing descriptors derived from bulk DFT calculations that are of lower computational cost. In previous work we demonstrated that the electronic structure of the bulk TMO, obtained as the crystal orbital Hamiltonian populations (COHP) of the M-O bond, is an excellent descriptor for both *O and *OH adsorption[1]. In this work, we extend our model to a ML-based prediction of adsorption across multiple materials and

oxidation states, with a low mean absolute error of 0.21 eV for the O-OH adsorption energy difference. These results will enable a more efficient screening of materials active for OER and ORR by enabling a more accurate prediction of adsorption energies (Figure 1) already at the bulk level of DFT computation.

Task 2: Fundamentals of Electrochemistry

The electrochemistry task focuses on developing tools and fundamental insights into electrochemical phenomena as to design optimal microenvironments and highly active and durable electrocatalysts. Our focus phenomena range from catalyst-liquid interfaces and reaction mechanisms to synthesizing and characterizing catalysts with unique binding motifs and tracking material dynamics during reactions.

Many electrochemical technologies, e.g. electrolyzer for hydrogen evolution and carbon dioxide reduction, rely on the sluggish oxygen evolution reaction on the anode of their device. Looking into alternative reactions or device con has led to the combined experimental and theoretical study of benzyl alcohol oxidation (BAO)[2] as an OER replacement, or the ammonia oxidation reaction (AOR) as a hydrogen carrier and fuel cell alternative. Focusing on BAO, in a recent study we electrodeposited nickel hydroxide electrocatalysts and tested their performance in alkaline media. Experimentally, our results indicated, that in similar to the OER, Fe contamination impacted BAO. However, in contrast to the OER activity enhancement seen with Fe incorporation, the contamination increased the overpotential for BAO. Notably, this trend was characterized by tracking the $Ni^{2+/3+}$ redox wave, which is hypothesized to facilitate the reaction. Our complimentary mechanistic DFT calculations supported this hypothesis and gave further insights into the nature of the adsorption site and the pathway (Figure 2A).

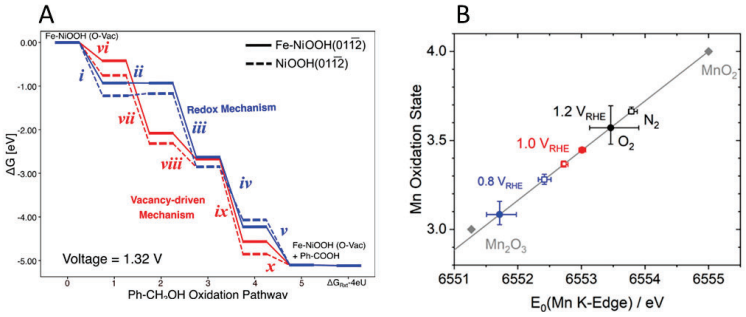

Figure 2. (A) Calculated free energy diagram for BAO at 1.32 vs RHE applied potential for Ni (dashed) and Ni-Fe (solid) oxyhydroxide. (B) Average Mn oxidation state for Ag-MnOx ORR electrocatalyst with (closed symbols) and without (open symbols) oxygen present in alkaline conditions.

In the past several years there has been a growing emphasis on the need to design durable materials. With the continued development of new tools capable of in situ and operando characterization, the field has gained many insights into the nature of the active site during reactions. In an effort to distill the knowledge that has already been acquired we focused on understanding Co-based materials for the OER and ORR. Broadly, based on our review of this material class we concluded that it is well known that starting structure, pH, and applied potential play a large role in the in situ/operando surface. However, there are still many outstanding questions for example, the specific surface composition, role of the support, catalysis, time, and the dynamics in a device-like microenvironment[3]. In an effort to address one of these areas we used in situ and operando x-ray absorption spectroscopy to characterize the Mn on the surface of a layered Ag-MnO_x thin film during electrochemistry[4]. By tracking the Mn oxidation state at a series of different potentials with and without oxygen present we were able to disentangle the relationship between oxygen reduction

and potential. We show that at the same potential (0.8 V vs RHE) that during ORR (e.g. with O_2 present) that the catalyst is more reduced (Figure 2B). This work highlights the importance of correlating the rate of catalysis to operando characterization.

Recently, we have expanded our suite of reactions to include reactive nitrogen species, and supplemented electrocatalysis approaches with selective electrochemical separations. Reactive nitrogen species include NH_3, NO_3^-, NO_2^-, NH_2OH, N_2H_4, N_2O, NO, and NO_2. The interconversion between these species plays critical roles in interactions between humans and the environment. For example, Haber-Bosch fertilizer production generates NH_3 and the Ostwald process converts NH_3 to NO_3^-. Reactive nitrogen emissions can also interconvert, leading to timely opportunities to valorize these emissions using electrocatalysis and electrochemical separations. We recently published a perspective in *ACS Catalysis* detailing efforts and an outlook on concentrating dilute emissions streams, using electrocatalysis to remove pollutants and/or generate valuable products, and creating high-purity commodities[5]. This perspective grounds our ongoing work on electrochemical nitrate reduction, as well as future work on carbon-nitrogen bond formation. The reactive separations approach will integrate polymer films (i.e., ionomers) onto electrode surfaces, as well as immobilize catalysts into membrane architectures for simultaneous catalysis and separations. We are particularly interested in the next funding period in closing nitrogen mass balances using gas and aqueous characterization and monitoring reactive intermediates with *operando* techniques.

Task 3: Fundamentals of Thermal Catalysis

During the past funding period, we have focused our attention on the dynamics of catalytic systems operating under conditions relevant to a variety of applications, and in particular to hydrocarbon activation in dehydrogenation and oxidation reactions. We developed the precise synthesis of bi- and trimetallic colloidal particles based on platinum and added with base metals to understand how surface chemistry evolves under reaction conditions and determines reactivity. This work is being done in strong connection with the alfa scheme developed by theory, with the goal to develop a predictive scheme able to determine the evolution of such multimetallic systems and their dynamics to identify valuable candidates for specific catalytic reactions.

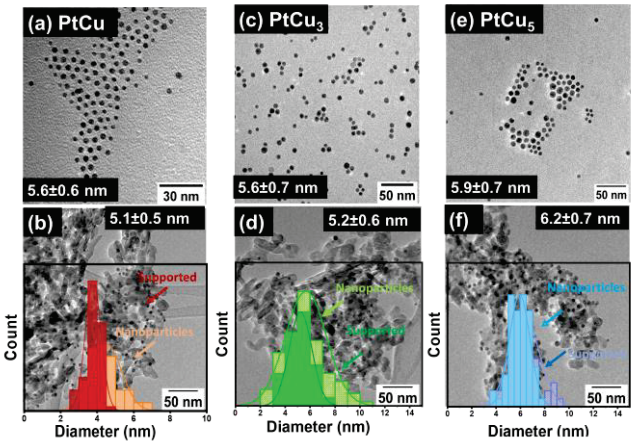

Figure 3. (a, c, e) TEM Images Of Pt/Cu bimetallic particles and obtained particle size distributions of the as-synthesized nanocrystal solutions, (b, d, f) representative TEM images after dispersion on Al_2O_3 with their respective particle size distribution of the nanoparticles drop casted from solution (dashed bars) and those supported on γ-Al_2O_3 (solid bars).

The synthesis of precise multimetallic particles was performed using seed-mediated approaches that rely on monodisperse Pt nanoparticles and that give us the opportunity to tune particle size through the initial seed size. The addition of base metals (Cu, Ni, Co, Zn) is then achieved by introducing their precursors into colloidal synthesis, thus tuning the Pt/metal ratio via simple control of precursor concentration. An example of a library of catalysts that can be produced with this method is reported in Figure 3. The particles are supported on a desired high-surface area oxide (e.g.,

alumina), and the catalysts are activated through a calcination process to remove ligands. The catalysts are probed with EDS mapping and XAS characterization before and after catalysis to determine dynamic behavior, in particular, how the alloying and dealloying at the bulk and surface level are related to their catalytic activity. These processes are connected to alfa schemes developed in tight collaboration with computational colleagues.

In these past few years of research, we demonstrated that the formation of surface alloys containing Cu, Ni and Co are beneficial for hydrocarbon C-H activation on Pt surfaces with low Pt content. The results demonstrate that the electronic structure of these surfaces is very sensitive to the composition, and that optimal arrangements of atoms deliver much greater rates of C-H activation. We put these results into perspective in a recent publication that highlights the needs in this community to develop tools that can give us more insight into the dynamic behavior of catalysts[6].

We also explored how dynamics can be controlled to determine selectivity in propane dehydrogenation catalysts. We found that Cu-rich Pt/Cu surfaces are very active in the reaction, but that dynamic changes restructure the surface and lead to deactivation. We controlled the surface structure by adding a third base metal, resulting in the stabilization of the dynamic behavior and an increase in rate and selectivity of dehydrogenation, confirmed by electronic structure calculations (Figure 4). The introduction of Co in Pt/Cu bimetallic catalysts stabilizes the surface structure of the particles, leading to isolated Pt sites that are electronically affected by the Cu and Co atoms as to reduce side-reaction of coke formation, and improve C-H activation towards propene.

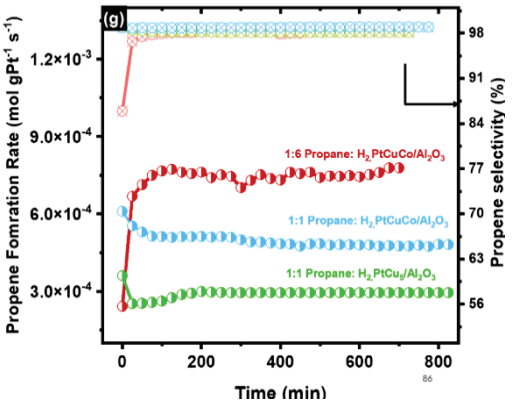

Figure 4. Predicted propane dehydrogenation rates and selectivity

We are continuing the work of describing the dynamic behavior in multimetallic systems and of predicting such dynamics using computational tools. The goal is to predict the dynamic behavior and its role in catalytic reactivity from first principles.

In addition, we made significant advances in understanding the connection between site stabilities and reaction rates (Figure 5). Our model approach connects instantaneously evaluated active site stabilities with the reaction energetics which then propagates through a microkinetic framework based on simple energy correlations to probe catalytic activity. To illustrate this, we modeled the simple NO decomposition reaction and identified a significant increase in rates when alloying Pt metal with Au. The ability to immediately obtain information about specific site activities also allows for the evaluation of rates as a function of particle size and shape thus enabling activity metrics of more realistic systems. The developed method is applicable not only for single element

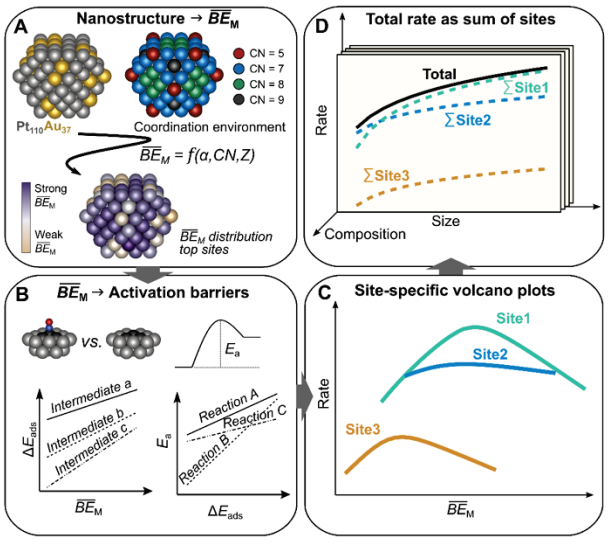

Figure 5. Stepwise approach for predicting active site-specific reaction rates on nanoparticles.

sites but also able to evaluate the catalytic activity of mixed metal sites in various coordination and chemical environments[7]. In a constant effort towards better understanding the effect of electronic properties on catalytic activity we have derived a physics-based chemisorption model for alloyed transition metal surfaces employing primarily metal *d*-band properties. In contrast to previous approaches this model accounts for perturbations in both the substrate and adsorbate electronic states upon interaction. We show that changes induced by the adsorbate on the adsorption site affects the chemical environment which again leads to a second-order response in the chemisorption energy proportional to changes in the *d*-filling of the neighboring atoms[8].

Task 4: The Consortium for Operando and Advanced Catalyst Characterization via Electronic Spectroscopy and Structure (Co-Access)

This past year has been a challenging year due to there being no beam available to users from December 2022 through to July 2023. Nevertheless, we took this opportunity to develop new data processing tools for our collaborators, design and construct new equipment, continue the development of BL 10-2, educate and teach, be intimately involved in the processing of XAS data and the subsequent writing of many manuscripts, and to develop closer ties with Tasks 1, 2 and 3. These are briefly summarized below.

One of our goals is to increase the standard in the application of XAS in the catalysis community. As such, we: (i) Informed the catalysis XAS community about some of the limitations in XAS for proving that single atoms are present on a catalyst. (ii) Developed a robust method for determining the presence of Ga(I) in a catalyst, and (iii) Wrote a perspective article on the current and future research directions of bridging the computational and experimental catalysis communities.

New Tools for Users| We have made significant progress on software and hardware for the XAS catalysis user community. We published and made available, *CatMass*, a software package used to calculate the ideal sample mass for X-ray measurements and guide detection schemes.

We have continued the development of *CatXAS* software (Hoffman) which allows for rapid processing of time resolved XAS data and correlating it to the process parameters and product analysis. The code has been able to characterize ligand exchange kinetics of single-site catalysts, identifying the rate limiting process (Hoffman), redox cycling and carburization of catalytic materials (Hoffman, Khatib, Genz, Roman, Scott). Combined with codes developed elsewhere (Scott) it has used to determine the enthalpy between reduced and oxidized single-site Ga used for PDH.

Equipment| We have upgraded our existing ambient and high-pressure flow systems expanding the safety infrastructure (more alarms and safe state triggers) and increasing functionality though reworking the interface with plans to expand the hardware to support more flow channels. We have designed a new *in-situ* XAS cell that allows the users to study multiple samples simultaneously, under various conditions, and purchased an XAS cell that can study samples under at temperatures close to LN2 temperatures (Linkam cell). We have also expanded our Echem ability by purchasing a 2-channel potentiostat for use in the Co-ACCESS lab or beamline. In the Co-ACCESS lab, we have purchased a low temperature DRIFTS cell to study samples at lower temperatures close LN2.

Outreach and Training| We have continued our efforts in outreach and training, driven by our goal to make the X-ray absorption spectroscopy technique at synchrotrons more accessible and effectively harnessed by the catalysis community for their research. We assist the research collaborators in writing competitive beamtime proposals and planning the actual beamtime to ensure the feasibility and safety of experiments. At the beamline, we provide extensive hands-on training for the students and postdocs in all aspects of an XAS experiment. Once the data are collected, we further mentor the students in data processing, data analysis, data interpretation, and data reporting. These mentoring sessions span from one-on-one meetings via Zoom or in-person, monthly office-hours via Zoom, group boot camp sessions to larger training sessions at national meetings. In the past year, Co-ACCESS has hosted XAS workshops at the 2022 SSRL Summer School, the 7th International Congress on Operando Spectroscopy, the 28th North American Catalysis Society Meeting, and the SUNCAT Summer Institute 2023. We also mentored a SULI student in summer 2023 and mentored two SCGSR students.

Collaboration with Other Tasks| We have continued our integration with the other three tasks in SUNCAT. We collaborate closely with all co-PI's in Task 2 and 3, and attend the sub-Task meetings. ASH collaborated with Michaela Stevens on an LDRD proposal, SRB and Kirsten Winther collaborated on a DOE proposal, and ASH led the planning and organization of the SUNCAT Summer Institute.

SSRL Beamline 10-2|At Beamline 10-2 SSRL is working on installing the optics for the beamline retrofit. The multi-element detector for characterizing dilute samples is on order and expected to be delivered in October 2023. SSRL had also installed the fire suppression and exhaust to the Co-ACCESS procured gas cabinets. We are actively working with Swagelok on the design and procurement of a permanent gas handling capability. Looking forward: 10-2 commissioning will occur in the winter 23/24, together with installation of the has handling system, first data will be collected in spring 24.

Subcontract with Prof. Ambarish Kulkarni, UC Davis| In the past year, we have worked on two major advancements related to QuantEXAFS. These are: (i) Adding new workflows to the QuantEXAFS code that can serve to enhance the knowledge acquired from XAS, and (ii) Extending the application of QuantEXAFS to a wider variety of supported catalysts to emphasize the approach of site identification for well-defined catalytic systems. For (i), related to code development, we have added capabilities of predicting site fraction in QuantEXAFS. Essentially, from the database of plausible structures the code uses density function theory (DFT) calculations and XAS features to predict the fraction of different sites present in the system including the minority species. This method is extremely useful to quantify the sites and this important information can be further utilized in understanding the reaction mechanisms, and synthesis of tailored catalytic sites. We benchmarked the code using the data that we collected from well-controlled beamline experiments. The code was further tested on simulated data and then on real catalytic samples.

Pertaining to (ii), we are working towards making QuantEXAFS available for the user community. While the current version of codes is released on GitHub, we have also worked towards consistent collaborations with members of the catalysis community to gain insights into their catalytic samples. Graduate students in the Kulkarni group have been trained to use the code to test zeolite

samples (Pt/ZSM5, Cr/Si-MFI, Mo/ZSM5 and atomically dispersed samples (Pt/MgO, Pd/MgO for ethylene hydrogenation). We are gradually working towards consistent improvements of the code to make it robust and eventually, we will soon release a packaged version for the user community. With the emphasis to synthesize tailored sites, we started exploring Ni sites supported on MgO. Currently, we have identified unique atomically dispersed Ni sites on MgO surface and subsurface using XAS experiments and QuantEXAFS analysis. We are in the process of testing the properties of these sites under reaction conditions using infrared spectroscopy in the Co-ACCESS lab and tracing the evolution of Ni using operando XAS experiments that can be analyzed using QuantEXAFS. This study will be an exemplary case to use a theory, synthesis and XAS analysis as an integrated approach for catalysis.

Subcontract with Prof. Fernando Vila, Univ. Washington |Theory-assisted interpretation of X-ray spectra for complicated systems like catalysts is essential to maximizing the amount of information extracted from experiments. Simulations provide a deeper understanding into the structure of the active site, and how changes due to chemical processes are correlated to spectral features. Given the complexity of some of these approaches, the main objective of this subcontract is to provide SUNCAT and Co-ACCESS users with end-to-end support in the optimal use of codes for X-ray spectroscopies, and their integration to density functional theory studies of structure. A few examples of how this support was used in the past year are: 1) We developed a rigorous analysis of Ga spectral signatures based on theoretical data. This allowed us to extract concentrations of Ga(I) during reduction processes. 2) The quick turnaround of theoretical results was used to compute *ab initio* EXAFS Debye-Waller (DW) factors for Lanthanide–EDTA complexes in solution. The theoretical DW factors can be used to both aid the EXAFS fits and assess the quality of the structural DFT simulations. 3) Theoretical insights formed the backbone of a "Perspective" published in ACS Catalysis where Co-ACCESS members highlighted how developments in analysis software, computational models, and data science can be used to improve the speed, accuracy, and reliability of EXAFS interpretation.

Statistics – Users, Beamtime, and Publications (Figure 6)

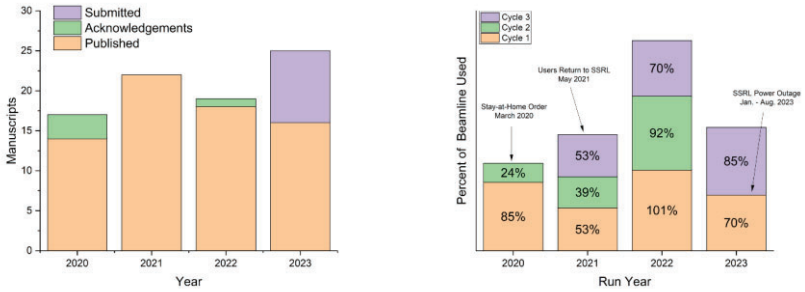

Figure 6. (left): Manuscripts submitted, published, or where Co-ACCESS was acknowledged in a given calendar year. (right): Beamtime use per cycle for each run year. Percent of a beamline used is determined by comparing the number of user-hours supported by Co-ACCESS staff and/or equipment to the user-hours of a beamline per year, approximately 1689 hours/cycle.

Cited Publications Acknowledging this Grant in 2020-2022

(1) Comer, B. M.; Li, J.; Abild-Pedersen, F.; Bajdich, M.; Winther, K. T. Unraveling Electronic Trends in O* and OH* Surface Adsorption in the MO2 Transition-Metal Oxide Series. *J. Phys. Chem. C* **2022**. https://doi.org/10.1021/acs.jpcc.2c02381.

(2) Wei, L.; Hossain, M. D.; Boyd, M. J.; Aviles-Acosta, J.; Kreider, M. E.; Nielander, A. C.; Stevens, M. B.; Jaramillo, T. F.; Bajdich, M.; Hahn, C. Insights into Active Sites and Mechanisms of Benzyl Alcohol Oxidation on Nickel–Iron Oxyhydroxide Electrodes. *ACS Catal.* **2023**, *13* (7), 4272–4282. https://doi.org/10.1021/acscatal.2c05656.

(3) Kreider, M. E.; Burke Stevens, M. Material Changes in Electrocatalysis: An In Situ/Operando Focus on the Dynamics of Cobalt-Based Oxygen Reduction and Evolution Catalysts. *ChemElectroChem* **2023**, *10* (3), e202200958. https://doi.org/10.1002/celc.202200958.

(4) Schröder, J.; Zamora Zeledón, J. A.; Kamat, G. A.; Kreider, M. E.; Wei, L.; Mule, A. S.; Torres, A.; Yap, K.; Sokaras, D.; Gallo, A.; Stevens, M. B.; Jaramillo, T. F. Tracking the Dynamics of a Ag-MnOx Oxygen Reduction Catalyst Using In Situ and Operando X-Ray Absorption Near-Edge Spectroscopy. *ACS Energy Lett.* **2023**, *8* (7), 2962–2969. https://doi.org/10.1021/acsenergylett.3c00823.

(5) Niemann, V. A.; Benedek, P.; Guo, J.; Xu, Y.; Blair, S. J.; Corson, E. R.; Nielander, A. C.; Jaramillo, T. F.; Tarpeh, W. A. Co-Designing Electrocatalytic Systems with Separations To Improve the Sustainability of Reactive Nitrogen Management. *ACS Catal.* **2023**, *13* (9), 6268–6279. https://doi.org/10.1021/acscatal.3c00933.

(6) Chavez, S.; Werghi, B.; Sanroman Gutierrez, K. M.; Chen, R.; Lall, S.; Cargnello, M. Studying, Promoting, Exploiting, and Predicting Catalyst Dynamics: The Next Frontier in Heterogeneous Catalysis. *J. Phys. Chem. C* **2023**, *127* (5), 2127–2146. https://doi.org/10.1021/acs.jpcc.2c06519.

(7) Halldin Stenlid, J.; Streibel, V.; Choksi, T. S.; Abild-Pedersen, F. Assessing Catalytic Rates of Bimetallic Nanoparticles with Active-Site Specificity: A Case Study Using NO Decomposition. *Chem Catal.* **2023**, *3* (5), 100636. https://doi.org/10.1016/j.checat.2023.100636.

(8) Saini, S.; Halldin Stenlid, J.; Abild-Pedersen, F. Electronic Structure Factors and the Importance of Adsorbate Effects in Chemisorption on Surface Alloys. *Npj Comput. Mater.* **2022**, *8* (1), 1–12. https://doi.org/10.1038/s41524-022-00846-z.

Publications Acknowledging this Grant in 2020-2023

(I) Intellectually led by SUNCAT FWP

1. Pillai, H. S.; Li, Y.; Wang, S. H.; Omidvar, N.; Mu, Q.; Achenie, L. E. K.; Abild-Pedersen, F.; Yang, J.; Wu, G.; Xin, H. Interpretable Design of Ir-Free Trimetallic Electrocatalysts for Ammonia Oxidation with Graph Neural Networks. *Nat. Commun. 2023 141* **2023**, *14* (1), 1–11. https://doi.org/10.1038/s41467-023-36322-5.
2. Schröder, J.; Zeledón, J. A. Z.; Kamat, G. A.; Kreider, M. E.; Wei, L.; Mule, A. S.; Torres, A.; Yap, K.; Sokaras, D.; Gallo, A.; Stevens, M. B.; Jaramillo, T. F. Tracking the Dynamics of a Ag-MnOx Oxygen Reduction Catalyst Using In Situ and Operando X-Ray Absorption

Near-Edge Spectroscopy. *ACS Energy Lett.* **2023**. https://doi.org/10.1021/ACSENERGYLETT.3C00823.
3. Kreider, M. E.; Burke Stevens, M. Material Changes in Electrocatalysis: An In Situ/Operando Focus on the Dynamics of Cobalt-Based Oxygen Reduction and Evolution Catalysts. *ChemElectroChem* **2023**, *10* (3), e202200958. https://doi.org/10.1002/CELC.202200958.
4. Oh, J.; Beck, A.; Goodman, E. D.; Roling, L. T.; Boucly, A.; Artiglia, L.; Abild-Pedersen, F.; van Bokhoven, J. A.; Cargnello, M. Colloidally Engineered Pd and Pt Catalysts Distinguish Surface- and Vapor-Mediated Deactivation Mechanisms. *ACS Catal.* **2023**, *13* (3), 1812–1822. https://doi.org/10.1021/ACSCATAL.2C04683
5. Wei, L.; Hossain, M. D.; Boyd, M. J.; Aviles-Acosta, J.; Kreider, M. E.; Nielander, A. C.; Stevens, M. B.; Jaramillo, T. F.; Bajdich, M.; Hahn, C. Insights into Active Sites and Mechanisms of Benzyl Alcohol Oxidation on Nickel-Iron Oxyhydroxide Electrodes. *ACS Catal.* **2023**, *13* (7), 4272–4282. https://doi.org/10.1021/ACSCATAL.2C05656
6. Zhao, W.; Xu, G.; He, Z.; Cai, C.; Abild-Pedersen, F.; Wang, T. Toward Carbon Monoxide Methanation at Mild Conditions on Dual-Site Catalysts. *J. Am. Chem. Soc.* **2023**. https://doi.org/10.1021/JACS.3C02180.
7. Craig, M. J.; Kleuker, F.; Bajdich, M.; García-Melchor, M. FEFOS: A Method to Derive Oxide Formation Energies from Oxidation States. *Catal. Sci. Technol.* **2023**, *13* (11), 3427–3435. https://doi.org/10.1039/D3CY00107E.
8. Baek, J.; Hossain, D.; Mukherjee, P.; Lee, J.; Winther, K.; Jiang, Y.; Chueh, W.; Bajdich, M.; Zheng, X. Synergistic Effects of Mixing and Strain in High Entropy Spinel Oxides for Oxygen Evolution Reaction. *Nat. Commun. (in print)* **2023**. https://doi.org/10.21203/RS.3.RS-1879578/V1.
9. Blair, S. J.; Nielander, A. C.; Stone, K. H.; Kreider, M. E.; Niemann, V. A.; Benedek, P.; McShane, E. J.; Gallo, A.; Jaramillo, T. F. Development of a Versatile Electrochemical Cell for in Situ Grazing-Incidence X-Ray Diffraction during Non-Aqueous Electrochemical Nitrogen Reduction. *1600-5775* **2023**, *30* (5), 917–922. https://doi.org/10.1107/S1600577523006331.
10. Jiang, D.; Wan, G.; Halldin Stenlid, J.; García-Vargas, C. E.; Zhang, J.; Sun, C.; Li, J.; Abild-Pedersen, F.; Tassone, C. J.; Wang, Y. Dynamic and Reversible Transformations of Subnanometre-Sized Palladium on Ceria for Efficient Methane Removal. *Nat. Catal. 2023 67* **2023**, *6* (7), 618–627. https://doi.org/10.1038/S41929-023-00983-8.
11. Koshy, D. M.; Hossain, M. D.; Masuda, R.; Yoda, Y.; Gee, L. B.; Abiose, K.; Gong, H.; Davis, R.; Seto, M.; Gallo, A.; Hahn, C.; Bajdich, M.; Bao, Z.; Jaramillo, T. F. Investigation of the Structure of Atomically Dispersed NiNx Sites in Ni and N-Doped Carbon Electrocatalysts by 61Ni Mössbauer Spectroscopy and Simulations. *J. Am. Chem. Soc.* **2022**. https://doi.org/10.1021/JACS.2C09825.
12. Trepte, K.; Voss, J. Data-Driven and Constrained Optimization of Semi-Local Exchange and Non-Local Correlation Functionals for Materials and Surface Chemistry. J. Comput. Chem. **2022**, 43, 1104–1112.https://doi.org/10.1002/jcc.26872
13. Comer, B. M.; Li, J.; Abild-Pedersen, F.; Bajdich, M.; Winther, K. T. Unraveling Electronic Trends in O* and OH* Surface Adsorption in the MO2 Transition-Metal Oxide Series. J. Phys. Chem. C **2022**, 126 (18), 7903–7909. https://doi.org/10.1021/acs.jpcc.2c02381
14. Voss, J. Hubbard-Corrected Oxide Formation Enthalpies without Adjustable Parameters. J. Phys. Commun. **2022**, 6 (3), 035009. https://doi.org/10.1088/2399-6528/ac6069

15. Koshy, D. M.; Hossain, M. D.; Masuda, R.; Yoda, Y.; Gee, L. B.; Abiose, K.; Gong, H.; Davis, R. C.; Seto, M.; Gallo, A.; Hahn, C.; Bajdich, M.; Bao, Z.; Jaramillo, T. Investigation of the Structure of Atomically Dispersed NiNx Sites in Ni, N-Doped Carbon Electrocatalysts by 61Ni Mössbauer Spectroscopy and Simulations. **2022**. https://doi.org/10.26434/chemrxiv-2022-hz7wc.
16. Zamora Zeledón, J. A.; Jackson, A.; Stevens, M.B.; Kamat, G.A.; Jaramillo, T.F. Methods—A Practical Approach to the Reversible Hydrogen Electrode Scale. *J. Electrochemical Soc.* **2022**, *169*, 066505. https://iopscience.iop.org/article/10.1149/1945-7111/ac71d1.
17. Resasco, J.; Abild-Pedersen, F.; Hahn, C.; Bao, Z.; Koper, M. T. M.; Jaramillo, T. F. Enhancing the Connection between Computation and Experiments in Electrocatalysis. *Nat Catal.* **2022**, *5* (5), 374–381. https://doi.org/10.1038/s41929-022-00789-0.
18. Lunger, J. R.; Lutz, N.; Peng, J.; Bajdich, M.; Shao-Horn, Y. Cation-Dependent Multielectron Kinetics of Metal Oxide Splitting. *Chem. Mater.* **2022**, 34, (8), 3872-3881. https://doi.org/10.1021/acs.chemmater.2c00602.
19. Kelly, S. R.; Heenen, H. H.; Govindarajan, N.; Chan, K.; Nørskov, J. K. OH Binding Energy as a Universal Descriptor of the Potential of Zero Charge on Transition Metal Surfaces. *J. Phys. Chem. C* **2022**, *126* (12), 5521-5528. https://doi.org/10.1021/acs.jpcc.1c10362.
20. Kamat, G. A.; Zamora Zeledón, J. A.; Gunasooriya, G. T. K. K.; Dull, S. M.; Perryman, J. T.; Nørskov, J. K.; Stevens, M. B.; Jaramillo, T. F. Acid Anion Electrolyte Effects on Platinum for Oxygen and Hydrogen Electrocatalysis. *Commun Chem.* **2022**, *5* (1), 1–10. https://doi.org/10.1038/s42004-022-00635-1.
21. Liu, M. J.; Guo, J.; Hoffman, A. S.; Stenlid, J. H.; Tang, M. T.; Corson, E. R.; Stone, K. H.; Abild-Pedersen, F.; Bare, S. R.; Tarpeh, W. A. Catalytic Performance and Near-Surface X-Ray Characterization of Titanium Hydride Electrodes for the Electrochemical Nitrate Reduction Reaction. *J. Am. Chem. Soc.* **2022**, 144 (13), 5739-5744. https://doi.org/10.1021/jacs.2c01274.
22. Hubert, M. A.; King, L. A.; Jaramillo, T. F. Evaluating the Case for Reduced Precious Metal Catalysts in Proton Exchange Membrane Electrolyzers. *ACS Energy Lett.* **2022**, *7* (1), 17–23. https://doi.org/10.1021/acsenergylett.1c01869.
23. Hubert, M. A.; Gallo, A.; Liu, Y.; Valle, E.; Sanchez, J.; Sokaras, D.; Sinclair, R.; King, L. A.; Jaramillo, T. F. Characterization of a Dynamic $Y_2Ir_2O_7$ Catalyst during the Oxygen Evolution Reaction in Acid. *J. Phys. Chem. C* **2022**, *126* (4), 1751–1760. https://doi.org/10.1021/acs.jpcc.1c07760.
24. Shi, X.; Peng, H.-J.; Hersbach, T. J.; Jiang, Y.; Zeng, Y.; Baek, J.; Winther, K. T.; Sokaras, D.; Zheng, X.; Bajdich, M. Efficient and Stable Acidic Water Oxidation Enabled by Low-Concentration, High-Valence Iridium Sites. *ACS Energy Letters* **2022**, *7*, 2228–2235. https://doi.org/10.1021/acsenergylett.2c00578.
25. Saini, S.; Halldin Stenlid, J.; Abild-Pedersen, F. Electronic Structure Factors and the Importance of Adsorbate Effects in Chemisorption on Surface Alloys. npj Comput. Mater. 2022 81 2022, 8 (1), 1–12. https://doi.org/10.1038/s41524-022-00846-z.
26. Wrasman, C. J.; Zhou, C.; Aitbekova, A.; Goodman, E. D.; Cargnello, M. Recycling of Solvent Allows for Multiple Rounds of Reproducible Nanoparticle Synthesis. J. Am. Chem. Soc. 2022, 144 (26), 11646–11655. https://doi.org/10.1021/JACS.2C02837.
27. Valle, E.; Duyar, M. S.; Snider, J. L.; Regli, S. K.; Rønning, M.; Gallo, A.; Jaramillo, T. F. In Situ Studies of the Formation of MoP Catalysts and Their Structure under Reaction Conditions for Higher Alcohol Synthesis: The Role of Promoters and Mesoporous

Supports. J. Phys. Chem. C **2022**, 126 (12), 5575–5583. https://doi.org/10.1021/acs.jpcc.2c00837.
28. Streibel V., Aljama H., Yang A.-C., Choksi T. S., Sánchez-Carrera R. S., Schäfer A., Li Y., Cargnello M., Abild-Pedersen F.,"Microkinetic modeling of propene combustion on a stepped, metallic palladium surface and the importance of oxygen coverage.", ACS Catalysis, **2022**, 12, 1742-1757. . https://doi.org/10.1021/acscatal.1c03699
29. Tahsini, N.; Yang, A.-C.; Streibel, V.; Werghi, B.; Goodman, E. D.; Aitbekova, A.; Bare, S. R.; Li, Y.; Abild-Pedersen, F.; Cargnello, M. Colloidal Platinum–Copper Nanocrystal Alloy Catalysts Surpass Platinum in Low-Temperature Propene Combustion. J. Am. Chem. Soc. **2022**, 144 (4), 1612–1621. https://doi.org/10.1021/jacs.1c10248.
30. Schlexer Lamoureux, P.; Choksi, T. S.; Streibel, V.; Abild-Pedersen, F. Combining Artificial Intelligence and Physics-Based Modeling to Directly Assess Atomic Site Stabilities: From Sub-Nanometer Clusters to Extended Surfaces. Phys. Chem. Chem. Phys. **2021**, 23, 22022-22034.https://doi.org/10.1039/D1CP02198B
31. Brown, K.; Maimaiti, Y.; Trepte, K.; Bligaard, T.; Voss, J. MCML: Combining Physical Constraints with Experimental Data for a Multi-Purpose Meta-Generalized Gradient Approximation. J. Comput. Chem. **2021**, 42 (28), 2004–2013. https://doi.org/10.1002/jcc.26732
32. Li, J.; Stenlid, J. H.; Ludwig, T.; Lamoureux, P. S.; Abild-Pedersen, F. Modeling Potential-Dependent Electrochemical Activation Barriers: Revisiting the Alkaline Hydrogen Evolution Reaction. *J. Am. Chem. Soc.* **2021**, *143* (46), 19341–19355. https://doi.org/10.1021/jacs.1c07276.
33. Ben-Naim, M.; Liu, Y.; Stevens, M. B.; Lee, K.; Wette, M. R.; Boubnov, A.; Trofimov, A. A.; Ievlev, A. V.; Belianinov, A.; Davis, R. C.; Clemens, B. M.; Bare, S. R.; Hikita, Y.; Hwang, H. Y.; Higgins, D. C.; Sinclair, R.; Jaramillo, T. F. Understanding Degradation Mechanisms in SrIrO3 Oxygen Evolution Electrocatalysts: Chemical and Structural Microscopy at the Nanoscale. *Advanced Functional Materials* **2021**, *31* (34), 2101542. https://doi.org/10.1002/adfm.202101542.
34. Koshy, D. M.; Nathan, S. S.; Asundi, A. S.; Abdellah, A. M.; Dull, S. M.; Cullen, D. A.; Higgins, D.; Bao, Z.; Bent, S. F.; Jaramillo, T. F. Bridging Thermal Catalysis and Electrocatalysis: Catalyzing CO2 Conversion with Carbon-Based Materials. *Angewandte Chemie International Edition* **2021**, *60* (32), 17472–17480. https://doi.org/10.1002/anie.202101326.
35. Lee, K.; Flores, R. A.; Liu, Y.; Wang, B. Y.; Hikita, Y.; Sinclair, R.; Bajdich, M.; Hwang, H. Y. Epitaxial Stabilization and Oxygen Evolution Reaction Activity of Metastable Columbite Iridium Oxide. *ACS Appl. Energy Mater.* **2021**, *4* (4), 3074–3082. https://doi.org/10.1021/acsaem.0c02788.
36. Zheng, X.; Tang, J.; Gallo, A.; Torres, J. A. G.; Yu, X.; Athanitis, C. J.; Been, E. M.; Ercius, P.; Mao, H.; Fakra, S. C.; Song, C.; Davis, R. C.; Reimer, J. A.; Vinson, J.; Bajdich, M.; Cui, Y. Origin of Enhanced Water Oxidation Activity in an Iridium Single Atom Anchored on NiFe Oxyhydroxide Catalyst. *PNAS* **2021**, *118* (36). https://doi.org/10.1073/pnas.2101817118.
37. Sanchez, J.; Stevens, M. B.; Young, A. R.; Gallo, A.; Zhao, M.; Liu, Y.; Ramos-Garcés, M. V.; Ben-Naim, M.; Colón, J. L.; Sinclair, R.; King, L. A.; Bajdich, M.; Jaramillo, T. F. Isolating the Electrocatalytic Activity of a Confined NiFe Motif within Zirconium Phosphate.

Advanced Energy Materials **2021**, *11* (20), 2003545. https://doi.org/10.1002/aenm.202003545.
38. Baeumer, C.; Li, J.; Lu, Q.; Liang, A. Y.-L.; Jin, L.; Martins, H. P.; Duchoň, T.; Glöß, M.; Gericke, S. M.; Wohlgemuth, M. A.; Giesen, M.; Penn, E. E.; Dittmann, R.; Gunkel, F.; Waser, R.; Bajdich, M.; Nemšák, S.; Mefford, J. T.; Chueh, W. C. Tuning Electrochemically Driven Surface Transformation in Atomically Flat LaNiO3 Thin Films for Enhanced Water Electrolysis. *Nat. Mater.* **2021**, *20* (5), 674–682. https://doi.org/10.1038/s41563-020-00877-1.
39. Asundi, A. S.; Nathan, S. S.; Hong, J.; Hoffman, A. S.; Pennel, M.; Bare, S. R.; Bent, S. F. Identifying Higher Oxygenate Synthesis Sites in Cu Catalysts Promoted and Stabilized by Atomic Layer Deposited Fe2O3. J. Catal. **2021**, 404, 210–223. https://doi.org/10.1016/j.jcat.2021.09.015.
40. Asundi, A. S.; Hoffman, A. S.; Nathan, S. S.; Boubnov, A.; Bare, S. R.; Bent, S. F. Impurity Control in Catalyst Design: The Role of Sodium in Promoting and Stabilizing Co and Co2C for Syngas Conversion. ChemCatChem **2021**, 13 (4), 1186–1194. https://doi.org/10.1002/cctc.202001703.
41. Nathan, S. S.; Asundi, A. S.; Singh, J. A.; Hoffman, A. S.; Boubnov, A.; Hong, J.; Bare, S. R.; Bent, S. F. Understanding Support Effects of ZnO-Promoted Co Catalysts for Syngas Conversion to Alcohols Using Atomic Layer Deposition. ChemCatChem **2021**, 13 (2), 770–781. https://doi.org/10.1002/cctc.202001630.
42. Upham, D. C.; Orazov, M.; Jaramillo, T. F. Phosphate-Passivated Mordenite for Tandem-Catalytic Conversion of Syngas to Ethanol or Acetic Acid. J. Catal. **2021**, 399, 132–141. https://doi.org/10.1016/j.jcat.2021.04.029.
43. Duyar, M. S.; Gallo, A.; Regli, S. K.; Snider, J. L.; Singh, J. A.; Valle, E.; McEnaney, J.; Bent, S. F.; Rønning, M.; Jaramillo, T. F. Understanding Selectivity in CO2 Hydrogenation to Methanol for MoP Nanoparticle Catalysts Using In Situ Techniques. Catalysts **2021**, 11 (1), 143. https://doi.org/10.3390/catal11010143.
44. Goodman, E. D.; Asundi, A. S.; Hoffman, A. S.; Bustillo, K. C.; Stebbins, J. F.; Bare, S. R.; Bent, S. F.; Cargnello, M. Monolayer Support Control and Precise Colloidal Nanocrystals Demonstrate Metal–Support Interactions in Heterogeneous Catalysts. Adv. Mater. **2021**, 33 (44), 2104533. https://doi.org/10.1002/adma.202104533.
45. Wang, T.; Li, G.; Cui, X.; Abild-Pedersen, F. Identification of Earth-Abundant Materials for Selective Dehydrogenation of Light Alkanes to Olefins. Proc. Natl. Acad. Sci. **2021**, 118 (11), e2024666118. https://doi.org/10.1073/pnas.2024666118.
46. D. Goodman, E.; Z. Carlson, E.; M. Dietze, E.; Tahsini, N.; Johnson, A.; Aitbekova, A.; Taylor, T. N.; N. Plessow, P.; Cargnello, M. Size-Controlled Nanocrystals Reveal Spatial Dependence and Severity of Nanoparticle Coalescence and Ostwald Ripening in Sintering Phenomena. Nanoscale **2021**, 13 (2), 930–938. https://doi.org/10.1039/D0NR07960J.
47. Wang, T.; Cui, X.; Winther, K. T.; Abild-Pedersen, F.; Bligaard, T.; Nørskov, J. K. Theory-Aided Discovery of Metallic Catalysts for Selective Propane Dehydrogenation to Propylene. ACS Catal. **2021**, 11 (10), 6290–6297. https://doi.org/10.1021/acscatal.0c05711.
48. Wang, T.; Abild-Pedersen, F. Identifying Factors Controlling the Selective Ethane Dehydrogenation on Pt-Based Catalysts from DFT Based Micro-Kinetic Modeling. J. Energy Chem. **2021**, 58, 37–40. https://doi.org/10.1016/j.jechem.2020.09.034.

49. Stenlid, J. H.; Streibel, V.; Choksi, T. S.; Abild-Pedersen, F. Assessing Catalytic Rates of Bimetallic Nanoparticles with Active Site Specificity - A Case Study Using NO Decomposition. **2021**. https://doi.org/10.26434/chemrxiv-2021-lmlmg.
50. Yang A.-C. , Streibel V. , Choksi T. S. , Aljama H. , Werghi B. , Bare S. R. , Sánchez-Carrera R. S., Schäfer A. , Li Y. , Abild-Pedersen F. , Cargnello M., "Insights and comparison of structure–property relationships in propane and propene catalytic combustion on Pd- and Pt-based catalysts.", Journal of Catalysis, **2021**, 401, 89-101. https://doi.org/10.1016/j.jcat.2021.06.018
51. Wang, T.; Abild-Pedersen, F. Achieving Industrial Ammonia Synthesis Rates at Near-Ambient Conditions through Modified Scaling Relations on a Confined Dual Site. Proc. Natl. Acad. Sci. **2021**, 118 (30), e2106527118. https://doi.org/10.1073/pnas.2106527118.
52. Mamun, O.; Winther, K. T.; Boes, J. R.; Bligaard, T. A Bayesian Framework for Adsorption Energy Prediction on Bimetallic Alloy Catalysts. Npj Comput. Mater. **2020**, 6 (1), 1–11. https://doi.org/10.1038/s41524-020-00447-8
53. Koshy, D.M.; Chen, S.; Lee, D. U.; Stevens, M.B.; Abdellah, A. M.; Dull, S. M.; Chen, G.; Nordlund, D.; Gallo, A.; Hahn, C.; Higgins, D. C.; Bao, Z.; Jaramillo, T. F. Understanding the Origin of Highly Selective CO_2 Electroreduction to CO on Ni, N-doped Carbon Catalysts. *Angewandte Chemie International Edition* **2020**, *59* (10), 4043-4050. https://doi.org/10.1002/anie.201912857.
54. Hubert, M. A.; Patel, A. M.; Gallo, A.; Liu, Y.; Valle, E.; Ben-Naim, M.; Sanchez, J.; Sokaras, D.; Sinclair, R.; Nørskov, J. K.; King, L. A.; Bajdich, M.; Jaramillo, T. F. Acidic Oxygen Evolution Reaction Activity–Stability Relationships in Ru-Based Pyrochlores. *ACS Catal.* **2020**, *10* (20), 12182–12196. https://doi.org/10.1021/acscatal.0c02252.
55. Mefford, J. T.; Zhao, Z.; Bajdich, M.; Chueh, W. C. Interpreting Tafel Behavior of Consecutive Electrochemical Reactions through Combined Thermodynamic and Steady State Microkinetic Approaches. *Energy Environ. Sci.* **2020**, *13* (2), 622–634. https://doi.org/10.1039/C9EE02697E.
56. Kelly, S. R.; Kirk, C.; Chan, K.; Nørskov, J. K. Electric Field Effects in Oxygen Reduction Kinetics: Rationalizing PH Dependence at the Pt(111), Au(111), and Au(100) Electrodes. *J. Phys. Chem. C* **2020**, *124* (27), 14581–14591. https://doi.org/10.1021/acs.jpcc.0c02127.
57. Gibbons, B. M.; Wette, M.; Stevens, M. B.; Davis, R. C.; Siahrostami, S.; Kreider, M.; Mehta, A.; Higgins, D. C.; Clemens, B. M.; Jaramillo, T. F. In Situ X-Ray Absorption Spectroscopy Disentangles the Roles of Copper and Silver in a Bimetallic Catalyst for the Oxygen Reduction Reaction. *Chem. Mater.* **2020**, *32* (5), 1819–1827. https://doi.org/10.1021/acs.chemmater.9b03963
58. Gallo, A.; Snider, J. L.; Sokaras, D.; Nordlund, D.; Kroll, T.; Ogasawara, H.; Kovarik, L.; Duyar, M. S.; Jaramillo, T. F. Ni5Ga3 Catalysts for CO2 Reduction to Methanol: Exploring the Role of Ga Surface Oxidation/Reduction on Catalytic Activity. Appl. Catal. B Environ. **2020**, 267, 118369. https://doi.org/10.1016/j.apcatb.2019.118369.
59. Duyar, M. S.; Gallo, A.; Snider, J. L.; Jaramillo, T. F. Low-Pressure Methanol Synthesis from CO2 over Metal-Promoted Ni-Ga Intermetallic Catalysts. J. CO2 Util. **2020**, 39, 101151. https://doi.org/10.1016/j.jcou.2020.03.001.

60. Asundi, A. S.; Hoffman, A. S.; Chi, M.; Nathan, S. S.; Boubnov, A.; Hong, J.; Bare, S. R.; Bent, S. F. Enhanced Alcohol Production over Binary Mo/Co Carbide Catalysts in Syngas Conversion. J. Catal. **2020**, 391, 446–458. https://doi.org/10.1016/j.jcat.2020.09.003.
61. Streibel, V.; Choksi, T. S.; Abild-Pedersen, F. Predicting Metal–Metal Interactions. I. The Influence of Strain on Nanoparticle and Metal Adlayer Stabilities. J. Chem. Phys. **2020**, 152 (9), 094701. https://doi.org/10.1063/1.5130566.
62. Choksi, T. S.; Streibel, V.; Abild-Pedersen, F. Predicting Metal–Metal Interactions. II. Accelerating Generalized Schemes through Physical Insights. J. Chem. Phys. **2020**, 152 (9), 094702. https://doi.org/10.1063/1.5141378.
63. Wrasman, C. J.; Riscoe, A. R.; Lee, H.; Cargnello, M. Dilute Pd/Au Alloys Replace Au/TiO2 Interface for Selective Oxidation Reactions. ACS Catal. **2020**, 10 (3), 1716–1720. https://doi.org/10.1021/acscatal.9b05227.
64. Boubnov, A.; Timoshenko, J.; Wrasman, C. J.; Hoffman, A. S.; Cargnello, M.; Frenkel, A. I.; Bare, S. R. Insight into Restructuring of Pd-Au Nanoparticles Using EXAFS. *Radiation Physics and Chemistry* **2020**, *175*, 108304.
65. Groden, K.; Vila, F. D.; Li, L.; Bare, S. R.; Scott, S. L.; McEwen, J. S. First-Principles Approach to Extracting Chemical Information from X-Ray Absorption Near-Edge Spectra of Ga-Containing Materials. *Journal of Physical Chemistry C* **2021**, *125* (51), 27901–27908.
66. Van Ravenhorst, I. K.; Hoffman, A. S.; Vogt, C.; Boubnov, A.; Patra, N.; Oord, R.; Akatay, C.; Meirer, F.; Bare, S. R.; Weckhuysen, B. M. On the Cobalt Carbide Formation in a Co/TiO2 Fischer-Tropsch Synthesis Catalyst as Studied by High-Pressure, Long-Term Operando X-Ray Absorption and Diffraction. *ACS Catal* **2021**, *11* (5), 2956–2967.
67. Chen, Y.; Rana, R.; Sours, T.; Vila, F. D.; Cao, S.; Blum, T.; Hong, J.; Hoffman, A. S.; Fang, C. Y.; Huang, Z.; Shang, C.; Wang, C.; Zeng, J.; Chi, M.; Kronawitter, C. X.; Bare, S. R.; Gates, B. C.; Kulkarni, A. R. A Theory-Guided X-Ray Absorption Spectroscopy Approach for Identifying Active Sites in Atomically Dispersed Transition-Metal Catalysts. *J Am Chem Soc* **2021**, *143* (48), 20144–20156.
68. Ben-Naim, M.; Liu, Y.; Stevens, M. B.; Lee, K.; Wette, M. R.; Boubnov, A.; Trofimov, A. A.; Ievlev, A. V.; Belianinov, A.; Davis, R. C.; Clemens, B. M.; Bare, S. R.; Hikita, Y.; Hwang, H. Y.; Higgins, D. C.; Sinclair, R.; Jaramillo, T. F. Understanding Degradation Mechanisms in SrIrO3 Oxygen Evolution Electrocatalysts: Chemical and Structural Microscopy at the Nanoscale. *Adv Funct Mater* **2021**, *31* (34), 2101542.
69. Aitbekova, A.; Wrasman, C. J.; Riscoe, A. R.; Kunz, L. Y.; Cargnello, M. "Determining Number of Sites on Ceria Stabilizing Single Atoms via Metal Nanoparticle Redispersion.", Chin. J. Catal. **2020**, 41, 998-1005.

(II) Jointly funded by this grant and other grants with intellectual leadership by other funding sources

70. Marin, D. H.; Perryman, J. T.; Hubert, M. A.; Lindquist, G. A.; Chen, L.; Aleman, A. M.; Kamat, G. A.; Niemann, V. A.; Stevens, M. B.; Regmi, Y. N.; Boettcher, S. W.; Nielander, A. C.; Jaramillo, T. F. Hydrogen Production with Seawater-Resilient Bipolar Membrane Electrolyzers. *Joule* **2023**, *7* (4), 765–781. https://doi.org/10.1016/j.joule.2023.03.005.
71. Blair, S. J.; Doucet, M.; Niemann, V. A.; Stone, K. H.; Kreider, M. E.; Browning, J. F.; Halbert, C. E.; Wang, H.; Benedek, P.; Mcshane, E. J.; Nielander, A. C.; Gallo, A.; Jaramillo, T. F.; Stanford, D. Combined, Time-Resolved, in Situ Neutron Reflectometry and X-Ray Diffraction Analysis of Dynamic SEI Formation during Electrochemical N2 Reduction. *Energy Environ. Sci.* **2023**, *16* (8), 3391–3406. https://doi.org/10.1039/D2EE03694K.
72. Niemann, V. A.; Benedek, P.; Guo, J.; Xu, Y.; Blair, S. J.; Corson, E. R.; Nielander, A. C.; Jaramillo, T. F.; Tarpeh, W. A. Co-Designing Electrocatalytic Systems with Separations To Improve the Sustainability of Reactive Nitrogen Management. *ACS Catal.* **2023**, *13* (9), 6268–6279. https://doi.org/10.1021/ACSCATAL.3C00933.
73. Kreider, M. E.; Kamat, G. A.; Zamora Zeledón, J. A.; Wei, L.; Sokaras, D.; Gallo, A.; Stevens, M.B. Jaramillo, T. F. Understanding the Stability of Manganese Chromium Antimonate Electrocatalysts through Multi-modal In Situ and Operando Measurements *JACS*. **2022**, 144,22549-22561. https://pubs.acs.org/doi/10.1021/jacs.2c08600
74. Wei, F.; Smeets, E. W. F.; Voss, J.; Kroes, G.-J.; Lin, S.; Guo, H. Assessing Density Functionals for Describing Methane Dissociative Chemisorption on Pt(110)-(2×1) Surface. Chin. J. Chem. Phys. **2021**, 34 (6), 883–895 https://doi.org/10.1063/1674-0068/cjcp2110207
75. Gerrits, N.; Geweke, J.; Smeets, E. W. F.; Voss, J.; Wodtke, A. M.; Kroes, G.-J. Closing the Gap Between Experiment and Theory: Reactive Scattering of HCl from Au(111). J. Phys. Chem. C **2020**, 124 (29), 15944–15960. https://doi.org/10.1021/acs.jpcc.0c03756
76. Kim, H. W.; Bukas, V. J.; Park, H.; Park, S.; Diederichsen, K. M.; Lim, J.; Cho, Y. H.; Kim, J.; Kim, W.; Han, T. H.; Voss, J.; Luntz, A. C.; McCloskey, B. D. Mechanisms of Two-Electron and Four-Electron Electrochemical Oxygen Reduction Reactions at Nitrogen-Doped Reduced Graphene Oxide. ACS Catal. **2020**, 10 (1), 852–863. https://doi.org/10.1021/acscatal.9b04106
77. Flores, R. A.; Paolucci, C.; Winther, K. T.; Jain, A.; Torres, J. A. G.; Aykol, M.; Montoya, J.; Nørskov, J. K.; Bajdich, M.; Bligaard, T. Active Learning Accelerated Discovery of Stable Iridium Oxide Polymorphs for the Oxygen Evolution Reaction. Chem. Mater. **2020**, 32 (13), 5854–5863. https://doi.org/10.1021/acs.chemmater.0c01894
78. Blair, S. J.; Doucet, M.; Browning, J. F.; Stone, K.; Wang, H.; Halbert, C.; Avilés Acosta, J.; Zamora Zeledón, J. A.; Nielander, A. C.; Gallo, A.; Jaramillo, T. F. Lithium-Mediated Electrochemical Nitrogen Reduction: Tracking Electrode–Electrolyte Interfaces via Time-Resolved Neutron Reflectometry. *ACS Energy Lett.* **2022**, *7*, (6), 1939–1946. https://doi.org/10.1021/acsenergylett.1c02833
79. Choi, S.-H.; Kreider, M. E.; Nielander, A. C.; Stevens, M. B.; Kamat, G.; Eung Koo, J.; Ho Bae, K.; Kim, H.; Young Yoon, I.; Un Yoon, B.; Hwang, K.; Un Lee, D.; Jaramillo, T. F.

Origins of Wear-Induced Tungsten Corrosion Defects in Semiconductor Manufacturing during Tungsten Chemical Mechanical Polishing. *Applied Surface Science* **2022**, *598*, 153767. https://doi.org/10.1016/j.apsusc.2022.153767

80. Gunasooriya, G.T.K.K.; Kreider, M. E.; Liu, Y.; Zamora Zeledón, J. A.; Wang, Z.; Valle, E.; Yang, Y-C.; Gallo, A.; Sinclair, R.; Stevens, M.B.; Jaramillo, T.F.; Nørskov, J.K. First-row Transition Metal Antimonates for the Oxygen Reduction Reaction. *ACS Nano*, **2022**, *16*, 6334-6348. https://pubs.acs.org/doi/full/10.1021/acsnano.2c00420
81. Zeledón, J. A. Z.; Gunasooriya, G. T. K. K.; Kamat, G. A.; Kreider, M. E.; Ben-Naim, M.; Hubert, M. A.; Acosta, J. E. A.; Nørskov, J. K.; Stevens, M. B.; Jaramillo, T. F. Engineering Metal–Metal Oxide Surfaces for High-Performance Oxygen Reduction on Ag–Mn Electrocatalysts. *Energy Environ. Sci.,* **2022**, *15,* 1611-1629. https://doi.org/10.1039/D2EE00047D
82. dos Santos, E. C., Araujo, R. B., Valter, M., Salazar-Alvarez, G., Johnsson, M., Bajdich, M., Abild-Pedersen, F., & Pettersson, L. G. M. Efficient Screening of Bi-Metallic Electrocatalysts for Glycerol Valorization. *Electrochimica Acta*, **2021**, 139283. https://doi.org/10.1016/J.ELECTACTA.2021.139283
83. Zamora Zeledón, J. A.; Kamat, G. A.; Gunasooriya, G. T. K. K.; Nørskov, J. K.; Stevens, M. B.; Jaramillo, T. F. Probing the Effects of Acid Electrolyte Anions on Electrocatalyst Activity and Selectivity for the Oxygen Reduction Reaction. *ChemElectroChem* **2021**, *8* (13), 2467–2478. https://doi.org/10.1002/celc.202100500
84. Zamora Zeledón, J. A.; Stevens, M. B.; Gunasooriya, G. T. K. K.; Gallo, A.; Landers, A. T.; Kreider, M. E.; Hahn, C.; Nørskov, J. K.; Jaramillo, T. F. Tuning the Electronic Structure of Ag-Pd Alloys to Enhance Performance for Alkaline Oxygen Reduction. *Nat Commun* **2021**, *12* (1), 620. https://doi.org/10.1038/s41467-021-20923-z
85. Koshy, D. M., Akhade, S. A., Shugar, A., Abiose, K., Shi, J., Liang, S., Oakdale, J. S., Weitzner, S. E., Varley, J. B., Duoss, E. B., Baker, S. E., Hahn, C., Bao, Z., & Jaramillo, T. FChemical Modifications of Ag Catalyst Surfaces with Imidazolium Ionomers Modulate H2Evolution Rates during Electrochemical CO2Reduction. Journal of the American Chemical Society, **2021**, 143(36), 14712–14725. https://doi.org/10.1021/JACS.1C06212
86. Winiwarter, A.; Boyd, M.J.; Scott, S. B.; Higgins, D. C.; Seger, B.; Chorkendorff, I.; Jaramillo, T. F. CO as a Probe Molecule to Study Surface Adsorbates during Electrochemical Oxidation of Propene. *ChemElectroChem*, **2021**, *8,* 250-256. https://doi.org/10.1002/celc.202001162
87. Chen, G.; Stevens, M.B.; Liu, Y.; King, L. A.; Park, J.; Kim, T.R.; Sinclair, R.; Jaramillo, T.F.; Bao, Z. Nanosized Zirconium Porphyrinic Metal-Organic Frameworks that Catalyze the Oxygen Reduction Reaction in Acid, *Small Methods*, **2020**, *4*, 2000085. https://doi.org/10.1002/smtd.202000085
88. Garcia-Esparza A. T., Park S.,Abroshan H., Paredes Mellone O. A., Vinson J., Abraham B., Kim T. R., Nordlund D., Gallo A., Alonso-Mori R., Zheng X., Sokaras D., "Local Structure of Sulfur Vacancies on the Basal Plane of Monolayer MoS2.", ACS Nano **2022**, 16, 4, 6725–6733. https://doi.org/10.1021/acsnano.2c01388
89. Ashbridge Z., Kreidt E., Pirvu L., Schaufelberger F., Halldin Stenlid J., Abild-Pedersen F., Leigh D. A., "Vernier template synthesis of molecular knots.", Science, **2022**, 375, 1035-1041. https://doi.org/10.1126/science.abm9247

90. Park S., Garcia-Esparza A. T., Abroshan H., Abraham B., Vinson J., Gallo A., Nordlund D., Park J., Kim T. R., Vallez L., Alonso-Mori R., Sokaras D., Zheng X., "Operando Study of Thermal Oxidation of Monolayer MoS2." Adv. Sci. **2021**,8, 2002768. https://doi.org/10.1002/advs.202002768
91. Riscoe, A. R.; Wrasman, C. J.; Menon, A.; Dinakar, B.; Goodman, E. D.; Kunz, L. Y.; Yacob, S.; Cargnello, M. "Chemically controllable porous polymer-nanocrystal composites with hierarchical arrangement show substrate transport selectivity.", Chem. Mater. **2020**, 32, 5904-5915.
92. Yang, A.-C.; Choksi, T.; Streibel, V.; Aljama, A.; Wrasman, C. J.; Roling, L. T.; Goodman, E. D.; Thomas, D.; Bare, S. R.; Sánchez-Carrera, R. S.; Schäfer, A.; Li, Y.; Abild-Pedersen, A.; Cargnello, M. "Revealing the structure of a catalytic combustion active-site ensemble combining uniform nanocrystal catalysts and theory insights.", Proc. Natl. Acad. Sci. USA **2020**, 117, 14721-14729.
93. Huang, W.; Zhang, X.; Yang, A.-C.; Goodman, E. D.; Kao, K.-C.; Cargnello, M. "Enhanced Catalytic Activity for Methane Combustion through In-Situ Water Sorption.", ACS Catal. **2020**, 10, 8157-8167.
94. Holm, A.; Goodman, E. D.; Stenlid, J. H.; Aitbekova, A.; Zelaya, R.; Diroll, B. T.; Johnston-Peck, A. C.; Kao, K.-C.; Frank, C. W.; Pettersson, L. G. M.; Cargnello, M. "Nanoscale Spatial Distribution of Supported Nanoparticles Controls Activity and Stability in Powder Catalysts.", J. Am. Chem. Soc. **2020**, 142, 14481-14494.
95. Ledbetter K., Reinhard M. E., Kunnus K., Gallo A., Britz A., Biasin E., Glownia J. M., Nelson S., Van Driel T., Weninger C., Zederkof D. B., Haldrup K., Cordones M. A., Gaffney K. J., Sokaras D., Alonso-Mori R., "Excited state charge distribution and bond expansion of ferrous complexes observed with femtosecond valence-to-core x-ray emission spectroscopy.", The Journal of Chemical Physics, **2020**, 152, 074203. https://doi.org/10.1063/1.5139441
96. Hamamoto Y., Wella S. A. , Inagaki K., Abild-Pedersen F., Bligaard T., Hamada I., Morikawa Y., "Enhanced CO tolerance of Pt clusters supported on graphene with lattice vacancies.", Physical Review B, **2020**, 102, 075408. https://doi.org/10.1103/PhysRevB.102.075408
97. Kunz, L. Y.; Hong, J.; Riscoe, A. R.; Majumdar, A.; Cargnello, M. Reducing Instability in Dispersed Powder Photocatalysis Derived from Variable Dispersion, Metallic Co-Catalyst Morphology, and Light Fluctuations. *J Photochem Photobiol* **2020**, *2*, 100004.
98. Rahman, M.; Infantes-Molina, A.; Hoffman, A. S.; Bare, S. R.; Emerson, K. L.; Khatib, S. J. Effect of Si/Al Ratio of ZSM-5 Support on Structure and Activity of Mo Species in Methane Dehydroaromatization. *Fuel* **2020**, *278*, 118290.
99. Guan, E.; Ciston, J.; Bare, S. R.; Runnebaum, R. C.; Katz, A.; Kulkarni, A.; Kronawitter, C. X.; Gates, B. C. Supported Metal Pair-Site Catalysts. *ACS Catal* **2020**, *10* (16), 9065–9085.
100. Asundi, A. S.; Hoffman, A. S.; Chi, M.; Nathan, S. S.; Boubnov, A.; Hong, J.; Bare, S. R.; Bent, S. F. Enhanced Alcohol Production over Binary Mo/Co Carbide Catalysts in Syngas Conversion. *J Catal* **2020**, *391*, 446–458.
101. Babucci, M.; Hoffman, A. S.; Debefve, L. M.; Kurtoglu, S. F.; Bare, S. R.; Gates, B. C.; Uzun, A. Unraveling the Individual Influences of Supports and Ionic Liquid Coatings on the Catalytic Properties of Supported Iridium Complexes and Iridium Clusters. *J Catal* **2020**, *387*, 186–195.

102. De Freitas, L. F.; Puértolas, B.; Zhang, J.; Wang, B.; Hoffman, A. S.; Bare, S. R.; Pérez-Ramírez, J.; Medlin, J. W.; Nikolla, E. Tunable Catalytic Performance of Palladium Nanoparticles for H2O2 Direct Synthesis via Surface-Bound Ligands. *ACS Catal* **2020**, *10* (9), 5202–5207.
103. Riley, C.; Canning, G.; De La Riva, A.; Zhou, S.; Peterson, E.; Boubnov, A.; Hoffman, A.; Tran, M.; Bare, S. R.; Lin, S.; Guo, H.; Datye, A. Environmentally Benign Synthesis of a PGM-Free Catalyst for Low Temperature CO Oxidation. *Appl Catal B* **2020**, *264*, 118547.
104. Fang, C. Y.; Valecillos, J.; Conley, E. T.; Chen, C. Y.; Castaño, P.; Gates, B. C. Synthesis of Rh6(CO)16 in Supercages of Zeolite HY: Reaction Network and Kinetics of Formation From Mononuclear Rhodium Precursors via Rh4(CO)12 Facilitated by the Water Gas Shift Half-Reaction. *Journal of Physical Chemistry C* **2020**, *124* (4), 2513–2520.
105. Azzam, S. A.; Boubnov, A.; Hoffman, A. S.; López-Ausens, T.; Chiang, N.; Canning, G.; Sautet, P.; Bare, S. R.; Simonetti, D. A. Insights into Copper Sulfide Formation from Cu and S K Edge XAS and DFT Studies. *Inorg Chem* **2020**, *59* (20), 15276–15288.
106. Qi, J.; Finzel, J.; Robatjazi, H.; Xu, M.; Hoffman, A. S.; Bare, S. R.; Pan, X.; Christopher, P. Selective Methanol Carbonylation to Acetic Acid on Heterogeneous Atomically Dispersed ReO4/SiO2 Catalysts. *J Am Chem Soc* **2020**, *142* (33), 14178–14189.
107. Resasco, J.; Derita, L.; Dai, S.; Chada, J. P.; Xu, M.; Yan, X.; Finzel, J.; Hanukovich, S.; Hoffman, A. S.; Graham, G. W.; Bare, S. R.; Pan, X.; Christopher, P. Uniformity Is Key in Defining Structure-Function Relationships for Atomically Dispersed Metal Catalysts: The Case of Pt/CeO2. *J Am Chem Soc* **2020**, *142* (1), 169–184.
108. Perez-Aguilar, J. E.; Chen, C. Y.; Hughes, J. T.; Fang, C. Y.; Gates, B. C. Isostructural Atomically Dispersed Rhodium Catalysts Supported on SAPO-37 and on HY Zeolite. *J Am Chem Soc* **2020**, *142* (26), 11474–11485.
109. Uzun, A.; Kurtoglu, S. F.; Hoffman, A. S.; Akgül, D.; Babucci, M.; Aviyente, V.; Gates, B. C.; Bare, S. R. Electronic Structure of Atomically Dispersed Supported Iridium Catalyst Controls Iridium Aggregation. *ACS Catal* **2020**, *10* (21), 12354–12358.
110. Yang, A. C.; Choksi, T.; Streibel, V.; Aljama, H.; Wrasman, C. J.; Roling, L. T.; Goodman, E. D.; Thomas, D.; Bare, S. R.; Sánchez-Carrera, R. S.; Schäfer, A.; Li, Y.; Abild-Pedersen, F.; Cargnello, M. Revealing the Structure of a Catalytic Combustion Active-Site Ensemble Combining Uniform Nanocrystal Catalysts and Theory Insights. *Proc. Natl. Acad. Sci. U. S. A.* **2020**, *117* (26), 14721–14729.
111. Felvey, N. W.; Meloni, M. J.; Kronawitter, C. X.; Runnebaum, R. C. Ethane Dehydrogenation over Cr/ZSM-5: Characterization of Active Sites through Probe Molecule Adsorption FTIR. *Catal. Sci. Technol.*, **2020**, *10*, 5069–5081.
112. Najmi, S.; Rasmussen, M.; Innocenti, G.; Chang, C.; Stavitski, E.; Bare, S. R.; Medford, A. J.; Medlin, J. W.; Sievers, C. Pretreatment Effects on the Surface Chemistry of Small Oxygenates on Molybdenum Trioxide. *ACS Catal* **2020**, *10* (15), 8187–8200.
113. Babucci, M.; Hoffman, A. S.; Bare, S. R.; Gates, B. C. Characterization of a Metal-Organic Framework Zr6O8Node-Supported Atomically Dispersed Iridium Catalyst for Ethylene Hydrogenation by X-Ray Absorption Near-Edge Structure and Infrared Spectroscopies. *Journal of Physical Chemistry C* **2021**, *125* (31), 16995–17007.
114. Chen, L.; Unocic, R. R.; Hoffman, A. S.; Hong, J.; Braga, A. H.; Bao, Z.; Bare, S. R.; Szanyi, J. Unlocking the Catalytic Potential of TiO2-Supported Pt Single Atoms for the Reverse Water-Gas Shift Reaction by Altering Their Chemical Environment. *JACS Au* **2021**, *1* (7), 977–986.

115. Jiang, D.; Yao, Y.; Li, T.; Wan, G.; Pereira-Hernández, X. I.; Lu, Y.; Tian, J.; Khivantsev, K.; Engelhard, M. H.; Sun, C.; García-Vargas, C. E.; Hoffman, A. S.; Bare, S. R.; Datye, A. K.; Hu, L.; Wang, Y. Tailoring the Local Environment of Platinum in Single-Atom Pt1/CeO2 Catalysts for Robust Low-Temperature CO Oxidation. *Angew. Chem. Int. Ed.* **2021**, *60* (50), 26054–26062.
116. Samira, S.; Hong, J.; Camayang, J. C. A.; Sun, K.; Hoffman, A. S.; Bare, S. R.; Nikolla, E. Dynamic Surface Reconstruction Unifies the Electrocatalytic Oxygen Evolution Performance of Nonstoichiometric Mixed Metal Oxides. *JACS Au* **2021**, *1* (12), 2224–2241.
117. Goodman, E. D.; Asundi, A. S.; Hoffman, A. S.; Bustillo, K. C.; Stebbins, J. F.; Bare, S. R.; Bent, S. F.; Cargnello, M. Monolayer Support Control and Precise Colloidal Nanocrystals Demonstrate Metal–Support Interactions in Heterogeneous Catalysts. *Advanced Materials* **2021**, *33* (44), 2104533.
118. Asundi, A. S.; Nathan, S. S.; Hong, J.; Hoffman, A. S.; Pennel, M.; Bare, S. R.; Bent, S. F. Identifying Higher Oxygenate Synthesis Sites in Cu Catalysts Promoted and Stabilized by Atomic Layer Deposited Fe2O3. *J Catal* **2021**, *404*, 210–223.
119. Yang, A. C.; Streibel, V.; Choksi, T. S.; Aljama, H.; Werghi, B.; Bare, S. R.; Sánchez-Carrera, R. S.; Schäfer, A.; Li, Y.; Abild-Pedersen, F.; Cargnello, M. Insights and Comparison of Structure–Property Relationships in Propane and Propene Catalytic Combustion on Pd- and Pt-Based Catalysts. *J Catal* **2021**, *401*, 89–101.
120. Wang, J.; Lu, Y.; Liu, L.; Yu, L.; Yang, C.; Delferro, M.; Hoffman, A. S.; Bare, S. R.; Karim, A. M.; Xin, H. Catalytic CO Oxidation on MgAl2O4-Supported Iridium Single Atoms: Ligand Configuration and Site Geometry. *Journal of Physical Chemistry C* **2021**, *125* (21), 11380–11390.
121. Qi, L.; Babucci, M.; Zhang, Y.; Lund, A.; Liu, L.; Li, J.; Chen, Y.; Hoffman, A. S.; Bare, S. R.; Han, Y.; Gates, B. C.; Bell, A. T. Propane Dehydrogenation Catalyzed by Isolated Pt Atoms in ≡SiOZn–OH Nests in Dealuminated Zeolite Beta. *J Am Chem Soc* **2021**, *143* (50), 21364–21378.
122. Nathan, S. S.; Asundi, A. S.; Singh, J. A.; Hoffman, A. S.; Boubnov, A.; Hong, J.; Bare, S. R.; Bent, S. F. Understanding Support Effects of ZnO-Promoted Co Catalysts for Syngas Conversion to Alcohols Using Atomic Layer Deposition. *ChemCatChem* **2021**, *13* (2), 770–781.
123. Simons, M. C.; Prinslow, S. D.; Babucci, M.; Hoffman, A. S.; Hong, J.; Vitillo, J. G.; Bare, S. R.; Gates, B. C.; Lu, C. C.; Gagliardi, L.; Bhan, A. Beyond Radical Rebound: Methane Oxidation to Methanol Catalyzed by Iron Species in Metal-Organic Framework Nodes. *J Am Chem Soc* **2021**, *143* (31), 12165–12174.
124. Asundi, A. S.; Hoffman, A. S.; Nathan, S. S.; Boubnov, A.; Bare, S. R.; Bent, S. F. Impurity Control in Catalyst Design: The Role of Sodium in Promoting and Stabilizing Co and Co2C for Syngas Conversion. *ChemCatChem* **2021**, *13* (4), 1186–1194.
125. Lopez Luna, M.; Timoshenko, J.; Kordus, D.; Rettenmaier, C.; Chee, S. W.; Hoffman, A. S.; Bare, S. R.; Shaikhutdinov, S.; Roldan Cuenya, B. Role of the Oxide Support on the Structural and Chemical Evolution of Fe Catalysts during the Hydrogenation of CO2. *ACS Catal* **2021**, *11* (10), 6175–6185.
126. Albrahim, M.; Thompson, C.; Leshchev, D.; Shrotri, A.; Unocic, R. R.; Hong, J.; Hoffman, A. S.; Meloni, M. J.; Runnebaum, R. C.; Bare, S. R.; Stavitski, E.; Karim, A. M. Reduction and Agglomeration of Supported Metal Clusters Induced by High-Flux X-Ray Absorption

Spectroscopy Measurements. *Journal of Physical Chemistry C* **2021**, *125* (20), 11048–11057.
127. Ouyang, M.; Papanikolaou, K. G.; Boubnov, A.; Hoffman, A. S.; Giannakakis, G.; Bare, S. R.; Stamatakis, M.; Flytzani-Stephanopoulos, M.; Sykes, E. C. H. Directing Reaction Pathways via in Situ Control of Active Site Geometries in PdAu Single-Atom Alloy Catalysts. *Nat Commun* **2021**, *12*, 1549.
128. Divins, N. J.; Kordus, D.; Timoshenko, J.; Sinev, I.; Zegkinoglou, I.; Bergmann, A.; Chee, S. W.; Widrinna, S.; Karslıoğlu, O.; Mistry, H.; Lopez Luna, M.; Zhong, J. Q.; Hoffman, A. S.; Boubnov, A.; Boscoboinik, J. A.; Heggen, M.; Dunin-Borkowski, R. E.; Bare, S. R.; Cuenya, B. R. Operando High-Pressure Investigation of Size-Controlled CuZn Catalysts for the Methanol Synthesis Reaction. *Nat Commun* **2021**, *12*, 1435.
129. Giannakakis, G.; Kress, P.; Duanmu, K.; Ngan, H. T.; Yan, G.; Hoffman, A. S.; Qi, Z.; Trimpalis, A.; Annamalai, L.; Ouyang, M.; Liu, J.; Eagan, N.; Biener, J.; Sokaras, D.; Flytzani-Stephanopoulos, M.; Bare, S. R.; Sautet, P.; Sykes, E. C. H. Mechanistic and Electronic Insights into a Working NiAu Single-Atom Alloy Ethanol Dehydrogenation Catalyst. *J Am Chem Soc* **2021**, *143* (51), 21567–21579.
130. Rorrer, J. E.; Ebrahim, A. M.; Questell-Santiago, Y.; Zhu, J.; Troyano-Valls, C.; Asundi, A. S.; Brenner, A. E.; Bare, S. R.; Tassone, C. J.; Beckham, G. T.; Román-Leshkov, Y. Role of Bifunctional Ru/Acid Catalysts in the Selective Hydrocracking of Polyethylene and Polypropylene Waste to Liquid Hydrocarbons. *ACS Catal* **2022**, *12* (22), 13969–13979.
131. Meloni, M.; Hong, J.; Hoffman, A. S.; Holton, S.; Kulkarni, A.; Bare, S. R.; Runnebaum, R. C. Nano-Sized Metallic Nickel Clusters Stabilized on Dealuminated Beta-Zeolite: A Highly Active and Stable Ethylene Hydrogenation Catalyst. *Journal of Physical Chemistry C* **2022**, *126* (50), 21213–21222.
132. Nathan, S. S.; Asundi, A. S.; Hoffman, A. S.; Hong, J.; Zhou, C.; Vila, F. D.; Cargnello, M.; Bare, S. R.; Bent, S. F. Surface Fe Clusters Promote Syngas Reaction to Oxygenates on Rh Catalysts Modified by Atomic Layer Deposition. *J Catal* **2022**, *414*, 125–136.
133. Babucci, M.; Conley, E. T.; Hoffman, A. S.; Bare, S. R.; Gates, B. C. Iridium Pair Sites Anchored to Zr6O8 Nodes of the Metal–Organic Framework UiO-66 Catalyze Ethylene Hydrogenation. *J Catal* **2022**, *411*, 177–186.
134. Kurtoğlu-Öztulum, S. F.; Yalçın, K.; Hoffman, A. S.; Jalal, A.; Zhao, Y.; Gates, B. C.; Bare, S. R.; Unal, U.; Uzun, A. Ionic Liquid Sheath Stabilizes Atomically Dispersed Reduced Graphene Aerogel-Supported Iridium Complexes during Ethylene Hydrogenation Catalysis. *ChemCatChem* **2022**, *14* (19), e202200553.
135. Aitbekova, A.; Zhou, C.; Stone, M. L.; Lezama-Pacheco, J. S.; Yang, A. C.; Hoffman, A. S.; Goodman, E. D.; Huber, P.; Stebbins, J. F.; Bustillo, K. C.; Ercius, P.; Ciston, J.; Bare, S. R.; Plessow, P. N.; Cargnello, M. Templated Encapsulation of Platinum-Based Catalysts Promotes High-Temperature Stability to 1,100 °C. *Nat Mater* **2022**, *21* (11), 1290–1297.
136. Qi, L.; Zhang, Y.; Babucci, M.; Chen, C.; Lu, P.; Li, J.; Dun, C.; Hoffman, A. S.; Urban, J. J.; Tsapatsis, M.; Bare, S. R.; Han, Y.; Gates, B. C.; Bell, A. T. Dehydrogenation of Propane and N-Butane Catalyzed by Isolated PtZn4Sites Supported on Self-Pillared Zeolite Pentasil Nanosheets. *ACS Catal* **2022**, *12* (18), 11177–11189.
137. Zhou, C.; Asundi, A. S.; Goodman, E. D.; Hong, J.; Werghi, B.; Hoffman, A. S.; Nathan, S. S.; Bent, S. F.; Bare, S. R.; Cargnello, M. Steering CO2 Hydrogenation toward C–C Coupling to Hydrocarbons Using Porous Organic Polymer/ Metal Interfaces. *Proc. Nat. Acad. Sci. U.S.* **2022**, *119* (7), e2114768119.

138. Acharya, P.; Manso, R. H.; Hoffman, A. S.; Bakovic, S. I. P.; Kekedy-Nagy, L.; Bare, S. R.; Chen, J.; Greenlee, L. F. Fe Coordination Environment, Fe-Incorporated Ni(OH)2 Phase, and Metallic Core Are Key Structural Components to Active and Stable Nanoparticle Catalysts for the Oxygen Evolution Reaction. *ACS Catal* **2022**, *12* (3), 1992–2008.
139. Lu, Y.; Thompson, C.; Kuo, C. Te; Zhang, X.; Hoffman, A. S.; Boubnov, A.; Bare, S. R.; Kovarik, L.; Xin, H.; Karim, A. M. CO Oxidation on MgAl2O4 supported Irn: Activation of Lattice Oxygen in the Subnanometer Regime and Emergence of Nuclearity-Activity Volcano. *J Mater Chem A Mater* **2022**, *10* (8), 4266–4278.
140. Felvey, N.; Guo, J.; Rana, R.; Xu, L.; Bare, S. R.; Gates, B. C.; Katz, A.; Kulkarni, A. R.; Runnebaum, R. C.; Kronawitter, C. X. Interconversion of Atomically Dispersed Platinum Cations and Platinum Clusters in Zeolite ZSM-5 and Formation of Platinum Gem-Dicarbonyls. *J Am Chem Soc* **2022**, *144* (30), 13874–13887.
141. Liu, M. J.; Guo, J.; Hoffman, A. S.; Stenlid, J. H.; Tang, M. T.; Corson, E. R.; Stone, K. H.; Abild-Pedersen, F.; Bare, S. R.; Tarpeh, W. A. Catalytic Performance and Near-Surface X-Ray Characterization of Titanium Hydride Electrodes for the Electrochemical Nitrate Reduction Reaction. *J Am Chem Soc* **2022**, *144* (13), 5739–5744.
142. Chen, Y.; Rana, R.; Huang, Z.; Vila, F. D.; Sours, T.; Perez-Aguilar, J. E.; Zhao, X.; Hong, J.; Hoffman, A. S.; Li, X.; Shang, C.; Blum, T.; Zeng, J.; Chi, M.; Salmeron, M.; Kronawitter, C. X.; Bare, S. R.; Kulkarni, A. R.; Gates, B. C. Atomically Dispersed Platinum in Surface and Subsurface Sites on MgO Have Contrasting Catalytic Properties for CO Oxidation. *Journal of Physical Chemistry Letters* **2022**, *13* (17), 3896–3903.
143. Le, T. T.; Shilpa, K.; Lee, C.; Han, S.; Weiland, C.; Bare, S. R.; Dauenhauer, P. J.; Rimer, J. D. Core-Shell and Egg-Shell Zeolite Catalysts for Enhanced Hydrocarbon Processing. *J Catal* **2022**, *405*, 664–675.
144. Tahsini, N.; Yang, A. C.; Streibel, V.; Werghi, B.; Goodman, E. D.; Aitbekova, A.; Bare, S. R.; Li, Y.; Abild-Pedersen, F.; Cargnello, M. Colloidal Platinum-Copper Nanocrystal Alloy Catalysts Surpass Platinum in Low-Temperature Propene Combustion. *J Am Chem Soc* **2022**, *144* (4), 1612–1621.
145. Paz Herrera, L.; Freitas de Lima e Freitas, L.; Hong, J.; Hoffman, A. S.; Bare, S. R.; Nikolla, E.; Medlin, J. W. Reactivity of Pd–MO2 Encapsulated Catalytic Systems for CO Oxidation . *Catal Sci Technol* **2022**, *12* (5), 1476–1486..
146. Lynch, T. J.; Birkner, N. R.; Christian, M. S.; Wrubel, J. A.; Schorne-Pinto, J.; Van Veelen, A.; Bargar, J. R.; Besmann, T. M.; Brinkman, K. S.; Chiu, W. K. S. *In Situ* Determination of Speciation and Local Structure of NaCl–SrCl2 and LiF–ZrF4 Molten Salts. *J Phys Chem B* **2022**, *126* (7), 1539–1550.
147. Meloni, M.; Hong, J.; Hoffman, A. S.; Holton, S.; Kulkarni, A.; Bare, S. R.; Runnebaum, R. C. Nano-Sized Metallic Nickel Clusters Stabilized on Dealuminated Beta-Zeolite: A Highly Active and Stable Ethylene Hydrogenation Catalyst. *Journal of Physical Chemistry C* **2022**, *126* (50), 21213–21222.
148. Kurtoğlu-Öztulum, S. F.; Kaan Yalçın; Zhao, Y.; Pelin Çağlayan, H.; Hoffman, A. S.; Gates, B. C.; Bare, S. R.; Ünal, U.; Uzun, A. Transformation of Reduced Graphene Aerogel-Supported Atomically Dispersed Iridium into Stable Clusters Approximated as Ir6 during Ethylene Hydrogenation Catalysis. *J Catal* **2022**, *413*, 603–613.
149. Thompson, C. B.; Liu, L.; Leshchev, D. S.; Hoffman, A. S.; Hong, J.; Bare, S. R.; Unocic, R. R.; Stavitski, E.; Xin, H.; Karim, A. M. CO Oxidation on Ir1/TiO2: Resolving Ligand Dynamics and Elementary Reaction Steps. *ACS Catal* **2023**, 7802–7811.

150. Acharya, P.; Hong, J.; Manso, R.; Hoffman, A. S.; Kekedy-Nagy, L.; Chen, J.; Bare, S. R.; Greenlee, L. F. Temporal Ni K-Edge X-Ray Absorption Spectroscopy Study Reveals the Kinetics of the Ni Redox Behavior of the Iron-Nickel Oxide Bimetallic OER Catalyst. *The Journal of Physical Chemistry C* **2023**, *127* (25), 11891–11901.
151. Das, S.; Anjum, U.; Lim, K. H.; He, Q.; Hoffman, A. S.; Bare, S. R.; Kozlov, S. M.; Gates, B. C.; Kawi, S. Genesis of Active Pt/CeO2 Catalyst for Dry Reforming of Methane by Reduction and Aggregation of Isolated Platinum Atoms into Clusters. *Small* **2023**, *19*, 2207272.
152. Zhang, Z.; Tian, J.; Lu, Y.; Yang, S.; Jiang, D.; Huang, W.; Li, Y.; Hong, J.; Hoffman, A. S.; Bare, S. R.; Engelhard, M. H.; Datye, A. K.; Wang, Y. Memory-Dictated Dynamics of Single-Atom Pt on CeO2 for CO Oxidation. *Nat Commun* **2023**, *14*, 2664.
153. Le, T. T.; Qin, W.; Agarwal, A.; Nikolopoulos, N.; Fu, D.; Patton, M. D.; Weiland, C.; Bare, S. R.; Palmer, J. C.; Weckhuysen, B. M.; Rimer, J. D. Elemental Zoning Enhances Mass Transport in Zeolite Catalysts for Methanol to Hydrocarbons. *Nat Catal* **2023**, *6* (3), 254–265.
154. Werghi, B.; Wu, L.; Ebrahim, A. M.; Chi, M.; Ni, H.; Cargnello, M.; Bare, S. R. Selective Catalytic Behavior Induced by Crystal-Phase Transformation in Well-Defined Bimetallic Pt-Sn Nanocrystals. *Small* **2023**, *19*, 2207956.
155. Yeh, B.; Chheda, S.; Prinslow, S. D.; Hoffman, A. S.; Hong, J.; Perez-Aguilar, J. E.; Bare, S. R.; Lu, C. C.; Gagliardi, L.; Bhan, A. Structure and Site Evolution of Framework Ni Species in MIL-127 MOFs for Propylene Oligomerization Catalysis. *J Am Chem Soc* **2023**, *145* (6), 3408–3418.
156. Albrahim, M.; Shrotri, A.; Unocic, R.; Hoffman, A.; Bare, S.; Karim, A. M. Size-Dependent Dispersion of Rhodium Clusters into Isolated Single Atoms at Low Temperature and the Consequences for CO Oxidation Activity. *Angew. Chem. Int. Ed.* **2023**, e202308002.
157. Chen, L.; Allec, S. I.; Nguyen, M.-T.; Kovarik, L.; Hoffman, A. S.; Hong, J.; Meira, D.; Shi, H.; Bare, S. R.; Glezakou, V.-A.; Rousseau, R.; Szanyi, J. Dynamic Evolution of Palladium Single Atoms on Anatase Titania Support Determines the Reverse Water–Gas Shift Activity. *J Am Chem Soc* **2023**, *145* (19), 10847–10860.
158. Shah, S.; Hong, J.; Cruz, L.; Wasantwisut, S.; Bare, S. R.; Gilliard-AbdulAziz, K. L. Dynamic Tracking of NiFe Smart Catalysts Using *In Situ* X-Ray Absorption Spectroscopy for the Dry Methane Reforming Reaction. *ACS Catal* **2023**, *13* (6), 3990–4002.

POSTER PRESENTATION ABSTRACTS

Frank Abild-Pedersen

Physics-based design principles for complex chemical reactions

Shyama Charan Mandal, Frank Abild-Pedersen

SUNCAT Center for Interface Science and Catalysis
SLAC National Accelerator Laboratory

Poster Abstract

The ability to predict the stability of complex intermediates in a chemical reaction is extremely important when designing new and more efficient catalysts. To gain more insights into the reaction mechanism of more complex processes, we have investigated correlation of various C_1 to C_3 hydrocarbon adsorbates on Pt-based catalysts. The local bonding nature of the hydrocarbons follow a similar pattern for certain adsorbates regardless of the chain length and can effectively be classified into a few categories based on their binding nature on the catalytic surface. The energy correlations between the elements in the class are linked entirely through the binding strength of the active site on the surface and since these energies can be obtained through a simple scheme based on parameters carrying information about the local chemical environment as well as the stability, we now have an efficient way of linking the catalyst surface structure to its reactivity.[1] The generality of this approach allows for an expansion of the methodology to include other metals and alloys and the established correlations and classification of intermediates will be immensely valuable for the accurate and efficient screening of numerous catalysts.

[1] Shyama Charan Mandal, Frank Abild-Pedersen 2023 ACS Catalysis (under review)

Líney Árnadóttir

Theoretical studies on BES Catalysis Core Program

Greg Collinge, [a] Jack Fuller, [a] Bojana Ginovska,[a] Mal-Soon Lee,[a] Simone Raugei, [a] Greg Schenter,[a] and Líney Árnadóttir[a,b]

[a] Pacific Northwest National Laboratory, Physical and Computational Sciences Directorate and Institute for Integrated Catalysis, Richland, WA 99354, USA

[b] School of Chemical, Biological, and Environmental Engineering, Oregon State University, Corvallis, Oregon 97331, USA

Presentation Abstract

Computational and theoretical studies are an integral part of the BES Catalysis core program at PNNL. This component seeks to provide atomistic insights and predictability into catalytic processes in close collaborations with experiments. To effectively describe the often complex experimental conditions, including dynamic active sites, confinements, and solvents, a multi-level approach is needed where the methods are tailored to the complexity of the problem. To better capture this complexity, we apply and combine computational methods that span multiple lengths and time scales. In this poster, we will highlight recent progress in different areas of the programs. DFT studies of CO oxidation of single-site Cu atoms on CeO_2 show how facile charge transfer between the active site and support opens different reaction channels and contributes to the catalyst adaptability under reaction conditions. Through AIMD free energy calculations we describe propanol interactions with H-MFI micropores and dimer and trimer species formation within the H-MFI micropores. Using a combination of in situ and MD Al K-edge XNAES we show the transition of the Al T-site with the formation of monomer, dimer, and trimer 1-propanol species. The importance of co-absorbates and solvent representation is illustrated in two separate studies, through combined STM and DFT study we show how neighboring OH helps facilitate acetic acid diffusion on TiO_2 and the formation of an ordered phase at higher coverage. The importance of QM dynamical representation of water is highlighted in the difference in predicted reaction energy landscape and rate-determining steps for CO_2 hydrogenation with a Rh molecular catalyst when modeled with QM and continuum solvent vs. adaptive QM/MM MD, coupled with AIMD for validation. The addition of explicit water through an adaptive QM/MM MD approach enables us to identify reaction paths that bypass the high-energy transition states identified using QM continuum model calculations. These highlights illustrate the integration of complexity and multiple level approaches to modeling and underscores the strong integration of computational and theoretical studies in the BES Catalysis core program at PNNL.

FWP 47319: Impact of catalytically active centers and their environment on rates and thermodynamic states along reaction paths

PI: Johannes Lercher

Co-PI's: Aaron Appel, Líney Árnadóttir, David Dixon (U Alabama), Zdenek Dohnálek, John Fulton, Bojana Ginovska, Jian-Zhi Hu, Enrique Iglesia (UC Berkeley), Abhi Karkamkar, Bruce Kay, Sungmin Kim, Gregory Kimmel, Libor Kovarik, Mal-Soon Lee, John Linehan, Greg Schenter, Wendy Shaw, Janos Szanyi, Ba Tran, Huamin Wang, Yong Wang (Washington State U), Eric Wiedner, Nancy Washton.

Jason D. Azoulay

Gold Catalyzed Polymerization Reactions of Unsaturated Substrates: Towards New Functional, Recyclable, and Upcycled Aromatic Polymers

Jason D. Azoulay, Eric King, and Naresh Eedugurala
Georgia Institute of Technology

Presentation Abstract

Synthetic aromatic polymers are ubiquitous and indispensable to modern life, industry, and the global economy. The presence of planar, rigid aromatic, or pseudo-aromatic heterocycles within these polymers imparts robust properties that enable their broad utility in commodity, specialty, and high-performance applications. Despite their vital technological roles, these macromolecules rarely possess the same fidelity in their chemistry when compared to their aliphatic counterparts, aromatic "plastics" are largely unsustainable, and the demands of emerging technologies require functionalities and forms that remain inaccessible. Thus, there remains a critical need to create new synthetic technologies that cannot be accommodated within the scope of traditional polymerization reactions, that revolutionize the lifecycle of these plastics, utilize unusable industrial and consumer waste, and which reduce environmental impacts. Here, we demonstrate new patterns of catalytic reactivity for homogenous gold catalysts that promote efficient and chemoselective transformations between traditionally unreactive bonds in monomers and polymers. This has enabled the direct *C*–*H* activation polycondensation of alkyne-containing comonomers and heteroarene nucleophiles with high reactivities to give high molecular weight (> 100 kg mol^{-1}) products. This represents *one of the first* examples of multiple successive intermolecular reactions mediated by Au. We further demonstrated a practical approach to functionalize aromatic polymers in a mild and chemoselective manner, activating unsaturated carbon-carbon (*C*–*C*) bonds towards the attack of a wide variety of nucleophiles in the presence of H_2O, O_2, acids, and functional groups that poison other catalysts. Results are consistent with the direct *C*(sp^2)–*H* functionalization of commercial polystyrene (PS), polyethylene terephthalate (PET), and polysulfone (PSU) using highly functionalized alkenes and alkynes. This reactivity is without precedent and opens completely new opportunities for the chemical transformation of aromatic polymers. Additional efforts have demonstrated that gold catalysis also offers completely new paradigms for monomer utilization, polymer synthesis, and advanced materials development.

Grant or FWP Number: DE-SC0021161
Gold Catalyzed Polymerization Reactions of Unsaturated Substrates: Towards New Functional, Recyclable, and Upcycled Aromatic Polymers

PI: Jason D. Azoulay
Postdoc: Naresh Eedugurala
Student(s): Eric King, Samuel Hunt
Affiliations: University of Southern Mississippi

RECENT PROGRESS

Gold Catalyzed C–H Functionalization Polycondensation for the Synthesis of Aromatic Polymers. Homogeneous gold (Au) complexes have demonstrated tremendous utility in modern organic chemistry; however, their application towards the synthesis of

polymers remains rare. Here, we demonstrate the first catalytic application of Au complexes toward the polycondensation of alkyne-containing comonomers and heteroarene nucleophiles. Polymerizations occur through successive intermolecular hydroarylations to produce high molecular weight aromatic copolymers with 1,1-disubstituted alkene backbone linkages. Clear correlations between the rate and degree of polymerization (DP) were established based on catalyst structure and counterion pairing enabling polymerizations that proceed with remarkable efficiency, high reactivities, and exceptional DPs. The reactivity is broad in scope, enabling the copolymerization of highly functionalized aromatic and aliphatic monomers. These results highlight the untapped utility of Au in the construction of new macromolecular chemistries.

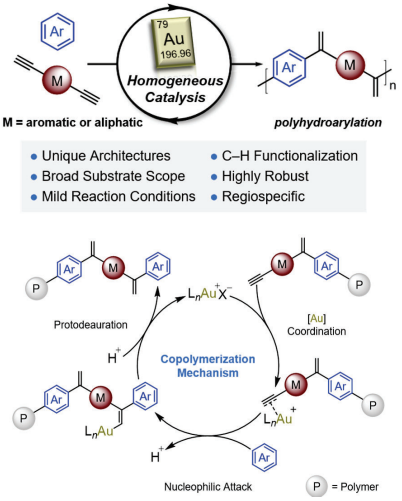

Figure 1. (Top) Gold catalyzed copolymerization using (hetero)arenes (Ar) and alkyne monomers (M). (Bottom) Proposed gold catalytic cycle for the copolymerization of arenes to generate polymers (P).

Gold-Catalyzed Post-Polymerization Modification of Commodity Aromatic Polymers

Synthetic aromatic polymers are ubiquitous and indispensable to modern life, industry, and the global economy. The direct functionalization of these materials remains a considerable challenge on account of their unreactive aromatic *C–H* bonds and robust physical properties. Despite the exploration of a vast chemical space, methods for the PPM of aromatic polymers are harsh, non-selective, necessitate multiple steps, and cause significant degradation (i.e., chain scission). Here, we demonstrate that homogenous gold catalysis offers a mild, chemoselective, and practical approach to functionalize high-volume commodity aromatic polymers. Utilizing a gold-catalyzed intermolecular hydroarylation between a highly functionalized alkyne, methyl propiolate, and nucleophilic arenes within polystyrene (PS) results in direct *C–H* functionalization of phenyl rings with 1,2-substituted methyl acrylate functional groups. The reactivity and functionalization depend on the steric and electronic environment of the catalyst, counterion pairing, and method of activation. The reactivity is broad in scope, enabling the functionalization of arenes within commercial polysulfone (PSU) and waste polyethylene terephthalate (PET). These reactions open new opportunities to chemically transform aromatic polymers and modify their physical properties.

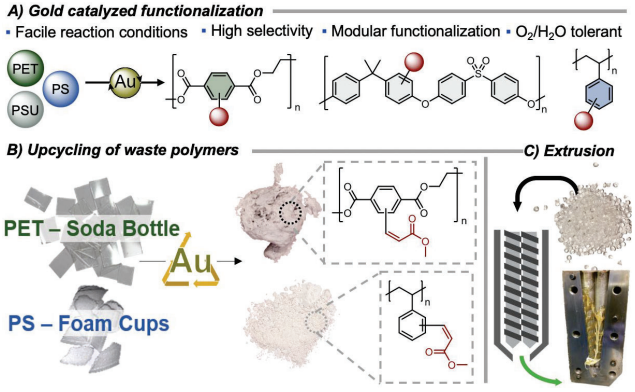

Figure 2. A) Gold-catalyzed post-polymerization modification of PET, PS, and PSU. B) Upcycling of waste PET and PS into methacrylate functionalized products. C) Functionalization of PS using reactive extrusion.

The facile modification of commodity polymers is advantageous since it makes use of optimized industrial processes for value-added materials and enables the use of discarded plastic as a resource. Several attributes of this reactivity are novel and noteworthy: (*i*) the reactions proceed using very mild conditions (i.e. 25–80 ºC); (*ii*) unprecedented levels of functionalization are achieved; (*iii*) the reactivity can be controlled using different catalysts and conditions; (*iv*) a very broad functional scope can be achieved; (*v*) the reaction proceeds in the presence of H_2O, O_2, acids and additives/contaminants–exemplified by the functionalization of commercial waste including PET (i.e. a soft-drink bottle) and PS foam (Fig. 2b). Moreover, the novel reactivity of Au enables new paths towards chemical cross-linking using commercial PS and a single monomer resulting in a highly functionalized network in a single step (Fig. 2). We have also demonstrated a practical and scalable reactive extrusion process (Fig. 2c). This reactivity is without precedent and opens completely new opportunities for the chemical transformation of aromatic polymers and manifold opportunities for chemical separation and upcycling.

Publications Acknowledging this Grant in 2020-2023

(I) Intellectually led by this grant

1. King, E.R.; Tropp, J.; Eedugurala, N.; Gonce, L. E.; Stanciu, S.; Azoulay, J. D.; "Gold-Catalyzed C–H Functionalization Polycondensation for the Synthesis of Aromatic Polymers" *Angew. Chem. Int. Ed.* **2020**, *59*, 21971–21975.
2. King, E.R.; Hunt, S.; Azoulay, J. D.; J. D. Azoulay "Post-Polymerization and Polymeric Material Modification Through Gold Catalysis" U.S. Provisional Application 63/105047 (**2020**).
3. King, E.R.; Hunt, S.; Hamernick, L. J.; Gonce, L. E.; Wiggins, J. S.; Azoulay J. D.; "Gold-Catalyzed Post-Polymerization Modification of Commodity Aromatic Polymers" *JACS Au* **2021**, *1*, 1342–1347.
4. Azoulay, J. D.; King, E.R.; Tropp, J.; "Gold Catalyzed Polymerization Reactions of Unsaturated Substrates" US Patent 11,359,049, **2022**.

Co-ACCESS at SSRL
Developing Synchrotron Operando Characterization Capabilities for the Catalysis Community

Simon R Bare[1], Adam S. Hoffman[1], Jiyun Hong[1], Jorge Perez-Aguilar[1], Rachita Rana[2], Fernando Vila[3]
[1]SSRL, SLAC National Accelerator Laboratory, [2]Department of Chemical Engineering, University of California at Davis, [3]Department of Physics, University of Washington

Presentation Abstract

Co-ACCESS (Task 4 of the SUNCAT FWP) focuses on developing *operando* catalysis characterization capabilities at SSRL that benefit the catalysis community at large. This poster will highlight a few of our developments, often in collaboration with our users in the following areas: (i) The limits of detection for X-ray absorption spectroscopy of heterogenous single atom catalysts where we make recommendations for the community to follow, (ii) The rigorous oxidation state assignments for supported Ga-containing catalysts using theory-informed XAS signatures from well-defined Ga(I) and Ga(III) compounds with a method that allows users to determine the amount of Ga(I) in their catalyst, and (iii) the development and application of CatMass and CatXAS as software tools to aid in the planning of their experiments and enhanced data processing, respectively.

Grant or FWP Number: FWP10049
SUNCAT Center for Interface Science and Catalysis FWP10049

PI: Thomas Jaramillo, Frank Abild-Pederson, Johannes Voss, Zhenan Bao, Stacey Bent, Matteo Cargnello, Michal Bajdich, Michaela B Stevens, Adam C Nielander Kirsten T Winther, William A. Tarpeh, Daniel Lee, Adam S Hoffman
Postdoc: Jiyun Hong
Research Associate: Jorge Perez-Aguilar
Student: Rachita Rana

Bart M. Bartlett

Rotating Ring-Disk Electrodes Show that Chloride-Mediated Electrochemical Ethanol Oxidation Occurs in Discrete One-Electron Steps

Bart M. Bartlett (PI), Siqi Li, Ryan D. Van Daele (Graduate Students), Katherine Morrissey (Undergraduate Student)
Department of Chemistry, University of Michigan, Ann Arbor, MI 48109-1055

Presentation Abstract

Combining redox mediators with photo- and/or electro-active materials is a promising strategy for synthesizing higher value products from biomass feedstocks. This poster presentation will highlight recent work in probing the kinetics for chloride-mediated ethanol oxidation on glassy carbon. Rotating-ring disk electrodes combined with UV-Vis spectroelectrochemistry reveal two distinct electron-transfer steps: a Volmer step in which chloride adsorbs to the glassy carbon followed by subsequent chloride-ion transfer to form an ethyl hypochlorite intermediate. This intermediate likely decomposes to acetaldehyde (not observed), which then rapidly condenses with ethanol solvent to form the product, 1,1-diethoxyethane. This mechanistic insight explains why no chlorinated products are observed and helps to direct future efforts in the broader class of mediated oxidation reactions.

DE-SC0006587: Tandem Electrocatalysis and Particle-based Catalysis as a Strategy for Mediated Alcohol Oxidation Reactions

RECENT PROGRESS

Chloride-Mediated Ethanol Oxidation

Recent work has focused on elucidating details of chloride-mediated ethanol oxidation on dark electrodes (glassy carbon). Koutecky-Levich analysis in **Figure 1** shows that the rate constant for the electrochemical chloride oxidation reaction (COR) is four order of magnitudes faster than that of direct alcohol oxidation (10^{-3} s^{-1} vs. 10^{-7} s^{-1}). This data corroborates the observed current density difference during cyclic voltammetry measurements in our previous publication (*J. Am. Chem. Soc.* **2021**, *143*, 15907). By varying the chloride ion concentration, we propose a one-electron transfer mechanism in which chloride adsorbs onto the glassy carbon electrode (a Volmer step). However, the lack of chlorinated products falsifies

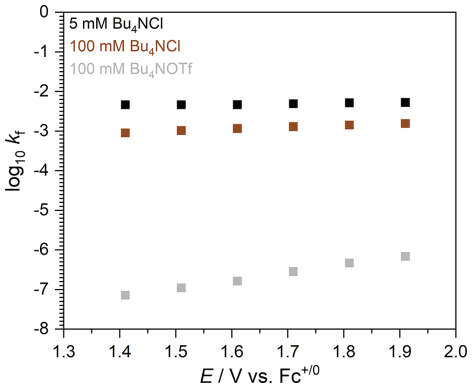

Figure 1. Forward rate constants as a function of applied potential for chloride oxidation in ethanol.

the formation of long-lived chlorine radical and suggests a fast or concerted reaction with ethanol solvent. This Volmer mechanism is further supported by observing a linear-dependence of peak current with scan rate after chloride adsorption in an inert solvent (**Figure 2**). UV-Vis spectroelectrochemistry in ethanol shows one sole chloride oxidation product (the ethyl hypochlorite intermediate with λ_{max} of 237 nm, data not shown) among the range of applied potentials 1.3 – 2.0 V vs. $Fc^{+/0}$, indicating that no mechanistic change occurs with increasing bias. Current efforts include expanding the hydrodynamic analysis towards oxidation reactions in other neat alcohol systems and using *in situ* IR spectroscopy to show adsorbed chlorine on the glassy carbon electrode.

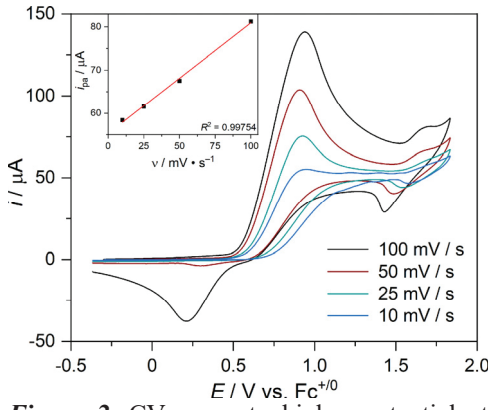

Figure 2. CV scans to higher potential at varying scan rate for 10 mM Bu_4NCl and 90 mM Bu_4NPF_6 dissolved in DCM. The working electrode is a GC disk with a Pt wire auxiliary electrode and a Ag wire pseudo-reference electrode normalized against the $Fc^{+/0}$ couple. **Inset**. i_{pa} vs. ν for the second oxidation wave.

Quantifying Surface Defects on Synthesized H_xWO_3 Particles

A second focus for recent work is establishing the titration methods needed to quantify surface defects on oxide materials. Lewis basic sites (surface oxygen vacancies) and Brønsted acidic sites (surface hydroxyl groups) can be distinguished by reactions with CO_3^{2-} (both a Lewis and Brønsted base) and lutidine (only a Lewis base). We prepare H_xWO_3 powders by spin coating ammonium metatungstate as a precursor and annealing in air according to the balanced equation:

$$(NH_4)_6H_2W_{12}O_{40} \cdot xH_2O(aq) + \frac{15}{2}O_2(g) \rightarrow 12WO_3(s) + 6NO(g) + (13+x)H_2O(g)$$

We find a nearly 10-fold greater density of Lewis acid sites than Brønsted acid sites at high temperatures, and not surprisingly, the density Lewis acid sites increases as annealing temperatu increases, illustrated in **Figure 3**. Together, these d suggest that the intercalated protons in the cubic si of H_xWO_3 are *not* strongly Brønsted acidic, and t there are few surface hydroxyls. Consequent oxygen vacancies dominate the surface chemist Current work focuses on decoupling electro structure imparted by the intercalated ion from t surface reactivity for both the chloride oxidation a oxygen evolution reactions by probing the activity f each reaction in electrolytes composed of varying alkali cations and on films annealed at varying temperatures.

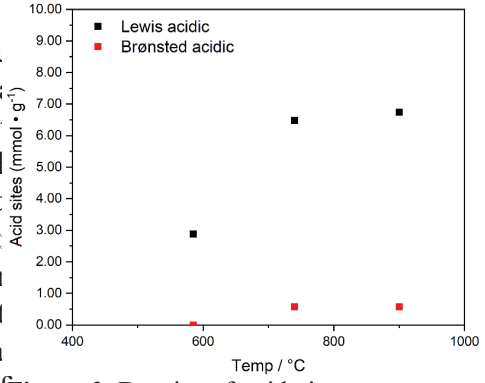

Figure 3. Density of acid sites on tungsten oxide as a function of annealing temperature.

Publications Acknowledging this Grant in 2019-2022

(I) Intellectually led by this grant

10. Breuhaus-Alvarez, A. G.; Li, S.; Hardin, N. Z.; Bartlett, B. M.* Oxidizing Ethanol and 2-Propanol by Hypochlorous Acid Generated from Chloride Ions on H_xWO_3 Photoelectrodes. *J. Phys. Chem. C* **2021**, *125*, 26307-26312.
9. Li, S.; Bartlett, B. M.* Selective Chloride-Mediated Neat Ethanol Oxidation to 1,1-Diethoxyethane via an Electrochemically Generated Ethyl Hypochlorite Intermediate. *J. Am. Chem. Soc.* **2021**, *143*, 15907-15911.
8. McDonald, K. D.; Bartlett, B. M.* Microwave synthesis of Spinel $MgFe_2O_4$ Nanoparticles and the Effect of Annealing on Photocatalysis. *Inorg. Chem.* **2021**, *60*, 8704-8709.
7. DiMeglio, J. L.; Terry, B. D.; Breuhaus-Alvarez, A. G.; Whalen, M. J.; Bartlett, B. M.* Base-Assisted Nitrate Mediation as the Mechanism of Electrochemical Benzyl Alcohol Oxidation. *J. Phys. Chem. C* **2021**, *125*, 8148-8154.
6. Breuhaus-Alvarez, A. G.; Cheek, Q.; Cooper, J. J.; Maldonado, S.; Bartlett, B. M.* Chloride Oxidation as an Alternative to the Oxygen Evolution Reaction on H_xWO_3 Photoelectrodes. *J. Phys. Chem C.* **2021**, *125*, 8543-8550.
5. Terry, B. D.; DiMeglio, J. L.; Cousineau, J. P.; Bartlett, B. M.* Nitrate Radical Facilitates Indirect Benzyl Alcohol Oxidation on Bismuth(III) Vanadate Photoelectrodes. *ChemElectoChem* **2020**, *7*, 3776-3782.
4. Proctor, A. D.; Bartlett B. M.* Hydroxyl Radical Suppression during Photoelectrocatalytic Water Oxidation on WO_3 | FeOOH. *J. Phys. Chem. C.* **2020**, *124*, 17957-19763.
3. McDonald, K. D.; Bartlett, B. M.* Photocatalytic Primary Alcohol Oxidation on WO_3 Nanoplatelets. *RSC Adv.* **2019**, *9*, 28688-28694.
2. DiMeglio, J. L.; Breuhaus-Alvarez, A. G.; Li, S.; Bartlett, B. M.* Nitrate Mediated Alcohol Oxidation on Cadmium Sulfide Photocatalysts. *ACS Catal.* **2019**, *9*, 5732-5741.
1. Breuhaus-Alvarez, A. G.; DiMeglio, J. L.; Cooper, J. J.; Lhermitte C. R.; Bartlett, B. M.* Kinetics and Faradaic Efficiency of Oxygen Evolution on Reduced H_xWO_3 Photoelectrodes. *J. Phys. Chem. C* **2019**, *123*, 1142-1150.

Elizabeth J. Biddinger

Speciation and Sources of Copper Electrocatalyst Fouling During Electrochemical Hydrogenation and Hydrogenolysis of Furfural in Acid

Andrew S. May and Elizabeth J. Biddinger*
Department of Chemical Engineering, The City College of New York, CUNY, New York, New York 10031, United States

Presentation Abstract

Understanding the electrocatalyst deactivation pathways and how deactivation impacts electrochemical reactions of biomass-derived species is important for continuing development and improvement of the reactions. The electrochemical hydrogenation and hydrogenolysis of furfural to furfuryl alcohol and 2-methyl furan, respectively, is a promising way to produce chemical intermediates and alternative fuel candidates. To produce 2-methyl furan, highly acidic electrolytes and copper electrocatalysts are required. This highly acidic condition also drives undesired homogeneous side reactions of the furanics and fouls the electrode surface. Through an intentional electrode fouling study, the fouling was identified as potential-dependent and coming from the starting material furfural, not the products. At less negative potentials at the cathode, poly(furfuryl alcohol) was formed as the deactivating layer. At more negative potentials at the cathode, coke was formed as the deactivating layer on the electrode. The polymerization and coking was found to be electrochemically-driven, not forming in the absence of an applied potential. Additionally, under an applied potential with only the furfuryl alcohol, which would mimic the products in the electrolyte, no fouling was observed. With the enhanced understanding of electrode fouling, mechanisms can be developed to incorporate the fouling and better systems can be designed to mitigate the fouling.

Grant or FWP Number: Grant Title
DE-SC0019134: Reaction Mechanism and Kinetics for Electrochemical Hydrogenation and Hydrogenolysis of Biomass-Derived Species

PI: Elizabeth J. Biddinger
Postdoc(s): N/A
Student(s): Andrew S. May[1], Steven M. Watt[1,2], Seoyeong Lee[1], Sarvar Talipov[1], Moses Chilunda[1], Hafiz M. Umar Farooq[1]
Affiliations(s): [1] Department of Chemical Engineering, The City College of New York; [2] PhD Program in Chemistry, CUNY Graduate Center

RECENT PROGRESS

Progress on understanding of electrode fouling and relation to electrochemical hydrogenation and hydrogenolysis

Electrochemical hydrogenation and hydrogenolysis (ECH) of furfural (FF) results in the formation of furfuryl alcohol (FA) and 2-methyl furan (MF) being formed. To form MF, copper electrocatalysis and acidic conditions are required. The very acidic conditions required to achieve high selectivities toward 2-methyl furan during ECH also drive undesired side reactions both in solution and on the electrode surface. To better understand the behavior of the side reactions at the electrode surface that result in electrode fouling, a study was performed to intentionally foul the electrode surface. High concentrations of furfural (200 mM) and highly acidic electrolyte (0.5M H_2SO_4 in 20:80 v:v acetonitrile:water) were used to drive the fouling. Copper foil electrodes were used in fresh electrolyte three times to increase the build-up of fouling for characterization (Fig. 1a). Two cathodic potentials were investigated: -560 mV vs. RHE and -700 mV vs. RHE. At both potentials the fouling worsened the reaction performance with electrode reuse (Fig. 1b-d). The resistance of the electrodes also increased with reuse, further supporting that fouling had occurred.

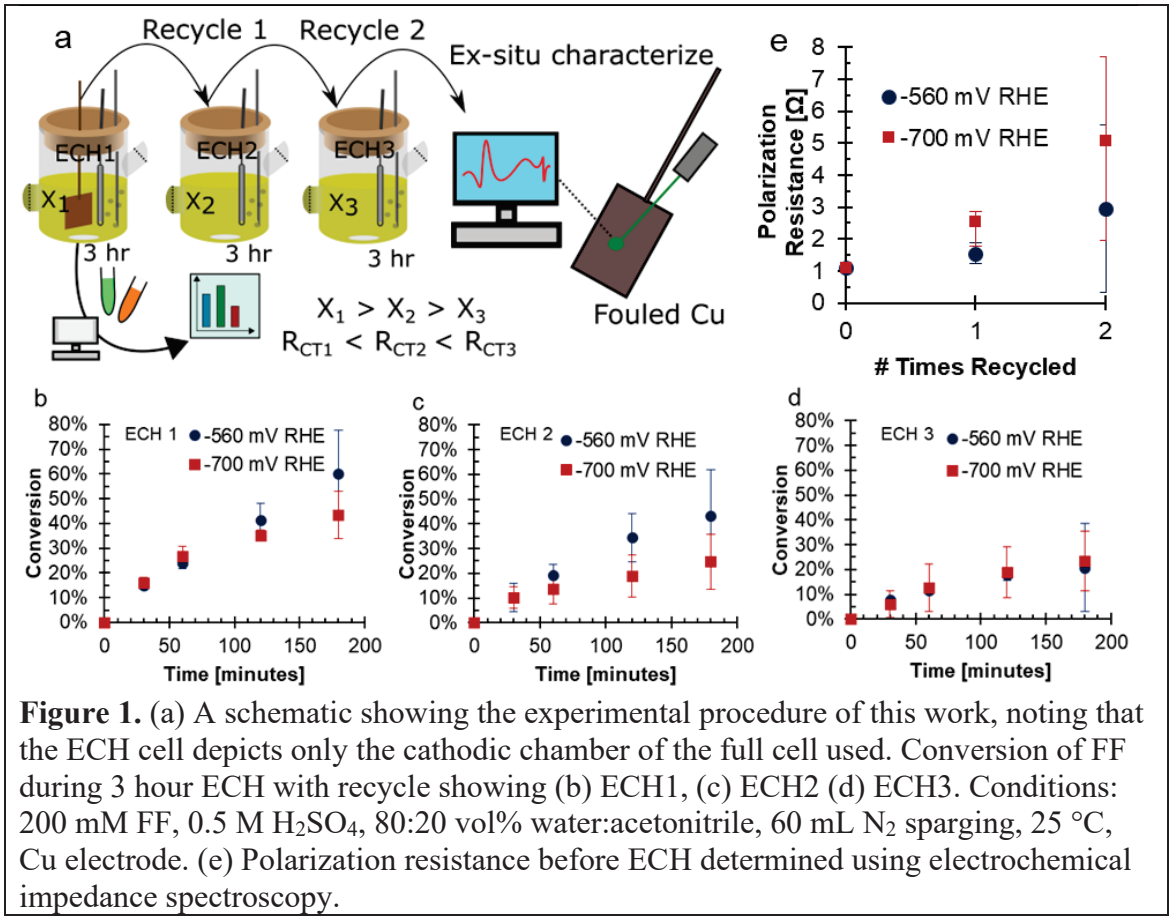

Figure 1. (a) A schematic showing the experimental procedure of this work, noting that the ECH cell depicts only the cathodic chamber of the full cell used. Conversion of FF during 3 hour ECH with recycle showing (b) ECH1, (c) ECH2 (d) ECH3. Conditions: 200 mM FF, 0.5 M H_2SO_4, 80:20 vol% water:acetonitrile, 60 mL N_2 sparging, 25 °C, Cu electrode. (e) Polarization resistance before ECH determined using electrochemical impedance spectroscopy.

The fouled Cu electrodes were characterized to identify the species present and the coverage. After the three uses, the Cu electrodes were completely covered in a carbonaceous material. At -560 mV vs. RHE, the material on the electrode was found to be polyfurfuryl alcohol, as evidenced via FTIR (Fig. 2.). The -700mV vs. RHE fouled electrode did not have a spectra that resembled polyfurfuryl alcohol, rather it behaved like a black body. Further analysis of the fouled electrodes using Raman spectroscopy (Fig. 3) revealed that coke or soot was formed on the -700 mV vs. RHE electrode, rather than a polymer.

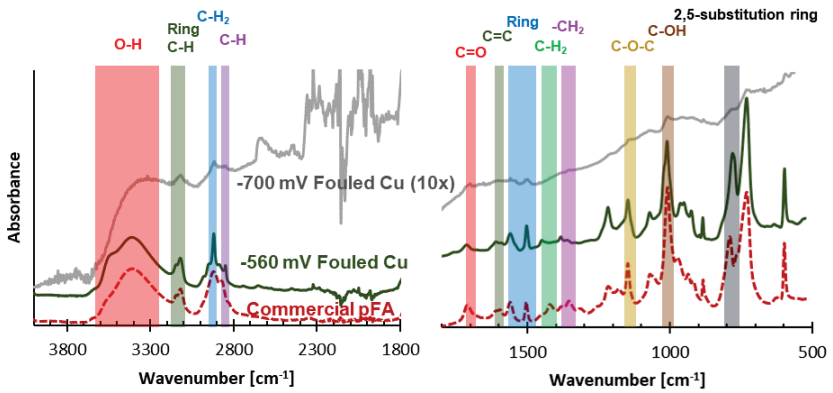

Figure 2. FTIR spectra of -560 mV RHE fouled Cu polymer, commercial pFA, and 10x magnified -700 mV RHE fouled Cu. Shaded areas indicate key pFA band.s

Additional experiments were performed to determine the source of the fouling. To determine if the fouling was electrochemically driven or if the fouling was a result of homogeneous reaction products adsorbing to the surface of the Cu electrode, the electrode was submerged in a simulated reaction electrolyte containing 100mM FF and 30mM FA (the MF during ECH of FF is in situ evaporated out of the electrolyte to a solvent trap using inert gas sparging). Species characteristic of humins were identified on the Cu electrode after the submersion experiment. No evidence of polymerization was observed, indicating that the polyfurfuryl alcohol formation was an electrochemically-driven reaction.

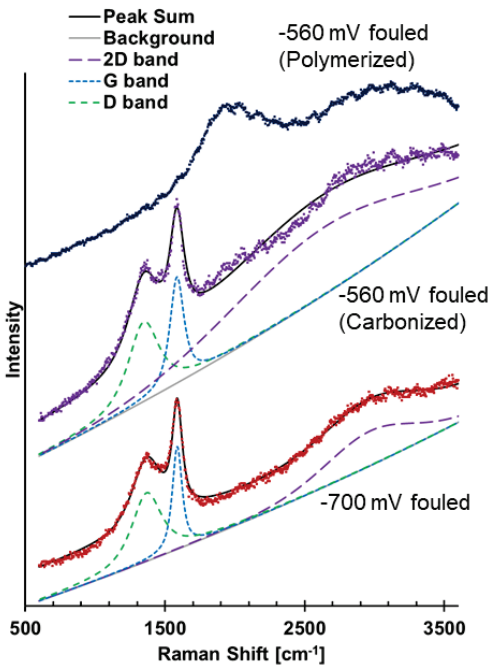

Figure 3. Raman spectra of -700 mV RHE fouled Cu showing D, G, and 2D bands, spectra of -560 mV RHE fouled Cu showing spectra from a carbonized area of electrode and a polymerized area of the electrode.

To better identify if furfural or furfuryl alcohol is the initiating species for the electrode fouling, ECH was performed on Cu electrodes with FA as the starting reactant instead of FF. Characterization of the electrodes did not reveal any polyfurfuryl alcohol, coke or humins. This result indicates that FA is not the source of

electrocatalyst fouling, rather FF is the source.

FA was significantly converted over the reaction periods during the ECH of FA experiments, however. Fig. 4 includes the conversion and mass balance for a single experimental run at -560 mV vs. RHE. Previously in our group and others, it has been shown that FA does not further react to form MF. Similarly, in this work, MF was not detected. During the ECH of FA experiment at -560 mV RHE, the conversion of FA reached an average of (40.9 ± 2.59)%. FA is known to undergo side reactions homogeneously due to the acidic conditions, and using the homogeneous kinetics from our previous work, the expected conversion in FA was found to be 39.4%. The unreacted FA and the estimated consumption due to side reactions accounted for 98.7% of the initial FA, showing that it was unlikely that mass was lost due to electrochemical reactions of FA.

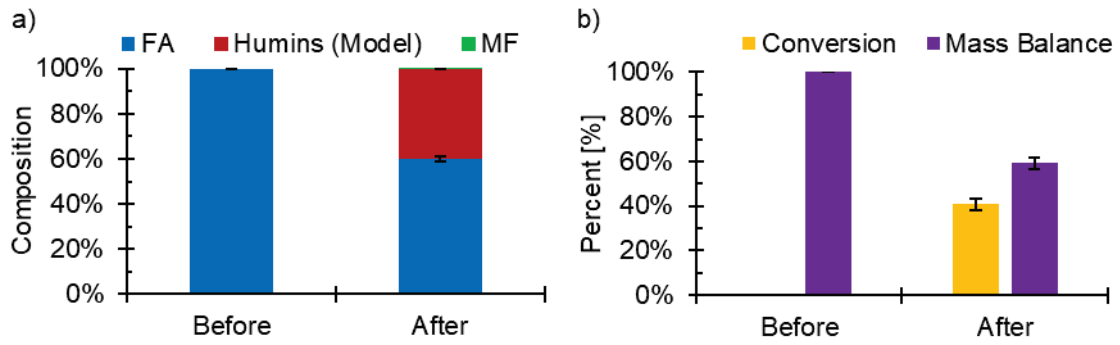

Figure 4. The composition of the FA ECH electrolyte before and after 3hr ECH. (b) The conversion and mass balance from FA ECH experiments. Conditions: -560 mV RHE, 80:20 vol% acetonitrile:water, 0.5M H_2SO_4, 15 mM FA, N_2 sparging 60 mL/min, Cu electrode.

Through this study, we were able to identify that FF, not FA is the source of the fouling and that the fouling is electrochemically-driven and the species are potential-dependent.

Publications Acknowledging this Grant in 2020-2023

(I) Intellectually led by this grant

1. May, A. S.; Biddinger, E. J., Strategies to control electrochemical hydrogenation and hydrogenolysis of furfural and minimize undesired side reactions. *ACS Catal.* **2020**, 10, 3212-3221.
2. May, A. S.; Watt S. M.; Biddinger E. J., Kinetics of furfural electrochemical hydrogenation and hydrogenolysis in acidic media on copper. *React. Chem. Eng.* **2021**, 6, 2075-2086.
3. May, A. S.; Biddinger, E. J. Modeling competing kinetics between electrochemical reduction of furfural on copper and homogeneous side reactions in acid. *Energy Fuels.* **2022**, 36, 11001–11011.

(II) Jointly funded by this grant and other grants with intellectual leadership by other funding sources

1. S. Sharifi Golru, A.S. May, E.J. Biddinger, "Modifying Copper Local Environment with Electrolyte Additives to Alter CO_2 Electroreduction vs Hydrogen Evolution," *ACS Catal.*, **2023,** 13, 7831-7843.

Jesse Q. Bond

Quantifying the activity of alloy catalysts under working conditions

Jesse Q. Bond, Robson Schuarca, and Yaqin Tang
Biomedical and Chemical Engineering, Syracuse University, Syracuse, NY 13244

Presentation Abstract

Catalytic metals are frequently combined with secondary, promoter metals to improve dispersion, enhance activity, and/or prevent side reactions. Unfortunately, when working with supported nanoparticles, mixing metals will usually create heterogeneous alloys. This makes it difficult to rigorously quantify reaction rates on these "technical catalysts." For most alloys, the concept of an active site is ambiguous. Moreover, individual components of an alloy may respond differently to their environment, so they are apt to restructure under reaction conditions. Dynamic, ill-defined active sites provide a challenging basis for defining turnover frequencies, which prevents a meaningful assessment of how nominal changes in alloy structure or composition impact catalytic activity. As a potential resolution, we consider the use of transient response methods, like steady state isotopic transient kinetic analysis (SSITKA), for characterizing catalyst activity. We compare results with those obtained through conventional packed bed experiments and titrant chemisorption. The aim is to develop a suite of tools that allow facile, accessible, and accurate determination of turnover rates for materials with poorly defined active sites. Coupling these techniques with appropriate in situ characterization methods should enable a better understanding of how the structure and composition of metal alloys impacts their function. Data are presented here for Pt and Pt_xSn_y alloys supported on SiO_2 and γ-Al_2O_3 and employed for the hydrogenation of CO and acetone, and we consider the impact of changes in alloy composition and the identity of the metal support.

Grant or FWP Number:
DE-SC0022071: Connecting surface structure with activity for alloy catalysts under working conditions.

PI: Jesse Q. Bond
Postdoc(s): None
Student(s): Robson Schuarca, Yaqin Tang
Affiliations(s): Syracuse University, Biomedical and Chemical Engineering

RECENT PROGRESS

We have characterized CO methanation over monometallic Pt/SiO_2, monometallic Pt/γ-Al_2O_3, and bimetallic Pt_xSn_y supported on SiO_2 and γ-Al_2O_3. Sn introduction is detrimental to the extensive rate of CO hydrogenation over Pt, but as long as alloys remain randomly ordered, it has little impact on the intrinsic activity of Pt. In most cases, Pt_xSn_y catalysts, resemble partially deactivated Pt catalysts. The one exception is that when we observe the formation of ordered, intermetallic phases, like PtSn. We find that these intermetallics have no activity for CO hydrogenation. FTIR spectra suggest that CO binds atop at Pt atoms comparably in monometallic Pt, random alloys, and intermetallics, whereas we see a loss of bridging CO bands in intermetallic phases. As such, we attribute the inactivity of intermetallics to the loss of Pt-Pt site pairs, which presumably lowers the rates of elementary steps that involve site pairs, such as C-O dissociation, C-H formation, and O-H formation. We thus conclude that loss of CO hydrogenation activity in PtSn intermetallics is more a geometric effect than an electronic one. For most samples, we observe agreement in turnover frequencies calculated from (1) steady state methane formation rates in a packed bed and (2) SSITKA experiments utilizing $^{12}CO/^{13}CO$ switches. We are developing open-source tools in Julia to enable a more rigorous quantification of elementary kinetic parameters (e.g., barriers and pre-exponential factors) by modelling reactor dynamics in response to isotope switching.

As we conclude analysis of CO methanation, we have shifted to acetone hydrogenation as a model system. Macroscopic trends are similar to those observed during CO methanation over Pt and Pt_xSn_y. Specifically, adding Sn reduces extensive rates of acetone hydrogenation. While evidence points to a geometric effect in CO methanation, the mechanistic origin of the activity loss is unclear during acetone hydrogenation. This system is more complex, and we see a prominent support effect, which makes resolving contributions from Pt and Sn considerably more difficult. Specifically, Pt/γ-Al_2O_3 is roughly 5 times more intrinsically active than Pt/SiO_2. To exclude potential impacts of heat transfer, mass transfer, and particle size effects (structure sensitivity), we considered a Madon-Boudart type plot for acetone hydrogenation rates measured over Pt/SiO_2 and Pt/γ-Al_2O_3 (Figure 1). In both systems, rates scale linearly with titrant (CO) uptake for a given sample—this is independent of average metal cluster sizes between 1 nm and 20 nm. This suggests that acetone hydrogenation is structure insensitive on both Pt/SiO_2 and Pt/γ-Al_2O_3 and that rates are kinetically controlled. We therefore attribute the factor of ~ 5 difference in rates observed over Pt/γ-Al_2O_3 to an intrinsic support effect that cannot be explained by dispersion effects, particle size effects, or transport control.

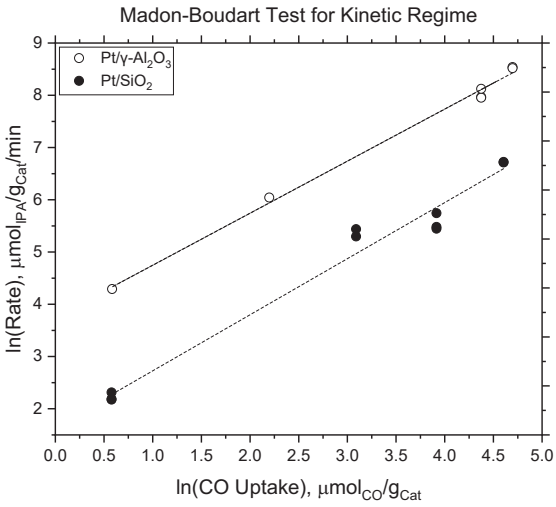

Figure 1: Madon-Boudart plot for acetone hydrogenation over Pt/SiO_2 and Pt/γ-Al_2O_3. Slopes of regressed lines are ≈1, indicating kinetic control and structure insensitivity.

Publications Acknowledging this Grant in 2019-2022

Please classify your publications into two categories according to the source of support for the work published:

(I) Intellectually led by this grant

1. (Conference Presentation) Bond, J.Q. "Modelling and analysis of transient phenomena in catalytic flow reactors," ACS Fall Meeting, August 2022
2. (Conference Workshop) Bond, J.Q., "Obtaining good kinetic insights from badly-behaved reactors," NAM 2023.

(II) Jointly funded by this grant and other grants with intellectual leadership by other funding sources

1. He, W, Potts, D.S., Zhang, Z., Liu, B., Schuarca, R.L., Hwang, S., Bond, J.Q., Flaherty, D.W., and Cybulskis, V.J., "Lewis acidity and substituent effects influence aldehyde enolization and C-C coupling in beta zeolites," *J. Catal*, **2023**, Article in Press.

Bert D. Chandler

The Role of Surface Hydroxyls and Entropy in Hydrogen Spillover

Akbar Mahdavi-Shakib,[1]† Todd N. Whittaker,[2,3]† Tae Yong Yun,[1] K. B. Sravan Kumar,[4]‡ Lauren C. Rich,[2] Shengguang Wang,[4] Robert M. Rioux,[1,5] Lars C. Grabow,[4] and Bert D. Chandler[1,5]

[1]Department of Chemical Engineering, The Pennsylvania State University, University Park, Pennsylvania 16802, United States

[2]Department of Chemistry, Trinity University, San Antonio, Texas 78212-7200, United States

[3]Department of Chemical and Biological Engineering, The University of Colorado, Boulder, Colorado 80303, United States

[4]Department of Chemical and Biomolecular Engineering, University of Houston, Houston, TX 77204-4004

[5]Department of Chemistry, The Pennsylvania State University, University Park, Pennsylvania 16802, United States

Presentation Abstract

Hydrogen spillover involves the migration of H atom equivalents from metal nanoparticles to a support. While well-documented, H spillover is poorly understood and largely unquantified. Here, we measure weak, reversible H_2 adsorption on Au/TiO_2 catalysts, and extract the surface concentration of spilled-over hydrogen. The spillover species (H*) is best described as a loosely coupled proton/electron pair distributed across the titania surface hydroxyls. In stark contrast to traditional gas adsorption systems, H* adsorption increases with temperature. This unexpected adsorption behavior has two origins. First, entropically favorable adsorption results from high proton mobility and configurational surface entropy. Second, the number of spillover sites increases with temperature, due to increasing hydroxyl acid-base equilibrium constants. Increased H* adsorption correlates with the associated changes in titania surface zwitterion concentration. This study provides a quantitative assessment of how hydroxyl surface chemistry impacts spillover thermodynamics and contributes to the general understanding of spillover phenomena.

DE-SC0022053: Tuning Hydrogenation & Hydrogenolysis Activity away from the H_2 Binding Site

Postdoc(s): Akbar Mahdavi-Shakib
Student(s): Tae Yong Yun

Supported Au catalysts have excellent selectivity for a number of important hydrogenations and semi-hydrogenations but have notoriously low activity. We have been studying hydrogen adsorption on Au/TiO_2 catalysts to better understand how to improve their activity. Hydrogen chemisorption on Au surfaces is widely recognized to be thermodynamically unfavorable; however, our recent work indicates hydrogen adsorption occurs via heterolytic activation at the metal support interface, not on the Au. To date no one has examined weak hydrogen adsorption on Au catalysts.

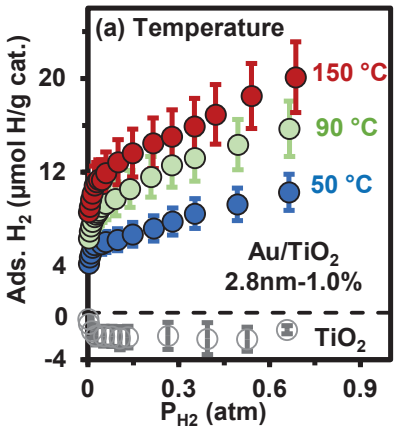

Figure 1. H_2 adsorption isotherms for Au/TiO_2.

Figure 1 shows isotherms for reversible hydrogen adsorption on a 1% Au/TiO_2 catalyst. Each isotherm was measured with a combination of volumetric adsorption and infrared spectroscopy to confirm no water was removed from the surface. Isotherms are completely reversible via evacuation at the adsorption temperature and was repeated at least four times (error bars show standard deviations). Weak, reversible adsorption shows a surprising trend: the total amount of adsorption increases with temperature.

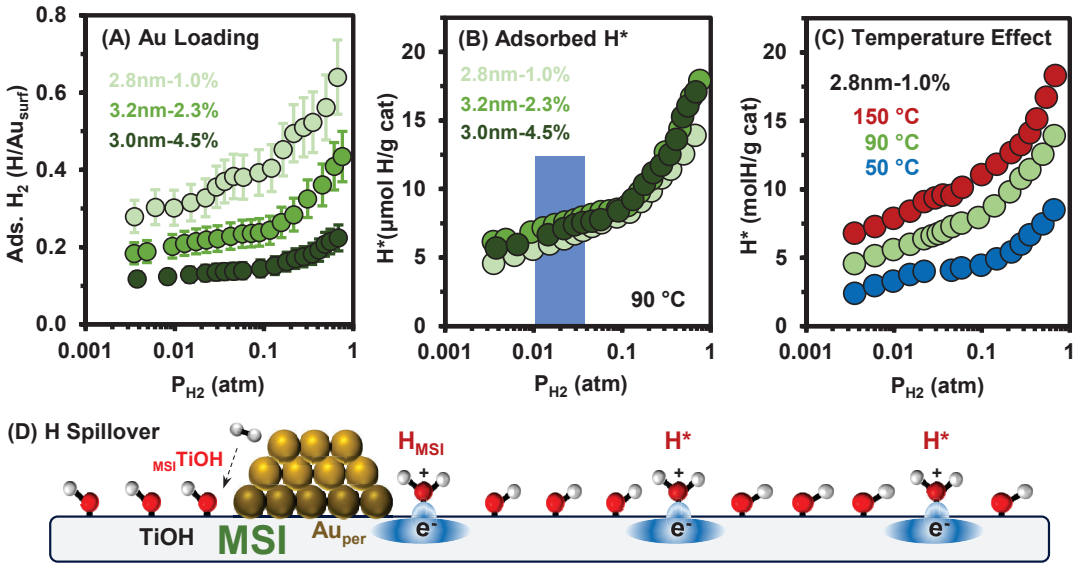

Figure 2. Determination and schematic of H_2 adsorption at the MSI and spillover H.

Figure 2A shows H_2 adsorption isotherms for three Au/TiO_2 catalysts in which the Au particle size was held constant, but the Au loading varied, normalized to the surface Au

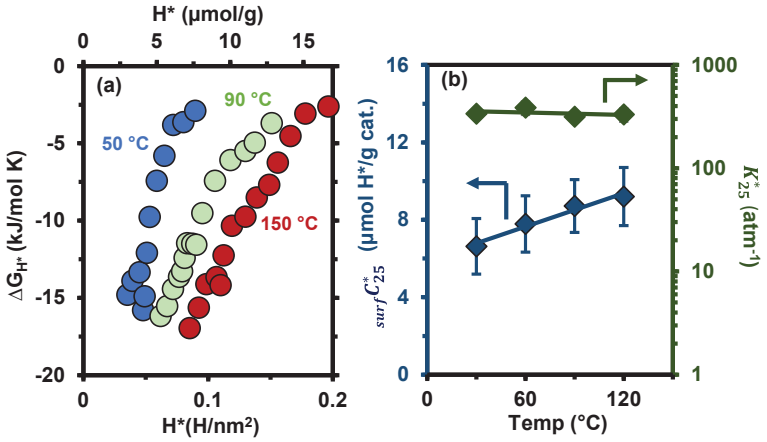

Figure 3. H* adsorption energetics and site density determined with a progressive Langmuir analysis.

fraction. The increase in total adsorption with decreasing Au loading indicates the adsorbed H does not migrate to the Au surface; rather, the adsorption occurs on the support. Normalizing the adsorption by accounting for the relatively stronger (but still readily reversible) adsorption at the metal-support interface (MSI) yields identical isotherms (**Figure 2B**), consistent with this conclusion. We therefore conclude these isotherms are a combination of H_2 adsorption at the MSI and spillover hydrogen (H*) on the support; to our knowledge, these are the first reported quantitative H* measurements in the literature. Adsorption at the MSI does not change across the temperature range in Figure 1, allowing us to extract the H* portion of the isotherms (**Figure 2C**); both types of adsorption are shown schematically in **Figure 2D**.

H* isotherms do not fit Langmuir or Temkin adsorption models; however, a progressive Langmuir analysis allows us to extract coverage dependent adsorption parameters. **Figure 3A** shows ΔG_{ads} values determined from extracted adsorption equilibrium constants. At constant H* coverage, the adsorption free energy increases with temperature; this suggests entropically favorable adsorption. A van't Hoff analysis (**Figure 3B**) shows the H* enthalpy of adsorption to be essentially thermoneutral. The van't Hoff analysis also suggests the number of adsorption sites populated at 25 Torr increases with temperature.

There are few reported similar cases of entropically favorable adsorption in the literature. **Figure 4** shows H_2 adsorption is entropically favorable when the surface entropy is greater than ~65 J/molK; this is a relatively small value. For H*, the surface entropy is composed of three components: vibrational, translational, and configurational entropy. Treating the adsorbed H* as a weakly coupled proton-electron pair (surface proton, sub-surface electron in the titania conduction band), we determined the generated surface $TiOH_2^+$ species to have a maximum vibrational entropy of ~10 J/molK. This value is small relative to the total surface

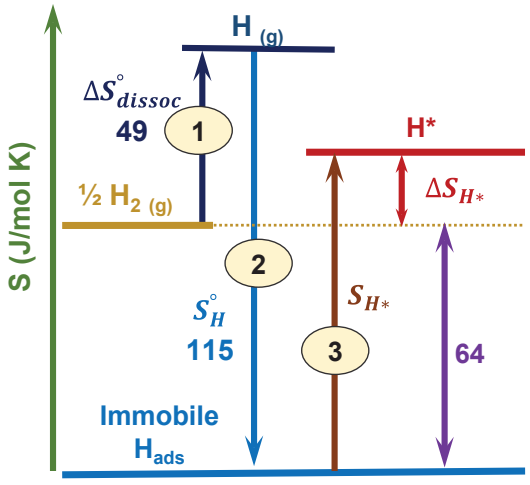

Figure 4. H_2 adsorption entropy diagram.

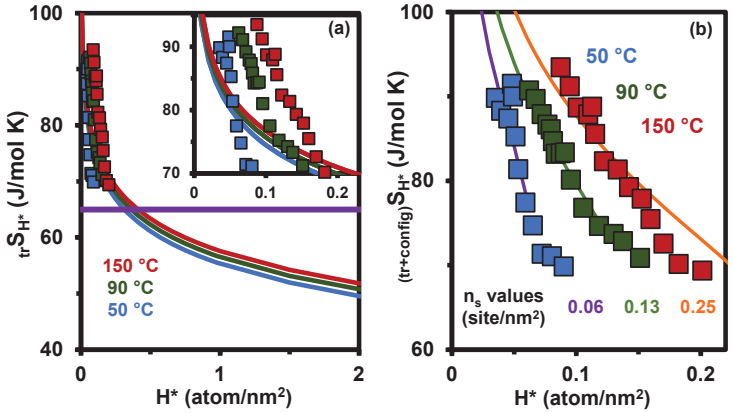

Figure 5. Translational (A) and Translational + configurational entropy contributions to the H* ΔS_{ads}.

entropy and on the order of our measurement errors. Vibrational entropy contributions were therefore excluded from our subsequent analysis.

Translational entropy is dominated by the average area per adsorbate; **Figure 5a** shows, translational entropy is sufficient to drive H* adsorption at very low coverages. The inset shows the experimental data are not well described by translational entropy alone. When a configurational entropy term is added (**Figure 5b**) the total surface entropy change is well described only when the number of adsorption sites increases with temperature. We note the number of adsorption sites is a fitted parameter likely describing the complex configurations of protons across the surface.

Aqueous slurry titrations (reported last year) previously showed significant changes in the surface point of zero charge as temperature increases. We surmised temperature-dependent changes to the surface protonation state might be associated with the observed increase in H* site density. Note, the surface equilibrium resulting in greater amounts of proton transfer at higher temperatures is essentially the same as the well-known increase in the water autodissociation constant (K_w) with temperature; this is also an effect of entropy. The autodissociation of surface hydroxyls results in the generation of a surface zwitterion; the surface concentration of these zwitterions depends on temperature dependent changes in the surface K_a and K_b values. The surface zwitterion concentration can be estimated based on the values determined in water; as **Figure 6** shows, the H* surface concentration is strongly correlated with both estimates of the surface zwitterion concentration.

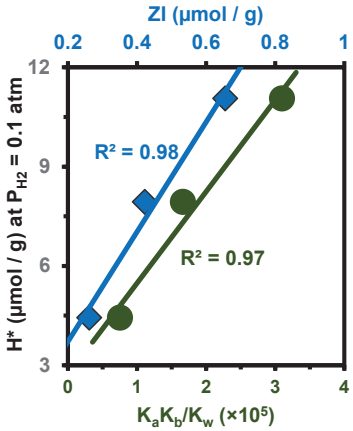

Figure 6. H* surface concentration plotted against two estimates of the surface zwitterion concentration.

Publications Acknowledging this Grant in 2020-2023

Please classify your publications into two categories according to the source of support for the work published:

(I) Intellectually led by this grant

1. Mahdavi-Shakib, A; Whittaker, T; Yun, TY Kumar, S; Rich, LC; Wang, S; Rioux, RM; Grabow, LC; Chandler, BD;* "The Role of Surface Hydroxyls in the Entropy Driven Adsorption and Spillover of H_2 on Au/TiO_2 Catalysts", *Nature Catalysis*, **2023**, v6, p710-719 (DOI: 10.1038/s41929-023-00996-3).
2. Yun, TY & Chandler, BD*; "Surface Hydroxyl Chemistry of Titania- and Alumina-Based Supports: Quantitative Titration and Temperature Dependence of Surface Brønsted Acid–Base Parameters", *ACS Applied Materials & Interfaces*, **2023**, v15, p6868–6876 (DOI: 10.1021/acsami.2c20370).

(II) Jointly funded by this grant and other grants with intellectual leadership by other funding sources

(*The length of the extended abstract, excluding the Publications list, is limited to 4 pages for university grants and 6 pages for laboratory FWPs. If multiple Presentations refer to the same Grant or FWP, include the Grant/FWP section in only one extended abstract.*)

Gas-Phase Hydrogenation and Hydroformylation with Metal-Organic Framework Catalysts

Donna A. Chen,[1] Juan D. Jimenez,[2] Sanjaya D. Senanayake,[2] Natalia B. Shustova,[1] Deependra M. Shakya,[1] Musbau Gbadamosi,[1] Konstantinos D. Vogiatzis,[3] and Gavin McCarver[3]
[1]University of South Carolina, Department of Chemistry and Biochemistry
[2]Brookhaven National Laboratory, Chemistry Division
[3]University of Tennessee at Knoxville, Department of Chemistry

Presentation Abstract

The $Cu_xRh_{3-x}(BTC)_2$ catalyst (abbreviated CuRhBTC, BTC^{3-} = benzene tricarboxylate) provides excellent dispersion of active metal sites coupled with well-defined structures for hydrogenation and hydroformylation reactions. This material therefore serves as a unique prototype for understanding catalytic activity in metal organic frameworks (MOFs). The mechanism of gas-phase hydrogenation at the bimetallic metal nodes of a MOF has been investigated in detail for the first time using in situ spectroscopy and diffraction experiments combined with density functional theory (DFT) calculations. The reaction occurs via a cooperative process in which the metal and linker sites play complementary roles; specifically, H_2 is dissociated at a Rh^{2+} site with a missing Rh-O bond, while protonation of the decoordinated carboxylate linker stabilizes the active sites and promotes H_2 dissociation. In situ Raman spectroscopy and diffuse reflectance infrared Fourier transform spectroscopy (DRIFTS) experiments demonstrate that propylene adsorbs at both Rh^{2+} and Cu^{2+} sites via π bonding. Cu^{2+} is catalytically inactive, but at Rh^{2+} sites, a propyl intermediate is observed when H_2 is introduced into the propylene feed. Furthermore, the appearance of the O-H stretch of COOH at ~3690 cm^{-1} in the DRIFT spectra is characteristic of defects consisting of missing Rh-O bonds. These experimental results are consistent with the reaction mechanism proposed by DFT, in which the decoordinated carboxylate linker is protonated, and the active Rh^{2+} site remains available for readsorption of reactants in the subsequent catalytic cycle. Gas phase ethylene hydroformylation studies have also been carried out on $Cu_xRh_{3-x}(BTC)_2$ as well as other Rh-containing MOFs with Rh in different coordination environments. Rh-containing MOFs have higher selectivity for the desired propanal product over ethane compared to oxide-supported metallic Rh particles.

DE-SC0019360: Multimetallic Metal-Organic Frameworks as Heterogeneous Catalysts for Gas Phase Hydroformylation and Hydrogenation Reactions

PIs: Donna A. Chen, Natalia B. Shustova, and Graeme Henkelman
Students: Deependra M. Shakya, Musbau Gbadamosi, Kyoungchul Park, Gina Wilson, Naman Katyal, and Ben Patterson

RECENT PROGRESS

Gas-phase hydroformylation of alkenes on Rh-containing MOFs were studied in order to design catalysts with high selectivity toward the aldehyde product. Given that gas-phase hydroformylation on supported metallic Rh particles results in the fully hydrogenated alkane as a major product, there is a need to develop catalysts with better selectivity to the more valuable aldehyde. Although solution-phase hydroformylation with Rh-containing organometallic compounds, such as Wilkinson's catalyst, have high selectivity to the aldehyde, heterogeneous gas-phase catalysis is more economical due to ease of separation. Rh-containing MOFs offer the synthetic flexibility to create the highly dispersed, isolated ionic Rh sites found in the organometallic catalysts while enabling heterogeneous catalysis in the gas phase.

The $Cu_xRh_{3-x}(BTC)_2$ (BTC^{3-}=benzene tricarboxylate, abbreviated CuRhBTC, Fig. 1) was the first MOF studied for hydroformylation since our previous studies of this system showed that this MOF is capable of hydrogen dissociation and hydrogenation of alkenes. The CuRhBTC MOF was synthesized by exposing $Cu_3(BTC)_2$ (HKUST-1, abbreviated CuBTC) to a solution of $RhCl_3$ at elevated temperature, and Raman spectroscopy experiments established that Rh ions were substituted for Cu ions in the paddlewheel node, based on the appearance of Cu-Rh and Rh-Rh stretches. Furthermore, X-ray photoelectron spectroscopy (XPS) and X-ray Absorption Near Edge Structure (XANES) experiments established that the Rh ions have an unusual +2 oxidation state in CuRhBTC. Ethylene was chosen as the reactant since it is a simple alkene and the rate of hydroformylation for ethylene is higher than that for larger alkenes. Reaction conditions were ethylene:hydrogen:CO=22:22:2 sccm at 80 °C and 3 atm. The exact conditions of temperature, pressure, feed gas composition were chosen to maximize activity and selectivity for propanal, while minimizing MOF decomposition via reduction of the metal nodes. Prior to reaction, the CuRh(3.4%)BTC was dried under N_2 for 90 min. Notably, in situ activation under He for 3 hrs at 100 °C to remove coordinating ethanol solvent resulted in substantial deactivation. Fig. 2 shows the rate of propanal and ethane production as a function of time on stream; no other products were detected although the residual ethanol solvent was observed for the first 10 hours on stream.

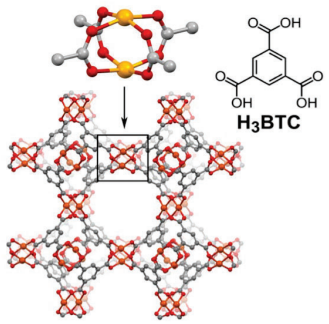

Fig. 1: Structure of the CuBTC MOF showing the paddle-wheel metal node and the structure of the H_3BTC linker.

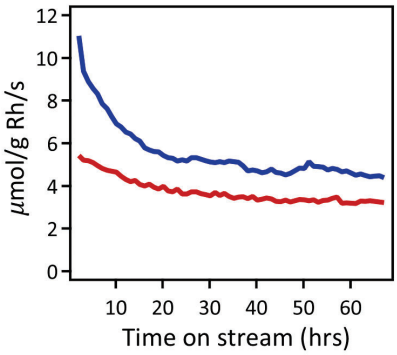

Fig. 2: Hydroformylation activity on CuRh(3.4%)BTC for propanal (red) and ethane (blue).

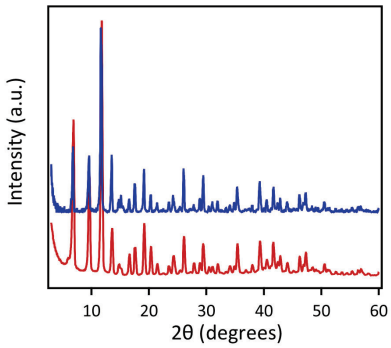

Fig. 3: PXRD of CuRh(3.4%)BTC before (red) and after (blue) hydroformylation.

During the period of time when ethanol is still desorbing from the MOF, the production of both propanal and ethane decreases. However, the rate of product formation is stable at longer times on stream, decreasing by less than 7% between 40 and 67 hours. Post-reaction solvent extraction of residual products retained in the MOF demonstrate that a small amount of diethyl ketone (DEK) is present (1% selectivity), while the trapped propanal accounts for only 2% of the total propanal production. Post-reaction powder X-ray diffraction (PXRD) shows that the MOF retains its crystallinity under reaction conditions, given that there is no evidence for metallic Rh formation or MOF degradation in the 2θ=40-50° region of the diffraction pattern (Fig. 3). Furthermore, *in situ* XPS experiments on the CuRhBTC illustrated that the Rh oxidation state did not change under reaction conditions even at temperatures as high as 140 °C although the maximum pressure that could be reached was only 50 mTorr due to experimental constraints. For hydroformylation on a CuRh(29%)BTC catalyst at 80 °C at 9 atm, the PXRD data indicate that MOF degradation occurs at this higher pressure, and the color of the post-reaction sample is black, in contrast to the green as-synthesized material. Activity for propanal formation increased by a factor of three at 9 atm, but this may be due to reaction on metallic Rh or Rh sites associated with the partially decomposed MOF. One question about the activity of Rh^{2+} at the paddlewheel node is whether there are sufficient Rh coordination sites to facilitate hydroformylation, given that only the axial position on Rh^{2+} is accessible to absorbates. Preliminary DFT calculations by the Henkelman group suggest that adsorption of ethylene, CO, and dissociation of H_2 can be achieved at a Rh site with only one cleaved Rh-O bond due to the small size of the adsorbed H.

A comparison of activity/g Rh for metallic Rh particles on SiO_2 vs. the CuRhBTC is presented in Fig. 4. Metallic Rh has a higher rate of propanal production, and the selectivity for propanal is greater compared to CuRh(3.4%)BTC (60% vs. 40%). However, the activity for metallic Rh continues decreases by 40% after 24 hours on stream, most likely due to fouling. CuBTC itself has no activity for hydroformylation under these conditions. The pure RhBTC was also studied but has both lower activity for propanal formation/g Rh and poorer selectivity for propenal; it should be noted that RhBTC is much less crystalline than CuRhBTC based on PXRD data. In addition, hydroformylation was investigated on the ionic Rh catalysts: Rh^{3+}/SiO_2, Rh^{2+}/SiO_2, and a Rh-Y zeolite prepared from exchange of Rh^{3+} into the Na-Y zeolite (Fig. 5). All of these catalysts have lower activity/g Rh than CuRhBTC, and all except Rh^{2+}/SiO_2 have lower selectivity to propanal. Diethyl ketone (DEK) is observed as a minor product for the ionic Rh catalysts (Fig. 6) and is also observed on RhBTC and the reduced Rh^{3+}/SiO_2(metallic Rh particles). DEK is not observed CuRhBTC catalysts that have been thoroughly washed in a Soxhlet extractor after Rh^{3+} transmetallation, but DEK is observed on less extensively washed materials. The amount of DEK

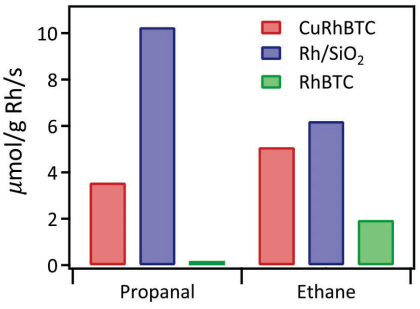

Fig. 4: Hydroformylation activity of CuRh(3.4%)BTC, Rh/SiO_2 and RhBTC.

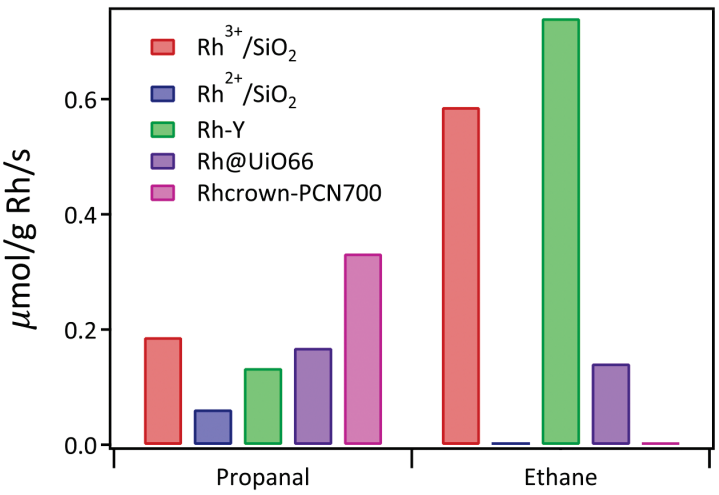

Fig. 5: Hydroformylation activities of various Rh-containing catalysts for propanal and ethane production at 80 °Cand 3 atm.

production also decreases with increasing reduction temperature and time for Rh^{3+}/SiO_2, and therefore DEK is believed to originate from reaction at ionic Rh sites.

Other Rh-containing MOFs were prepared in order to create Rh sites that are more accessible to adsorbates and can incorporate the Rh^{3+} oxidation state that is known to be active for hydroformylation in homogeneous catalysts. Rh^{3+} ions were coordinated at missing linker defect sites in UiO66, which is comprised of $Zr_6O_4(OH)_8(H_2O)_4$ nodes with 4,4-biphenyldicarboxylate linkers (Rh^{3+}@UiO66(defective)). At 80 °C and 3 atm, Rh^{3+}@UiO66(defective) had no activity for hydroformylation, but activity was observed at 9 atm, and a return to 3 atm resulted in the formation of propanal and ethane (Fig. 5), suggesting that an activation process occurred at 9 atm. However, both the activity/g Rh and selectivity were not as high as for the CuRhBTC. For comparison, the undefective UiO66 was also exposed to $RhCl_3$ to the MOF pores directly with Rh^{3+} ions ($RhCl_3$-UiO66(nondefective). This MOF did not have any activity for hydroformylation at either 3 atm or 9 atm, which suggests that the activity of Rh^{3+}@UiO66(defective) is not due to the reduction of Rh^{3+} to metallic Rh under reaction conditions. Furthermore, metallic Rh was not detected in the post-reaction PXRD for either MOF.

A MOF containing highly dispersed Rh^{3+} ions that are stable under reducing conditions was also prepared. Specifically, Rh^{3+} was coordinated in 18-crown-6-based organic linker (4,4′ -(2,3,5,6,8,9,11,12,14,15-decahydrobenzo[*b*][1,4,7,10,13,16]hexaoxacycloocta-decine-17,20-diyl)dibenzoicacid, Fig. 7) This Rh^{3+}-crown ether complex was incorporated into the PCN700 MOF structure ($Zr_6O_4(OH)_8(Me_2BPDC)_4$ where H_2Me_2BPDC= 2,2′ -dimethyl-4,4′ -biphenyldicarboxylicacid), as shown in Fig. 7 via coordination of terminal carboxylate groups of the linkers at the unsaturated metal nodes. Although the rate of propanal production/g Rh was lower than for CuRhBTC (Figs. 4 and 5), the activity was extremely stable over time with 100% selectivity for propanal over ethane at 80 °C and 3 atm. XPS and EXAFS

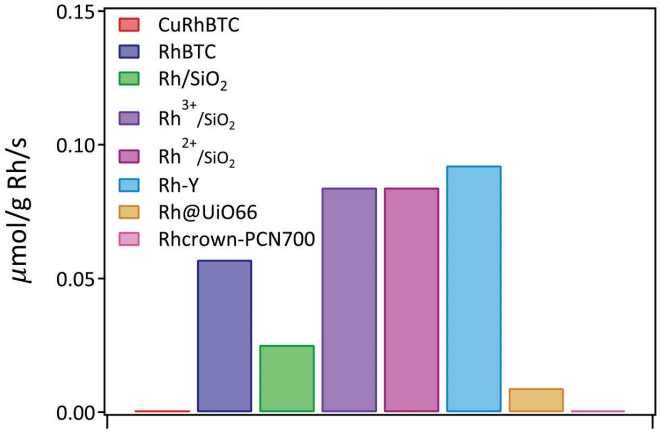

Fig. 6: DEK production in the hydroformylation reaction on various Rh-containing catalysts at 80 °Cand 3 atm.

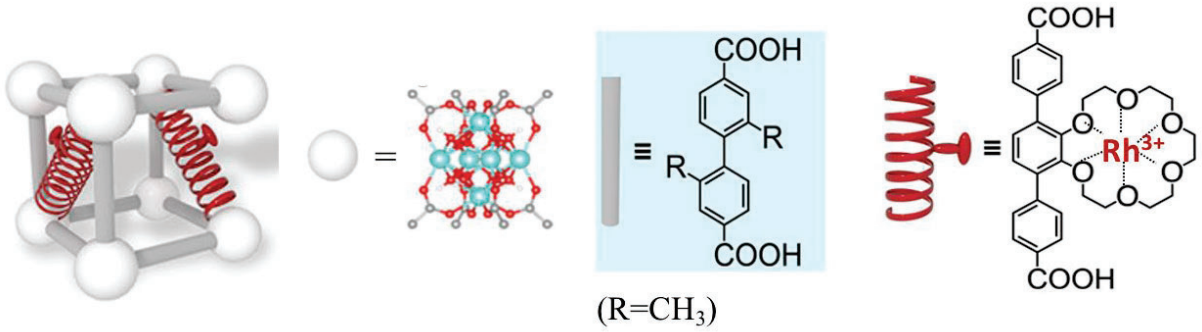

Fig. 7: Structure of the Rh-crown-PCN700 MOF.

experiments are underway on the post-reaction MOF to characterize the properties of the active Rh sites.

Publications Acknowledging this Grant in 2019-2023

(I) Intellectually led by this grant

Shakya, D. M; Ejegbavwo, O. A.; Rajeshkumar, T.; Senanayake, S. D.; Brandt, A. J.; Farzandh, S.; Acharya, N.; Ebrahim, A. M.; Frenkel, A. I.; Rui, N.; Tate, G. L.; Monnier, J. R.; Vogiatzis, K. D.; Shustova, N. B.; Chen, D. A. Metal Nodes in Bimetallic Metal-Organic Frameworks as Sites for Hydrogenation Reactions. *Angewante Chemie*, **2019**, *58*, 16533-16537.

Brandt, A.J.; Shakya, D.M.; Metavarayuth, K.; Dolgopolova, E.; Hensley, L.; Duke, A.S.; Farzandh, S.; Stefik, M.; Shustova, N.B.; Chen, D.A. Growth of Crystalline Bimetallic Metal-Organic Framework Films Via Transmetalation. *Langmuir* **2020,** *36,* 9900-9908.

Metavarayuth, K.; Ejegbavwo, O.; McCarver, G.; Myrick, M.L.; Makris, T.M.; Vogiatzis, K.D.; Senanayake, S.D.; Manley, O.M.; Ebrahim, A.M.; Frenkel, A.I., et al. Direct Identification of Mixed-Metal Centers in Metal-Organic Frameworks: $Cu_3(BTC)_2$ Transmetalated with Rh^{2+} Ions. *J. Phys. Chem. Lett.* **2020,** *11,* 8138-8144.

Ejegbavwo, O.A.; Berseneva, A.A.; Martin, C.R.; Leith, G.A.; Pandey, S.; Brandt, A.J.; Park, K.C.; Mathur, A.; Farzandh, S.; Klepov, V.V., et al. Heterometallic Multinuclear Nodes Directing MOF Electronic Behavior. *Chem. Sci.* **2020,** *11,* 7379-7389.

McCarver, G.A.; Rajeshkumar, T.; Vogiatzis, K.D. Computational Catalysis for Metal-Organic Frameworks: An Overview. *Coordination Chemistry Reviews* **2021**, *436*, 213777/

Kittikhunnatham, P.; Leith, G.A.; Mathur, A.; Naglic, J.K.; Martin, C.R.; Park, K.C.; McCullough, K.; Jayaweera, H.; Corkill, R.E.; Lauterbach, J., et al. A Metal-Organic Framework (MOF)-Based Multifunctional Cargo Vehicle for Reactive-Gas Delivery and Catalysis. *Angew. Chem. Int. Edit.* **2022,** *61,* e2021139.

Chen, D.A.; Jimenez, J.D.; Senanayake, S.D.; Stetzler, J.P.; Shakya, D. M.; McCarver, G. A.; Rajeshkumar, T.; Vogiatzis, K.D.; Mathur, A. Shustova, N.B. et al. Mechanistic Investigations of Gas-Phase Catalytic Hydrogenation in Metal-Organic Frameworks: Cooperative Activity of the Metal and Linker Sites in $Cux Rh_{3-x}(BTC)_2$. *J. Phys. Chem. C* **2022**, *126*, 11553.

Eugene Y.-X. Chen

Redesigning Polymers to Leverage A Circular Economy (RePLACE)

Eugene Y.-X. Chen,[1] Garret M. Miyake,[1] Linda J. Broadbelt,[2] Tobin J. Marks,[2] and Yuriy Román-Leshkov[3]
[1] Colorado State University, [2] Northwestern University, and [3] Massachusetts Institute of Technology

Presentation Abstract

The central objective of this five-PI team project for Redesigning Polymers to Leverage A Circular Economy (RePLACE) is to design, discover, and develop next-generation circular polymers (CPs) with either intrinsic chemical circularity or catalysis-enabled chemical recyclability that can replace today's non-recyclable or hard-to-recycle commodity polymers including thermoplastics and thermosets. To accomplish this objective, RePLACE's three-institution, five-PI cross-disciplinary team will conduct transformative, hypothesis-driven fundamental research towards CPs and work collaboratively and synergistically to achieve the following tightly integrated goals over the three-year project period: (a) Establish fundamental design principles for kinetically trapped, intrinsically circular polymers with tunable properties (Research Thrust Area 1); and (b) Develop innovative strategies for catalysis-enabled circularity designed for thermodynamically controlled polymers not having intrinsic recyclability (Research Thrust Area 2). Key results that RePLACE has achieved to date include: closed-loop upcycling of mixed plastics into reprocessable living graft multiblock copolymers via compatibilization by dynamic crosslinking (*Nature*, 2023); circular polyethylene-like polyester platform (*Nature Chemistry*, 2023); dual recycling of depolymerization catalyst and biodegradable polyester that markedly outperforms polyolefins (*Angew. Chem. Int. Ed.* 2023); selective catalytic Nylon-6 depolymerization to monomer ε-caprolactam (*Angew. Chem. Int. Ed*. 2023); understanding of kinetics of aldol addition in microporous media towards biomass-derived monomer synthesis (*ACS Catal.* 2023); mechanistic understanding of Nylon-6 depolymerization and catalyst design (*under revision*, 2023); chemically recyclable polyolefin-like multiblock polymers (*under revision*, 2023); and predictive thermodynamic design and machine learning for the discovery of CPs (*in preparation*).

Grant or FWP Number: DE-SC0022290
Title: Redesigning Polymers to Leverage A Circular Economy (RePLACE)

PI(s): Eugene Chen (Lead), Linda Broadbelt, Tobin Marks, Garret Miyake, Yuriy Román-Leshkov
Postdoc(s): Wilf Diment, Zhitao Hu, Alexander Khechfe, Yosi Kratish, Kun Liu, Xiaoyan (Shelly) Liu, Liwei Ye
Student(s): Kristen Becket, Ryan Clark, Francesca Eckstrom, Kevin Franklin, Shivani Kozerekar,
Affiliations(s): Colorado State University, Northwestern University, Massachusetts Institute of Technology

RECENT PROGRESS

I. Closed-loop upcycling of immiscible mixed plastics via compatibilization by dynamic crosslinking

Mixed plastics waste presents the biggest challenge for recycling, upcycling, or repurposing, and there is no current, effective closed-loop solution. This challenge lies to the fact that most polymer mixtures are immiscible, primarily because the entropy of mixing is dramatically reduced in polymers – in fact, this quantity scales inversely with the length of the chains, and for typical chains of length ~1000, the entropy of mixing, which favors miscibility, is essentially zero. Thus, even a small energetic dislike between the segments of the two polymers, especially polar/apolar polymer mixtures, readily yields an immiscible system in which phase separation leads to materials with significantly inferior properties. From a recycling viewpoint, there is thus a pressing need to compatibilize generally immiscible mixed plastic "dead" chains. To address this key barrier, we developed a novel compatibilization strategy that installs dynamic crosslinkers into several classes of binary, ternary, and post-consumer immiscible polymer mixtures in situ. Our combined experimental and modeling studies show that specifically designed classes of universal dynamic crosslinkers (UDCs) can reactivate essentially any mixed plastic "dead" chains (as long as they contain C–H bonds) represented here by apolar polyolefins and polar polyesters, by compatibilizing them via dynamically forming living graft multiblock copolymers (**Fig. 1**). The resulting in-situ generated dynamic thermosets exhibit intrinsic reprocessability and enhanced tensile strength and creep resistance, relative to virgin plastics. This approach avoids the need for de/reconstruction and thus potentially provides an alternate, facile route towards the recovery of the endowed energy and materials value of the individual plastics. The paper was published in *Nature*: Clarke, R. W.; Sandmeier, T.; Franklin, A. Kevin; Reich, D.; Zhang, X.; Vengallur, N.; Patra, T. K.; Tannenbaum, R. J.; Adhikari, S.; Kumar, S. K.; Rovis, T.; Chen, E. Y.-X. Dynamic Crosslinking Compatibilizes Immiscible Mixed Plastics. *Nature* **2023**, *616*, 731−739.

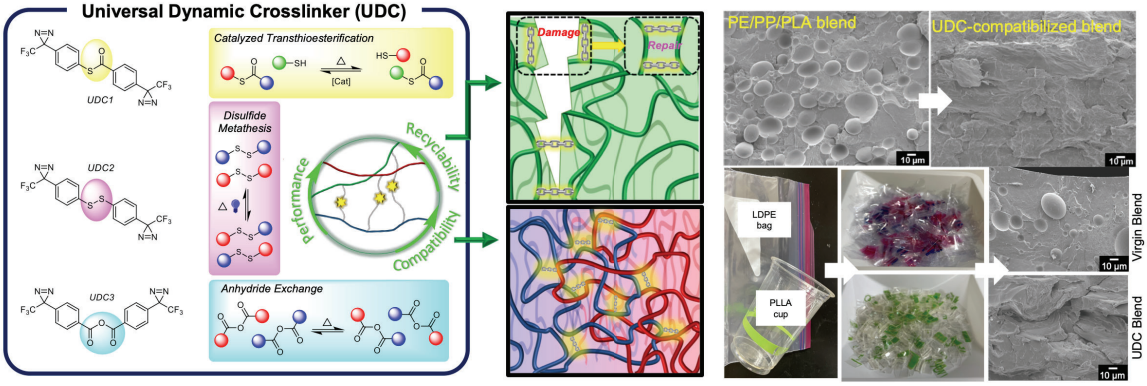

Figure 1. Designed UDCs **1-3** embedded with dynamically exchangeable bonds between the crosslinking sites (left), illustrated thermoset reprocessability via dynamic bond exchange enabled by UDCs and compatibilisation effect on otherwise immiscible polymer blend domains rendered by regenerative formation of living, tethered graft multi-block copolymer architectures (middle), SEM cross-sectional images revealing degree of UDC compatibilisation of immiscible ternary LDPE-*i*PP-PLLA virgin blend and UDC-compatibilized LDPE-*i*PP-PLLA blend, and compatibilisation of real-world mixed-plastics of a LDPE bag and a PLLA cup, subsequent flakes by mechanical shredding for melt-extrusion highlighting included colorants and additives, and cross-sectional SEM images revealing degree of UDC compatibilisation of the immiscible LDPE bag-PLLA cup blend and the UDC-compatibilized LDPE bag-PLLA cup blend (right).

II. Circular polyethylene-like polyester platform

We developed a circular PE-like polyester platform based on gem-dialkyl-substituted valerolactones (VL^{R2}), which generated the corresponding polyesters PVL^{R2} that exhibit not only complete chemical recyclability, by closing the monomer-polymer-monomer loop under mild conditions (ambient temperature for metal-catalyzed polymerization and 150 °C with a metal-based catalyst for depolymerization), but also PE-like thermal (T_m up to 140 °C), mechanical (ultimate strength up to 47 MPa, elongation at break up to 320%), and transport (low water-vapor transmission rate and oxygen permeability) properties (**Fig. 2**). The paper was published in *Nature Chemistry*: Li, X.-L.; Clarke, R. W.; Jiang, J. -Y.; Xu, T.-Q.; Chen, E. Y.-X. A Circular Polyester Platform Based on Simple Gem-disubstituted Valerolactones. *Nat. Chem.* **2023**, *15*, 278−285.

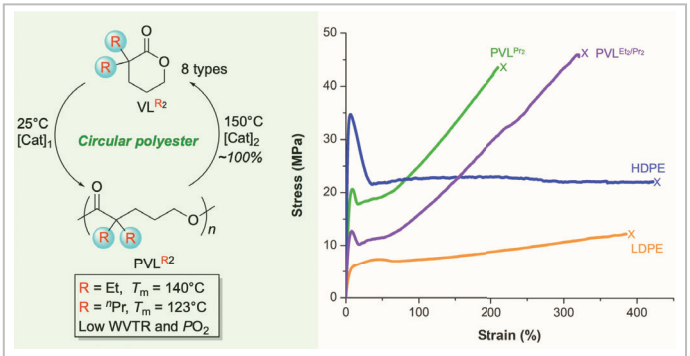

Figure 2. Circular PE-like polyester platform based on α,α-disubstituted valerolactones, PVL^{R2} (left) and overlay plots of stress/strain curves of PVL^{Pr2} and $PVL^{Et2/Pr2}$ as compared to LDPE and HDPE standards (right, break point indicated by ×).

III. Dual recycling of depolymerization catalyst and biodegradable polyester that markedly outperforms polyolefins

Chemically recyclable, circular polymers continue to attract increasing attention, but rendering catalysts for both depolymerization and high-performance polymers recyclable is a more sustainable yet challenging goal. Here we developed a dual catalyst/polymer recycling system in that recyclable inorganic phosphomolybdic acid catalyzes selective depolymerization of high-ceiling-temperature biodegradable poly(*δ*-valerolactone) (PVL), which, upon reaching suitable molecular weight from the ring-opening polymerization (ROP) of *δ*-valerolactone with catalysts such as $[La(OBn)_3]_x$, exhibits outstanding mechanical performance with a high tensile strength of ~66.6 MPa, fracture strain of ~904%, and toughness of ~308 MJ m^{-3}, and thus markedly outperforms commodity polyolefins, recovering its monomer in pure state and quantitative yield at only 100 °C (**Fig. 3**). In sharp contrast, the uncatalyzed depolymerization not only requires a high temperature of >310 °C but is also low yielding and non-selective. Importantly, the recovered monomer can be repolymerized as is to reproduce the same polymer, thereby closing the circular loop, and the recycled catalyst can be reused repeatedly for depolymerization runs without loss of

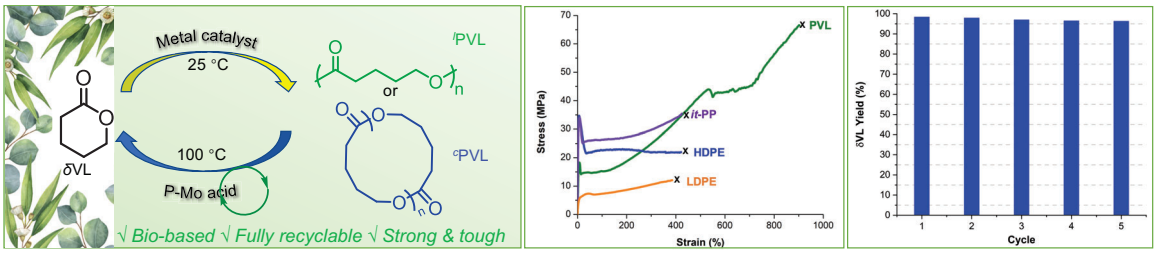

Figure 3. Closing the chemical loop of bio-based PVL under mild conditions (left), outstanding mechanical properties far superior to those of LDPE, HDPE, and *it*-PP (middle), and excellent catalyst recyclability of phosphomolybdic acid for catalyzed bulk depolymerization at remarkably low temperature of 100 °C (right).

its catalytic activity and efficiency. Li, X.-L.; Clarke, R. W.; An, H.-Y.; Gowda, R. R.; Jiang, J. -Y.; Xu, T.-Q.; Chen, E. Y.-X. Dual Recycling of Depolymerization Catalyst and Biodegradable Polyester that Markedly Outperforms Polyolefins. *Angew. Chem. Int. Ed.* **2023**, e202303791 (*Designated "Hot Paper"*).

IV. Development of chemically recyclable polyolefin-like multiblock polymers

We have developed an approach for synthesizing multiblock polyolefin-like materials constructed from hard and soft aliphatic oligomeric building blocks possessing identical chain-end groups to plastics possessing highly tunable materials properties dictated by the ratio of the two types of blocks (**Fig. 4A**). The crystallizable hard PE block was designed to imbue high T_m and modulus (E) into the polymer while the hexyl-branched soft bPE block was designed to introduce controlled short-chain C6 branching to create non-crystallizable, elastomeric soft domains. The oligomers were polymerized in high yields (>90%) with varying ratios of hard and soft blocks to modulate the hard PE content from 0 to 100% using ruthenium catalyzed dehydrogenation polymerization to high molecular weight polymers (M_w = 62.7 to 90.4 kDa) with high dispersity ($Đ$ > 2.2), as expected for polymers produced through a step-growth polymerization (**Fig. 4B**). Importantly, the different multiblock polymers can be mixed and efficiently depolymerized back to their building blocks for purification and repolymerization for recycling these different plastics. With increasing PE content, the crystallinity of the polymers increased from 0 to 68% (**Fig. 5B**). Polymers with hard PE content less than 80% exhibited low glass transition temperatures (T_g = -58 to -67 °C) while a high melting transition temperature (T_m = 106 to 124 °C) was observable for all multiblock polymers containing hard blocks. Thus, the multiblock polymers possessed both a low T_g and high T_m to allow for thermoplastic and elastic properties across a wide operating temperature. Rheology was performed to investigate the melt flow properties of the multiblock polymers. Generally, the zero-shear viscosity (η_o) and complex viscosity increased with increasing hard content from PE0 to PE100 (η_o = 3.45 to 447 $\times 10^5$ Pa·s) indicating that the introduction of short chain branching generally reduced entanglement (**Fig. 5C**). The mechanical properties of the multiblock polymers were investigated by uniaxial tensile testing (**Fig. 5D**). Polymer properties spanned drastic regimes, from elastomers to plastomers to thermoplastics by increasing the hard content. Both Young's modulus (E) and tensile strength (σ_{UTS}) increased by over three orders of magnitude (E = 580 kPa for PE0 to E = 802 MPa for PE100; σ_{UTS} = 40.5 kPa for PE0 to σ_{UTS} = 24.7 MPa for PE100) (**Fig. 5E**). Furthermore, all samples spanning these regimes demonstrated excellent extensibility, with the average strain at break (ε_b) for all multiblock polymers exceeding 700%, while achieving over 1000% for PE20 and PE40. These materials also exhibited high toughness (U_T), ranging from 0.19 to 150 MJ•m^{-3} (**Fig. 5F**).

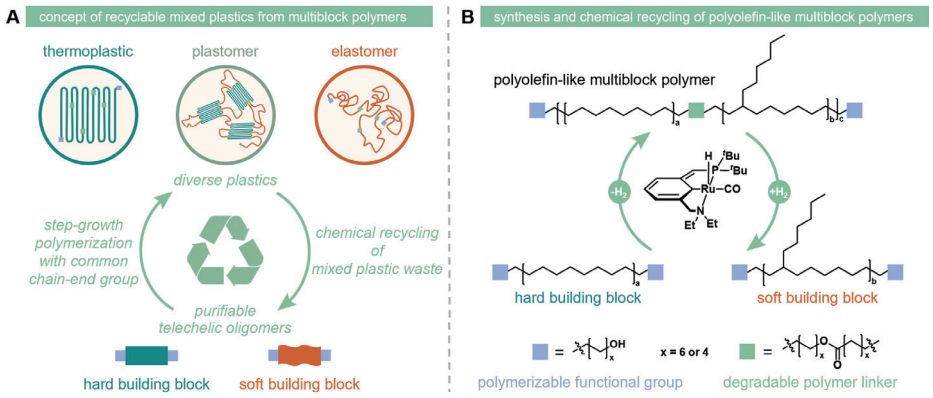

Figure 4. Overview of chemically recyclable multiblock polyolefins with tunable properties from polymerization of hard and soft oligomers. This strategy (**A**) successfully builds on a new approach for the synthesis of ester-linked multiblock polyolefin-like polymers to create a platform for closed-loop recycling of mixed plastics catalyzed by a ruthenium complex (**B**).

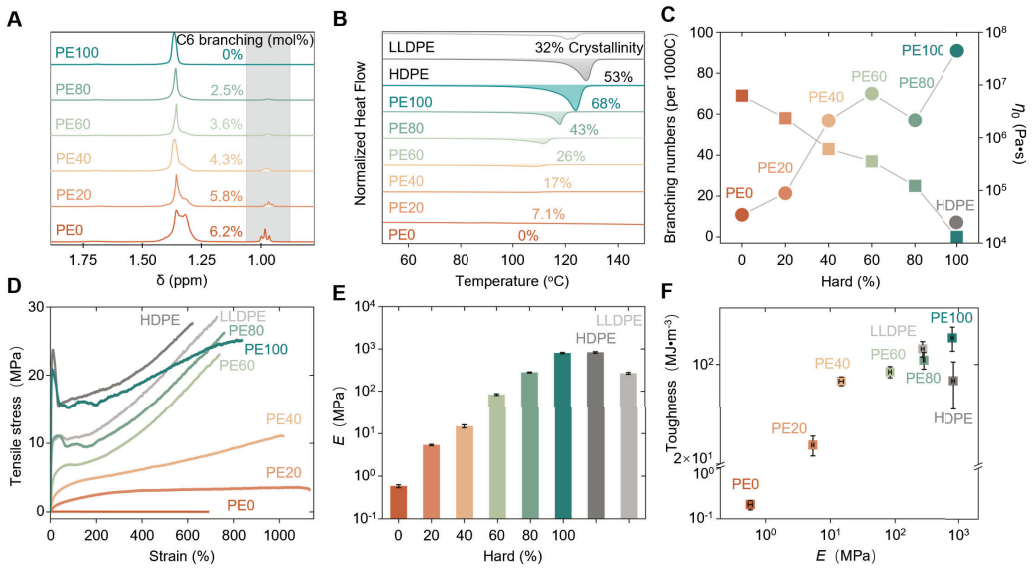

Figure 5. Properties of multiblock polymers can be modulated over diverse regimes. Stacked ^{1}H NMR (**A**), normalized differential scanning calorimetry (DSC) traces (**B**), relationship between branching number (per 1000 carbons) and zero shear viscosity measured at 150 °C (**C**), representative stress-strain curves (**D**), modulus (**E**), and property comparison of toughness and modulus (**F**) between multiblock polymers, HDPE and LLDPE.

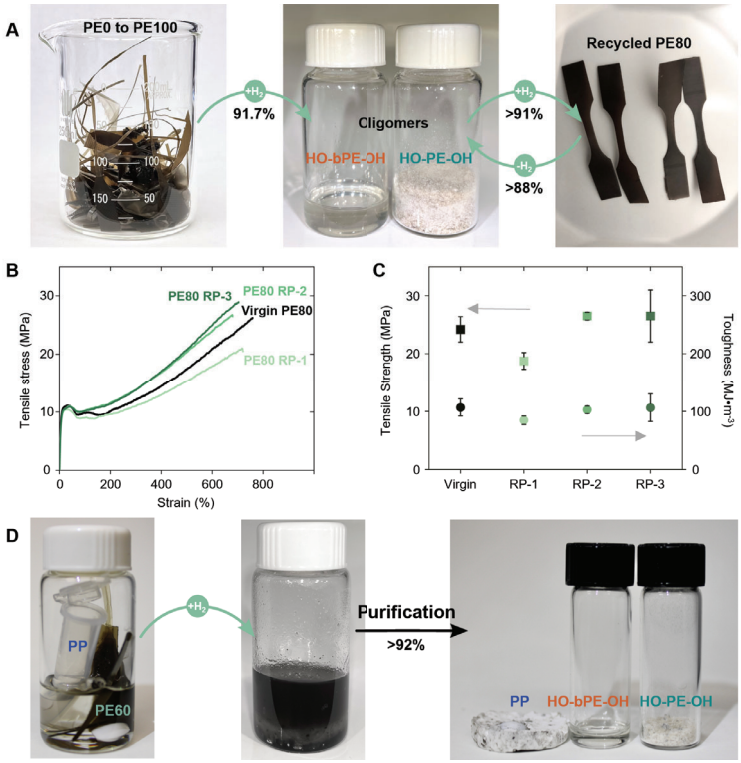

Figure 6. Chemical recycling of multiblock polymers. (**A**) Photographs of the chemical recycling of mixed multiblock polymers. (**B**) Representative stress-strain curves of virgin PE80 and repolymerized PE80 RP-1, PE80 RP-2, and PE80 RP-3. (**C**) Tensile strength and toughness of virgin PE80 and repolymerized PE80 RP-1, PE80 RP-2, and PE80 RP-3. (**D**) A mixture of polypropylene (PP) and PE60 as an example of a potential polyolefin waste stream. Photographs of mixed plastics in toluene (left), reaction after 72 h (middle), and the separated PP, HO-PE-PH, HO-bPE-OH (right).

To complete the closed-loop chemical recycling process, the multiblock polymers of all compositions following tensile testing were combined for simultaneous depolymerization (>99% conversion) and the hard and soft oligomeric building blocks were separated and purified in 91.7% isolated yield with no observable signs of oligomer decomposition by ^{1}H NMR (**Fig. 6A**). The hard and soft blocks were readily separated through selective solvent isolation by precipitation of the hard block and successfully repolymerized to PE80, which was subsequently depolymerized and repolymerized back into PE80 for two additional cycles with all steps proceeding in high yields. The molecular weights of the recycled PE80 multiblock polymers remained consistent (M_w = 73.8 to 96.6 kDa), demonstrating the robustness of this closed-loop recycling process. Significantly, tensile testing of all recycled PE80 samples revealed that the modulus, tensile strength, elongation at break, and toughness were comparable to the virgin PE80 sample (**Fig. 6B**,**C**). Lastly, we demonstrated that these multiblock polymers can be separated from technologically important isotactic polypropylene (PP), (**Fig. 6D**). In the presence of commercially available PP, the depolymerization of PE60 was efficient and the oligomers were readily separated from the PP in high yield (92%).

V. Nylon-6 deconstruction and upcycling

Gen 1 catalysts. In continuing activities begun in Year 1 in which, we discovered that commercially available lanthanide trisamido catalysts Ln(N(TMS)$_2$)$_3$ (Ln = lanthanide) can efficiently depolymerize Nylon-6 to ε-caprolactam (CLM) in a solvent-free, near quantitative, highly selective process, we sought to increase our mechanistic understanding of the catalytic process. To fulfill these goals, we have conducted kinetic and computational studies to understand the catalysis on a molecular level better. This paper was recently published in *Angewandte Chemie*: Wursthorn, L.; Beckett, K.; Rothbaum, J.O.; Cywar, R.M.; Lincoln, C.; Kratish, Y.; Marks, T.J.; Selective Lanthanide-Organic Catalyzed Depolymerization of Nylon-6 to ε-Caprolactam, *Angew. Chem.* **2023**, *62*, e202212543.

Since La(N(TMS)$_2$)$_3$ (**La^{NTMS}**) exhibits the highest activity in this study, it was chosen for the mechanistic investigations. Plotting the CLM yield vs. time reveals a linear dependence (**Fig. 7A**), indicating that the reaction is zero-order in Nylon-6 under the present conditions and suggesting that in the catalyst resting state, the polyamide is bound to La center, probably after a Nylon amide (p*K*a = ~25.5) /bis(trimethylsilyl)amine (p*K*a = ~30) exchange. The La catalytic centers likely bind to the Nylon terminal amide moiety since, at this position, the free amine group at the chain end can also coordinate and stabilize it (**Fig. 7B**). To understand the fate of the Nylon-6 during the reaction,

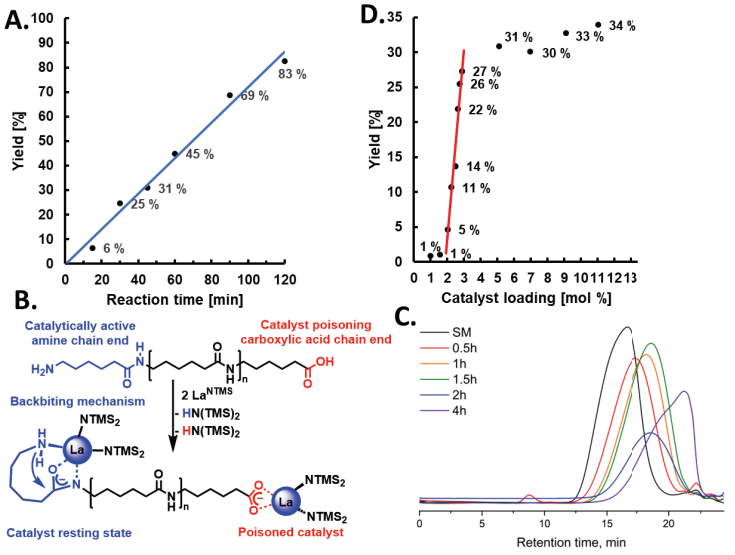

Figure 7. A. Effect of reaction time on CLM yield. Conditions: 100 mg Nylon-6, 5 % catalyst loading, 50 mL Schlenk flask, 240 °C, static vacuum (10^{-3} Torr) **B.** Structure of Nylon-6 and binding of the La^{NTMS} catalyst. **C.** Effect of catalyst loading on CLM yield. Reaction conditions: 100 mg Nylon-6, 50 mL Schlenk flask, 240 °C, 45 min, 10^{-3} Torr. Yield determined by ^{1}H-NMR using mesitylene as internal standard. **D.** GPC of solid fractions from Nylon-6 depolymerization experiments.

we collaborated with Dr. Robin Cywar of NREL, who carried out a Gel permeation chromatographic (GPC) analysis of our Nylon deconstruction products. Thus, we found as a function of reaction time, a gradual fall in the average molecular mass without significant changes in the dispersity, supporting a backbiting mechanism in which an CLM molecule is eliminated from the polymer-activated end on each catalytic cycle (**Fig. 7C**). The dependence of the depolymerization yield on catalyst concentration reveals an interesting and informative picture (**Fig. 7D**). No activity is observed from 0 to 1.5 mol% catalyst loading. This initial feature can be explained by catalyst deactivation involving the reactive carboxylic acid (p*K*a = 5) chain ends, as shown in **Fig. 7B**. Indeed, in the case of 1 mol % **La**$^{\mathbf{NTMS}}$ loadings and Nylon-6 (M_n = 11930 g/mol), the calculated carboxylic acid : La ratio is ~ 1:1 assuming one carboxylic acid unit per 1 polymer chain. To test this hypothesis, a Nylon-6 sample was treated with 1 M aqueous KOH to deprotonate the acidic chain ends. After washing and drying, catalytic depolymerization experiments were conducted with the KOH-treated Nylon-6. Rapid quantitative depolymerization is observed with only 1 mol% **La**$^{\mathbf{NTMS}}$ (96 % isolated yield after 4h; 94% yield after 1h), supporting a scenario where the carboxylic acid groups deactivate a fraction of the catalytic units. Between 1.5 and 3 mol%, a steep near-linear activity increase is observed, implying the rate is first order in [catalyst]. Beyond 3 mol% catalyst, the system evidences Michaelis-Menten-like saturation and even large increases in catalyst loading only marginally affect the reaction rate; in 45 min, 31 % conversion for 5 mol% catalyst vs. 34 % conversion for 11 mol% catalyst). Catalyst saturation would be achieved when every amide chain end was bound by a catalytic center, and another step becomes turnover-limiting. This observation also supports the proposed catalyst resting state shown in **Fig. 7B**. Thermogravimetric analysis (TGA) experiments were next conducted on Nylon-6 + catalyst mixtures to estimate the activation energy using the Flynn-Wall-Ozawa (FWO) method. The apparent depolymerization activation energy is E_a = 31.4 ± 3.1 kcal/mol.

To further probe the Nylon-6 reaction mechanism and energetic landscape, a detailed solution-phase enthalpy profile was computed by DFT for the **La**$^{\mathbf{NTMS}}$-catalyzed Nylon-6 depolymerization.

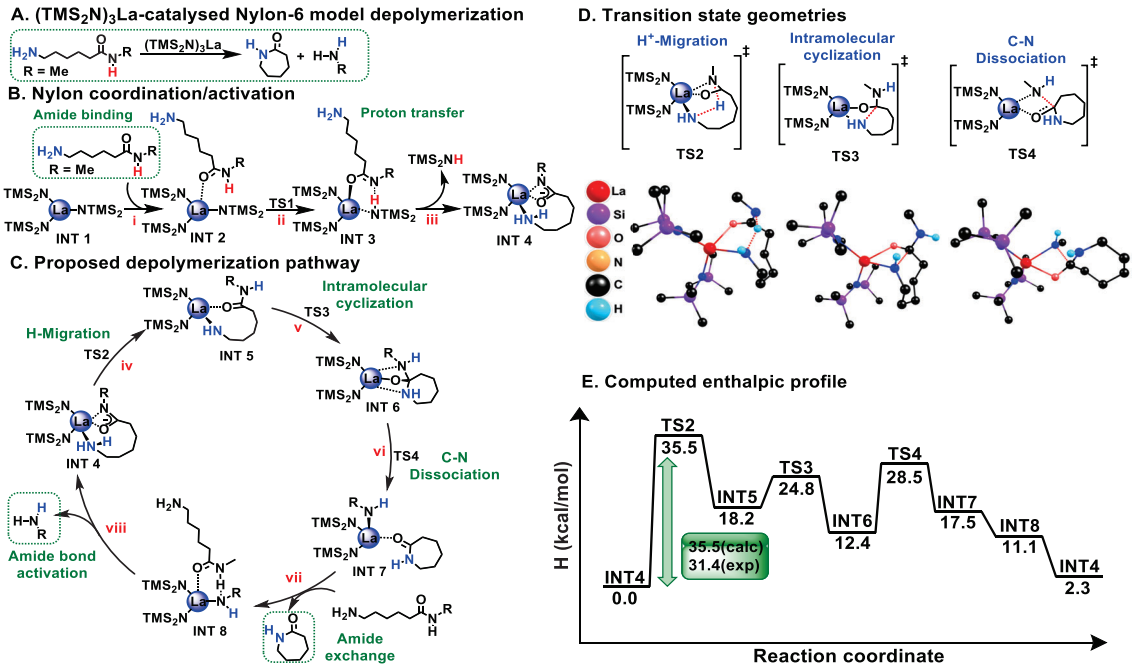

Figure 8. A. Mechanistic DFT analysis of Nylon-6 depolymerization. **A**. Computed Nylon-6 model reaction. **B**. Nylon coordination. **C**. Proposed depolymerization mechanism. **D**. Calculated transition state geometries. **E**. Computed solution-phase enthalpic profile in kcal/mol.

Catalysis proceeds via a novel mechanism involving initial deprotonation of the Nylon amide N-H bond, which binds the catalyst covalently to the polymer and is followed by predominant chain-end backbiting steps in which CLM units are sequentially excised from the chain ends (**Fig. 8**). The overall computed barrier of 35.5 kcal/mol is in good agreement with the TGA-derived E_a = 31.4± 3.1 kcal/mol (**Fig. 8**). Next, since most plastic streams are composed of mixed plastics and polymer additives, we sought to test whether these catalysts are compatible with plastics mixtures and post-consumer products. To investigate the applicability of the **La^{NTMS}** catalyst to such scenarios, the depolymerization of Nylon-6 was carried out on 1:1 mixtures (by weight) with the common polymers PE, PP, and PET. It is found that the PP and PE admixture has no adverse effects on the Nylon-6 depolymerization, affording CLM in 93% and 91 % yield, respectively (Table 1, entries 1 and 2), while unreacted PE or PP are recovered unchanged. The admixture of PET induces a slight decrease in catalytic activity, probably reflecting the presence of additional PET carboxylic acid or hydroxyl end groups (Table 1, entry 3). This process is also compatible with post-consumer fine-powder cryomilled Nylon-6 yarn yielding CLM in 78 % yield (Table 1, entry 4). Note that, unlike the reaction with Nylon-6 powder, the reaction with Nylon-6 yarn experiences heat and mass transfer issues in the form of slow melting and minimal stirring, leading to a significant decrease in the reaction rate. In many cases, when large particle size post-consumer Nylon-6 is used, the catalysis produces negligible yields. We find that when there is poor contact between the polymer and the catalysts during the melting stage, most of the **La^{NTMS}** catalyst sublimes away from the reaction hot zone leading to poor activity. Thus, we decided to redesign our catalysts to make them more compatible with post-consumer products.

Table 1. The effect of mixed plastics and post-consumer yarn on the catalytic Nylon-6 depolymerization process.

Entry	Polymer	Catalyst loading	Reaction time	Yield [a]
1	1:1 mixture Nylon-6:PP	5 %	6 h	93 %
2	1:1 mixture Nylon-6:PE	5 %	6 h	91 %
3	1:1 mixture Nylon-6:PET	5 %	6 h	77 %
4[b]	Post-consumer Nylon-6	4 %	24 h	78 %

Conditions: 100 mg untreated Nylon-6, 50 mL Schlenk flask, solventless, 240 °C, static vacuum (10^{-3} Torr). [a] Yield determined by ^{1}H-NMR using mesitylene as an internal standard. [b] Inert atmosphere instead of vacuum.

Gen 2 catalysts. In Year 2, we aimed to develop and implement a fundamental understanding of the Nylon-6 catalytic process, such as ligand effects. Our initial screening study discussed above indicated that, although >90 % yields of the ε-caprolactam are achieved, a substantial 5 mol% of La^{NTMS} (**1**) is required. For more attractive Ln metals with smaller sizes, the catalytic system exhibits significantly suppressed activities. To address these issues, we surveyed a series of lanthanocenes and identified extremely efficient, non-volatile catalysts for the chemical recycling of pre- and post-consumer Nylon-6 in a solventless, scalable process (**Fig. 9**). A detailed full paper manuscript has been submitted for publication.

In initial attempts to lower the catalyst loading of **1** from 5 mol% to 1 mol%, a moderate ε-caprolactam yield was obtained (69%, Table 2, entry 1) in 0.5 h reaction time at 240 °C. Further

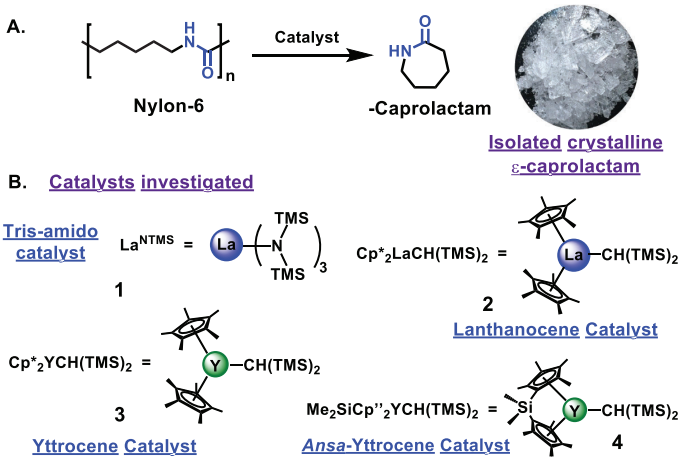

Figure 9. A. Reaction scheme for Nylon-6 depolymerization to CLM. **B.** Structures of catalysts investigated here.

decreasing the catalyst loading of **1** to 0.2 mol% depressed the depolymerization yield to 5.6% (Table 2, entry 2). In addition to the high volatility of **1**, we hypothesized that, after depolymerization is initiated, the three reactive La-amide linkages may promote macromolecule crosslinking and catalyst immobilization (supported by ^{1}H NMR analysis). In contrast, we find that lanthanocene complex **2** is a highly effective depolymerization catalyst, affording 93% yield of the monomer CLM with catalyst loadings as low as 0.2 mol% (Table 2, entry 3). We hypothesize that the non-dissociable Cp* ligands sterically shield the La center and likely hinder the undesired cross-linking/catalyst immobilization, and may promote effective interchain catalyst hopping at low catalyst loadings. To validate this mechanistic hypothesis, ^{1}H NMR analysis at the depolymerization process onset was performed. The data reveal gradual La-CH(TMS)$_2$ linkage protonolysis with ~95% of the expected CH$_2$(TMS)$_2$ yield obtained. Only trace amounts (<5% yield) of a Cp*H protonolysis product are detected, in accord with the stability the Ln-Cp* ligation.

In an effort to lower the reaction temperature, catalytic studies were next conducted at 220 °C with 0.2 mol% catalyst **3** loading for 4 h affording a 95% yield (Table 2, entry 4). Note that this temperature is, to our knowledge, the lowest reported Nylon-6 depolymerization temperature under solvent-free conditions in the peer-reviewed literature, with a 238× increase in depolymerization rate at 220 °C *vs.* catalyst **1** (0.5 *vs.* 118.8 (mol CLM)·(mol La)$^{-1}$·(h)$^{-1}$). In comparison, catalyst **1** is ineffective at 220 °C (2.4% yield after 24 h; Table 2, entry 5). Remarkably, these conditions are the mildest to date for Nylon-6 depolymerization to CLM in the peer-reviewed literature. Yttrium complexes with lower cost, higher thermal stabilities, and lower toxicities are attractive candidates for the deconstruction of more recalcitrant "real-world" Nylon-6 products. While the catalytic activity of **3** suffers from the smaller ionic radius of Y^{3+} (Table 2, entry 6), *ansa*-metallocene catalyst **4** with chelating ancillary π-ligands and larger "bite" angles dramatically increases the depolymerization yield (from 2.2% to 94 %; 43× enhanced rate; Table 2, entry 7). The "opening" of the Y coordination sphere essentially imbues a more desirable Y center with La center catalytic properties, illustrating the effects of ancillary ligand "engineering". We also computed steric effect quantification in free volume contours ($\%V_{free}$) computationally for catalysts **2** (37.9%), **3** (32.3%), and **4** (35.1%), in strong parallel with their respective experimental activity trend.

Table 2. Catalyst screening for Nylon-6 depolymerization.

Entry	Catalyst	Loading (mol%)	Time (h)	Temperature (°C)	Yield (%) [a]
1	**1**	1.0	0.5	240	69
2	**1**	0.2	1.0	240	5.6
3	**2**	0.2	1.0	240	93
4	**1**	0.2	4.0	220	95
5	**2**	0.2	24	220	2.4
6	**3**	1	1.0	240	2.2
7	**4**	1	1.0	240	94

Conditions: 100 mg pristine Nylon-6 powder, 10^{-3} Torr. [a] Yield determined by ^{1}H-NMR using mesitylene as internal standard.

Table 3. Depolymerization of post-consumer Nylon plastics.

Entry	Nylon plastic	Catalyst	Time (h)	Yield (%)
1 [a]	Fishing net	**1**	24	0
2 [a]	Fishing net	**2**	24	65
3 [a]	Fishing net	**3**	24	95
4	Fishing net	**4**	6.0	94
5	Carpet fiber	**4**	6.0	>99
6	Nylon yarn	**4**	6.0	87
	T-shirt	**4**	6.0	99
6 [b]	Gloves	**4**	12	89
7 [c]	Fishing net + water bottle cap	**4**	12	95

Conditions: 1 mol% catalyst, 240 °C, 100 mg scissor-chopped end-of-life Nylon. [a] 5 mol% loading was used. [b] Contains 31 wt.% Nylon-6. [c] Fishing net : water bottle cap in 1:1 mass ratio.

Encouraged by the high activities of the lanthanocene catalysts for pristine powdered Nylon-6, the chemical recycling of "real-world" post-consumer Nylon-6 products was next examined (Table 3). With relevance to ocean pollution, an end-of-life fishing net used for 2 years was first investigated. Note that catalyst **1** rapidly sublimes from the catalyst + finely chopped fishing net mixture, yielding negligible ε-caprolactam (Table 3, entry 1) after 24 h/ 240 °C. For catalyst **2**, a modest yield at high loadings is observed (Table 3, entry 2), likely reflecting poor mixing and the known

thermal instability of this catalyst; in contrast, thermally more robust Y catalyst **3** delivers a higher yield (Table 3, entry 3), and coordinatively more open chelated *ansa*-metallocene Y catalyst **4** achieves a remarkable 94% yield in only 6 h (Table 3, entry 4), paralleling the results with pristine powdered Nylon-6. Pleasingly, catalyst **4** achieves >99% conversion of other diverse end-of-life articles into ε-caprolactam, such as carpets, gloves, yarn, clothing, as well as in a mix-plastic case (Table 3, entries 2-7). Next, in a collaborative study with NREL, we showed that the ε-caprolactam collected from end-of-life fishing nets is re-polymerizable to pristine Nylon-6 with M_n = 43.6 kg mol^{-1} and yield of 99.3%. Note that the upcycled Nylon-6 offers has higher molecular mass *vs* the original fishing net (M_n = 21.7 kg mol^{-1}), highlighting the attractions of Nylon chemical recycling by efficient monomer recovery (**Fig. 10**).

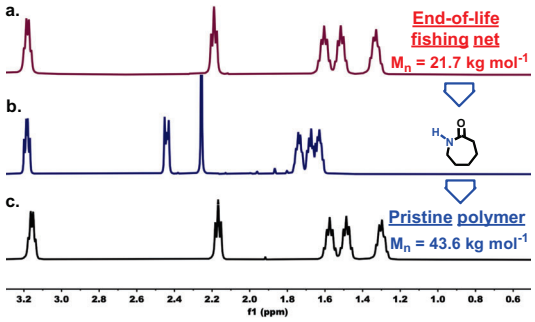

Figure 10. ^{1}H NMR ($CDCl_3$, 500 MHz) spectra of **a**) End-of-life fishing net; **b**) CLM collected from depolymerization of the fishing net; **c**) Pristine Nylon-6 obtained from the subsequent re-polymerization of the CLM.

Catalytic studies are now being extended to the deconstruction of other C-N containing plastics such as Nylon-6,6 and polyurethanes. In preliminary work, we find that catalysts **2**, **3**, and **4** are effective for the chemical deconstruction of Nylon-6,6, achieving full conversion, but modest selectivity for reasons we don't yet understand. Preliminary results on polyurethane depolymerization demonstrate that a $M(OTf)_4$ catalytic system affords moderate yields of pure monomers. Currently, we are optimizing the reaction conditions (metals, catalyst loadings, temperatures, H_2 pressures, etc.).

VI. Biomass-derived monomer synthesis

Kinetic study of aldol addition kinetics in microporous media. Solvent identity and pore polarity are known to influence Lewis acidic catalysis in zeolite pores for a variety of liquid-phase chemistries. We investigated how these parameters alter the rates of self-aldol addition of ethyl pyruvate (EP), a biomass-derived compound that we have proposed upgrading to MMBL and MVL monomers, over hydrophobic and hydrophilic Hf-BEA zeolites in both toluene and acetonitrile solvents. Reactions were performed in batch using hydrophobic Hf-BEA-F and hydrophilic Hf-BEA-OH and were free of internal and external mass transfer artifacts. Rates were observed to be first-order with respect to solution-phase ethyl pyruvate activity and were fit to first-order rate laws to obtain apparent first order rate constants (**Fig. 11a**). Apparent rate constants could then be decomposed into their respective enthalpic and entropic contributions using non-ideal transition state theory. The calculated values are tabulated in **Fig. 11b**.

(a)

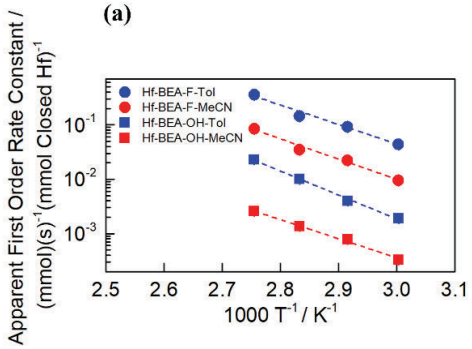

(b)

Catalyst	Solvent	ΔH_{app} / kJ mol^{-1}	ΔS_{app} / J mol^{-1} K^{-1}
Hf-BEA-F	Toluene	67.9±6	-68.5±19
	Acetonitrile	70.2±6	-74.0±18
Hf-BEA-OH	Toluene	83.8±4	-47.0±10
	Acetonitrile	67.7±4	-109±11

Figure 11. (**a**) Apparent first order rate constants for EP aldol addition (k_{app}, normalized per closed Hf) regressed from reaction rate data measured on Hf-BEA-F and Hf-BEA-OH in toluene and acetonitrile as functions of inverse temperature. Dashed lines are exponential fits to the data. (**b**) ΔH_{app} and ΔS_{app} values for EP aldol addition in Hf-BEA-F and Hf-BEA-OH in toluene and acetonitrile, extracted from apparent first order rate constants.

Despite the substantial rate constant variation across the four systems, apparent enthalpies in Hf-BEA-F in both solvents and Hf-BEA-OH in acetonitrile were within error of each other (~70 kJ mol^{-1}). Reactions performed using Hf-BEA-OH with toluene featured a higher apparent enthalpic barrier of 83.8 kJ mol^{-1}. The differences between the systems are attributed to hydrogen-bonding interactions between the EP molecules and polar silanol nests during catalysis in toluene using Hf-BEA-OH, which hinder EP adsorption to the active site in the hydrophilic framework. These hydrogen-bonding interactions are not present when acetonitrile is used as the solvent, as acetonitrile itself binds to and blocks silanol groups. Equilibrium EP absorption measurements indicate that while both toluene and acetonitrile are present in pores during catalysis, neither solvent forms a tight solvation shell around EP in the pores that must be disrupted prior to EP adsorption. These findings show that aldol addition kinetics are not significantly modified by solvent polarity in hydrophobic frameworks beyond site-blocking effects; however, silanol nests in hydrophilic frameworks significantly alter substrate adsorption to the active site. These results can be applied to other liquid-phase aldol condensation chemistries of relevance to RePLACE and will inform future studies in these types of systems.

Continuous vapor-phase catalytic synthesis of MVL from DVL and formaldehyde. We have demonstrated the continuous, vapor-phase synthesis of α-methylene-δ-valerolactone (MVL) from δ-valerolactone (DVL) and formaldehyde (FA) over alkaline earth oxides supported on silica. To our knowledge, this is the first time this chemistry has been performed over a heterogeneous catalyst in flow, as other MVL synthesis procedures reported in the literature have been in batch and required the use of expensive, stoichiometric, and non-biobased reagents to obtain MVL. In our system, a mixture of formalin (37 wt% FA in water) and DVL is vaporized in an N_2 gas flow and passed over a bed of 100-300 mg of catalyst diluted in inert silicon carbide. Three supported alkaline earth oxides were tested, and their selectivity to MVL at DVL conversions of ~60% are shown in **Fig. 12a**. MVL was produced by all three catalysts, with CaO and BaO showing 90% or higher selectivity to MVL under the conditions tested. Reactivity decreased with increasing basicity of the catalyst (i.e., downward on the periodic table), while selectivity toward the desired MVL product generally increased. Side products observed in GC included γ-valerolactone (GVL) and α-methyl-δ-valerolactone (methyl-DVL).

(a)

Catalyst	Contact Time / h	DVL Conversion / %	MVL Selectivity / %
MgO/SiO_2	2.9	60	41
CaO/SiO_2	4.4	66	90
BaO/SiO_2	12.1	57	100

(b)

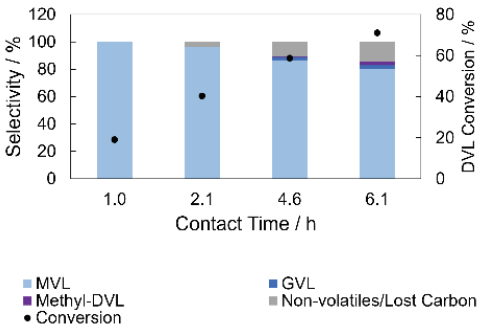

Figure 12. (**a**) Table comparing selectivities of different alkaline earth oxides toward MVL at comparable conversions. Contact time is defined as $m_{catalyst}/F_{DVL}$. (**b**) DVL conversion and product distributions as functions of contact time for 5 wt% CaO/SiO_2 catalyst, which was identified as both highly reactive and selective to MVL. Conditions: 0.4 mol% DVL, 1.2 mol% FA, 613 K, 101 kPa, 100 mg of 5 wt% catalyst.

Due to its high selectivity to MVL and overall reactivity, CaO/SiO_2 was selected for further study. By modifying the contact time (m_{cat}/F_{DVL}), we studied how the MVL selectivity changed at increasing DVL conversions (Figure 2b). As contact time is decreased, the selectivity toward MVL monotonically increases and becomes ~100% at contact times of 1.0 h with a DVL conversion of 19%. While methyl-DVL and GVL are formed at higher contact times to some extent, most of the side products at higher conversions seem to be non-volatiles that deactivate the catalyst over time. We believe that these are from parallel DVL-DVL aldol condensations and a series MVL-DVL aldol condensation that poison the catalyst over time and consume both the reactant and desired product. Calcination in air at 500 °C for 4 h regenerates all lost reactivity.

VII. Modeling

DFT calculations for chemical recycling of post-consumer nylons. In order to gain deeper insights into the reaction mechanism of Nylon-6 catalyzed by $Cp^*_2LaCH(TMS)_2$, a detailed Gibbs free energy profile for the depolymerization of Nylon-6 was computed using a dimer model of Nylon-6 (as illustrated in **Fig. 13**) in solution phase. The initial step involves the transfer of a hydrogen atom from the Cp* ligand to the $-CH(TMS)_2$ ligand, which occurs during the pre-catalyst thermolysis process. This results in the formation of the "Tuck-in" structure, as previously reported. Once the "Tuck-in" structure is formed, the Nylon-6 polymer chain coordinates to the pre-catalyst to form **INT3**. Next, the hydrogen atom in the $-NH_2$ group of the polymer chain transfers to the pre-catalyst to form **INT4**. **INT4** then enters the catalytic depolymerization cycle, where it undergoes intramolecular cyclization to form **INT5**. Following this, a C-N dissociation step in **INT5** converts it to **INT6**. Finally, ε-caprolactam is spontaneously released from **INT6**, while another secondary amide substrate coordinates to the La center, yielding **INT7**.

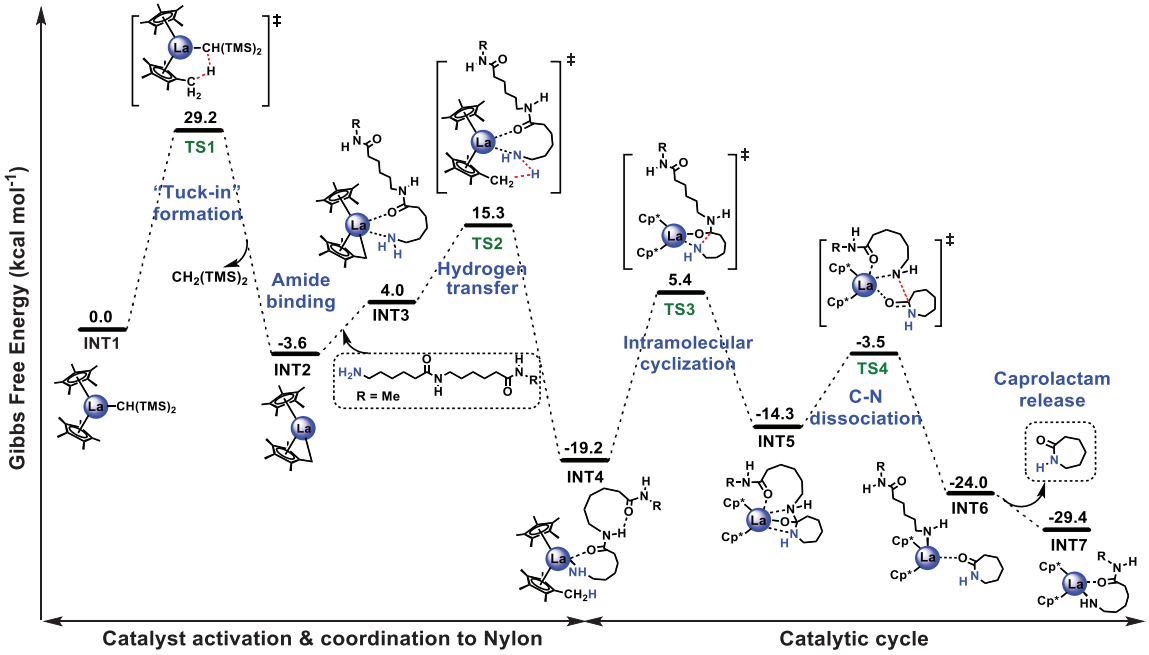

Figure 13. DFT-derived energetic (Gibbs free energy) profile in solution phase (kcal mol^{-1}). Reaction pathways are highlighted in dashed lines.

Developing the workflow to predict ΔH_P and ΔS_P for ring-opening polymerization. Towards estimating T_c values to design recyclable polymers, the Broadbelt group has developed a workflow based on multiscale simulations starting from semi-empirical molecular dynamics simulations

(GFN0-xTB) to density functional theory calculations using a recently developed composite method B97-3c. This workflow considers multiple configurations of polymer chains to improve calculation accuracy. The calculations of ΔH_P and ΔS_P for 2-allyloxymethyl-2-ethyl-trimethylene carbonate appear to be well representative of the bulk liquid phase (-0.66 kcal/mol vs. -0.86 kcal/mol of ΔH_P and -1.96 cal/mol/K vs. -1.65 cal/mol/K of ΔS_P for the calculated vs. experimental values, respectively). However, the calculated results in the solution phase are do not agree with experimental values well due to the lack of capturing the configurational changes of polymer chains in solution using an implicit solvent model. A similar workflow has been applied to δ–valerolactone, which shows good agreement with the values of ΔH_P and ΔS_P compared to the experimental results for monomer to polymer transition from the liquid phase to the high elastic phase at 298.15 K (-2.39 kcal/mol vs. -2.51 kcal/mol of ΔH_P and -1.35 cal/mol/K vs. -3.59 cal/mol/K of ΔS_P for the calculated vs. experimental values, respectively).

Assessing the thermodynamic design space for the discovery of circular polymers. Based on findings summarized in above, it has been demonstrated that using DFT to calculate T_c can be a costly process that may not yield a quantitative agreement with experimental outcomes. This is true even when considering the DFT chemical accuracy boundaries established by Grimme for small molecules. To quantify how much T_c deviates with small changes in enthalpy and entropy, we quantified the standard deviation and maximum absolute error within a thermodynamic design space, using the limits of chemical accuracy for the best achievable small molecules. The equations used are listed as followed:

Standard deviation: $\sigma_{T_C} = \frac{H}{S}\sqrt{(\frac{\sigma_H}{H})^2 + (\frac{\sigma_S}{S})^2}$, Maximum absolute error: $\sigma_{T_C} = \left|\frac{H-\sigma_H}{S+\sigma_S} - \frac{H}{S}\right|$

σ_{T_C} is either the standard deviation of the error or the maximum absolute error. σ_H and σ_S are the best-possible errors in enthalpy and entropy, respectively. In the error distribution represented in **Fig. 14**, the darkest colors depict an error range of >±100 °C compared to the expected T_c. Furthermore, the error distribution includes data points of various reported circular polymers, with special emphasis placed on the disubstituted lactones synthesized by the Chen group, denoted by the highlighted white markers.

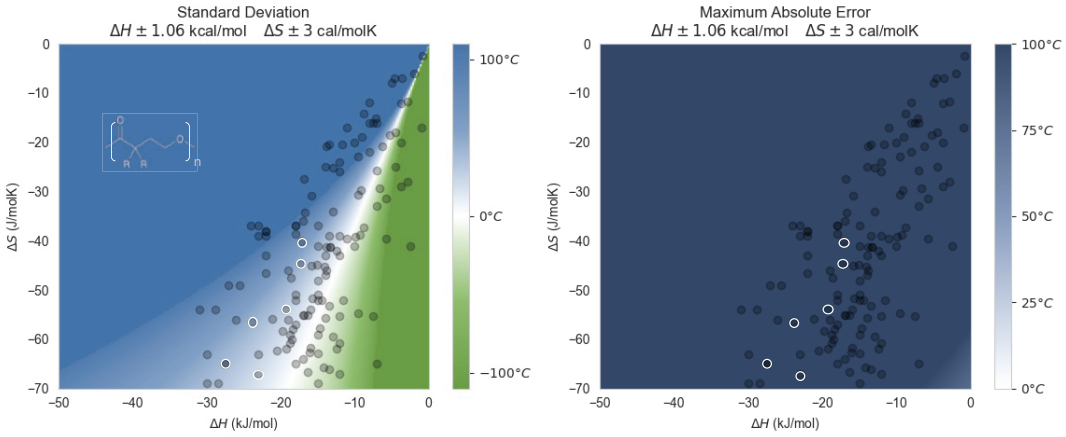

Figure 14. Standard error and maximum absolute errors associated with calculating T_c.

As evident from the presented data, even if we were to successfully predict thermodynamic properties within this defined limit, accurately calculating T_c remains challenging. This observation leads us to conclude that there are additional factors to be considered beyond T_c alone when assessing the circularity of a polymer, such as desirable ranges for enthalpy and entropy or other reaction conditions.

Machine learning for the discovery of circular polymers. Considering the complexity of this problem and the computationally intensive workflow involved in utilizing DFT to achieve only moderate accuracy, the application of machine learning techniques presents an opportunity to employ more cost-effective methods while achieving comparable results. By condensing simulation corrections into low-cost input features, a single machine learning workflow could be applied to a diverse range of polymers. The field of polymer property prediction has witnessed significant progress, leading to the availability of numerous open-source software solutions. To address this problem, we divided it into two parts: the first part focuses on using machine learning to predict the enthalpy of polymerization, while the second part involves predicting the entropy of polymerization using machine learning techniques. The workflow is seen in **Fig.15**. To predict the enthalpy of polymerization, we assembled a novel dataset comprising over 800 enthalpies of polymerization, encompassing a wide range of structures, states, and polymerization mechanisms. Various structural and reaction condition-related features were calculated for the dataset. Initially, we tested a few simple models employing solely structural features. We obtained a promising result with a Mean Absolute Error (MAE) of 2.45 kcal/mol (compared to Grimme's limit of 2 kcal/mol) using a Morgan fingerprint representation of the structure and neural networks. This outcome motivated us to proceed with a more sophisticated model employing message passing neural networks. Currently, we are working on modifying a standard message passing neural network to incorporate solvent effects and reaction conditions, thus enhancing the accuracy of our predictions.

Figure 15. Machine learning workflow used for Tc prediction.

Publications Acknowledging this Grant in 2020-2023

(I) Intellectually led by this grant

Clarke, R. W.; Sandmeier, T.; Franklin, A. Kevin; Reich, D.; Zhang, X.; Vengallur, N.; Patra, T. K.; Tannenbaum, R. J.; Adhikari, S.; Kumar, S. K.; Rovis, T.; Chen, E. Y.-X. Dynamic Crosslinking Compatibilizes Immiscible Mixed Plastics. *Nature* **2023**, *616*, 731−739. DOI: 10.1038/s41586-023-05858-3.

Li, X.-L.; Clarke, R. W.; Jiang, J. -Y.; Xu, T.-Q.; Chen, E. Y.-X. A Circular Polyester Platform Based on Simple Gem-disubstituted Valerolactones. *Nat. Chem.* **2023**, *15*, 278−285. DOI: 10.1038/s41557-022-01077-x.

Li, X.-L.; Clarke, R. W.; An, H.-Y.; Gowda, R. R.; Jiang, J. -Y.; Xu, T.-Q.; Chen, E. Y.-X. Dual Recycling of Depolymerization Catalyst and Biodegradable Polyester that Markedly Outperforms Polyolefins. *Angew. Chem. Int. Ed.* **2023**, e202303791. DOI: 10.1002/anie.202303791 (*Designated "Hot Paper"*).

Wursthorn, L.; Beckett, K.; Rothbaum, J.O.; Cywar, R.M.; Lincoln, C.; Kratish, Y.; Marks, T.J. Selective Lanthanide-Organic Catalyzed Depolymerization of Nylon-6 to ε-Caprolactam, *Angew. Chem.* **2023**, *62*, e202212543. DOI: 10.1002/anie.202212543.

Khechfe, A. A.; Matha, T. B. M.; Román-Leshkov, Y. Solvent Polarity and Framework Hydrophobicity of Hf-BEA Zeolites Influence Aldol Addition Rates in Organic Media, *ACS Catal.* **2023**, *13*, 6474–6485. DOI: 10.1021/acscatal.3c00787.

Ye, L.; Liu, X.; Beckett, K.; Rothbaum, J. O.; Lincoln, C.; Broadbelt, L. J.: Kratish,Y.; Marks, T.J. Catalyst Ligand Design to Address Nylon Plastics Recycling, **2023**, *Under revision*.

Zhao, Y., Rettner, E. R., Harry, K. L., Hu, Z., Miscall, J., Rorrer, N. A., Miyake, G. M. Chemically Recyclable Polyolefin-Like Multiblock Polymers, **2023**, *Under revision*.

Jingguang Chen

Grant number: DE-FG02-13ER16381
Grant Title: Metal Carbides/Nitrides and Bimetallic Alloys as Low-cost Electrocatalysts

PI: Jingguang Chen

Student(s): Neal Biswas (graduated in December 2022)
Hansen Mou (partial support; NSF Fellow)
Kevin Turaczy (partial support; NSF Fellow)
Samay Garg (partial support; NSF Fellow)

Postdoc: Qiaowan Chang (3 months)

Collaborators: Prof. Shyam Kattel (Florida A&M University)
Prof. Feng Jiao (University of Delaware)

Affiliations(s): Department of Chemical Engineering, Columbia University
Joint Appointment: Chemistry Division, Brookhaven National laboratory

RECENT PROGRESS

Motivation

It is well known that the electronic and catalytic properties of transition metals can be modified by the formation of carbides, nitrides and bimetallic alloys, which often demonstrate properties that are distinctively different from those of the parent metals. In particular, in some cases transition metal carbides (TMCs) and nitrides (TMNs) of Groups 4-6 elements show catalytic properties that are characteristic of Pt-group metals (PGM: Pt, Pd, Ir, Rh, Ru).

Many electrochemical devices, such as electrolyzers, fuel cells and photoelectrochemical cells, currently require PGM electrocatalysts. The high costs and limited supplies of these precious metals create potentially prohibitive barriers to market penetration and scale-up production of devices requiring large catalyst loadings. **The ultimate goal of our research program is to identify TMC, TMN and bimetallic catalysts to either substantially reduce or completely replace PGM in electrocatalysis.** We aim to achieve this goal by exploring the electrochemical properties of TMCs and TMNs, using them either as electrocatalysts or as catalytic supports for low loadings of PGM for several types of electrocatalytic reactions. In addition, we also explore the utilization of TMCs/TMNs-supported PGM and bimetallic catalysts for tandem catalytic reactions that couple electrocatalysis and thermocataysis.

Recent Results

Results from the current funding have led to 20 publications in the past 3 years, as listed at the end of this report. The topics of these publications include the utilization of

TMC, TMN and earth-abundant metals as catalytic materials, as well as our recent efforts in exploring tandem electrocatalytic-thermocatalytic processes. In this report we will briefly summarize our work in developing a tandem process for converting CO_2 to C_3 oxygenates (propanol and propanal).

The conversion of CO_2 is inherently challenging because of the stability of the carbon-oxygen double bonds. Effective catalytic processes are necessary to lower the activation barrier and minimize energy inputs. Various CO_2 conversion approaches, such as thermochemical, electrochemical, photochemical, and biological, are currently being explored. A purely thermocatalytic approach relies upon fossil fuel derived feedstocks (for example, the production of hydrogen via high-temperature steam methane reforming), which have their own associated CO_2 emissions. This results in an overall process that does not necessarily have net-negative CO_2 emissions. Alternatively, an electrocatalytic route can convert CO_2 by exploiting carbon-free electricity sources, such as wind or solar. However, direct electrochemical CO_2 conversion into high-value products with more than two carbons has low product selectivity and yields, as well as requiring large energy inputs to separate dilute oxygenate products from an aqueous electrolyte.

We instead propose a tandem two-stage electrocatalytic and thermocatalytic approach, wherein CO_2 (and water) are electrochemically reduced into ethylene, CO, and H_2, which are then directly fed to an ambient pressure thermochemical hydroformylation reactor to produce multi-carbon oxygenates, propanal and 1-propanol (Figure 1). Oxygenated products, such as aldehydes and alcohols, are important feedstocks used in plastics, automotive, pharmaceutical, and other chemical industries. At present, the precursors to oxygenate production are typically obtained from fossil fuel-based sources (e.g., alkenes are produced from alkane/naphtha cracking, and syngas is produced from coal/heavy hydrocarbon gasification or steam reforming). Instead, the proposed process can be powered by renewable energy and uses CO_2 as the carbon source to generate the intermediate precursor molecules. Directly coupling the two reactors also eliminates the need for intermediate separation of gaseous products from the CO_2 electrolyzer, as well as avoids safety risks associated with the transportation and storage of flammable and toxic feedstocks for hydroformylation reactions. To our knowledge, the tandem electrochemical-thermochemical production of C_3 oxygenated species from CO_2 has not yet been demonstrated.

We explore the possibility of achieving the tandem strategy to produce C_3 oxygenates from CO_2. We first perform electrochemical CO_2 reduction reaction (CO_2RR) experiments using commercial Cu catalysts in a vapor-fed membrane electrode assembly (MEA) device. Then, the thermochemical hydroformylation reaction is tested separately with a Rh_1Co_3/MCM-41 catalyst and using a $C_2H_4/CO/H_2$ feed ratio that matches the product ratio obtained from the CO_2RR experiments. Following the individual CO_2RR and hydroformylation catalytic tests, the reactors are connected in a tandem configuration to validate the feasibility of the proposed reaction strategy, as illustrated in Figure 1. Additionally, in situ X-ray absorption spectroscopy is used to identify the oxidation states of Cu and Rh during CO_2RR and hydroformylation reactions, respectively.

Initially, the electrochemical CO_2RR and thermochemical hydroformylation reactions were evaluated separately to test catalytic performance and optimize operating conditions. CO_2RR experiments were conducted in a zero-gap, vapor-fed 5 cm^2 electrolyzer with an MEA consisting of a cathode (Cu-coated carbon gas diffusion layer),

a Sustainion anion exchange membrane, and an anode (IrO_2 on a platinized titanium fiber felt). Due to its intermediate binding energies of H^* and CO^*, Cu is the only monometallic catalyst that is able to electrochemically produce ethylene with appreciable selectivity. In this work, we study CO_2RR on commercial Cu catalysts with different oxidation states (i.e., Cu and oxide-derived Cu catalysts), as well as with modifications to the gas diffusion layer (GDL) hydrophobicity (i.e., fluorinated ethylene propylene (FEP) reinforced carbon).

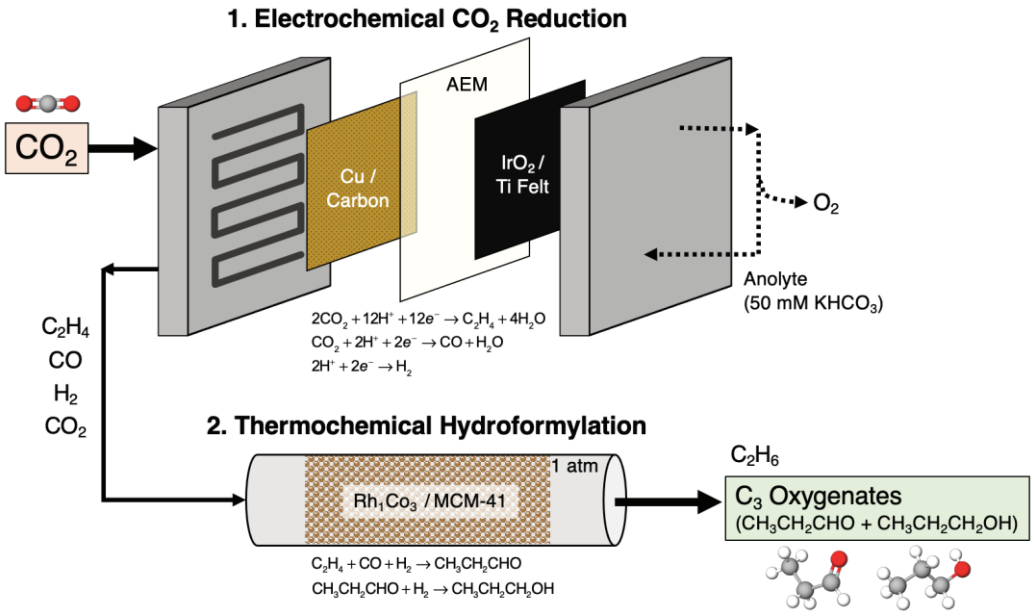

Figure 1. Tandem electrochemical-thermochemical reactors for CO_2 conversion to C_3 oxygenates.

Electrochemical experiments were conducted in a 5 cm^2 electrolyzer to determine the optimal current density and CO_2 feed rate. In general, higher current densities and lower CO_2 flowrates favored increased ethylene Faradaic efficiencies (FE); however, mass transport limitations were observed at current densities above –220 mA cm^{-2} and CO_2 flowrates below 10 sccm, which consequently resulted in excessive hydrogen production and cell instability. Changes in the Cu catalyst oxidation state and GDL hydrophobicity altered the CO_2RR product selectivities, as both the oxide-derived Cu catalyst (59.9% ethylene FE) and reinforced carbon GDL (55.9%) cathodes demonstrated increased ethylene Faradaic efficiencies relative to the Cu/C cathode (50.1%). The FEP-reinforced carbon GDL was also able to suppress the hydrogen evolution reaction (HER), lowering the H_2 Faradaic efficiency from 26.6% to 19.2%. For the oxide-derived Cu catalyst, the enhanced ethylene production was accompanied by a decreased CO Faradaic efficiency of 5.3%. electrolyzer operation is evident in all cases, which is essential for the downstream thermochemical reactor to achieve a steady state production of C_3 oxygenates.

Next, the hydroformylation reaction was investigated using a thermochemical reactor with C_2H_4/CO/H_2 feed ratios mimicking those from the CO_2 electrolyzer. A Rh_1Co_3 bimetallic catalyst supported on a high surface area MCM-41 substrate was selected. Our group has previously performed an in-depth study on the heterogenous hydroformylation reaction at ambient pressure, which included optimization of Rh/Co metal ratio in the bimetallic catalyst, in situ X-ray absorption analysis, and density functional theory

calculations. In the current study, we primarily focus on the effect of the $C_2H_4/CO/H_2$ feed gas ratio, which may vary as a result of the upstream electrochemical performance. Depending on experimental conditions, the product ratios obtained from electrochemical CO_2RR experiments were 1:1.1:3.2, 1:0.5:2.2, and 1:1.3:2.0 $C_2H_4/CO/H_2$. These molar ratios, along with a benchmark test of a 1:1:1 $C_2H_4/CO/H_2$ ratio, were simulated as the feed to the hydroformylation reactor with a total feed rate of 15 sccm.

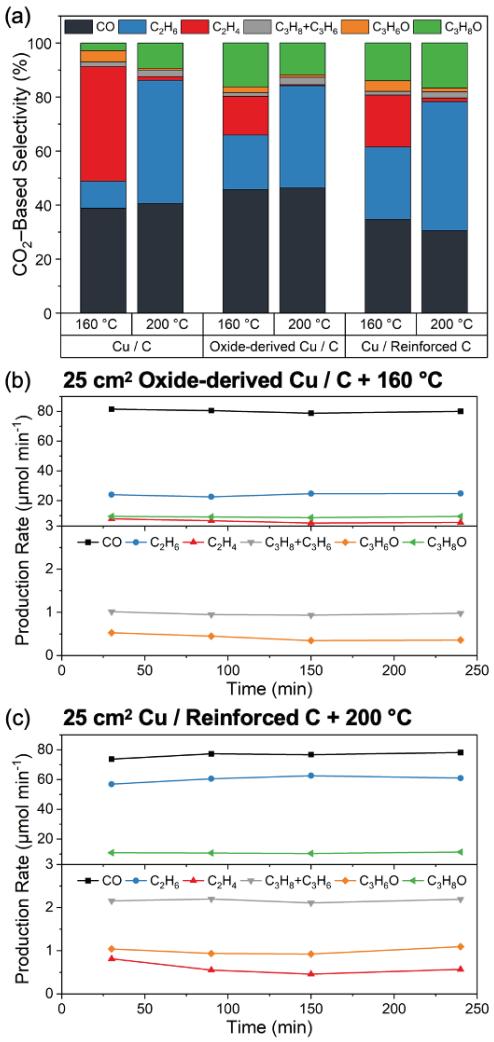

Figure 2. Tandem electrochemical-thermochemical performance. (a) CO_2-based selectivity of products for 5 cm^2 Cu/C, oxide-derived Cu/C, and Cu/reinforced C cathodes at –220 mA cm^{-2} in combination with 160 °C and 200 °C hydroformylation temperature. Production rate of species as a function of time on stream for (b) 25 cm^2 oxide-derived Cu/C and (c) 25 cm^2 Cu/reinforced C.

Following the independent CO_2RR and hydroformylation studies, the two reactors were coupled together in a tandem configuration, with the outlet from the CO_2 electrolyzer being directly fed as the inlet to the thermochemical hydroformylation reactor. The same CO_2RR cathodes (Cu/C, oxide-derived Cu/C, Cu/reinforced C) at –220 mA cm^{-2} and hydroformylation temperatures (160 °C, 200 °C) from the single reactor tests were used. Unlike the single reactor experiments, the tandem system contained a small concentration of unconverted CO_2 in the feed to the hydroformylation reactor. Additionally, the limitations of using a lab-scale electrolyzer resulted in a lower product flowrate (and therefore, higher residence times) than the flowrates used in the single hydroformylation reactor tests.

Figure 2a shows the selectivity on a reduced CO_2-basis of products for the tandem 5 cm^2 CO_2 electrolyzer and the thermochemical hydroformylation reactor. The largest C_3 oxygenate selectivities observed were 18.4% (16.2% 1-propanol, 2.2% propanal) for the oxide-derived Cu/C cathode + 160 °C hydroformylation, and 18.0% (16.7% 1-propanol, 1.3% propanal) for Cu/Reinforced C cathode + 200 °C hydroformylation. The conditions with the greatest C_3 oxygenate production were also consistent with that of the hydroformylation-only tests (i.e., 1:0.5:2.2 $C_2H_4/CO/H_2$ ratio at 160 °C and 1:1.3:2.0 $C_2H_4/CO/H_2$ ratio at 200 °C). Although the primary focus of this work was to demonstrate the production of C_3 oxygenates, the conversion of CO_2 to ethylene, ethane, and other multi-carbon products is also valuable. The total selectivity of C_{2+} products varied between 54% to 70% among all tandem reaction conditions.

The tandem system was also tested with a 25 cm^2 CO_2 electrolyzer to increase the C_3

oxygenate production rate and demonstrate scalability (Figure 2b and 2c). The CO_2 feed rate was increased to 40 sccm to avoid mass transfer limitations in the larger area device. The production rates of the major and minor products for 25 cm^2 oxide-derived Cu/C + 160 °C and Cu/Reinforced C + 200 °C are shown in Figure 3b and Figure 3c, respectively. The steady state production of total C_3 oxygenates from the tandem system was 9.3 μmol min^{-1} for oxide-derived Cu/C + 160 °C, and 11.8 μmol min^{-1} for Cu/Reinforced C + 200 °C. Previous studies have also independently shown stable CO_2RR-to-ethylene for up to 150 hours and heterogenous hydroformylation for up to 60 hours, further demonstrating the potential for long-term C_3 oxygenate production.

In order to make an equivalent comparison with the direct electrochemical CO_2 reduction to C_3 oxygenates, the FEs and current densities reported in literature were converted to selectivities (based on the total amount of CO_2 being reduced) and molar production rates. Compared with direct CO_2RR in flow cells, the tandem system exhibited higher C_3 oxygenate production rates, as well as improvements in C_3 oxygenate selectivity by nearly a factor of 5. State-of the-art CO_2RR H-cell studies have demonstrated higher 1-propanol FEs (~15%) than flow cells, however their production rates are 1–2 orders of magnitude smaller and cannot be easily scaled. Moreover, purely electrochemical systems would require highly energy-intensive separations to isolate dilute C_3 oxygenate quantities from a mixture of other liquid products (i.e., formate, acetate, methanol, ethanol) in an aqueous catholyte solution. In contrast, the tandem electrochemical-thermochemical system allows for easily separable liquid oxygenate products from the gaseous outlet stream of the second hydroformylation reactor. More research efforts will be needed to further improve the overall efficiency of the tandem electrochemical-thermochemical process, such as increasing the CO_2 utilization by suppressing carbonate formation and enhancing C_3 oxygenate selectivity by optimizing catalyst compositions in both electrochemical and thermochemical reactions.

In summary, this work validates the feasibility of the proposed electrochemical-thermochemical reactor scheme to convert CO_2 into C_3 oxygenate products. The tandem system achieved C_3 oxygenate selectivities up to 18.4% and production rates up to 11.8 μmol min^{-1}, demonstrating a distinct advantage over direct electrochemical CO_2 conversion. This work serves as a useful proof-of-concept. Similar tandem approaches can also be explored by encompassing other reactions, such as CO_2RR followed by the thermocatalytic aromatization ($3C_2H_4 \rightarrow C_6H_6 + 3H_2$) or hydrocarboxylation ($C_2H_4 + CO + H_2O \rightarrow CH_3CH_2COOH$) reactions. There remain many opportunities for future optimizations and innovations in tandem electrochemical-thermochemical CO_2 conversion processes.

Future Plans

In the next year we will further explore the activity, selectivity and stability of TMC/TMN and non-precious bimetallic catalysts. We will also explore the utilization of these catalysts for the electrochemical-thermochemical conversion of CO_2 to produce value-added products, paying particular attention in identifying reaction descriptors from the correlation between experimental results and DFT calculations.

Publications Acknowledging this Grant in 2020-2023

(I) Intellectually led by this grant

1. A.N. Biswas, L.R. Winter, Z. Xie and J.G. Chen*, "Utilizing CO_2 as a Reactant for C_3 Oxygenate Production via Tandem Reactions", *JACS Au*, 3 (2023) 293.
2. A.N. Biswas, Z. Xie, R. Xia, S. Overa, F. Jiao* and J.G. Chen*, "Tandem Electrocatalytic-Thermocatalytic Reaction Scheme for CO_2 Conversion to C_3 Oxygenates", *ACS Energy Letters*, 7 (2022) 2904.
3. Q. Chang, Y. Liu, J.-H. Lee, D. Ologunagba, S. Hwang, Z. Xie, S. Kattel*, J.H. Lee* and J.G. Chen*, "Metal-coordinated Phthalocyanines as Platform Molecules for Understanding Isolated Metal Sites in Electrochemical Reduction of CO_2", *Journal of the American Chemical Society*, 144 (2022) 16131.
4. X. Yang, J.H. Lee, S. Kattel, B. Xu* and J.G. Chen*, "Tuning Reaction Pathways of Electrochemical Conversion of CO_2 by Growing Pd Shells on Ag Nanocubes", *Nano Letters,* 22 (2022) 4576.
5. Z. Lin, S.C. Ammal, S.R. Denny, S.A. Rykov, K.-E. You, A. Heyden* and J.G. Chen*, "Unraveling Unique Surface Chemistry of Transition Metal Nitrides in Controlling Selective C-O Bond Scission Pathways of Glycerol", *JACS Au*, 2 (2022) 367.
6. H. Mou, Q. Chang, Z. Xie, S. Hwang, S. Kattel and J.G. Chen, "Enhancing Glycerol Electrooxidation from Synergistic Interactions of Platinum and Transition Metal Carbides", *Applied Catalysis B: Environmental*, 315 (2022) 121648.
7. S.R. Denny, Z. Lin, W.N. Porter, N. Artrith and J.G. Chen, "Machine learning prediction and experimental verification of Pt-modified nitride catalysts for ethanol reforming with reduced precious metal loading", *Applied Catalysis B: Environmental*, 312 (2022) 121380.
8. Y. Nian, Y. Wang, A.N. Biswas, X. Chen, Y. Han* and J.G. Chen*, "Trends and descriptors for tuning CO_2 electroreduction to synthesis gas over Ag and Au supported on transition metal carbides and nitrides", *Chemical Engineering Journal*, 426 (2021) 130781.
9. D. Tian, S.R. Denny, K. Li*, H. Wang*, S. Kattel* and J.G. Chen*, "Density Functional Theory Studies of Transition Metal Carbides and Nitrides as Electrocatalysts", *Chemical Society Reviews*, 50, (2021) 12338.
10. Y. Wang, Y. Nian, A.N. Biswas, W. Li, Y. Han* and J.G. Chen*, "Challenges and Opportunities in Utilizing MXenes of Carbides and Nitrides as Electrocatalysts", *Advanced Energy Materials*, 11 (2021) 2002967.
11. L.R. Winter and J.G. Chen*, "N_2 Fixation by Plasma-Activated Processes", *Joule*, 5 (2021) 300.
12. Q. He, J.H. Lee, D. Liu, Y. Liu, Z. Lin, Z. Xie, S. Hwang, S. Kattel*, L. Song*, J.G. Chen*, "Accelerating CO_2 Electroreduction to CO over Pd Single-Atom Catalyst", *Advanced Functional Materials*, 30 (2020) 2000407.
13. Q. He, D. Liu, J.H. Lee, Y. Liu, Z. Xie, S. Hwang, S. Kattel*, L. Song*, J.G. Chen*, "Electrochemical Conversion of CO_2 to Syngas with Controllable CO/H_2 Ratios over Co and Ni Single-Atom Catalysts", *Angewandte Chemie International Edition*, 59 (2020) 3033.

14. B.M. Tackett, J.H. Lee and J.G. Chen*, "Electrochemical Conversion of CO_2 to Syngas with Palladium-Based Electrocatalysts", *Accounts of Chemical Research*, 53 (2020) 1535.
15. Y. Liu, D. Tian, A.N. Biswas, Z. Xie, S. Hwang, J.H. Lee*, H. Meng* and J.G. Chen*, "Transition Metal Nitrides as Promising Catalyst Supports for Tuning CO/H_2 Syngas Production from Electrochemical CO_2 Reduction", *Angewandte Chemie International Edition*, 59 (2020) 11345.

(II) Jointly funded by this grant and other grants with intellectual leadership by other funding sources

16. P. Cao, X. Quan*, X. Nie, K. Zhao, Y. Liu, S. Chen, H. Yu and J. G. Chen*, "Metal single-site catalyst design for electrocatalytic production of hydrogen peroxide at industrial-relevant currents", *Nature Communications*, 14 (2023) 172.
17. Q. Chang, Y. Hong, H.J. Lee, J.H. Lee, D. Ologunagba, Z. Liang, J. Kim, M.J. Kim, J.W. Hong, L. Song, S. Kattel, Z. Chen*, J.G. Chen* and S.-I. Choi*, "Achieving complete electrooxidation of ethanol by single atomic Rh decoration of Pt nanocubes", *Proceedings of the National Academy of Sciences of United States*, 119 (2022) e2112109119.
18. R. Xia, D. Tian, S. Kattel, B. Hasaa, H. Shina, X. Ma*, J.G. Chen* and F. Jiao*, "Electrochemical Reduction of Acetonitrile to Ethylamine", *Nature Communications*, 12 (2021) 1949.
19. Q. Chang, J. Kim, J.H. Lee, S. Kattel, J.G. Chen*, S.-I. Choi*, Z. Chen*, "Boosting Activity and Selectivity of CO_2 Electroreduction by Pre-hydridizing Pd Nanocubes", *Small*, 16 (2020) 2005305.
20. Q. Chang, P. Zhang, A.H.B. Mostaghimi, X. Zhao, S.R. Denny, J.H. Lee, H. Gao, Y. Zhang, H. Xin, S. Siahrostami*, J.G. Chen* and Z. Chen*, "Promoting H_2O_2 Production via 2-Electron Oxygen Reduction by Coordinating Partially Oxidized Pd with Defect Carbon", *Nature Communications*, 11 (2020) 2178.

Zhongfang Chen

Theory-guided Innovation of High-performance Electrocatalysts for CO_2 Reduction

Zhongfang Chen (PI), Department of Chemistry, University of Puerto Rico at Rio Piedras
William E. Mustain (Co-PI), Department of Chemical Engineering, University of South Carolina

Presentation Abstract

This project aims to advance the understanding and identification of single-atom catalysts (SACs), bi-atom catalysts (BACs), and single-cluster catalysts (SCCs) for the electrochemical CO_2 reduction reaction (CO_2RR). We will combine theoretical (density functional theory, machine learning) and experimental (synthesis, electrochemical characterization) techniques to enable practical CO_2RR catalysts from computational discovery. Our goal is to show how these catalysts can selectively produce value-added chemicals like HCOOH, CO, CH_3OH, CH_3CH_2OH, CH_3CHO, and C_2H_4. Additionally, this project offers training and education in chemistry, catalysis, and applied science for CO_2RR.

In this reporting period (since September 2022), we have achieved the following: i) theoretically identified a new class of bi-atom catalysts with unique inverse sandwich structures; ii) designed an electrocatalyst for CO_2-to-C_2H_4 conversion by anchoring a Cu_5 cluster to a MoS_2 monolayer; iii) contributed to a collaborative experimental project by providing insights into the mechanisms for developing new CO_2 reduction-active platinum complexes; iv) made significant progress in synthesizing Pt and Fe-based catalysts with high density of single atoms; v) initiated the synthesis of non-Pt catalysts with the goal of realizing the structures predicted by theory.

Grant Number: DE-SC0023418

Student(s):

Graduate students

UPR, Linguo Lu, Alvaro J Guerrero; USC, Hanna Soucie

Undergraduate students:

UPR: Alana S. Cabrera Minier, Abraham L. Nicholson Carro; USC: Ian Street, Nathan Thornburg, Valerie Heimer (summer intern from Virginia Tech)

High school students:

UPR: Saleh Yassin, Jerry Chen, Guan Kevin Shan

Double-Atom Catalysts Featuring Inverse Sandwich Structure for CO_2 Reduction Reaction: A Synergetic First-Principles and Machine Learning Investigation.

To maximize metal atom utilization and enhance electrocatalytic performance, two-dimensional (2D) material-supported single/double atom catalysts (SACs/DACs) have been widely explored. However, current studies on DACs are limited to those with double metal atoms loaded in the same plane of the 2D substrates.

We explored a new family of DACs supported on defective graphene featuring an inverse sandwich structure, utilizing a synergistic approach of density functional theory (DFT) and machine learning (ML) techniques (Figure 1). More specifically, we first explored 132 DACs on graphene (gra) for CO_2RR, including five homonuclear M_2⊥gra and 127 heteronuclear MM′⊥gra, among which 1 homonuclear (Rh_2⊥gra) and 14 heteronuclear DACs (particularly RhIr⊥gra and RhPt⊥gra) showed excellent catalytic activity for converting CO_2 to CH_3OH/CH_4 (with limiting potential <0.70 eV). Using an ML approach, we predicted 154 stable DACs with $|U_L|$ values < 0.60 V from 784 inverse sandwich configurations, including 40 < 0.50 V and 3 < 0.40 V.

This work not only reveals the promise of unprecedented DACs configurations with metal dimers vertically anchored in defective graphene as CO_2RR electrocatalysts, but also demonstrates the power of combining traditional DFT computations and the emerging ML techniques for catalyst design. This design strategy is not limited to graphene, as vertical metal dimers can also be anchored onto other suitable 2D materials. As such, our study introduces a versatile and innovative design strategy for DACs for CO_2RR and beyond.

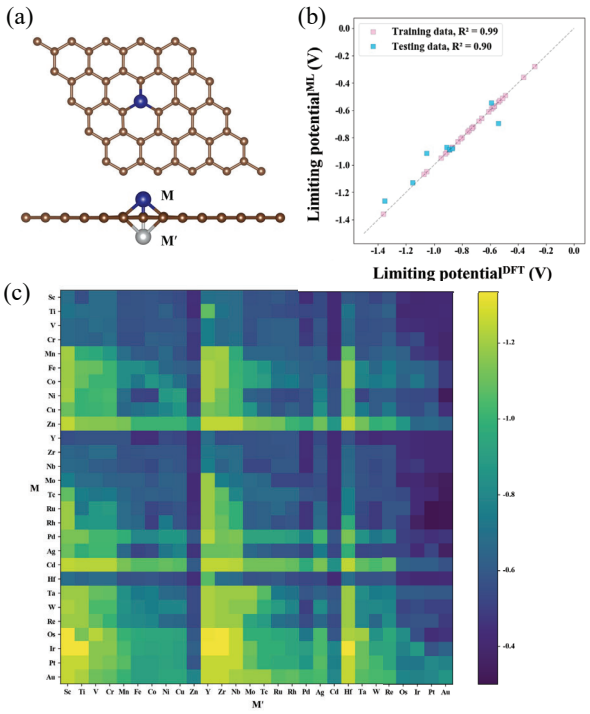

Figure 1. (a) Top and side view of DACs featuring an inverse sandwich structure. Machine learning (ML) training and prediction. (b) Comparison of U_L obtained by DFT with ML predicted values. (c) The ML-predicted heat map of U_L values for the 784 MM′⊥gra.

Computational Design of Cu-Based Clusters on MoS_2 for Highly Selective Electrocatalytic CO_2 Reduction to Ethylene

Electrochemical CO_2RR into value-added fuels and chemicals by using excess renewable electricity has been widely regarded as a promising strategy to solve energy and environment problems, among which C_2H_4 is an important product due to its wide applications. Copper has been widely reported as the most promising catalyst to be capable of yielding multicarbon (C_{2+}) compounds due to its moderate adsorption strength with $^*CO$ intermediate, but which is greatly hampered by its high overpotential and low selectivity. Thus, it is highly attractive to further develop novel Cu-based catalysts for the

electrocatalytic conversion of CO_2 to C_2H_4 with high selectivity, high activity, good stability, and low cost.

Systematic DFT computations were performed to design Cu-based clusters anchored on defective molybdenum disulfide (MoS_2) monolayer with sulfur (S) vacancy as an effective and highly selective catalyst for the reduction of CO_2 to C_2H_4. Our results showed that the Cu_5 cluster anchored on S vacancy site ($Cu_5@MoS_2$) features a square-like structure (Figure 2a). Moreover, $Cu_5@MoS_2$ not only has excellent structural stability and high electrical conductivity, but also its square-like sites facilitate the C−C coupling reaction between two adsorbed $^*CO$ species to $^*C_2O_2$ intermediate with a low kinetic barrier of 0.56 eV and low limiting potential (about -0.32 V), which can be further enhanced under alkaline conditions (Figure 2b). Therefore, $Cu_5@MoS_2$ can perform as a compelling electrocatalyst with high activity, high selectivity, and low cost for CO_2 reduction to the special C_2H_4 product.

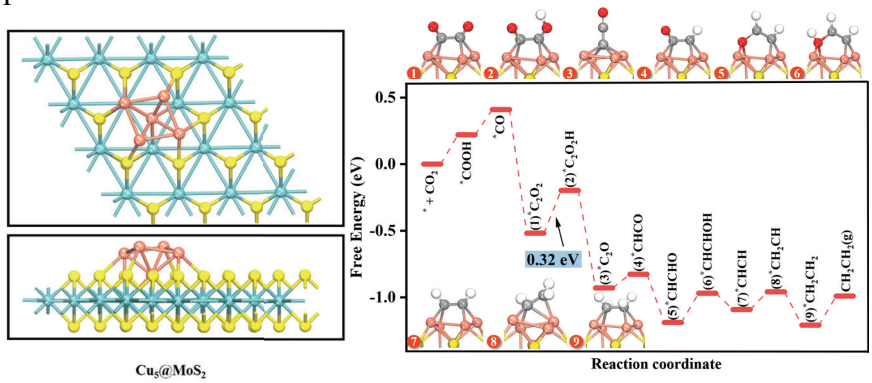

(a) (b)

Figure 2. (a) Top and side views of ($Cu_5@MoS_2$). (b) Free energy diagram for C_2H_4 generation along the most favorable pathway, along with the corresponding configurations of the reaction intermediates.

Synthesis of Pt and Fe-based catalysts with high density of single atoms

The first catalyst synthesized was Pt single atoms (Pt-SAs) on defect-free C-supports. Despite the poor CO_2RR performance (which was verified experimentally), it was chosen for its relevance to future DAC research, which may encompass Pt or other noble metals such as Rh, as suggested by our DFT predictions. Pt-SAs were fabricated through chelate fixation. Figure 3A shows XRD patterns for a catalyst with primarily SAs with that of a Pt nanoparticle catalyst with a similar mass loading. The absence of metallic Pt peaks (2θ=39°, 46°, 68°) corresponding to (111), (200), and (220) planes in the Pt-SAC indicates its low crystallinity and a predominantly single-atom structure. STEM images for this catalyst are shown in Figure 3B.

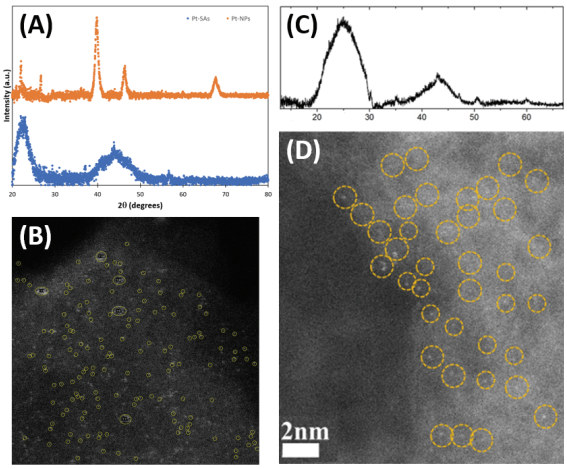

Figure 3. A) XRD patterns for nanoparticle and chelate fixation (single-atom) catalysts. B) STEM image of a Pt-single atom catalyst supported on Norit Rox. C) XRD pattern, and D) STEM image for the MOF-derived Fe-N-C.

We also incorporated transition metal single atoms in N_4-C structures. XRD analysis of Fe-N_4-C (Figure 3C) revealed weak diffraction peaks at 35°, 43°, 47°, 50° and 60°, typical for such catalysts. These patterns indicate low crystallinity, confirming successful single-atom catalyst formation, as further evidenced by STEM images (Figure 3D) where Fe single atoms are highlighted in orange circles. Line scan analysis affirmed the presence of single atoms through color intensity variations along the scans.

Preliminary Electrochemical Analysis of Pt- and Fe-SACs

Linear Sweep Voltammetry (LSV) was used to assess both catalysts in Ar-saturated and CO_2-saturated 0.1 M $KHCO_3$ electrolyte. For Pt-SAC, LSVs in CO_2-saturated electrolyte showed a lower current response than in Ar-saturated electrolyte (Figure 4A). This was expected as it is well-known that Pt undergoes CO_2RR through a CO pathway and strong CO adsorption on Pt sites leads to CO accumulation, deactivating and suppressing Pt activity. Thus, Pt is generally inactive for CO_2RR, and less studied than other transition metals such as Ag and Cu. But, it does show that a method has been developed that is able to put single atoms of noble metals onto carbon supports at a high density.

For Fe-N_4-C, there was a clear region where the HER was not a significant competing reaction (Figure 4B). Despite often being done in the literature, it is not rigorous to estimate the CO_2RR selectivity by comparing the measured current in the Ar- versus CO_2-saturated electrolytes. A much more quantitative method is to measure the gas-phase and liquid-phase products that are made as a result of the CO_2RR, which will be done be in the second year of this project. A GC-MS system has been set up to be highly quantitative (ppm-level accuracy for most C-1 products) and will be used to determine the faradaic efficiency in future work in this project.

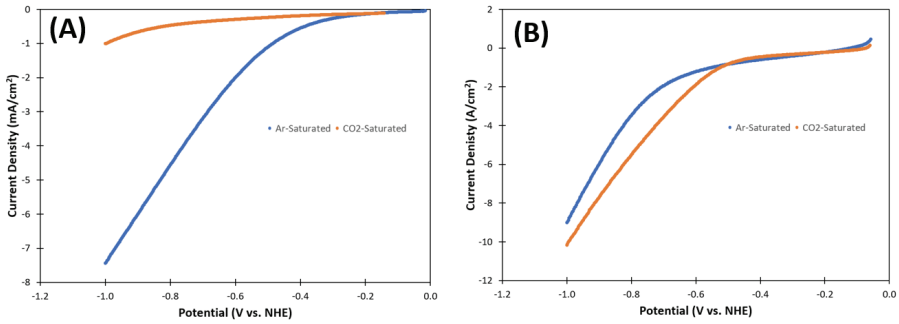

Figure 4. LSVs for A) Pt-SAC and B) Fe-N_4-C catalyst in Ar-saturated and CO_2-saturated 0.1 M $KHCO_3$ electrolyte. Both curves were collected at an electrode rotation rate of 1600 RPM at room temperature.

Publications Acknowledging this Grant in 2022-2023

(I) Intellectually led by this grant

(II) Jointly funded by this grant and other grants with intellectual leadership by other funding sources

(1) Yu, L.; Li, F.; Huang, J.; Sumpter, B. G.; Mustain, W. E.; Chen, Z. Double-Atom Catalysts Featuring Inverse Sandwich Structure for CO_2 Reduction Reaction: A Synergetic First-Principles and Machine Learning Investigation. *ACS Catalysis, ACS Catal.* **2023**, *13*, 14, 9616–9628

(2) Zhao, T.; Yan, T.; Sun, Y.; Wang, Z.; Cai, Q.; Zhao, J.; Chen, Z. Constructing the Square-Like Copper Cluster to Boost C-C Coupling for CO_2 Electroreduction to Ethylene, *J. Mater. Chem. A.* **2023**, ASAP, https://doi.org/10.1039/D3TA03630H

(3) Rivera, J.; Soto-Pérez, J.; Sepulveda Pagán, M.; Lu, L.; Borrero, J.; Luna, A.; Trinidad, P.; Pagan, Y.; Chen, Z.; Cabrera, C.; West, W.; Jones, J.; Piñero Cruz, D. M.; New platinum complexes from a salen- and a hydroxy-substituted salpn-naphthalene ligands with CO_2 reduction activity. Catalysts, *Catalysts* **2023**, *13,* 911

(4) Gao, Z.; Ma, F.; Wu, H.; Ge, Y.; Zhu, Z.; Liu, Y.; Jiao, Y.; Chen, Z. Two-dimensional Ruthenium Boride: A Dirac Nodal Loop Quantum Electrocatalyst for Efficient Hydrogen Evolution Reaction. *J. Mater. Chem. A*, **2023**,*11*, 3717-3724.

(5) He, G.; Lu, L.; Zhang, N.; Liu, W.; Chen, Z.; Li, Z.; Zou, Z. Narrowing the Band Gap and Suppressing Electron–Hole Recombination in β-Fe_2O_3 by Chlorine Doping, *Phys. Chem. Chem. Phys.*, **2023**, *25*, 3695-3701.

Paul J. Chirik

Approaches to the Catalytic Synthesis of Weak Chemical Bonds

Paul J. Chirik, Junho Kim and Matthew Pecoraro
Department of Chemistry, Princeton University, Princeton, New Jersey 08544

Presentation Abstract

The synthesis of weak chemical bonds at or near thermodynamic potential without the generation of chemical waste is a long-standing challenge in synthesis and catalysis. This is particularly relevant in the hydrogenation of molecular nitrogen to ammonia using molecular catalysts. The formation of metal nitrides from N_2 cleavage is often driven by the formation of strong M≡N bonds which in turn results in weak, "non-classical" M=N–H bonds that are often below the thermodynamic threshold for H_2 formation. Our program is focused on the development of metal-hydride catalysts that are designed to serve the dual function of activating H_2 and promoting N–H bond formation under thermal or photochemical conditions. As part of these efforts, an understanding of N_2 cleavage by well-defined metal complexes to generate metal nitrides most compatible with hydrogenation is under exploration. As part of this effort, a series of group 6 transition metal nitrides have been prepared by oxidative N_2 cleavage and the mechanism of this reaction has been investigated. Bridging intermediates with appropriate electronic driving force have been identified as key to the reaction. With this small library of substrates in hand, nitride hydrogenation by both thermal and photochemical means has been investigated and structure-activity relationships and the mechanism of N–H bond formation under study. The results of these studies will be presented.

DE-SC00066498: Approaches to the Catalytic Synthesis of Weak Chemical Bonds: Ammonia and Beyond.

Student(s): Junho Kim, Matthew Pecoraro

RECENT PROGRESS

Catalytic Approaches to Weak Bond Formation. The principal motivator of this research is to synthesize weak element-hydrogen (E–H) bonds encountered during the activation of small molecules (N_2, CO_2, arenes) using H_2 as a terminal reductant. This approach minimizes both waste and chemical overpotential. With previous DOE support, methods involving proton-coupled electron transfer (PCET) with visible light as an external driving force have been developed. Piano-stool iridium hydride compounds are effective for harnessing photonic energy as a driving force and efficiently deliver net H-atom to targeted weak E–H bonds, such as various organic molecules, metal imido complexes and metal nitrides. A general scheme outlining this approach is illustrated in the Figure below:

This work:

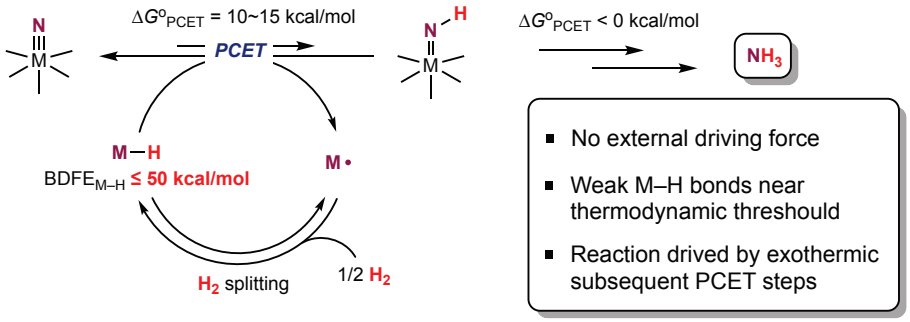

Our approach simultaneously explores new metal-hydride catalysts for the dual role of H_2 activation and subsequent hydrogen atom transfer or PCET. Recent efforts have focused on a new class of piano-stool ruthenium hydride compounds with neutral, bidentate supporting ligands. These molecules were targeted because of their robustness to C–H reductive elimination, a common deactivation pathway for group 9 metal hydride complexes. The Figure below illustrates recent progress in this area and the application to the catalytic hydrogenation to form new N–H bonds.

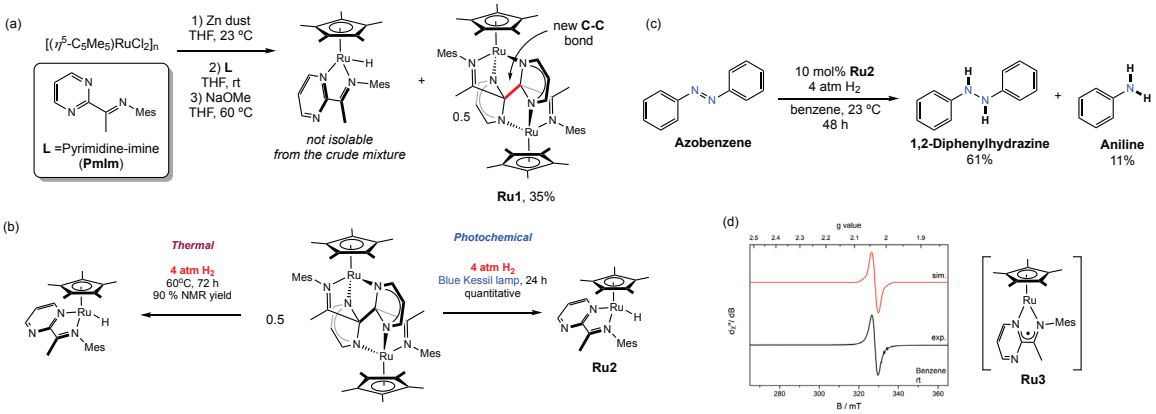

Ammonia Synthesis from N_2-Derived Metal Nitrides. A second area of research is the synthesis of N_2-derived metal nitrides for ammonia synthesis. When successful, these reactions represent the catalytic formation of ammonia from N_2 and H_2. We have previously demonstrated that $[(depe)_2MoN][BAr^F{}_4]$ is an effective substrate for this purpose using visible light and an iridium hydride photocatalyst. Recent efforts have focused on substrate optimization with the following guiding questions – what are the factors of the metal complex that promote N_2 cleavage? With respect to this question, rare examples of chromium(IV) and tungsten(IV) nitrides have been obtained. A second question is what are the properties of the resulting metal nitride that enable the highest yielding and most efficient ammonia synthesis reaction? We are currently establishing structure-reactivity relationships among the group 6 congeners and evaluating what if any correlation there is between N–H bond dissociation free energies and efficiency in ammonia synthesis. A general scheme outlining this approach is shown in the Figure below:

With respect to these goals, we are currently optimizing the yield of ammonia as a function of metal, ligand and metal-hydride photocatalyst. Motivation features of this work is to understand the mechanism of N–H bond formation. Pathways under consideration include:

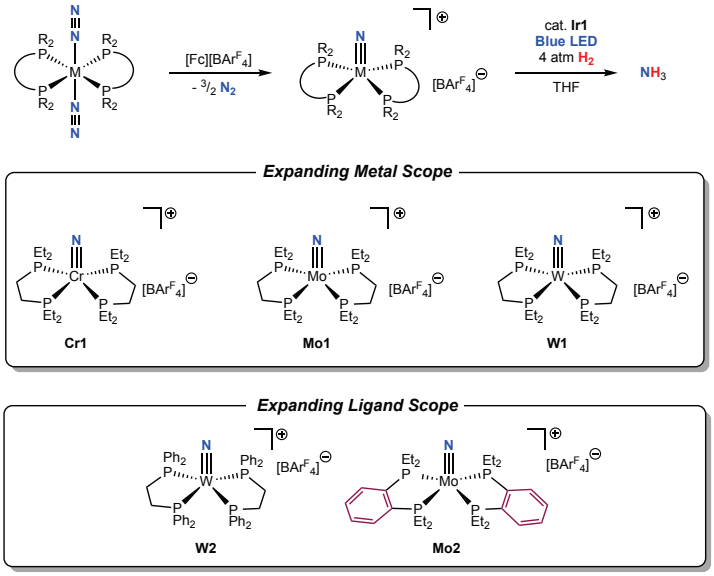

(i) photodriven PCET from the metal hydride where the resulting 17-electron metalloradical is responsible for the activation of H_2 and(ii) photocatalysis whereby the metal complex serves as a photosensitizer and activates the metal nitride by phosphine dissociation and 1,2-addition of dihydrogen. For the second pathway, we have explored other potential photosensitizers and discovered with the first generation molybdenum nitride that ammonia synthesis is possible. While not definitive for the case of metal hydrides, this suggests that pathways involving phosphine dissociation are plausible. Current studies are focusing on the type and photophysical properties of these compounds that are required to promote catalytic ammonia formation. For the first possibility, we have initiated a program at understanding the synthesis, stability and hydrogen activation ability of metalloradical compounds with the goal of realizing more long-lived catalysts.

Publications Acknowledging this Grant in 2020-2023

(I) Intellectually led by this grant
(II) Jointly funded by this grant and other grants with intellectual leadership by other funding sources

(I) Park, Y.; Zhong, H.; Pabst, T. P.; Kim, J.; Chirik, P. J. Pentamethylcyclopentadienyl Metalloradical Iron Complexes Containing Redox Noninnocent α-Diimine-Type Ligands: Synthesis, Molecular, and Electronic Structures. *Organometallics* **2023**, *42*, 465–472.

(I) Kim, S.; Kim, J.; Zhong, H.; Panetti, G. B.; Chirik, P. J. Catalytic N–H Bond Formation Promoted by a Ruthenium Hydride Complex Bearing a Redox-Active Pyrimidine-Imine Ligand. *J. Am. Chem. Soc.* **2022**, *144*, 20661–20671.

(I) Kim, S.; Park, Y.; Kim, J.; Pabst, T. P.; Chirik, P. J. Ammonia Synthesis by Photocatalytic Hydrogenation of a N_2-derived Molybdenum Nitride. *Nature Synthesis* **2022**, *1*, 297–303.

(I) Park, Y.; Tian, L.; Kim, S.; Pabst, T. P.; Kim, J.; Scholes, G. D.; Chirik, P. J. Visible-Light-Driven, Iridium-Catalyzed Hydrogen Atom Transfer: Mechanistic Studies, Identification of Intermediates, and Catalyst Improvements. *JACS Au* **2022**, *2*, 407–418.

(I) Park, Y.; Semproni, S. P.; Zhong, H.; Chirik, P. J. Synthesis, Electronic Structure, and Reactivity of a Planar Four-Coordinate, Cobalt-Imido Complex. *Angew. Chem. Int. Ed.* **2021**, *60*, 14376–14380.

(I) Park, Y.; Kim, S.; Tian, L.; Zhong, H.; Scholes, G. D.; Chirik, P. J. Visible Light Enables Catalytic Formation of Weak Chemical Bonds with Molecular Hydrogen. *Nature Chemistry* **2021**, *13*, 969–976.

(II) Mendelsohn, L. N.; MacNeil, C. S.; Tian, L.; Park, Y.; Scholes, G. D.; Chirik, P. J. *ACS Catal*. **2021**, *11*, 1351–1360.

(I) Kim, S.; Zhong, H.; Park, Y.; Loose, F.; Chirik, P. J. Catalytic Hydrogenation of a Manganese(V) Nitride to Ammonia. *J. Am. Chem. Soc.* **2020**, *142*, 9518–9524.

(I) Margulieux, G. W.; Kim, S.; Chirik, P. J. Determination of the N–H Bond Dissociation Free Energy in a Pyridine(diimine)molybdenum Complex Prepared by Proton-Coupled Electron Transfer. *Inorg. Chem.* **2020**, *59*, 15394–15401.

(I) Bezdek, M. J.; Pelczer, I.; Chirik, P. J. Coordination-Induced N–H Bond Weakening in a Molybdenum Pyrrolidine Complex: isotopic Labeling Provides Insight into the Pathway for H_2 Evolution. *Organometallics* **2020**, *39*, 3050–3059.

(I) Kim, S.; Loose, F.; Chirik, P. J. Beyond Ammonia: Nitrogen–Element Bond Forming Reactions with Coordinated Dinitrogen. *Chem. Rev.* **2020**, *120*, 5637–5681.

Chemically Recyclable Polyolefins

Paul J. Chirik, Emily Davidson, Rodney Priestley, Richard Register, Michael Webb,
Department of Chemistry & Department of Chemical and Biological Engineering,
Princeton University, Princeton, New Jersey 08544

Presentation Abstract

Polyolefins are essential materials in modern society yet their end of life poses an environmental challenge. Our research is focused on the development of chemically recyclable polyolefins whereby commodity monomers are enchained in such a manner that the resulting product undergoes, in the presence of a catalyst, selective regeneration of monomer. During the past period of support, we have synthesized a microstructure of polybutadiene arising from [2+2] cycloaddition polymerization of butadiene followed by acyclic diene metathesis. The resulting polymer can be tuned by the number of cyclobutyl repeat units to unsaturated or saturated linkages, allowing direct control over the crystallinity of the material. This new material is currently being studied by our team for its physical, mechanical and chemical properties and is complemented by a modeling effort that provides molecular level insights into the observed properties. This material provides two modes of chemical recycling. Ethenolysis in the presence of a ruthenium catalyst cleaves the unsaturated connections while iron-catalyzed retrocycloaddition selectivity returns butadiene. Results on the synthesis of new chemically recyclable materials, catalyst development for the forward and reverse reactions and modeling efforts will be presented.

DE-SC0022303: Chemically Recyclable Polyolefins

Co-PI(s): Emily Davidson, Rodney Priestley, Richard Register, Michael Webb
Postdoc(s): William Archer, Coralie Duchemin, Shawn Maguire,
Student(s): John Koleng, Cherish Nie, Hang Zhang, Shannon Zhang

RECENT PROGRESS

Structure-Activity Investigations and Expanding Catalyst Space for [2+2]-Cycloaddition. The influence of steric and electronic parameters was studied for a series of C_{2v}-symmetric iron pyridine(diimine) (PDI) butadiene complexes in the [2+2]-cycloaddition of butadiene and ethylene to divinylcyclobutane (VCB). Notably, two similarly electron poor pincer ligands exhibited divergent behavior with ^{Me}BPDIFe(C_4H_6) and $^{Me}P^{Z}$DIFe(C_4H_6) giving the highest and lowest yield of VCB, respectively (Scheme 1A). Examination of the relative rates of oxidative cyclization and reductive coupling revealed that the difference arises from a substantial change in the reductive coupling rate. The reductive coupling was investigated by density functional theory methods that established that the spin crossover process is less facile for $^{Me}P^{Z}$DIFe(C_4H_6) than for ^{Me}BPDIFe(C_4H_6), suggesting that the energy difference of the singlet and triplet states may contribute to the differences in reductive coupling rate and catalytic turnover.

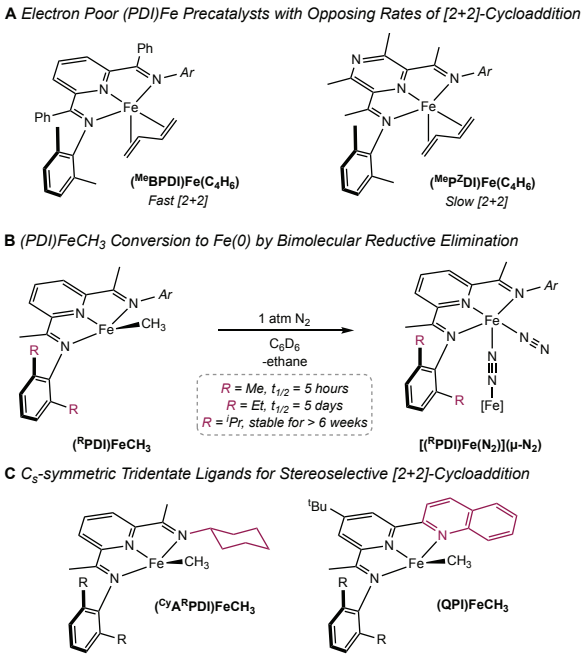

Scheme 1. Mechanistic investigation and catalyst development for Fe-catalyzed [2+2]-cycloaddition.

Despite the abundance of PDI ligands, the scope of PDI iron(0) dinitrogen complexes remains limited while iron (I) alkyl complexes are able to support a wide range of PDI ligands and are a promising platform to expand the catalyst space for [2+2] cycloadditions. A suite of (^{R}PDI)FeCH$_3$ (R = Me, Et, ^{i}Pr) complexes was synthesized to understand the activation of iron(I) alkyl complexes to catalytically-active iron(0) complexes (Scheme 1B). Both (^{Me}PDI)FeCH$_3$ and (^{Et}PDI)FeCH$_3$ underwent bimolecular reductive elimination of ethane under a dinitrogen atmosphere to generate corresponding iron dinitrogen complexes. The more sterically-hindered (^{iPr}PDI)FeCH$_3$ complex was stable under identical conditions but generated the iron butadiene complex in the presence of butadiene. As precatalysts, (^{R}PDI)FeCH$_3$ achieved results consistent with catalysis initiated from dinitrogen complexes. Furthermore, the readily accessible (*meso*-^{tBu}PDI)FeCH$_3$ generated vinylcyclobutane with 95% selectivity, demonstrating successful [2+2]-cycloaddition from a complex for which the corresponding dinitrogen complex was inaccessible.

To control [2+2]-cycloaddition stereochemistry, new iron catalysts were explored that operate by enantiomorphic site control (Scheme 1C). A series of C_S-symmetric (aryl,alkyl)-substituted PDI iron methyl complexes ((^{Cy}A^{R}PDI)FeCH$_3$) were evaluated for [2+2]-cycloaddition, resulting in mixtures of VCB and (*Z*)-hexa-1,4-diene. Despite the loss of chemoselectivity, this work revealed that hydrovinylation products arise from reversible oxidative cyclization leading to an accessible *cis*-metallacycle, while vinylcyclobutane formation proceeds via irreversible reductive elimination from a *trans*-metallacycle. A series of iron methyl complexes were also prepared with quinoline pyridine(imine) (QPI) ligands which feature a more accessible iron center. Bimolecular reductive elimination afforded an iron crotyl complex bearing a cyclometallated ligand which was a competent

catalyst for hydrovinylation, but not [2+2]-cycloaddition. These studies have shown that opening the coordination site of iron led to undesirable reactivities.

Characterization and Chemical Recycling of pDVOCB and Copolymers. Having achieved the successful acyclic diene metathesis (ADMET) polymerization of a series of pDVOCB polymers, an in-depth study of their properties was conducted to understand their structure-property relationships. Differential scanning calorimetry (DSC) of pDVOCB revealed highly crystalline behavior and multiple endothermic events including a rotator phase which was confirmed by variable-temperature WAXS (Scheme 2A). Notably, *n* has a major role in dictating the melting temperature of the polymers which ranged from 210 °C to 260 °C. Dynamic mechanical analysis (DMA) showed that pDVOCB exhibits a storage modulus comparable to HDPE and iPP, and Instron testing revealed the strain at break of pDVOCB(5, 67) (31%) was more than three times higher than that of pDVOCB(5, 40) (9%), suggesting that achieving higher molecular weight improves ductility.

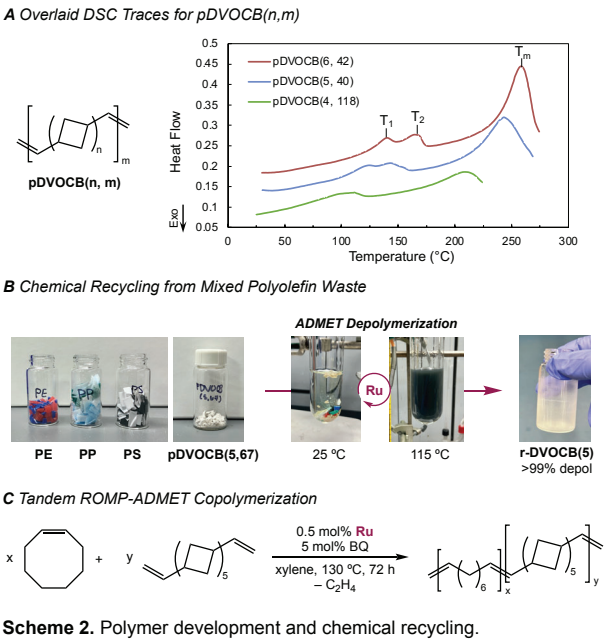

Scheme 2. Polymer development and chemical recycling.

An optimized method for the depolymerization of pDVOCB by reverse ADMET was developed which enabled the recovery of recycled DVOCB in >99% depolymerization and >99% yield. The chemical recycling of pDVOCB was also successfully conducted from mixed post-consumer plastic waste (Scheme 2B). The recycled DVOCB was polymerized again to yield recycled polymer with no deterioration of thermal properties. To establish a chemical recycling pathway to feedstock olefin, an improved method for the deoligomerization of DVOCB back to butadiene was developed. To overcome the inhibitory effects of free-butadiene coordination, an experimental setup using liquid nitrogen to trap evolving butadiene was designed, which enabled complete deoligomerization of DVOCB to butadiene (79%) and 1,3-divinylcyclobutane (21%).

Also of interest is the synthesis of chemically recyclable elastomers through simultaneous ring-opening metathesis polymerization (ROMP) of cyclooctene (COE) and ADMET of DVOCB, enabling access to copolymers containing hard (DVOCB) and soft (COE) segments that retain chemical recyclability (Scheme 2C). A series of copolymers synthesized with varying weight percent of DVOCB were studied by DSC and showed melting transitions at low temperatures characteristic of PCOE crystallinity in soft materials. The PCOE melting transitions broaden with increasing loadings of DVOCB, where DVOCB crystallinity also appears to contribute.

Modeling and Computational Studies. As current existing force fields cannot properly describe the conformational structure and dynamics of DVOCB, our recently developed TAFFI (topology-automated force-field interactions) framework was used as a potential solution for parameterizing models for DVOCB and polymeric derivatives. Using this

framework, we have completed the parameterization work of our novel DVOCB/pDVOCB force field, which properly handles details such as ring-flipping behavior and stereochemical considerations. A series of validation exercises and refinement protocols were used to benchmark and improve correspondence of the models to realizable experimental systems. Simulation infrastructure was also developed to support the simulation and study of thermomechanical characteristics of polymers.

Publications Acknowledging this Grant in 2020-2023

(I) Intellectually led by this grant
(II) Jointly funded by this grant and other grants with intellectual leadership by other funding sources

(I) Kovel, C. B.; Darmon, J. M.; Stieber, S. C. E.; Pombar, G.; Pabst, T. P.; Theis, B.; Turner, Z. R.; Üngör, Ö; Shatruk, M.; DeBeer, S.; Chirik, P. J. Bimolecular Reductive Elimination of Ethan from Pyridine(diimine) Iron Methyl Complexes: Mechanism, Electronic Structure, and Entry into [2+2] Cycloaddition Catalysis. *J. Am. Chem. Soc.* **2023**, *145*, 5061–5073.

(II) Zhang, H.; Sundaresan, S.; Webb, M. A. Molecular Dynamics Investigation of Nanoscale Hydrophobicity of Polymer Surfaces: What Makes Water Wet? *J. Phys. Chem. B* **2023**, *127*, 5115–5127.

(I) Duchemin, C.; Kim, J.; Chirik, P. J. C_s-Symmetric Pyridine(diimine) Iron Methyl Complexes for Catalytic [2+2] Cycloaddition and Hydrovinylation: Metallacycle Geometry Determines Selectivity. *JACS Au* **2023**, *3*, 2007–2024.

Catalytic production of hydrogen and solid carbon from methane over MgO supported catalysts

Steven Crossley,[1] Daniel Resasco,[1] Bin Wang,[1] Anibal Boscoboinik[2]

1) University of Oklahoma, Department of Sustainable Chemical, Biological and Materials Engineering
2) Brookhaven Naitonal Laboratory, Center for Functional Nanomaterials

Presentation Abstract

The catalytic conversion of methane to hydrogen and solid carbon involves multiple interfaces that evolve during the various stages of carbon nucleation and growth. Designing a catalyst that retains metal catalysts on the support throughout growth while also exhibiting rapid rates of methane activation and slow rates of catalyst deactivation is a daunting challenge. Here we show the importance of strong metal support interactions that manifest through mixed oxides with MgO, coupled with bimetallic mixtures of active metal particles. We explore how the interface between the metal and support influences base growth mechanisms, and how coupling of different metals with metal oxides, such as MoO_3, that form carbides during growth leads to exsolution of stable nanoparticles. We further show how this combination of strong interfaces is critical to ensuring that the catalysts exhibit high rates of methane activation while also remaining adhered to the surface fo the catalyst and thus promoting base growth. A combination of methane conversion rates with accompanying deactivation rates are contrasted with XRD, TEM, TPR, and operando XPS results to reveal the dynamic nature of these promising catalysts under reaction conditions. We show how critical the pre-reduction step is, as slight over-reduction leads to particle segregation but excessively mild prereduction leads to carbon encapsulation prior to nanotube nucleation and growth. We further show how alteration of reaction conditions and catalyst ratios can lead to remarkably high yields of carbon per gram of catalyst.

DE‐SC0023497: Interrogating complex and dynamic interfaces during carbon‐free H2 production

Postdoc(s): Laura Alejandra Gomez (3 months)

RECENT PROGRESS

Influence of metal support combination

First, catalyst screening with known active metals was carried out to evaluate the most appealing metal-support combinations. Table 1 reveals the fascinating synergistic benefits upon combining Ni with Mo and MgO. Ni alone on various supports results in modest yields. Ni on MgO alone under these conditions results in no measurable growth, which we hypothesize is due to excessively strong Ni interactions with the support. Mo

incorporation, however forms a unique interface upon which Ni anchors, and during the exsolution process results in nanoparticles that lead to enhanced growth, orders of magnitude higher than the metal-support combinations alone. Altering the Ni to Mo ratio reveals an optimal amount of Mo incorporation upon which exsolution results in stable particles that yield high amounts of hydrogen and solid carbon as can be seen in Figure 1. Increased temperature results in much higher yields as well, which alters both the evaluation of the catalyst as well as steady state growth and deactivation rates. We plan to work at temperatures within this range to avoid additional contributions from noncatlaytic thermal reactions that occur at temperatures above 1000°C.

Increasing reaction temperatures reveals drastically enhanced rates with increased temperautres, with rates in excess of 3000% yield (g carbon per gram of catalyst) at elevated temperatures, with less than 50% loss in catalyst life after 3 hours time on stream.

Catalyst Support	**Ratio Ni:Mo**	**Reaction Temperature**	**C Yield/ g catalyst (%)**
ZrO_2	Ni	800	10%
SiO_2	Ni	700	32%
TiO_2	Ni	700	18%
MgO	Ni	700	0%
MgO	Mo	700	0%
MgO-Al_2O_3	Ni	700	0%
Al_2O_3	Ni,Mo (1:5)	700	0%
MgO	Ni,Mo (1:5)	700	305%

Table 1: catalyst screening over various supports, Reduction tempearature 650°C, reaaction temperature 700°C in flowing methane.

Dynamic role of Ni/MoOx/MgO interactions

Catalyst particles undergo a series of significant transformations during growth, including the formation of a mixed $MgMoO_4$ phase after initial calcination which is disrupted upon the addition of Ni. As seen in Figure 1, as the Ni loading is increased, the appearance of a mixed oxide phase becomes less pronounced, with no observed peak observed at Ni to Mo ratios of 1:1 or in excess Ni. This implies that the initial catalyst, prior to reduction exhibits widely differing metal support interactions as the strong affinity of Ni for both the Mo as well as the MgO support alter the starting state of the catalyst. Upon reduction, even in instances of minority Ni concentration where a clear $MgMoO_4$ phase is present (**Figure 2a**), this oxide phase is reduced. It is important to note that these pre-reduction conditions are too mild to reduce Mo alone in the absence of Ni, and pre-reduction of catalysts in the absence of Ni results in no measurable reduction in the mixed $MgMoO_4$ phase XRD peaks.

Not only does the mixed Mo-support interface evolve during reduction, but new carbide phases begin to form during reaction as well. After only 5 minutes of reaction, one observes the presence of Mo carbide features that often occur during carbon nanotube growth on supports that do not interact strongly with Mo, such as silica (**Figure 2b**). This, in turn, results in exsolution of small Ni metal particles which serve as nucleation centers for carbon nanotube growth.

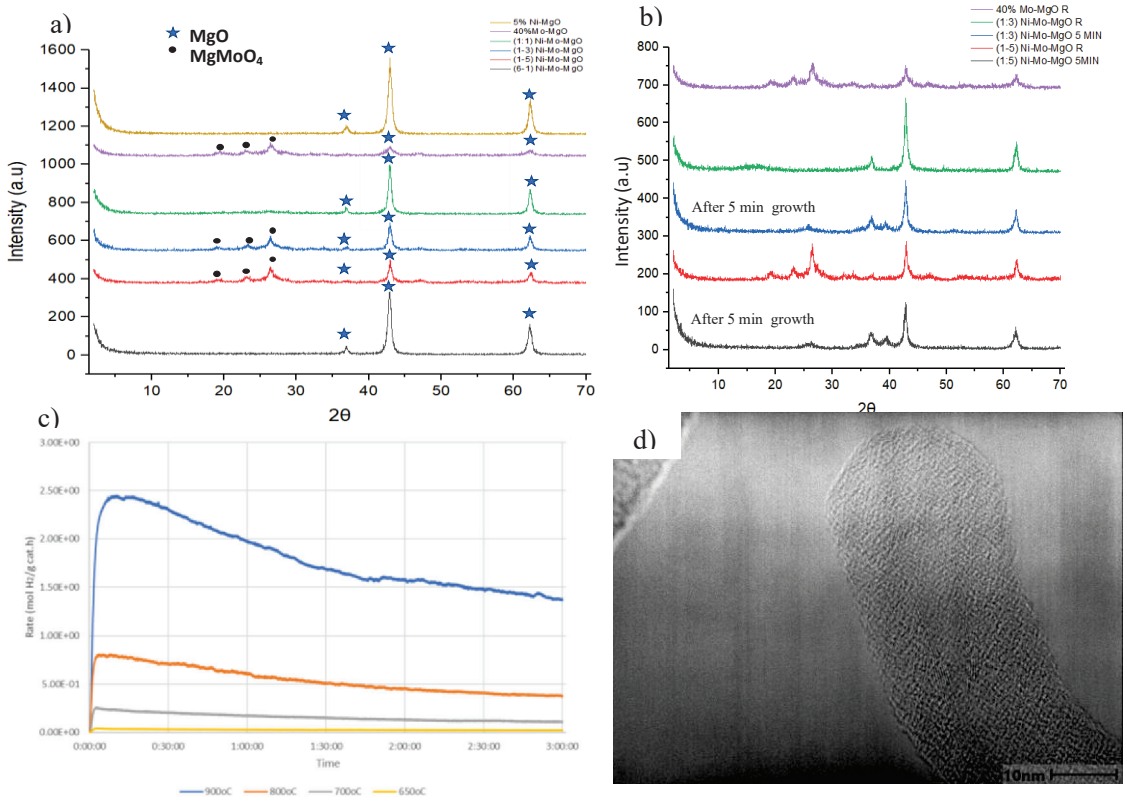

Figure 1: a) XRD of calcined Ni-Mo-MgO catalysts at different ratios, b) XRD after reduction (R) and methane introduction after 5 minutes reaction time, highlighted region revealing Mo carbide features, c) reaction rate of hydrogen production as a function of time on stream for a (1:5) Ni-Mo catalyst at differen reaction temperatures d) representative TEM image revealing the lack of encapsulated metal particle at the tip of growing nanotube.

The catalyst particle dynamics and growth is a complex process, which we illustrate by modifying the initial pre-reduction temperature. Literature reports vary widely regarding approaches to pre-reduce catalysts. One may hypothesize that excessive reduction temperatures will lead to large metal particles, while no-pre-reduction delays methane activation and increases the risk of carbon encapsulation prior to nanotube growth. For this series of catlaysts, pre-reduction plays a significant role in this reaction, with significantly higher yields observed with a mild pre-reduction step which serves to activation methane molecules and inhibit particle encapsulation.

Growth kinetics follow an induction period followed by gradual decline in catalyst activity with time. We have carried out reactions at varying temperatures as well as methane partial pressures, and constructed a preliminary kinetic model involving said induction period, steady state rates, as well as deactivation constants. This will be coupled with in-situ characterization in coming months to reveal predominant mechanisms of catalyst deactivation. This catalyst combination has proven to be quite promising thus far, with yields of carbon per gram of catalyst exceeding 3,000%. Further, as revealed in a representative image in Figure 2d, catalyst particles remain anchored to the support during growth as opposed to retained within the tips of the nanotubes as would be observed in tip growth mechanisms. Achieving catalsyts that are active, stable, and also exhibit base growth are essential factors for promising catalytic pyrolysis

experiments. Coupling our kinetic results with in-situ characterization in the coming months will allow for great advances in our fundamental understanding of these promising but highly dynamic catalyst particles under reaction coniditons.

Varying behavior of base metal in MoOx/MgO systems

Table 2: Carbon yields after 3 hours growth with different metal combinations over MgO supports

Metal	Support	Reduction Temperature	Reaction Temperature	Yield (%)
5% Ni	MgO	650	700	0
5% Co	MgO	650	700	5
5% Fe	MgO	650	700	0
5%Ni-40%Mo	MgO	650	700	199
5%Fe-40%Mo	MgO	650	700	245
5%Co-40%Mo	MgO	650	700	231
Mo	MgO	650	700	0

An interesting finding regarding the metal combinations, is that while Ni is generally believed to be one of the most active metals for methane pyrolysis, Co and Fe when combined with Mo offer similar benefits as can be seen in Table 2, with Fe outperforming Ni at a reaction temperature of 700°C. Further, not shown here, the catalyst lifetimes are markedly different in these systems, with not only enhanced rates, but greatly improved stability over the Ni catlaysts in some cases. We plan on exploring these metals in much more detail in coming months, as the inclusion of Fe is appealing for many reasons, both due to its low cost and reduced toxicity. While in-situ XPS and XRD will reveal the dynamics of the system in much more detail, simple characterization of the catalysts reveals that the system is quite intriguing.

Dr. Lisandro F. Cunci

Catalysts Research in Oxygen Reduction and Oxidation Reactions to Increase Representation in Energy Science in Puerto Rico

Dr. Lisandro Cunci
Department of Chemistry, School of Natural Sciences, University of Puerto Rico – Rio Piedras Campus

Presentation Abstract

Dr. Cunci's lab works in the development and understanding of non-platinum group metal (non-PGM) and non-metal catalysts for the oxygen reduction reaction (ORR) and oxygen evolution reaction (OER), which are essential for the mass production and use of alkaline membrane fuel cell and green hydrogen production. These reactions are currently limited by sluggish kinetics and catalyst degradation, and platinum group-based catalysts are the most active but also the most expensive and scarce. By gaining a deeper understanding of how electrochemical reactions affect the atom-atom distances in catalysts under in situ and operando conditions, our lab hopes to improve the activity and durability of non-platinum group catalysts and reduce the reliance on expensive and scarce materials. By doping onion-like carbon (OLC) nanoparticles with heteroatoms, carbon-based supports can enhance the activity of non-PGM catalysts. Nitrogen-doped and phosphorus-doped OLC/FeCo catalysts have shown catalytic activities similar to Vulcan/Pt catalysts for the ORR. Our group has found an increase in interatomic distances at potentials where ORR is more active, suggesting that the higher interatomic distances in the surface of FeCo nanoparticles may be responsible for the enhanced ORR activity.
Dr. Cunci is the Lead PI of the BES RENEW project titled ***"Partnership to Increase Representation in Energy Research in Puerto Rico"***. This project was approved in February, 2024 and started in April, 2023. One graduate student and six undergraduate students were recruited from underrepresented populations and 57% are women. During the last summer we co-organized the Electrochemistry Hands-On (ECHO) Workshop at the National Renewable Energy Laboratory with Dr. Bryan Pivovar. One graduate student and three undergraduate students participated in this workshop during an entire week (May 22-26, 2023) with seminars, tours, hands-on work, and demonstrations at NREL. After the first week, the students worked for 9 more weeks at NREL in different projects with four mentors from NREL.

DE-SC0023686: Partnership to Increase Representation in Energy Research in Puerto Rico
PI: Dr. Lisandro F Cunci
Co-PIs: Dr. Jorge Colon, Dr. Lymari Fuentes Claudio, Dr. Mitk'El Santiago, Dr. Miguel Goenaga, and Dr. Juan Santana.
Student(s): Ambar Maldonado Santos (Graduate Student); Alannisse Santos, Daniella Gibson Colon, Hector Gonzalez Velez, Alejandra Rodriguez Nazario, Kevin Torres, and Yaneiska Ruiz Torres (Undergraduate Students).
Affiliations(s): University of Puerto Rico – Rio Piedras, Humacao, and Cayey Campus; Universidad Ana G. Mendez – Cupey and Gurabo Campus.

RECENT PROGRESS

Summer Electrochemistry Hands-On Workshop (ECHO) at the National Renewable Energy Laboratory (NREL)

Figure 1 – Final presentation in Sumer Internship at NREL.

Our project Partnership to Increase Representation in Energy Research in Puerto Rico (PIRES-PR) started last April, 2023 to increase the number of Hispanic students working in basic energy research. We were able to recruit one graduate student and six undergraduate students with 57% of them women starting in the right direction toward one of our main objectives of increase the number of women in energy science in Puerto Rico. During the Summer Internship 2023 at NREL, the graduate student and three undergraduate students (50% women) did research under the mentorship of four researchers and under the supervision of Dr. Bryan Pivovar (Co-PI of PIRES-PR) and Dr. Shaun Alia, two experts in hydrogen research. Figure 1 shows a picture of the final poster presentation at NREL. From left to right: Dr. Bryan Pivovar (Co-PI of PIRES-PR, NREL), mentor Dr. Carlos Baez-Cotto (NREL) and his mentee Kevin Torres (UAGM-Cupey), mentor Dr. Audrey Taylor (NREL) and her mentee Alejandra Rodriguez (UPR-Cayey), mentor Dr. Melissa Kreider (NREL) and her mentee Ambar Maldonado (UPR-Rio Piedras), mentor Emily Volk (NREL) and her mentee Hector Rodriguez (UPR-Humacao), and Dr. Shaun Alia (NREL).

Kick-off Meeting for PIRES-PR in Puerto Rico

Figure 2 – Kick-off Meeting for PIRES-PR on March 10th, 2023

In March 8-10, 2023, we organized the Kick-off Meeting for PIRES-PR. We had researchers from NREL traveling to Puerto Rico for three days. The first and second day, we organized several presentations at different universities in Puerto Rico to help recruit students and promote the participation in DOE-funded programs in Puerto Rico, NREL, and other National Laboratories. The third day, March 10th, we hosted the Kick-off Meeting for PIRES-PR where each of the researchers presented their proposed projects and their preliminary results. Moreover, our students were able to network with researchers from NREL and paired each potential mentee with their respective mentor for the Summer Internships 2023 at NREL. Figure 2 shows pictures of the Kick-off Meeting and presentations at different universities in Puerto Rico.

Seminar Series in Energy Research with NREL Researchers

We have also organized a series of seminars at different universities of Puerto Rico in April 26-29, 2023. During these four days, we brought researchers from NREL, SLAC, UCDavis, and Stanford University to several universities spanning the entire Puerto Rico, from UPR – Mayaguez in the far west to the University of Puerto Rico – Humacao in the far east. We were able to promote the research efforts and DOE-funded programs in energy research in Puerto Rico and US mainland to underrepresented students in primarily undergraduate institutions as well as research universities. During the seminars, researchers talked about different projects, and we had the opportunity to have Dr. Murali Baggu, who oversees the Puerto Rico Grid Resilience and Transitions to 100% Renewable Energy Study (PR100) led by the U.S. Department of Energy's Grid Deployment Office and six national laboratories, give talks about this important study. Figure 3 shows pictures of the different activities as well as the flyers shared to the universities of the different talks.

Figure 3 – Pictures and flyers of presentations organized between PIRES-PR and universities in Puerto Rico and the US mainland.

Synergistic Activities between Energy-based Research Efforts in Puerto Rico

We have devised a training program during the academic year for the students to take advantage of synergistic activities with other energy research projects in Puerto Rico. We have joined three research efforts together, namely the Partnership to Increase Representation in Energy Research in Puerto Rico (i.e., this BES RENEW project), Center for Interfacial Electrochemistry of Energy Materials (NSF-PREM), and the students from the Puerto Rican effort that is part of the High Magnetic Field X-Ray Beamline Development of the Cornell High Energy Synchrotron Source (Mid-scale RI-2). The students that are part of these three research efforts in energy meet every other Friday to participate of research seminars, professional development workshops, presentation practice, and networking with other researchers in Energy Science.

Publications Acknowledging this Grant in 2020-2023

Nothing to report. This project started in April 2023.

Awards or leadership activities during 2020-2023 calendar years

We are currently partnering with the Puerto Rico ACS Local Section to help organize the ACS Senior Technical Meeting, an annual research meeting, that will be held at the beginning of November 2023. We will have two researchers from NREL give plenary talks in Puerto Rico and network with researchers to foster collaborations.

Paul J. Dauenhauer

Electrocatalytic Oxygen Evolution (OER) via Catalytic Condensers

Paul J. Dauenhauer and C. Daniel Frisbie
Department of Chemical Engineering and Materials Science, University of Minnesota

Presentation Abstract

Heterogeneous catalysis is well-known to be sensitive to electron accumulation or depletion on surfaces, but electron density is usually controlled by chemical doping (e.g., promoters) in the case of thermocatalysis, or electrochemical potential in the case of electrocatalysis. The recent advent of ultrathin two dimensional (2D) catalysts prepared either by exfoliation or thin film growth methods opens up new opportunities to exploit the transverse field effect—so central to silicon CMOS technology—to modulate the carrier density in the catalyst (or electrocatalyst). In this approach the 2D catalyst material is deposited on top of a metal/dielectric stack to make a condenser; application of a voltage between the catalyst and the metal causes positive or negative charge to accumulate in the catalyst, depending on the sign of the voltage. This charge in turn tunes the reactivity of active sites in the catalytic layer, accelerating the rate of reaction on its top surface. Here, we describe results for catalytic condensers applied to electrocatalysis for the oxygen evolution reaction (OER) via kinetic modeling, device fabrication, and experimental evaluation. In general, catalytic condensers provide a platform for fundamental investigation of electronic effects in electro- and thermocatalysis, as well as a strategy for dynamic control of reaction rates.

Grant or FWP Number: DE-SC0021163
Title: Electronically-Controlled Electrocatalytic Interfaces: Optimizing Surface Chemistry by Means of the Field Effect and Dynamic Resonance
Student(s): Sallye Gathman, Amber Walton, Shreya Singh, Yuxin Wang

RECENT PROGRESS

1. A Microkinetic Model for Dynamic Potential Control in OER.

The key bottleneck in water electrolysis is the sluggish kinetics of the oxygen evolution reaction (OER: $2H_2O \rightarrow O_2 + 4H^+ + 4\ e^-$), which occurs in tandem with hydrogen evolution (HER: $2H^+ + 2e^- \rightarrow H_2$) and which accounts for the majority of applied overpotential and low H_2 production rates. **Figure 1A** shows data (★) and our kinetic model (line) of the Sabatier or 'volcano' plot depicting electrocatalytic activity for different metal oxide electrodes versus a key descriptor of OER activity, namely $\Delta G_{volc} = \Delta G^{0}_{O*} - \Delta G^{0}_{OH*}$. The volcano plot results from two rate-limiting surface reactions in the multi-step OER mechanism, namely (1) OH* scission (step 2), and (2) OOH* formation (step 3). The left side of the volcano plot describes a surface covered in O* such that increasing ΔG_{volc} leads to faster rates of OOH* formation; the right side of the volcano describes a surface

covered in OH* that exhibits faster rates of OH* scission with decreasing ΔG_{volc}. IrO_2, the best known electrocatalyst for OER, exists at the peak of the plot where ΔG_{volc} has been optimized with respect to both steps; this is known as the Sabatier limit.

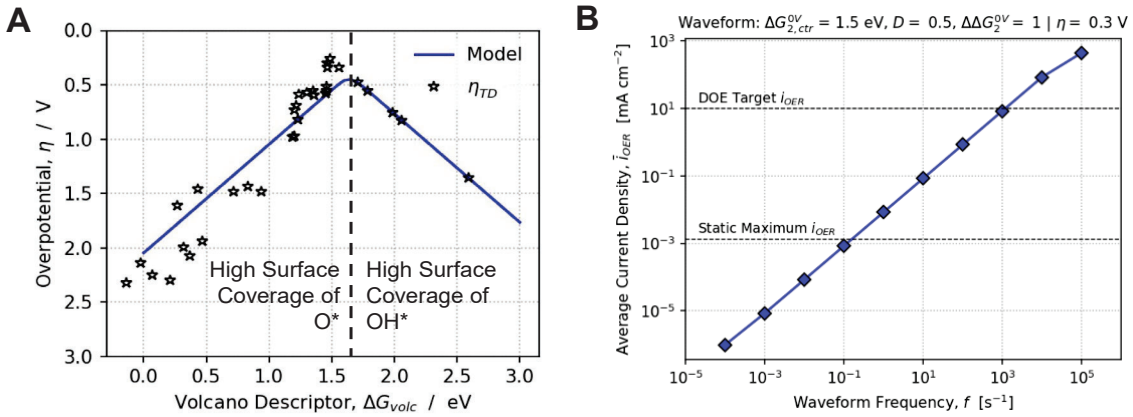

Figure 1. Microkinetic modeling of the oxygen evolution reaction. (A) Static kinetic model of OER fit to experimental data. **(B)** Programmable dynamic model with variable applied frequency and average current density exceeds the Sabatier peak and DOE target.

In the simulated dynamic trials, we leveraged recently postulated dynamic control of surface energy to accelerate OER beyond the Sabatier limit, **Figure 1B**. The idea was to switch a catalyst between two (or more) electronic states that sequentially favor one rate limiting step (e.g., surface reaction 2) and then the other (e.g., surface reaction 3), but the inclusion in the microkinetic model accounted for the possibility of any elementary reaction contributing to the overall rate (current density). Simulation at variable frequencies of square waveforms indicated proportional catalytic rate current response, with catalytic rates exceeding the Sabatier volcano at 0.1 Hz and exceeding the DOE target at ~1000 Hz, ultimately providing significant catalytic rate benefit for oxygen evolution.

2. Accelerating Electron Transfer Rate Constants by 30X with Enhanced Condenser Capacitance.

We report steady-state voltammetry of outer-sphere redox species (TCNQ) at back-gated ultrathin ZnO working electrodes in order to determine electron transfer rate constants k_{ET} as a function of independently-controlled gate bias, V_G, see Figure 2. We demonstrate that k_{ET} can be modulated as much as 30-fold by application of $V_G \leq 8$ V. The reason is that V_G shifts the band alignment between ZnO and the redox accepter states in solution, making it more favorable. Key to this demonstration was integrating the ultrathin (5 nm) ZnO on a high dielectric constant insulator, HfO_2 (30 nm), which was grown on a Pd metal gate. The high-k HfO_2 dramatically decreased the required V_G values and increased the gate induced charge in ZnO compared to previous studies. Importantly, the enhanced gating power of the Pd/HfO_2/ZnO stack meant it was also possible to observe a non-monotonic dependence of k_{ET} on V_G, which reflects the inherent density of redox acceptor states in solution. This work adds to the growing body of literature that demonstrates that electrochemical kinetics (i.e., rate constants and overpotentials) at ultrathin working electrodes can be tuned by V_G, independent of the conventional electrochemical working electrode potential.

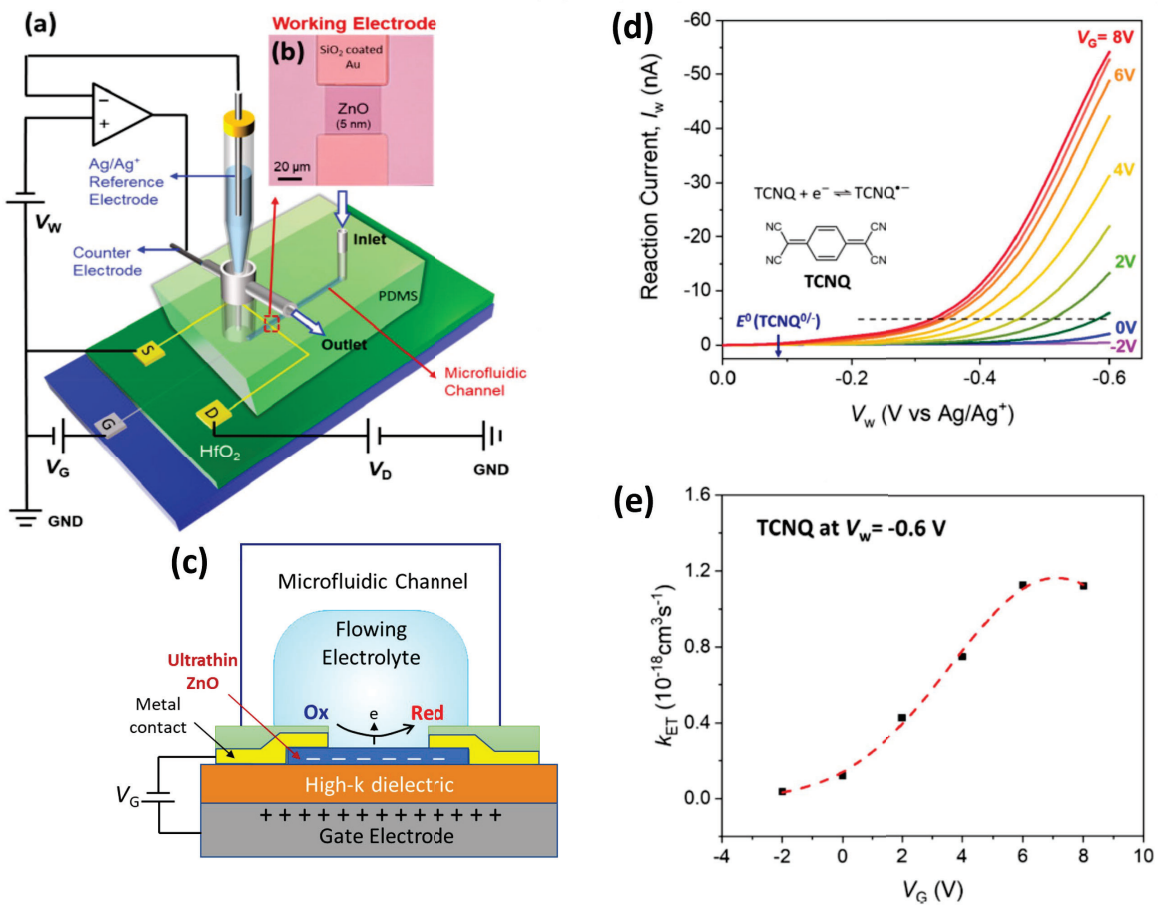

Figure 2. **Catalytic condenser increases electron transfer rates**. (a) Electrochemical setup for voltammetry at ZnO based catalytic condenser. Location of device is shown by red box. (b) Photo of ZnO catalytic condenser showing source and drain contacts. (c) Cross-sectional scheme of the catalytic condenser showing microfluidic channel with flowing electrolyte. (d) Steady state voltammetry of TCNQ redox chemistry at ZnO as a function of V_W and V_G. Redox reaction is shown. (e) Analysis of the reaction current in (d) yields the electron transfer rate constant k_{ET} vs V_G for the reaction. It is clear that k_{ET} increases strongly as V_G increases.

3. Growth of electroactive Co_3O_4 *films by atomic layer deposition.*

OER catalysts such as Co_3O_4 are being integrated as ultrathin films into catalytic condensers. We grow films of Co_3O_4 as thin as a few nm by atomic layer deposition, Figure 3. Film growth optimization has allowed us to achieve good linear growth of Co_3O_4 vs ALD cycle number. We have also been able to verify the stoichiometry by XPS and XRD.

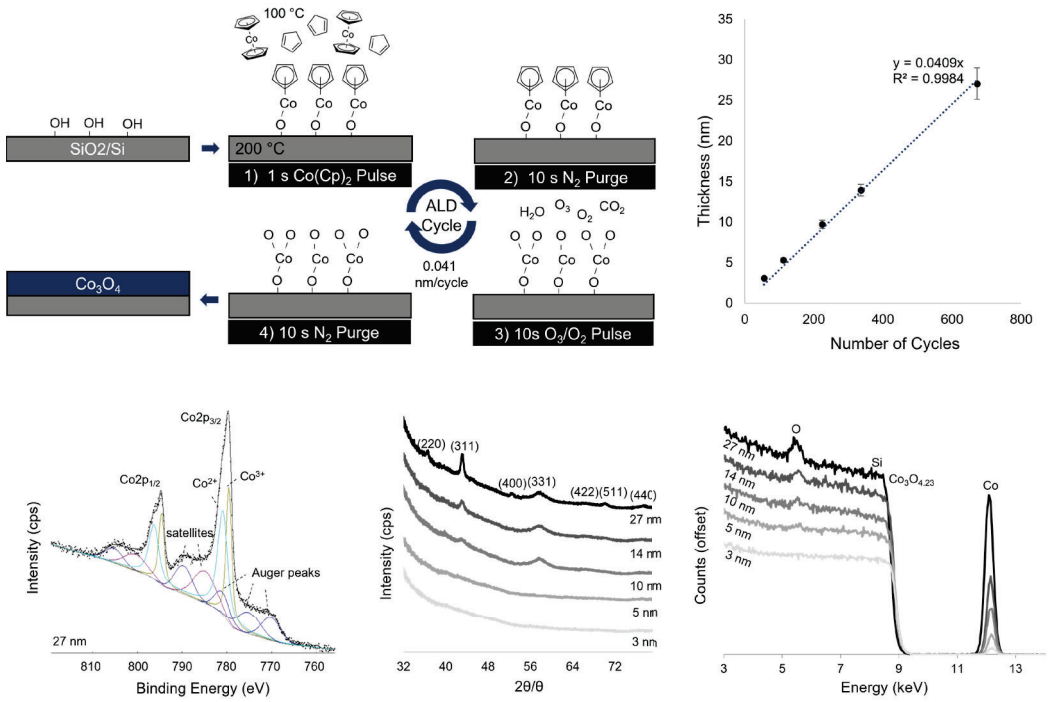

Figure 3. Growth of ultrathin Co3O4 OER catalyst by atomic layer deposition.

The XRD in particular confirms the presence of spinel Co_3O_4. These films are OER active and gating experiments for OER films in condensers (p+-Si/HfO2/Co3O4) are underway.

Publications Acknowledging this Grant in 2020-2023

(I) Intellectually led by this grant

Wang, Y.; Wang, Y.; Frisbie C.D. Electrochemistry at Back-Gated, Ultrathin ZnO Electrodes: Field Effect modulation of Heterogeneous Electron Transfer Rate Constants by 30X with Enhanced Gate Capacitance. *ACS Appl. Mater. Interfac*. **2023**, *15*, 9554-9562.

Wang, Y.; Frisbie, C.D. Four Terminal Electrochemistry: A Back-Gate Controls the Electrochemical Potential of a 2D Working Electrode. *ACS Appl. Mater. Interfac*. **2023**, submitted.

S. Gathmann, O. Abdelrahman, C. Bartel, C.D. Frisbie, P.J. Dauenhauer, "Catalytic Resonance of the Oxygen Evolution Reaction" In preparation.

(II) Jointly funded by this grant and other grants with intellectual leadership by other funding sources

None

David A. Dixon

The Development of Hydricity and Ligand Binding Energy Scales for Homogeneous Catalyst Applications

David A. Dixon,[1] Yiqin Hu,[1] Damian Duda,[1] Kyle C. Edwards,[1] Aaron Appel,[2] Eric Wiedner,[2] Andrei Chirila,[2] Ba Tran,[2] Morris Bullock[2]
[1]Department of Chemistry & Biochemistry, The University of Alabama
[2]Pacific Northwest National Laboratory

Presentation Abstract

Hydride transfer is an important reaction in stoichiometric and catalytic transformations with applications in hydrogen storage, hydrogenation and dehydrogenation of CO_2, and petrochemicals; transition metal hydrides often play a crucial role in such processes. Hydricity is the energy for heterolytic bond cleavage of A-H to remove a hydride (H^-) where A is the hydride acceptor. A hydricity scale for esters and ketones in MeCN and THF has been built using the G3MP2 method for the gas phase calculations and COSMO/ωB97X-D/aug-cc-pVDZ(-PP) for the self-consistent reaction field solvation energy calculations in MeCN and THF. The absolute values are referenced to that of BH_3. The binding energy between the organic molecules and BH_3 with THF and MeCN was calculated as the hydricity can depend on this quantity. This leads to a free energy hydricity scale. The correlation between the Gibbs free reaction energies and Gibbs free transition barrier energies was explored for the hydride transfer reaction between $[Co(dmpe)_2]H$ and $[Rh(dmpe)_2]H$ and the ketones. Following Hammond's postulate, the more exothermic the reaction, the lower the transition barrier energy. Two near parallel sets of trendlines were found between transition state energy barriers and reaction energies for ketones with the functional group R-PhC(O)Ph-R/R-PhC(O)CH_3 and R-PhC(O)CF_3 for both metal catalysts. The reactivity of highly sterically hindered $(carbene\text{-}CuH)_2$ dimers for hydride transfer has been explored. NHC carbene and phosphine binding energy scales with metals are being developed and have led to a novel binding motif for alkali and alkaline earth metal ions binding to PPh_3.

FWP 47319: Impact of catalytically active centers and their environment on rates and thermodynamic states along reaction paths

PI: Johannes Lercher[2]
Student(s): Yiqin Hu, Damian Duda, Sarah Sprouse
Affiliations(s): [2]Pacific Northwest National Laboratory

Keary M. Engle

Catalytic Dicarbofunctionalization for Production of Sequence-Encoded Cyclooctene ROMP Monomers

Van T. Tran[1], Anne K. Ravn[1], Camille Z. Rubel[1], Mizhi Xu[2], Yue Fu[3], Ethan M. Wagner[2], Steven R. Wisniewski[4], Peng Liu[3], Will R. Gutekunst[2], Keary M. Engle[1]

[1] Department of Chemistry, The Scripps Research Institute, 10550 N. Torrey Pines Rd., La Jolla, CA 92037, USA
[2] School of Chemistry and Biochemistry, Georgia Institute of Technology, Atlanta, GA 30332, USA
[3] Department of Chemistry, University of Pittsburgh, Pittsburgh, PA 15260, USA
[4] Chemical Process Development, Bristol Myers Squibb, 1 Squibb Drive, New Brunswick, NJ 08903, USA

Presentation Abstract

A one-step, nickel-catalyzed synthesis of 5,6-diaryl cyclooctene monomers from the feedstock chemical 1,5-cyclooctadiene is described. The reaction proceeds in a modular, regio- and diastereo-selective fashion, granting access to both homo- and hetero-diaryl cyclooctene monomers that smoothly undergo ROMP. The resulting 1,2-diaryl-substituted polymers possess head-to-head dyads that have not been previously explored, giving rise to unique and tunable properties. DFT calculations highlight mechanistic aspects of the nickel-catalyzed diarylation reaction and the ruthenium-catalyzed ROMP process, revealing a previously unappreciated role of the boronic ester in promoting migratory insertion which was leveraged to provide enantioinduction.

DE-SC0023205: Catalytic Difunctionalization of Cyclic Dienes: Direct Entry to Novel ROMP Monomers

PI: Keary M. Engle; Will R. Gutekunst
Postdoc(s): Anne K. Ravn
Student(s): Camille Z. Rubel, Ethan M. Wagner
Affiliations(s): The Scripps Research Institute; Georgia Institute of Technology

RECENT PROGRESS

During the past funding period, we developed a method to perform selective 1,2-diarylation of 1,5-cyclooctadiene and related cyclic dienes under nickel catalysis without competitive alkene isomerization or over functionalization (Figure 1). The resulting "sequence encoded" monomers are reactive in controlled ring-opening metathesis polymerization using Grubb-type initiators, granting access (after reduction) to styrene–ethylene copolymer products with branching architectures that are otherwise impossible

to access using known methods. Using this workflow, we were able to quickly prepare a library of novel polymers, and we demonstrated that by adjusting the structure of the aryl groups, the thermal properties of the resulting materials could be tuned over a broad range of glass transition temperatures (54–108 °C). In-depth mechanistic studies established the important role of dynamic ligand exchange processes along the productive catalytic cycle. This progress sets the stage for future progress to expand the scope of coupling partners that be integrated into sequence-encoded monomers using this approach and refined understanding the of the mechanistic intricacies of the reaction towards improved catalyst designs.

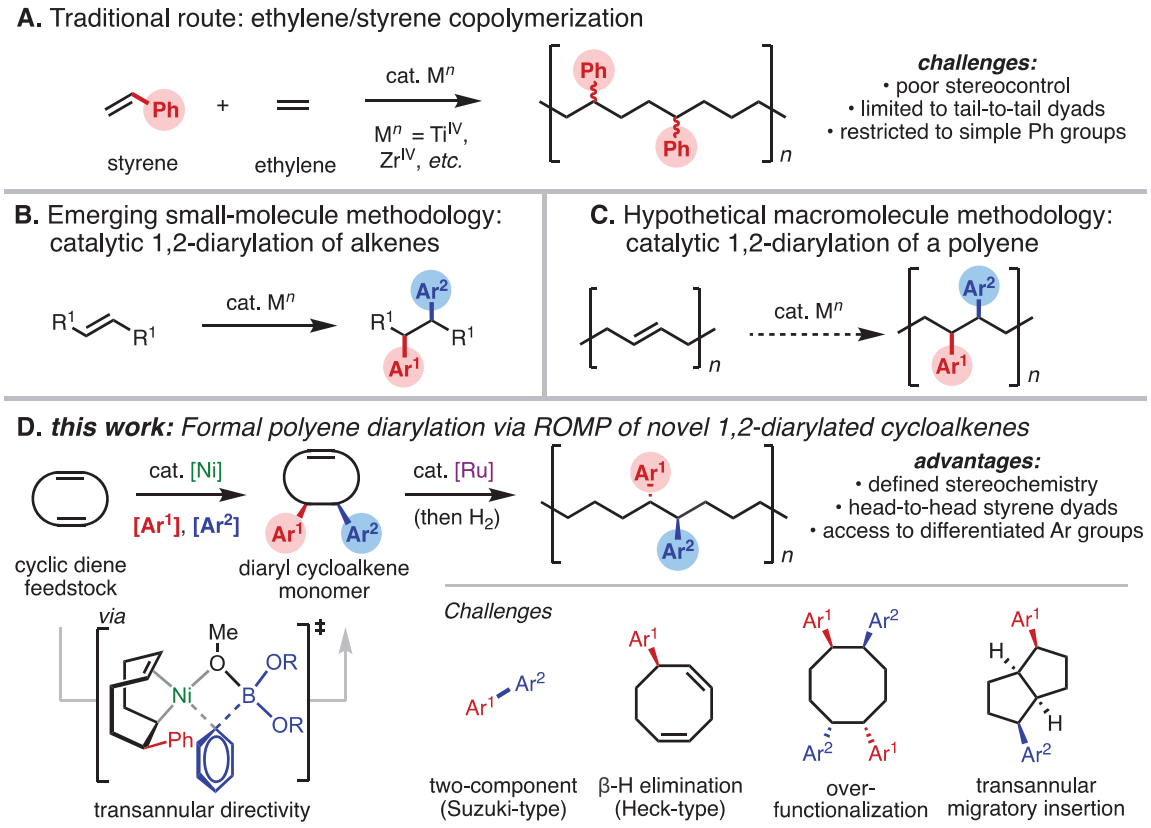

Figure 1: Overview of progress in this funding period.

Publications Acknowledging this Grant in 2020-2023

(I) Intellectually led by this grant

Tran, V. T.†; Ravn, A. K.†; Rubel, C. Z.†; Xu, M.†; Fu, Y.†; Wagner, E. M.; Wisniewski, S. R.; Liu, P.; Gutekunst, W. R.; Engle, K. M. "Catalytic Dicarbofunctionalization for Production of Sequence-Encoded Cyclooctene ROMP Monomers," *Nat. Synth. Submitted for publication in 2023, reviewed favorably, currently in revision*. (†Authors contributed equally)

(II) Jointly funded by this grant and other grants with intellectual leadership by other funding sources

None

Interplay Between Solvent Molecules and Alkyl Chains and Consequences on Epoxidation Catalysis

David S. Potts[1], Ohsung Kwon,[1] Chris Torres,[1] David W. Flaherty[1,2]*
[1]*University of Illinois at Urbana-Champaign, Urbana, Illinois 61801 (USA)*
[2]*Georgia Institute of Technology, Atlanta, Georgia 30332 (USA)*

*dflaherty3@gatech.edu

Solvents play a significant role in mediating catalysis, especially in confined environments (e.g., microporous zeolites), through interactions with reactive species nearby active sites. However, kinetics within confined structures often reflects the convoluted effects of solvents, including dispersive interactions ("solvation") and thermodynamic non-idealities that depend on micropore topology, solvent organization, and the physical properties of reactive species. Here, we combine rate measurements, liquid-phase isothermal titration calorimetry, and *in situ* spectroscopy to demonstrate that the apparent enthalpy and entropy changes for activation and adsorption processes scale in proportion to the quantities of solvent molecules displaced by formation of reactive surface intermeditates. This is exemplified both by liquid-phase initial product formation rates acquired in batch reactors but also within fixed bed reactors, in which the intentional condensation of gaseous acetonitrile (CH_3CN) leads to changes in the vapor-phase alkene epoxidation kinetics. The enthalpy and entropy changes scale with both the density of hydrogen bond interactions (donors, acceptors) but also the chain length of reactant alkenes.

We synthesized Ti-BEA zeolites with varying intrapore silanol ($(SiOH)_x$) densities and controlled CH_3CN partial pressures to introduce different densities of intrapore CH_3CN, varying from 0.4 to 10 molecule·(unit cell)$^{-1}$. Turnover rates of longer-chain alkenes (C_6-C_{10}) epoxidation increase systematically by 3-fold with intrapore CH_3CN density. However, rates for short-chain alkenes (C_3-C_4) weakly depend on CH_3CN density. Apparent activation enthalpies and entropies for epoxidations (at a fixed CH_3CN density) decrease with carbon numbers from C_3 to C_6, then increase from C_6 to C_{10}, and these changes range between 30 kJ·mol^{-1} and 80 J·mol^{-1}·K^{-1}, respectively. These results infer that the stabilization by condensing CH_3CN onto the reactive species depends on the substrate sizes. Solvation by CH_3CN surrounding reactive species leads to an enthalpic stabilization of short-chain alkene substrates, while more significant reorganization of CH_3CN to accommodate bulkier transition states results in entropic benefits to the epoxidation kinetics. Dynamic vapor sorption and *in situ* infrared spectroscopy reveal that the CH_3CN reorganization depends systematically on the chain length and intrapore CH_3CN densities. Collectively, these results demonstrate the role of solvents during catalysis within confined structures, and the effects strongly depend on the proximity and substrate properties.

[1] D. S. Potts, D. T. Bregante, J. S. Adams, C. Torres, D. W. Flaherty, "Influence of Solvent Structure and Hydrogen Bonding on Catalysis at Solid-Liquid Interfaces", Chem. Soc. Rev. 2021, 50, 12308-12337

[2] D. S. Potts, V. Jeyaraj, O. Kwon, R. Ghosh, A. M. Mironenko, D. W. Flaherty, "Effect of Interactions Between Alkyl Chains and Solvent Structures on Lewis-Acid Catalyzed Epoxidations", ACS Catal. 2022, 12, 21, 13372–13393.

[3] O. Kwon, E. Z. Ayla, D. S. Potts, D. W. Flaherty, "Effects of Solvent-Pore Interaction on Rates and Barriers for Vapor-Phase Alkene Epoxidation with Gaseous H_2O_2 in Ti-BEA Catalysts", ACS Catal. 2023, 13, 6430–6444.

[4] C. Torres, D. S. Potts, D. W. Flaherty, "Solvent Mediated Interactions on Alkene Epoxidations in Ti-MFI: Effects of Solvent Identity and Silanol Density", ACS Catal. 2023, 13, 8925–8942.

Oxyanion Reduction Catalysis

Alison R. Fout, Kelly L. Gullett, Jewel M. Moore, Hsien-Liang Cho
Texas A&M University

Presentation Abstract

Despite its apparent simplicity, the reduction of a substrate by an electron and/or a hydrogen atom is a surprisingly complex reaction. This complexity stems from the fact that both proton(s) and electron(s) need to be delivered to the substrate to complete the reduction. Biology often uses synchronous proton delivery from an amino acid residue with an electron delivery pathway. In this context, we have developed ligands to promote similar proton/electron delivery into our catalyst design. Systematically we have built ligands that can facilitate the proton/electron delivery pathways and reduce the residual charge burden on the metal center. We have explored the reduction of new substrates with these modified ligands and have continued our mechanistic studies on reduction catalysis. Oxyanions, like nitrate, nitrite, (per)chlorate, sulfite, selenate, and arsenate are potent groundwater contaminants that Nature has evolved to be able to reduce. We will present our work toward the reduction of seleniferous oxyanions, the conversion of nitrate to ammonia, and the development of new complexes for oxyanion reduction.

Grant or FWP Number: DOE DE-SC002
Grant Title: Aspatial Oxyanion Reduction Catalysis

Student(s): Kelly Gullett,[1] Jewel M. Moore,[2] Hsien-Liang Cho[2]
Affiliations(s): [1]University of Illinois at Urbana-Champaign and [2]Texas A&M University

RECENT PROGRESS

Selenium Oxyanion Reduction

Seleniferous oxyanions, selenate (SeO_4^{2-}) and selenite (SeO_3^{2-}), are of interest due to their bioavailability and toxicity as well as the usefulness of the reduced product, red Se^0. Selenium is an essential micronutrient to living organisms on Earth, but only one order of magnitude separates healthy and toxic concentrations of selenium in aquatic environments. We have successfully demonstrated the catalytic reduction of both selenate and selenite to elemental red selenium.

Conversion of Nitrate and Nitrite to Ammonia

The conversion of nitrate and nitrite to ammonia is well vetted in biological systems. Previously we reported the catalytic reduction of nitrate and nitrite to NO(g). Now we have discovered a route to stoichiometrically reduce these oxyanions to ammonia ultimately completing one part of the global nitrogen cycle with our iron catalyst.

New Ligand Development

We have been working toward developing new ligands that feature both a primary and secondary coordination sphere capable of tautomerizing to be both hydrogen bond donating and hydrogen bond accepting. These new ligands include and anionic variant, and multiple metal binding pockets.

Publications Acknowledging this Grant in 2019-2022

(I) Intellectually led by this grant

1. Gullett K, Ford C, Garvey I, Miller T, Leahy C, Awaitey L, Hofmann D, Woods T, Fout A. Formation of Red Elemental Selenium from Seleniferous Oxyanions: Deoxygenation by Homogenous Iron Catalyst. *Journal of the American Chemical Society* **2023,** Accepted.
2. Park, Yun Ji; Peñas-Defrutos, Marconi N.; Drummond, Michael J.; Gordon, Zachary; Kelly, Oscar ; Garvey, Ian J.; Gullett, Kelly L. ; Garcia-Melchor, Max; Fout, Alison R. Secondary Coordination Sphere Influences the Formation of Fe(III)-O or Fe(III)-OH in Nitrite Reduction: A Synthetic and Computational Study. *Inorg. Chem*. **2022**, *61*, 8182-8192.
3. Leahy, C. A.; Drummond, M. J.; Vura-Weis, J.; Fout, A. R. "Synthesis of a series of M(II) (M = Mn, Fe, Co) chloride complexes with both inter- and intra-ligand hydrogen bonding interactions." *Dalton Trans*. **2021**.
4. Ford, C. L.; Miller, T. J.; Park, Y.; Iranmanesh, N.; Gray, D. L. "Varying the Secondary Coordination Sphere: Synthesis of Cobalt and Iron Complexes of a Tripodal Ligand Featuring Two Hydrogen Bond Donors or Acceptors." *J. Coord. Chem.*, **2020**, *73*, 2195- 2208.

Anatoly I. Frenkel

Speciation of Nanocatalysts Using X-ray Absorption Spectroscopy Assisted by Machine Learning

Anatoly I. Frenkel
Stony Brook University and Brookhaven National Laboratory (Joint Appointment)

Presentation Abstract

X-ray absorption fine structure (XAFS) spectroscopy, despite being a leading technique for local structural analysis, is hampered by its ensemble-averaging nature, which often leads to a bias toward a single "representative" structure. Learning heterogeneous distributions of nanostructures at the inter- and intraparticle levels from the average spectrum is challenging. We review recent developments at the Frenkel group relying on the neural network approach such as the determination of the distribution of local compositional motifs in dilute bimetallic nanocatalysts [1], atomically dispersed catalysts and coordination complexes [2] and embedding-based approach for dimensionality reduction and descriptor modeling [3]. In the end, we will outline the common limitations, caveats and future directions for machine learning – based applications in XAFS.
[1] N. Marcella, A. I. Frenkel, et al. *Nature Commun*. **2022,** *13***,** 832
[2] N. Marcella, S. Lam, V. Bryantsev, S. Roy, A. I. Frenkel, *Phys. Rev. Lett*. (in review)
[3] P. K. Routh, N. Marcella, A. I. Frenkel, *J. Phys. Chem. C (Perspective)*, **2023**, *127*, 5653

DE-SC0022199: Machine Learning for Accelerated Understanding of Dynamic Catalysis

PI: Boris Kozinsky (Harvard)
Postdoc(s): Prahlad Routh (Stony Brook), Nicholas Marcella (University of Illinois)
Student(s): Kaifeng Zheng (Stony Brook), Haodong Wang (Stony Brook)

RECENT PROGRESS

- *Unraveling the catalytic effect of hydrogen adsorption on Pt nanoparticle shape-change*
- *Speciation of nanocatalysts by X-ray absorption spectroscopy assisted by machine learning*
- *Neural network -based analysis of multimodal bond distributions using their EXAFS spectra*
- *Migration and aggregation of Pt atoms on metal oxide-suppored ceria nanodomes control reverse water gas shift reaction activity*
- *Tuning the placement of Pt "single atoms" on a mixed CeO2-TiO2 support*
- *Dynamic restructuring of supported metal nanoparticles and its implication for structure insensitive catalysis*

Publications Acknowledging this Grant in 2020-2023

(I) Intellectually led by this grant

1. C. J. Owen, N. Marcella, Y. Xie, J. Vandermause, **A. I. Frenkel**, R. G. Nuzzo, B. Kozinsky
Unraveling the catalytic effect of hydrogen adsorption on Pt nanoparticle shape-change
arXiv:2306.00901 [cond-mat.mtrl-sci], 2023

2. P. K. Routh, N. Marcella, **A. I. Frenkel**
Speciation of nanocatalysts by X-ray absorption spectroscopy assisted by machine learning
J. Phys. Chem. C (Perspective) **2023**, *127*, 5653-5662

3. H. Wang, N. Rui, S. D. Senanayake, L. Zhang, Y. Li, **A. I. Frenkel**
Tuning the placement of Pt "single atoms" on a mixed CeO2-TiO2 support
J. Phys. Chem. C **2022**, *126*, 16187-16193

4. Y. Li , J. J. Rehr, R. G. Nuzzo, **A. I. Frenkel**
Nanoclusters
in: X-ray Absorption Spectroscopy and Related Techniques,
Int. Tables. Crystallogr. I, 2022

5. H. Wang, M. Kottwitz, N. Rui, S. Senanayake, N. Marinkovic, Y. Li, R. G. Nuzzo, **A. I. Frenkel**
Aliovalent doping of CeO2 improves the stability of atomically dispersed Pt
ACS Appl. Mater. Interf. **2021**, *13*, 52736-52742

(II) Jointly funded by this grant and other grants with intellectual leadership by other funding sources

1. A. Raut, H. Fang, Y.-C. Lin, S. Fu, D. Sprouster, R. Shimogawa, **A. I. Frenkel**, J. C. Douglin, J. Lilloja, K. Tammeveski, Z. Zeng, S. Bliznakov, M. Rafailovich, D. R. Dekel
Migration and precipitation of Platinum in anion-exchange membrane fuel cells
Angew. Chem. Int. Ed. (2023), in press. DOI: 10.1002/anie.202306754

2. C. Vogt, F. Meirer, M. Monai, E. Groeneveld, D. Ferri, R. A. van Santen, M. Nachtegaal, R. R. Unocic, **A. I. Frenkel**, B. M. Weckhuysen
Dynamic restructuring of supported metal nanoparticles and its implication for structure insensitive catalysis
Nature Commun. **2021**, *12*, 7096

Rachel B. Getman

Descriptors of Solvation at Water-Solid Catalyst Interfaces and Their Dependence on Both Adsorbate and Interfacial Properties

Xiuting Chen, Ricardo A. García Cárcamo, Jiexin Shi, Xiaohong Zhang, and Rachel B. Getman
Department of Chemical and Biomolecular Engineering, The Ohio State University

Presentation Abstract

Solvents have profound influences on catalysis, for example, altering free energies of interfacial species and hence energies and barriers of interfacial reactions. In this work, we use our previously developed method of multiscale sampling (MSS) to investigate how free energies of solvation depend on adsorbate and interfacial properties. MSS combines density functional theory (DFT) with force-field molecular dynamics (MD) to generate explicit configurations of solvent at a solid interface. It is both tractable and reliable for computing enthalpies and entropies of solvation of interfacial species. In this work, we use it to determine descriptors of enthalpies and entropies of solvation of C1-C3 oxygenate and hydrocarbon species at metal single crystal, supported metal nanoparticle, metal electrode, hydrophobic zeolite, and hydrophilic zeolite catalyst interfaces. We then correlate the results to adsorbate, interface, and solvent properties to identify possible descriptors of solvation thermodynamics. Our results indicate that enthalpies are determined about equally by adsorbate and solvent properties, while entropies also have a large contribution from interfacial properties. Some key descriptors are the polarity and size of the adsorbate; hydrophobicity/hydrophilicity, structure, and field at the interface; and polarity of and extent of hydrogen bonding within the solvent. Interestingly, we find key differences in the descriptors of confined versus unconfined interfaces. Further, within confined interfaces, we find key differences depending on if the interface is hydrophobic or hydrophilic. While performing these calculations with explicit solvation is necessary and can be done tractably using multiscale methods such as MSS, it is still computationally demanding. Hence, we additionally use what we have learned about descriptors in a machine learning analysis to deploy a tool that estimates enthalpies of solvation. This tool has an uncertainty less than 10 kJ/mol and provides values in a fraction of the time required to calculate them with explicit solvation in DFT.

DE-SC0021170: Discerning Influences from Enthalpy and Entropy at Aqueous Interfaces Involved in Biomass Conversions in Porous Catalysts
PI: Rachel Getman
Postdoc(s): N/A
Student(s): Xiuting Chen, Jiexin Shi
Affiliations(s): The Ohio State University

RECENT PROGRESS

Descriptors of solvation thermodynamics in Ti-FAU zeolites

Using MSS, we calculated enthalpies, entropies, and free energies of solvation for 20 C1-C3 oxygenates and hydrocarbons in Ti-FAU with both hydrophobic and hydrophilic pores (**Figure 1**). Models of hydrophilic pores included 4 hydroxyl groups in the same pore as the adsorbate, while models of hydrophobic pores included the same number of hydroxyl groups, but in a different pore than the adsorbate. We specifically investigated alcohol, aldehyde, and polyol adsorbates. We found that while free energies of solvation are for the most part negative in hydrophobic pores, they are mostly positive in hydrophilic pores. The reason for this depends on the type of adsorbate. For alcohols, enthalpies of solvation are significantly stronger in hydrophobic pores than in hydrophilic pores, while entropies of solvation are the same. In contrast, for aldehydes, enthalpies of solvation are similar in hydrophobic and hydrophilic pores, but hydrophobic pores induce a larger entropy penalty than in hydrophilic pores. The behavior for polyols is more complicated and cannot be generalized without incorporating details about the specific adsorbate properties.

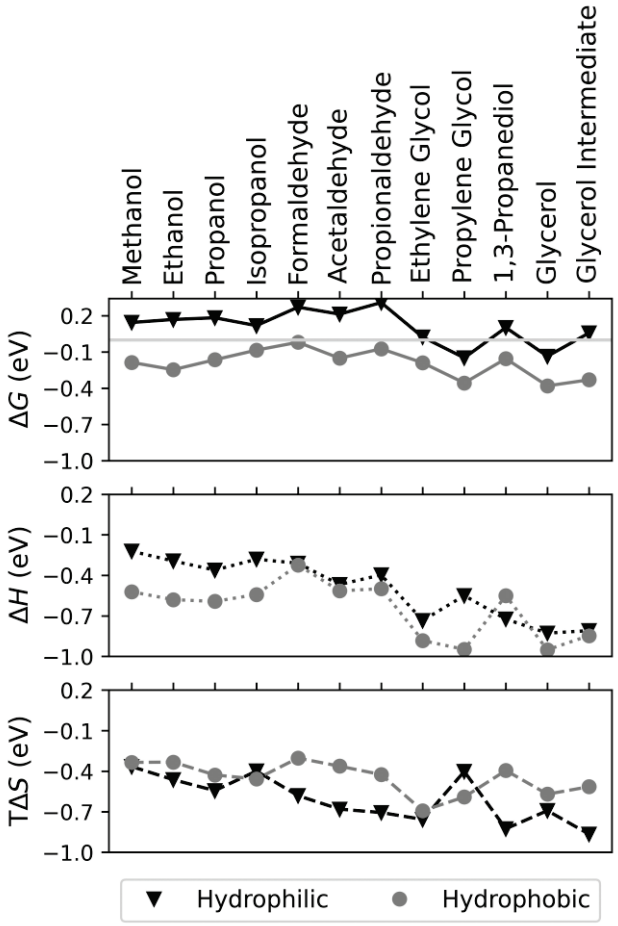

Figure 1. Free energies (top), enthalpies (middle), and entropies (bottom; multiplied by 300 K) of representative alcohol, aldehyde, and polyol species in hydrophilic (triangles) and hydrophobic (circles) models of Ti-FAU.

To understand this, we plotted calculated enthalpies and entropies of solvation against various adsorbate, solvent, and zeolite properties. The properties that we found give the best correlation are the number of water-adsorbate hydrogen bonds, the solvent accessible surface area (SASA), the adsorbate dipole moment, and the partial charge of the adsorbate. Similar to correlations uncovered in our prior work, none of these properties gives "good" correlation, since solvation thermodynamics do not depend linearly on any one property and instead are more complex functions of multiple properties. That said, solvation enthalpy shows decent correlation with number of hydrogen bonds and SASA.

Solvation entropy is more complicated and hence shown in **Figure 2**. One, it exhibits weaker correlation with all properties. Two, the properties that show good correlation are different depending on if the adsorbate is in a hydrophobic or a hydrophilic pore. Specifically, in hydrophobic pores, entropy correlates best to the number of adsorbate-water hydrogen bonds and SASA, whereas in hydrophilic pores, it correlates best with dipole moment and partial charge. The physical phenomena underpinning these findings have to do with the mobilities of the water molecules and disorder within the water structure, which depend on interactions with the adsorbate and pore surface and confinement within the pore. In general, hydrogen bonding decreases the mobilities and increases the degrees of order of water molecules, since hydrogen bonds are strong and directional. However, water molecules in the vicinity of other hydrogen bond donors/acceptors can exhibit increased disorder, since they have more "options" for forming hydrogen bonds. For example, water molecules in a hydrophobic pore without an adsorbate will tend to form a cluster. The individual water molecules in the cluster will lack mobility; however, the cluster itself may be mobile and/or configurationally disordered. In contrast, water molecules in a hydrophilic pore with a hydrophilic adsorbate can hydrogen bond with the adsorbate, the pore, or the other water molecules. In this case, there is a balance between the increased configurational disorder and the loss of mobility (caused by decreases in enthalpy due to formation of strong hydrogen bonds). Entropy hence depends on interactions with the adsorbate *and* the pore surface. Our ongoing work involves more precisely defining these contributions, with the aim of building fundamental understanding of how they determine interfacial solvation behavior.

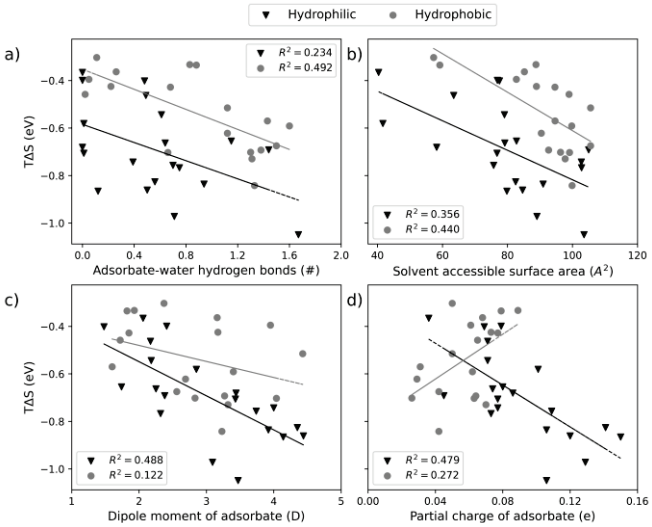

Figure 2. Calculated entropy of solvation (multipled by 300 K) of adsorbates in hydrophilic (triangles) and hydrophobic (circles) pores plotted against various adsorbate and solvent properties.

Development of a tool to estimate enthalpy of solvation

Computing solvation free energies requires explicit solvation methods based on quantum mechanics for all but the simplest of systems and is hence computationally demanding. Hence, a tool that could estimate these values in a computationally tractable way would be quite valuable. To this end, we have used machine learning to build a tool to estimate solvation enthalpies. To see if this would be viable, we started with a database that we had previously calculated for C1-C3 oxygenate species adsorbed to Pt(111) surfaces. Specifically, the database includes 90 distinct adsorbates, each with DFT-calculated interaction energies for 5 uncorrelated configurations of liquid water, for a total of 450 datapoints. We used machine learning to correlate these energies to a variety of features

related to properties of the adsorbate and local solvent structure. These models gave good performance ($R^2 > 0.8$, rMSE in the test set < 0.1 eV, and comparable rMSE between the test and train sets). An example parity plot is shown in **Figure 3**. In agreement with our results in Ti-FAU, machine learning analysis indicates that the number of hydrogen bonds formed between the solvent and the adsorbate and the adsorbate size contribute significantly to the solvation enthalpy. Other important properties include the adsorbate polarity and the local density and orientation of solvent molecules around the adsorbate. The machine learning tool is promising, since it predicts the interaction energy between an adsorbate and interfacial water in a fraction of a second, compared to multiple hours (or more) using DFT. Further, the uncertainty of less than 0.1 eV is within the uncertainty of DFT itself. Properly sampled values computed with machine learning could thus be averaged to obtain solvation enthalpies, hence significantly reducing the time needed to compute solvation free energies at liquid/solid interfaces. A next step is to test the transferability of this tool. For example, can it be used to predict enthalpies of solvation of C1-C3 adsorbates in Ti-FAU zeolites, or other systems with more complex solvent-interface interactions and environments? Answering these questions is a topic of our ongoing work.

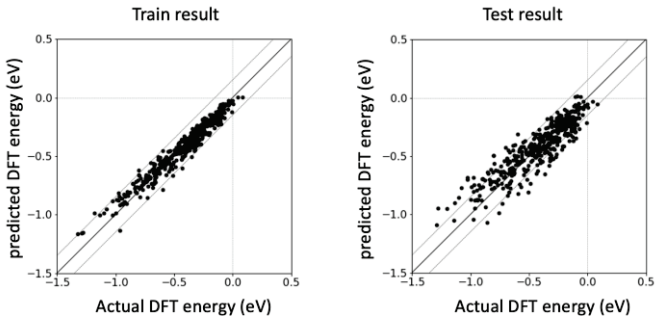

Figure 3. Parity plots showing predicted versus DFT-calculated energies of interaction between liquid water and adsorbates on a Pt(111) surface.

Publications Acknowledging this Grant in 2020-2023

(I) Intellectually led by this grant

Chen, X. and Getman, R. B. Free Energies of Solvation of C1-C3 Oxygenates in Hydrophilic versus Hydrophobic Pores of Ti-FAU Zeolite. *In preparation.*

Shi, J.; Zhang, X.; Getman, R. B. Prediction of Solvation Free Energies of Adsorbates at Pt(111)/Liquid Water Interfaces Using Machine Learning. *In preparation.*

García Cárcamo, R. A.; Chen, X.; Estejab, A.; Biswas, S.; Shi, J.; Getman, R. B. Strategies for Modeling Chemical and Physical Phenomena at Liquid/Solid Interfaces. *In preparation.*

(II) Jointly funded by this grant and other grants with intellectual leadership by other funding sources

None.

Karen I. Goldberg

Gold Pincer Complexes for Aerobic Oxidations

Alexander Phearman, Yotam Ardon and Karen Goldberg
Department of Chemistry, University of Pennsylvania

Presentation Abstract

The use of molecular oxygen as an oxidant in chemical production has significant environmental and economic benefits, however, numerous large-scale reactions currently employ more hazardous or expensive oxidants. Homogeneous organometallic compounds have proved to be exceptionally selective catalysts for organic transformations. Late transition metals in particular are promising for selective aerobic oxidations. Their high electronegativity and low oxophilicity suggest that the release of oxygenated products should be facile, enabling catalyst turnover. In this presentation, we report on organometallic gold compounds and their potential for application in aerobic oxidations of organics.

The synthesis and full characterization of a rare Au^{III}–H supported by a diphosphine pincer ligand, [(^{t}BuPCP)Au^{III}-H]OTf (^{t}BuPCP = 2,6-bis-(di-*tert*butylphosphinomethyl)benzene), is described. [(^{t}BuPCP)Au^{III}-H]OTf was found to cleanly react with molecular oxygen to yield a stable Au^{III}–OOH complex which was also fully characterized. The results of extensive kinetic studies on the O_2 insertion reaction are found to be consistent with an autoaccelerating radical chain mechanism. The observed kinetic behavior exhibits some similarities to that of previously reported Pd^{II}–H and Pt^{IV}–H reactions with O_2, but is not fully consistent with any known O_2 insertion mechanism, thus expanding our nascent knowledge of the pathways of late metal hydride aerobic oxidation reactions.

Oxygen atom transfer from [(^{t}BuPCP)Au^{III}-OOH]OTf generates the hydroxide complex, [(^{t}BuPCP)Au^{III}-OH]OTf. The hydrogenolysis reaction of [(^{t}BuPCP)Au^{III}-OH]OTf to regenerate the gold hydride, [(^{t}BuPCP)Au^{III}-H]OTf, has also been studied. In contrast to the analogous reaction of (^{t}BuPCP)Pd^{II}-OH, the reaction of [(^{t}BuPCP)Au^{III}-OH]OTf requires an acid catalyst. Kinetic and mechanistic studies have been completed and a viable pathway for the reaction is proposed. Overall, our studies on this Au^{III} system indicate that similar reactions as previously demonstrated for the analogous Pd^{II} system are observed but the mechanistic pathways deviate. This mechanistic insight is important as we seek to develop efficient catalysts for selective aerobic oxidation.

DE-SC0018057**:** Strategic Design of Homogenous Catalysts for Selective Aerobic Oxidation

Student(s): Alexander Phearman, Yotam Ardon, Anant Jain, Amitesh Soni

RECENT PROGRESS

Au Chemistry:

In our studies of homogeneous Au^{III} systems for aerobic epoxidation reactions, we have carried out detailed investigations of two of the reactions steps in our proposed catalytic cycle: oxygen insertion into a Au^{III}-H bond (eq. 1) and hydrogenolysis of the corresponding Au^{III}-OH complex (eq. 2). The ancillary ligand in this system is $^{t\text{Bu}}$PCP (2,6-bis-(di-*tert*butylphosphinomethyl)benzene) and complexes **1**-**3** (eq 1 and 2) have all been fully characterized. The results of our experimental and computational studies of the mechanism of the reaction shown in eq. 1 are consistent with a radical chain pathway. Hydrogen atom abstraction by O_2 generates a Au^{II} radical cation species that then reacts with oxygen to form a AuOO radical cation which acts as a radical chain carrier (Scheme 1).

Eq. 1

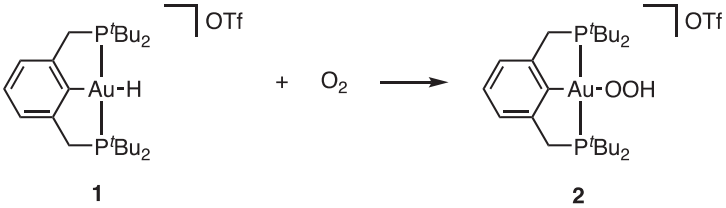

1 **2**

Eq. 2

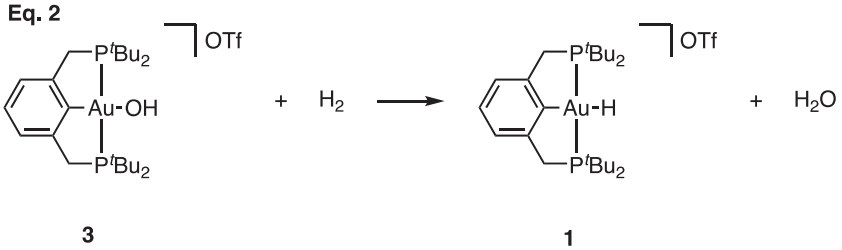

3 **1**

Scheme 1

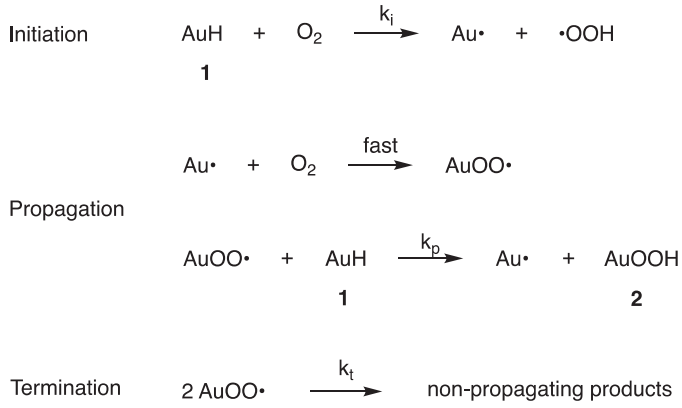

The hydrogenolysis of [($^{t\text{Bu}}$PCP)Au^{III}-OH]OTf (eq. 2) was found to require an acid catalyst and evidence supports that the reaction involves the generation of a Au^{III} aquo complex intermediate, [($^{t\text{Bu}}$PCP)Au(OH_2)]($OTf)_2$. The aquo species has also been isolated and fully characterized. Kinetic and computational studies are consistent with a

mechanism involving displacement of the aquo ligand by H_2 and deprotonation to generate the Au^{III} hydride product.

Protic and hemilabile ligands:

Di-*tert*butyl imidazolyl phosphine Ir and Rh complexes with halide anions (**4-Ir**, **4-Rh** respectively) were prepared and all exhibit a square planar M^I configuration with one bidentate ligand and an outer-sphere halide in the solid state.[1] Characterization of these complexes in solution revealed that the low valent ligand-protonated Ir^I complexes equilibrate with their metal protonated Ir^{III}-H congeners (eq. 3). The position of the equilibrium is dependent on both the steric and the electronic profile of the halide anion. No formation of the Rh^{III}-H analogs is observed under any conditions. Reactions of both Ir and Rh complexes with oxygen resulted in phosphine oxidation, with the rates of reaction dependent on the halide anion.

Eq. 3

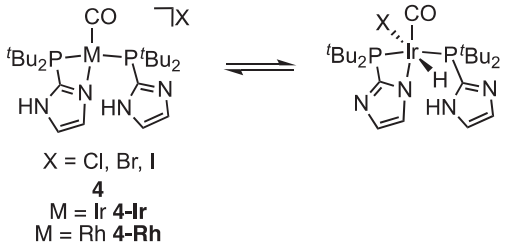

The same di-*tert*butyl imidazolyl phosphine was investigated with palladium and complex **5** was prepared and characterized. In contrast to the reaction of many Pd bisphosphine complexes which generate peroxo species, when **5** was exposed to oxygen, a mixture of cis and trans Pd^{II} complexes with two κ^2 ligands were formed (eq. 4). Current efforts are directed at exploring the mechanism of this reaction, identifying an observed intermediate, and determining the fate of the oxygen atoms.

Eq. 4

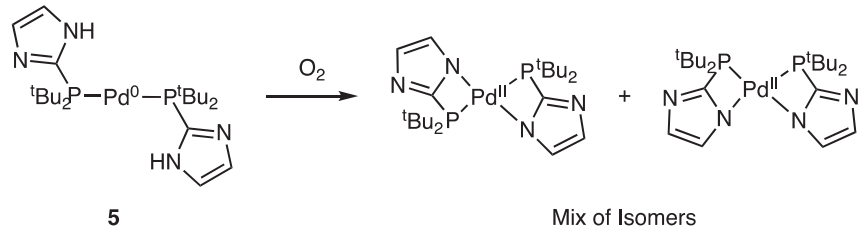

To investigate the potential of non-phosphine proton-responsive ligands to promote efficient aerobic oxidations, we have been exploring the bispyrazolyl pyridine ligand (**6a**). As metal-ligand proton tautomerization was invoked in the mechanism of dinuclear reductive elimination observed from an Ir^{III}-H complex bearing this ligand,[2] we sought to study analogous complexes that lacked the NH moiety for comparison purposes. Thus we prepared the isoelectronic and isosteric aprotic analogs, the bisisoxazolyl pyridine ligand (**6b**) and the monoprotic isoxazolyl pyrazolyl pyridine variant (**6c**). Cationic Rh-carbonyl

complexes of all three NNN ligands were synthesized (**7**) and comparison of the CO stretching frequencies of these "isoelectronic complexes" suggests that the donor ability of these ligands differ significantly. Ligand substitution reactions to open the chelates were also strongly influenced by the differences in donor strength. Thus, the differences in donor ability must be considered alongside the protic functionality as the hemilability of the ligands varies significantly with the differing donor abilities.

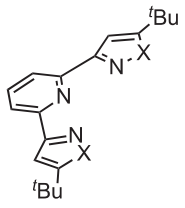

X = NH, NH **6a**
X = O, O **6b**
X = NH, O **6c**

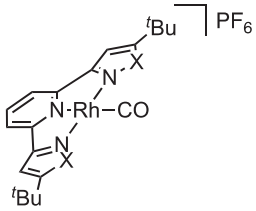

7

References

(1) (a) Jain, A. K.; Gau, M. R.; Carroll, P. J.; Goldberg, K. I. "The Underappreciated Influence of Ancillary Halide on Metal-Ligand Proton Tautomerism", *Chem. Sci.* **2022***, 13,* 7837-7845 (b) Jain, A. K.; Gau, M. R.; Carroll, P. J.; Goldberg, K. I. "Comparing Square Planar Rh^I and Ir^I: Metal-Ligand Proton Tautomerism, Fluxionality, and Reactivity", *Organometallics* **2022**, *41*, 3341-3348.
(2) Kuo, J. L; Goldberg, K. I. "Metal/Ligand Proton Tautomerism Facilitates Dinuclear H_2 Reductive Elimination", *J. Am. Chem. Soc.* **2020**, *142*, 21439-21449.

Publications Acknowledging this Grant in 2020-2023

(I) Intellectually led by this grant

1. Kuo, J. L; Goldberg, K. I. "Metal/Ligand Proton Tautomerism Facilitates Dinuclear H_2 Reductive Elimination", *J. Am. Chem. Soc.* **2020**, *142*, 21439-21449.
2. Jain, A. K.; Gau, M. R.; Carroll, P. J.; Goldberg, K. I. "The Underappreciated Influence of Ancillary Halide on Metal-Ligand Proton Tautomerism", *Chem. Sci.* **2022***, 13,* 7837-7845.
3. Jain, A. K.; Gau, M. R.; Carroll, P. J.; Goldberg, K. I. "Comparing Square Planar Rh^I and Ir^I: Metal-Ligand Proton Tautomerism, Fluxionality, and Reactivity", *Organometallics* **2022**, *41*, 3341-3348.

(II) Jointly funded by this grant and other grants with intellectual leadership by other funding sources

1. Phearman, A. S.; Moore, J. M.; Bhagwandin, D. D.; Goldberg, J. M.; Heinekey, D. M.; Goldberg, K. I. "(Hexamethylbenzene)Ru Catalysts for the Aldehyde-Water Shift Reaction", *Green Chem*. **2021**, *23*, 1609-1615.

Catalytic alkane dehydrogenation: "Non-classical" approaches

Alan S. Goldman
Rutgers University, Department of Chemistry, New Brunswick, NJ

Presentation Abstract

Our laboratory and others have extensively developed and exploited low-valent transition metal complexes, particularly those of the type (PCP)Ir, for catalytic alkane dehydrogenation. Alternative approaches to alkane dehydrogenation under investigation in our laboratory will be presented. Electrochemical oxidation of metal hydrides is one such theme. High oxidation state dehydrogenation catalysts have been developed and these may hold particular promise in this context. A novel pincer ligand has been developed which promotes metal-ligand proton tautomerization, leading to autodeprotonation of an Ir(III) hydride and facile one-electron oxidation, for a net oxidatively induced cleavage of a very strong M-H bond (thus loss of H•). This ultimately leads to a second oxidation, for a net electrochemical abstraction of hydride, which then results in C(sp^3)-H activation. Efforts to exploit this for catalysis are underway.

A new approach to the development of improved low-valent catalysts for alkane dehydrogenation is illustrated with a triphosphorus ("PPP") pincer ligand. The architecture of this ligand selectively destabilizes the resting state and favors a "sideways-directed" pathway for dehydrogenation, resulting in extremely high turnover frequencies and regioselectivity for dehydrogenation of the terminal position of *n*-alkanes.

Grant: Alkane Dehydrogenation and Related Reactions Catalyzed by Transition Metal Complexes (DE-SC0020139)

PI: Alan S. Goldman
Postdoc(s): Xiaoguang Zhou
Student(s): Tariq Bhatti, Ashish Parihar, Santanu Malakar, Arun Shada, Benjamin Gordon, Soumyadipa Das, Soham Chakraborty

Publications Acknowledging this Grant in 2020-2023

(I) Intellectually led by this grant

Bhatti, T. M.; Kumar, A.; Parihar, A.; Moncy, H. K.; Emge, T. J.; Waldie, K. M.; Hasanayn, F.; Goldman, A. S. Metal–Ligand Proton Tautomerism, Electron Transfer, and C(sp^3)–H Activation by a 4-Pyridinyl-Pincer Iridium Hydride Complex. *J. Am. Chem. Soc.* **2023**, *145*, 18296–18306.

Bhatti, T. M.; Kumar, A.; Parihar, A.; Emge, T. J.; Hasanayn, F.; Goldman, A. S. Metal-Ligand Tautomerism, Electron-Transfer, and C(sp^3)-H Activation by a 4-Pyridinyl-Pincer Iridium Hydride Complex *ChemRxiv* **2023**. DOI: 10.26434/chemrxiv-2023-8sbll-v2

Malakar, S.; Gordon, B. M.; Mandal, S.; Emge, T. J.; Goldman, A. S. Ruthenium Complexes of a Triphosphorus-Coordinating Pincer Ligand: Ru–P Ligand-Substituent Exchange Reactions Driven by Large Variations of Bond Energies *Inorg. Chem.* **2023**, *62*, 4525–4532.

Bhatti, T. M.; Yasmin, E.; Kumar, A.; Goldman, A. S. Historical perspective and mechanistic aspects of C-H bond functionalization In *Transition-Metal-Catalyzed C-H Functionalization of Heterocycles*; Punniyamurthy, T., Kumar, A., Eds.; John Wiley and Sons: 2023.

Gordon, B. M.; Parihar, A.; Hasanayn, F.; Goldman, A. S. High Activity and Selectivity for Catalytic Alkane–Alkene Transfer (De)hydrogenation by (^{tBu}PPP)Ir and the Importance of Choice of a Sacrificial Hydrogen Acceptor *Organometallics* **2022**, *41*, 3426–3434.

Gordon, B. M.; Lease, N.; Emge, T. J.; Hasanayn, F.; Goldman, A. S. Reactivity of Iridium Complexes of a Triphosphorus-Pincer Ligand Based on a Secondary Phosphine. Catalytic Alkane Dehydrogenation and the Origin of Extremely High Activity *J. Am. Chem. Soc.* **2022**, *144*, 4133-4146.

Zhou, X.; Malakar, S.; Dugan, T.; Wang, K.; Sattler, A.; Marler, D. O.; Emge, T. J.; Krogh-Jespersen, K.; Goldman, A. S. Alkane Dehydrogenation Catalyzed by a Fluorinated Phebox Iridium Complex *ACS Catal.* **2021**, *11*, 14194-14209.

Biswas, S.; Blessent, M. J.; Gordon, B. M.; Zhou, T.; Malakar, S.; Wang, D. Y.; Krogh-Jespersen, K.; Goldman, A. S. Origin of Regioselectivity in the Dehydrogenation of Alkanes by Pincer–Iridium Complexes: A Combined Experimental and Computational Study *ACS Catal.* **2021**, *11*, 12038-12051.

Shada, A. D. R.; Miller, A. J. M.; Emge, T. J.; Goldman, A. S. Catalytic Dehydrogenation of Alkanes by PCP–Pincer Iridium Complexes Using Proton and Electron Acceptors *ACS Catal.* **2021**, *11*, 3009-3016.

Sheludko, B.; Castro, C. F.; Khalap, C. A.; Emge, T. J.; Goldman, A. S.; Celik, F. E. Regioselective Gas-Phase *n*-Butane Transfer Dehydrogenation via Silica-Supported Pincer-Iridium Complexes *ChemCatChem* **2021**, *13*, 407-415.

Sheludko, B.; Castro, C. F.; Khalap, C. A.; Emge, T. J.; Goldman, A. S.; Celik, F. E. Regioselective gas-phase n-butane transfer dehydrogenation via silica-supported pincer-iridium complexes *ChemRxiv* **2020**, 1-9. DOI: 10.26434/chemrxiv.12885491.v1

(II) Jointly funded by this grant and other grants with intellectual leadership by other funding sources

Sheludko, B.; Castro, C. F.; Goldman, A. S.; Celik, F. E. Poison or Promoter? Investigating the Dual-Role of Carbon Monoxide in Pincer-Iridium-Based Alkane Dehydrogenation Systems via Operando Diffuse Reflectance Infrared Fourier Transform Spectroscopy *ACS Catal.* **2020**, *10*, 12425-12436.

Sheludko, B.; Wegener, E. C.; Celik, G.; Kropf, A. J.; Castro, C. F.; Delferro, M.; Goldman, A. S.; Kaphan, D. M.; Celik, F. E. In situ formation of a sub-nanometer iridium phosphide catalyst from supported organometallic species *ChemRxiv* **2020**, 1-9.
DOI: 10.26434/chemrxiv.12935585.v1

First Principles Studies of Solvation and Electrocatalytic Reactivity Trends

Jeffrey Greeley

Davidson School of Chemical Engineering, Purdue University, West Lafayette, IN 47907

Presentation Abstract

Fundamental principles of electrocatalysis and electrocatalytic reaction mechanisms at electrified solid/liquid interfaces are explored using periodic Density Functional Theory methodologies. This continuing effort seeks to identify and exploit efficient methods to elucidate complex electrocatalytic reaction mechanisms under realistic in-situ conditions, estimate the statistical thermodynamics and kinetics of charge transfer at interfaces, generate pH/potential-dependent phase diagrams of multifunctional interfaces in aqueous environments, and investigate new approaches for applying these fundamental insights to enhance the properties of electrocatalysts for energy-relevant chemistries.

In this abstract, we describe work-in-progress relating to a subproject of the above efforts. We have sought to develop simple strategies to improve estimation of solvation energies of adsorbed electrocatalytic reaction intermediates at solid/water interfaces using two distinct strategies. First, we have explored the use of simulated annealing, combining ab-initio molecular dynamics simulations with tailored Born-Haber cycles and analysis of hydrogen bonding characteristics, to estimate structures of water molecules surrounding large, adsorbed intermediates at water/catalyst interfaces. Second, we have used neural network-based schemes, combined with transfer learning methodologies, to initiate training of water/solid/adsorbate force fields, based on inputs from DFT calculations, to capture subtleties of the water/solid interfaces that may be missed by the simulated annealing strategies. These analyses are relevant both to the determination of more realistic reaction enthalpies in aqueous electrochemical environments and to the identification of robust structures for electrochemical double layers that, in turn, control the voltage dependence of electrochemical reaction energetics.

DE-SC0010379: Electrocatalysis at Liquid-Solid Interfaces: Principles and Reactivity Trends

Postdoc(s): Zhenhua Zeng
Student(s): Ankita Morankar, Anwin John

RECENT PROGRESS

Water-adsorbate interactions on transition metal surfaces

As discussed briefly above, the interplay between covalent and non-covalent interactions at the solid-liquid interface strongly influences electrocatalytic reactions. Although methods to determine the former interactions have been rigorously developed, the latter are often described with static bilayer models or similarly approximate methods. To improve upon these approximations, we seek to account for disorder and dynamics at complex electrochemical interfaces with a simple theory to estimate the enthalpy of solvation for adsorbed intermediates. In a strategy reminiscent of Born-Haber cycles, the enthalpy of solvation is expressed in terms of two sub-processes: vacancy creation by water reorganization, and adsorbate interaction with solvent molecules. The magnitude of the solvation enthalpy is then determined as a mean value from statistical sampling of hydrated adsorbate-catalyst configurations obtained from simulated annealing with *ab initio* molecular dynamic (AIMD) simulations. This approach provides a more accurate treatment of water reorganization and interaction than is found with simple calculations of adsorbates in the presence of static water bilayers at the catalyst surface and, at the same time, avoids the need for AIMD simulations of extremely long duration. The details of this method are described in a recently submitted paper, and we have tested it on several electrocatalytic reaction systems, ranging from the classic oxygen reduction reaction (ORR) on non-precious metal catalyst surfaces to ethanol electrooxidation on platinum surfaces. Below, we briefly summarize two key tests of the approach.

First, we have calculated the solvation stabilization energies of two well-known reaction intermediates for the ORR on Pt(111), the most studied electrocatalyst for this chemistry. In this case, the calculated stabilization (~ -0.56 eV per OH* adsorbate) agrees well with a variety of other values determined using static bilayer models (-0.56, -0.50, -0.58, -0.66, and -0.56 eV, from various literature sources). This is expected, since the small OH* adsorbate does not significantly perturb the structure of surrounding water molecules, under static or dynamical conditions, and the result points to the accuracy of our scheme. On the other hand, the calculated stabilization for the OOH* intermediates (~ -0.27 eV per OOH* group) is on the lower end of a range of energies calculated from static bilayer methods (-0.16, -0.25, -0.54, -0.70, and -0.79 eV, from literature). The large deviation in literature values suggests that OOH* introduces more complex perturbations into the surrounding water structure, thus limiting reproducibility in calculations and making the static bilayer analysis less accurate. Our calculated result, in turn, suggests that the stabilization of OOH* is less significant than has been previously estimated using static bilayer models, likely because those models do not account for the disruption and destabilization of the bilayer structure by the OOH* species itself.

A second example focuses on the elementary reaction thermodynamics of ethanol electrooxidation on Pt(111). This chemistry is of interest in the development of low temperature fuel cells powered by ethanol and related liquid fuels, and there is ongoing interest in establishing the detailed reaction mechanisms and potential-limiting steps platinum and platinum alloys, which are the state-of-the-art catalysts for the chemistry. Figure 1 shows the calculated reaction energetics for ethanol electrooxidation to acetic acid,

a commonly observed product. This figure shows the free energy diagrams for the acetic acid formation at 1.16 V_{RHE} (the voltage where all the elementary steps are downhill when no water is included in the simulations) at gas-solid interfaces with no water and with our AIMD-based approach. The energy stabilization through solvation is highlighted with green arrows. The solvation stabilization is seen to be non-negligible for the EOR intermediates, and $CH_3CH_2OH^*$ and CH_3COOH^*, in particular, have large magnitudes of solvation enthalpies that, in turn, have a significant impact on the EOR mechanism. The onset potential for the EOR with the dynamical liquid water analysis drops to 0.81 V_{RHE}, indicating that solvation effects substantially reduce the voltage for acetic acid formation. This potential is consistent with experimental results showing that the onset voltage for acetic acid is approximately 0.60 V_{RHE} (Cantane et al., *J. Electrochem Soc*., 2012).

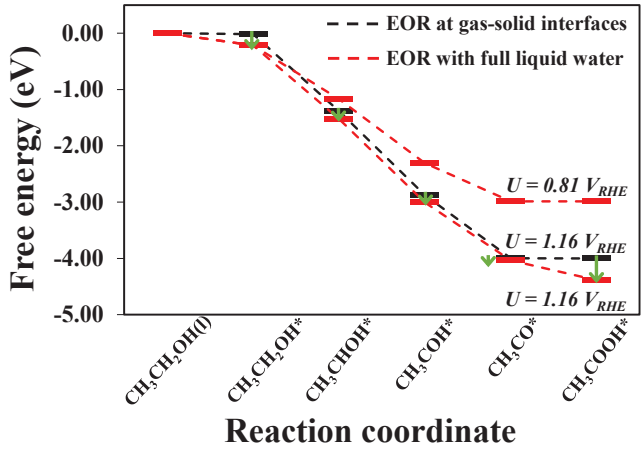

Figure 1. DFT-calculated thermodynamics of ethanol electrooxidation on Pt(111) without solvation effects (black line) and accounting for such effects using our Born-Haber scheme (red lines). The onset potential for the reaction is seen to shift from 1.16 V to 0.81 V due to solvation stabilization.

Solvation of adsorbates using DFT-aided machine learning strategies

Classical molecular dynamics (MD) simulations offer access to larger system sizes (consisting of millions of atoms) and longer timescales (approximately ranging from 100 to thousands of nanoseconds) than are possible with purely ab-initio-based molecular dynamics (AIMD). However, the interatomic potentials used in these simulations are derived from empirical approximations and frequently fail to capture accurate mechanistic details. Machine learning potentials (MLPs) have, however, emerged as a hybrid solution to bridge the gap between AIMD and classical MD calculations. MLPs accomplish this by training a nonlinear function with millions of parameters, enabling a direct mapping from atomic structure to DFT-calculated energies and forces (Batzner et al., 2021). Here, we adapt these schemes, and seek to provide a convenient framework in which solvation enthalpies and entropies of reaction intermediates adsorbed at solid/liquid interfaces may be determined, to propose an on-the-fly active learning approach coupled with gaussian mixture model uncertainty estimation to determine solvation energies of common adsorbates using explicit solvent molecules. We use O*, OH*, OOH* intermediates on various Pt and Mo doped Pt step surface terminations (which we have been exploring as alternate ORR catalysts in independent work) in a water environment as a model system to test our methodology.

To demonstrate the feasibility of our approach, we initially focused on the MoO_3OH/Pt(211) model system. We exploited the independence of Pt-Pt, H_2O-H_2O, and Pt-H_2O interactions from Mo, allowing us to train these interactions separately (this

strategy can be extended to other adsorbates as well, considering that Pt and water are common components in all calculations). Consequently, instead of training an MLP from scratch, we initiated with a pretrained model involving water on bare Pt(211). The mean absolute error is summarized in Table 1.

Table 1: The mean absolute error in energies and forces for MoO_3OH/Pt(322) system on the validation dataset with and without pretraining with water on bare Pt(221) calculations.

	Mean Absolute error in energy (eV)	**Mean Absolute Error in Forces (eV/A)**			
		O	**H**	**Pt**	**Mo**
Model from scratch	0.10	0.077	0.053	0.067	0.089
Model pretrained with water	0.04	0.039	0.020	0.018	0.056

As anticipated, pretraining significantly reduced the error in the forces of O, H, and Pt atoms, as the model has been exposed to more structures containing these atoms. Interestingly, pretraining also improves the force error for Mo atoms, despite the equal number of Mo-containing images in both cases. This improved transferability and accuracy can be attributed to the model's ability to focus more on Mo interactions, as it gains confidence in the pretrained interactions. As expected, the pretrained model exhibits superior performance in energy evaluations. Therefore, in current work, we are consistently starting with a pretrained model based on a system involving water on bare Pt(211). *These results suggest that exciting possibility that the concept of transfer learning, which is closely tied to the pretraining approach described above, can be used to greatly accelerate the training of ML-based potentials for specific electrocatalytic systems of interest, thereby providing a fast and accurate method to estimate solvation enthalpies and entropies for energy-critical elementary reactions.*

Publications Acknowledging this Grant in 2019-2022

Intellectually led by grant

1) B. Bukowski, J. Bates, R. Gounder, and J. Greeley, "Defect-Mediated Ordering of Condensed Water Structures in Microporous Zeolites," *Angewandte Chemie-International Edition* **58** (2019) 16422-16426.
2) F. Dionigi *et. al.*, "In-situ Structure and Catalytic Mechanism of NiFe and CoFe Layered Double Hydroxides During Oxygen Evolution," *Nature Communications* **11** (2020) 2522.
3) S. Deshpande and J. Greeley, "First-Principles Analysis of Coverage, Ensemble, and Solvation Effects on Selectivity Trends in NO Electroreduction on Pt_3Sn Alloys," *ACS Catalysis* **10** (2020) 9320-9327.
4) H. Chun, Z. Zeng, and J. Greeley, "Direct Demonstration of Unified Brønsted-Evans-Polanyi Relationships for Proton-Coupled Electron Transfer Reactions on Transition Metal Surfaces," *Journal of the Electrochemical Society* **167** (2020) 166516.
5) F. Dionigi, J. Zhu, Z. Zeng, …, J. Greeley, P. Strasser, "Intrinsic electrocatalytic activity for oxygen evolution of crystalline 3d-transition metal layered double hydroxides," *Angewandte Chemie International Edition* **60** (2021) 14446-14457.
6) H. Chun, Z. Zeng, J. Greeley, "DFT Insights into NO Electrochemical Reduction: A Case Study of Pt(211) and Cu(211) Surfaces," *ACS Catalysis* **12** (2022) 1394-1402.

Jointly funded by this grant and other grants

7) D. Bregante, A. Johnson, A. Patel, E. Ayla, M. Cordon, B. Bukowski, J. Greeley, R. Gounder, and D. Flaherty, "Cooperative Effects between Hydrophilic Pores and Solvents: Catalytic Consequences

of Hydrogen Bonding on Alkene Epoxidation in Zeolites," *Journal of the American Chemical Society* **141** (2019) 7302-7319.
8) J. Bates, B. Bukowski, J. Greeley, and R. Gounder, "Distinct Catalytic Reactivity of Sn Substituted in Framework Locations and at Defect Grain Boundaries in Sn-Zeolites," *ACS Catalysis* **7** (2019) 6146-6168.
9) J. Bates, B. Bukowski, J. Greeley, and R. Gounder, "Structure and Solvation of Confined Water and Water-Ethanol Clusters within Microporous Bronsted Acids and Their Effects on Ethanol Dehydration Catalysis," *Chemical Science* **11** (2020) 7102-7122.

T. Brent Gunnoe

Understanding Molecular Catalysts for Oxidative Arene Alkenylation: A Comparison of Rh and Pd Catalysis

T. Brent Gunnoe[a], Marc T. Bennett[a], Kwanwoo Park[a], Xiaofan Jia[a], Hannah E. Ketcham[a], Charles B. Musgrave III[b], William A. Goddard III[b], Sen Zhang[a]

[a] Department of Chemistry, University of Virginia
[b] Materials & Process Simulation Center, California Institute of Technology

Presentation Abstract

Experimental and computational investigations have been used to compare and understand catalytic arene alkenylation using $Pd(OAc)_2$ and $[(\eta^2\text{-}C_2H_4)_2Rh(\mu\text{-}OAc)]_2$ as catalyst precursors with arene, olefin and Cu(II) carboxylate at elevated temperature (> 120 °C). Under specific conditions, previous computational and experimental efforts have identified heterotrimetallic complexes $PdCu_2(\eta^2\text{-}C_2H_4)_3(\mu\text{-}OPiv)_6$ and $[(\eta^2\text{-}C_2H_4)_2Rh(\mu\text{-}OPiv)_2]_2(\mu\text{-}Cu)$ (OPiv = pivalate) as possible active catalysts for these processes. Further studies of catalyst speciation suggest a complicated equilibrium between Cu(II)-containing complexes containing one Rh or Pd atom and complexes containing two Rh or Pd atoms. At 120 °C, Rh catalysis produces styrene > 20-fold more rapidly than Pd. Regardless of arene functionality, the regioselectivity for alkenylation of mono-substituted arenes with the Rh catalyst gives an approximate 2:1 *meta:para* ratio with minimal *ortho* C–H activation. In contrast, Pd selectivity is significantly influenced by arene electronics with electron-rich arenes giving an approximate 1:2:2 *ortho:meta:para* ratio while the electron deficient (α,α,α)-trifluorotoluene gives a 3:1 *meta:para* ratio with minimal *ortho* functionalization. Kinetic intermolecular arene ethenylation competition experiments find that Rh reacts most rapidly with benzene, and the rate of mono-substituted arene alkenylation does not correlate with arene electronics. In contrast, with Pd catalysis, electron-rich arenes react more rapidly than benzene while electron-deficient arenes react less rapidly than benzene. Our studies are consistent with the arene C–H activation step for Pd catalysis involving significant η^1-arenium character due to Pd-mediated electrophilic aromatic substitution character. In contrast, the mechanism for Rh catalysis is not sensitive to arene substituent electronics, which we propose indicates less electrophilic aromatic substitution character for the Rh-mediated arene C–H activation.

Grant Number: DE-SC0000776
Grant Title: Development of Transition Metal Catalysts for the Functionalization of Carbon-Hydrogen Bonds: Fundamental Studies of Catalytic Hydroarylation of Olefins
PI: T. Brent Gunnoe
Postdocs: N/A
Students: Hannah Ketcham (G), Marc Bennett (G), Chris Reid (G), Kwanwoo Park (U)
Collaborators: William Goddard III (Cal. Inst. of Tech.), Sen Zhang (U. of Virginia)

RECENT PROGRESS

We have completed a combined experimental and computational investigation to compare and understand catalytic arene alkenylation using the Pd(II) and Rh(I) precursors $Pd(OAc)_2$ and $[(\eta^2\text{-}C_2H_4)_2Rh(\mu\text{-}OAc)]_2$ with arene, olefin and Cu(II) carboxylate at elevated temperature (> 120 °C). The computational studies were completed by the Goddard group, and these results of these efforts have been published (*J. Am. Chem. Soc.* **2023***, 145*, 15507-15527. DOI: 10.1021/jacs.3c04295). Our studies compared:

1. selectivity and rate of catalytic styrene production from benzene and ethylene,
2. quantification of competitive ethylene functionalization to give vinyl acetate,
3. catalytic conversion of vinyl esters and arenes to form alkenyl arenes (including a proposed mechanism for the Pd-catalyzed process),
4. selectivity for catalytic alkenylation of mono-substituted arenes (toluene, chlorobenzene and anisole) using ethylene, styrene and methyl acrylate as the olefins,
5. comparative kinetics for the ethenylation of mono-substituted arenes relative to benzene
6. and comparative kinetics for the ethenylation of toluene relative to *para*-xylene, *ortho*-xylene and *meta*-xylene.

Under specific conditions, previous computational and experimental efforts have identified heterotrimetallic cyclic $PdCu_2(\eta^2\text{-}C_2H_4)_3(\mu\text{-}OPiv)_6$ and $[(\eta^2\text{-}C_2H_4)_2Rh(\mu\text{-}OPiv)_2]_2(\mu\text{-}Cu)$ (OPiv = pivalate) species as likely active catalysts for these processes Scheme 1). Further studies of catalyst speciation suggest a complicated equilibrium between Cu(II)-containing complexes containing one Rh or Pd atom with complexes containing two Rh or Pd atoms (Scheme 2 and Figure 1). At 120 °C, Rh catalysis produces styrene > 20-fold more rapidly than Pd (Figure 2). Also, at 120 °C, Rh is ~98% selective for styrene formation while Pd is ~82% selective. Our studies indicate that Pd catalysis has a higher predilection toward olefin functionalization to form undesired vinyl ester, while Rh catalysis is more selective for arene/olefin coupling. However, at elevated temperatures, Pd converts vinyl ester and arene to vinyl arene, which is proposed to occur through low valent Pd(0) clusters that are formed *in situ*. Regardless of arene functionality, the regioselectivity for alkenylation of mono-substituted arenes with the Rh catalyst gives an approximate 2:1 *meta:para* ratio with minimal *ortho* C–H activation. In contrast, Pd selectivity is significantly influenced by arene electronics with electron-rich arenes giving an approximate 1:2:2 *ortho:meta:para* ratio while the electron deficient (α,α,α)-trifluorotoluene gives a 3:1 *meta:para* ratio with minimal *ortho* functionalization. Kinetic intermolecular arene ethenylation competition experiments find that Rh reacts most rapidly with benzene, and the rate of mono-substituted arene alkenylation does not correlate with arene electronics. In contrast, with Pd catalysis, electron-rich arenes react more rapidly than benzene while electron-deficient arenes react less rapidly than benzene. These experimental findings, in combination with computational results, are consistent with the arene C–H activation step for Pd catalysis involving significant η^1-arenium character due to Pd-mediated electrophilic aromatic substitution character. In contrast, the mechanism for Rh catalysis is not sensitive to arene substituent electronics, which we propose indicates less electrophilic aromatic substitution character for the Rh-mediated arene C–H activation.

Rhodium-catalyzed arene alkenylation using Cu(II) carboxylates as the *in situ* oxidant and mono-substituted olefins has been previously reported (e.g., *J. Am. Chem. Soc.* **2019,** *139,* 5474; *J. Am. Chem. Soc.* **2018,** *140*, 17007; *Organometallics* **2019,** *38*, 3860; *J. Am. Chem. Soc.* **2020,** *142*, 10534). Recently, we completed studies of arene alkenylation using multi-substituted olefins with the goal of evaluating the effect of olefin substitution pattern and substituent identity on selectivity and turnover frequency. This work has been published (*Organometallics* **2023**, *42*, 908-920. DOI: 10.1021/acs.organomet.3c00073).

The influence of olefin substitution is probed by comparing the conversion of benzene to alkenyl arenes with ethylene, propylene, 1-butene, *cis*-2-butene, *trans*-2-butene, isobutene, 2-methyl-2-butene and tetramethylethylene as well as the phenyl-substituted olefins and isomers of propenylbenzene (Scheme 3). The rate of oxidative hydrophenylation for multi-substituted olefins follows the trend monosubstituted > disubstituted > trisubstituted, and tetrasubstituted olefins are unreactive. To probe the effect of substituent size on Markovnikov/anti-Markovnikov regioselectivity, cyclohexyl, *tert*-butyl, isopropyl, ethyl and methyl substituted α-olefins are compared. Selectivity for anti-Markovnikov products generally increases as substituent steric bulk is increased. Tolerance for some functionalized olefins is demonstrated. The *ortho/meta/para* regioselectivity with mono-substituted arenes reveals arene and olefin identity influences selectivity. Further mechanistic studies provide evidence for Curtin-Hammet control of *ortho/meta/para* regioselectivity with monosubstituted arenes. Our findings include:

1. Internal olefin substrates undergo isomerization to terminal olefins *in situ* to produce terminal-arylated products. This process is more significant for tri-substituted and *trans*-di-substituted olefins than for *cis*-di-substituted olefins.
2. For multiple-substituted olefin substrates, mono-substituted olefins react more rapidly than di-substituted olefins, and tri-substituted olefins are minimally reactive.
4. Increasing the steric bulk of mono-substituted olefin substituents lead to higher selectivity for linear (i.e., anti-Markovnikov) alkenyl arene products.
5. The chemistry is sensitive to olefin substituent identity: coordinating groups on the olefin result in decreased reactivity. For example, vinyl pivalate, vinyl ethyl ether, vinyl ethyl sulfide and acrylonitrile are minimally reactive. Linear selectivity is observed for most olefin functional groups.
6. For reactions with mono-substituted arenes, *meta:para* selectivity ranges from 1:1 to 2:1 as a function of HOPiv concentration, olefin concentration and substituents on the olefin and arene. This is likely the result of a kinetic advantage for the *para* position of mono-substituted arenes, but no thermodynamic preference for either position.

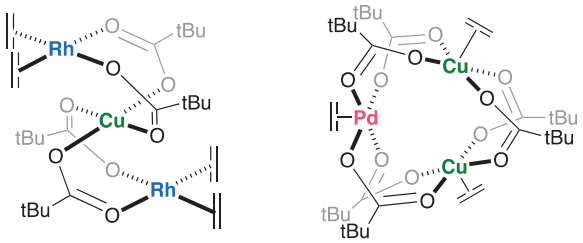

$[Rh(\mu\text{-}OPiv)_2(\eta^2\text{-}C_2H_4)_2]_2(\mu\text{-}Cu)$ $PdCu_2(\eta^2\text{-}C_2H_4)_3(\mu\text{-}OPiv)_6$

Scheme 1. Structures of $[Rh(\mu\text{-}OPiv)_2(\eta^2\text{-}C_2H_4)_2]_2(\mu\text{-}Cu)$ (left) and $PdCu_2(\eta^2\text{-}C_2H_4)_3(\mu\text{-}OPiv)_6$ (right) that we have proposed as likely catalysts for oxidative arene alkenylation using arene, olefin and Cu(II) carboxylate and Pd(II) or Rh(I) carboxylate salts as starting materials.

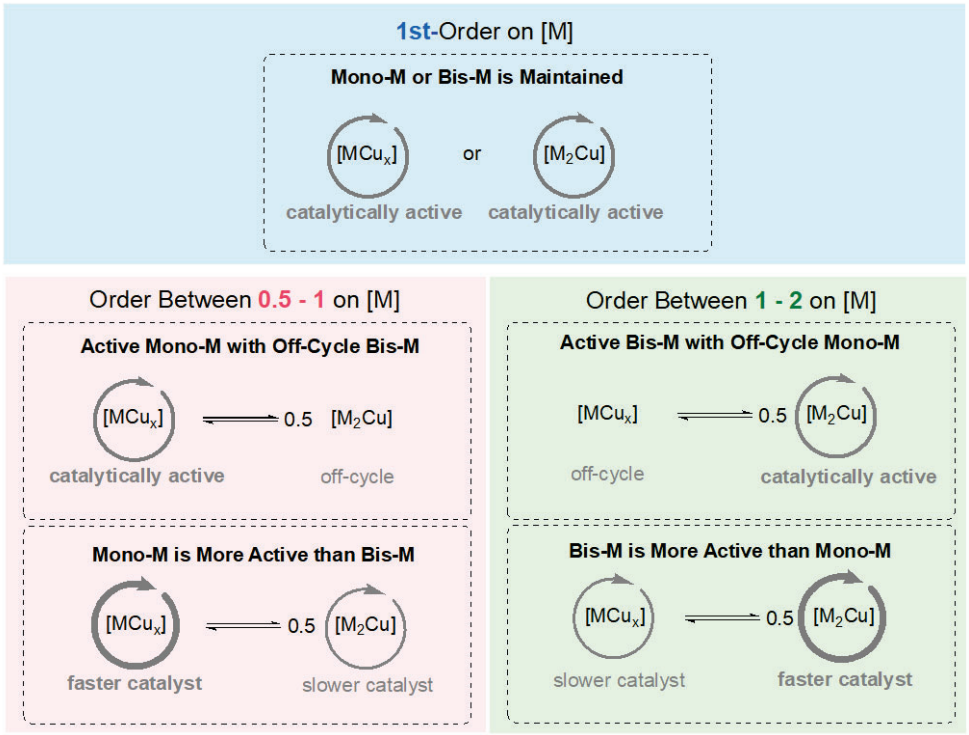

Scheme 2. Possible speciation of Rh or Pd (denoted generically as "M") and the consequent order based on M concentration.

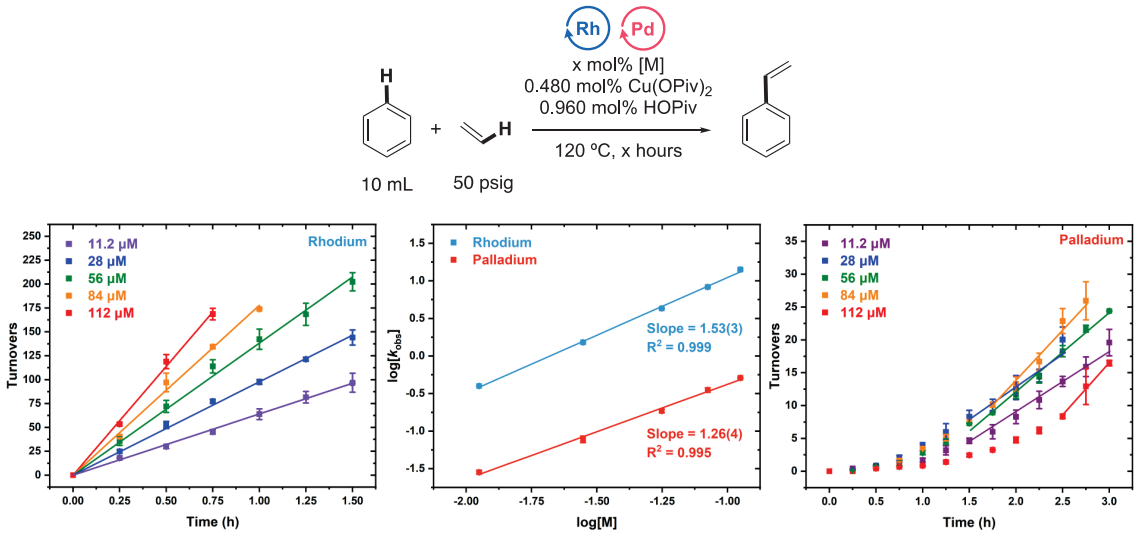

Figure 1. Turnovers of styrene versus time plots and log-log plots used to determine the order on $[(\eta^2\text{-}C_2H_4)_2Rh(\mu\text{-}OAc)]_2$ and $Pd(OAc)_2$ concentration. Reaction conditions: 10 mL benzene, 0.001 mol% of [Rh] or [Pd] per single Rh or Pd atom ([Rh] = $[(\eta^2\text{-}C_2H_4)_2Rh(\mu\text{-}OAc)]_2$; [Pd] = $Pd(OAc)_2$), 0.480 mol% $Cu(OPiv)_2$ (relative to benzene), 0.960 mol% HOPiv, 50 psig ethylene. For reactions using $Pd(OAc)_2$ as the catalyst precursor, and induction period is observed, which was previously attributed to the conversion of $Pd(OAc)_2$ to $Pd_2Cu(\eta^2\text{-}C_2H_4)_3(\mu\text{-}OPiv)_6$. After the induction period, the linear region of catalysis was fit to a linear regression, which was used to calculate turnover frequency and $k_{obs.}$ Error bars represent the standard deviation for a minimum of three independent reactions.

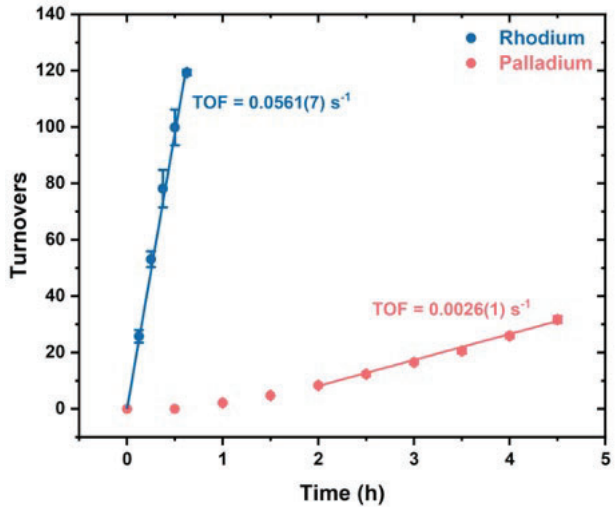

Figure 2. Kinetics of styrene production using Rh or Pd catalysts. Conditions: 10 mL benzene, 50 psig of ethylene, 0.001 mol% of [Rh] or [Pd] per single Rh or Pd atom ([Rh] = $[(\eta^2\text{-}C_2H_4)_2Rh(\mu\text{-}OAc)]_2$; [Pd] = $Pd(OAc)_2$), 480 equiv. of $Cu(OPiv)_2$, 960 equiv. of HOPiv, 120 °C. Turnover frequencies (TOFs) for the linear region of the catalysis are given in the plot, and were calculated by fitting the data from 0 to 0.625 hours (for Rh) and 2 to 4.5 hours (for Pd) using linear regressions. Each data point is the average of at least three independent experiments, and error bars represent the standard deviations based on a minimum of three independent experiments (note: error bars on Pd experiments are too small to be observed at the plot scale presented above).

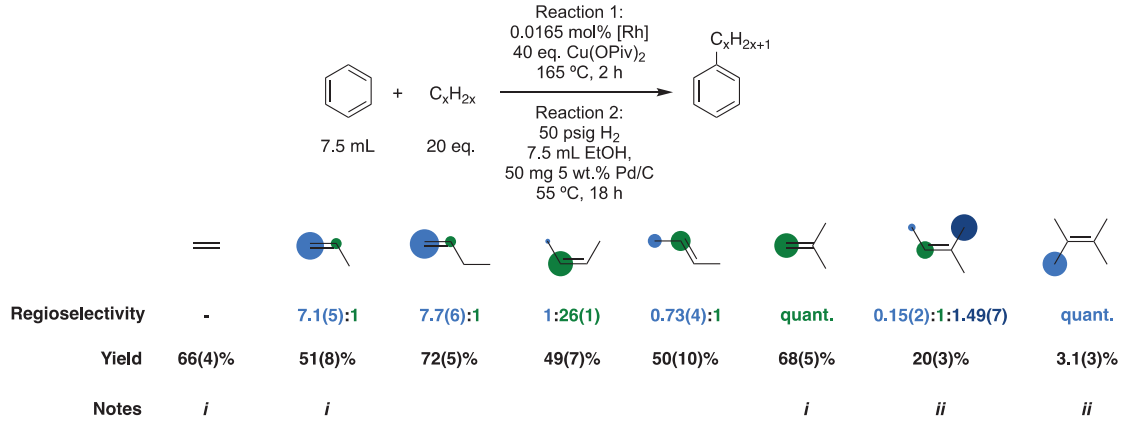

Scheme 3. Regioselectivity and yield for oxidative hydrophenylation of multi-substituted olefin substrates. Green and blue shaded circles represent the ratio of oxidative hydrophenylation at each olefin carbon. Reaction conditions: Reaction 1: 0.0165 mol% $[(\eta^2\text{-}C_2H_4)_2Rh(\mu\text{-}OAc)]_2$, 40 eq. $Cu(OPiv)_2$, 20 eq. olefin, 165 °C, 2 h. Reaction 2: 50 mg of 5 wt.% Pd/C, 7.5 mL EtOH, 18 h, 55 °C. Catalyst loading is relative to benzene per single Rh atom. Yields were quantified by GC-FID analysis of the product mixture relative to external standard hexamethylbenzene and is relative to the olefin, which is the limiting regent in each reaction. Reported yields and regioselectivities represent the averages and standard deviations from at least three independent experiments. *i.* yield and selectivity quantified using calibration curves for the unsaturated products, *ii.* 4-hour reaction time used.

Publications Acknowledging this Grant in 2020-2023

I. Intellectually led by this grant

12. "Pd(II) and Rh(I) Catalytic Precursors for Arene Alkenylation: Comparative Evaluation of Reactivity and Mechanism Based on Experimental and Computational Studies" Bennett, M. T., Jia, X., Musgrave III, C. X., Zhu, W., Goddard III, W. A.*, Gunnoe, T. B.* *J. Am. Chem. Soc.* **2023***, 145*, 15507-15527. DOI: 10.1021/jacs.3c04295

11. "Rhodium-Catalyzed Alkenylation of Arenes with Multi-Substituted Olefins: Comparison of Selectivity and Reaction Rate as a Function of Olefin Identity" Bennett, M. T., Reid, C. W., Musgrave III, C. B., Godard III, W. A.*, Gunnoe, T. B.* *Organometallics* **2023**, *42*, 908-920. DOI: 10.1021/acs.organomet.3c00073

10. "Advances in Arene Alkenylation Catalyzed by Transition Metal Complexes Based on Ruthenium, Nickel, Palladium, Platinum, Rhodium and Iridium" Ketcham, H. E., Bennett, M. T., Reid, C. W., Gunnoe, T. B.* *Adv. Organomet. Chem.* **2023**, *80*, 93-176. DOI: 10.1016/bs.adomc.2023.01.002

9. "The Reaction Mechanism Underlying Pd(II) Catalyzed Oxidative Coupling of Ethylene and Benzene to Form Styrene: Identification of a cyclic Mono-Pd^{II} Bis-Cu^{II} Complex as the Active Catalyst" Musgrave III, C. B., Bennett, M. T., Ellena, J. F., Dickie, D. A., Gunnoe, T. B.* Goddard III, W. A.* *Organometallics* **2022**, *41*, 1988-2000. DOI: 10.1021/acs.organomet.2c00183

8. "Electron-Deficient Cationic Ru(II) Catalyst Precursors for Ethylene Hydrophenylation" Jia, X., Tian, S., Shivokevich, P. J., Harman, W. D., Dickie, D. A., Gunnoe, T. B.* *Inorganics* **2022**, *10*, 76 (14 pages). DOI: 10.3390/inorganics10060076 (selected as a Feature Paper and for the issue cover feature)

7. "Advances in Group 10 Transition Metal-Catalyzed Arene Alkylation and Alkenylation" Zhu, W., Gunnoe, T. B.* *J. Am. Chem. Soc.* **2021**, *143*, 6746-6766. DOI: 10.1021/jacs.1c01810

6. "Mechanistic Studies of Styrene Production from Benzene and Ethylene using $[Rh(\mu\text{-}OAc)(\eta^2\text{-}C_2H_4)_2]_2$ as Catalyst Precursor: Identification of a Bis-Rh^{I} Mono-Cu^{II} Complex as Catalyst" Musgrave III, C. B., Zhu, W., Coutard, N., Ellena, J. F., Dickie, D. A., Gunnoe, T. B.*, Goddard III*, W. A. *ACS Catal.* **2021**, *11*, 5688-5702. DOI: 10.1021/acscatal.1c01203

5. "Oxidative Alkenylation of Arenes Using Supported Rh Materials: Evidence that Active Catalysts are Formed by Rh Leaching" Luo, Z., Whitcomb, C., Kaylor, N., Zhang, Y., Zhang, S., Davis, R. J.*, Gunnoe, T. B* *ChemCatChem* **2021**, *13*, 260-270. DOI: 10.1002/cctc.202001526

4. "Transition Metal-Catalyzed Arene Alkylation and Alkenylation: Catalytic Processes for the Generation of Chemical Intermediates" Gunnoe, T. B.*, Schinski, W. L.*, Jia, X. *ACS Catal.* **2020**, *10*, 14080-14092. DOI: 10.1021/acscatal.0c03494

3. "Rhodium-Catalyzed Arene Alkenylation Using Only Dioxygen as Oxidant" Zhu, W., Gunnoe, T. B.* *ACS Catal.* **2020**, *10*, 11519-11531. DOI: 10.1021/acscatal.0c03439

2. "Synthesis of Stilbenes by Rhodium-Catalyzed Aerobic Alkenylation of Arenes via C–H Activation" Jia, X., Frye, L. I., Zhu, W., Gu S., Gunnoe, T. B.* *J. Am. Chem. Soc.* **2020**, *142*, 10534-10543. DOI: 10.1021/jacs.0c03935

1. "Advances in Rhodium Catalyzed Oxidative Arene Alkenylation" Zhu, W., Gunnoe, T. B.* *Acc. Chem. Res.* **2020**, *53*, 920-936. DOI: 10.1021/acs.accounts.0c00036

Patents and Patent Applications

5. "Methods of Arene Alkenylation" U. S. Patent Application 17/999,273 (US 2023/0234900 A1) Full patent filed on May 19, 2021 (published Jul. 27, 2023) Gunnoe, T. B., Jia, X., Frye, L.

4. "Catalyst and Methods for Forming Alkenyl and Alkyl Substituted Arenes" U.S. Patent Application 18/163,647 (US 2023/0173476 A1) Full patent application filed on Feb. 2, 2023 (published Jun. 8, 2023) Gunnoe, T. B., Webster-Gardiner, M. S., Vaughn, B. A.

3. "Catalyst and Methods for Forming Alkenyl and Alkyl Substituted Arenes" U.S. Patent Application 17/188,535 (US 2021/0283587 A1) Full patent application filed on Mar. 1, 2021 (published Sept. 16, 2021) Gunnoe, T. B., Webster-Gardiner, M. S., Vaughn, B. A.

2. "Catalytic Synthesis of Super Linear Alkenyl Arenes Using Rhodium Catalysts" U.S. Patent 11,306,041, Schinski, W., Goldman, A., Gunnoe, T. B., Webster-Gardiner, M. S., Schwartz, N. Issued April 19, 2022.

1. "Catalyst and Methods for Forming Alkenyl and Alkyl Substituted Arenes" U.S. Patent 10,967,364 B2, Gunnoe, T. B., Webster-Gardiner, M. S., Vaughn, B. A. Issued April 6, 2021.

II. Jointly funded by this grant and other grants with intellectual leadership by other funding sources

1. "Studies of C–H Activation and Functionalization: Combined Computational and Experimental Efforts to Elucidate Mechanisms, Principles and Catalysts" Schwartz, N. A., Gu, S., McKeown, B. A., Huang, X., Boaz, N. C., Gunnoe, T. B., Groves, J. T. invited chapter in "Computational Materials, Chemistry, and Biochemistry: From Bold Initiatives to the Last Mile: In Honor of William A. Goddard's Contributions to Science and Engineering" **2021**, 767-801.

Thomas W. Hamann

Oxidation of Amines Coordinated to Ruthenium Metal Centers: Our Quest for Mechanistic Insight

Chuan-Pin Chen, Milton R. Smith, III, Thomas W. Hamann

Department of Chemistry, Michigan State University, 578 South Shaw Lane, East Lansing, MI 48824, USA

Presentation Abstract

This poster will present our recent investigation into the ammonia oxidation mechanism by the catalyst $[Ru^{III}(tpy)(dmabpy)NH_3]^{3+}$ ($[Ru(NH_3)]^{3+}$). Stoichiometric reactions of $[Ru(NH_3)]^{3+}$ were carried out with exogeneous non-coordinating Lewis bases to trigger a proposed redox disproportionation reaction, which was followed using variable temperature NMR. An intermediate species was identified as a dinitrogen bridged complex using ^{15}N NMR and Raman spectroscopy on isotopically labeled complexes. This intermediate is proposed to derive from coupling of nitridyl species formed upon sequential redox disproportion reactions. Acetonitrile displaces the dinitrogen bridge to yield free N_2. DFT calculations support this lower energy pathway versus that previously reported for ammonia oxidation by the parent $[Ru^{III}(tpy)(bpy)NH_3]^{3+}$ complex. These experimental and computational results are consistent with the interpretation of redox disproportionation involving sequential hydrogen atom transfer reactions by an amide/aminyl intermediate, $[Ru(NH_2)^-]^+ \Leftrightarrow [Ru(NH_2)^\bullet]^+$, formed upon deprotonation of the parent complex. Analogous methylamine complexes, $[Ru(NH_2CH_3)]^{2+/3+}$, were also prepared to test the proposed mechanism. Treating $[Ru(NH_2CH_3)]^{3+}$ with a Lewis base was found to cleanly yield two products $[Ru(NH_2CH_3)]^{2+}$ and $[Ru(CN)]^+$ in ~3:1 ratio, fully consistent with our proposed mechanism. In addition, preliminary results of next-generation catalyst systems will be presented.

Following Ultrafast Reaction Dynamics and Capturing Rare Intermediates in Heterogeneous Catalysis

Frank Abild-Pedersen, Tony F. Heinz, Alan Luntz, Anders Nilsson,
Hirohito Ogasawara, and Johannes Voss
SLAC National Accelerator Laboratory, 2575 Sand Hill Road, Menlo Park, CA 94025

Abstract

This project aims to address fundamental issues in heterogeneous catalysis using ultrafast measurement techniques, particularly exploiting capabilities of ultrafast pulses from x-ray free electron lasers as chemically specific probes with femtosecond time resolution. The approach is applied to examine underlying dynamics issues in gas-surface interactions, and the formation of new chemical species through surface and interface reactions. Processes to be investigated include the nature of ultrafast charge and energy transfer, the identification and analysis of short-lived intermediate states in surface reactions, and characterization of transition states. Surface processes will be initiated by ultrafast laser pulses, either through rapid heating or through non-equilibrium photoexcitation. Research will also rely on laboratory-based measurements of ultrafast dynamics, and the development of theoretical approaches to model ultrafast excitation and dynamics and to interpret transient spectroscopic signatures.

We have recently completed and published several studies on ultrafast adsorbate-substrate dynamics probed with femtosecond x-ray absorption spectroscopies using x-ray free electron lasers. We investigated three systems, involving different forms of carbon relevant for heterogeneous catalysis using carbon core level transitions: graphene supported on a copper substrate, atomic carbon chemisorbed on Ni(100), and CO on Ru(0001) with co-adsorbed O and CO. The former systems allowed us to investigate fundamental issues of adsorbate-substrate coupling for physisorbed and chemisorbed systems; the latter permitted us to examine competing desorption and reaction channels. We also made significant progress on the experimental infrastructure for measurements of ultrafast dynamics in heterogeneous catalysis using LCLS-II at SLAC through commission of our user-supplied endstation, as well as our theoretical capabilities for analyzing transient x-ray spectra.

FWP 100435: Following Ultrafast Reaction Dynamics and Capturing Rare Intermediates in Heterogeneous Catalysis
PIs: Tony F. Heinz (lead), Frank Abild-Pedersen, Alan Luntz, Anders Nilsson, Hirohito Ogasawara, and Johannes Voss
Postdocs: Joergen Gladh, Henrique Ribeiro, Markus Soldemo, Han Wang

RECENT PROGRESS

Probing ultrafast adsorbate dynamics with x-ray free electron lasers

We recently completed studies probing adsorbate-substrate dynamics and the behavior of heterogeneous catalytic reactions in which competing reaction channels were present. In both cases, the experimental approach was based on ultrafast probing of the systems by means of femtosecond x-ray absorption spectroscopy using capabilities of free-electron lasers. We briefly summarize each of these efforts below.

One system under study has been graphene adsorbed on a copper substrate, which may be taken as representative of weakly bound adsorbates and similar to adsorption of molecular systems with extended aromatic structures. In our investigations [1], we examined the dynamics of ultrafast charge and energy transfer between the copper substrate and the adsorbed graphene layer when excited by an ultrafast visible laser pulse. In the investigations carried out at the PAL free-electron laser, the time resolution from such optical pumping and X-ray probing was approximately 100 fs. Our x-ray probe of the response was based on X-ray absorption (XAS) of the carbon K-edge of the atoms in the graphene layer, particularly in the C1s→π* transition region. We observed ultrafast signatures of both electronic excitation in the graphene and of the energy flow from the hot carriers in graphene/copper to the vibrational degree of freedom of the graphene adlayer, as shown in representative experimental data and modeling in Fig. 1.

In our measurements, the ultrafast optical laser pulse rapidly heated the electrons in the copper substate to temperature as high as 10000 K, which was followed by a thermalization with the substrate phonon modes over several picoseconds to produce an equilibrium temperature rise of a few hundred Kelvins. The initial very high electron temperature was found not only to couple effectively to the electronic excitation of graphene, but also, on time scales of ~200 fs, to particular graphene vibrational modes. These modes, the strongly coupled optical phonons (SCOPs) subsequently relaxed to the other graphene vibrational modes over several picoseconds. The evolution of charge and energy flow was revealed in distinct features of the

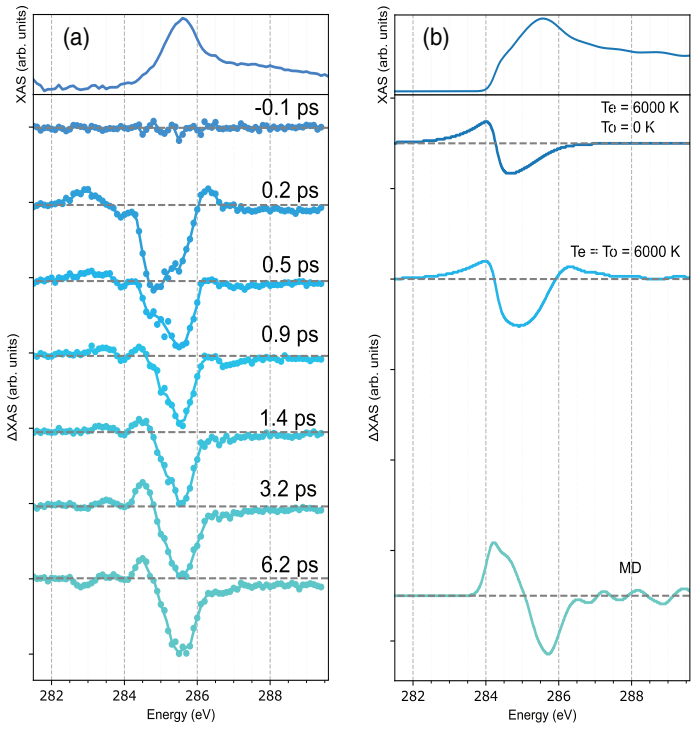

Figure 1: Transient X-ray absorption spectra from the carbon K transitions in a graphene sheet adsorbed on to a copper substrate. The top panel in the left column initial X-ray absorption spectrum, while the traces below indicate the differential change in this spectrum for the indicated time delays in picoseconds following excitation of the system by a 100-fs optical excitation pulse. Both photo-induced increases (at lower x-ray energies) and decreases are observed. The right column shows the result of modeling. The initial photoexcited state is compared with the behavior for only electronic excitation, then with a rapidly appearing state with electronic excitation and selected strongly coupled vibrational excitations in the carbon later. and finally to a thermally equilibrated state as analyzed by molecular dynamics (MD) simulations.

transient XAS spectra recorded as a function of delay time following excitation of the system by the ultrafast optical pump pulse, as shown in representative time-resolved transient x-ray absorption data.

Hole transfer from the copper substrate to the occupied graphene π-band yielded essentially instantaneous growth of a low-energy feature in the XAS, while substrate electron transfer to populate the graphene π* band produced a prompt decrease in higher-energy peaks in the XAS. The somewhat slower ensuing phonon dynamics led to well-defined shifts in the spectral features in the XAS, which correlated well with the expected changes in the XAS calculated from displacements of the carbon atoms induced by the corresponding vibrations. The long-time behavior could be modeled by full thermal equilibration where the C atom vibrations led to a shift in the corresponding X-ray absorption spectrum.

The second investigation expanded on earlier studies of the catalytic oxidation of CO induced by an excitation pulse on a Ru(0001) surface with co-adsorbed O and CO [2]. Here we investigated the competing channel of CO desorption occurring during CO oxidation at higher CO concentrations. The measurements were carried out at the FERMI free-electron laser and made use of time- and polarization-resolved C1*s* XAS measurements. In the investigations we observed two distinct transient XAS peaks during the desorption process, each having different dynamics and polarization dependence. From density-functional theory calculations, we were able to assign the spectral features to CO molecules in a precursor state. The spectra revealed increased interaction with the surface due to the co-adsorbed atomic O, producing a shift in C1*s*→2*p** polarized XAS features for perpendicular-aligned and parallel-aligned CO molecules. These findings differed notably from those of the previous studies of O+CO/Ru(0001) at lower CO surface coverage in which no precursor state in the desorption channel was observed. The results, reveal the clear impact of modest changes in adsorbate-adsorbate interactions on the dynamics and chemical pathways in heterogeneous catalysis when competing reaction channels are accessible.

User-supplied endstation for ultrafast catalysis experiments at LCLS

As a central component of this research program, a user-supplied endstation has been developed and authorized for installation in the Near-Experimental Hall at SLAC's LCLS free electron laser, existing standard LCLS endstations in their standard configurations not being suitable to support the planned investigations of heterogeneous catalysis. The custom-designed ultrahigh vacuum (UHV) system in this endstation will permit us to study the dynamics and pathways of model catalytic reactions under highly controlled surface and dosing conditions. The desired femtosecond time resolution is achieved using the pump-probe approach, with both ultrafast optical/infrared pump and x-ray probe pulses provided by LCLS and guided onto the sample surface in our endstation. The endstation will permit us to perform ultrafast measurements using time-resolved x-ray absorption spectroscopy (XAS), x-ray emission spectroscopy/resonant inelastic x-ray scattering (XES/RIXS), and x-ray photoelectron spectroscopy (XPS). In addition, our complementary laboratory-based instrument will permit adsorbates on catalyst surfaces to be characterized by mass spectrometry using temperature-programmed thermal desorption measurements or ultrafast-laser-excited reactions.

With these capabilities, we have recently been conducting scientific commissioning studies on the hot electron-driven nitrogen activation on Ni surfaces and hot hole-driven nitrogen activation on Cu surfaces. In these measurements we will employ time-resolved XAS and XES/RIXS to follow the initial charge transfer to and recombination desorption of adsorbed nitrogen atoms. In preparation, we have utilized beamline 13-1 of SLAC's SSRL synchrotron for characterization of the systems in their initial state using X-ray spectroscopy of the 1*s* level of the adsorbed N atoms. In complementary measurements in the SLAC laser laboratory, we have performed further experiments to optimize conditions for both dosing the sample and driving recombinative desorption by ultrafast laser pulses. These synchrotron- and laboratory-based studies prepare us for scientific commissioning and time-resolved experiments at LCLS.

Theoretical capabilities for and research on ultrafast surface dynamics

We have continued to expand our capabilities in supporting the analysis of the ultrafast catalysis experiments in our FWP. We extended our approach to capture vibrational excitation of adsorbed species on the catalyst surface from molecular adsorbates in the previous fiscal years to phononic excitations. Following particular phonon modes in graphene that display very strong electron-phonon coupling allowed us to explain the early XAS response in our XFEL experiments on copper-supported graphene . These results were published in Physical Review Materials [1]. We further extended our simulations to include models for valence electronic excitations by assuming highly-elevated electronic temperatures. With this approach we identified hot holes in our paper on graphene and we also helped analyze the XAS and XES spectral evolution for atomic carbon chemisorbed on nickel; this was published in Physical Review Letters [3]. We additionally assisted the analysis of this experiment by providing molecular dynamics snapshot-averaged X-ray spectra, capturing the response of the system after thermal equilibration.

To broaden our theoretical capabilities, we performed tests of time-dependent density functional theory (TDDFT) simulations and Ehrenfest dynamics, confirming that it is now possible to perform such simulations for metal surfaces due to the Brillouin zone sampling capabilities of select TDDFT implementations. Such simulations will allow us to capture coupling between catalyst substrate electrons and adsorbate nuclear motion beyond the perturbative approaches that we have recently employed. Using Ehrenfest dynamics and selectively tracing adsorbate vibrational modes, these simulations will provide us with models for non-equilibrium electronic occupations that these forced oscillations will excite. Such an understanding of the catalyst electronic structure will greatly improve on the simplified models using elevated temperatures we employed in our experimental analysis to date.

Publications Acknowledging this Grant in 2019-2023

(I) Publications intellectually led by this grant

1. Ogasawara, H.; Wang ,H.; Gladh, J.; Gallo, A.; Page, R. H.; Voss, J.; Luntz, A. C. ; Diesen, E.; Abild-Pedersen, F.; Nilsson, A.; Soldemo, M.; Zajac, M.; Attar, A.; Chen, M. E.; Cho, S. W.; Katoch, A.; Kim, K.-J.; Kim, K. H.; Kim, M.; Kwon, S.; Park, S. H.; Ribeiro, H.; Sainio, S.; Wang, H.-Y.; Yang, C.; Heinz, T. F. X-ray free electron laser studies of electron and phonon dynamics of graphene adsorbed on copper. *Phys. Rev. Mater.* **2023**, *7*, 024005.
2. LaRue, J.; Liu, B.; Rodrigues, G. L. S.; Liu, C.; Torres, J. A. G.; Schreck, S.; Diesen, E.; Weston, M.; Ogasawara, H.; Perakis, F.; Dell'Angela M.; Capotondi, F.; Ball, D.; Carnahan, C.; Zeri, G.; Giannessi, L.; Pedersoli, E.; Naumenko, D.; Amann, P.; Nikolov, I.; Raimondi, L.; Spezzani, C.; Beye, M.; Voss, J.; Wang, H.-Y.; Cavalca, F.; Gladh, J.; Koroidov, S.; Abild-Pedersen, F.; Kolb, M.; Miedema, P. S.; Costantini, R.; Heinz, T. F.; Luntz, A. C.; Pettersson, L. G. M.; Nilsson, A. Symmetry-resolved CO desorption and oxidation dynamics on O/Ru(0001) probed at the C K-edge by ultrafast X-ray spectroscopy. *J. Chem. Phys*. **2022**, *157,* 164705.
3. Schreck, S.; Diesen, E., Dell'Angela, M., C. Liu, M. Weston, M.; Capotondi, F.; H. Ogasawara; LaRue, J.; Costantini, R.; Beye, M.; Miedema, P. S.; Halldin, J. H.; Gladh, J.; Liu, B.; Wang, H-Y.; Perakis, F.; Cavalca, F.; Koroidov, S.; Amann, P.; Pedersoli, E.; Naumenko, D.; Nikolov, I.; Raimondi, L.; Abild-Pedersen, F.; Heinz, T. F.; Voss, J.; Luntz, A. C.; Nilsson, A. Atom-Specific Probing of Electron Dynamics in an Atomic Adsorbate by Time-Resolved X-ray Spectroscopy. *Phys. Rev. Lett.* **2022**, *129*, 276001.
4. Rodrigues, G. L. S.; Diesen E.; Voss J.; Norman P., Pettersson L. G. M. Simulations of x-ray absorption spectra for CO desorbing from Ru(0001) with transition-potential and time-dependent density functional theory approaches, *Struct. Dynamics* **2022,** *9,* 014101.

5. Diesen, E.; Wang, H.-Y.; Schreck, S.; Weston, M.; Ogasawara, H.; LaRue, J.; Perakis, F.; Dell'Angela, M.; Capotondi, F.; Giannessi, L.; Pedersoli, E.; Naumenko, D.; Nikolov, I.; Raimondi, L.; Spezzani, C.; Beye, M.; Cavalca, F.; Liu, B.; Gladh, J.; Koroidov, S.; Mediema, P. S.; Costantini, R.; Heinz, T.F.; Abild-Pedersen, F.; Voss, J.; Luntz, A. C.; Nilsson, A. Ultrafast adsorbate excitation probed with subpicosecond-resolution x-ray absorption spectroscopy. *Phys. Rev. Lett*. **2021**, *127*, 016802.
6. Diesen, E.; Rodrigues, G. L. S.; Luntz, A. C.; Abild-Pedersen, F.; F.; Pettersson, L. G. M.; Voss, J. Accuracy of XAS theory for unraveling structural changes of adsorbates: CO on Ni(100). *AIP Advances* **2020**, *10*, 115014.
7. Wang, H. Y.; Schreck, S.; Weston, M.; Liu, C.; Ogasawara, H.; LaRue, J.; Perakis, F.; Dell'Angela, M.; Capotondi, F.; L. Giannessi, L.; Pedersoli, E.; Naumenko, D.; Nikolov, I.; Raimondi, L.; Spezzani, C.; Beye, M.; Cavalca, F.; Liu, B., Gladh, J.; Koroidov, S.; Miedema, P. S., Costantini, R.; Pettersson, L. G. M.; Nilsson, A. Time-resolved observation of transient precursor state of CO on Ru(0001) using carbon K-edge spectroscopy. *Phys. Chem. Chem. Phys.* **2020**, *22*, 2677.

(II) Publications jointly funded by this grant and other grants with intellectual leadership by other funding sources

1. Reinhard, M.; Gallo. A.; Guo, M; Garcia-Esparza, A. T.; Biasin, E.; Qureshi, M.; Britz, A.; Ledbetter, K.; Kunnus K.; Weninger C.; van Driel, T.; Robinson, J.; Glownia, J. M.; Gaffney, K. J.; Kroll, T.; Weng, T.-C.; Alonso-Mori, R.; Sokaras D. Ferricyanide photo-aquation pathway revealed by combined femtosecond Kβ main line and valence-to-core x-ray emission spectroscopy. *Nat. Commun.* **2023**, *14*, 2443.
2. Singh S. K.; Takeyasu K.; Homma K., Ito S.: Morinaga T.; Endo Y.; Furukawa M.; Mori T., Ogasawara H.; Nakamura J.; Activating nitrogen-doped graphene oxygen reduction electrocatalysts in acidic electrolytes using hydrophobic cavities and proton-conductive particles. *Angew. Chem. Int. Ed.* e202212506 (2022).
3. Britz, A.; Attar, A. R.; Zhang, X.; Chang, H.-T.; Nyby C.; Krishnamoorthy, A.; Park, S. H.; Kwon, S.; Kim, M.; Nordlund, D.; Sainio, S.; Heinz, T. F.; Leone, S. R.; Lindenberg, A. M..; Nakano, A.; Ajayan, P.; Vashishta, P.; Fritz, D.; Lin, M.-F.; Bergmann, U. Carrier-specific dynamics in 2H-$MoTe_2$ observed by femtosecond soft x-ray absorption spectroscopy using an x-ray free-electron laser. *Struct. Dyn.* **2021,** *8,* 014501.
4. Solati, N.; Mobassem, S.; Kahraman, A.; Ogasawara, H.; Kaya, S. A comprehensive study on the characteristic spectroscopic features of nitrogen doped graphene. *Appl. Surf. Sci*. **2019,** *495*, 143518.

Simon M. Humphrey

Poster: Well-Defined Single-Site Catalysts Supported on Phosphine-, Arsine- and Stibine-based MOFs as Solid-State Ligands

Simon M. Humphrey
University of Texas at Austin, Department of Chemistry, Welch Hall 4.424, 105 E. 24th St. Stop A5300, Austin TX 78712-0165

Presentation Abstract

We continue to utilize the triphenylphosphine-based metal-organic framework (MOF) material, PCM-101, as a platform to post-synthetically attach a range of low-valent metal sites, which yields single-crystalline MOF-catalysts with periodic structures that can be interrogated by X-ray diffraction. Examples to be presented include material functionalized with Rh^{I}, Ir^{I} and Pt^{II} centers bearing alkyl and/or carbonyl terminal moieties. In some cases, the resulting MOF-coordinated catalyst species consist of structurally unusual dimeric species that are not accessible by traditional coordination chemistry approaches. The catalysts have been studied in model reactions as heterogeneous catalysts for gas- and liquid- phase hydroformylation using a range of alkenes (*e.g.*, ethylene, styrene, cyclohexene, 1-hexene). Unique pore-confinement effects imposed by the MOF micropores, coupled to the pore topology and hydrophobicity is shown to result in interesting and non-standard variations in product regio- and chemo-selectivity. The same materials have also been interrogated in C–C coupling reactions.

To improve site occupancy of catalyst loading within the MOFs, we have also synthesized pre-metallated phosphine MOF linkers to afford the materials PCM-201-Os_2 and AsCM-201-Os_2 which are isoreticular with the PCM-101 platform but contain a diosmium(I) tetracarbonyl complex bridging between adjacent 2-D sheets. This material has been studied in dihydrogen activation by experiment and with DFT, in order to understand how frontier orbitals and HOMO-LUMO levels change (sometimes dramatically) when a molecular complex is embedded within a MOF solid-state scaffold.

Thirdly, we present new results relating to an expanded MOF library that provides access to new As- and Sb-based scaffolds. R_3Sb ligands in particular are often too labile to be utilized in molecular catalysis, but in the solid-state setting, leaching can be greatly reduced. We observe that changing the identity of the pnictogen in a series of isostructural MOFs can in fact change the preferred coordination environment of a given low-valent metal ion, due to changes in Lewis basicity of the linker, as well as structural changes due to the changing cone angle of the local ligand environment. We have studied this through DFT studies to compare molecular orbital environments of the two isostructural materials Ag-PCM-201 and Ag-SbCM-201 in which the incorporated Ag(I) complex has changed its coordination mode from linear to trigonal, respectively.

Grant or FWP Number: DOE-0000250630
Grant Title: Phosphine Metal-Organic Frameworks as Solid-State Ligands to Support Single-Site Catalysts in Persistent Non-Equilibrium States

PI: Simon M. Humphrey
Postdoc: Venkatesh Piradi

Collaborators: Graeme Henkelman (UT Austin), Gregory Powell (ACU).
Students: Samuel K. Emslie, , Naman Katyal, Benjamin Patterson, Benjamin Siu, Joseph Willoughby.

RECENT PROGRESS

Over the past 18 months, we have studied new synthetic routes toward pre- and post-synthetic metalation of previously known triphenylphosphine-based MOFs that are proprietary to our group. The MOFs are used as solid-state ligands to support a range of low-valent catalytic metal species, in sterically pressured and/or geometrically strained coordination environments. Specifically, we have recently targeted functionalization of the isoreticular PCM-101 and -201 platforms (PCM = phosphine coordination material) using Ru^{II}, Rh^{I}, Ir^{I} and Pt^{II} complexes. Previous preparative methods had suffered from low total metal loading within the MOF (*i.e.*, incomplete functionalization of periodic donor sites by secondary low-valent metal complexes), with the exception of a Rh-PCM-101 analogue, which achieved unity loading under facile post-synthetic treatment using $[Rh(CO)_2Cl]_2$. Current strategies are focusing on an alternative one-pot (peri-synthetic) method using modified solvent conditions, which has been found to afford new Ru^{II}- and Ir^{I}-supported catalysts with high (> 90%) site occupancies. These materials have been studied as novel hydrogenation and hydroformylation heterogeneous catalysts using both light olefins and aromatic feedstocks as model probes. We have focused on understanding how the MOF-supported catalysts function and degrade in both the vapor and liquid phases using batch-type reactions in pressurized reactors, under a range of reaction conditions. In general, as summarized below, the catalysts offer an unrivalled level of structural information via single crystal diffraction studies, and, as catalysts also show: (a) unusual and important regioselectivity versus their homogeneous analogues; (b) good resistance to leaching of the low-valent metal(s) under forcing reaction conditions; and, (c) unique coordination environments that are inaccessible and/or not previously represented by traditional molecular organometallic complexes.

The post-metallation of PCMs such as the *tris*(aryl)-based PCM-101 platform provides new insights into large-scale industrial reactions, since catalytic intermediates that may be transient in molecular catalysis can be isolated using MOF matrices, which permit in-depth structural studies using single crystal X-ray diffraction. One such example is observed when PCM-101 is treated with $[Rh(CO)_2Cl]_2$ in DMF at 60 ºC under N_2, overnight. This relatively simple method results in complexation between pairs of trans phosphine sites. The resulting Rh_2 dimers are unique in their coordination environment, being bridged by a single chloride ligand (Figure 1), along with 4,4′-bipyridine as a secondary pillaring ligand. The resulting Rh^{I}-functionalized PCM-101 shows a distortion of the trans-P_2 sites to accommodate the Rh^{I} dimers with shared μ_2-bridging Cl anion (Figure 1). This is possible since the MOF itself is also monoanionic per repeat unit, meaning that the MOF is itself the 'counterion', but the catalyst is, in essence, counterion-free. As such, when the catalyst is activated, *e.g.*, under 10 atm of CO gas, we find that pairs of asymmetric Rh^{I} centers are

generated (*i.e.*, [P–Rh(bipy)$(CO)_2]^+$ and P–Rh(bipy)(CO)Cl). Extensive batch hydroformylation studies have been conducted thus far using this novel catalyst material and notable results are summarized in Table 1.

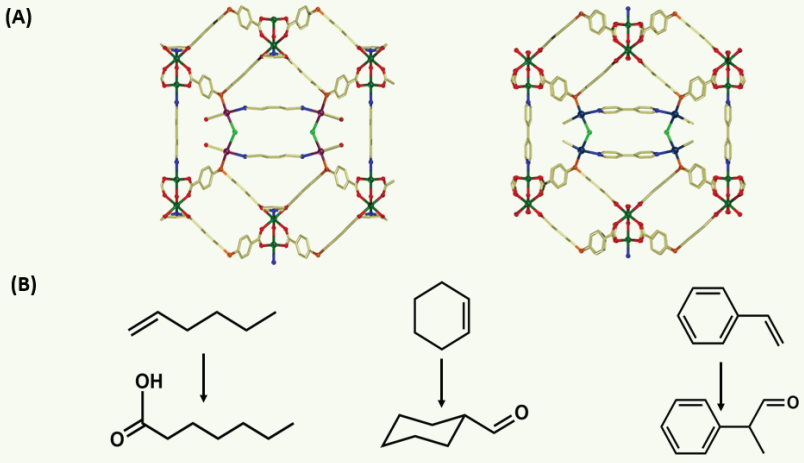

Figure 1. (A) Structures of isostructural Rh-PCM-101 (left) and Ir-PCM-101 (right). **(B)** Selection of olefin substrates and their respective MOF-catalyzed major hydroformylation products and n/iso ratios.

First, Rh-PCM-101 was pre-activated by heating at 80 °C for 15 h in a sealed 300 mL Anton Paar 4760 pressure vessel. Then, unsaturated organic substrates (*e.g.,* styrene, 1-hexene, cyclohexene) in toluene solvent were introduced to the dry activated MOF crystals, and the reactor was subsequently charged with a 1:1 $CO:H_2$ gas mixture at pressures between 10–55 atm. In the case of cyclohexene at 50 bar, a single aldehyde product was formed in high seslectivity. By comparison, 1-hexene showed no product formation at 50 bar, but when the total pressure was raised to 55 bar, a 4:1 *n*/*iso* ratio of the aldehyde product was obtained, along with the corresponding carboxylic acid as a minority byproduct. In contrast, styrene was converted to the aldehyde product under the same conditions with an inverted 1:24 *n*/*iso* product ratio. For all reactions, the extent of potential catalyst leaching was determined using ICP-OES analysis of the solvent (in addition to PXRD), which showed only minimal or modest loss of the active species (varying between 1–12%). The steric pressure and asymmetric nature of the catalyst dimers ultimately results in inverted *n:iso* selectivity compared to what is usually obtained using molecular Rh^I catalysts. Before this work is completed for publication, we are awaiting advanced structural analysis (by XAS) to pinpoint the structures of different catalyst intermediates and resting states.

Substrate	Catalyst Loading (wt%)[a]	*t* (h)	*T* (°C)	*P* (bar)	Yield (%)	*n* : *iso*
Styrene	0.20	20	80	55	90	0.4
1-hexene	0.21	18	80	50	55	4.0
Cyclohexene	0.17	18	80	50	85	N/A

Table 1. Comparison of Rh-PCM-101 hydroformylation results with a range of substrates with a 1:1 ratio of $CO:H_2$. [a]Values determined by ICP-MS analysis.

In parallel studies, we have been continuing to study the reactivity of our material, Os_2-PCM-201, which contains the dimeric complex $[Os_2(\mu_2\text{-}OCH)_2(CO)_2]$ encapsulated between the *trans*-

phosphine Lewis base sites, catalyst loading and occupancy within the material was improved *via* pre-synthetic metalation of the phosphine ligand prior to MOF formation. Experimentally, we have investigated this material thoroughly with a range of hydride- and methyl-sourcing substrates and reagents, however, only limited reactivity was observed at the osmium sites. Activated samples with overpressures of H_2 gas (1,5, 10 bar), as well as treatment with hydride and halide sources (*i.e.,* hydrazine, I_2), were found by XPS analysis to yield a maximum of 15% conversion from Os(I) to the expected Os(II) states. Notably, we were also able to synthesize the arsine-osmium analogue of this material, AsCM-201-Os_2, which was found to display similar catalytic activity at the osmium site as we have observed with the phosphine complex.

To investigate the reasons for the apparent reduced activity of this complex within both PCM and AsCM scaffolds compared to the molecular structure, we hav collaborated with the Henkelman group (UT Austin) to study the material computationally. We optimized Os_2-PCM-201 and Os_2-AsCM-201 unit-cells and tolyl molecular analogues of the MOF Os sites in the VASP program. Both MOFs were found to have unfavorable binding energies for trifluoroacetic acid (TFA), contrary to their respective molecular analogues. To better understand this, we compared the frontier orbitals of the pristine MOFs and molecular analogues which led us to the conclusion that the Co atoms in the MOF pull electron density away from the Os site. The density of states (DOS) for the MOFs and molecular analogues imply that Co orbitals energetically shield the orbitals with density at the Os site in the MOF by filling empty energy levels between the highest occupied and lowest unoccupied orbitals in the MOF with Os density. Both effects cause the Os site to be a worse Lewis base when installed in the MOF than when free in solution. There also exists a geometry constraint to the reaction that the MOF framework imposes which manifests as a smaller change in the MOF Os bite angle before and after acid introduction compared to the molecular analogue. A manuscript for this project is currently under peer review, in which the interesting structures and chemical reactivity of these two novel osmium materials are presented alongside our computational investigation of the MOF-imposed effects onto the encapsulated osmium dimer.

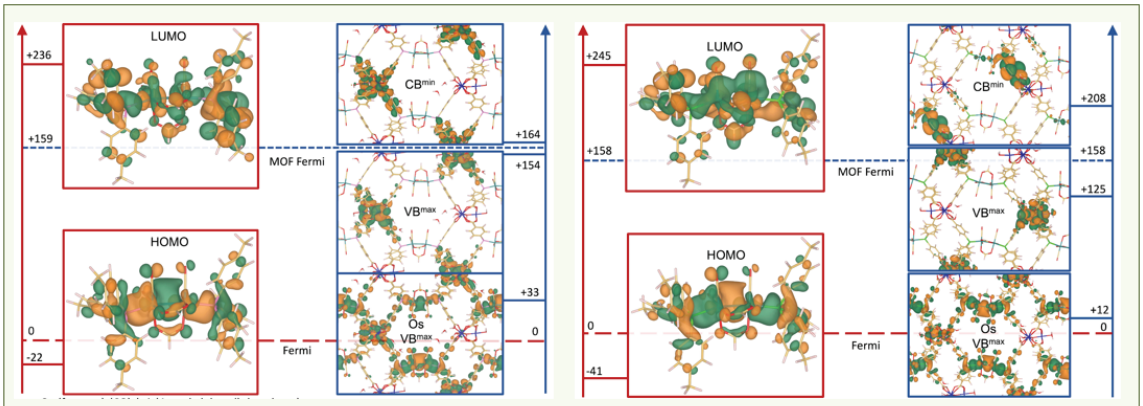

Figure 2. Comparisons of the calculated HOMO-LUMO energy levels in the molecular and MOF electronic states for Os_2-PCM-201 (left) and Os_2-AsCM-201 materials.

Thirdly, we have successfully expanded our library of MOF-forming ligands to include triaryl(antimony) and triaryl(bismuth) compounds, which enable the forward access to new classes of materials, referred to as SbCMs and BiCMs. Thus far, we have been successful in forming a range of materials isostructural to our PCMs and AsCMs, which have been metalated at the softer stibine Lewis basic site. Interestingly, we have observed that the change in identity of the pnictogen donor in isoreticular materials can affect the coordination geometry of the encapsulated metal complex. In

one key example under current study, coordination of Ag^{I} ions in an Sb analogue of PCM-201 gives the new catalyst species Ag-SbCM-201, wherein the geometry of the Ag^{I} cation is markedly changed from a common, linear (P–Ag–P) coordination mode to a trigonal (P_2Ag–X) species (X = coordinating solvent). To our surprise, DFT studies suggest that the Sb donors induce an open-shell $4d^9 6s^1$ electronic structure at each Ag^{I} center, meaning that the Ag functions as an open-shell ion, capable of formal coordination of the solvent molecule, X. DFT calculations that explore relative P vs. Sb energy states in the isostructural materials show that the LUMO state in the Ag-SbCM is significantly lowered in energy and has greater contribution from the silver 4*d* orbitals. We are continuing to investigate these antimony catalysts, both experimentally and through computational techniques, to further explore the effect of changing pnictogen identity on the encapsulated metal states.

Publications Acknowledging this Grant in 2020-2023

1. Juan L. Obeso, J. L.; Huxley, M. T.; de los Reyes, J. A.; Humphrey, S. M.; Ibarra, I. A.; Peralta R., "Low-Valent Metals in Metal-Organic Frameworks Via Post-Synthetic Modification," *Angew. Chem. Int. Ed.* **2023**, e202309025. DOI: 10.1002/anie.202309025.

2. Emslie, S. K.; Patterson, B.; Sikma, R. E.; Powell, C. B.; Henkelman, G.; Powell, G. L.; Humphrey, S. M., "Phosphine and Arsine MOFs with stabilized diosmium(I) carbonyl sawhorse pillars," *Under Review (J. Am. Chem. Soc.)* **2023.**

Ayman M. Karim

Fluxionality of Supported Pt Clusters and Consequences for H_2 Adsorption and Reaction

Ricardo Pool Mazun[1], Vinson Liao[2], Hung-Ling-Yu[1], Md Raian Yousuf[1], Salman Khan[2], Dionisios G. Vlachos[2], Ayman M. Karim[1]

[1] Virginia Polytechnic Institute and State University
[2] University of Delaware

The ability to activate hydrogen is important for many reactions including hydrogenation, hydrogenolysis, hydrodeoxygenation, hydroformylation, etc. Given the interest in maximizing the use of precious metals used for these reactions in the form of subnanometer clusters and single atoms, understanding the effect of metal nuclearity on the activation of H_2 and selective hydrogenation is crucial. Additionally, understanding the effect of the support and temperature on the Pt electronic and geometric is equally important. Using a combination of microcalorimetry, in-situ/operando infrared and X-ray absorption spectroscopies, we quantified the binding of adsorbates and studied the effect of adsorbates and temperature on the electronic and geometric properties of different sized Pt clusters on Al_2O_3 and on CeO_2. The results show a strong effect of temperature and adsorbate on the shape of the clusters and the electron density on Pt. The heats of adsorption of H_2 vs. size and temperature show unexpected trend and the activity/selectivity of acetylene hydrogenation to ethylene exhibited a volcano dependence on size. We introduce a computational methodology to access spectroscopically relevant timescales of particle dynamics using molecular dynamics and thermodynamic sampling of geometric quantities at finite temperatures using force biased Monte Carlo simulations. This methodology allows for accurate Pt cluster structure predictions consistent with experimental data.

DE-SC0022144: Molecularly Tailored Subnanometer Hydrogenation Catalysts

PI: Ayman M. Karim **co-PI:** Dionisios G. Vlachos
Postdoc(s): Salman Khan
Student(s): Ricardo Pool Mazun, Vinson Liao, Hung-Ling-Yu, Md Raian Yousuf

Reversible Temperature-Induced Shape Transition of Pt Nanoparticles Supported on Al_2O3 (*to be submitted*)

In this work, we use in-situ X-ray absorption near edge spectroscopy (XANES) and extended X-ray absorption fine structure spectroscopy (EXAFS), and theoretical calculation to study the effect of H_2 and temperature on the shape and electronic properties of 1.9 nm Pt nanoparticles supported on Al_2O_3. The coordination numbers from EXAFS show that the nanoparticles reversibly change shape, in both H_2 and in He, from 3D

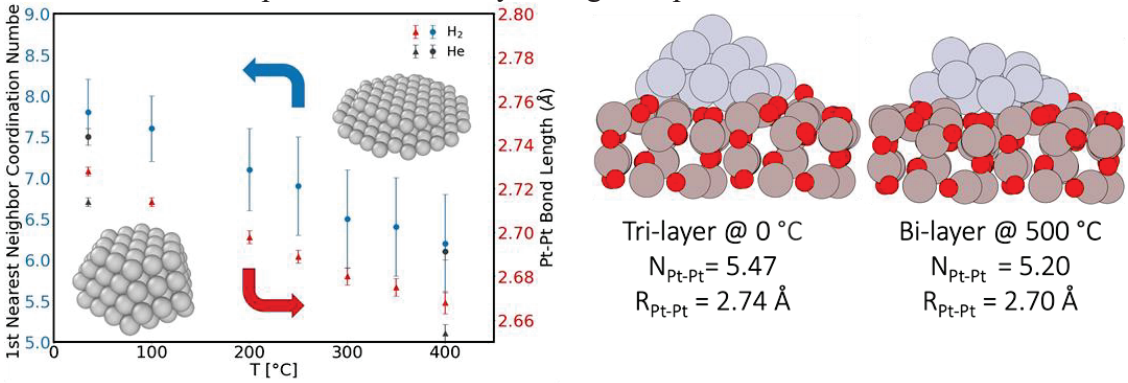

Figure 1: Effect of temperature on Pt-Pt coordination and bond distance from EXAFS (left) and MD simulations showing the flattening of a Pt_{15} cluster at higher temperature.

nanoparticles at low temperatures (35-100 °C) to 2D rafts at higher temperatures (200-400 °C). Our density functional theory and molecular dynamics calculations of $Pt_{15}/Al_2O_3(110)$ show that the distribution of nanoparticle shapes/structures change with temperature and shift to being flatter at the higher temperatures. Furthermore, the experiments and theoretical results indicate that the contraction in Pt-Pt bond distances at higher temperatures is attributed primarily to the change in nanoparticle shape and secondarily to lower H_2 coverage. The results show the fluxional nature of supported Pt nanoparticles with varying temperatures.

Effect of Pt Nanoparticles Shape on Binding with H_2 (*in preparation*)

The shape of supported Pt nanoparticles is strongly affected by temperature. We recently showed that Al_2O_3 supported 1.9 nm Pt nanoparticles change shape reversibly from hemispherical (3D) to flat (2D) shape as the temperature increases from 35 to 400 °C. Additionally, the shape change was observed in both He and H_2 environments. The change in the shape of Pt nanoparticles results in

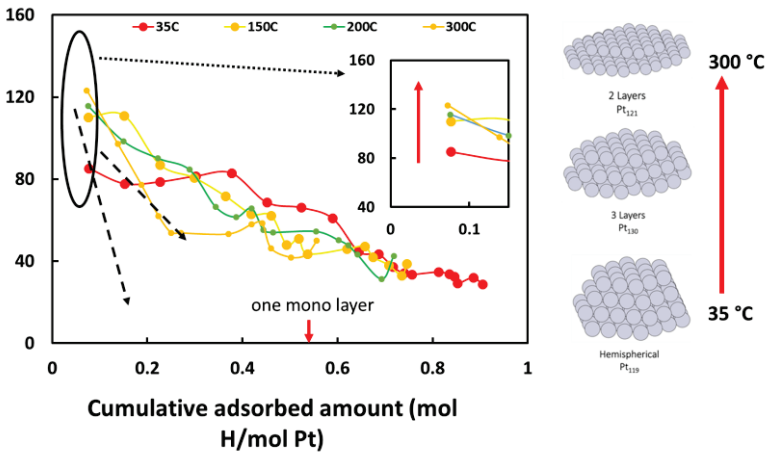

Figure 2: Effect of temperature on shape and H_2 binding on $Pt_{1.8nm}/Al_2O_3$.

new type of sites being exposed as shown in the cartoon in Figure 2. The newly exposed sites should have different properties, specifically their binding with H_2 should have different heat of adsorption. Therefore, in this work we measured the H_2 heat of adsorption at different temperatures corresponding to the shape change of the Pt nanoparticles. Figure 2 shows the heat of adsorption as a function of coverage at different temperatures. At low temperatures the shape remains hemispherical based on our EXAFS (Figure 1) and MD simulations. The heat of adsorption is ~85 kJ/mol which is consistent with previous reports on Pt nanoparticles of similar size. However, as the temperature increases, the initial heat of adsorption increases from 85 kJ/mol to 110 and 123 kJ/mol at 150 °C and 300 °C, respectively. Furthermore, as would be expected, the coverage of H_2 decreases significantly at higher temperatures as reflected in the faster drop in heat of adsorption with coverage. The results strongly indicate the presence of new type of sites, which according to our geometric models (based on EXAFS) and the MD calculations are more undercoordinated as the nanoparticles changes from a hemispherical shape to a 2D "flat" shape.

Publications Acknowledging this Grant in 2020-2023

Two manuscripts are about to be submitted and one is in preparation:

- *(I) Reversible Temperature-Induced Shape Transition of Pt Nanoparticles Supported on Al_2O_3 (to be submitted)*
- *(II) Theoretical Insights into H2 Activation over Anatase TiO2 Supported Single Atom Catalysts (to be submitted)*
- *(III) Effect of Pt Nanoparticles Size and Shape on Binding with H2 (in preparation)*

Sheima J. Khatib

Catalyst design strategies for multifunctional metal-promoted zeolites in methane dehydroaromatization

Sheima J. Khatib[1], Md Sifat Hossain[1], Gagandeep Singh Dhillon[2,3], Liping Liu[1], Hongliang Xin[1], Apoorva Sridhar[2,4], Emanuele J. Hiennadi[1], Jiyun Hong[5], Simon R. Bare[5],

[1] Department of Chemical Engineering, Virginia Tech, Blacksburg, VA 24061, USA

[2] Department of Chemical Engineering, Texas Tech University, Lubbock, TX 79409, USA

[3] Lydian Labs Inc., Cambridge, MA-02139, USA

[4] Intel Co, Hillsboro, OR 97124, USA

[5]SSRL, SLAC National Accelerator Laboratory, Menlo Park, CA 94025, USA

Presentation Abstract

We have studied the catalytic activity of iron molybdate ($Fe_2(MoO_4)_3$) supported on ZSM-5 for the first time in non-oxidative methane dehydroaromatization (MDA). Literature shows that adding Fe in oxidic or metallic form as a separate phase to Mo/ZSM-5 catalysts can improve benzene selectivity, but only when added in a small quantity, making it difficult to properly characterize the state of Fe in the catalyst to understand the possible role of Fe-Mo interactions on the catalytic properties. Here, we explore how the nature of the Mo-Fe interactions in the catalyst precursor can influence the stability and product selectivity in MDA, by employing $Fe_2(MoO_4)_3$/ZSM-5 as a catalyst precursor. We have compared the activity of $Fe_2(MoO_4)_3$/ZSM-5 catalyst with monometallic MoO_3/ZSM-5 and mixed $MoO_3 + Fe_2O_3$/ZSM-5 catalysts containing equivalent Mo and Fe loadings and found that $Fe_2(MoO_4)_3$/ZSM-5 shows higher benzene selectivity than the mixed $MoO_3 + Fe_2O_3$/ZSM-5 catalyst under the same reaction conditions, as well as exhibiting higher stability compared to the monometallic MoO_3/ZSM-5 catalyst. Structural characterization suggests that $Fe_2(MoO_4)_3$ partially segregates to amorphous MoO_x and Fe_2O_3 during thermal pretreatment in helium. The MoO_x species migrate into the zeolite channels during pretreatment, while the Fe oxides remain on the external surface of the zeolite. Gas adsorption/desorption techniques and DFT calculations demonstrate that the preexisting Fe_2O_3 phases on the external surface of the zeolite in the mixed $MoO_3 + Fe_2O_3$/ZSM-5 precursor trap $(MoO_3)_3$ clusters preventing them from migrating into the zeolite channels during pretreatment, whereas gradual formation of an amorphous layer of MoO_x simultaneously to the segregation of the Fe_2O_3 phase in a $Fe_2(MoO_4)_3$ precursor results in less trapping of $(MoO_3)_3$ clusters and in consequent enhancement in migration and anchoring of the MoO_x species at the Brønsted acid sites in the zeolite channels, hence boosting the selectivity to benzene. Characterization of used catalysts suggests that when Fe is present in the catalyst, structured carbon nanofibers, presumably nanotubes, formed in reaction lead to a decrease in the rate of catalyst deactivation.

Grant or FWP Number: DE-SC0019074

PI: Sheima J. Khatib
Student(s): Md Sifat Hossain, Emanuele J. Hiennadi, Apoorva Sridhar

RECENT PROGRESS

Ex-situ formation of metal carbide species in Mo-X/ZSM-5 (X=Fe,Co, Ni) catalysts

Zeolite-supported molybdenum catalysts are the most effective MDA catalysts studied so far, but they do not possess conversion and stability requirements for commercialization. A catalyst design strategy employed to improve catalyst performance in MDA is the addition of metal promoters (X) to Mo/ZSM-5 catalysts. Based on our literature review, we have identified Fe, Co, and Ni as promising additives given their capacity to enhance both benzene yield and catalyst stability, and their relatively cheap price compared to other noble metal promoters. Most work in the literature shows that despite the improvement achieved in catalyst stability and benzene yield in presence of these promoters, the enhancement is short-lived. Our group has found that Mo carbides formed by temperature programmed reduction and carburization (TPR&C) under softer conditions (before reaction) (ex situ) lead to a much higher stability in reaction, and enhanced benzene yield. Based on this discovery, we investigated how this activation method would affect Fe-promoted Mo/ZSM-5 catalysts[2]. We found that for a certain loading of Mo (6wt% Mo), there is an optimum loading of Fe (0.2 wt% Fe) that results in enhanced production of benzene and better catalyst stability. Furthermore, if the as-prepared catalyst is treated by the TPR&C activation protocol, the enhancement measured in presence of Fe additive is larger. Analysis of the conversion-selectivity plots suggest that the nature of the active sites is different in Mo versus Mo-Fe samples, but no bimetallic species were directly detected with the characterization techniques we employed. This was not surprising given the extremely low Fe loadings employed. TPR and XRD data did suggest that there was some interaction between Mo and Fe, given that the presence of Fe seems to affect the reducibility of Mo and the crystallinity of the MoO_3 clusters on the external surface of the zeolite. We extended our studies to employing Co and Ni additives with Mo/ZSM-5 catalysts[3]. We synthesized Mo-X (X = Co, Ni) catalysts using ZSM-5 as support and tested various loadings of X: 0.2, 0.6 and 1 wt% for a constant 6wt% loading of Mo. We found that the effect of adding Co and Ni to Mo/ZSM-5 catalysts varies depending on the type of pretreatment received. When Mo carbides were formed *in situ*, during the reaction induction period (after He pretreatment) the presence of additives was detrimental to their catalytic activity and benzene yield (see blue points in **Figure 1**). However, when the catalysts were treated in H_2+CH_4, a synergy between Mo and X was established for optimum loadings of both Co (0.6 wt%) and Ni (0.2 wt%) (red points in **Figure 1**), rendering catalysts that produced higher and more stable benzene yields. To confirm that indeed we had a synergy and not a sum of the performance of Mo and X sites in the Mo-X catalysts, we measured the catalytic activity of the single metal Co/ZSM-5 and Ni/ZSM-5 catalysts in MDA with the same loadings used in the Mo-X catalysts; the results showed that in absence of Mo, these catalysts were just active to methane cracking, and no, or close to no products resulting from C-C coupling were detected (open symbols in **Figure 1**).

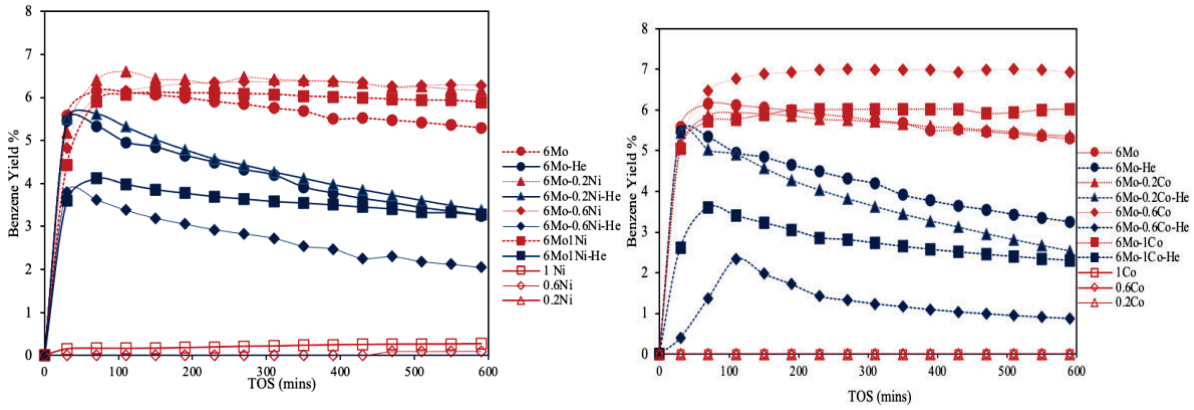

Figure 1. Benzene yield versus time on stream (TOS) for (a) Co-modified and (b) Ni-modified 6Mo/ZSM-5 catalysts. The blue symbols correspond to He-pretreated catalysts and red symbols correspond to precarburized catalysts. (The data points for unmodified 6Mo/ZSM-5, and single Co/ZSM-5 and Ni/ZSM-5 are included in both graphs as reference.). After ref. [3].

Structural characterization of the as-prepared catalysts by XRD[3] showed that when Mo and the additive species coexist, no crystalline mixed phases were observed. Similarly, the XRD patterns of the precarburized catalysts showed broad peaks corresponding to the Mo_2C phase detected on the external surface in presence of both Ni and Co additives. TPR profiles of the catalysts[3] suggested that the presence of Co promotes the location of Mo oxides inside the zeolite channels since the intensity of the peak assigned to these species (at 580 °C) increased with Co loading, while Ni increases the reducibility of the Mo oxide species on the external surface of the zeolite and promotes the location of Mo oxides inside the channels. TPR profiles of the single metal Co and Ni/ZSM-5 samples showed no H_2 consumption in the case of Co, due to its high dispersion and low loading, and in the case of Ni, only a reduction peak attributed to reduction of unbound NiO was detected at the highest Ni loading employed. Further proof of the effect of X on Mo was observed by TGA of the as-prepared Mo-X catalysts (**Table 1**): with additive loading, the temperature at which the Mo species evaporate increases, thus the presence of additives further decreases the volatility and mobility of the Mo species, possibly enhancing the retention of the Mo species inside the zeolite channels and reducing catalyst deactivation.

Table 1 Evaporation temperature of metals in as-prepared catalysts. determined by TGA. After ref. [3].

Catalyst	Weight drop temperature (°C)
6Mo	750
6Mo-0.2Co	800
6Mo-0.6Co	815
6Mo-1Co	820
6Mo-0.2Ni	830
6Mo-0.6Ni	810
6Mo-1Ni	855

Elucidating the role of Fe-Mo interactions in the metal oxide precursors for Fe promoted Mo/ZSM-5 catalysts in non-oxidative methane dehydroaromatization References

Despite the encountered improvements with addition of Fe to Mo/ZSM-5 catalysts, the nature of the Mo-Fe interactions is more difficult to determine given the small quantities of Fe present at the optimum compositions. In this regard, it has been suggested that the presence of a binary Mo-Fe phase such as $Fe_2(MoO_4)_3$ or a binary Mo-Fe carbide could

promote catalyst stability in MDA[4,5]. Yet, direct spectroscopic evidence of the existence of an active binary $Fe_2(MoO_4)_3$ or reduced binary Mo-Fe phase on ZSM-5 in MDA has not been reported to date. With the aim to understand the role that Mo-Fe interactions can play in MDA we have studied for the first time $Fe_2(MoO_4)_3$/ZSM-5 as a catalyst precursor, where those interactions evidently pre-exist in the presence of the ZSM-5 support[6].

We have contrasted the catalytic activity and structures of catalysts consisting of $Fe_2(MoO_4)_3$/ZSM-5 with those of catalysts where MoO_3 and Fe_2O_3 phases coexist on ZSM-5 but do not form a binary phase (similar to Fe promoted Mo/ZSM-5 catalysts presented in the literature). In **Figure 2** we observe that both Fe-containing catalysts, $Fe_2(MoO_4)_3$/ZSM-5_2x and 3.7Mo-1.4Fe/ZSM-5, showed stable and similar benzene yield, at approximately 4.5 %, over the 11 h time on stream. In contrast, the benzene yield obtained with the monometallic 3.7Mo/ZSM-5 sample started off showing higher values but dropped at a faster rate within three hours of reaction and continued to drop to below 4 % after 11 h of reaction time. The lower stability of this catalyst in producing benzene is not surprising given the higher selectivity to heavier hydrocarbons which act as precursors to carbon deposits that are thought to cause catalyst deactivation. While the evolution and value of the benzene yield was similar for both Fe-containing catalysts, analysis of the selectivity and product distribution shows variations between the two catalysts. At similar methane conversion values, the $Fe_2(MoO_4)_3$/ZSM-5_2x catalyst presents 15 % higher benzene selectivity values and lower selectivity to toluene, naphthalene, and heavier hydrocarbons, compared to the 3.7Mo-1.4Fe/ZSM-5 catalyst. The variations in the product distributions between the

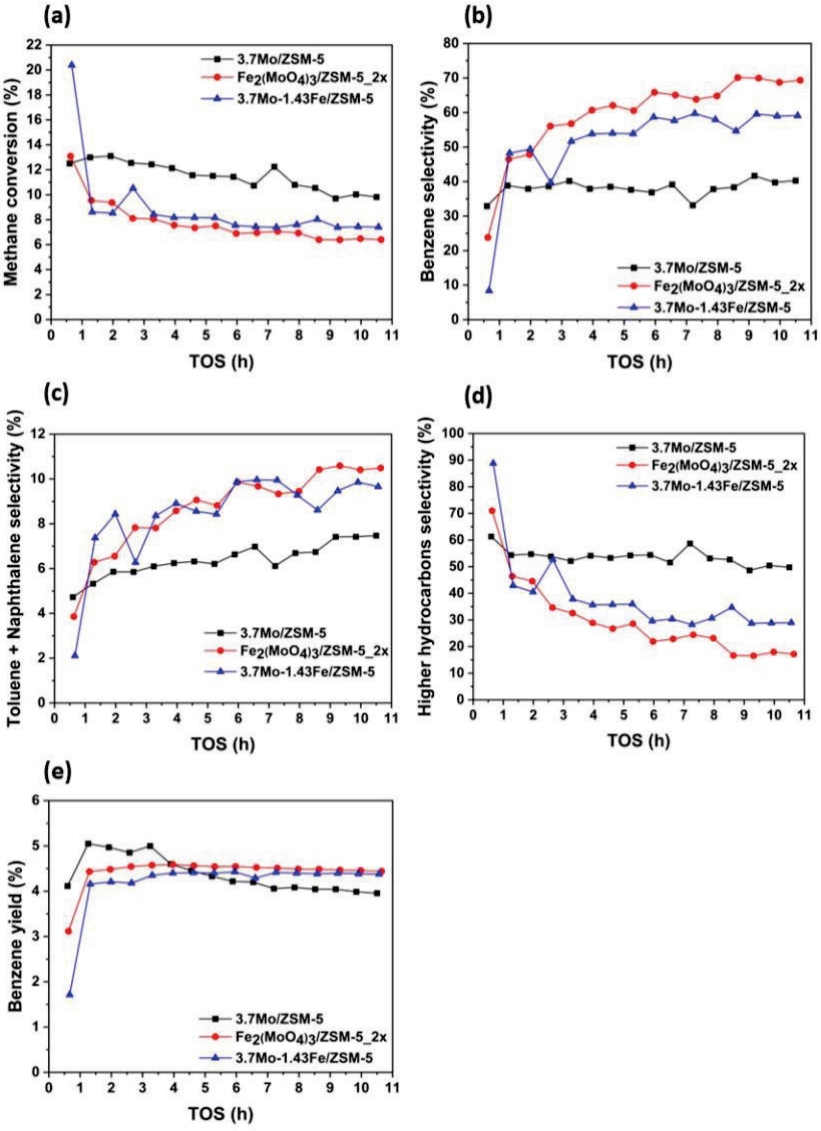

Figure 2. Activity as a function of time on stream over 3.7Mo/ZSM-5, 3.7Mo-1.43Fe/ZSM-5, and $Fe_2(MoO_4)_3$/ZSM-5_2x catalysts. (a) methane conversion over time on stream, (b) benzene selectivity over time on stream, (c) toluene + naphthalene selectivity over time on stream, (d) higher hydrocarbons selectivity over time on stream, (e) benzene yield over time on stream.

two Fe-containing catalysts suggest that there could be differences either in the nature, or the distribution, of the active sites, of these two catalysts. It is possible that the difference in the nature of the Mo-Fe interactions existing in the $Fe_2(MoO_4)_3$ precursor before pretreating the catalyst affects their subsequent evolution under He pretreatment and favors benzene selectivity. The structural characterization (XRD, XAS) of the as-prepared and He-pretreated catalysts indicates that during the high temperature pretreatment $Fe_2(MoO_4)_3$/ZSM-5 undergoes a partial segregation to Fe_2O_3 and amorphous MoO_x (**Figure 3**). These segregated MoO_x species then migrate and anchor at the Brønsted acid sites inside the zeolite channels (similar to the modus operandi in monometallic MoO_3/ZSM-5 catalysts), while Fe_2O_3 phases persist on the external surface of the zeolites. We determine experimentally via water evolution studies during catalyst calcination (**Figure 4**) that the extent of migration and anchoring of MoO_x species inside the zeolite channels is higher when we start with $Fe_2(MoO_4)_3$/ZSM-5 compared to the MoO_3/ZSM-5 or mixed MoO_3-Fe_2O_3/ZSM-5 samples, explaining its higher benzene selectivity. DFT calculations suggest that the interactions between Mo and Fe present different energetics in $Fe_2(MoO_4)_3$ and MoO_3+Fe_2O_3. The presence of a Fe_2O_3 phase acts as a trap for $(MoO_3)_3$ clusters, decreasing MoO_x migration inside the channels in the case of the MoO_3+Fe_2O_3/ZSM-5 catalyst, while the more complex and dynamic structure of the $Fe_2(MoO_4)_3$ phase enables a gradual Fe_2O_3 segregation in parallel to MoO_x formation, reducing the extent to which trapping of $(MoO_3)_3$ clusters on the Fe_2O_3 can occur.

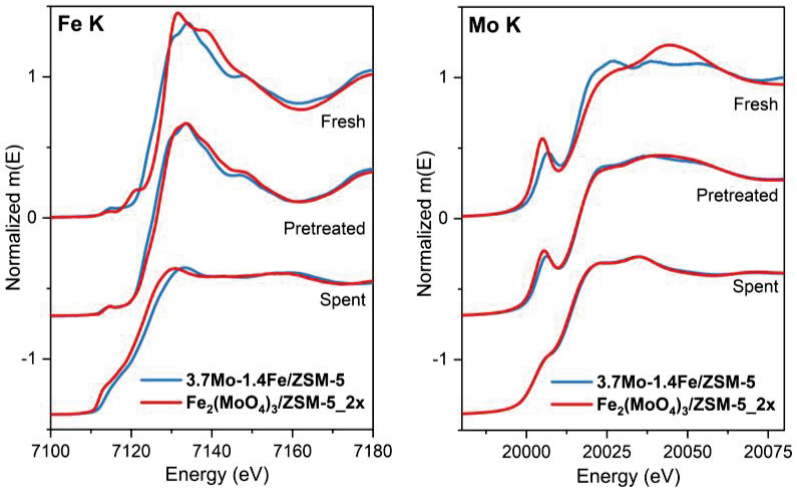

Figure 3. Normalized Fe and Mo K-edge XAS spectra of as-prepared, He-pretreated, and used 3.7Mo-1.4Fe/ZSM-5 and $Fe_2(MoO_4)_3$/ZSM-5_2x catalysts.

The work we present here answers some fundamental questions on the role that Mo-Fe interactions play in MDA catalysis, while also identifying bimetallic $Fe_2(MoO_4)_3$/ZSM-5 as a promising alternative catalyst for the MDA reaction.

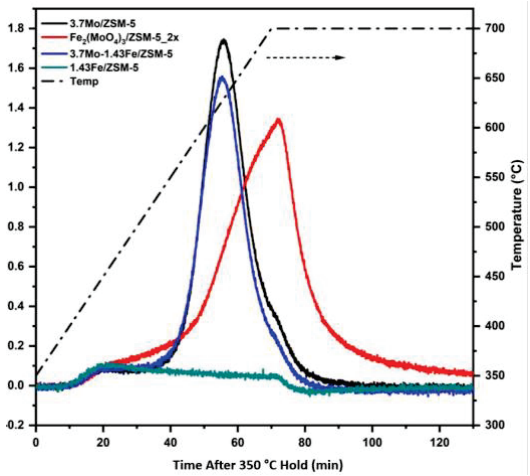

Figure 4. Evolution of H_2O during temperature-programmed calcination under Ar flow.

[1] Rahman, M.; Infantes-Molina, A.; Hoffman, A.S.; Bare, S. R.; Emerson, K.L.; Khatib, S.J. *Fuel,* **2020**, *278*, 118290.

[2] Sridhar, A.; Rahman, M.; Khatib, S.J.; *ChemCatChem*, **2018**,*10*, 2571–2583
[3] Sridhar, A., Rahman, M., Infantes-Molina, A., Wylie, B. J., Borcik, C.G., Khatib, S.J., *Appl. Catal. A: Gen.* **2020***, 589*, 117247.
[4] Masiero, S.S; Marcilio, N.R.; Perez-Lopez, O.W.; *Catal Letters*, **2009**, *131,* 194–202.
[5] Liu, S.; Dong, Q.; Ohnishi, R.; Ichikawa, M.; *Chem. Commun.* **1997**, 1455–1456.
[6] Hossain, M.S.; Dhillon, G.S.; Liu, L.; Sridhar, A.; Hiennadi, E.J.; Hong, J.,; Bare, S.R.; Xin, H.; Ericson, T.; Cozzolino, A.; Khatib*, S.J., *CEJ,* **2023** (under review).

Publications Acknowledging this Grant in 2019-2022

(I) Intellectually led by this grant

(1) Hossain, M.S.; Dhillon, G.S.; Liu, L.; Sridhar, A.; Hiennadi, E.J.; Hong, J.,; Bare, S.R.; Xin, H.; Ericson, T.; Cozzolino, A.; Khatib*, S.J. Elucidating the role of Fe-Mo interactions in the metal oxide precursors for Fe promoted Mo/ZSM-5 catalysts in non-oxidative methane dehydroaromatization, *CEJ,* **2023** (under review).

(2) Menon, U.; Rahman, M.; Khatib*, S.J. A Critical Literature Review of the Advances in Methane Dehydroaromatization over Multifunctional Metal-Promoted Zeolite Catalysts, *Applied Catalysis A: General*, **2020**, *608*, 117870.

(3) Rahman, M.; Infantes-Molina, A.; Hoffman, A.; Bare, S.R; Emerson, K.L.; Khatib*, S.J. Effect of Si/Al ratio of ZSM-5 support on structure and activity of Mo species in methane dehydroaromatization, *Fuel*, **2020**, *278*, 118290.

(4) Sridhar, A.; Rahman, M.; Infantes-Molina, A.; Wylie, B. J.; Borcik, C.G.; Khatib*, S.J. Bimetallic Mo-Co/ZSM-5 and Mo-Ni/ZSM-5 Catalysts for Methane Dehydroaromatization: A Study of the Effect of Pretreatment and Metal Loadings on the Catalytic Behavior, *Applied Catalysis A: General*, **2020**, *589,* 117247.

(5) Rahman, M.; Infantes-Molina, A.; Boubnov, A.; Bare, S.R.; Stavitski, E.; Sridhar, A.; Khatib*, S. J. Increasing the catalytic stability by optimizing the formation of zeolite-supported Mo carbide species ex situ for methane dehydroaromatization, *Journal of Catalysis*, **2019**, *375,* 314-328.

Clemens Krempner

Polydentate Lewis Acids in FLP Catalyzed Hydrogenations of Aldehydes and Organosuperbase Catalyzed Sb-C Bond Formation

Jacob Culvyhouse, Elin Sarkissian
Department of Chemistry & Biochemistry, Texas Tech University, Lubbock, TX, 79409

Presentation Abstract

The last decade has witnessed significant interest in the design and synthesis of Frustrated Lewis Pairs (FLPs) as metal-free hydrogenation catalysts [1]. FLPs are sterically encumbered Lewis pairs unable to form classical Lewis acid-base adducts due to unfavorable repulsive interactions (frustration). Key to this mode of bond activation is the unquenched Lewis acidity and basicity of an FLP, which upon interaction with for example molecular hydrogen polarizes the H-H bond and facilitates its heterolytic cleavage. In this context, we recently demonstrated that sterically congested organosuperbases in combination with relatively weak Lewis acids generate so-called "inverse" FLPs, which are capable of catalyzing the hydrogenation of a range of imines and ketones [2].

Herein, we report the design and application of "inverse" FLPs composed of organosuperbases and tri and tetradentate boron-based Lewis acids. These novel systems were demonstrated to effectively catalyze the selective metal-free hydrogenation of a range of aromatic aldehydes to primary alcohols under mild conditions and with low catalyst loadings of 0.5 mol%. Initial mechanistic studies support the notion that these polydentate Lewis acids act cooperatively in activating both molecular hydrogen and the carbonyl substrate.

In addition, we discovered that organosuperbases can catalyze highly selective Sb-C bond formation reactions. The superbase catalyzed reaction of $Sb(C_6F_5)_3$, an electron-deficient organostibine, with the weakly acidic hydrocarbons phenylacetylene, 2-cyano-thiazole, benzoxazole, benzothiazole, and N-methyl-benzimidazole, resp., resulted in the quantitative formation of C_6F_5H and the desired trisubstituted organostibines, SbR_3 [R = phenylethinyl, cyano-thiazolyl, benzoxazolyl, benzothiazolyl, N-methyl-benzimidazolyl], in good isolated yields. Also, the significantly less electron-deficient stibines, $Ph_2SbC_6F_5$ and $PhSb(C_6F_5)_2$ smoothly underwent base-catalyzed exchange reaction with a range of terminal alkynes to generate the stibines $PhSb(C{\equiv}CPh)_2$, and $Ph_2SbC{\equiv}CR$ [R = C_6H_5, C_6H_4-NO_2, COOEt, CH_2Cl, CH_2NEt_2, CH_2OSiMe_3, $Sb(C_6H_5)_2$], respectively. Kinetic studies of the base-catalyzed reaction of $Ph_2SbC_6F_5$ with phenylacetylene to form $Ph_2SbC{\equiv}CPh$ and C_6F_5H showed the empirical rate law to be of first-order dependence with respect to the base catalyst, alkyne, and stibine suggesting σ-bond metathesis to be the most probable reaction mechanism.

[1] a) Welch, G. C.; San Juan, R. R.; Masuda, J. D.; Stephan, D. W. *Science* **2006**, *314*, 1124; b) Welch, G. C.; Stephan, D. W. *J. Am. Chem. Soc.* **2007**, *129*, 1880.

[2] a) Mummadi, S.; Unruh, D. K.; Zhao, J.; Li, S.; Krempner, C. *J. Am. Chem. Soc.* **2016**, *138*, 3286; b) Mummadi, S.; Brar, A.; Wang, G.; Kenefake, D.; Diaz, R.; Unruh, D. K.; Li, S.; Krempner, C., *Chem. Eur. J.* **2018**, *24*, 16526.

Smaranda C. Marinescu

Dithiolene-Based Coordination Complexes and Polymers For H_2 Evolution and CO_2 Reduction

Smaranda C. Marinescu
University of Southern California, Los Angeles, CA 90089, Chemistry Department

Presentation Abstract

Research in the Marinescu group focuses on the development of novel catalytic systems for efficient *solar-to-fuel* technologies. Inspired by biological systems, we design molecular catalysts that involve hydrogen bonding networks capable of small molecule activation through multiple proton and electron transfers. Given the scale of potential applications, we focus our studies on species that contain abundant elements, require benign (aqueous) solvents, and display high activity, selectivity, and stability during the catalytic process. We have demonstrated the successful integration of metal dithiolene units into one and two-dimensional frameworks by using dinucleating and trinucleating thiolate-based ligand scaffolds. The developed metal dithiolene frameworks display high activity and selectivity for the electrocatalytic HER in acidic aqueous media. Preliminary studies in the Marinescu group indicate that a biologically inspired cobalt phosphinothiolate complex (**CoPS**) catalyzes the electrochemical reduction of CO_2 to a mixture of H_2 and CO (syngas) in the ratio of ~3:1 with excellent Faradaic Efficiencies (FEs) (>99%). Inspired by this promising result, the activity of a cobalt phosphino-thiolate complex (**[Co(triphos)(bdt)]$^+$**) towards the selective reduction of CO_2 to formate was explored. In the presence of an exogenous proton source such as H_2O, selective electrochemical conversion of CO_2 to $HCOO^-$ is observed with faradic yields as high as 94% at an overpotential of 750 mV. The catalyst displays robust stability, with 8 and 24 hour CPE experiments displaying negligible reduction in current and no evidence of deposition on the electrode during electrolysis. Chemical reduction studies of **[Co(triphos)(bdt)]$^+$** indicate that deligation of the apical phosphine likely occurs before catalysis. A mechanism is proposed to occur through a hydride transfer pathway, and DFT calculation indicate an additional reduction of the **[Co(triphos)(bdt)(H)]^0** to **[Co(triphos)(bdt)(H)]$^-$** is necessary for turnover, suggesting an overall ECEC mechanism. This study provides additional experimental evidence towards the beneficial role sulfur-based moieties play in molecular metal complexes as a method to increase their selectivity as electrocatalysts towards CO_2RR.

Jean-Sabin McEwen

Bimetallic Catalysts for Bio-oil Upgrading: A Multi-Scale Modeling Approach

Naseeha Cardwell[a], Isaac Onyango[a], Neeru Chaudhary[a], Alyssa J. R. Hensley[a,b], Xianghui Zhang[a], Sten Lambeets[c], Megan Rose Hawkins[a], Greg Collinge[c], Cody B. Cockreham[a], Junnan Shangguan[d], Reinhard Denecke[e], Yong Wang[a,c], Cathy Chin[d], Di Wu[a], Pierre Gaspard[f], Thierry Visart de Bocarmé[f], Daniel Perea[c], Jean-Sabin McEwen[a,c]*

[a]Washington State University (WSU), Pullman, WA 99164, USA
[b]Stevens Institute of Technology, Hoboken, New Jersey 07030 USA
[c]Pacific Northwest National Laboratory, Richland, WA 99352, USA
[d] University of Toronto, ON M5P 2G8, Canada
[e]University of Leipzig, Leipzig, D-04103, Germany
[f]Université Libre de Bruxelles, Brussels, B-1050, Belgium

Presentation Abstract

One aspect crucial to the design of effective catalysts is knowledge of the elementary reaction mechanisms, which is difficult to divine from experiment alone. However, first principles-based modeling techniques can be used to address this knowledge gap. An area currently in need of such fundamental insight is the hydrodeoxygenation (HDO) of bio-oil to create useable biofuels, where precious metal promoted Fe catalysts are effective for selective HDO. Currently, the role of the promoter remains elusive. In this work, we predict the cooperative effects and concerted behavior of several facets at the surface of a single catalytic grain when it is exposed to oxygen, hydrogen, and oxygenated aromatic compounds. We model these effects on several-crystal facets using a combination of density functional theory (DFT) calculations and cluster expansion techniques, which can then be compared to the experimental results to gain insights for effective catalyst design.

Results indicate that the clustering tendency of precious metal promoters is predictive of their ability to promote HDO. The energetics for Pd/Fe, Ru/Fe, Pt/Fe and Rh/Fe in terms of both coverage and configuration space are also parametrized, which provides atomic insights into the catalytically relevant structures for a range of heterogeneous reactions. Further, the coverage dependence of the adsorbate−adsorbate interactions for a series of phenolics on Pd(111) is determined. We find that for most adsorbates investigated, the data fits the linear mean field model well. The linear slopes are highly dependent on the size and number of functional groups present, where the only aromatics seemingly not dependent on increasing coverage are those with free radicals and those containing carboxylic acid functional groups. We construct a multi-scale mean field model for a single multi-faceted catalytic Fe grain using four Fe facets for a 110-oriented field emitter tip in the presence of an external electric field, comparing with experimental operando atom probe tomography results. We find that the oxygen coverage is lowest on the Fe(024) and Fe(013) facets, whereas it is highest for the flatter facets. These simulations are also compared between two different models: one that uses data from only three facets and one using data from four facets. We find that the four-facet model more accurately captures the operando atom probe tomography measurements, indicating the importance of combining theoretical and experimental investigations for fully capturing catalyst behavior.

DE-SC0014560: Developing Multi-Scale Models for the Effective Design of Bimetallic Catalysts for the Targeted Refinement of Bio-oil to Usable Biofuel

Students: Isaac Onyango, Naseeha Cardwell, Neeru Chaudhary, Xianghui Zhang, Megan Rose Hawkins, Cody B. Cockreham

RECENT PROGRESS

Specific Aim 1: Determine the chemical nature of the synergetic properties between the two metals of a bimetallic catalyst and the lateral interactions between the phenolic compounds.

Fe-based catalysts have been shown to be highly selective for hydrodeoxygenation of biomass derived oxygenates but are prone to oxidative deactivation. Promotion with a noble metal has been shown to improve oxidative resistance and also improve catalytic activity. We use DFT-parameterized Lattice Gas Cluster Expansions (LG CE) to account for the lateral interactions of noble metals (Pd, Pt, Rh and Ru) within HDO-active Fe(100). The resulting LG CEs are highly predictive with predictive errors below 10 meV/site over a noble metal coverage range of 0 to 2 monolayers (top two layers of Fe(100)). We also identified ground state (GS) configurations. An analysis of the GSs together with the LG CEs, particularly the 2-body cluster terms with their respective Effective Cluster Interactions (ECIs), provides insights into the distribution of these noble metals within Fe(100). For example, for Pd, the ECIs of the 1-body terms in the LG CE shows that it is more favorable to have Pd on the surface than go subsurface by about 0.7 eV (**Figure 1a**) thus having exclusively surface occupation up to 1 ML for the GSs. Additionally, we observe a GS with at least a fourth nearest neighbor (4NN) interaction (**Figure 1b, cluster 30**) between the atoms at 0.2 ML (**Figure 1c**), but an appearance of first nearest neighbor (1NN) interaction (**Figure 1b, cluster 27**) in a GS at 0.5 ML (**Figure 1d**). We therefore posit that structures below 0.2 ML for Pd would resist agglomeration and remain dispersed, but there would be both dispersed and agglomerated phases for between 0.2 and 0.5 ML, and only agglomeration beyond 0.5 ML.

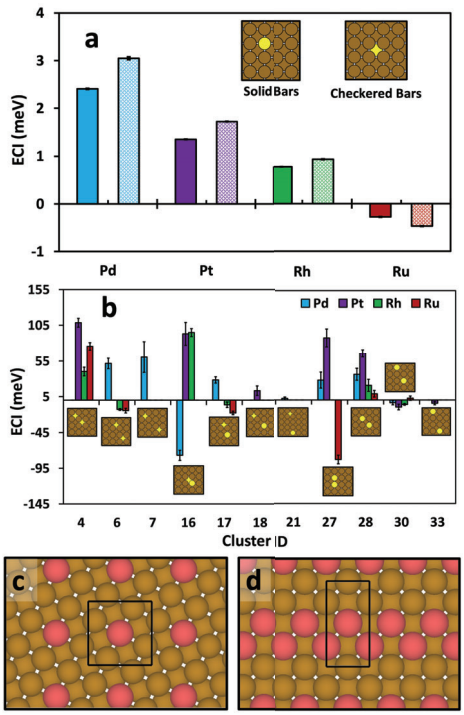

***Figure 1**: **a** and **b** are 1-body and 2-body terms in the LG CEs for the noble metals systems (M/Fe(100), M = Pd, Pt, Fe, Rh and Ru), respectively. **c** is the ground state structure at 0.2 ML while **d** is the ground state structure at 0.5 ML.*

Specific Aim 2: Predict the cooperative effects and concerted behavior on several facets at the surface of a single catalytic grain under hydrodeoxygenation conditions.

We elucidated the influence of applied electric fields on the oxidation of an Fe catalyst by correlating the experimental results to first principles-based models of a single catalytic

grain. We compared the experimental Fe oxidation results (**Figure 2A, B**) with the theoretical surface oxygen distribution on the Fe grain, simulated at an oxygen partial pressure of 1.1×10^{-9} mbar and temperature of 700K (**Figure 2C**). We see that the experimental and theoretical results agree with one another at these conditions—the oxygen coverage is lowest on the more rigid facets, like Fe(024) and Fe(013), whereas it is highest for flatter facets, like Fe(244) and Fe(011). The theoretical results are based on coverage dependent first principles-based oxygen adsorption energies and kubic harmonic expansions, allowing us to use the symmetry of the Fe bcc lattice to expand the adsorption energy of oxygen over the full Fe grain, taking advantage of the underlying symmetry of the grain. Our results indicate that Fe(024) is most sensitive to positive applications of the electric field as compared to the other facets tested.

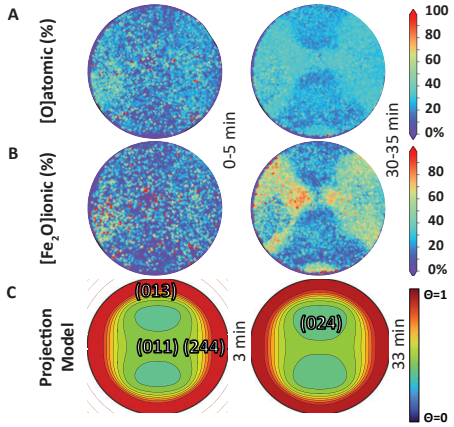

***Figure 2**: 2D projection composition maps of **A** $O(\%)_{atomic}$, **B** $Fe_2O^{n+}{}_{ionic}$ of a Fe specimen exposed to 1.2×10^{-7} mbar of pure O_2 with a constant 23 V/nm applied external electric field (EEF). 2D projection composition maps of **C** corresponding first principles-based model of the evolution of oxygen over a field emitter tip when an EEF of 30.5 V/nm. The experimental composition maps shown are displaying the average composition detected over a 5 min time laps.*

These simulations are also compared between two different models: a model that uses the data from only three facets (termed the '3-facet' model) and a model that uses the theoretical data from all four facets ('4-facet' model) (**Figure 3**). At the lower applied electric field of 25 V/nm, there are differences between the 3-facet and 4-facet models in terms of the overall coverage (**Figure 3 A** and **B**, respectively). The distinct differences in terms of the anisotropy start at the 30.5 V/nm case (**Figure 3 C** and **D**, respectively). The general coverage is the similar in the {244} regions, it seems, but at the (011) and {024} facets, the trends are completely different. At 25 V/nm, the 3-facet model shows a significant decrease in overall oxygen coverage compared to the 4-facet model (i.e., more blue coloring). At 30.5 V/nm, the 3-facet model also indicates no anisotropy on the surface of the tip while there is a clear anisotropy on the 4-facet model where the coverage around the {024} facets is depleted. Experimentally, the Fe grain sees a minimal oxygen coverage at the {024} facets and a higher coverage at the (011) facet under these conditions, so the 4-facet model more

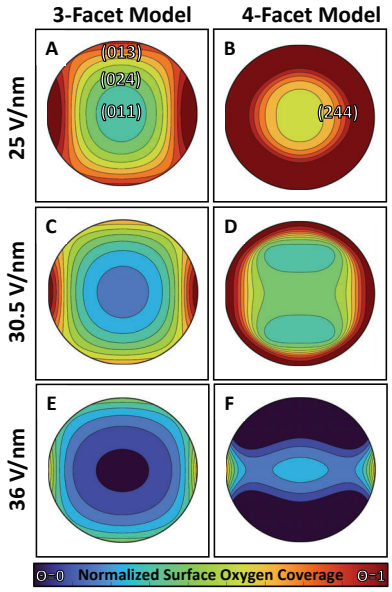

***Figure 3**: Normalized surface oxygen distribution on the Fe grain under equilibrium at 1.1×10^{-8} mbar and 700 K.*

accurately captures that scenario. This comparison highlights the importance of combining theory and experiment together to guide one another through the investigation.

Specific Aim 3: Determine the dominant mechanism for the deoxygenation of phenol on Fe-based catalysts in the presence of Pd, Pt, Rh, Ni, Cu and alkali metal promoters with surface oxygen and water.

The coverage dependence for the adsorption of a series of phenolics was modeled on a Pd(111) catalyst using the mean-field (MF) approach. The aromatics studied here varied in complexity with respect to their functional groups. For most adsorbates investigated, the data fits the linear MF model well, where the only adsorbates with Root-Mean-Square-Errors (RMSE) larger than 50 meV are benzoic acid and salicylic acid. Both adsorbates have a −COOH functional group, suggesting that the MF approach does not work well for carboxylic acids. The Leave-One-Out Cross-Validation (LOO-CV) scores are also under 50 meV for all but those two adsorbates.

For most adsorbates, the adsorption energy values decrease with increasing coverage (**Figure 4**). This is expected since the metal *d*-bands become more filled as the coverage increases, making it harder for subsequent aromatics to adsorb onto the surface. However, for phenoxy and guaioxy, open-shelled aromatics with a free radical, the slopes are nearly-zero, indicating that their adsorption energies have a minimal dependence on the changing coverage. This is likely a result of the stronger impact from the free radical that renders the aromatic highly reactive.

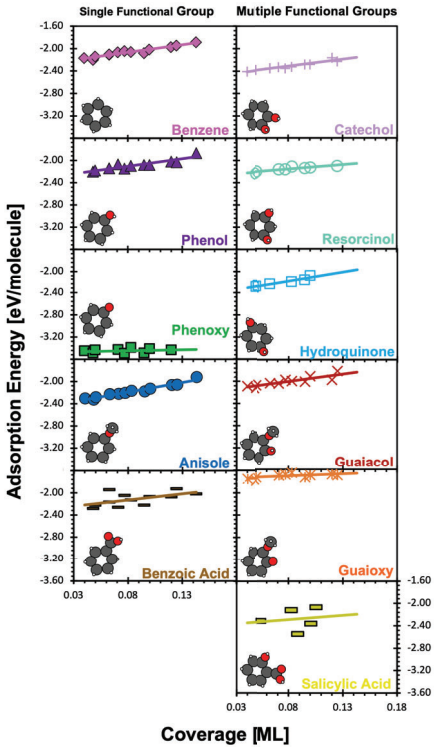

Figure 4: *Adsorption energies as a function of coverage for various aromatics on Pd(111).*

Comparing phenol to benzene, we note that the MF slopes are nearly the same, suggesting that the addition of an −OH functional group has a minimal impact on the coverage-dependent adsorption energies. Anisole has a MF slope that is ~1.5 times larger than that of benzene or phenol (a result of its larger methoxyl functional group), while anisole and guaiacol also have similar slope values, further confirming that the addition of the −OH functional group has a minimal impact on the coverage-dependent adsorption energies. Benzoic acid has a smaller slope than either anisole or phenol despite its much larger functional group, potentially because the large size of −COOH causes the functional group to move farther away from the Pd surface as compared to anisole or phenol, limiting the surface-adsorbate interactions, and thus lowering the MF slope. Catechol, resorcinol, and hydroquinone are also studied here, which represent ortho, meta, and para positions of the secondary hydroxyl functional group. As of now, there are no congruent conclusions to remark on as both resorcinol and hydroquinone are missing half their adsorption data. The aim for including these three aromatics is to determine how the position of the secondary functional group affects the ability to capture the adsorbate-adsorbate lateral interactions.

Publications Acknowledging this Grant in 2019-2023

(I) Intellectually led by this grant

1. Chaudhary, N.; Onyango, I.; Wang, Y.; McEwen, J.-S. Determining Catalytically-Relevant Surfaces Through Coverage-Dependent Lattice Gas Models: Carbon Adsorption on Fe(100) *J. Phys. Chem. C*, **2023**, 127, 14163-14176.

2. Collinge, G.; Hensley, A. J. R.; McEwen, J.-S. Quantifying Errors in Effective Cluster Interactions of Lattice Gas Cluster Expansions *J. Phys. Chem. C*, **2022**, 126, 1289-1302.

3. Shangguan, J.; Hensley, A. J. R.; Morgenstern, L.; Li, Z.; McEwen, J.-S.; Ma, W.; Chin, Y.-H. Bronsted Acidity of H-adatoms at Protic Solvent-Transition Metal Interfaces and its Kinetic Consequences in Electrophilic Addition Reactions *J. Catal.*, **2022**, 408, 179-195.

4. Groden, K.; Vila, F. D.; Li, L., Bare, S. R.; Scott, S. L.; McEwen. J.-S. First Principles Approach to Extracting Chemical Information from X-Ray Absorption Near-Edge Spectra of Ga-Containing Materials *J. Phys. Chem. C,* **2021**, 125, 27901-27908.

5. Hensley, A. J. R; Collinge, G.; Wang, Y.; and McEwen, J.-S. Guiding the Design of Oxidation-Resistant Fe-based Single Atom Alloy Catalysts with Insights from Configurational Space *J. Chem. Phys.*, **2021**, 154, 174709.

6. Hensley, A. J. R.; deJoode, I.; Wang, Y.; McEwen, J.-S. Identifying Trends in the Field Ionization of Diatomic Molecules over Adsorbate Covered Pd(331) Surfaces *Top. Catal.*, **2020**, 63, 1510-1521.

7. Zhang, X.; Chaudhary, N.; Hawkins, M. R.; Cockreham, C. B.; Yang, C.; Shangguan, J.; Hensley, A. J. R.; Chin, Y.-H.; Ha, S.; McEwen, J.-S. Wu, D. Determining the Hydration Energetics on Carbon-Supported Ru Catalysts: An Adsorption Calorimetry and Density Functional Theory Study *Catal. Today*, **2020**, 365, 172-180.

8. Hensley, A. J. R.; Bray, J.; Shangguan, J.; Chin, Y.-H.; McEwen, J.-S. Catalytic Consequences of Hydrogen Addition Events and Solvent-Adsorbate Interactions during Guaiacol-H_2 Reactions at the H_2O-Ru(0001) Interface *J. Catal.*, **2020**, 395, 467-482.

9. Shangguan, J.; Hensley, A. J. R.; Gradiski, M. V.; Pfriem, N.; McEwen, J.-S.; Morris, R. H.; Chin, Y.-H. The Role of Protons and Hydrides in the Catalytic Hydrogenolysis of Guaiacol at the Ruthenium Nanoparticle-water Interface, *ACS Catal.*, **2020**, 10, 12310-12332.

10. Hensley, A. J. R.; Collinge, G.; Wang, Y.; McEwen, J.-S. Coverage Dependent Adsorption of Hydrogen on Fe(100): Determining Catalytically Relevant Surface Structures via Lattice Gas Models, *J. Phys. Chem. C*, **2020**, 124, 7254-7266.

11. Collinge, G.; Groden, K.; Stampfl, C.; McEwen J.-S. Formulation of Multicomponent Lattice Gas Model Cluster Expansions Parameterized on Ab Initio Data: An Introduction to the Ab Initio Mean-Field Augmented Lattice Gas Model Code, *J. Phys. Chem. C*, **2020**, 124, 2923-2938.

12. Chaudhary, N.; Hensley, A.J.R.; Collinge, G.; Wang, Y.; McEwen, J.-S. Coverage-Dependent Adsorption of Phenol on Pt (111) from First Principles, *J. Phys. Chem. C*, **2020**, 124, 356-362.

13. Hensley, A. J. R.; Wang, Y.; McEwen, J.-S. The Partial Reduction of Clean and Doped -Fe_2O_3(0001) from First Principles, *Appl. Catal. A: Gen.*, **2019**, 582, 116989.

14. Wong, B.; Collinge, G.; Hensley, A. J. R.; Wang, Y.; McEwen, J.-S. Benchmarking the Accuracy of Coverage-Dependent Models: Adsorption and Desorption of Benzene on Pt(111) and Pt_3Sn(111) from First Principles, *Prog. Surf. Sci.*, **2019**, 94, 100538.

(II) Jointly funded by this grant and other grants with intellectual leadership by other funding sources

1- Gray, J.; Che, F.; McEwen, J.-S.; Ha, S. Field-Assisted Suppression of Coke in the Methane Steam Reforming Reaction, *Appl. Catal. B: Environ.*, **2020**, 260, 118132.

2- Gray, J.; Wook Kang, S.; Yang, J.-I.; Kruse, N.; McEwen, J.-S.; Chan Park, J., Ha, S. Unravelling the Reaction Mechanism of Formic Acid Decomposition on Highly Dispersed Mo_2C/graphene Nanoparticles Supported on Graphene Flakes, *Appl. Catal. B: Environ.*, **2020**, 264, 118478.

3- Song, J.; Zheng, J.; Zhang, R.; Fu, S.; Zhu, C.; Feng, S.; McEwen, J.-S.; Du, D.; Li, X.; Yuehe, L. Enhancing Chemical Interaction of Polysulfide and Carbon through Synergetic Nitrogen and Phosphorus Doping, *ACS Sustain. Chem. Eng.*, **2020**, 8, 806-813.

4- Bkour, Q.; Che, F.; Lee, K.-M.; Zhou, C.; Akter, N.; Boscoboinik, J. A.; Zhao, K.; Gray, J.; Saunders, S. R.; Norton, M. G.; McEwen, J.-S.; Kim, T.; Ha, S. Enhancing the partial oxidation of gasoline with Mo-doped Ni catalysts for SOFC applications: An integrated experimental and DFT study, *Appl. Catal. B.: Environ.*, **2020**, 266, 118626.

5- Hu, S.; Che, F.; Bita, K.; Mina, J.; Chang Won, Y.; McEwen, J.-S.; Scudiero, L.; Ha, S. Improving the Electrochemical Oxidation of Formic Acid by Tuning the

Electronic Properties of Pd-Based Bimetallic Nanoparticles, *Appl. Catal. B: Environ.*, **2019**, 254, 685-692.

J. Will Medlin

Tailoring the near-surface environment of Rh single-atom catalysts for selective CO_2 hydrogenation

Alex Jenkins, Erin Dunphy, Charles Musgrave, Michael Toney, Will Medlin
Dept. of Chemical and Biological Engineering, University of Colorado

Presentation Abstract

Modification of oxide-supported, atomically dispersed metals with support-bound ligands is a promising strategy towards improving the sintering resistance of these catalysts. It also offers the opportunity to precisely control the positioning of functional groups in the vicinity of a well-defined active site, potentially enabling a new level of control over active site design. We used a combination of experimental spectroscopies, density functional calculations, and vapor-phase reaction studies to investigate the effects of functionalized phosphonic acid (PA) monolayers on CO_2 hydrogenation with Rh_1/TiO_2 single atom catalysts. We found that deposition of specific amine-functionalized ligands resulted in overall improvements to CO_2 reduction turnover frequency and on-stream stability. The effect of the modifier on reactivity was highly sensitive to the proximity of the amine functional group to the surface, which was controlled by adjusting the length of the PA tail. Furthermore, deposition of alkyl PAs without an amine functional group resulted in blocked CO_2 adsorption and a near-complete loss of catalytic activity. Infrared spectroscopy studies suggested that the amine group provided binding sites for CO_2 that enabled hydrogenation when the amine was positioned near a Rh_1 site. PA-modified catalysts exhibited high selectivity to CO over the series product methane; the selectivity effect was traced to modification of the Rh_1 sites to favor CO desorption. PA deposition resulted in a significant loss in accessible Rh_1 sites, likely due to blocking by tail groups. However, even with the loss of sites, under low-temperature reaction conditions the rates of CO_2 hydrogenation were improved with the coatings, indicating that the remaining sites are highly efficient.

DE-SC0005239: Controlling chemistry on atomically dispersed metals with using organic monolayers

PI: Will Medlin, Daniel Schwartz (co-PI)
Postdoc(s): Alex Jenkins
Student(s): Ezra Baghdady, Zachary Meduna

RECENT PROGRESS

Controlling catalyst selectivity with organic monolayers

Coadsorbed organic species including thiolates can promote direct synthesis of hydrogen peroxide from H_2 and O_2 over Pd particles. In work recently published in *Angewandte Chemie*, density functional theory based kinetic modeling (conducted by our collaborator, Henrik Grönbeck),

augmented with activity measurements and vibrational spectroscopy (conducted by our group) were used to provide atomistic understanding of direct H_2O_2 formation over alkylthiolate(RS) Pd. RS species were oxidized during reaction conditions yielding RSO_2 as the effective ligand. The RSO_2 ligand shows superior ability for proton transfer to the intermediate surface species OOH, which accelerates the formation of H_2O_2. The ligands promote the selectivity also by blocking sites for unselective water formation and by modifying the electronic structure of Pd. The work rationalizes observations of enhanced selectivity of direct H_2O_2 formation over ligand-funtionalized Pd nanoparticles and shows that engineering of organic surface modifiers can be used to promote desired hydrogen transfer routes.

Use of monolayers to control surface hydrophobicity in catalysis

Our work over the past year has continued to emphasize using organic monolayers to understand the role of near-surface environment effects on catalysis. We have chiefly
Transfer hydrogenation (TH) of unsaturated hydrocarbons with formic acid (FA) is an attractive processing pathway for the reduction of lignocellulosic pyrolysis oils. The low solubility of hydrophobic bio-oil species in water and FA in oil necessitates the use of a biphasic system as the reaction environment. In a publication last year in *ACS Applied Materials and Interfaces*, we reported the effects of Pd/silica catalyst surface wettability on the TH reaction rate. Modification of the surface with short chain (C1–C4) alkyl silanes resulted in an increase in the reaction rate as compared to the unmodified catalyst. In contrast, modification of the surface with sulfonate (hydrophilic) and C18 alkyl silanes (hydrophobic) resulted in a decrease in the reaction rate as compared to the unmodified catalyst. The results are discussed in terms of the catalyst interfacial activity and relative affinity of the reagents to the Pd active sites. An observed change in the apparent reaction order in styrene for a hydrophilic catalyst suggests that changing catalyst surface wettability from hydrophilic to hydrophobic resulted in a switch from a transport-limited to a kinetic-limited reaction regime.

Tracking particle active motion to understand catalysis

Adsorbate molecules present in a reaction mixture may bind to and block catalytic sites. Measurement of the surface coverage of these molecules via adsorption isotherms is critical for modeling and design of catalytic reactions on surfaces. However, it is challenging to measure isotherms in solution in a way that is directly relevant to catalytic activity under reaction conditions, particularly since adsorbates may bind with an enormous range of surface affinity parameters. In a paper published last year in the *Journal of Colloid and Interface Science*, we used the motion of self-propelled catalytic Janus particles, which employ the decomposition of hydrogen peroxide fuel as a propulsion mechanism, to determine the effective surface coverage of thioglycerol, furfural, and ethanol on a platinum surface as a function of concentration in aqueous solution by measuring the decrease in active motion due to the blocking of active sites. For strongly adsorbing thioglycerol, this effective coverage was compared and contrasted to the total adsorbed amount measured using inductively-coupled plasma analysis. Demonstrating the broad applicability of this approach, the surface affinity of the three adsorbates spanned more than four orders of magnitude. For each species, the adsorbate-mediated attenuation of active motion occurred over a wide concentration range and was well-described by a Langmuir isotherm. The

strongly interacting thioglycerol had the highest affinity towards the surface and fully deactivated the active particle motion at surface saturation. Furfural had an intermediate affinity but did not fully block H_2O_2 access to the surface at apparent saturation, consistent with a maximum fractional surface coverage of $\theta_{max} = 0.67$. Ethanol exhibited even lower affinity and its coverage saturated at only $\theta_{max} = 0.38$. Analysis of isotherms at elevated temperatures enabled direct extraction of the enthalpies of adsorption. The degree of surface coverage at adsorbate saturation appeared to correlate with the relative energies of adsorption for the different adsorbate species and was consistent with adsorbate saturation of one of multiple active site populations towards H_2O_2 decomposition. Moreover, computational investigations into solvent effects on furfural adsorption showed good quantitative agreement with the experimental results. This work leverages unique properties of active particles to explore fundamental catalysis questions and demonstrates a novel paradigm for significant and experimentally accessible multidisciplinary research.

The adsorption strengths of organic compounds on metal surfaces are sensitive to the metal composition, and they play a central role in many catalytic reactions, helping to control the coverage of the reactant and altering the overall reaction rate. While adsorption energies are straightforward to measure and calculate in vacuum and gas-phase environments, adsorption energetics can be dramatically altered by the presence of solvent in liquid-phase reactions. However, the effects of metal composition on binding strengths in a liquid environment are less well understood, primarily due to the difficulty of accurate *in situ* measurements of organic binding on metal surfaces in the liquid phase. In a paper recently published in the *Journal of Physical Chemistry C*, we utilize the motion of active particles in water to probe the adsorption energies of an organic adsorbate (furfural) on a range of metal surfaces (pure Pd, pure Pt, and four PdAu alloy compositions) to elucidate the effect of metal composition. Janus particles with catalytic caps of particular metal compositions all exhibited active motion resulting from consumption of H_2O_2; adsorbate binding was inferred through the decrease in the velocity of active motion and was modeled by a Langmuir adsorption isotherm. The measured adsorption affinities were used to extract the adsorption enthalpy of furfural on the different metals. The Pd surface was found to bind furfural more strongly than the Pt surface by some 10 kJ/mol. Furthermore, the adsorption of furfural on the alloys was found to increase monotonically in magnitude with Pd content.

Publications Acknowledging this Grant in 2020-2023

(I) Intellectually led by this grant

(1) Zhang, J.; Asokan, C.; Zakem, G.; Christopher, P.; Medlin, J. W. Enhancing sintering resistance of atomically dispersed catalysts in reducing environments with organic monolayers. *Green Energy & Environment* **2022**, *7* (6), 1263-1269.
(2) Greydanus, B.; Saleheen, M.; Wu, H.; Heyden, A.; Medlin, J. W.; Schwartz, D. K. Probing surface-adsorbate interactions through active particle dynamics. *J. Colloid Interface Sci.* **2022**, *614*, 425-435.
(3) Chen, L.; Moura, P.; Medlin, J. W.; Grönbeck, H. Multiple Roles of Alkanethiolate‐Ligands in Direct Formation of H2O2 over Pd Nanoparticles. *Angew. Chem.* **2022**, e202213113.

(4) Baghdady, E. A.; Schwartz, D. K.; Medlin, J. W. Effects of Surface Hydrophobicity on Catalytic Transfer Hydrogenation of Styrene with Formic Acid in a Biphasic Mixture. *ACS Appl. Mater. Inter.* **2022**, *14* (29), 33457-33462.
(5) Jenkins, A. H.; Musgrave, C. B.; Medlin, J. W. Altering Linear Scaling Relationships on Metal Catalysts via Ligand–Adsorbate Hydrogen Bonding. *J. Phys. Chem. C* **2021**, *125* (43), 23791-23802. DOI: 10.1021/acs.jpcc.1c07550.
(6) Jenkins, A. H.; Medlin, J. W. Controlling Heterogeneous Catalysis with Organic Monolayers on Metal Oxides. *Acc. Chem. Res.* **2021**, *54* (21), 4080-4090. DOI: 10.1021/acs.accounts.1c00469.
(7) Coan, P. D.; Farberow, C. A.; Griffin, M. B.; Medlin, J. W. Organic Modifiers Promote Furfuryl Alcohol Ring Hydrogenation via Surface Hydrogen-Bonding Interactions. *ACS Catal.* **2021**, *11*, 3730-3739.
(8) Blanchette, Z.; Zhang, J.; Yazdi, S.; Griffin, M. B.; Schwartz, D. K.; Medlin, J. W. Investigating deposition sequence during synthesis of SAM-modified Pd/Al2O3 catalysts. *Catalysis Science and Technology* **2022**, *12*, 2306-2314.
(9) Zhang, J.; Deo, S.; Janik, M. J.; Medlin, J. W. Control of Molecular Bonding Strength on Metal Catalysts with Organic Monolayers for CO2 Reduction. *J. Am. Chem. Soc.* **2020**, *142* (11), 5184-5193.
(10) Greydanus, B.; Medlin, J. W.; Schwartz, D. K. Elucidating the Influence of Metal Surface Composition on Organic Adsorbate Binding Using Active Particle Dynamics. *J. Phys. Chem. C* **2023**, *127* (2), 1006-1014. DOI: 10.1021/acs.jpcc.2c05907

(II) Jointly funded by this grant and other grants with intellectual leadership by other funding sources

(12) Slot, T. K.; Riley, N.; Shiju, N. R.; Medlin, J. W.; Rothenberg, G. An experimental approach for controlling confinement effects at catalyst interfaces. *Chemical Science* **2020**, *11* (40), 11024-11029.

Homocoupling of CE_2 (E = O, S) by polynuclear metal complexes

William R. Buratto, Maria Victoria Lorenzo Ocampo, Bradley W. Musselman, and **Leslie J. Murray***

Homogeneous catalytic reduction of CO_2 to C2 compounds remains rare for molecular species, although well evidenced in heterogeneous chemistry. Arguably, C–C bond formation starting from CO_2 presents a unique opportunity in accessing carbon-neutral chemical precursors. Our lab reported the chemical conversion of CO_2 to oxalate using a chemical reductant and chalcogen-bridged tricopper clusters housed within a cyclophane ligand. Here, advances in understanding the mechanism of that transformation will be presented. Relatedly, we report our discovery of an iron-sulfur cluster supported by a cyclophane ligand that acts as a catalyst for CO_2 homocoupling to oxalate using chemical reductants or under applied potentials. Electrocatalysis occurs with no apparent loss in performance (tested up to 10 h). Reaction conditions can be tuned to alter the product distribution, reminiscent of Saveant's prior proposed work on CO_2 electrolysis and the work of others on metallocarboxylates.

Tunning Cationic Sites in Nonstoichiometric Mixed Metal Oxides for Oxygen Electrocatalysis at Solid/Liquid Interfaces

Eranda Nikolla
Department of Chemical Engineering
University of Michigan-Ann Arbor, Michigan, 48109

Oxygen electrocatalysis at solid/liquid interfaces, which revolves around the reduction and evolution of molecular oxygen (ORR/OER), has become very critical toward shaping the future energy landscape. Nonstoichiometric mixed metal oxides have been explored as promising alternative to precious metal electrocatalysts for these electrochemical transformations given their compositional versatility, providing numerous opportunities to tune their catalytic performance. However, while promising, identification of robust nonstoichiometric metal oxides for these reactions has been often limited by their complexity and lack of effective descriptors of their activity and stability.

Herein, we discuss our efforts, which combine controlled synthesis, advanced characterization, electrochemical kinetic studies, and theory, toward obtaining a fundamental understanding of the underlying factors that govern the energetics of ORR/OER at solid/liquid interfaces. We show that (i) the electronic structure of the transition metal cations in these oxides can be systematically tuned via oxide compositional variations to achieve the outmost reactivity, and (ii) the oxide framework can act as a platform for *in situ* generation of highly catalytically active surfaces under oxidative electrochemical conditions. We highlight the aspects that present opportunities and challenges for using nonstoichiometric, mixed metal oxides for oxygen electrocatalysis at solid/liquid interfaces.

DE-SC0023645/SC0020953: Tuning Catalytically Active Single Sites in Non-stoichiometric, Mixed Metal Oxides for Oxygen Electrocatalysis

PI: Eranda Nikolla
Student(s): Hyungdon Joo (University of Michigan), John Carl A. Camayang (Wayne State University)
Institution: Wayne State University, Detroit, MI (2020/2022), University of Michigan (2022-current)

RECENT PROGRESS

We have focused on developing structure-activity-stability relationships for electrochemical oxygen reduction and evolution (ORR/OER) chemistries on B- and A-site modified nonstoichiometric mixed metal oxides with various crystal structures (R-P oxides, perovskites and pyrochlores) at solid/liquid interfaces. These efforts have involved a combination of controlled synthesis, advanced characterization, and experiments. Below we highlight some of the recent progress.

We have probed the structural changes in nonstoichiometric mixed metal oxides ($A_{n+1}B_nO_{3n+1}$; n=1 (R-P oxide) and n=∞ (perovskite)) that governed their OER activity and

stability as a function of the oxide composition (A=La, Sr, Ca; B=Mn, Fe, Co, and Ni) in alkaline media. These studies were conducted in purified alkaline electrolytes in the absence of meaningful Fe impurities (Fe content <1ppb). We found that the oxides containing alkaline earth metal cations, independent of their composition or crystal phase (R-P oxides or perovskites), underwent surface restructuring as a consequence of alkaline earth metal cation dissolution in the electrolyte, resulting in an *in situ* generation of an amorphous 3*d* transition metal (TM) oxyhydroxide shell on top of the parent oxide core. We attributed the extent of A-site alkaline earth metal dissolution from the oxide to: (i) the oxide crystal phase, with n=1 R-P phases exhibiting higher rates of dissolution as opposed to the n=∞ perovskite phase; (ii) the oxide reducibility (the strength of the metal-oxygen bonds in the oxide structure); and (iii) the lattice strain induced by the differences in the ionic radii of the rare earth and alkaline earth metal cations in mixed A-site compositions. We found that the extent of B-site TM cation dissolution was significantly lower with highly oxophilic metal cations, such as Fe and Mn, exhibiting higher dissolution than Co and Ni. Among all the oxide compositions that we considered in this study, alkaline earth metal containing $A_{n+1}Co_nO_{3n+1}$ exhibited the highest improvement in OER performance as a consequence of restructuring, leading to electrochemical rates (normalized per geometric surface area of the oxide) that were even higher than as-synthesized bulk Co- oxyhydroxide (Co-OOH). The *in situ* generated Co-OOH surface structurers from mixed metal oxide cores were shown to be stable under extended 1000 OER cycles. The insights from this study are critical toward understanding the surface dynamics of nonstoichiometric mixed ion-electronic conducting metal oxides under OER conditions and pave the way for identification of effective design criteria for describing their OER performance in alkaline media.

We have also interrogated the cation compositional effect of Ru-based nonstoichiometric mixed metal oxides on their OER activity and stability in acidic electrolytes. We have considered an array of nonstoichiometric mixed metal oxides with pure Ru in the B-site and variations in the A site cation composition (i.e., $A_xRu_yO_z$; A = Ca, Sr, La, Pr, Sm, Gd; x = 1, 2; y = 1, 2; z = 3, 7) and variations in crystal structures from perovskites to pyrochlores. A modified sol-gel approach was used to synthesize all the oxides explored using $Ru(NO_3)_3NO$ as the Ru precursor. We found that oxide reducibility had an inverse relationship with oxide stability under acidic OER conditions, in which more reducible Ru-based oxides demonstrated inferior stability with higher extent of cation dissolution. Our electrochemical data also showed that oxides with higher measured extent of cationic dissolution also demonstrated onset currents at lower oxidizing potentials, which were consistent with these current contributions stemming from lattice oxygen evolution leading to cation dissolution. To understand the underlying mechanism that governed structural changes of Ru-based nonstoichiometric mixed metal oxides during acid OER, we used detailed characterization to show that these oxides undergo similar structural transformations independent of the A-site composition, however different rates of restructuring were observed dictated by the oxide reducibility.

Publications Acknowledging this Grant in 2019-2022

(I) Intellectually led by this grant:

- Samira S., Camayang J. C. A., Patel K., Gu X-K, Nikolla E.*, "Modulating Catalytic Properties of Targeted Metal Cationic Centers in Nonstochiometric Mixed Metal Oxides for Electrochemical Oxygen Reduction", **ACS Energy Lett.** 2021, 6, 1065−1072.
- Samira S., Hong J., Camayang J. C. A., Sun, K., Hoffman A. S., Bare S. R.*, Nikolla E.*, "Dynamic Surface Reconstruction Unifies the Electrocatalytic Oxygen Evolution Performance of Nonstoichiometric Mixed Metal Oxides", **JACS Au,** 2021, 1, 2224-2241.
- Gu X-K, Camayang J. C. A., Samira S., Nikolla E., "Oxygen evolution electrocatalysis using mixed metal oxides under acidic conditions: Challenges and opportunities"., **J. Catalysis**, 2020, 388, 130-140.
- Joo D., Camayang J. C. A., Hong J., Sun, K., Hoffman A. S., Bare S. R., Nikolla E.*, "Insights on the Factors that Govern the Activity and Stability of Ru-based Mixed Metal Oxides during Acidic Oxygen Evolution Reaction", in preparation.

Highly Reactive Main Group Cations and C-F Activation

Oleg V. Ozerov*, Derek W. Leong, S. Olivia Gunther, Nattamai Bhuvanesh
Department of Chemistry, Texas A&M University, College Station, TX 77842

Presentation Abstract

Our group is exploring advanced strategies for hydrodefluorination of perfluoroalkyl substances (PFAS) utilizing highly Lewis acidic main group cations (e.g., X_3Si^+) as catalysts. We have determined that in order to target fully fluorinated alkanes (such as CF_4, C_2F_6, etc.) in hydrodefluorination, silylium cations more reactive (Lewis acidic) than trialkylsilylium (X= alkyl) are necessary, possible with X = halogen instead of X = alkyl. Silylium cations are typically generated by hydride abstraction from an X_3Si-H silane with a carbocation, most commonly Ph_3C^+. However, the hydride affinity of Ph_3C^+ is insufficient for abstraction of a hydride from X_3Si-H with X groups more electron-withdrawing than an alkyl. To this end, we have devised syntheses of fluorinated trityl salts [(*m,m*-$F_2C_6H_3)_3C$][$HCB_{11}Cl_{11}$] (**F_6Tr^+**) and [$(C_6F_5)_3C$][$HCB_{11}Cl_{11}$] (**$F_{15}Tr^+$**). This presentation will highlight the remarkably high hydride affinities for these "bottlable" **F_6Tr^+** and **$F_{15}Tr^+$** in reactions with silanes, hydrocarbons, and other relevant small molecules. In addition, the presentation will explore the influence of the introduction of main group element halides into hydrodefluorination reaction mixtures

Grant or FWP Number: **New Challenges for C-F Activation with Cationic Main Group Electrophiles, *DE-SC0023280***

Students: Derek W. Leong, Jovanny J. Contreras

RECENT PROGRESS

Preparation of perfluorinated activator

A part of our proposal focuses on the synthesis of silylium (and other main group) cations that are more reactive than trialkylsilylium cations. We view this as necessary for lowering the barrier for reactions with highly electron-poor perfluoroalkanes and perfluoroalkyl chains. In order to access the more reactive silylium cations, we need more reactive but isolable carbocations, to be able to abstract the hydride from more electron-deficient silanes. To this end, we recently reported the preparation of a hexafluorotrityl cation F_6Tr^+ as a $[HCB_{11}Cl_{11}]^-$ salt.[1] It possesses ca. 20% higher hydride affinity than its parent $Tr^+ = [(C_6H_5)_3C^+]$. An even higher hydride affinity is predicted[2] for the perfluorotrityl $F_{15}Tr^+$. Besides, its high hydride affinity, the advantage of $F_{15}Tr^+$ is in that $F_{15}Tr$-H, the product of hydride abstraction, does not possess any aromatic C-H bonds, and thus is not subject to Friedel-Crafts substitution. Friedel-Crafts alkylation can lead to alkylarenes with benzylic positions which can give rise to carbocations that are too stable for the desired HDF reactivity.

Riedel and coworkers recently reported the preparation of $F_{15}Tr^+$ partnered with a $[Al(OTeF_5)_4]^-$ anion. [3] Unfortunately, this anion is not compatible with hydrodefluorination strategies. In addition, the Riedel work largely handled $F_{15}Tr^+$ in solution at low temperature and did not isolate bulk solid samples. We targeted the preparation of $F_{15}Tr[HCB_{11}Cl_{11}]$ and have been able to succeed (Figure 1). The silylium abstraction of trifluoroacetate from $F_{15}Tr\text{-}O_2CCF_3$ works well and the apparently pure solid samples of $F_{15}Tr[HCB_{11}Cl_{11}]$ can be isolated at ambient temperature. $F_{15}Tr[HCB_{11}Cl_{11}]$ is soluble in SO_2Cl_2 and can be characterized by solution NMR techniques.

Figure 1. Synthesis of the perfluorotrityl cation $[HCB_{11}Cl_{11}]$salt.

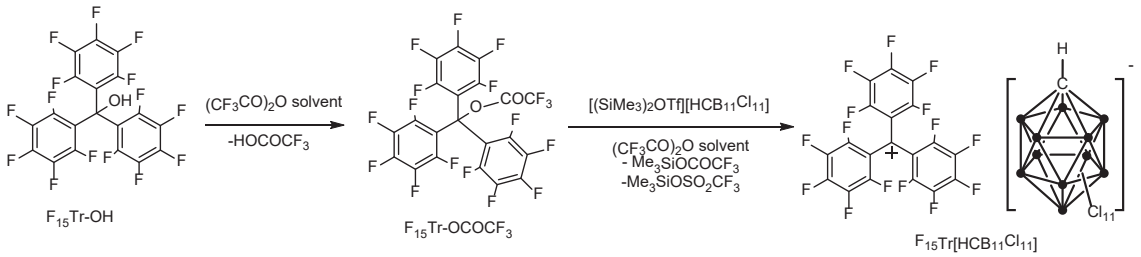

Analysis of additives for perfluoroalkane activation

As part of our attempts to access chloro-substituted silylium cations, we explored HDF reactions involving mixed H/Cl-substituted silanes such as Me_2SiHCl and also mixtures of Et_3SiH with Me_3SiCl or $SiCl_4$. While HDF was possible in the presence of Si-Cl bonds, we observed at best an incremental improvement in some reactions, and worsening of performance in others. We set out to empirically test for the influence of other halides and other fluoridophilic main group elements. Addition of I_2 (produces Si-I and H-I in situ from Si-H), Me_3SiI, BI_3 or AlI_3 to catalytic mixtures using Et_3SiH also had at best a modest positive effect, but often a deleterious one.

Figure 2. HDF of perfluorohexane with a BBr_3 additive.

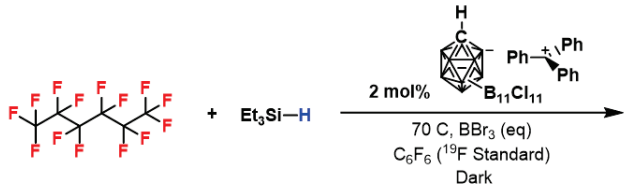

	BX_3	Time (h)	C–F (% conv)[a]	TON
1	BBr_3 (4.66 eq)	120	27	189
		336	27	189
2	BBr_3 (9.32 eq)	120	58	406
		336	74	519

However, we observed improvement of performance under certain scenarios where BBr_3 and $SiBr_4$ was added as a bromine source. In fact, with this additive, for the first time, we observe consumption of a perfluoroalkane (perfluorohexane)! We do not yet have

a complete understanding of the mass balance in these reactions, or of the nature of the influence of the additives. Under catalytic conditions, extensive redistribution of substituents on Si and B can take place. This leads to a rather intimidating number of potential species (both neutral and cationic) that can form in a Et_3SiH/BBr_3/perfluorohexane/Et_3Si^+ mixture. The characterization of the products is also a significant challenge. Although we document disappearance of perfluorohexane, we see only traces of B-F or Si-F bonds formed. Glass is clearly a non-innocent culprit here, but mass balance is difficult even in reactions in hydrocarbon plastics. A certain amount of solid tends to form and we cannot rule out formation of fluorinated polymeric material. Nonetheless, these are very encouraging results.

---

[1] "Isolable fluorinated triphenylmethyl cation salts of $[HCB_{11}Cl_{11}]^-$: demonstration of remarkable hydride affinity", Gunther, S. O.; Lee, C.-I; Song, E.; Bhuvanesh, N.; Ozerov, O. V. *Chem. Sci*. **2022**, *13*, 4972-4976.

[2] "Is the Perfluorinated Trityl Cation Worth a Revisit? A Theoretical Study on the Lewis Acidities and Stabilities of Highly Halogenated Trityl Derivatives", Couchman, S. A.; Wilson, D. J. D.; Dutton, J, L. *Eur. J. Org. Chem*. **2014**, 3902-3908.

[3] "The Tris(pentafluorophenyl)methylium Cation: Isolation and Reactivity", Hoffmann, K. F.; Battke, D.; Golz, P.; Rupf, S. M.; Malischewski, M.; Riedel, S. *Angew. Chem. Intl. Ed*. **2022**, *61*, e202203777.

Publications Acknowledging this Grant in 2020-2023

I. Publications with DOE grant being the lead:

1. Davidson, J. J.; Gunther, S. O.; Leong, D. W.; Ozerov, O. V. Synthesis of Fluorinated Aminium Cations Coupled with Carborane Anions For Use as Strong One-Electron Oxidants, submitted to *Dalton Trans*. (in revision).

Umit S. Ozkan

Fundamental studies of multifunctional electrocatalysis on heteroatom-doped carbon nanostructures (CNx)

Umit S. Ozkan, Dishari Basu, Niharika Vennala, Aravind Asthagiri, Anne Co[1]
The Ohio State University, Department of Chemical and Biomolecular Engineering
[1]The Ohio State University, Department of Chemistry and Biochemistry

Presentation Abstract

Nitrogen-doped carbon nanostructures (CNx) are widely studied for electrocatalytic technologies such as PEM fuel cells and PEM electolyzers, owing to their economic feasibility and versatility. Although they have shown significant activity and stability, they are not as active as their precious metal counterparts. Heteroatom doping with electronegative elements such as oxygen and halogens is an effective strategy to enhance oxygen reduction reaction (ORR) activity of CNx catalysts. In our recent work, we have shown CNx to have potential as both an anode catalyst for bromine evolution reaction (BER) and a cathode catalyst for ORR using oxygen depolarized cathode (ODC) technology. In this reporting period, we have focused on exploring a facile electrochemical bromine doping technique via BER to enhance the ORR activity of CNx. Our results indicate a marked enhancement in the ORR kinetics after CNx was subjected to an intermediate BER treatment.

In our previous work, we also reported CNx to be a potential bifunctional ORR and OER catalyst for regenerative fuel cell applications. It was suggested that oxygenated intermediates adsorbed on CNx at mild potentials during OER. Thus, we focused on tailoring the surface of CNx via oxygen doping through OER to explore the effect on its ORR performance. Our results indicated an improvement in its ORR activity after conducting OER by scanning potentials with a concomitant increase in the relative distribution of pyridinic nitrogen. Pyridinic nitrogen is widely considered to either be an ORR active site or a marker for the true active sites i.e. the adjacent carbon atoms.

While continuing the quest to understand the nature of active sites on CNx for ORR, we have used pos-reaction surface characterization, DFT calculations and used CO_2 as a molecular probe for investigating the nature of ORR active centers in CNx. Thus, our work is targeted towards gaining a fundamental insight into ORR activity over CNx via characterization techniques, molecular probes and DFT calculations.

Grant Number: DE-FG02-07ER15896; **Grant Title:** Fundamental studies of the multifunctional electrocatalysis on heteroatom-doped carbon (CNx) catalysts
PIs: Umit Ozkan (PI), Aravind Asthagiri (Co-PI), Anne Co (Co-PI)
Students: Deeksha Jain, Dishari Basu, Niharika Vennala

RECENT PROGRESS

CO_2 poisoning of CNx for ORR

In this phase of the study, CO_2 was used to probe ORR active sites over CNx in conjunction with DFT models and NAP-XPS experiments. The Lewis basic ORR active sites were reported to have an affinity for acidic CO_2 based on computational results[1, 2]. Electrochemical measurements showed a decrease in the ORR activity of CNx after exposure to CO_2 bubbling in the electrolyte (Fig. 1).

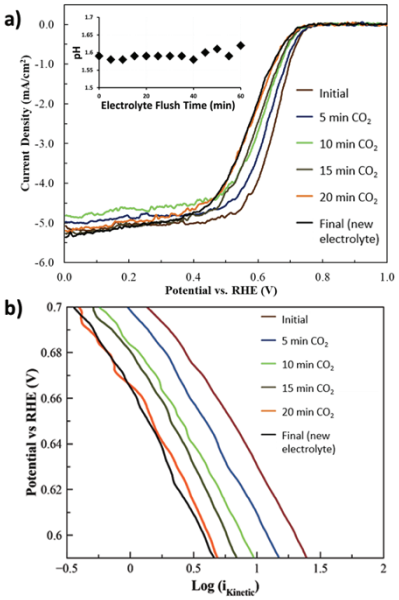

Figure 1: a) Polarization curves b) Tafel Plots for CNx incrementally exposed to CO_2 (1600 rpm, 10 mV/s and 800 $\mu g_{catalyst}/cm^2_{geometric}$). Inset: pH measurements of 0.1 M $HClO_4$ during 70 mL/min CO_2 exposure

NAP-XPS was used to study the differences in nitrogen species distribution of pristine and CO_2-exposed CNx. Fig. 2a -b shows a decrease in the pyridinic N content under UHV conditions for the CO_2-exposed sample. When the two samples are exposed to 2mbar O_2 atmosphere (Fig. 2c-d), pristine CNx shows an increase in N^+O^- species whereas CO_2-exposed CNx shows a decrease. Another observation is that the pristine sample shows a decrease in pyridinic N species when exposed to oxygen, possibly due to oxygenation of these sites whereas the CO_2-poisoned sample shows no difference. These results may suggest a decrease in the O_2 adsorption ability of CNx once it was exposed to CO_2 in a medium similar to the electrolyte for ORR reaction. These results were further corroborated using DFT insights. Based on free energies of reaction to convert CO_2-derived species at ORR onset potentials at 1.1V-RHE, most sites on CNx favor CO_2 (CO_2^*) with only the armchair and basal quaternary sites favoring bicarbonate (HCO_3*) species. Upon comparing the formation of OOH*(first step in ORR) to the stability of the preferred species of CO_2 on the surface, DFT predicts that CO_2* can poison (delay the onset potential of OOH* formation) for basal quaternary, zigzag oxide, and zigzag quaternary, while HCO_3* poisons the armchair and basal quaternary sites. The DFT results suggest that CO_2 can partially poison the ORR on CNx, and both CO_2* and HCO_3* species could play a role, but on different sites.

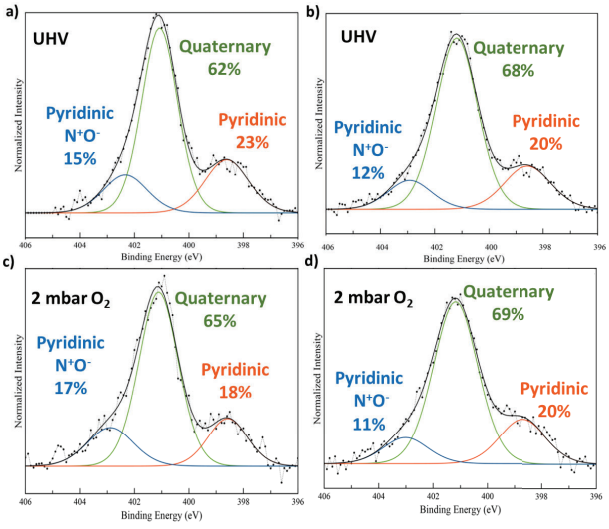

Figure 2: NAP-XPS N1s spectra of a) pristine CNx UHV; b) CO_2- exposed CNx UHV; c) pristine CNx 2 mbar O_2 and d) CO_2-exposed CNx 2 mbar O_2

Effect of electrochemical bromine doping on the performance of CNx for ORR

The ORR performance of CNx was found to be significantly enhanced when the catalyst coated electrode was subjected to an intermediate BER step. After performing the initial ORR step in 0.1M $HClO_4$, 100mM of HBr was added to the electrolyte and the catalyst was subjected to oxidative potentials up to 1.3V under Argon saturation to conduct electrochemical BER. The intermediate potentials after the initial ORR were applied stepwise and holding for 10 minutes at each potential: 1.1 V, 1.2 V and 1.3 V (Fig. 3a). After this BER step, the half-cell vessel was switched and ORR was performed in a fresh 0.1M $HClO_4$ electrolyte. Fig. 3b presents the ORR activity results before and after CNx was subjected to an intermediate BER step.

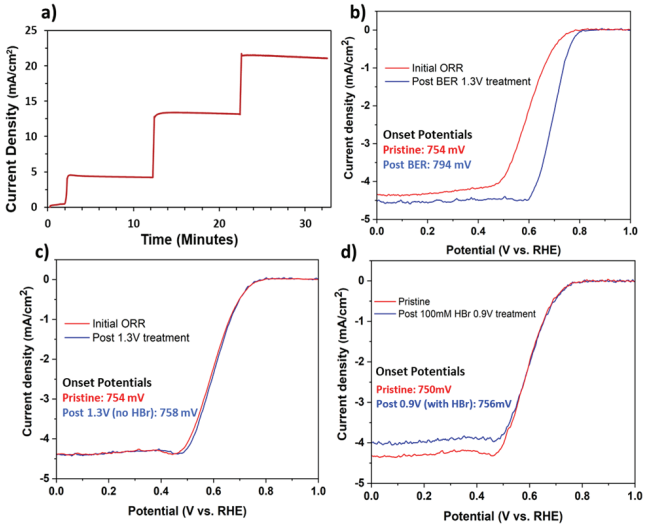

Figure 3: a) The intermediate electrochemical steps for part b) such that potentials after the initial ORR step were applied as chronoamperometric holds in argon saturated 0.1M $HClO_4$ containing 100mM HBr at 1600rpm. Cathodic ORR polarization curves over CNx b) pre and post BER c) pre and post potential application without HBr, d) pre and post BER at 0.9V (O_2 saturated, 1000 rpm, 10 mV/s and 800 $\mu g_{catalyst}/cm^2_{geometric}$)

There is a clear improvement in the ORR activity, likely due to the incorporation of electronegative Br atoms and/or due to creation of defects. Similar observations were made in our earlier work as well as in the other reports[3-5]. To probe if the improved performance was due to the formation of C-Br bonds or simply due to exposure to oxidizing potentials[6], electrochemical ORR activity measurements were performed in 0.1M $HClO_4$ electrolyte before and after subjecting CNx to the intermediate electrochemical steps without dissolved HBr. Fig. 3c shows that the observed ORR activity enhancement in Fig. 3b does not stem from the application of oxidative potentials alone. Another control test was performed to understand the role of the applied potential on BER induced enhancement by performing the intermediate BER step at 0.9V vs RHE. The results indicate that the applied potential of the intermediate BER step plays a role in modulating surface composition for optimum ORR activity as no enhancement is observed when the intermediate BER step is performed at 0.9V which is below the thermodynamic potential of BER i.e., 1.07V. In all cases the selectivity of CNx towards complete reduction to water, determined using Koutecky−Levich technique, remained unchanged after application of potentials with or without dissolved HBr.

Previously ORR activity over CNx has been linked to the presence of pyridinic nitrogen which was said to either be the ORR active site or a marker for the active (carbon adjacent to it) site[7]. XPS was performed on catalysts that went through the same electrochemical histories shown in Fig. 3 and the N1s spectra are presented in Fig. 4. The sample which went through a BER electrochemical step also showed the highest pyridinic N content. While these results provide interesting leads, the mechanism by which the surface is modified by BER electrochemical step is not known and needs further investigation.

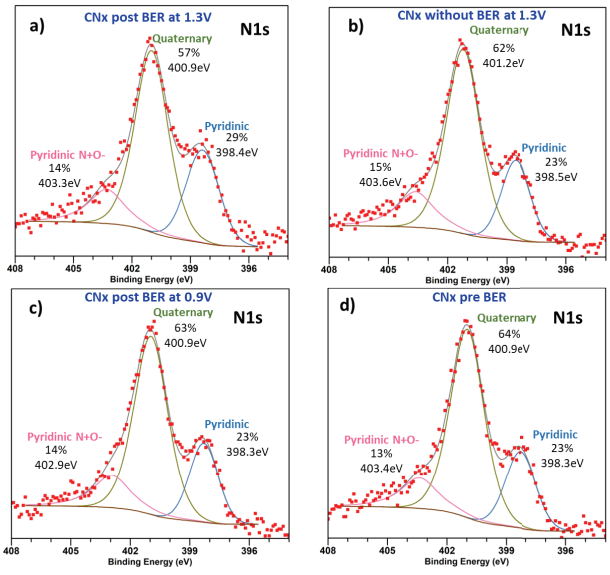

Figure 4: Deconvoluted post reaction N1s spectra of CNx post a) BER at 1.3V for 10 minutes with 100mM HBr b) applying potential at 1.3V for 10 minutes without HBr c) BER at 0.9V for 10 minutes with 100mM HBr d) pre-BER

Enhancement of ORR performance over CNx by anodic activation in acidic medium

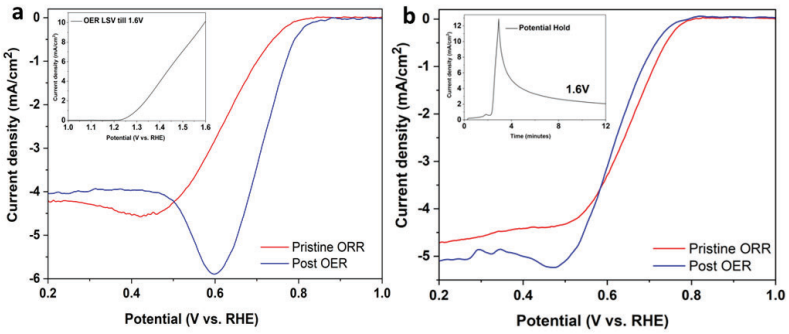

Figure 5: ORR cathodic polarization plots collected at 1000 rpm in O_2-saturated 0.1 M $HClO_4$ (10 mV/s, 800 $\mu g_{catalyst}/cm^2_{geometric}$) over CNx pre and post a) OER LSV till 1.6V b) OER potential hold at 1.6V for 10 minutes

In this work we have shown that OER may be used to "activate" CNx for enhanced ORR activity based on surface changes that occur under oxidative potentials applied during the intermediate anodic OER step. Fig. 5 shows the polarization curves obtained during ORR in oxygen saturated 0.1M $HClO_4$ before and after subjecting CNx to an intermediate OER linear sweep voltammogram (LSV) and chronoamperometric hold at 1.6V for 10 minutes. While a significant improvement was observed in ORR activity following an OER LSV, the effect disappeared upon increasing the duration under oxidative potential. Moreover, this enhancement is lower than that observed over the BER treated sample in the previous section pointing to a different mechanism at play here. Few reports have detailed the changes that occur over carbon based catalysts with application of oxidative potentials which include increase in the electrochemically active surface area and formation of oxygen functional groups [6, 8]. Electrochemical oxidation also leads to surface roughening and creation of surface functional groups resulting in increased capacitance [6, 9, 10]. Post-reaction characterization also revealed that the anodic treatment led to an increase in the surface oxidation levels while tuning the relative composition of nitrogen species. Further insights obtained from DFT computation in conjunction with spectroscopic analysis will be used to decipher the OER-led ORR activation mechanism.

REFERENCES CITED:

1. D. Guo, R. Shibuya, C. Akiba, S. Saji, T. Kondo and J. Nakamura, Science, 2016, 351, 361–365.
2.H. Metiu, S. Chrétien, Z. Hu, B. Li and X. Sun, J. Phys. Chem. C, 2012, 116, 10439–10450.
3.Jain, D.; Hightower, J.; Basu, D.; Gustin, V.; Zhang, Q.; Co, A. C.; Asthagiri, A.; Ozkan, U. S., Journal of Catalysis 2022, 413, 1005-1016.
4.T. Ishizaki, Y. Wada, S. Chiba, S. Kumagai, H. Lee, A. Serizawa, O. L. Li and G. Panomsuwan, Phys. Chem. Chem. Phys., 2016, 18, 21843–21851.
5.Y.-G. Lee and H.-J. Ahn, Applied Surface Science, 2019, 487, 389–397.
6.Y. Yi, J. Tornow, E. Willinger, M. G. Willinger, C. Ranjan and R. Schlögl, ChemElectroChem, 2015, 2, 1929–1937.
7.Mamtani, K.; Jain, D.; Zemlyanov, D.; Celik, G.; Luthman, J.; Renkes, G.; Co, A. C.; Ozkan, U. S., ACS catalysis 2016, 6 (10), 7249-7259.
8.C. Lei, Q. Zheng, F. Cheng, Y. Hou, B. Yang, Z. Li, Z. Wen, L. Lei, G. Chai and X. Feng, Adv. Funct. Mater., 2020, 30, 2003000.
9.Jain, D.; Mamtani, K.; Gustin, V.; Gunduz, S.; Celik, G.; Waluyo, I.; Hunt, A.; Co, A. C.; Ozkan, U. S., ChemElectroChem 2018, 5 (14), 1966-1975.
10.E. Leppänen, S. Sainio, H. Jiang, B. Mikladal, I. Varjos and T. Laurila, ChemElectroChem, 2020, 7, 4136–4143

PUBLICATIONS ACKNOWLEDGING THIS GRANT IN 2020-2023

I. Intellectually led by this grant

1. Jain, D.; Hightower, J.; Basu, D.; Gustin, V.; Zhang, Q.; Co, A. C.; Asthagiri, A.; Ozkan, U. S. Highly Active Nitrogen – Doped Carbon Nanostructures as Electrocatalysts for Bromine Evolution Reaction: A Combined Experimental and DFT Study. *Journal of Catalysis* **2022**, *413*, 1005–1016.

2. Jain, D.; Zhang, Q.; Gustin, V.; Hightower, J.; Gunduz, S.; Co, A. C.; Miller, J. T.; Asthagiri, A.; Ozkan, U. S. Experimental and DFT Investigation into Chloride Poisoning Effects on Nitrogen-Coordinated Iron–Carbon (FeNC) Catalysts for Oxygen Reduction Reaction. *J. Phys. Chem. C* **2020**, *124* (19), 10324–10335.

3. Jain, D.; Gustin, V.; Basu, D.; Gunduz, S.; Deka, D. J.; Co, A. C.; Ozkan, U. S. Phosphate Tolerance of Nitrogen-Coordinated-Iron-Carbon (FeNC) Catalysts for Oxygen Reduction Reaction: A Size-Related Hindrance Effect. *Journal of Catalysis* **2020**, *390*, 150–160.

4. Jain, D.; Ozkan, U. S. Electrocatalytic Applications of Heteroatom-Doped Carbon Nanostructures: Thinking beyond PEM Fuel Cells. In *Catalysis*; Spivey, J., Han, Y.-F., Shekhawat, D., Eds.; *Royal Society of Chemistry: Cambridge*, **2020;** Vol. 32, pp 44–80.

II. Jointly funded by this grant and other grants with intellectual leadership by other funding sources

1. Kim, J.; Kim, Y. J.; Ferree, M.; Gunduz, S.; Co, A. C.; Kim, M.; Ozkan, U. S. In-Situ Exsolution of Bimetallic CoFe Nanoparticles on (La,Sr)FeO3 Perovskite: Its Effect on Electrocatalytic Oxidative Coupling of Methane. *Applied Catalysis B: Environmental* **2023**, *321*, 122026.

2. Kim, J.; Ferree, M.; Gunduz, S.; Co, A. C.; Ozkan, U. S. Sr2Fe2–XMoXO6 Double Perovskites as Electrocatalysts for Oxidative Dehydrogenation of Ethane: Effect of B-Site Stoichiometry. *Electrochimica Acta* **2023**, *461*, 142633.

3. Kim, J.; Ferree, M.; Gunduz, S.; Millet, J. M.; Aouine, M.; Co, A. C.; Ozkan, U. S. Electrocatalytic Oxidative Coupling of Methane on NiFe Exsolved Perovskite Anode: Effect of Water. *ChemCatChem* **2023**, *15* (7), e202201336.

4. Kim, J.; Deka, D. J.; Gunduz, S.; Co, A. C.; Ozkan, U. S. Synergy between the Proton Conducting and a Mixed Electronic and Oxygen Ionic Conducting Phases in a Composite Anode for Electrocatalytic Propane ODH. *Applied Catalysis A: General* **2023**, *658*, 119169.

5. Ferree, M.; Gunduz, S.; Kim, J.; LaRosa, R.; Khalifa, Y.; Co, A. C.; Ozkan, U. S. Enhanced N $_2$ Activation on a Composite Co $_3$ Mo $_3$ N Nitride and La $_{0.6}$ Sr $_{0.4}$ Co $_{0.2}$ Fe $_{0.8}$ O $_3$ Perovskite Cathode for High-Temperature Electrochemical Ammonia Synthesis. *ACS Sustainable Chem. Eng.* **2023**, *11* (13), 5007–5013.

6. Kim, J.; Ferree, M.; Gunduz, S.; Millet, J.-M. M.; Aouine, M.; Co, A. C.; Ozkan, U. S. Exsolution of Nanoparticles on A-Site-Deficient Lanthanum Ferrite Perovskites: Its Effect on Co-Electrolysis of CO $_2$ and H $_2$ O. *J. Mater. Chem. A* **2022**, *10* (5), 2483–2495.

7. Gunduz, S.; Deka, D. J.; Ferree, M.; Kim, J.; Millet, J.-M. M.; Co, A. C.; Ozkan, U. S. Composite Cathodes with Oxide and Nitride Phases for High-Temperature Electrocatalytic Ammonia Production from Nitrogen and Water. *ECS Adv.* **2022**, *1* (1), 014501.

8. Gunduz, S.; Deka, D. J.; Kim, J.; Wilson, M.; Warren, M.; Ozkan, U. S. Incident-Angle Dependent *Operando* XAS Cell Design: Investigation of the Electrochemical Cells under Operating Conditions at Various Incidence Angles. *RSC Adv.* **2021**, *11* (12), 6456–6463.

9. Deka, D. J.; Kim, J.; Gunduz, S.; Aouine, M.; Millet, J.-M. M.; Co, A. C.; Ozkan, U. S. Investigation of Hetero-Phases Grown via in-Situ Exsolution on a Ni-Doped (La,Sr)FeO3 Cathode and the Resultant Activity Enhancement in CO2 Reduction. *Applied Catalysis B: Environmental* **2021**, *286*, 119917.

10. Deka, D. J.; Kim, J.; Gunduz, S.; Jain, D.; Shi, Y.; Miller, J. T.; Co, A. C.; Ozkan, U. S. Coke Formation during High-Temperature CO2 Electrolysis over AFeO3 (A = La/Sr) Cathode: Effect of A-Site Metal Segregation. *Applied Catalysis B: Environmental* **2021**, *283*, 119642.

11. Deka, D. J.; Kim, J.; Gunduz, S.; Ferree, M.; Co, A. C.; Ozkan, U. S. Temperature-Induced Changes in the Synthesis Gas Composition in a High-Temperature H2O and CO2 Co-Electrolysis System. *Applied Catalysis A: General* **2020**, *602*, 117697.

Gerard Parkin

Reactivity of Terminal Magnesium Hydride and Methyl Complexes towards Carbonyl Compounds: Access to Terminal Alkoxide and Enolate Complexes and Catalytic Activity

David Vaccaro and Gerard Parkin
Columbia University, Department of Chemistry

Presentation Abstract

The insertion of unsaturated groups into M–H and M–R bonds are important steps in many catalytic cycles for the conversion of organic compounds. For example, the insertion of CO_2 into M–H and M–Me bonds is of relevance to developing the use of carbon dioxide as a C_1 building block and we have investigated such chemistry with respect to zinc and magnesium compounds. To develop further this chemistry, we have examined the reactivity of terminal Mg–H and Mg–Me bonds in well-defined monomeric compounds, namely [Tism$^{Pr^iBenz}$]MgH and [Tism$^{Pr^iBenz}$]MgMe, towards other carbonyl compounds. In this regard, both [Tism$^{Pr^iBenz}$]MgH and [Tism$^{Pr^iBenz}$]MgMe undergo insertion reactions with non-enolizable carbonyl compounds. For example, Ph_2CO reacts with [Tism$^{Pr^iBenz}$]MgH and [Tism$^{Pr^iBenz}$]MgMe to afford the alkoxide compounds, [Tism$^{Pr^iBenz}$]MgOCHPh_2 and [Tism$^{Pr^iBenz}$]MgOCMePh_2, respectively. In contrast, enolizable carbonyl compounds afford enolate complexes, as illustrated by the reactions of [Tism$^{Pr^iBenz}$]MgH and [Tism$^{Pr^iBenz}$]MgMe to afford [Tism$^{Pr^iBenz}$]MgOC(Me)=CH_2. However, despite that fact that both the hydride and methyl compounds afford the same enolate product, the reactions involve different pathways. Specifically, while the methyl complex [Tism$^{Pr^iBenz}$]MgMe reacts with acetone by protolytic cleavage of the Mg–Me bond to release CH_4 and form the enolate [Tism$^{Pr^iBenz}$]MgOC(Me)=CH_2 directly, the corresponding reaction of the hydride complex [Tism$^{Pr^iBenz}$]MgH occurs by insertion of acetone to afford the isopropoxide [Tism$^{Pr^iBenz}$]MgOPr^i that undergoes a subsequent reaction with acetone to afford the enolate. The observation of two different reaction pathways is associated with the barrier for insertion of a carbonyl group into a Mg–H bond being lower than that for insertion into the Mg–Me bond.

DE-SC0019204: Metal Catalyzed Transformations involving C–X bonds for the Conversions of Carbon Dioxide and Organic Chemicals

Students: David Vaccaro, Aaron Loo and Ran Yan

RECENT PROGRESS

1. Insertion of Carbonyl Compounds into Mg–H and Mg–Me Bonds: Alkoxide Formation

As part of our efforts to develop C_1 chemistry of carbon dioxide we have investigated the insertion of CO_2 into M–H and M–Me bonds in zinc and magnesium compounds. To develop further this chemistry, we have examined the reactivity of [Tism$^{Pr^iBenz}$]MgH and [Tism$^{Pr^iBenz}$]MgMe towards a variety of aldehydes and ketones. Both [Tism$^{Pr^iBenz}$]MgH and [Tism$^{Pr^iBenz}$]MgMe undergo insertion reactions with Ph_2CO to afford the alkoxide compounds, [Tism$^{Pr^iBenz}$]MgOCHPh_2 and [Tism$^{Pr^iBenz}$]MgOCMePh_2, respectively (Figure 1). Likewise, [Tism$^{Pr^iBenz}$]MgH reacts with PhCHO to afford [Tism$^{Pr^iBenz}$]MgOCH_2Ph, while [Tism$^{Pr^iBenz}$]MgMe reacts with PhCHO to afford [Tism$^{Pr^iBenz}$]MgMOCH(Me)Ph. Although the formation of magnesium alkoxide derivatives

from carbonyl compounds is precedented by the well-known reactivity of Grignard reagents, there are very few examples of the insertion of aldehydes and ketones into a terminal Mg–H bond.

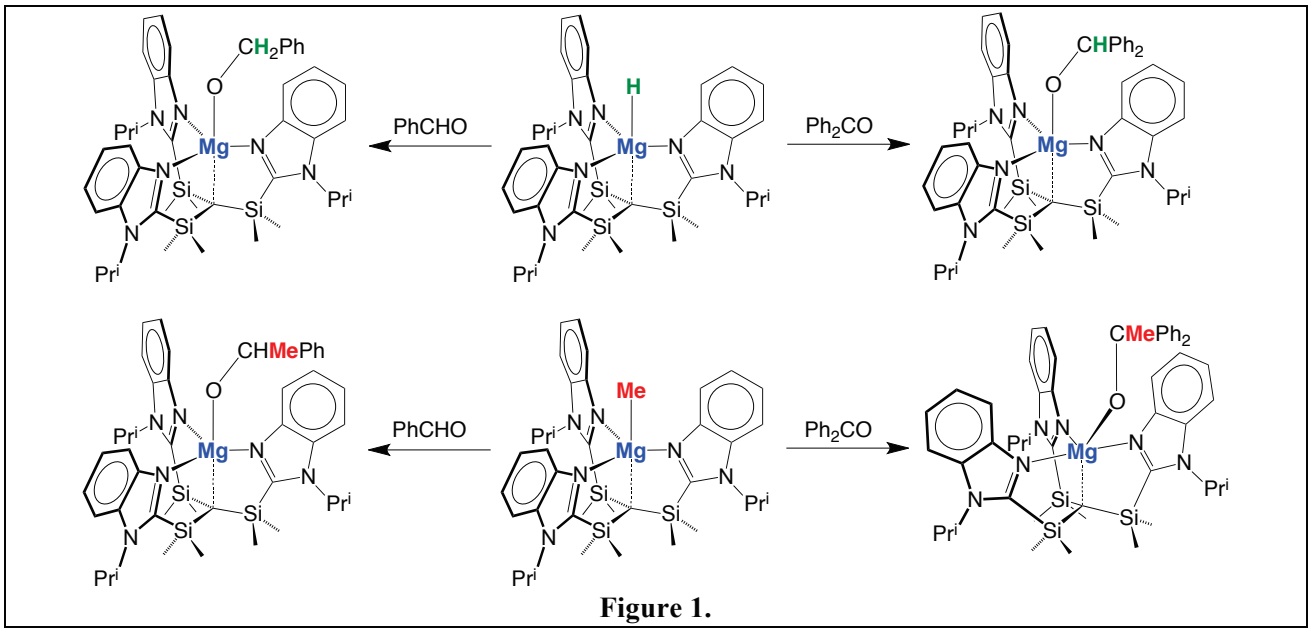

Figure 1.

The molecular structures of [Tism$^{Pri Benz}$]MgOCH$_2$Ph, [Tism$^{Pri Benz}$]MgOCHPh$_2$ and [Tism$^{Pri Benz}$]MgOCMePh$_2$ have been determined by X-ray diffraction and the M–O–R bond angles for [Tism$^{Pri Benz}$]MgOR range from 140.6(6)˚ to 149.21(17)˚, with the largest value corresponding to that for [Tism$^{Pri Benz}$]MgOCMePh$_2$. Although these bond angles are larger than the CSD average [140.0˚], they are much smaller than that observed for other L$_n$MgOCMePh$_2$ compounds that possess an almost linear Mg–O–R bond angle. To address the impact of varying the Mg–O–R bond angle on the stability of a magnesium alkoxide compound, the energy of [Tism$^{Pri Benz}$]MgOCH$_2$Ph as a function of Mg–O–C bond angle was evaluated by DFT geometry optimization, as illustrated in Figure 2. Significantly, the energy of the molecule varies relatively little on bending the Mg–O–C moiety; for example, the energy of the molecule changes by less than 1 kcal mol^{-1} over the range 130˚ to 175˚. Thus, the M–O–R moiety is rather flexible.

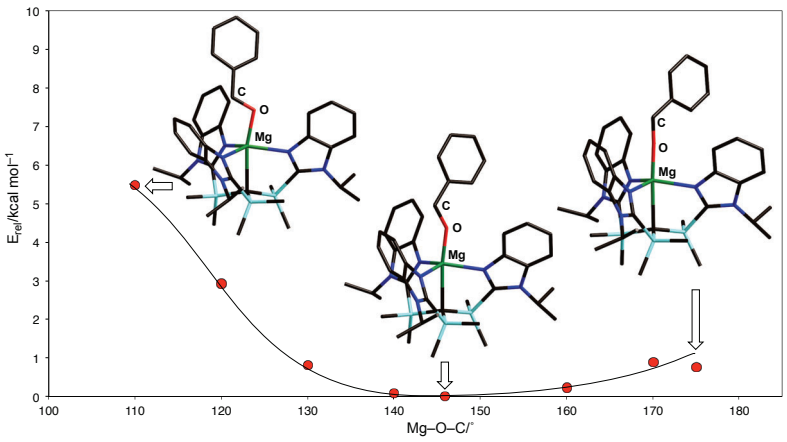

Figure 2.

2. Reactivity of Mg–H and Mg–Me Bonds Towards Enolizable Ketones: Magnesium Enolate Formation

In contrast to insertion of the carbonyl groups of Ph_2CO and PhCHO into the Mg–Me bond, [Tism^{PriBenz}]MgMe reacts with acetone to form the enolate compound, [Tism^{PriBenz}]MgOC(Me)=CH_2, and eliminate CH_4 (Figure 3).

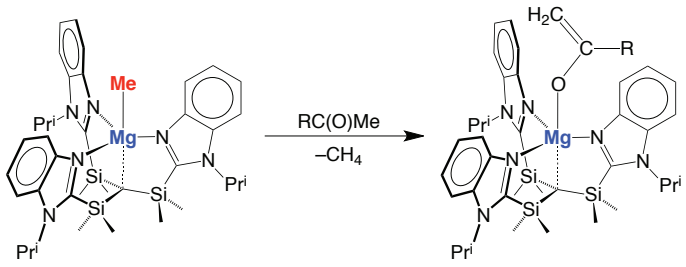

Figure 3.

The molecular structure of [Tism^{PriBenz}]MgOC(Me)=CH_2 has been determined by X-ray diffraction and is not only of significance because there are no other structurally characterized magnesium enolate compounds derived from acetone but also because there are few structurally characterized derivatives for other metals, in contrast to *C*–bound acetonyl isomers, $L_nMCH_2C(O)Me$, that are relatively common. While a variety of pathways are possible for formation of an enolate, it must be emphasized that the formation of [Tism^{PriBenz}]MgOC(Me)=CH_2 is atypical for the reaction of Grignard reagents with acetone, which preferentially form t-butoxide derivatives.

The hydride compound, [Tism^{PriBenz}]MgH, also reacts with acetone and acetophenone to yield the enolate compounds, [Tism^{PriBenz}]MgOC(Me)=CH_2 and [Tism^{PriBenz}]MgOC(Ph)=CH_2; interestingly, however, the enolate compounds are not the initially formed products (Figure 4). Specifically, acetone and acetophenone undergo preferential insertion into the Mg–H bond to generate the corresponding alkoxide, [Tism^{PriBenz}]MgOPr^i and [Tism^{PriBenz}]MgOCH(Me)Ph, which convert to the respective enolate in the presence of excess ketone. These observations indicate that insertion of the C=O group into the Mg–H bond is more facile than insertion into the Mg–Me bond relative to protolytic cleavage of the Mg–H and Mg–Me bonds.

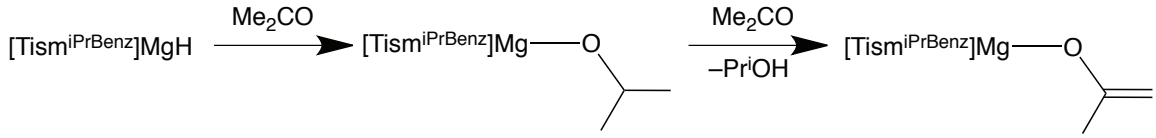

Figure 4.

3. Comparison of the Insertion of Carbonyl Compounds into Mg–H and Mg–Me Bonds

The relative ability of the hydride and methyl compounds to undergo insertion of carbonyl compounds into the Mg–H and Mg–Me bonds has been addressed computationally, with the transition states for acetone being illustrated Figure 5. In each case, the four-membered transition states are approximately planar and, as would be expected, the shape of the four-membered structures for insertion of the carbonyl moiety into the Mg–H and Mg–Me moieties differ considerably as a consequence of the different size of Me *versus* H. For example, the Mg–C–C bond angle (68.9˚) for insertion of acetone into the Mg–Me bond is much more acute than the Mg–H–C bond angle (83.6) for insertion into the Mg–H bond.

The barrier for insertion of the carbonyl group into the Mg–H bond is calculated to be considerably lower than that for insertion into the Mg–Me bond (Figure 5). The significantly higher barrier for insertion of acetone into the Mg–Me bond than the Mg–H bond is consistent with the observation that, rather than undergo insertion, acetone forms the enolate derivative, [Tism^{PriBenz}]MgOC(Me)=CH_2 with elimination of methane.

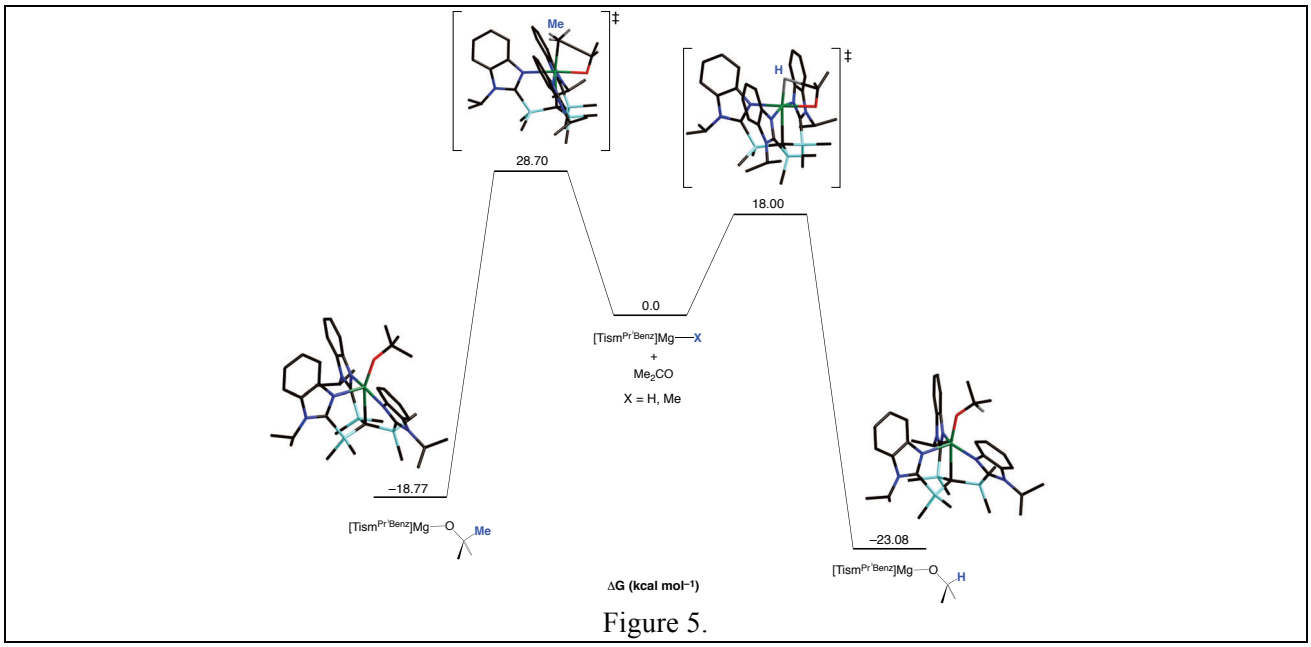

Figure 5.

4. Catalytic Activity of [Tism^{PriBenz}]MgOR Derivatives

[Tism^{PriBenz}]MgOR derivatives also participate in catalytic transformations. For example [Tism^{PriBenz}]MgX (X = H, Me) reacts with diacetone alcohol to form the enolate derivative resulting from C–C bond cleavage, [Tism^{PriBenz}]MgOC(Me)=CH_2, in contrast to ketolate derivatives that have been observed in other systems; as such it is a very efficient catalytic system for the retro-aldol conversion (Figure 6).

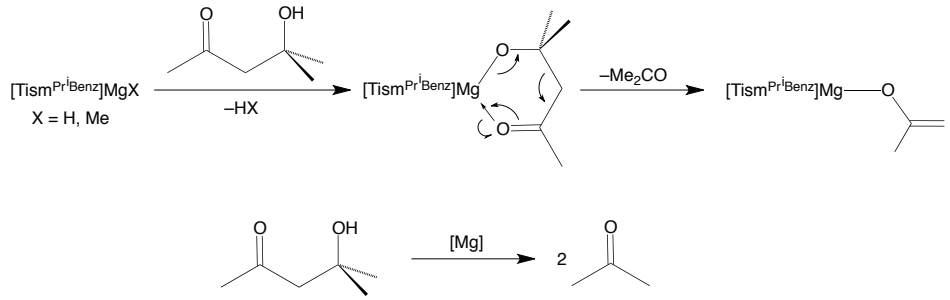

Figure 6.

In addition, [Tism^{PriBenz}]MgOR also catalyze (i) the Tishchenko reaction, converting ArCHO to $ArC(O)OCH_2Ar$, and (ii) hydroboration of ketones, converting Ph_2CO to $Ph_2C(H)OBpin$.

5. Catalytic Reduction of CO_2 and Carbonyl Compounds Mediated by Terpyridine Zinc Formate

Our previous investigations have demonstrated that zinc hydride compounds are capable of effecting catalysis of the reduction of CO_2 and carbonyl compounds. For example, the catalytic reduction of CO_2 by the tris(pyridyl)methylzinc hydride compound, [Tptm]ZnH, occurs *via* the initial insertion of CO_2 into the Zn–H bond to generate the formate complex, $[Tptm]ZnO_2CH$. In view of this participation of zinc formate species in catalytic cycles, we have evaluated the potential of other zinc formate compounds. For example, we have used terpyridine (terpy) to synthesize and structurally characterize the zinc formate compound, $(terpy)Zn(O_2CH)_2$, which serves as a catalyst for reducing CO_2 to the formic acid and methanol oxidation levels. For example, in the presence of $(terpy)Zn(O_2CH)_2$, CO_2 reacts with pinacolborane (HBpin) to afford HCO_2Bpin and MeOBpin. In addition, $(terpy)Zn(O_2CH)_2$ catalyzes the reduction of PhC(O)Me by $PhSiH_3$ to afford $PhSiH[OC(Me)Ph]_2$ and $PhSi[OC(Me)Ph]_3$.

Publications Acknowledging this Grant in 2020-2023

(I) Intellectually led by this grant

1. Shlian, D. G.; Amemiya, E.; Parkin, G. Synthesis and Structural Characterization of *Bis*(2-pyridylthio)methyl Zinc Hydride and the Catalytic Hydrosilylation and Hydroboration of CO_2 *Chem. Commun.* **2022**, 58, 4188-4191.
2. Ruccolo, S.; Sambade, D.; Shlian, D. G.; Amemiya, E.; Parkin, G. Catalytic Reduction of Carbon Dioxide by a Zinc Hydride Compound, [Tptm]ZnH, and Conversion to the Methanol Level *Dalton Trans.* **2022**, 51, 5868–5877
3. Sambade, D.; Collins, C.; Parkin, G. Structure and Bonding of 1,2,4-Triazole Thiones Derived from Nitron *J. Mol. Struct.* **2021**, *1231*, 129682.
4. Ruccolo, S.; Amemiya, E.; Shlian, D. G.; Parkin, G. Hydrosilyation of CO_2 Using a Silatrane Hydride: Structural Characterization of a Silyl Formate Compound *Can. J. Chem.* **2021**, *99*, 259-267.
5. Quinlivan, P. J.; Loo, A.; Shlian, D. G.; Martinez, J.; Parkin, G. *N*-heterocyclic Carbene Complexes of Nickel, Palladium and Iridium Derived from Nitron: Synthesis, Structures and Catalytic Properties *Organometallics* **2021**, *40*, 166-183.
6. Rauch, M.; Strater, Z.; Parkin, G. Methods for Preparing Formaldehyde from Carbon Dioxide US Patent # 11,111,199 (September 7, 2021).
7. Sattler, W.; Shlian, D. G.; Sambade, D.; Parkin, G. Synthesis and Structural Characterization of *Bis*(2-pyridylthio)(*p*-tolylthio)methyl Zinc Complexes and the Catalytic Hydrosilylation of CO_2 *Polyhedron* **2020**, *187*, 114542.
8. Amemiya, E.; Loo, A.; Shlian, D. G.; Parkin, G. Rhenium versus Cadmium: An Alternative Structure for a Thermally Stable Cadmium Carbonyl Compound *Chem. Sci.* **2020**, *11*, 11763-11776.

(II) Jointly funded by this grant and other grants with intellectual leadership by other funding sources

1. Parkin, G. Impact of the Coordination of Multiple Lewis Acid Functions on the Electronic Structure and v^n Configuration of a Metal Center *Dalton Trans.* **2022**, *51*, 411-427.

PCET Mediators for Reductive Electrocatalysis

Jonas C. Peters*, Pablo Garrido-Barros, Matthew J. Chalkley, Joseph Derosa, Mengdi Li, Enric Adillon, John Ovian, Alexander I. Alabugin, Jonas Baumgärtner
California Institute of Technology, Division of Chemistry and Chemical Engineering

Presentation Abstract

Proton-coupled electron transfer (PCET) reactions can provide a powerful strategy for mediating reductive transformations, with new approaches being pursued to generate *in situ* highly reactive H-atom equivalents as intermediates. Conceptually related PCET approaches also hold promise for reductive small molecule catalysis, as for N_2-to-NH_3 conversion (N_2RR), where high barriers can otherwise result in kinetically inefficient pathways. The development of new classes of highly reactive organometallic species featuring homolytically very weak (20 – 40 kcal•mol^{-1}) X–H bonds has therefore been of interest to us. Such species can facilitate reductive PCET reactions with challenging substrates, including unsaturated organic derivatives to generate synthetically versatile α-radical intermediates. Mediators we have pursued most recently as part of this DOE award facilitate the rapid co-localization of a proton and an electron equivalent, affording strong substrate reduction capacity via PCET from an N-H bond ($BDFE_{N-H}$< 40 kcal•mol^{-1}), while kinetically suppressing the hydrogen evolution reaction (HER). They are therefore attractive in terms of reductive electrocatalysis; preferential substrate selectivity relative to HER is a major challenge in reductive electrocatalysis. To achieve this goal our mediator design combines a redox active center (e.g., a metallocene) with a tethered but electronically insulated Brønsted base. This approach allows us to drive multi-electron/proton reductive transformations at an applied bias tuned to the redox center and anodic of background HER catalyzed by the electrode in the presence of partner Brønsted acid. We have studied examples of reductive transformations catalyzed by the mediator, as well as reductive transformations that feature a tandem transition metal co-catalyst. We are also studying second generation mediators to expand their scope, and probing fundamental aspects of how these reactions proceed.

Grant or FWP Number: Organometallic PCET mediators for reducing unsaturated substrates (DE-0235032)

Postdocs: Joseph Derosa, John Ovian, Pablo Garrido-Barros,
Students: Alexander I. Alabugin, Jonas Baumgärtner, Mengdi Li, Enric Adillon, Matthew J. Chalkley

Publications Acknowledging this Grant in 2020-2023 (the following publications are under the primary scope of this DOE Award)**:**

Deegan, M. M.; Hannoun, K. I.; Peters, J. C. Dihydrogen Adduct (Co–H_2) Complexes Displaying H-Atom and Hydride Transfer. *Angew. Chem. Int. Ed.* **2020**, 59, 22631–22637.

Gu, N. X.; Oyala, P. H.; Peters, J. C. H2 Evolution from a Thiolate-Bound Ni(III) Hydride. *J. Am. Chem. Soc.* **2020**, 142, 7827–7835.

Chalkley, M. J.; Drover, M. W.; Peters, J. C. Catalytic N_2-to-NH_3 (or -N_2H_4) Conversion by Well-Defined Molecular Coordination Complexes. *Chem. Rev.* **2020**, 120, 5582–5636.

Chalkley, M. J.; Garrido-Barros, P.; Peters, J. C. A molecular mediator for reductive concerted proton-electron transfers via electrocatalysis. *Science*. **2020**, 369, 850-854.

Schild, D. J.; Drover, M. W.; Oyala, P. H.; Peters, J. C. Generating Potent C–H PCET Donors: Ligand-Induced Fe-to-Ring Proton Migration from a Cp*Fe^{III}–H Complex Demonstrates a Promising Strategy. *J. Am. Chem. Soc.* **2020**, *142*, 18963-18970.

Derosa, J.; Garrido-Barros, P.; Peters, J.C. Electrocatalytic Reduction of C–C π-Bonds via a Cobaltocene-Derived Concerted Proton–Electron Transfer Mediator: Fumarate Hydrogenation as a Model Study. *J. Am. Chem. Soc.* **2021**, 143**,** 9303-9307.

Garrido-Barros, P.; Derosa, J.; Chalkley, M.J.; Peters, J.C. Tandem electrocatalytic N_2 fixation via concerted proton-electron transfer. *Nature* **2022**, 609, 71-76.
Note: This publication was jointly funded by NIGMS (075757), an award focused on aspects of Fe- (and other metal) mediated nitrogen fixation. The study falls within the primary intellectual domain of this DOE award given its focus.

Derosa, J.; Garrido-Barros, P.; Peters, J.C. Electrocatalytic Ketyl-Olefin Cyclization at a Favorable Applied Bias Enabled by a Concerted Proton-Electron Transfer Mediator. *Inorg. Chem.* **2022**, 61, 6672-6678.

Derosa, J.; Garrido-Barros, P.; Li, M.; Peters, J.C. Use of a PCET mediator enables a Ni-HER electrocatalyst to Act as a Hydride Delivery Agent. *J. Am. Chem. Soc.* **2022***,* 144, 20118-20125.

Ibrahim, A.F.; Garrido-Barros, P.; Peters, J.C. Electrocatalytic Nitrogen Reduction on a Molybdenum Complex Bearing a PNP Pincer Ligand. *ACS Catal.* **2023**,13, 72-78.
Note: This publication was jointly funded by NIGMS (075757), an award focused on aspects of Fe- (and other metal) mediated nitrogen fixation. The study intellectually prioritized by the NIH Award but with overlap and support via this DOE award.

Peters, J.C. Advancing electrocatalytic nitrogen fixation: insights from molecular systems. *Faraday Discuss.* **2023**, 243, 450-472.
Note: This publication was jointly funded by NIGMS (075757), an award focused on aspects of Fe- (and other metal) mediated nitrogen fixation. The study intellectually prioritized by the NIH Award but with overlap and support via this DOE award

Development of an integrated multiscale methodology for simulating electrocatalysis at the metal oxide – electrolyte interface

Craig Plaisance
Louisiana State University, Cain Department of Chemical Engineering

Presentation Abstract

We are currently working to formulate and implement a multiscale simulation for electrocatalysis at the metal oxide – electrolyte interface. The first aim of this work is to develop an efficient framework for performing tight binding molecular dynamics (TBMD) simulations of the aqueous electrolyte. The TB Hamiltonian will be constructed using a machine learning (ML) based approach that parametrizes the short-range one- and two-electron integrals as sums of nonlinear two- and three-body terms. Long-range interactions are treated by a linear scaling multipole expansion approach that we have formulated and implemented in Python withing the Atomic Simulation Environment. A unique aspect of the TB Hamiltonian is that a machine-learned perturbative polarization scheme is utilized to account for distortion of the valence atomic orbitals from their spherically symmetric forms in the reference atomic configuration.

After implementing the method for calculating the TB Hamiltonian within Python and VASP, we will then focus on implementing a method for solving for the TB wave function. This will be done using a linear scaling operator expansion form of the wave function that can be expressed in terms of local interactions. The result will be an efficient TB calculation that scales linearly with system size. Once the approach is functioning for the bulk electrolyte, we will begin working on the description of the oxide surface and its interaction with the electrolyte.

Grant or FWP Number: Development of an integrated multiscale methodology for simulating electrocatalysis at the metal oxide – electrolyte interface

Postdoc(s): Ujjal Sardar
Student(s): Nkechi Kingsley

RECENT PROGRESS

Implementation of an efficient linear-scaling multipole expansion method for computing long range electrostatic interactions

A key part of our approach is that the energy and TB Hamiltonian are separated into long-range and short-range contributions according to,

$$E = E_{\mathrm{SR}} + E_{\mathrm{H}}[\tilde{\rho}]$$
$$H_{\mu\nu} = H_{\mu\nu}^{\mathrm{SR}} + \widetilde{H}_{\mu\nu}$$

The long-range contributions are due to Coulombic interactions between non-overlapping charge densities and can therefore be calculated using a multipole expansion method. To due this, we construct a *soft charge density* $\tilde{\rho}$ according to,

$$\tilde{\rho}(r) = \sum_i \tilde{\rho}_i^{\mathrm{ref}}(r) + \sum_{\mu\nu} \Delta P_{\mu\nu} \tilde{\rho}_{\mu\nu}(r)$$

where $\tilde{\rho}_i^{\mathrm{ref}}$ is the soft charge density of atom i in the atomic reference state and $\tilde{\rho}_{\mu\nu}$ is the soft overlap charge density between TB orbitals μ and ν. This latter quantity is constructed to have the same moments as $\rho_{\mu\nu}(r) = \phi_\mu^*(r)\phi_\nu(r)$ but a much longer radial extent that is based on the distance cutoff R_{cut} for the short-ranged interactions. The elements of the TB Hamiltonian based on these soft charge densities are given by,

$$\widetilde{H}_{\mu\nu} = \langle \tilde{\rho}_{\mu\nu} \widehat{U} \tilde{\rho} \rangle$$

where $\widehat{U}$ is the Coulomb operator.

The soft charge density is constructed in real space using a linear-scaling algorithm that takes advantage of the limited radial extent R_{cut} of the contribution from each atom. The electrostatic potential is then computed in reciprocal space, making use of fast Fourier transforms. Finally, the elements of $\widetilde{H}_{\mu\nu}$ are evaluated in real space using a similar linear-scaling algorithm used to construct the charge density. The algorithm has been implemented in Python and is found to require less than 10 s for a 100-time step AIMD trajectory on a system of 96 water molecules, running on a single laptop core. It was found that using R_{cut} values greater than 3 Å does not result in a sufficient increase in computational speed. This corresponds to a grid spacing of 0.3 Å, which is similar to the spacing used in VASP to represent the soft charge density.

Formulation of a machine-learning framework for calculating atomic orbital integrals

The short-range contributions to the energy and Hamiltonian are given by,

$$E_{\mathrm{SR}} = E_{\mathrm{ref}} + \sum_{\mu\nu} \Delta P_{\mu\nu} h_{\mu\nu}^{\mathrm{SR}} + \frac{1}{2} \sum_{\mu\nu\alpha\beta} \Delta P_{\mu\nu} W_{\mu\nu,\alpha\beta}^{\mathrm{SR}} \Delta P_{\alpha\beta}$$

$$H_{\mu\nu}^{\mathrm{SR}} = h_{\mu\nu}^{\mathrm{SR}} + \sum_{\alpha\beta} W_{\mu\nu,\alpha\beta}^{\mathrm{SR}} \Delta P_{\alpha\beta}$$

and require the evaluation of atomic orbital integrals $h_{\mu\nu}^{\mathrm{SR}}$ and $W_{\mu\nu,\alpha\beta}^{\mathrm{SR}}$ in the tight binding basis along with evaluation of the energy E_{ref} in the reference electronic configuration. PI Plaisance recently formulated a framework for efficiently evaluating these integrals within a ML framework that is based on decomposition of the tight binding orbitals into a valence component $|\phi_\mu^{\mathrm{val}}\rangle$ and a polarization component. The assumption is made that the polarization component can be treated as a first order perturbation and expressed linearly in terms of the tight binding occupancy matrix $\Delta P_{\kappa\lambda}$ as,

$$|\phi_\mu\rangle = |\phi_\mu^{\mathrm{val}}\rangle + \sum_{\kappa\lambda} \Delta P_{\kappa\lambda} |\Delta^{\kappa\lambda} \phi_\mu\rangle$$

Using this form, the short-range integrals can be expressed in terms of valence contributions and polarization contributions,

$$h_{\mu\nu}^{\mathrm{SR}} = h_{\mu\nu}^{\mathrm{SR,val}} + \sum_{\kappa\lambda} \Delta P_{\kappa\lambda} \Delta^{\kappa\lambda} h_{\mu\nu}^{\mathrm{SR}}$$

$$W^{\mathrm{SR}}_{\mu\nu,\alpha\beta} = W^{\mathrm{SR,val}}_{\mu\nu,\alpha\beta} + \sum_{\kappa\lambda} \Delta P_{\kappa\lambda}\, \Delta^{\kappa\lambda} W^{\mathrm{SR}}_{\mu\nu,\alpha\beta}$$

An additional assumption is made that the valance and polarization contributions in these expressions can be expressed as a sum of nonlinear two- and three-atom contributions,

$$f = f_0 + \sum_{ij} f_{ij}(r_{ij}) + \sum_{ijk} f_{ijk}(r_{ij}, r_{jk}, r_{ik})$$

where r_{ij} is the distance between atoms i and j. The sums only extend over the atoms on which the relevant atomic orbitals ($\mu\nu\alpha\beta\kappa\lambda$) are centered. This corresponds to the approximation that the joint spatial overlap between a set of atomic orbitals centered on more than two atoms is negligible. The integrals can be evaluated during an ab initio molecular dynamics (AIMD) simulation performed in VASP, making use of the quasi-atomic orbital method implemented previously by PI Plaisance to define the tight binding basis. Subtracting off the long-range contribution (calculated using the multipole expansion method discussed above) gives the short-range integrals,

$$h^{\mathrm{SR}}_{\mu\nu} = h_{\mu\nu} - \langle \tilde{\rho}_{\mu\nu} \hat{U} \tilde{\rho}_{\mathrm{ref}} \rangle$$
$$W^{\mathrm{SR}}_{\mu\nu,\alpha\beta} = W_{\mu\nu,\alpha\beta} - \langle \tilde{\rho}_{\mu\nu} \hat{U} \tilde{\rho}_{\alpha\beta} \rangle$$

The next step is to implement the method for calculating the TB Hamiltonian within Python and train the ML model using AIMD performed in VASP.

Publications Acknowledging this Grant in 2020-2023

N/A

Anchoring Active Sites for Enhanced Catalyst Performance in Dry Reforming of Methane

Junyan Zhang[1], Meijia Li[1], Yuanyuan Li[1], Zili Wu[1,2], Zhenzhen Yang[1], Sheng Dai[1,3], Felipe Polo-Garzon[1]

[1]Chemical Sciences Division, [2]Center for Nanophase Materials Sciences, Oak Ridge National Laboratory, Oak Ridge, TN 37831; [3]Department of Chemistry, University of Tennessee, Knoxville, TN 37996

The overarching goal of our catalysis program is to control reaction pathways and enhance catalyst stability through detailed tuning of active sites and their local and extended environment. In dry reforming of methane (DRM), two greenhouse gases, CH_4 and CO_2, are converted into syngas ($CO+H_2$), which is a platform mixture to produce a variety of chemicals. DRM is highly endothermic and is conducted at high temperature. Thus catalysts must be resistant to sintering and coke formation. State-of-the-art catalysts for DRM are Ni-based and despite they offer stable performance for at least 500 h of TOS at 800 °C, however, they still present deactivation at moderate temperatures (650 °C). At these moderate temperatures, coke formation is more thermodynamically favorable. Here, we present our current research on strategies to control the metal-support interaction of Ni active sites to limit sintering and coke formation in DRM reaction.

Spatial confinement strategy: Dealuminated Beta zeolite (BEA) was chosen as the catalyst support for Ni active sites. Dealumination of the structure served two purposes: reduction of the acid sites, where coke is typically generated, and creation of anchoring sites for Ni sites. The confinement of Ni sites in the zeolitic structure was hypothesized to provide enhance stability towards sintering, along with hindered coke formation on Ni single atoms (SA). By means of a finely tuned synthesis procedure, we were able to tune the structure of Ni sites as (SA) or nanoparticles (NP). Kinetic isotopic experiments showed the intrinsically higher reactivity of Ni NP compared to Ni SA; however, the SA dispersion balances out the higher reactivity of NPs to provide similar macroscopic conversion. Furthermore, the interaction of Ni SA with the zeolite structure provided enhance stability with time-on-stream, and negligible coke deposition. XAS experimentation unveiled the details of the synthesis process that allow enhancing the Ni SA-zeolite interaction and led to remarkable catalytic performances for DRM.

Configurational entropy confinement strategy: In an alternative strategy to stabilize Ni active sites, high entropy oxides (HEOs) were used as DRM catalysts, where the entropy of mixing in a multi-component solid solution is hypothesized to provide enhanced catalyst stability. To test the hypothesis, we studied DRM over an HEO catalyst ($NiMgCuCoZnO_x$) where 5 elements were included. XAS of the spent samples showed mixed valence states of Ni species, indicating a high resistance to reduction of the Ni sites stabilized in HEO. This resistance could potentially decelerate the commonly observed sintering of Ni species during DRM. When only Cu was removed from the structure (NiMgCoZnOx), the catalyst exhibited superior reactivity and stability in comparison to the HEO, even surpassing the widely-studied NiMgOx sample with higher Ni loading. Understanding the bonding and electronic structure of the operating HEO and HEO-derived catalysts is currently underway.

Research supported by the U.S. Department of Energy, Office of Science, Basic Energy Sciences, Chemical Sciences, Geosciences, and Biosciences Division, Catalysis Science Program. This research is part of FWP ERKCC96: Fundamentals of Catalysis and Chemical Transformations. For a full description of recent progress see Extended Abstract for ERKCC96.

Robert M Rioux

Catalytic Reactions at Solid-Liquid Interfaces: Solvent Effects on Activity, Selectivity and Reaction Mechanisms

Robert M Rioux[1,2] (PI), Yanyu Mu[1], Tianze Xie[1], Jeonghwan Lee[1], Kathryn MacIntosh[1]
[1]Department of Chemical Engineering and [2]Department of Chemistry, The Pennsylvania State University, University Park, PA 16802

Presentation Abstract

The impact of solvent effects during acid- and metal-catalyzed heterogeneous reactions are explored through a combination of explicit thermodynamic and kinetic measurements. Liquid-phase isothermal titration calorimetry (ITC) is used to probe the interaction of acid site titrants and alkanol substrates (for eventual catalytic dehydration) in solvents and solvent mixtures of different character to quantify the thermodynamic description of adsorption from the solvent phase. Thermochemical Born-Haber cycles to rationalize the influence of solvent on apparent thermodynamics have been constructed utilizing additional information from gas-phase adsorption calorimetry, equilibrium adsorption isotherms and solution thermodynamics. Reaction rates quantified per available acid site and selectivity for alkanol dehydration will be measured under conditions of variable intrapore solvent concentration and structure, from solvent-free (gas-phase) to the incipient intrapore condensation. Reaction rates will be rigorously defined utilizing non-ideal thermodynamic formalisms for each intrapore environment examined. Apparent differences in acid site availability based on the solvent type and structure included in zeolite pores have been probed by liquid-/gas- phase calorimetry and *in-situ* titration during catalytic turnover. We examine the impact of a unique solvent environment – molten metal – during the catalytic hydrogenation of ethylene. The metallic Ga solvent containing low quantity of Pd serves as an ample reservoir for ethylene, while the absorption of H_2 is deficient in the bulk Ga phase. The catalytic reaction occurs in the bulk Ga liquid under ethylene-rich conditions regardless of the gas-phase ethylene and H_2 partial pressures.

DE-SC0016192: Catalytic Reactions at Solid-Liquid Interfaces: Solvent Effects on Activity, Selectivity and Reaction Mechanisms

PI: Robert M Rioux
Postdoc(s): Kathryn MacIntosh, Jeonghwan Lee
Student(s): Yanyu Mu, William Elliott
Affiliations(s): The Pennsylvania State University

RECENT PROGRESS

Dependence of aqueous phase acid-base interactions on the Si/Al ratio

ITC thermograms for the adsorption of pyridine on three different H-ZSM-5 samples (Si/Al=11.5, Si/Al=40 and Si/Al=140) at 25°C in water are shown in **Figure 1** Apparent enthalpies do not vary with coverage for all three zeolites when the titration ratio is less than 0.1 – 0.2 mol base/mol BAS. The apparent enthalpy depends on the hydrophilicity of zeolites and increases with increasing the Si/Al ratio of zeolites when water is used as

solvent. The enthalpy of acid-base interaction for the most hydrophilic H-ZSM-5 (Si/Al=11.5) is slightly less negative compared to the H-ZSM-5 (Si/Al=40), but is ~20 kJ/mol less than the value for the most hydrophobic H-ZSM-5 (Si/Al=140). The heat associated with dilution, hydrogen bonding between pyridine and silanol groups of zeolites and van der Waals interactions between pyridine and zeolite framework during the injection of aqueous pyridine into the zeolite suspension in ITC is small compared to the heat released due to acid-base interactions (Figure S10) and is not considered when calculating the reaction enthalpy. The concentration of silanol groups of H-ZSM-5 (Si/Al=40) is similar to BAS, however, ^{15}N SS NMR characterization of adsorbed pyridine on H-ZSM-5 (Si/Al=40) from aqueous solution at room temperature (Figure S11) only shows a signal associated with pyridinium (~200 ppm). There is no resonances associated with pyridine adsorption on silanol groups (~290 ppm) since silanol groups are unable to protonate pyridine and interact weakly with pyridine through hydrogen bonding, similar to pyridine interactions with water. The ^{15}N pyridine chemical shift associated with Si-O-H-pyridine (~290 ppm) is similar to the chemical shift associated with H_2O-pyridine (~300 ppm).

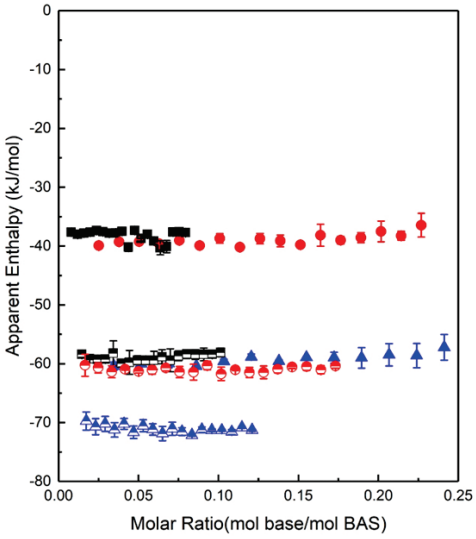

Figure 1. ITC thermograms for adsorption of pyridine (filled points) and isopropylamine (semi-transparent points) on H-ZSM-5 (Si/Al = 11.5 (black square), Si/Al = 40 (red circle) and Si/Al = 140 (blue triangle)) at 25°C in water. Error bars represent the standard deviations of three to five independent measurements in three different ITC instruments.

Gas-phase enthalpies for pyridine adsorption on three H-ZSM-5 zeolites were measured to be about -200 kJ/mol and were similar between the zeolites with different Si/Al ratio (the difference is less than 5%). According to the gas-phase Born-Haber cycle, the experimentally measured gas-phase adsorption enthalpy of pyridine on H-ZSM-5 is the sum of the deprotonation energy of the BAS, an intrinsic property of the zeolites and can only be estimated from calculations, gas-phase proton affinity of the probe base and interactions between gas-phase ion and framework anion which is orientation-dependent and includes hydrogen bonding, electrostatic and van der Waals interactions. The enthalpy measured in ITC is determined by the proton affinity of pyridine and interactions between pyridinium and zeolite framework in the presence of surrounding water molecules as well as the energetic penalty to displace water molecules from BAS inside zeolite pores to bulk water. Water molecules adjacent to the zeolite proton stabilize the proton by forming water clusters, therefore inhibiting the transfer of the proton to pyridine. Water molecules also stabilize pyridinium but to a lesser extent than the proton because the larger size of pyridinium leads to a higher degree of charge delocalization. The adsorption of pyridine on BAS leads to displacement of water molecules inside zeolite pores which also decreases the extent to which pyridinium is stabilized by water molecules. Compared to the adsorption enthalpy measured in the gas phase, the enthalpy measured in aqueous phase is about 150 kJ/mol lower which arises from a different extent of enthalpic stabilization of

relevant gas-phase states by water molecules. It has been reported that water stabilizes the acidic proton to a greater extent relative to the protonated transition state which leads to lower reactivity of a Brønsted acid catalyst, lower proton transfer equilibrium constant during the process of pyridine adsorption on acidic zeolites and higher temperature required to desorb pyridine from acidic zeolites in aqueous phase.

Enthalpies of adsorption of pyridine from the aqueous phase on zeolites with different Si/Al ratio do not reflect differences in intrinsic acidity of the zeolite BAS which has been widely accepted to be their deprotonation energy and independent of Si/Al ratio, locations of BAS and framework type. The measured enthalpy of adsorption of pyridine on BAS of zeolites in water increases with increased hydrophobicity of zeolites due to the lower quantity of adsorbed water inside hydrophobic zeolite pores, therefore decreasing the extent of enthalpic stabilization of proton and pyridinium by water molecules. Water adsorption isotherms and adsorption enthalpies on zeolites before and after pyridine adsorption were measured to understand how the hydrophobicity of zeolites influences the uptake of water molecules and the interaction between adsorbed water molecules and zeolites. For all three zeolites, the enthalpy of adsorption of pyridine on BAS of zeolites in water are about 10 - 20 kJ/mol lower than the adsorption enthalpy of isopropylamine (IPA). However, the gas-phase adsorption enthalpy of pyridine is -200 kJ/mol, similar to the value for IPA (-205 kJ/mol) due to similar gas-phase proton affinity of the probe bases. The pKa of the conjugate acid for pyridine and IPA are 5.23 and 10.63, respectively, indicating IPA is more basic than pyridine in water. The enthalpy of protonation of bases in dilute aqueous solution ($\Delta H_{prot,s0}$) is another scale to characterize aqueous basicity of bases, the values for pyridine and IPA are -20 kJ/mol and -58 kJ/mol, respectively. The higher basicity of IPA in aqueous solution leads to higher adsorption enthalpy on BAS of zeolites. Another possible reason why the adsorption of IPA releases more heat is the smaller effective ionic radius of IPA which leads to higher heat of hydration than pyridinium. Fewer water molecules are displaced from zeolite pores after IPA is adsorbed on BAS, therefore, a decreased enthalpic penalty incurs to displace water molecules from BAS inside zeolite pores to bulk water.

Influence of ACN-water mixture composition on the thermodynamic parameters and the uptake of pyridine by H-ZSM-5 (Si/Al=40)

The apparent enthalpies and stoichiometry of pyridine adsorption on BAS of H-ZSM-5 (Si/Al=40) in ACN-water mixtures obtained from the single-site fitting model are presented in Figure 2. In the case of water, the apparent enthalpy (ΔH_1) and stoichiometry (n_1) were obtained using multiple-sites fitting. The multiple-sites model does not fit well in the first sigmoid region which leads to lower estimation of n_1 (data not shown). We believe the adsorption stoichiometry of pyridine on BAS of H-ZSM-5 (Si/Al=40) in water is as high as 1 which can be clearly proved using the modified single-site model. The adsorption enthalpies of pyridine on BAS of H-ZSM-5 (Si/Al=40) in ACN-water mixtures are lower than the value in pure water or pure ACN. We also measured the initial adsorption enthalpies by titrating low concentration of pyridine solutions (5mM) to zeolite suspensions to control the titration ratio (mol pyridine/mol BAS) less than 0.1 and compared initial enthalpies with the fitted enthalpies obtained from the single-site model as shown in Figure 2a. The initial enthalpies are consistent with the fitted enthalpies over the whole examined range of concentrations which proves there isn't mass transportation limit during the process of pyridine adsorption on BAS of H-ZSM-5 (Si/Al=40) at 25 °C.

The apparent enthalpy is the lowest in the ACN-rich solutions (99mol% ACN mixtures) which is about 15 kJ/mol lower than the value in pure ACN.

The lower adsorption enthalpies indicate the difference between solvating initial state and final state by solvent molecules is greater. It is influenced by (1) the different uptake of solvent mixtures before and after pyridine adsorption and (2) different local solvation conditions of BAS and pyridinium. The existence of microheterogeneity in ACN-water mixtures may enhance the structure of water clusters around BAS which leads to more stabilized initial state. Therefore, the enthalpy penalty of pyridine displacing water clusters to be adsorbed on BAS is higher and apparent adsorption enthalpy is lower. The Gibbs energy of transfer of proton from water to ACN-water mixtures is negative indicating the mixtures (X_{ACN} < 70 mol%) are more basic than water, therefore, proton is more stabilized in water.

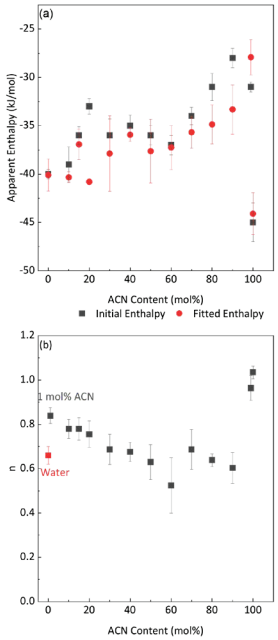

Figure 2.(a) Apparent enthalpies of adsorption of pyridine on BAS of H-ZSM-5 (Si/Al=40) in ACN-water mixtures at 25 °C. Red data points are obtained from the single-site model fitting. Black data points are initial adsorption enthalpies obtained by controlling the titration ratio less than 0.1. (b) Adsorption stoichiometry obtained from the single-site model fitting (black data points). For water, the stoichiometry (n_1) was obtained from the multiple-sites model fitting.

The adsorption stoichiometries of pyridine on BAS of H-ZSM-5 (Si/Al=40) in ACN-water mixtures are lower than the water-rich and ACN-rich solutions. In 1 mol% ACN, 99 mol% and pure ACN, the adsorption stoichiometries are 0.84, 0.96 and 1.03, respectively (Figure 2B). In other ACN-water mixtures, the adsorption stoichiometry is lower than 1 and the minimum value is 0.52 in 60 mol% ACN mixtures. Lower apparent adsorption enthalpies in ACN-water mixtures are possibly contributing to the low adsorption stoichiometries. There are solvated BAS not accessible to pyridine anymore in ACN-water mixtures due to preferential solvation environment and large enthalpy penalty involved in the adsorption process. But in the case of 99 mol% ACN mixture, the stoichiometry is as high as 0.96 even though the apparent enthalpy is only -30.8 kJ/mol. It indicates the re-arrangement of solvent molecules as reflected in favorable entropy also plays roles in the adsorption of pyridine on BAS of H-ZSM-5 (Si/Al=40) in ACN-water mixtures. In the case of mixtures with high ACN content, even though the apparent adsorption enthalpy is lower, but the re-arrangement of water clusters around the BAS possibility leads to favorable entropy change. The addition of water to acetonitrile leads to microheterogeneity in the solution where each of the components are preferentially surrounded by molecules of the same kind. The microstructure of water-acetonitrile changes with the mole fraction of acetonitrile which has been widely studied. Therefore, the structure of acetonitrile after mixing with water becomes more disordered than before mixing.

Publications Acknowledging this Grant in 2019-2022

(I) Intellectually led by this grant

1. Xie T., Rioux, R. M., Catalytic influence of light element incorporation in the lattice of palladium. *Catal. Today* **2021**, *371*, 29-39.
2. J. W. Chang, A. Armaou, R. M. Rioux. Continuous-injection isothermal titration calorimetry for in-situ evaluation of thermodynamic binding properties of ligand-receptor binding models. *J. Phys. Chem. B* **2021**, *125*, 8075-8087.
3. Mu, Y., Elliott, W.A., Lee, J., Zaman, Z., Rioux, R. M. Effect of Water on Acid-Base Interactions in Solid Acids: A Comprehensive Calorimetric Evaluation. Nature Chemistry **2023** resubmitted, under review
4. Chang, J. W., Mu, Y., Armaou, A., Rioux, R. M. Direction determination of high affinity binding constants by continuous injection isothermal titration calorimetry. *J. Phys. Chem. B* **2023** under review.

(II) Jointly funded by this grant and other grants with intellectual leadership by other funding sources

1. Mellmer, M. A., Sanpitakseree, C., Ma, K., Demir, B., Elliott, W. A., Bai, P., Johnson, R. L., Shanks, B. H., Rioux, R. M., Neurock, M., Dumesic, J.A. Effects of Chloride Ions in Acid-Catalyzed Biomass Dehydration Reactions in Polar Aprotic Solvents. *Nature Comm*. **2019**, *10*, 1132.
2. Garg, A., Goncalves, D., Liu, Y., Wang, Z., Wang, L., Yoo, J. S., Kolpak, A., Rioux, R. M., Zanchet, D., Román-Leshkov, Y. Impact of Transition Metal Carbide and Nitride Supports on the Electronic Structure of Thin Platinum Overlayers. *ACS Catal.* **2019**, *9*, 7090-7098.
3. Wang, Z., Garg, A., Wang, L., He, H., Dasgupta, A., Zanchet, D., Janik, M. J., Rioux, R. M., Román-Leshkov, Y., Enhancement of Alkyne Semi-Hydrogenation Selectivity by Electronic Modification of Platinum. *ACS Catal.* **2020**, *10*, 6763-6770.
4. Guo, Y., He, H., Liu, X., Chen, Z., Rioux, R. M., Janik, M. J., Savage, P. E., Ring-opening and hydrodenitrogenation of indole under hydrothermal conditions over Ni, Pt, Ru and Ni-Ru bimetallic catalysts. *Chem. Eng. Sci*. **2021**, *406*, 126853.
5. Mahdavi-Shakib, A., Sravan Kumar, K. B., Whittaker, T. N., Xie, T., Rioux, R. M., Grabow, L. C., Chandler, B. D., Kinetics of H_2 Adsorption at the Metal-Support Interface of Au/TiO_2 Catalysts using the Broad Background IR Absorbance. *Angew. Chem. Int. Ed*. **2021**, *60*, 7735-7743.
6. Mahdavi-Shakib, A., Whittaker, T. N., Yun, T. Y., Sravan Kumar, K. B., Rich, L. C., Wang, S., Rioux, R. M., L. C. Grabow, B. D. Chandler. The role of surface hydroxyls in the entropy-driven adsorption and spillover of H_2 on Au/TiO_2 catalysts. *Nature Catal*. **2023***, 6*, 710-719.

Caroline T. Saouma

Towards electrostatic modulation of the thermochemistry of a Ru hydrogenation catalyst

Caroline T. Saouma, Abhijit Bera
University of Utah, Department of Chemistry

Presentation Abstract

The advancement of fuel cells and chemical hydrogen batteries are promising technologies to advance clean energy. These technologies necessitate that both reductive and oxidative reactions be feasible, ideally using the same catalyst that can be tuned to favor each reaction type. For example, a chemical hydrogen battery may require the interconversion of CO_2 and H_2 with formic acid. Towards this end, we are exploring how electrostatic fields impact the thermodynamic parameters of a Ru hydrogenation catalyst. We hypothesize that when appended at an electrode and a potential is applied, the resulting electrostatic field will modulate the hydricity of acidity of the catalyst. We propose that the rate of catalysis and/or the rate determining step can be controlled by the electrostatic field, allowing for oxidative and reductive reactions to occur from the same catalyst. My poster will describe the rationale for our approach, as well as our progress on preparing catalysts that are amenable to electrode attachment.

Grant or FWP Number: Electric Fields to Modulate Catalyst Thermochemical Properties for Multi-Electron/Multi-Proton Redox Reactions

PI: Caroline T. Saouma
Postdoc(s): Abhijit Bera
Affiliations(s): University of Utah, Department of Chemistry

RECENT PROGRESS

Synthesis of ligands for surface attachment.
Work on this new project has focused on the preparation of ligands suitable for attachment to a gold surface. Our target ligand is 6-((ditertbutylphosphaneyl)methyl)-2,2'bipyridine, with a thiolate (or thioester) at either the 4 or 4' position of the bipyridine ring. Over the past few months, progress has been made on developing high-yielding syntheses of the ligand precursors; each ligand is made in 3-4 steps. We are cautiously optimistic that we have prepared 2 of the 4 ligands, and are now in position to metalate Ru with them and initiate our studies on how electrostatic fields impact catalysis and catalyst thermodynamics.

Publications Acknowledging this Grant in 2020-2023
None.

Fluxional Nature of Heterogeneous Catalysts

Philippe Sautet, Geng Sun, Simran Kumari, Anastassia N. Alexandrova
Chemical and Biomolecular Engineering dep., University of California Los Angeles
Chemistry and Biochemistry dep., University of California Los Angeles

Presentation Abstract

We will show that heterogeneous catalysts are not static but dynamic, fluxional, metastable and that they strongly evolve under reaction conditions, creating new active sites, not present for the as prepared catalysts. The first example will concern Pt clusters (Pt_7 to Pt_{13}) under hydrogen pressure and their reactivity for alkane dehydrogenation. The approach combines Density Functional Theory, high-dimensional Neural Networks and evolutionary techniques. It also includes grand canonical global optimization to study variable amount of adsorbed hydrogen and novel constrained global optimization methods to determine the structure of the cluster active site that provides the lowest barrier for the reaction. We show, with methane activation on supported Pt clusters and by an explicit sampling of cluster configurations at the transition state, that important restructuring is required to reach the most active transition state. The capability of the cluster to reconstruct, simultaneously with the C-H dissociation, is a key aspect for catalytic activity. The second example deals with the nature of the zirconia on copper inverse catalyst under the conditions of CO_2 hydrogenation to methanol. We consider a model three atom Zr cluster on a Cu(111) surface decorated with various O, OH and formate ligands, noted $Zr_3O_x(OH)_y(HCOO)_z$/Cu(111), revealing major changes in the active site induced by various reaction parameters such as the gas pressure, temperature, conversion levels, and CO_2:H_2 feed ratios. Calculations provide insights into the dynamic behavior of the catalyst. Specifically, under reaction conditions, we observe a large number of compositions and structures with similar free energy for the catalyst, with respect to changing the type, number, and binding sites of the ligands, suggesting that the active site should be regarded as a statistical ensemble of diverse structures that easily interconvert.

DE-SC0019152: Ensemble Representation for the Realistic Modeling of Cluster Catalytic Reactivity at Heterogeneous Interfaces

PI: Anastassia Alexandrova, Philippe Sautet
Postdoc(s): Harry Morgan, Geng Sun, Han Guo
Student(s): Simran Kumari, Vaidish Sumaria, Patricia Poths, Edison Cummings, Santiago Vargas, Robert Lavroff, Zisheng Zhang

RECENT PROGRESS

Methodological advances:

• We have developed GOCIA, a Python package for global optimization of clusters, interfaces, and adsorbates, with the following features: (1) Highly flexible and customizable generation of random cluster and surface configurations. (2) Grand canonical genetic algorithm (GCGA), which can efficiently explore the vast chemical space of off-

stoichiometric restructuring of supported clusters or general surfaces under a specific condition. (3) Polyatomic adsorbate configuration sampling scheme, which keeps track of the adsorbate molecules.

• We are developing potentials for alumina-supported Pt-clusters; we were able to successfully train highly-accurate neural networks with <0.2 meV/Atom energy errors and < 0.1 eV/Ang force errors. We are currently refining the dataset to include more out-of-domain data points to increase where the neural network can accurately predict.

• We have developed GAS, a novel constrained global optimization methods to determine the structure of the cluster active site that provides the lowest barrier for the reaction.

New chemistry, new phenomena at dynamic catalytic interfaces:

i) hydrogenation of CO_2 to methanol on zirconia-modified Cu.

The hydrogenation of CO_2 to value added products such as methanol has numerous benefits such as mitigating the greenhouse gas emissions by capturing CO_2 and re-using it to make alternative liquid fuels. Zirconia-modified copper catalysts have been shown to be effective in CO_2/H_2 conversion to methanol with a good water tolerance, high thermal stability, and high ability to reduce CO_2 and other reaction intermediates.

We use our Grand Canonical Basin Hopping (GCBH) code to find the energetically relevant structures in reaction conditions. Under the conditions of CO_2 hydrogenation ($CO_2 + 3H_2 \rightarrow CH_3OH + H_2O$), it is very important to determine the right H and O coverage of the Zirconia clusters deposited on Cu(111), to correctly identify the catalytic environment of the reaction. Using the GCBH code, we have identified the potential energy surface of these clusters under varying O and H chemical potential. In order to accurately replicate the reaction conditions for the CO_2 hydrogenation reaction, it is essential to calculate the chemical potentials of all species involved as a function of (a) Initial feed pressure of CO_2 and H_2, (b) the ratio of CO_2: H_2 in the initial feed, (c) the temperature at which the reaction is conducted, and (d) the total conversion to methanol.

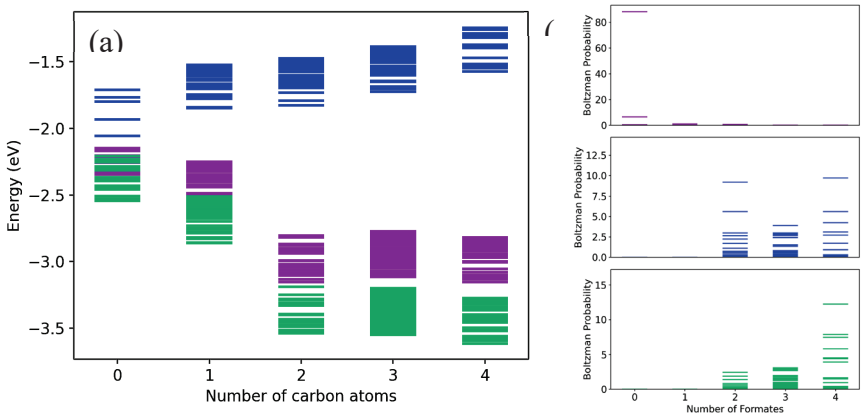

Figure 1. (a) Adsorption energies of the $Zr_3O_xOH_yHCOO_z$ cluster at three different reaction conditions corresponding to experimental works. Blue: P = 0.013 atm, conv = 2%, CO2/H2 ratio = 9, and T = 500K, Purple: P = 4.93 atm, conv = 0.8%, CO_2/H_2 ratio = 1:3, and T = 493.15K and Green: pressure = 30 atm, conv = 19.7%, CO_2/H_2 ratio = 3, and T = 493.15 K . The x axis represents the number of formates on the cluster. (b) The corresponding Boltzmann probability of each structure.

The Cu(111) surface was selected, along with a Zr cluster consisting of three Zr atoms, as the model for studying the catalytic properties of the highly dispersed Zirconia-Copper inverse catalyst under CO_2 hydrogenation conditions. Using this model, the optimum coverage of oxygen, hydroxyl, and formate species on the Zirconia-Copper inverse catalyst under CO_2 hydrogenation conditions was investigated. Under reaction conditions, we observe a large number of composition and structures with similar free energy for the catalyst (Fig. 1), with respect to changing the type, number, and binding sites of adsorbates, suggesting that the active site should be regarded as a statistical ensemble of diverse structures that easily interconvert.

ii) hydrogenation of CO_2 to methanol on Zinc-modified Cu.
Copper/zinc/zinc oxide interfaces remain the most effective known catalyst for thermal CO_2 hydrogenation to methanol; however, the active site(s) of this system are poorly understood. Beginning with a 20% ZnO coverage on Cu(100), we sample hydrogen and oxygen coverage under a range of reaction conditions and observe restructuring in the form of surface alloying, water and hydroxyl adsorption, and zinc oxide partial reduction. This is accomplished through a grand-canonical genetic algorithm in which minimum free-energy structures are determined under given chemical potentials of oxygen and hydrogen.

iii) Fractal like structure of Titanium oxide on Au (coll. with Mike White (BHNL))
We have determined how sub-stoichiometric titanium oxide clusters on stepped Au(111), an inverse catalytic system for high performance CO oxidation., follow the canonical mechanism of diffusion limited aggregation (DLA) to form fractal-like structures observed experimentally by scanning-tunneling microscopy (Fig. 2). These Ti_3O_5 clusters contrast from their stoichiometric counterparts (Ti_3O_6), which form wires along under-coordinated step edges, due to inability to polymerize along the step in an energetically favorable way as well as entropic contributions from terrace diffusion. DLA is confirmed as a mechanism via very low diffusion barriers and binding energetics of fractal nucleation sites and propagation from them.

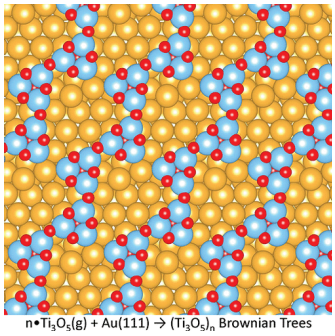

Figure 2 : Organization of Ti_3O_5 clusters on Au

iv) kinetics of isomerization of catalytic clusters
We constructed exhaustive isomerization networks for Pt_4 in the gas phase (Fig. 3) and on alumina support, under varying amount of H-coverage, with two goals: 1) to see if the presence of ligands affects fluxionality (we found that it does, and in particular both the H and the support tends to increase the isomerization barriers and also make the potential energy surface more complicated and richer in minima); 2) to determine the extent to which the Boltzmann statistics holds up, and the time required to equilibrate the ensemble. For the latter, we have

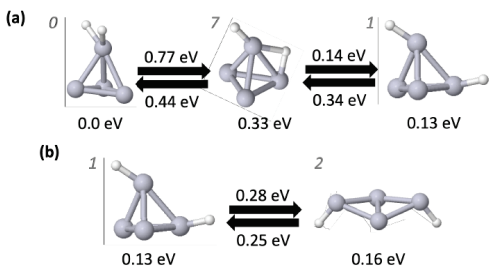

Figure 3 : Representative isomerization pathways between Pt_4H_2 isomers.

been using the Boltzmann statistics, and we found that in a large number of studies we cannot agree with, nor predict the experiment without ensemble averaging. However, the accuracy of Boltzmann statistics can be questioned. Indeed, we found that kinetic trapping of some isomers is not uncommon, and for some systems the exit from the trapped state requires more than 450K and more than 100 μs. Our current goal is to develop descriptors that would permit identifying such off-Boltzmann cases quickly, in order to formalize the approach to their modeling beyond Boltzmann.

v) boride catalysts for oxidative dehydrogenation of propane

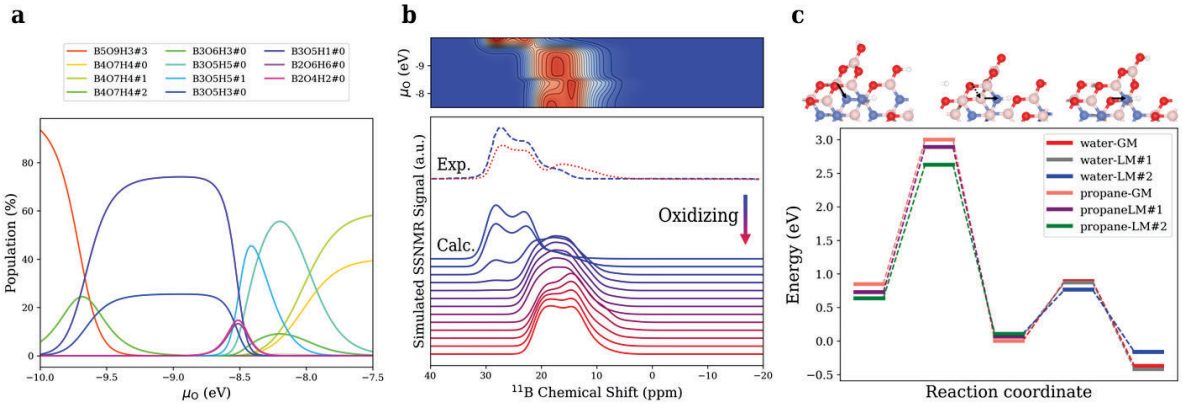

Figure 4. Off-stoichiometric restructuring and sliding dynamics of hBN edges. (a) The evolution of population of accessible surface phases as a function of oxygen chemical potential μ_O. $B_xO_yH_x$#n denotes the n-th local minima (zeroth is the global minimum) of the surface stoichiometry of $B_xO_yH_z$. (b) Evolution of the ^{11}B SSNMR spectra as a function of μ_O. The experimental data are also shown in the lower panel for comparison. (c) The energy diagram of a restructured h-BN armchair edge interconverting among the three sliding configurations of the lowest energy.

Using GCGA, we have searched for the global minimum and low-energy local minima structures of hBN armchair and zigzag edges under relevant conditions of oxidative dehydrogenation of propane (ODHP). Surface phase diagrams are constructed from the grand canonical ensemble of surface states, and the evolution of surface structure as a function of chemical potential (Figure 4a, corresponding to temperature and partial pressure) can be used to simulate condition-dependent ^{11}B chemical shift spectra, which is in good agreement with previous experimental reports (Figure 4b) and offers detailed atomistic insights. The effects of sliding dynamics of hBN sheets on the reactivity of restructured edges are studied by AIMD simulations. Multiple sliding configurations are found to be accessible at timescale of a few ps, and each has differently strained B-O linkages at the edges. The metastable sliding configurations are found to be more active towards propane and water activation as compared to the global minimum sliding configuration (Figure 4c). Such phenomenon is likely the origin of hBN's higher ODHP activity than those of the metal borides.

Tungsten boride has also been investigated as a metal boride with lower activity but similar selectivity in ODHP compared with hBN. We sample stoichiometries and configurations of the B_xO_y layer on WB with GCGA. Key minima are investigated for the activation of propane and analyzed for structural differences in the B_xO_y layer.

Publications Acknowledging this Grant in 2020-2023

(I) Intellectually led by this grant

1. Zhang, Z.; Hermans, I.; Alexandrova, A. N. Off-stoichiometric Restructuring and Sliding Dynamics of Hexagonal Boron Nitride Edges in Conditions of Oxidative Dehydrogenation of Propane. J. Am. Chem. Soc., **2023**, 145, 17265-17273.
2. Morgan, H. W. T.; Alexandrova, A. N., Structures of LaH_{10}, EuH_9, and UH_8 superhydrides rationalized by electron counting and Jahn–Teller distortions in a covalent cluster model. Chem. Sci. **2023**,14, 6679
3. Lavroff, R. H.; Wang, J.; White, M.G.; Sautet, P.; Alexandrova, A. N. Mechanism of Stoichiometrically Governed Titanium Oxide Brownian Tree Formation on Stepped Au(111). J. Phys. Chem. C **2023**, 127, 8030–8040.
4. Lavroff, R. H.; Morgan, H. W. T.; Zhang, Z.; Poths, P.; Alexandrova, A. N. Ensemble representation of catalytic interfaces: soloists, orchestras, and everything in-between. Chem. Sci. **2022**, 2022,13, 8003.
5. Poths, P.; Sun, G.; Sautet, P.; Alexandrova, A. N. Interpreting operando XANES of supported Cu and CuPd clusters in conditions of oxidative dehydrogenation of propane: dynamic changes in composition and size. J. Phys. Chem. C **2022**, 126, 1972–1981.
6. Morgan, H. W. T.; Alexandrova, A. N. Electron Counting and High Pressure Phase Transformations in Metal Hexaborides. Inorg. Chem. **2022**, 61, 18701-18709
7. Guo, H.; Poths, P; Sautet, P; Alexandrova, A. N. Oxidation Dynamics of Supported Catalytic Cu Clusters: Coupling to Fluxionality, ACS Catalysis **2022**, 12, 818-827
8. Sun, G; Sautet, P. Active Site Fluxional Restructuring as a New Paradigm in Triggering Reaction Activity for Nanocluster Catalysis, Acc. Chem. Res., **2021**, 54, 3841-3849
9. Hülsey, M.J.; Sun, G.; Sautet, P.; Yan, N. Observing Single-Atom Catalytic Sites During Reactions with Electrospray Ionization Mass Spectrometry, Angew. Chem. Int. Ed. **2021**, 60, 4764–4773
10. Sun, G.; Fuller, J. T.; Alexandrova, A. N.; Sautet, P. Global Activity Search Uncovers Reaction Induced Concomitant Catalyst Restructuring for Alkane Dissociation on Model Pt Catalysts, ACS Catalysis **2021** 11, 1877-1885
11. Zhang, Z.; Zandkarimi, B.; Alexandrova, A. N. Ensembles of metastable states govern heterogeneous catalysis on dynamic interfaces. Acc. Chem. Res. **2020**, 53, 447-458.
12. Sun, G.; Alexandrova, A. N.; Sautet, P. Structural Rearrangements of Subnanometer Cu Oxide Clusters Govern Catalytic Oxidation, *ACS Catal.* **2020**, 10, 5309−5317
13. Guo, H.; Sautet, P.; Alexandrova, A. N. Reagent-Triggered Isomerization of Fluxional Cluster Catalyst via Dynamic Coupling. *J. Phys. Chem. Lett.* **2020**, 11, 3089−3094
14. Zandkarimi, B.; Sun, G.; Halder, A.: Seifert, S.; Vajda, S.; Sautet, P.; Alexandrova, A. N. Interpreting the Operando XANES of Surface-Supported Subnanometer Clusters: When Fluxionality, Oxidation State, and Size Effect Fight. *J. Phys. Chem. C* **2020**, 124, 10057-10066
15. Halder, A.; Ha, M.-A.; Zhai, H.; Alexandrova, A. N.; Vajda, S. Oxidative Dehydrogenation of Cyclohexane on Pd vs. Cu Clusters: Selectivity Control by Specific Cluster Dynamics. *ChemCatChem* **2020**, 12, 1307-1315.

16. Zhai, H.; Sautet, P.; Alexandrova, A. N. Global Optimization of Adsorbate Covered Supported Cluster Catalysts: the Case of $Pt_7H_{10}CH_3$on alpha-Al_2O_3. *ChemCatChem* **2020**, 12, 762-770.
17. Venegas, J. M.; Zhang, Z.; Agbi, T. O.; McDermott, W. P.; Alexandrova, A. N.; Hermans, I. Why Boron Nitride is such a Selective Catalyst for the Oxidative Dehydrogenaiton of Propane. *Angew. Chem. Int. Ed*. **2020**, 14, 16527-16535.
18. Zhang, Z.; Cui, Z. H.; Jimenez-Izal, E.; Sautet, P.; Alexandrova, A. N. Hydrogen Evolution on Restructured B-rich WB: Metastable Surface States and Isolated Active Sites. *ACS Catal.* **2020**, 10, 13867
19. Liu, J.-Y.; Gong, X.-Q.; Li, R.; Shi, H.; Cronin, S. B.; Alexandrova, A. N. (Photo)electrocatalytic CO_2 reduction at the defective anatase TiO_2 surface. *ACS Catal.* **2020**, 10, 4048-4058.
20. Liu, G.; Poths, P.; Zhang, X.; Zhu, Z.; Marshall, M.; Blankenhorn, M.; Alexandrova, A. N., Bowen, K. H. CO_2 Hydrogenation to Formate and Formic Acid by Bimetallic Palladium-Copper Hydride Clusters. *J. Am. Chem. Soc.* **2020**, 142, 7930-7936

(II) Jointly funded by this grant and other grants with intellectual leadership by other funding sources

21. Wan, C.; Zhang, Z.; Dong, J.; Xu, M.; Pu, H.; Baumann, D.; Lin, Z.; Wang, S.; Huang, J.; Shah, A. H.; Pan, X.; Hu, T.; Alexandrova, A. N.; Huang, Y.; Duan, X. Amorphous nickel hydroxide proton sieve tailors local chemical environment on Pt surface for high-performance hydrogen evolution reaction in alkaline medium. Nat. Mater. 2023, 22, 1022-1029
22. Shah, A. H.; Zhang, Z.; Huang, Z.; Wang, S.; Zhong, G.; Wan, G.; Alexandrova, A. N.; Huang, Y.; Duan, X. Unriddling the role of alkali metal cations and Pt-surface hydroxide in alkaline hydrogen evolution reaction. Nature Catal., 2022, 5, 923-933
23. Zhang, R.; AthariBorojeny, M.; Collinge, G.; Iablokov, V.; Shumilov, K.; Alexandrova, A. N.; Kruse, N.; McEwen, J.-S. Promoting the cleavage of C-O bonds at the interface between a metal oxide cluster and a Co(0001) support. *ACS Catal.* **2020**, 10, 14722–14731.

Biocatalytic Nanoparticles that Enable Supra-biological Cascade Reactions

Daniel K. Schwartz and Joel L. Kaar
University of Colorado Boulder

Presentation Abstract

In this new project, we are developing biohybrid catalytic materials that expand the performance limits of enzymes far beyond what can be achieved through conventional enzyme engineering approaches. These biocatalysts exhibit greatly enhanced catalytic activity, enabling one-pot multi-step cascade reactions that are relevant to fuel production and polymer upcycling applications. In the process, we will develop insights into the mechanisms by which abiotic materials interact with enzymes to stabilize and/or "heal" them. These biocatalysts will also serve as highly tunable systems to test fundamental questions about how the efficiency of one-pot cascade reactions depends on the selectivity and activity of catalysts for independent steps. The catalysts will comprise complex materials as enzyme supports, including random copolymer brushes and mixed lipid bilayers. A critical requirement for this research involves the need to understand complex, dynamic, and heterogeneous environments, where biomolecules interact with material interfaces via both covalent and non-covalent interactions. In particular, to understand the mechanisms by which abiotic materials enhance the performance of biocatalysts, it is necessary to directly probe the relevant dynamic behavior of enzymes, in particular the conformational changes that reflective catalytic activity. Notably, we have developed single-molecule FRET methods that are uniquely capable of this type of analysis, which is performed in a highly multiplexed manner, resulting in large datasets that are analyzed using statistical methods and machine learning algorithms to provide insights into the mechanisms that underlie complex behavior.

DE-SC0023449
Biocatalytic Nanoparticles that Enable Supra-biological Cascade Reactions
PI: Daniel K. Schwartz and Joel L. Kaar
Student(s): David Kelaita and Evan Bissiri
Affiliations(s): University of Colorado Boulder

RECENT PROGRESS

Aim 1: Catalyst Design, Preparation, and Activity Screening

We have prepared biohybrid catalytic nanoparticles by incorporating enzymes of interest into tunable complex support materials, and we are functionally screening these chimeric materials, by measuring catalytic activity under harsh conditions, to identify promising candidates, that demonstrate strong (or weak) performance-enhancing effects. Parameters of particular interest for use in cascade reactions, are thermal and pH denaturation resistance. Notably, in this period, we found that incorporation of small amounts of aromatic monomers into polymer brush supports greatly enhanced the thermal stability and activity of LipA lipase, which has a particularly high fraction of surface exposed aromatic residues. We hypothesize that this remarkable stabilization is related to aromatic pi-stacking interactions between support and enzyme surface moieties, and this hypothesis will be explored in ongoing work. To impart supra-biological performance in the context of extreme pH, we are incorporating anionic / cationic monomers into polymer brush supports to shift the local pH while maintaining or enhancing enzyme stability and activity.

We have developed a protocol for making supported lipid bilayers (SLBs) using silica-coated magnetic nanoparticles as the support, enhancing our ability to purify nanoparticle catalyst without the needs for centrifugation and/or vortexing for re-suspension. Successful coating of these particles has been confirmed using dynamic light scattering and zeta potential measurements. We have successfully used these SLBs to immobilize LipA, one of the proposed cascade components. After immobilizing LipA to mixed lipid SLBs, the activity of immobilized particles was comparable to a soluble enzyme control at room temperature. Studies are underway to compare the activity of LipA immobilized to SLBs vs. lipid liposomes.

Aim 2: Mechanistic Information from SM-FRET

Here we are studying and understanding the mechanisms of biocatalytic performance enhancement using highly multiplexed single-molecule Förster Resonance Energy Transfer characterization of enzyme conformational dynamics, distinguishing between chemical stabilization of the native state, rescue of inactivated biocatalytic sites, and physical stabilization through nanoconfinement. We have developed a dual labeled Lipase A construct for use in single molecule FRET experiments to interrogate the mechanisms of enzyme stabilization on surface grafted polymer brushes, and supported lipid bilayers. In this period, we used this method to understand the mechanisms by which polymer brush supports containing aromatic monomers enhance the thermal stability and activity of LipA. SM-FRET microscopy experiments revealed that these supports maintained catalytic LipA activity in thermally denaturing environments by preserving the folded and catalytically-active state of LipA. A Markov chain analysis demonstrated that this effect was achieved via simultaneous stabilization of the folded state and chaperone-like acceleration of refolding, both due to interactions with aromatic moieties. SM-FRET also revealed that optimally composed supports restricted LipA's unfolded state to a constrained partially unfolded conformation, resulting in the effective acceleration of enzyme refolding.

Aim 3: and Biocatalytic Cascade Reactions

Here we are employing the knowledge from Aims 1 and 2 to create biocatalytic systems that perform selective and efficient one-pot multi-step enzymatic reactions. The systems describe above are used to develop knowledge about the connections between biocatalyst and process design and cascade reaction efficiency. The performance of biohybrid catalytic nanoparticles are compared to soluble enzymes in cascade reactions under extreme conditions. Moreover, we are comparing the effects of employing multi-enzyme nanoparticles (where each particle catalyzes the full cascade reaction) vs. mixing multiple types of single-enzyme nanoparticles (where each particle catalyzes a single reaction step). We have developed an activity assay for the lipase + lyase cascade reaction using high performance liquid chromatography (HPLC) and are in the process of comparing the performance of cascade reactions using soluble vs. immobilized enzyme catalysts.

Publications Acknowledging this Grant in 2020-2023

None to report.

Carsten Sievers

Mechanocatalytic Oxidative Cracking of Poly(ethylene) via a Heterogeneous Fenton Process

Van Son Nguyen, Yuchen Chang, Erin V. Phillips, Jacob A. DeWitt, Carsten Sievers
Georgia Institute of Technology – School of Chemical & Biomolecular Engineering

Presentation Abstract

Plastics upcycling poses significant challenges for chemist and engineers due to the chemical and physical stability of these materials. The present work addresses these challenges with mechanocatalytic processes in ball mills. In these reactors, collisions with milling provide reactive environments through a combination of localized heating, strain and surface modification of impacted materials and triboelectric effects (i.e., mechanically induced charge separation). In addition, they can induce intimate interactions of solid surfaces by sheering them.
Specifically, poly(ethylene) (PE) was partially oxidized by ball milling in a steel vessel with steel balls in the presence of a Fenton system consisting of an Fe_2O_3 catalyst and an aqueous hydrogen peroxide solution as oxidant. The insertion of oxygenated functional groups activated PE to allow for cracking adjacent to the oxidized carbon atom to produce linear hydrocarbon products. FTIR spectroscopy showed that the residual polymer contained increased amounts of carbonyl (1705 – 1735 cm^{-1}), alcohol and ester (1080 – 1220 cm^{-1}) functional groups. High temperature gel permeation chromatography showed the formation of hydrocarbons with carbon numbers in the C_{14} – C_{30} range. Evidently, the fragments were formed via oxidation of the PE chain which weakened the chemical inertness of the carbon-carbon bonds in PE, followed by subsequent cracking at these functionalized locations and removal of oxygen containing groups as CO_2 or CO.

DE-SC0016486: Selective Oxidation of Methane over Lewis Acidic and Redox - Active Catalysts under Transient Conditions

PI: Carsten Sievers, Andrew J. Medford (co-PI)
Postdoc(s): Dr. Kinga Golabek
Student(s): Van Son Nguyen, Yuchen Chang, Neung-Kyung Yu

RECENT PROGRESS

Selective Oxidation of Hydrocarbons under Transient Conditions

In mechanochemical processes, collisions in a ball mill or similar device create short-lived activated domains (hot spots) that can have extraordinary catalytic activity until they decay. We hypothesized that these environments should be suitable for selective oxidation of hydrocarbon because the limited lifetime of the hot spot will help limit overoxidation. Unfortunately, very limited oxidation of methane was observed during balling with a ceria-zirconia catalysts and O_2. We hypothesized that the issue was insufficient surface interactions of methane.

Therefore, we shifted our attention to the conversion of heavier hydrocarbons leveraging the fact that mechanochemical processes can induce intimate surface interaction between solid reactants and solid catalysts. Specifically, the partial oxidation of poly(ethylene) (PE) was utilized as a way of activating this recalcitrant polymer to allow for cracking adjacent to the activated carbon atom to produce linear hydrocarbon products. In these reactions, PE was processed inside a vibratory ball mill with a steel vessel and steel ball in the presence of a Fenton system consisting of an Fe_2O_3 catalyst and an aqueous hydrogen peroxide solution as oxidant. FTIR spectroscopy showed that the residual polymer contained increased amounts of carbonyl (1705 – 1735 cm^{-1}), alcohol and ester (1080 – 1220 cm^{-1}) functional groups. High temperature gel permeation chromatography of milled PE exhibited a bimodal molecular weight (MW) distribution compared to the unimodal distribution of the feedstock, indicating that a portion of polymer had been converted to low MW fragments (Figure 1). This low MW fraction was found to be partially soluble in hexanes. Gas chromatography-mass spectrometry analysis of the hexanes extract illustrated the presence of linear hydrocarbons with carbon numbers in the C14 – C30 range. Evidently, the fragments were formed via oxidation of the PE chain which weakened the chemical inertness of the carbon-carbon bonds in PE, followed by subsequent cracking at these functionalized locations and removal of oxygen containing groups as CO_2 or CO.

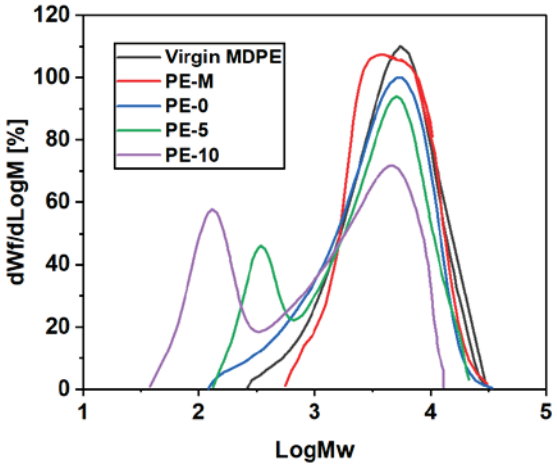

Figure 1: Gel permeation chromatography traces for virgin mid-density poly(ethylene) (MDPE), MDPE after milling without additives (PE-M), MDPE after milling with H_2O_2 (PE-0), MDPE after milling with H_2O_2 and 5 wt% Fe_2O_3 (PE-5), MDPE after milling with H_2O_2 and 10 wt% Fe_2O_3 (PE-10).

Mechanochemical Transformations and Redox Reactions of MoO_x

Our past work indicated that substantial reduction of MoO_3 can be achieved by heating it under inert gas (*ACS Catalysis,* 10 (2020) 8187–8200). Based on this reactivity we hypothesized that molybdenum oxide is a promising for mechanocatalytic redox reaction that involve a Mars-van Krevelen mechanism. Mechanocatalytic water splitting is a promising "test reaction" for gaining a more fundamental understanding of the generation and consumption of active oxygen species under mechanocatalytic conditions. Molybdenum oxide (MoO_x) is a reducible oxide that is hypothesized to be capable of mechanocatalytic water splitting. In the first phase of the project, we have explored how to use computational techniques to understand water splitting on MoO_x. Ball milling delivers the mechanical energy necessary to activate and potentially reduce MoO_x. The mechanical impact and resulting high local heat are expected to induce changes in the crystal phase, stoichiometry, and surface morphology of MoO_x. The current aim of the study is to gain insights into the prevalent MoO_x structures during mechanocatalysis, which we seek to

achieve in an effort led by density functional theory (DFT) calculations and ab-initio thermodynamics.

First, we explored the possible crystal phases and stoichiometries of bulk MoO_x by constructing bulk phase diagrams as a function of hydrogen and oxygen chemical potentials (Figure 2). The phase diagram at the top was generated using the data from the Materials Project database. The two distinct mu_O resulting from different reactions, O_2 and

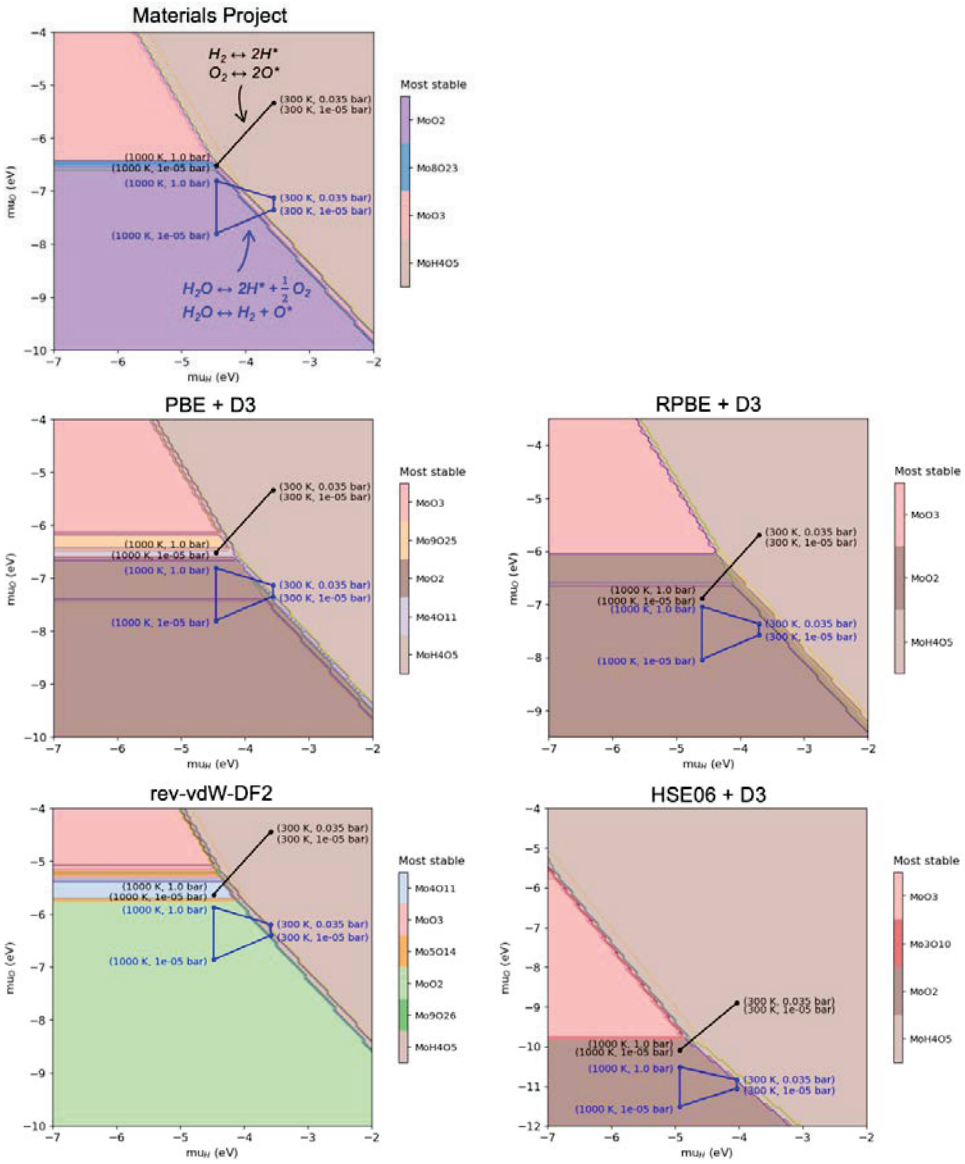

Figure 2: MoO_x bulk phase diagrams as a function of hydrogen and oxygen chemical potentials (mu_H and mu_O), based on the Materials Project database and our calculations using different functionals, PBE+D3, RPBE+D3, rev-vdW-DF2, and HSE06+D3. Each colored areas correspond to the most stable bulk structures and the contour lines represent the second most stable structures at given chemical potentials. Dots correspond to the chemical potentials at given experimental conditions (gas temperature and H_2O partial pressure). mu_H and mu_O for black dots are determined based on the dissociation reaction of H_2 and O_2, whereas for blue dots, mu_O involve H_2O decomposition.

H_2O dissociation, define separate areas of interest enclosed by black or blue lines connecting the dots in the phase diagram. These dots correspond to the experimental conditions that are expected during the oxidation step (water partial pressure equals water vapor pressure, $P_{H2O} = P_{vap,H2O}$) and reduction step ($P_{H2O} = 10^{-5}$ bar) at temperatures of 300 K and 1000 K. Based on the Materials Project database, we identified seven stable MoO_x structures, including the second most stable ones within the plotted chemical potential ranges. Additionally, we considered 18 experimentally discovered structures, resulting in a total of 25 MoO_x bulk structures used to construct the phase diagrams using different density functionals. The functionals employed include generalized gradient approximation (GGA) functionals PBE+D3BJ (PBE with Grimme's D3 dispersion correction with Becke-Johnson damping) and RPBE+D3BJ, nonlocal van der Waals functional rev-vdW-DF2, and hybrid functional HSE06+D3BJ. The phase diagrams generated from different functionals exhibit similar trends, with MoO_3 favored over MoO_2 as mu_O increases, and MoH_4O_5 preferred over non-hydrated MoO_x as mu_H increases. However, the choice of functional sometimes leads to different stable bulk structures or stoichiometries within the range of relevant chemical potentials. This inconsistency arises due to the inherent limitation of DFT formalism, as the exact exchange-correlation functional is not known. To address this ambiguity from DFT results, experimental validation will be conducted to determine which bulk MoO_3 structures are observed during ball milling.

Prior testing the effectiveness of MoO_x for mechanocatalytic water splitting, we investigated the mechanochemical stability of the study oxide. Based on literature, MoO_3 crystallizes with different structures. The most common and thermodynamically stable phase is orthorhombic α-MoO_3. However, the metastable monoclinic phase of MoO_3 shows higher activity in red-ox catalysis, especially in methanol oxidation, but it can be transformed into the α-phase by heating above 400 °C. Therefore, since the β-MoO_3 is less sable compared to the α-phase we focused on commercially α-MoO_3 as benchmark material. The MoO_3 sample was activated at 450 °C for 2 h to transform any potentially present β phase into α-MoO_3 as well as to remove adsorbates from the catalyst surface. The activated sample was subjected to ball milling for 5, 30 and 120 min. The phase composition and crystal structure were probed by powder X-ray diffraction (pXRD).

In pXRD pattern of both fresh activated and non-activated MoO_3 no characteristic diffraction peaks of the β-phase were found, confirming the high purity of the catalysts. Milling the samples for 5 min resulted in the significant increase in the intensity for all major diffraction peaks. This suggests a crystallization process of the MoO_3 samples. With increasing the milling time, the intensity of all diffraction peaks decreased while the lines broadened, which is indicative of loss of crystallinity due to amorphization or particle size reduction. Interestingly, this effect is more pronounced for the diffraction peaks with contributions from h or l Miller indices. The loss of coherence is probably in a and c directions, whereas the b direction stays relatively unchanged indicating that the changes of the crystals are anisotropic. We calculated the crystal sizes from Scherrer equation using the (210) diffraction peak. The size reduction of crystals was observed for both activated and non-activated samples. In addition, a decrease in the crystal size of 12% was observed right after activation process.

Publications Acknowledging this Grant in 2020-2023

(I) Intellectually led by this grant

1. Lyu, Y.; Jocz, J. N.; Xu, R.; Stavitski, E.; Sievers, C., Nickel Speciation and Methane Dry Reforming Performance of $Ni/Ce_xZr_{1-x}O_2$ Prepared by Different Synthesis Methods. *ACS Catalysis* **2020**, *10*, 11235−11252.
2. Lyu, Y.; Jocz, J. N.; Xu, R.; Williams, O. C.; Sievers, C., Selective Oxidation of Methane to Methanol over Ceria-Zirconia Supported Mono and Bimetallic Transition Metal Oxide Catalysts. *ChemCatChem* **2021**, *13*, 2832– 2842.
3. Lyu, Y.; Xu, R.; Williams, O. C.; Wang, Z.; Sievers, C., Reaction Paths of Methane Activation and Oxidation of Surface Intermediates over Nio on Ceria-Zirconia Catalysts Studied by in-Situ Ftir Spectroscopy. *J. Catal.* **2021**, *404*, 334-347.
4. Williams, O. C.; Sievers, C., Active Oxygen Species in Heterogeneously Catalyzed Oxidation Reactions *Applied Catalysis A: General* **2021**, *614*, 118057.
5. Jocz, J. N.; Lyu, Y.; Hare, B. J.; Sievers, C., Characterization of Surface Species During Benzene Hydroxylation over a Nio-Ceria-Zirconia Catalyst. *Langmuir* **2022**, *38*, 458–471.
6. Nguyen, V. S.; Chang, Y.; Phillips, E. V.; DeWitt, J. A.; Sievers, C., Mechanocatalytic Oxidative Cracking of Poly(Ethylene) Via a Heterogeneous Fenton Process. *ACS Sustainable Chem. Eng.* **2023**, *11*, 7617–7623.

(II) Jointly funded by this grant and other grants with intellectual leadership by other funding sources

7. Najmi, S.; So, J.; Stavitski, E.; McDermott, W. P.; Lyu, Y.; Burt, S. P.; Hermans, I.; Sholl, D. S.; Sievers, C., In-Situ IR Spectroscopy Study of Reactions of C_3 Oxygenates on Heteroatom (Sn, Mo, and W) Doped Bea Zeolites and the Effect of Co-Adsorbed Water *ChemCatChem* **2021**, *13*, 445– 458.

Jeremy M. Smith

A Nucleophilic Imido Ligand Enables New Catalytic Transformations of an Iron Complex

Yafei Gao, Maren Pink, Veronica Carta, and Jeremy Smith
Department of Chemistry, Indiana University

Presentation Abstract

Reduction of a three-coordinate iron(III) imido complex affords the corresponding iron(II) imido complex. The high spin ($S = 2$) state of the iron(II) complex attenuates the iron-nitrogen multiple bond character. Combined with the anionic nature of the complex, this helps create an electrophilic imido ligand that has reactivity patterns akin to those of early transition metals. In addition to previously observed transformations such as such as [2+2] cycloadditions, the iron(II) imido is active in new reactions, including the first ene-like reactivity of an imido ligand. For example, reaction with 3-hexyne generates the corresponding iron(II) amido allenyl complex. These new reactions form the basis of new catalytic processes, including selective alkyne and nitrile α-deuteration and pK_a-dictated alkene transposition. Mechanistic studies reveal the critical role of metal-ligand cooperativity in facilitating these unusual transformations, which extend beyond classical nitrene transfer reactivity of late metal imido complexes.

DE-SC0019466: Harnessing Spin as a Design Element in Low Valent Iron Catalysis

Postdoc(s): Yafei Gao, Bin Feng
Student: Arya Sree Ajay

RECENT PROGRESS

Catalytic Alkene Transposition Enabled by Iron Imido Cooperativity. The Fe(II) imido complex $[Ph_2B(^tBuIm)_2Fe{=}NDipp]^-$ catalyzes the regioselective isomerization of 1-alkenes. Kinetics, competition, and isotope labeling studies, supported by stoichiometric reactions, strongly implicate a unique, non-hydridic mechanism for alkene isomerization, in which the alkene coordinates to iron, and the basic imido ligand acts as a proton shuttle. Computational studies further support the proposed mechanism. As dictated by substrate pK_a, this mechanism enables the regioselective isomerization of allylarenes and 1,4-dienes, , even in the presence of other 1-alkenes. The catalyst tolerates a variety of functional groups, including potential ligands such as phosphines, amines and imidazoles.
Oxidation State Dependence of Hydrogen Atom Abstraction. One electron oxidation of the Fe(III) imido complex occurs at the imido ligand to afford $[Ph_2B(^tBuIm)_2Fe(THF)(=NDipp)]^+$ in which high spin ($S = 5/2$) Fe(III) is antiferromagnetically coupled to an imidyl radical ($S = 1/2$). While attempts to divert the hydrogen atom abstraction reactivity of this complex away from an intramolecular dehydrogenation reaction have been unsuccessful, the three-coordinate Fe(II) and Fe(III) imido complexes are active in intermolecular hydrogen atom abstraction reactions.

Despite a stronger thermodynamic driving force for hydrogen atom abstraction, the Fe(III) imido displays more sluggish kinetics.

Publications Acknowledging this Grant in 2020-2023

Intellectually led by this grant

1. Gao, Y.; Li, X.; Stevens, J.E.; Tang, H.; Smith, J.M. Catalytic 1,3-Proton Transfer in Alkenes Enabled by Fe═NR Bond Cooperativity: A Strategy for pK_a-Dictated Regioselective Transposition of C═C Double Bonds *J. Am. Chem. Soc.* **2023**, *145*, 11978-11987.
2. Gao, Y.; Lee, W.-T..; Carta, V.; Chen, C.-H.; Telser, J.; Smith, J.M. Heteroleptic Square Planar Cobalt(I/II) Complexes, *Eur. J. Inorg. Chem.* **2023**, e202200675.
3. Gao, Y.; Pink, M.; Carta, V.; Smith, J.M., Ene Reactivity of an Fe=NR Bond Enables the Catalytic α-Deuteration of Nitriles and Alkynes, *J. Am. Chem. Soc.* **2022***, 144*, 17165-17172.
4. Gao, Y.; Pink, M.; Smith, J.M., Alkali Metal Ions Dictate the Structure and Reactivity of an Iron(II) Imido Complex, *J. Am. Chem. Soc.* **2022**, *144*, 1789-1794.
5. Gao, Y.; Carta, V.; Pink, M.; Smith, J.M., Catalytic Carbodiimide Guanylation by a Nucleophilic, High Spin Iron(II) Imido Complex, *J. Am. Chem. Soc.* **2021**, *143*, 5324-5329.
6. Gao, Y.; Pink, M.; Smith, J.M., Iron(II) Complexes of an Anionic Bis(ylide)diphenylborate Ligand, *Inorg. Chem.* **2020**, *59*, 17303-17309.
7. Martinez, J.L.; Lutz, S.A.; Yang, H.; Xie, J.; Telser, J.; Hoffman, B.M.; Carta, V.; Pink, M.; Losovyj, Y.; Smith, J.M., Structural and Spectroscopic Characterization of an Fe(VI) Bis(imido) Complex, *Science* **2020**, *370*, 356-359.
8. Lutz, S.A.; Hickey, A.K.; Gao, Y.; Chen, C.-H.; Smith, J.M. Two-State Reactivity in Iron-Catalyzed Alkene Isomerization Confers σ-Base Resistance, *J. Am. Chem. Soc.* **2020**, *142*, 15527-15535.

Brian M. Tackett

Low-Temperature Electrocatalytic Manufacturing of Essential Chemical Building Blocks

B. M. Tackett (Lead PI), B. W. Boudouris, R. Gounder, J. P. Greeley, J. T. Miller,
Purdue University, Chemical Engineering

Presentation Abstract

Electrocatalytic dehydrogenation of light alkanes to their alkene counterparts has potential to drastically decarbonize production of olefins, which are among the most ubiquitous industrial chemical building blocks. The electrochemical dehydrogenation process generates the olefin product on one electrode and the hydrogen product on the other electrode, making the reaction irreversible, thus avoiding equilibrium limitations of thermal dehydrogenation routes. This substantially reduces the amount of downstream separations required, and, if successful at the industrial scale, could consequently avoid hundreds of millions of tons of CO_2 emissions per year. There are few examples of low-temperature aqueous alkane electrocatalysis, so our team is developing the fundamental science necessary to achieve efficient electrocatalytic alkane dehydrogenation, from the atomic scale to the device scale, by combining experiment and theory in this multidisciplinary project. In the first year of the project, we developed new polymer materials to enhance mass transport with gas diffusion electrodes, quantified alkane adsorption on smooth electrodes at room temperature, and developed a preliminary microkinetic model.

DE SC0023257: Low-Temperature Electrocatalytic Manufacturing of Essential Chemical Building Blocks

Postdoc(s): None
Student(s): Ashutosh Bhadouria, Joseph Heil, Hwiyoon Noh, Ryoh-Suke Sekiya, Brandon Bolton, Ho Joong Kim, Hyunki Yeo, Durvesh Parab, Wei-Ling Huang

RECENT PROGRESS

Optimizing Mass Transport with Next Generation Gas Diffusion Electrode

Efficient and stable gas diffusion electrodes are required to overcome low solubility of alkanes in aqueous electrolyte to enable continuous electrochemical reactions at the gas-solid-liquid interface. We selected PTFE membranes as our gas diffusion media, due to their robustness and hydrophobicity. We then modified the membranes by coating them with a PEDOT:PSS conductive polymer to make them suitable for gas diffusion electrodes. Post-treating the PEDOT:PSS with concentrated sulfuric acid enhanced conductivity by

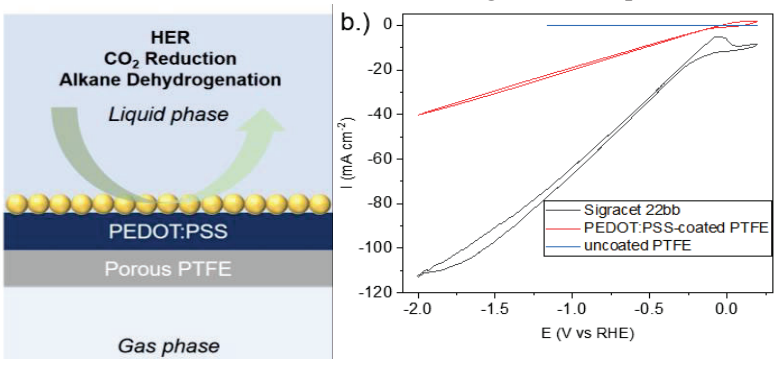

Figure 1. (left) Cross-section schematic of conductive polymer gas diffusion electrode. (right) Hydrogen evolution reaction electrocatalytic polarization curves.

a factor of 10 and also increased gas permeability to a level comparable with commercial carbon-based gas diffusion electrodes. In addition to conductivity, we verified the suitability of this material to enable electrocatalytic reactions by casting Pt nanoparticles onto the PEDOT:PSS film and demonstrating successful hydrogen evolution reaction in acid.

Designing Active and Selective Electrocatalysts for Alkane Dehydrogenation

In parallel to gas diffusion electrode development, we also quantified fundamental alkane adsorption behavior on smooth Pt electrodes under aqueous, room temperature conditions. We utilized a recently developed electrochemical mass spectrometer (EC-MS) to perform TPD-like experiments to investigate adsorption behavior. We quantified both time-dependence and potential-dependence on the fractional coverage of adsorbed propane. We also applied both oxidizing and reducing potential sweeps to adsorbed propane to understand the chemical structure and relative amounts of adsorbed species by combining coulometry with simultaneous mass spectrometry. We showed that propane readily adsorbs on smooth Pt at 0.3 V vs RHE in acid electrolyte with fractional coverage between 0.06 and 0.25 C/Pt. We also showed that adsorbed propane can either be desorbed as propane or completely oxidized to CO_2, depending on the applied potential. This indicates that it should be possible to design an electrocatalytic system (catalyst, electrolyte, potential) that selectively dehydrogenates alkanes without over-oxidation. We are using our analytical kinetic model along with density functional theory calculations to develop descriptors that will enable rational selection of electrocatalyst to achieve this selective dehydrogenation. Our current model assumes that the activation barrier of C-H bond breaking in propane is a critical parameter in determining the rate, and this barrier may further be estimated using linear (BEP) correlations with corresponding binding energies. These results will be iteratively refined with the fundamental experimental catalysis studies which will ultimately interface with the device-scale gas diffusion electrode development.

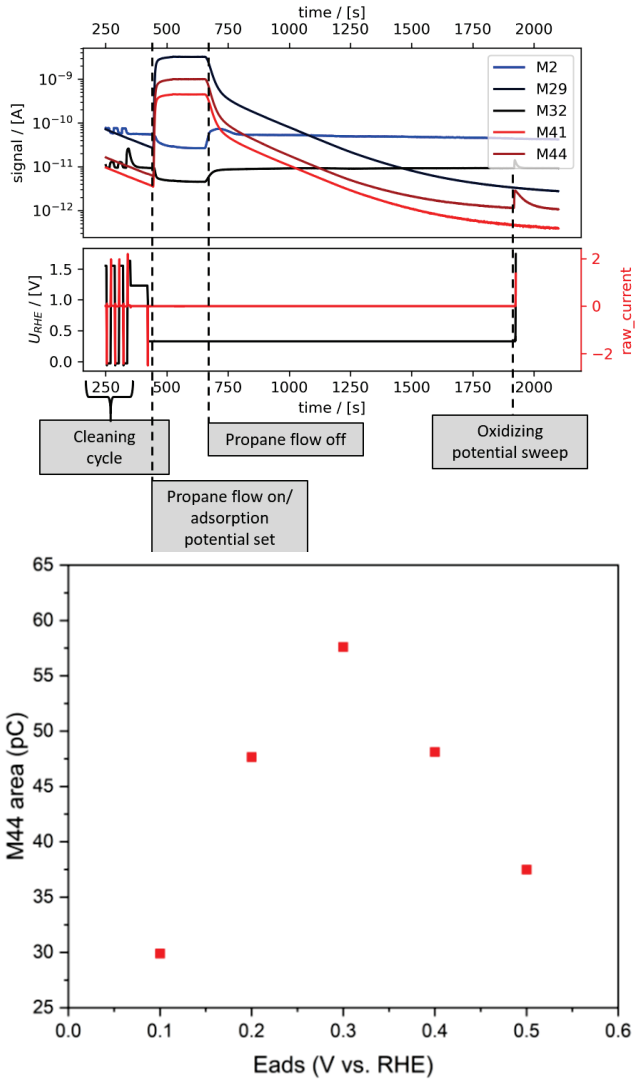

Figure 2. (top) Electrochemical mass spectrometer profile for a propane dose, purge, and reaction protocol. (bottom) Quantified CO_2 produced upon oxidation from propane adsorbed at various potentials.

Publications Acknowledging this Grant in 2020-2023: *N/A*

Converting Carbon and Nitrogen Waste Products to Valuable C-N Compounds

V. Sara Thoi
Johns Hopkins University, Department of Chemistry

Presentation Abstract

We investigated the electrochemical C-N coupling using waste products, carbon dioxide and nitrate, to form urea as a value-added product. Urea, which is an important fertilizer for agriculture, is industrially synthesized by the Bosch-Meiser process using ammonia generated from the Haber-Bosch process. As both of these processes require high heat and/or pressure, the discovery of an energy-efficient synthetic pathway to urea can thus have large environmental impacts. Herein, we report a series of Au- and Cu-based catalysts that can achieve up to 60% selectivity for urea at a current density of up to 300 μA cm^{-2} upon optimization. In particular, we explored pulsed potential electrolysis to obtain high selectivity and activity. We hypothesized that pulsing the potential anodically allows for rearrangement of the electrochemical double layer and promotes NO_3^- diffusion and activation. Moreover, we used *in situ* electrochemical, spectroscopic, and computational techniques to elucidate potential mechanisms for electrocatalytic C-N coupling.

RECENT PROGRESS

Electrochemical C-N Coupling

We have continued our focus on electrochemical C-N coupling through the co-reduction of nitrate and carbon dioxide. We have completed our electrochemical study on Au-catalyzed urea formation, where in the presence of carbon dioxide (pH 3, -0.4 V vs. RHE), we achieved up to 30% Faradaic efficiency and an activity of 175 μA cm^{-2} (**Figure 1a**). We have also shown that urea selectivity can be further optimized by pulsed potential electrolysis, achieving a urea selectivity of 60% with a cathodic pulse of -0.2 V (1 s) and an anodic pulse of 0.2 V (200 ms) (**Figure 1b**). These results are remarkable as previous literature has shown that Au does not catalyze C-N coupling at least at high cathodic potentials (-1.5 V vs. SHE).[1] Through several iteration of optimization, we found that potassium cations are critical for efficient coupling, with selectivity in the order of K > Cs > Na > Li. Using a crown ether to sequester potassium led to poor nitrate reduction (**Figure 1c,d**), leading us to believe that alkali cations play a crucial role in stabilizing N intermediates at the electrode surface.

We dedicated significant effort in the last award period towards mechanistic understanding for C-N coupling. *In situ* surface-enhanced IR spectroscopy (SEIRAS) was conducted, where a static cathodic potential is applied under catalytic conditions. We observed the rise and fall of a new band at 1410 cm^{-1} that we attribute to an intermediate C-N species resembling carbamate (**Figure 2**). Time-resolved SEIRAS under constant and pulsed potential electrolysis show the diffusion of NO_2^- and NO_3^- species may be important for enhancing C-N coupling. To offer further mechanistic support, we conducted density functional theory (DFT) calculations with our collaborator, Dr. Peter Zapol, at Argonne National Lab (**Figure 3**) showing that urea formation is favored over

ammonia production in the presence of CO_2 and NO_3^-. Current investigations are focused on electrodeposited AuCu alloys that can simultaneously activate carbon and nitrogen substrates.

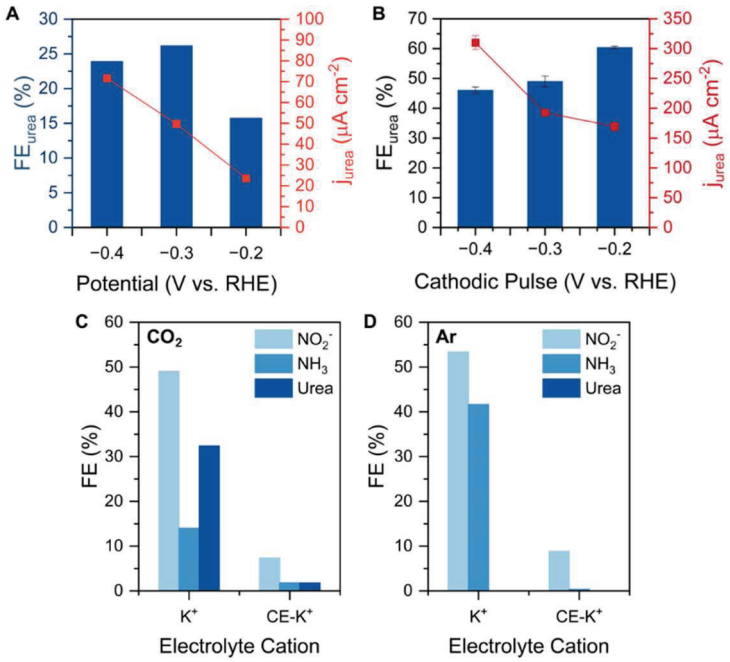

Figure 1. (a) Faradaic efficiency and current density for urea production on a Au foil electrode (a) under static controlled potential electrolysis and (b) pulsed potential electrolysis where the anodic potential was optimized to +0.2 V. Faradaic efficiency for (c) C-N coupling and (d) NO_3RR in the presence and absence of 18-crown-6-ether (CE)

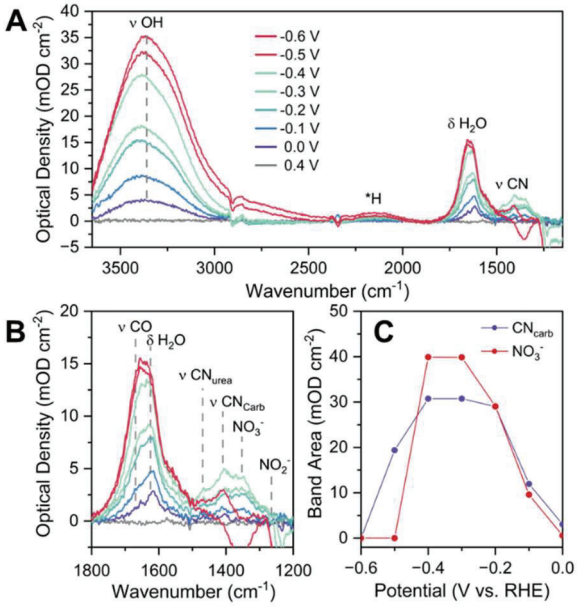

Figure 2. (a) *In situ* SEIRAS spectra showing the presence of a C-N intermediate resembling carbamate at 1410 cm^{-1} in the (b) expanded view, and (c) integrated area of the C-N intermediate and NO_3^- bands.

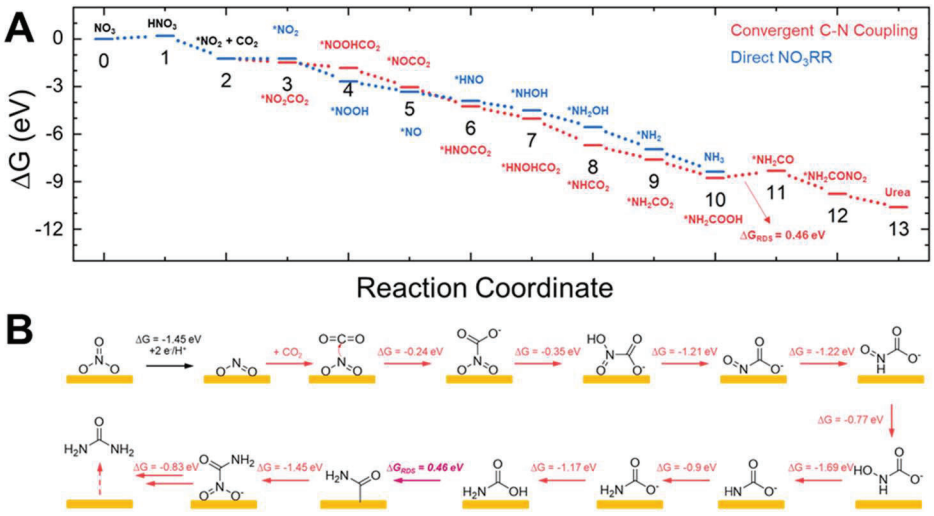

Figure 3. (a) Free energy diagram of the reduction steps towards urea production on an Au {111} facet at 0 V vs. SHE in comparison to NH_3 production indicating slightly lower energy at step 4 for the urea pathway. One electron and one proton are added at each step, and the overall highest energy step is from 10 to 11. (b) Molecular configurations along the reaction coordinate from CO_2 and NO_3^- to urea via C-N coupling.

Publications Acknowledging this Grant in 2020-2023

Intellectually led by this grant

- Banerjee, S.,[#] Gorham, J. M.,Beccar-Varela, P., Hackbarth, H. G., Siegler, M. A., Drichko, N., Write, J. T., Bedford, N. M.,* Thoi, V. S.* Atomically Dispersed CuN_x Sites from Thermal Activation of Boron Imidazolate Cages for Electrocatalytic Methane Generation, *ACS Appl. Energy Mater.*, **2022**, *in press*. **DOI: 10.1021/acsaem.2c01174**
- Davis, J., Banerjee, S., Beccar-Varela, P., Thoi, V. S., Drichko, N.* Raman Scattering Spectra of Boron Imidazolate Frameworks Containing Paramagnetic Ions, **2023,** *158*, 214707. **DOI: 10.1063/5.0152070**
- Singh, K. K., Saund, S. S., Zito, A. M., Siegler, M. A., **Thoi, V. S.*** CO_2 Activation with Manganese Tricarbonyl Complexes via an H-Atom Responsive Benzimidazole Ligand, *Chem. Eur. J.,* **2023**, *in press.* **DOI: 10.1002/chem.202300796**

YuYe J. Tong

Sustained Low-Temperature Electrochemical Methane Reforming Reaction on Commercial Pt/C and PtRu/C Electrocatalysts

Dejun Chen, Rachel A. Aterrado, Tianyu Ma, Thomas C. Allison, YuYe J. Tong (PI)
Georgetown University

Presentation Abstract

Methane activation under mild conditions of promising practical outlook is highly desirable economically as methane still is the main stock source for industrial hydrogen production. Yet, even after decades-long intensive research, it remains stubbornly on the short list of holy grails in chemistry. Herein, we report the observation of sustained *l*ow-*t*emperature (~80 °C) *e*lectro*c*hemical *m*ethane *r*eforming *r*eaction (LT-ECMRR), $CH_4 + 2H_2O \rightarrow CO_2 + 4H_2$, on both commercial carbon-supported Pt/C and PtRu/C electrocatalysts. Interestingly, although the observed specific activity of the LT-ECMRR on the Pt/C is about ten times higher than that on the PtRu/C, its apparent activation energy is almost same and surprisingly moderate: 46 kJ/mol on Pt/C vs 42 kJ/mol on PtRu/C. Preliminary density functional calculations suggest that the active sites for the LT-ECMRR are likely the Pt corner- and edge-like sites as experimental evidence shows that pure Ru/C electrocatalyst is inactive for low-temperature methane activation. A rough estimate using the specific chronoamperometric current obtained at 0.5V (vs normal hydrogen electrode – NHE) and 3600 s gives a price of hydrogen production by the LT-ECMRR at ~\$15/kg H_2. A 10-time improvement in its specific activity (a reasonably achievable aspiration) would bring the cost down to \$1.5/kg H_2, which is in the current cost range of industrial hydrogen production.

Grant Title: Exploring Electrocatalysis of Methane on Transition Metal Surfaces
DOE Grant #: DE-SC0021218
Student(s): Rongfeng Zheng, Rachel A. Aterrado, Tianyu Ma

RECENT PROGRESS

Sustained Low-Temperature Electrochemical Methane Reforming Reaction on Commercial Pt/C and PtRu/C Electrocatalysts

Figure 1 compares the cyclic voltammograms of the *l*ow-*t*emperature *m*ethane *e*lectro*c*hemical *r*eforming *r*eaction (LT-ECMRR), $CH_4 + 2H_2O \rightarrow CO_2 + 4H_2$, at 80 °C and 300 kPa back pressure on the 25-cm^2 metal-membrane-assembly consisting of commercial Pt/C (a, 4 mg/cm^2) vs PtRu/C (d, 12 mg/cm^2) and the corresponding in-line GCMS detected CO_2: b for on Pt/C and c on PtRu/C. The cathode was a hydrogen-fed normal hydrogen reference electrode (NHE). Both anode and cathode gas feeds were humidified with a relative humidity (RH) of 100%. Sustained LT-ECMRR current was observed on both electrocatalysts at 10 mV/s potential scan rate under very mild condition, i.e., at 80 °C and about 4 atmospheric pressure, with activity appeared much higher on Pt/C

than on PtRu/C. Using ^{13}C-labeled $^{13}CH_4$ confirmed unambiguously that the MS-observed CO_2 came directly from the LT-ECMRR.

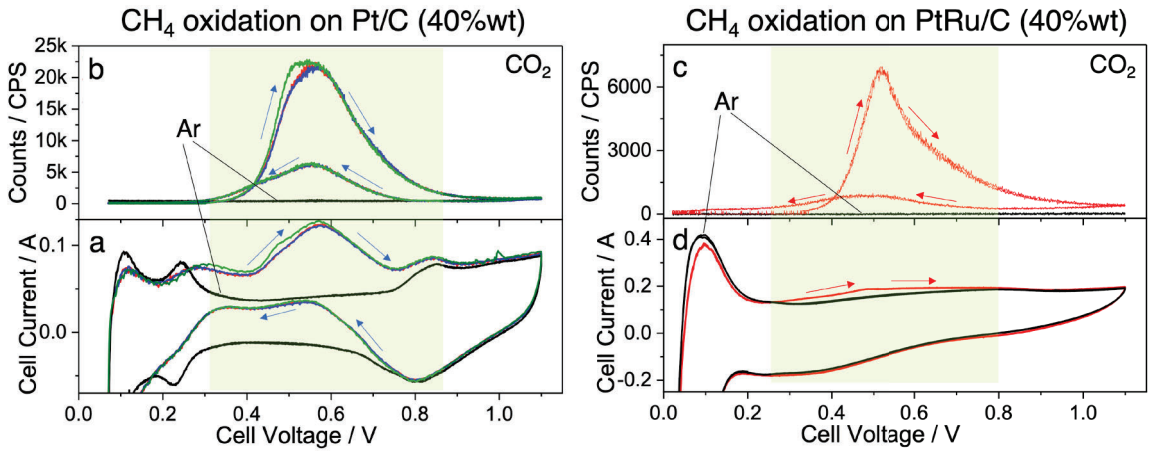

Figure 1. (a) Cyclic voltammograms (10 mV/s) obtained on the MEA of Pt/C (4 mg/cm^2, anode)|PtRu/C (12 mg/cm^2, cathode) with CH_4 and (b) the corresponding CO_2 mass (m/z=44) CVs obtained simultaneously by in-line GCMS. (d) Cyclic voltammograms (10 mV/s) obtained on the MEA of PtRu/C (12 mg/cm^2, anode)|Pt/C (4 mg/cm^2, cathode) with CH_4 and (c) the corresponding CO_2 mass (m/z=44) CVs obtained simultaneously by in-line GCMS. The black traces in the figures were obtained under Ar feed. The cell temperature was 80 °C and back pressure was 300 kPa. All gas feed were humidified at RH of 100%.

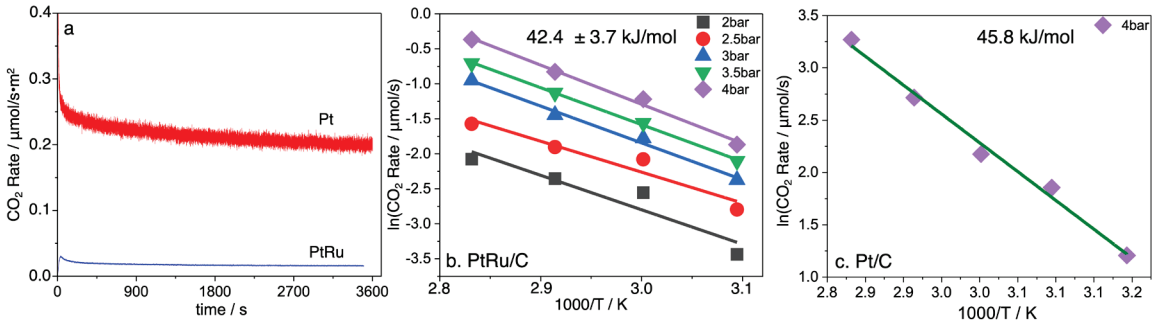

Figure 2. (a) The specific chronoamperometric current associated CO_2 on the Pt/C (red) and the PtRu/C (blue) measured at 0.5 V, 80 °C cell temperature, and 300 kPa back pressure. (b) Back pressure dependent measurements of the activation energy of CH_4 EO on the PtRu/C. (c) The measurements of the activation energy of CH

Figure 2a compares the chronoamperometric current associated CO_2 production measured at 0.5 V, 80 °C and 300 kPa back pressure on Pt/C (red) vs PtRu/C (blue). The results indicate that the LT-ECMRR activity was about 10 times higher on the Pt/C than on the PtRu/C, even though the evidence indicates that the surface Ru atoms of the latter anode were largely etched away. Figure 2b shows back-pressure dependent measurements of the activation energy of the LT-ECMRR on the PtRu/C and Figure 2c is that on Pt/C at the back pressure of 4 bar. The results reveal a largely back-pressure independent activation energy of the LT-ECMRR on the PtRu/C whose measured value is 42.4 kJ/mol (or 0.44 eV). A very similar value, 45.8 kJ/mol (or 0.47 eV), was also observed on the Pt/C. Notice

that the onset potential for the LT-ECMRR was almost the same on both anodes and lower than 0.3 V (vs. NHE), which is only slightly higher than the standard potential (0.17 vs RHE) for $CH_4 + 2H_2O \leftrightarrow CO_2 + 8H^+ + 8e^-$. *This indicates that for the active sites that enabled the observed LT-ECMRR, the reaction is rather counter-intuitively easy.*

By comparing CO_2 from the adsorbed LT-ECMRR intermediate stripping to that from the adsorbed CO stripping, we estimated that the number of active sites on the anode surface was about 14% on the Pt/C and about 3% on the PtRu/C. The preliminary DFT calculations presented in Figure 3 below suggest that the active sites are likely the Pt corner-/edge-like sites.

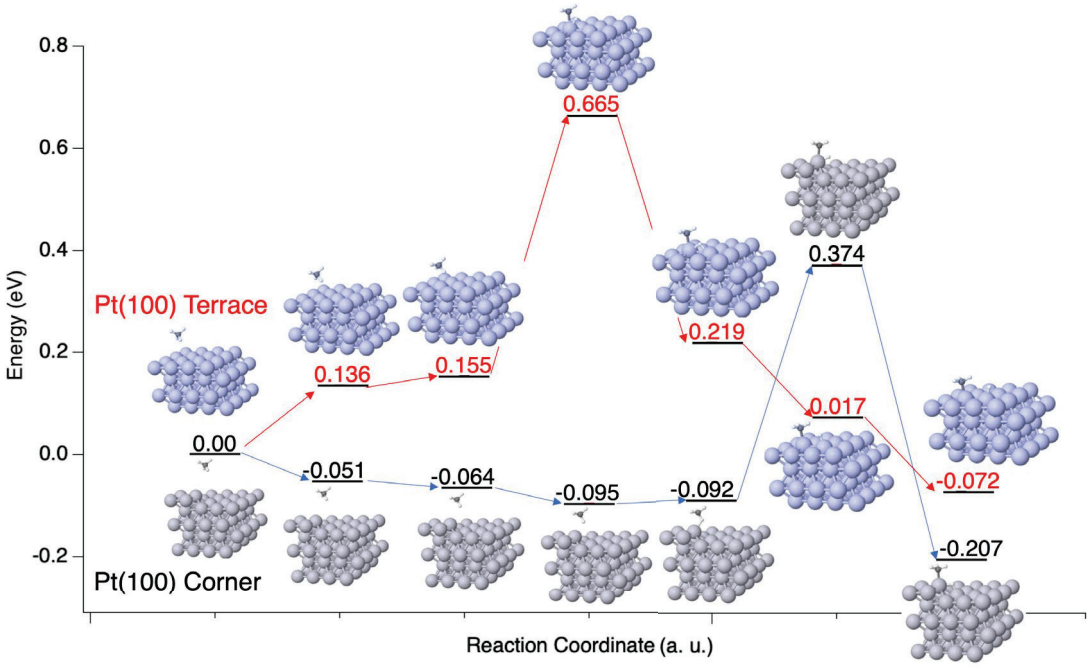

Figure 3. The preliminary energetic results of the DFT nudged elastic band calculations of C–H dissociation reaction of CH_4 on a Pt(100) corner site (black) vs on a Pt(100) terrace site (red).

Figure 3 shows the results of preliminary DFT nudged elastic band calculations of C–H dissociation reaction of CH_4 on a Pt(100) corner site (black) vs on a Pt(100) terrace site. For the Pt(100) corner site, the calculations reveal a shallow energy well before reaching the transition state. Its existence would significantly increase the surface residence time of CH_4 thus facilitate C–H bond dissociation. However, no such well exists for C–H dissociation on the Pt(100) terrace site. Moreover, the activation energy is much lower at the Pt(100) site (0.47 eV) than that at the Pt(100) terrace site (0.67 eV). The former compares extremely well with the experimentally determined value (0.44 eV) on the PtRu/C, Fig. 2b. Also, the dissociation products are more stable at the Pt(100) corner site (-0.21 eV) than at the terrace site (-0.072 eV). The above discussed comparison suggests strongly that the Pt corner/edge sites are likely the active sites for the LT-ECMRR.

Josh Vura-Weis

Ni and Fe photocatalysis revisited with transient XANES spectroscopy

Josh Vura-Weis
University of Illinois at Urbana-Champaign, Department of Chemistry

Presentation Abstract

We have applied steady-state and ultrafast XANES spectroscopy to re-evaluate the photophysics and photochemistry of transition metal complexes. The core-to-valence spectra at the K-edge (1s→valence), $L_{2,3}$-edge (2p→valence), and $M_{2,3}$-edge (3p→valence) are diagnostic of the spin state, oxidation state, and ligand field of the metal center. This element-specific probe, combined with femtosecond to picosecond time resolution, allowed us to disentangle excited-state pathways that were ambiguous when observed using visible-light probes. In our first subtask, we used tabletop femtosecond M-edge XANES to show that the primary photoproduct of μ-oxo Fe^{III} bisporphyrins is not the catalytically-active PFe^{II}/PFe^{IV}=O state, but instead an inactive PFe^{III+}/PFe^{III}-O^{-} state. No Fe^{IV}=O state was observed within the limits of our detection, suggesting that development of this class of photocatalysts should focus on altering the excited-state branching ratios and not on extending the lifetime of the scarcely-formed Fe^{IV}=O. In the second subtask, we performed picosecond K-edge and L-edge spectroscopy of the Ni^{II} center of (dtbbpy)Ni(*o*-tol)Cl. We confirm that the nanosecond lifetime of this complex observed in transient UV/Vis and IR spectroscopy is the ^{3}dd state, and not the once-postulated MLCT state. Furthermore, we show via ground-state XANES and magnetometry that the ground state has partial triplet character, which may influence the lifetime of the ^{3}dd state. Finally, we published the first XUV spectra of molecular 5d coordination complexes, showing that the 5p→5d and 4f→5d transitions in the 40-70 eV energy range are sensitive probes of the metal charge and ligand field.

DE-SC0018904: Catalytic Reaction Intermediates Revealed with Femtosecond M-edge XANES

PI: Josh Vura-Weis, Liviu Mirica (Co-PI)
Student(s): Lauren Boedicker, Jubyeong Chae, Laura Smith, Rachel Wallick

RECENT PROGRESS

Photochemistry of μ-oxo Fe(III) bisporphyrins revisited with M-edge XANES

μ-oxo iron^{III} bisporphyrins have been widely studied as earth-abundant and atom-economical photocatalysts for hydrocarbon oxidation using only light and molecular oxygen In the proposed catalytic pathway (Figure 1A, "Pathway A"), absorption of a visible or UV photon creates a LMCT state with one Fe^{II} and one Fe^{III}. This state then disproportionates into a free Fe^{II} porphyrin and a free Fe^{IV}=O porphyrin ("PFe^{II}/PFe^{IV}=O", where "P" represents the porphyrin). The PFe^{IV}=O reacts with a substrate to give an oxidized product. Although the reaction yields (product molecules formed vs reactants consumed) are high, the quantum yields (product molecules formed vs photons absorbed) are extremely low ($\leq 10^{-4}$). The predominant explanation for this poor performance is rapid reclamping of the PFe^{II}/PFe^{IV}=O species to reform the starting PFe^{III}-O-PFe^{III} dimer. However, an alternate hypothesis proposes that instead of the metal-centered oxidation/reduction discussed above, the LMCT state separates into a charge-separated state PFe^{III+}/PFe^{III}-O^{-}. Visible-light transient absorption spectroscopy revealed a few-ns excited state lifetime but the nature of this excited state could not be definitively assigned, with different research groups assigning the same spectrum to either PFe^{II}/PFe^{IV}=O or to PFe^{III+}/PFe^{III}-O^{-}. The central difficulty of this assignment is that only the porphyrin π-π* transitions in the visible region have appreciable oscillator strength, so changes to the metal electronic structure

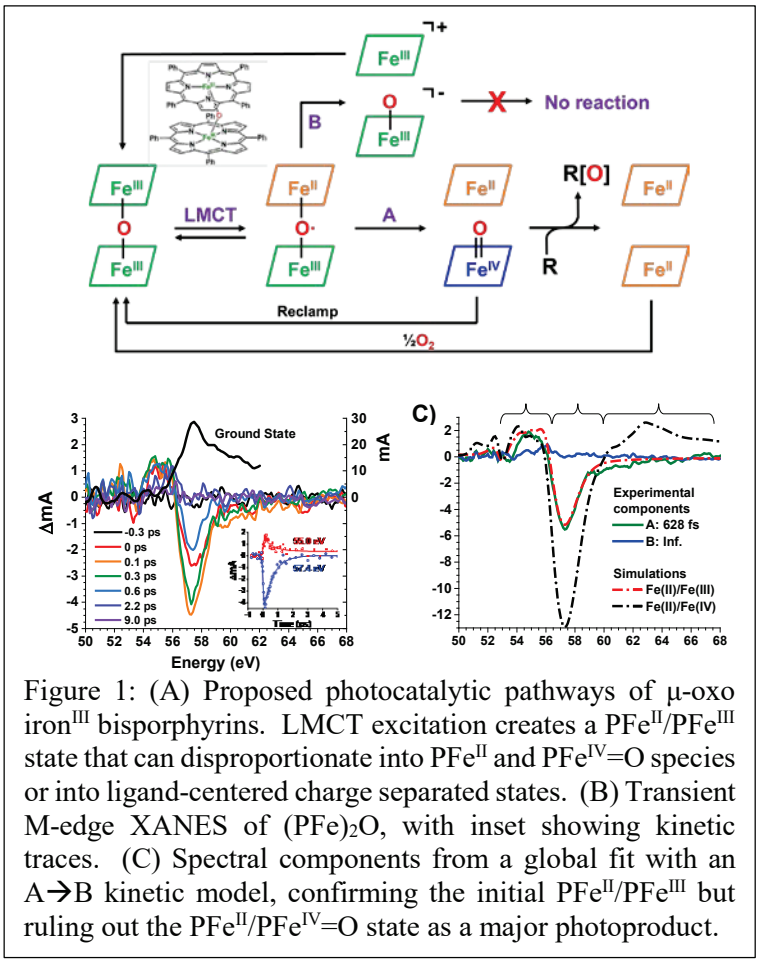

Figure 1: (A) Proposed photocatalytic pathways of μ-oxo iron^{III} bisporphyrins. LMCT excitation creates a PFe^{II}/PFe^{III} state that can disproportionate into PFe^{II} and PFe^{IV}=O species or into ligand-centered charge separated states. (B) Transient M-edge XANES of $(PFe)_2O$, with inset showing kinetic traces. (C) Spectral components from a global fit with an A→B kinetic model, confirming the initial PFe^{II}/PFe^{III} but ruling out the PFe^{II}/PFe^{IV}=O state as a major photoproduct.

must be deduced from subtle variations in the ligand spectrum

In order to resolve these competing hypotheses, we performed visible-pump, XUV-probe spectroscopy on μ-oxo bis [tetraphenylporphyrinato iron(III)]. As shown in Figure 1B, photoexcitation at 400 nm causes a bleach of the Fe^{III} ground-state peak at 57.5 eV and formation of a redshifted absorption feature at 55.0 eV. A global fit was performed using an A→B kinetic model, giving the component spectra in Figure 1C. The initial State A has a lifetime of 628 fs, and the nearly XUV-dark final State B lasted long past the 10 ps time window probed. These spectra were then compared to ligand field multiplet simulations of the LMCT (PFe^{II}/PFe^{III}) state and PFe^{II}/PFe^{IV}=O states. The LMCT state is a nearly quantitative match State A. However, the PFe^{II}/PFe^{IV}=O simulation predicts a factor-of-two stronger bleach at 57.4 eV (due to loss of the second Fe^{III}) and a new positive feature from 60-68 eV (due to the newly-formed Fe^{IV}). These changes are not observed in State B, which has only a weak positive signal at 56 eV. Pathway A is therefore ruled out as the majority photochemical pathway. The weak State B signal is consistent with Pathway B, in which both of the irons have reverted to high-spin Fe^{III} with a slightly modified ligand field. Given the signal-to-noise level of this experiment, the quantum yield of the catalytically-active PFe^{IV}=O must be a few percent or lower, placing a severe constraint on the overall yield of the photochemical reaction. Most importantly, this use of element- and oxidation-state spectroscopy provides clear guidance for optimization of this reaction: instead of seeking to increase the lifetime of the PFe^{IV}=O state, the branching ratio between the two pathways should be shifted by tuning the relative energies of the PFe^{III+}/PFe^{III}-O^{-} and PFe^{II}/PFe^{IV}=O pairs and the barriers to each dissociation pathway.

Evidence for ground-state triplet character in (dtbbpy)Ni(o-tol)Cl

Photo-assisted catalysis using Ni complexes is an emerging field for cross-coupling reactions in organic synthesis. We present L- and K-edge XAS, supported by Evans method nuclear magnetic resonance (NMR) and superconducting quantum interference device (SQUID) magnetometry, of a characteristic Ni photocatalyst, (dtbbpy)Ni(*o*-tol)Cl (dtb = 4,4'-di-*tert*-butyl, *o*-tol = *ortho*-tolyl). We show that at room temperature, the (dtbbpy)Ni(*o*-tol)Cl complex contains a mixture of singlet and triplet character, rather than adopting a pure singlet state as previously assumed. Our initial clue to this unusual spin state was L-edge XANES of the complex, as shown in Figure 2. A low-energy shoulder at 852.6 eV could only be modeled in semiempirical ligand field multiplet calculations using a ground-state electronic structure that contained ~30% triplet character. Intrigued by these results, we performed variable-temperature Evans-method NMR and SQUID magnetometry, and in both cases observed $\chi_M T$ values of ~0.4 cm^3 K mol^{-1}, intermediate between expected singlet and triplet values. Furthermore, NMR spectroscopy with an internal standard (benzodioxole) and spin integrating with respect to the standard peaks reveals a significantly decreased integration

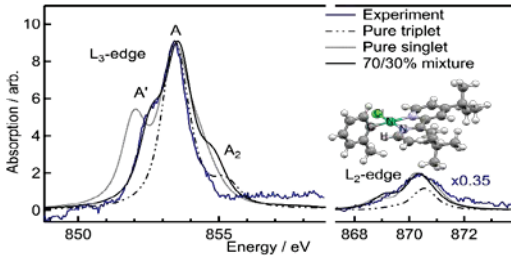

Figure 2: Experimental L_3- and L_2-edge XAS spectra with simulated spectra featuring different ratios between singlet and triplet character.

of the peaks corresponding to the diamagnetic, singlet-state complex, suggesting that the complex may contain only ~45% of diamagnetic material.

We then performed picosecond transient L-edge XANES to determine the electronic structure of a ~5 ns excited state observed Doyle et al in a series of reports, which first assigned this long-lived state as MLCT and later refined as ^{3}dd. After excitation at 343 nm, we observe a redshifted transient spectrum that lives for 4890 ps. By comparison to simulated excited state spectra, we assign this state as a tetrahedral ^{3}dd species. The admixture of triplet character is expected to increase the relaxation rate for distorted triplet excited states back to the ground state by making the transition partially spin-allowed.

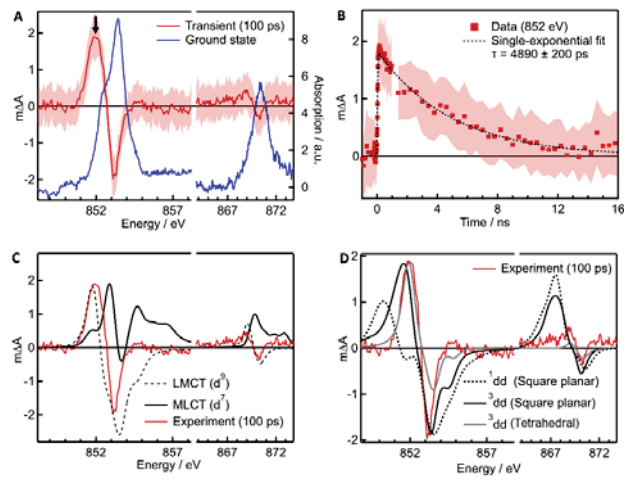

Figure 3: (A) L_3-edge transient spectrum of (dtbbpy)Ni(o-tol)Cl in DMF at after photoexcitation at 343 nm; (B) Kinetic trace collected at 852 eV (C) Simulations of MLCT and LMCT states (D) Simulations of high-lying ^{3}dd and ^{1}dd states

Tabletop XUV spectroscopy of 5d metals

Finally, we broadened the scope of XUV spectroscopy for catalytic applications to include 5d metals. Figure 4A shows XUV spectrum of $Ir^{III}(ppy)_3$, with O_3-edge (5p→5d) and $N_{6,7}$-edge (4f→5d) transitions. An energy level diagram of Ir^{III} and Ir^{IV} complexes with allowed transitions from the core orbitals to unoccupied valence orbitals is shown in Figure 4B. Upon MLCT excitation, a hole opens up in the t_{2g} orbital set, creating a new allowed transition at low energy. Oxidation of the metal center also stabilizes the core orbitals, blueshifting the core→e_g transitions. We then performed visible-pump, XUV-probe spectroscopy on this complex, giving the $N_{6,7}$-edge transient absorption spectrum shown in Figure 4C. The new 4f→t_{2g} peak appears at 60 eV, and derivative-shaped features at ~64 and 68 eV reflect the transient blueshift of the 4f→e_g peaks. This work opens up an entirely new class of molecules that can be studied with this tabletop technique.

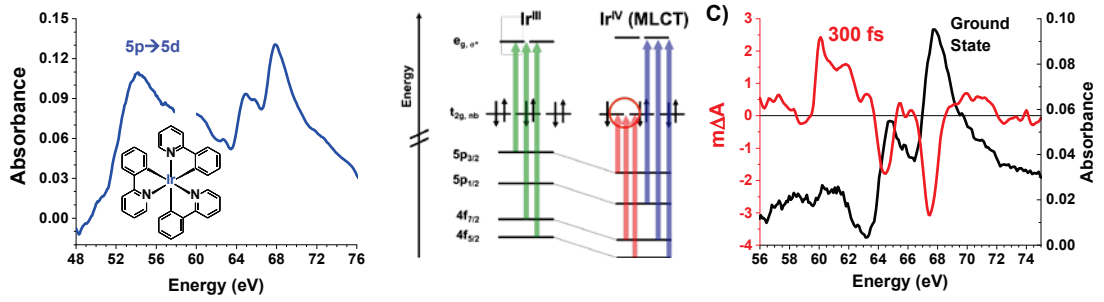

Figure 4. A) XUV spectrum of $Ir(ppy)_3$. B) Allowed transitions for Ir(III) and Ir(IV) in an octahedral ligands field. C) Transient $N_{6,7}$-edge XANES of $Ir(ppy)_3$ after 400 nm excitation.

Publications Acknowledging this Grant in 2020-2023

(I) Intellectually led by this grant

1. Wallick, R.F.; Chakrabarti, S.; Burke, J.H.; Gnewkow, R.; Chae, J.; Rossi, T.C.; Mantouvalou, I.; Kanngießer, B.; Fondell, M.; Eckert, S.; Dykstra, C.; Smith, L.E.; Vura-Weis, J.; Mirica, L.M.; van der Veen, R.M. Ground- and Excited-State Structure and Spin State of a Nickel-Bipyridine Photocatalyst Revealed by X-ray Absorption Spectroscopy. *Submitted*; ChemRxiv: 10.26434/chemrxiv-2023-3ckq3
2. Leahy, C.A.; Vura-Weis, J. Femtosecond extreme ultraviolet spectroscopy of an iridium photocatalyst reveals oxidation state and ligand field specific dynamics. *J. Phys. Chem. A*; **2022**; 126; 9510-9518
3. Sye, K.S.; Leahy, C.A.; Vura-Weis, J. Low quantum efficiency of μ-oxo iron bisporphyrin photoacatalysts explained with femtosecond M-edge XANES. *Catalysis Science and Technology*; **2022**; 12, 6097
4. Shari'ati, Y.; Vura-Weis, J. Ballistic ΔS= 2 Intersystem Crossing in a Cobalt Cubane Following Ligand-Field Excitation Probed by Extreme Ultraviolet Spectroscopy. *Phys. Chem. Chem. Phys*; **2021**; 23; 26990-26996
5. Shari'ati, Y.; Vura-Weis, J.Polymer thin films as universal substrates for extreme ultraviolet absorption spectroscopy of molecular transition metal complexes. *J. Sync. Rad*; **2021**;28; 1850

(II) Jointly funded by this grant and other grants with intellectual leadership by other funding sources

1. Cavedon, C.; Gisbertz, S.; Reischauer, S.; Vogl, S.; Sperlich, E.; Burke, J.H.; Wallick, R.F.; Schrottke, S.; Hsu, W.-H.; Anghileri, L.; Pfeifer Y.; Richter, N.; Teutloff, C.; Müller-Werkmeister, H.; Cambié, D.; Seeberger, P.H.; Vura-Weis, J.; van der Veen, R.M.; Thomas, A.; Pieber, B. Intraligand Charge Transfer Enables Visible-Light-Mediated Nickel-Catalyzed Cross-Coupling Reactions. *Angew. Chemie. Int. Ed.*; **2022**; 61; e202211433
2. Leahy, C.A.; Drummond, M.J.; Vura-Weis, J.; Fout, A.R. Synthesis of a series of M(II) (M = Mn, Fe, Co) chloride complexes with both inter- and intra-ligand hydrogen bonding interactions. *Dalton Trans*; **2021**; 50; 12088

Huamin Wang and Johannes A. Lercher

Towards a polyolefin-based refinery: Understanding and controlling the critical reaction steps

Johannes A. Lercher

Institute for Integrated Catalysis, Pacific Northwest National Laboratory, Richland, WA 99352, USA.

Presentation Abstract

Waste polymers pose a significant environmental challenge due to their durability and pervasive presence in contemporary products. Instead of viewing discarded polymers merely as waste, we should recognize them as untapped reservoirs of carbon. Rather than discarding them, these polymers should be repurposed, leveraging the carbon and energy originally invested in their production. Achieving this vision mandates a deep understanding of the foundational processes that enable the low-temperature transformation of spent plastics into a diverse array of products, from fuels and lubricants to the building blocks of new polymers. This project primarily targets polyolefins, which, while being among the most resilient, are also the most produced and thus, most prevalent in plastic waste. Polyolefins will be converted by kinetically and thermodynamically coupling the endothermic cleaving of C-C bonds with the exothermicity of the formation of new C-H and C-C bonds, enabling a low operation temperature. Specifically, we link the primary C-C bond cleavage to alkylation, metathesis, and hydrocracking. While the kinetic coupling enables complete conversion from a thermodynamic perspective, we use reactant environments, interactions with Lewis acid sites, tailored solvents and catalysts to accelerate the kinetic events that convert the polyolefin strands and intermediates at lower temperatures than currently practiced.

FWP 78459: Towards a polyolefin-based refinery: Understanding and controlling the critical reaction steps

PI: Johannes A. Lercher
Co-PI: Jianzhi Hu, Mal-Soon Lee, Jingguang Chen (Columbia University), Michele L. Sarazen (Princeton University), Susannah Scott (UC Santa Barbara)

RECENT PROGRESS

Low-temperature upcycling of polyolefins into liquid alkanes via tandem cracking-alkylation

Selective upcycling of polyolefin waste has been hampered by the relatively high temperatures that are required to cleave the carbon-carbon (C-C) bonds at reasonably high

rates. We present a distinctive approach that uses a highly ionic reaction environment to increase the polymer reactivity and lower the energy of ionic transition states. Combining endothermic cleavage of the polymer C-C bonds with exothermic alkylation reactions of the cracking products enables full conversion of polyethylene and polypropylene to liquid isoalkanes (C_6 to C_{10}) at temperatures below 100 °C (Figure 1). Both reactions are catalyzed by a Lewis acidic species that is generated in a chloroaluminate ionic liquid. The alkylate product forms a separate phase and is easily separated from the reactant catalyst mixture. The process can convert unprocessed post-consumer items to high-quality liquid alkanes with high yields. Acidic chloroaluminate-based ionic liquids as emerging alkylation catalysts have already been industrially used in the paraffin alkylation process. We thus envision that this upcycling strategy can be rapidly implemented not only in newly designed plants but also in existing refining technology. The synchronous release of alkenes via polyolefin cracking in the presented cascade cracking-alkylation conceptually allows for better control of product distribution and minimization of the formation of red oil waste, making polyolefins potential feed for refining alkylation. This work opens a transformative scalable approach to convert polyolefins and enables a critical contribution to a circular carbon economy.

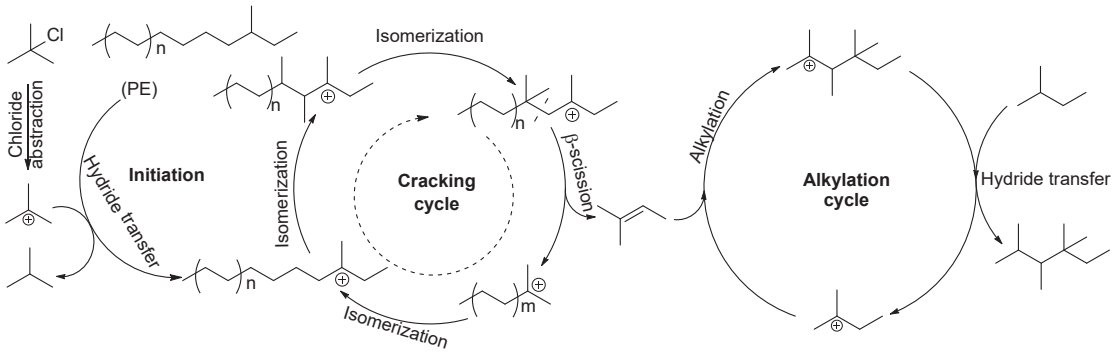

Figure 1. Upon initiation enabled by tertbutyl chloride, the C-C bond scission in the cracking cycle couples with the C-C bond formation in the alkylation cycle.

Conversion of polyethylene waste to short-chain hydrocarbons under mild temperature and hydrogen pressure with metal-free and metal-loaded MFI zeolites

Catalytic hydrocracking on supported metal zeolites promisingly converts waste plastics into more valuable hydrocarbons. Although the presence of metal sites on solid acids is typically considered necessary for C-C bond cleavage of alkanes at modest temperatures, polyethylene depolymerization on metal-free MFI zeolites proceeds at higher rates than analogous metal-loaded MFI zeolites (Pt, Ni) under mild reaction conditions (Figure 2). Higher rates on metal-free MFI are consistent with higher ratios of alkenes to alkanes, leading to subsequent alkene-mediated beta-scission events that form smaller molecules. Under varied reaction conditions both metal-free and metal-loaded MFI catalysts demonstrate high selectivity to C_3-C_7 gaseous hydrocarbons, likely due to the 10-MR channel structure. Collectively, these findings demonstrate the importance of deconvoluting metal and acid site contributions for polyethylene hydrocracking. We are currently working on performing such deconvolution and on studying the roles of the

zeolite structure and the composition, and size, of the metal phase on polymer conversion via hydrogenolysis and hydrocracking.

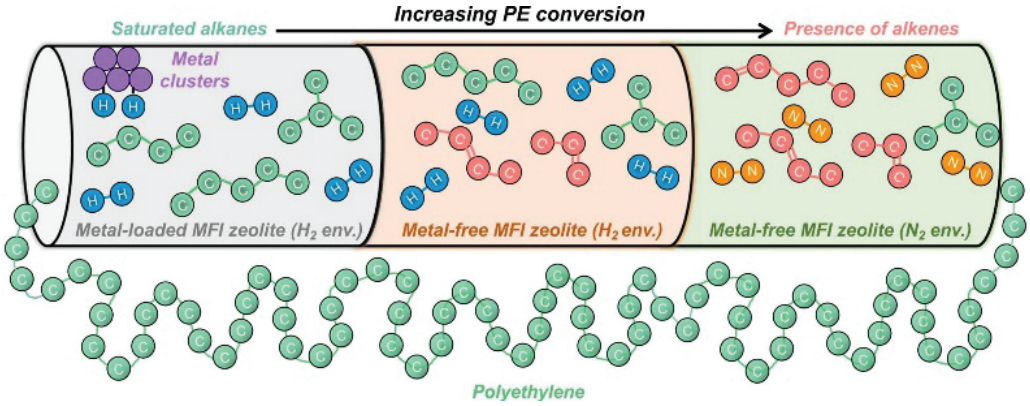

Figure 2. Catalytic cracking of polyethylene on metal-free zeolites under both H_2 and N_2 environments is significant even at mild reaction temperatures, producing small quantities of alkenes that further catalyze C-C bond scission events in polyethylene.

Publications Acknowledging this Grant in 2020-2023

1) Publications intellectually led by this FWP

1. Zhang, W.; Kim, S.; Wahl, L.; Khare, R.; Hale, L.; Hu, J.; Camaioni, D.M.; Gutiérrez, O.Y.; Liu, Y.; Lercher, J.A. Low-temperature upcycling of polyolefins into liquid alkanes via tandem cracking-alkylation. *Science* **2023**, *379*, 807–811
2. Tan, J. Z.; Hullfish, C. W.; Zheng, Y.; Koel, B. E.; Sarazen M. L. Conversion of polyethylene waste to short chain hydrocarbons under mild temperature and hydrogen pressure with metal-free and metal-loaded MFI zeolites. *Appl. Catal. B: Environ.* **2023**, *338*, 123028-123039
3. Chen, L.; Zhu, Y.; Meyer, L. C.; Hale, L. V.; Le, T. L.; Karkamkar, A.; Lercher, J. A.; Gutiérrez, O. Y.; Szanyi, J. Effect of reaction conditions on the hydrogenolysis of polypropylene and polyethylene into gas and liquid alkanes. *React. Chem. Eng*. **2022**, *7*, 844.

2) *Publications jointly funded by this grant and other grants with intellectual leadership by other funding sources:*

1. Chen, L.; Meyer, L. C.; Kovarik, L.; Meira, D.; Pereira-Hernandez, X. I.; Shi, H.; Khivantsev, K.; Gutiérrez, O. Y.; Szanyi J. Disordered, Sub-Nanometer Ru Structures on CeO_2 are Highly Efficient and Selective Catalysts in Polymer Upcycling by Hydrogenolysis. *ACS Catal.* **2022,** *12,* 4618-4627

Timothy H. Warren

Electrocatalytic Ammonia Oxidation by Earth-Abundant Metal Complexes

Md Estak Ahmed, Pokhraj Ghosh, Danushka Ekanayake, Fatimah Alsultan, and Timothy H. Warren*

Department of Chemistry, Michigan State University, East Lansing, MI 48824, United States

Presentation Abstract

Molecular catalysts for ammonia oxidation to dinitrogen represent enabling components to utilize ammonia as a fuel and/or source of hydrogen. Ammonia oxidation requires not only the breaking of multiple strong N-H bonds, but also controlled N-N bond formation. Owing to its high energy density and established global production and distribution networks, ammonia (NH_3) is an appealing fuel, particularly when synthesized by green methods. On a per-hydrogen atom basis, ammonia contains nearly the same chemical energy as hydrogen (H_2). Thus, sustainable catalysts that electrocatalytically oxidize ammonia for fuel cells or on-demand hydrogen production with only nitrogen (N_2) as a byproduct are highly desirable.

We describe electrocatalytic ammonia oxidation using molecular systems based on Earth-abundant copper and iron. Each approach focuses on enabling the conversion of NH_3 to masked forms of the amidyl radical $\bullet NH_2$ via PCET. Copper(I) β-diketiminate catalysts [Cu^I] enable ammonia oxidation via deprotonation of oxidized copper(II) ammine complexes $\{[Cu^{II}]\text{-}NH_3\}^+$ to form copper(II) amide species [Cu^{II}]-NH_2. The significant unpaired electron density on the amide N atom in [Cu^{II}]-NH_2 facilitates N-N coupling to dicopper(I) hydrazine species [Cu^I]-NH_2NH_2-[Cu^I]. While experimental studies reveal that ferrocenium (Fc^+) can stoichiometrically oxidize NH_3, a combination of mechanistic and computational studies suggests that outersphere oxidation of H-bonded ammonia dimers or trimers $[NH_3]_x$ (x = 2 or 3) occurs. To encourage H-bonding near the Fc^+ center, we synthesized a family of ferrocene complexes that feature pendant pyridine bases that serve as efficient electrocatalysts for ammonia oxidation. We hypothesize that a pendant pyridyl base engages in H-bonding to ammonia that facilitates PCET of the H-bonded ammonia molecules to give an amidyl radical ($\bullet NH_2$) stabilized by a protonated pyridinium base en route to hydrazine ($H_2N\text{-}NH_2$) that undergoes facile oxidation to nitrogen (N_2).

Grant or FWP Number: Grant or FWP Number: DE-SC001779
Catalytic Interconversion of Ammonia and Dinitrogen at Base Metals

Student(s): Josalyne A. M. Beringer, Fatimah Alsultan

Postdoc(s): Dr. Estak Ahmed, Dr. Pokhraj Ghosh, Dr. Danushka Ekanayake

RECENT PROGRESS

Electrocatalytic ammonia oxidation by copper β-diketiminates

Using [^{i}Pr$_2$NN$_{F6}$]Cu as a model electrocatalyst for ammonia oxidation by copper(I) β-diketiminate complexes [Cu^{I}], we outline a rate law from a detailed analysis of NMR and electrochemical data. NMR spectroscopy indicates that the catalyst system rests as [Cu^{I}]-NH$_3$ and the response of the catalytic current due to changes in the catalyst concentration and the ammonia concentration provides for the expression: rate = k[[Cu^{I}]-NH$_3$][NH$_3$]. Moreover, monitoring electrocatalysis by varying the concentration of ND$_3$ indicates a KIE of 2.4(2), indicating that there is some N-H/N-D bond breaking before or in the turnover limiting step. Importantly, controlled potential electrolysis indicates that this catalytic system generates N$_2$ and H$_2$ with faradaic efficiencies of 84 and 74%, respectively over multiple hours.

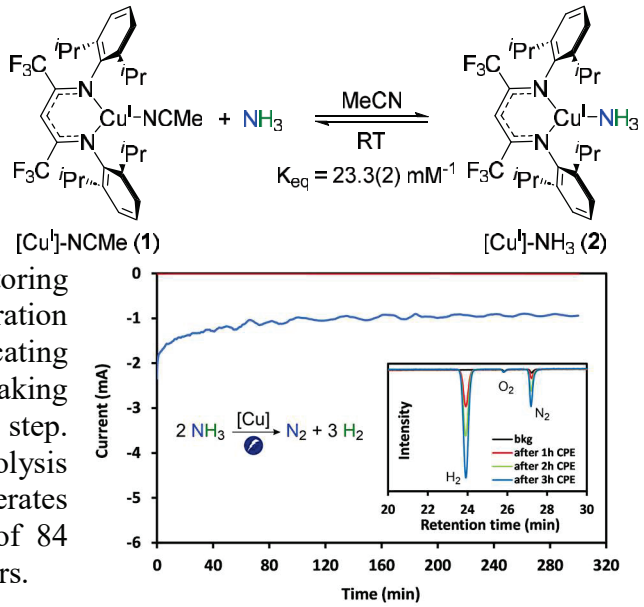

We have been able to isolate a number of intermediates in this reaction that include the novel three coordinate{[Cu^{II}]-NH$_3$}PF$_6$ that undergoes ready deprotonation by NH$_3$ to give the dicopper(I) hydrazine complex [Cu^{I}]$_2$(μ-NH$_2$NH$_2$). Combined with electrochemical data, this allows us to construct a detailed electrocatalytic cycle that involves oxidation of [Cu^{I}]-NH$_3$ to {[Cu^{II}]-NH$_3$}$^+$, deprotonation of {[Cu^{II}]-NH$_3$}$^+$ by NH$_3$ to form [Cu^{II}]-NH$_2$ and NH$_4^+$ followed by N-N dimerization of [Cu^{II}]-NH$_2$ to form [Cu^{I}]$_2$(μ-NH$_2$NH$_2$). Hydrazine is oxidized at the glassy carbon electrode under these catalytic conditions. Moreover, in an open cell set up, NH$_4^+$ is reduced to NH$_3$ and ½ H$_2$ at the counter electrode that serves as the cathode in the electrochemical cell used for CPE experiments.

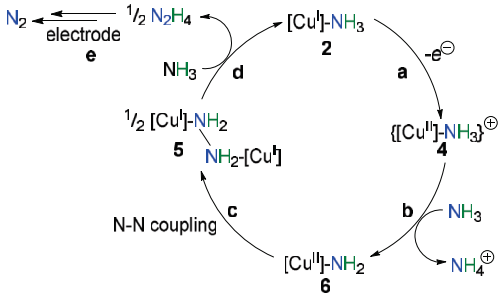

DFT studies allow a mapping of the energetic landscape for the productive transformations that enable oxidation of ammonia to hydrazine. Importantly, the highest energy step is deprotonation of {[Cu^{II}]-NH$_3$}$^+$ to form [Cu^{II}]-NH$_2$, consistent with electrochemical rate data. Curiously, binding of NH$_3$ to {[Cu^{II}]-NH$_3$}$^+$ to form {[Cu^{II}](NH$_3$)$_2$}$^+$ is a bit uphill, but this bisammine complex is very difficult to deprotonate to [Cu^{II}](NH$_2$)(NH$_3$). Thus, the reversible redox wave we observe with increasing intensity as the ammonia concentration is increased from 0.5 – 1.3 M signals the formation of the {[Cu](NH$_3$)$_2$}$^{0/+}$ redox couple.

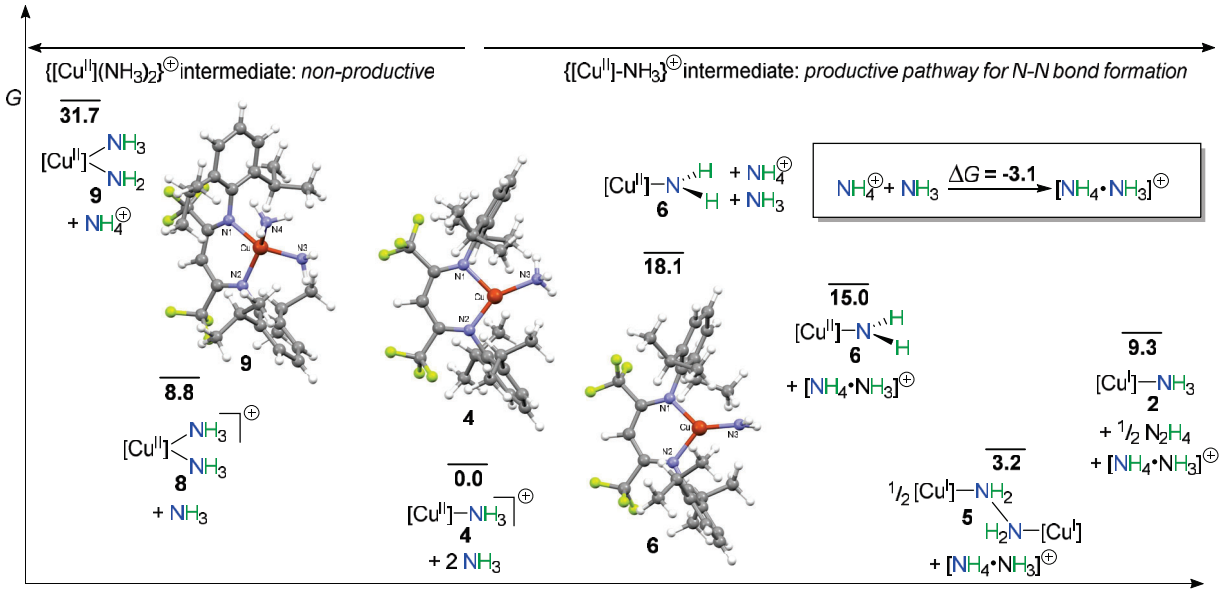

Lastly, addition of small, increasing amounts of DBU – a non-coordinating, strong base – also enhances the rate of electrocatalysis, signaling that deprotonation of $\{[Cu^{II}]\text{-}NH_3\}^+$ is likely the turnover limiting step.

Ammonia oxidation via ferrocene derivatives

Ferrocenium (Fc^+) stoichiometrically and catalytically oxidizes NH_3 to N_2. While first order in $[Fc^+]$, kinetic studies reveal a mixed 2nd / 3rd order in $[NH_3]$: rate = $(k_2[NH_3]^2 + k_3[NH_3]^3)[Fc^+]$. Additionally, there is evidence for ion pairing with the PF_6^- anion as the observed rate exhibits an inverse first-order dependence on $[PF_6]^-$. Employing simple ferrocene derivatives that include 1,1'-dimethylferrocene (1,1'-Me_2Fc) and the sulfonated species 1,1'-Me_2FcSO_3K, this electrocatalytic system that generates N_2 exhibits modest overpotentials (0.81 - 0.94 V) for catalytic ammonia oxidation compared to other reported molecular electrocatalysts. Perhaps more importantly, some of these robust catalysts operate in energy-dense, liquid ammonia in which many coordination compounds would be converted to Werner complexes $[M(NH_3)_6]^{n+}$ inactive towards ammonia oxidation.

We interpret the 2nd and 3rd order dependence of $[NH_3]$ in stoichiometric ammonia oxidation to reflect the need to pre-assemble ammonia dimers $[NH_3•NH_3]$ and trimers $[NH_3•NH_3•NH_3]$ around ferrocenium prior to 1-electron oxidation. While the B3LYP level of theory predicts that the formation of these aggregates are endergonic at +6 and +13 kcal/mol, respectively, they are *much* easier to ionize than free NH_3 giving overall thermodynamic barriers of 25.0 and 26.7 kcal/mol vs. the Fc^+/Fc couple in MeCN.

We have recently discovered that DMSO is a useful solvent for electrocatalytic ammonia oxidation due to its ability to support higher concentrations of ammonia at room temperature. In the presence of 0.1M $[Bu_4N]PF_6$ as electrolyte, DMSO enables formation of 2.4 M saturated solutions of ammonia at 1 atm NH_3 whereas MeCN only allows 1.3 M saturated solutions.

Ammonia oxidation via ferrocenes with pendant amine arms

We have begun to explore strategies to encourage NH_3 to engage in related H-bonding interactions near the ferrocenium catalyst that could accelerate ammonia oxidation by thermodynamically lowering the oxidation potential of NH_3 while accelerating outer-sphere electron transfer. Tethering of an oxidation of a 2-pyridyl group to ferrocene in ^{py}Fc results in a much more active ammonia oxidation catalyst than ferrocene alone. Due to the slightly greater electron-richness of the iron center, the onset potential for ammonia oxidation is lower at ca. -0.120 V vs. Fc^+/Fc corresponding to a lower overpotential for ammonia oxidation η = 820 mV. Analysis by cyclic voltammetry in DMSO indicates that the reaction is both first order ^{py}Fc and NH_3 to give a rate law: rate = $k[^{py}Fc][NH_3]$ with TOF_{max} = 125 h^{-1} ($[NH_3]$ = 2.4 M). Moreover, we observe a primary kinetic isotope effect k_H/k_D = 2.05(8) in electrocatalysis of NH_3 and ND_3.

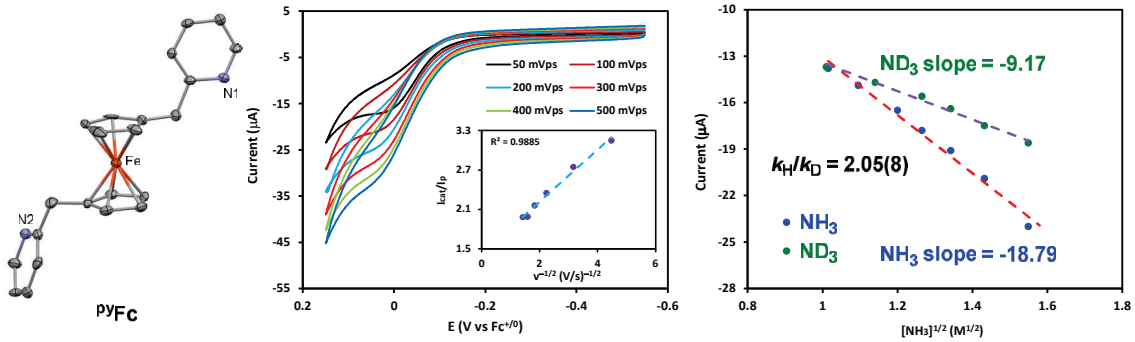

Enabling rates much higher than ferrocene alone, the pendant pyridyl group plays a crucial role in ammonia oxidation. We hypothesize that ammonia engages in H-bonding with the pendant pyridyl group [py···H-NH_2] near the ferrocene center. Once the ferrocene center is oxidized, this interaction facilitates proton-coupled electron transfer (PCET) of this H-bonded entity to form a pyridinium cation H-bonded to an amidyl radical $[pyH\cdots NH_2]^{+/\bullet}$ that enables rapid N-N bond formation to give H_2N-NH_2 that is rapidly oxidized to N_2 under electrocatalytic conditions.

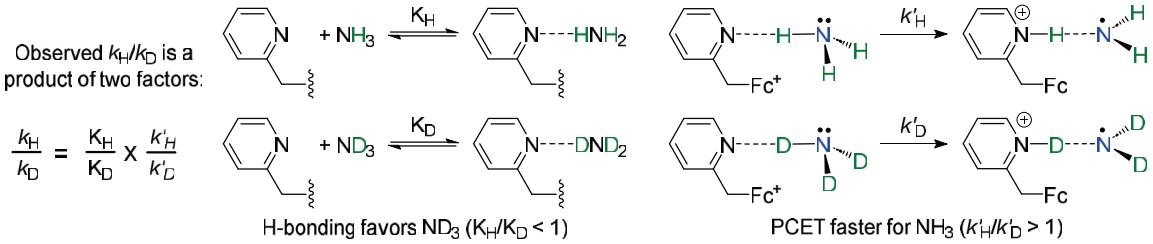

Survey of a small range of pyridyl substituents reveal that the use of more electron-rich pyridine groups both enhances the rate and lowers the overpotential. Moreover, the experimentally measured isotope effect decreases with increasing electron-richness of the pyridyl substituents. We view this as a combination of an equilibrium thermodynamic isotope effect that favors H-bonding by electron-rich pyridine groups (K_H/K_D < 1) preceding the PCET step with a primary kinetic isotope effect (k_H/k_D > 1).

These studies reveal the profound effect that H-bonding of ammonia to a base can have in electrocatalytic ammonia oxidation, suggesting the possibility of metal-free catalysts that take advantage of this interaction near an anode surface.

Publications Acknowledging this Grant in 2020-2023

(I) Intellectually led by this grant

Gardner, E. J.; Marguet, S. C.; Cobb, C. R.; Pham, D. M.; Beringer, J. A. M.; Bertke, J. A.; Shafaat, H. S.*; Warren, T. H.* Uncovering Redox Non-Innocent H-Bonding in Cu(I)-Diazene Complexes. *J. Am. Chem. Soc.* **2021**, *143*, 15960-15974.

Ahmed, M. E.; Boroujeni, M. R.; Ghosh, P.; Greene, C.; Kundu, S.; Bertke, J. A.; Warren, T. H.* Electrocatalytic Ammonia Oxidation by a Low Coordinate Copper Complex. *J. Am. Chem. Soc.* **2022**, *144*, 21136-21145.

Boroujeni, M. R.; Greene, C.; Bertke, J. A.; Cundari, T. R.; Warren, T. H.* Chemical and Electrocatalytic Ammonia Oxidation by Ferrocenium, *ChemRxiv* **2023**, doi: 10.26434/chemrxiv-2023-l1dtg-v2.

Linking operando spectroscopy with microkinetic modeling to unravel the catalytic mechanism for CH_4 oxidation on $IrO_2(110)$

Jovenal Jamir[1,†], Minkyu Kim[2,†], Connor Pope[1], Aravind Asthagiri[3*] and Jason F. Weaver[1*]

[1]Department of Chemical Engineering, University of Florida, Gainesville, FL 32611, USA

[2]School of Chemical Engineering, Yeungnam University, 280 Daehak-Ro, Gyeongsan 38541, Republic of Korea

[3]William G. Lowrie Chemical & Biomolecular Engineering, The Ohio State University, Columbus, OH 43210, USA

Operando surface spectroscopy can play a key role in developing first-principles microkinetic models that accurately represent the mechanism of heterogenous catalytic reactions and identify the roles of various surface species in the catalytic chemistry. The kinetics of the catalytic oxidation of CH_4 on the $IrO_2(110)$ surface was investigated both experimentally and using a first-principles microkinetic model that was revised to incorporate pathways for the formation of CHO_2 surface species observed under catalytic conditions using high-resolution, ambient pressure x-ray photoelectron spectroscopy (AP-XPS). Our results show that including pathways for surface CHO_2 formation is necessary for reproducing observations of a transition from CH_4 promotion to inhibition of the catalytic oxidation rate on $IrO_2(110)$ as the reactant mixture becomes enriched in CH_4 as well as the formation of high coverages of surface CHO_2 and HO species during the catalytic reaction. Analysis of the microkinetic simulations reveals that the catalytic oxidation of CH_4 on $IrO_2(110)$ occurs through a pathway in which CH_4 oxidizes to adsorbed CO prior to CO_2 and H_2O formation while surface CHO_2 species inhibit this pathway by occupying active surface sites. Only modest destabilization of the dominant CHO_2 surface species is needed to significantly improve agreement between the simulated and experimentally-determined kinetics and species coverages, demonstrating the critical role of CHO_2 in influencing catalytic CH_4 oxidation on $IrO_2(110)$. This study shows how operando AP-XPS measurements and molecular simulations can be used cooperatively to develop a mechanistic description of a complex heterogeneous catalytic reaction in which the roles of various surface species are accurately determined.

Christopher W Jones

Non-Orthogonal Tandem Catalysis in Compartmentalized Nanoreactors

Eman Ahmed (NYU), Jinwon Cho (GT), Seung Soon Jang (GT), Christopher W. Jones (GT), Fangbei Liu (NYU), Joshua Polster (NYU), Marcus Weck (NYU), Jules Zambito (NYU), and Wenyang Zhao (GT)

(NYU) Department of Chemistry and Molecular Design Institute, New York University, New York, NY 10003
(GT) School of Chemical & Biomolecular Engineering and School of Materials Science & Engineering, Georgia Institute of Technology, Atlanta, GA 30332

Presentation Abstract

In living systems, different catalytic reactions occur simultaneously in separated domains without interference due to a process known as compartmentalization. The creation of artificial systems with multiple compartments, however, hasn't been extensively documented. Developing these compartmentalized catalysts mimicking the biological systems can potentially advance the synthesis of intricate molecules more efficiently. Such catalysts can lead to better resource use, easier purification processes, cost reductions, waste reductions, and environmentally-friendly chemical conversions. By studying and replicating aspects of living systems, like isolating reaction sites and directing substrates, the research team is exploring the possibilities of compartmentalized nanoreactors, both theoretically and experimentally, where different chemical transformations, catalytic active sites, and reaction intermediates are present in distinct spaces. This collaborative work is focusing on the catalyst design and performance evaluation, such as polymers and inorganic substances, utilized for fixing catalysts and creating compartments. We are delving into unique nanoreactors crafted for sequential reactions that are generally incompatible. By tuning factors such as the nature, composition, and the functionality of the polymers, as well as characteristics of porous inorganic materials, our aim is to understand how to design compartmentalized catalysts for incompatible reactions effectively.

DE-FG02-03ER15459: Multi Compartment Nanoreactors as Supports for Incompatible Molecular Catalysts

PI: Seung Soon Jang, Christopher W. Jones, Marcus Weck
Postdoc(s): Wenyang Zhao
Student(s): Eman Ahmed, Jinwon Cho, Fangbei Liu, Joshua Polster, Jules Zambito

RECENT PROGRESS

Multicompartment Copolymer Nanoreactors

Nanostructured materials, inspired by nature, often consist of multiple discrete domains. Classic examples are the membrane-bond organelles or microcompartments in eukaryotic cells. These compartments enable incompatible chemical transformations to occur simultaneously and in close proximity. Multicompartment micelles (MCMs) mimic this concept by compartmentalizing three or more mutually incompatible blocks in one pot for potential use in non-orthogonal cascade catalysis.

Our functionalized MCM design contains hydrophilic (**H**), lipophilic (**L**), and fluorophilic (**F**) bottlebrush copolymers that spontaneously self-assemble in aqueous media (Figure 1). The bottlebrush copolymers have been synthesized using living ring-opening metathesis polymerization (ROMP). The MCMs are comprised of a hydrophobic poly(styrene) and poly(pentafluorostyrene) blocks in the core, surrounded by a hydrophilic carboxylic acid block and a hydrophilic poly(ethylene glycol) solubilizing block as the shell. We explored the catalytic activity for the incompatible transformations of a deacetalization-Knoevenagel reaction and a condensation-Michael addition. We synthesized three polymers: an acid-functionalized polymer **COOH**$_{40}$-**H**$_{60}$-**L**$_{15}$-**F**$_{15}$ (**P1**), a base-functionalized polymer **H**$_{60}$-**L**$_{15}$-**Proline**$_{36}$-**F**$_{15}$ (**P2**), and an acid-base bifunctional polymer **COOH**$_{40}$-**H**$_{60}$-**L**$_{15}$-**Proline**$_{36}$-**F**$_{15}$ (**P3**). All bottlebrush copolymers were assembled by solvent exchange, using THF and water to form **MCMs 1-3**. Catalytic tests showed that a physical mixture of **MCM 1** and **2** promoted the cascade reaction, but with lower efficiencies in comparison to **MCM 3,** which contains both domains in a single polymer particle. Furthermore, the substrate scope of bifunctional **MCM 3** was investigated using nitro-substituted acetals and benzaldehyde-substituted diethyl acetals. All catalytic tests above resulted in high conversions and excellent yields. These results demonstrate the first advanced application of MCMs in nonorthogonal cascade transformations.

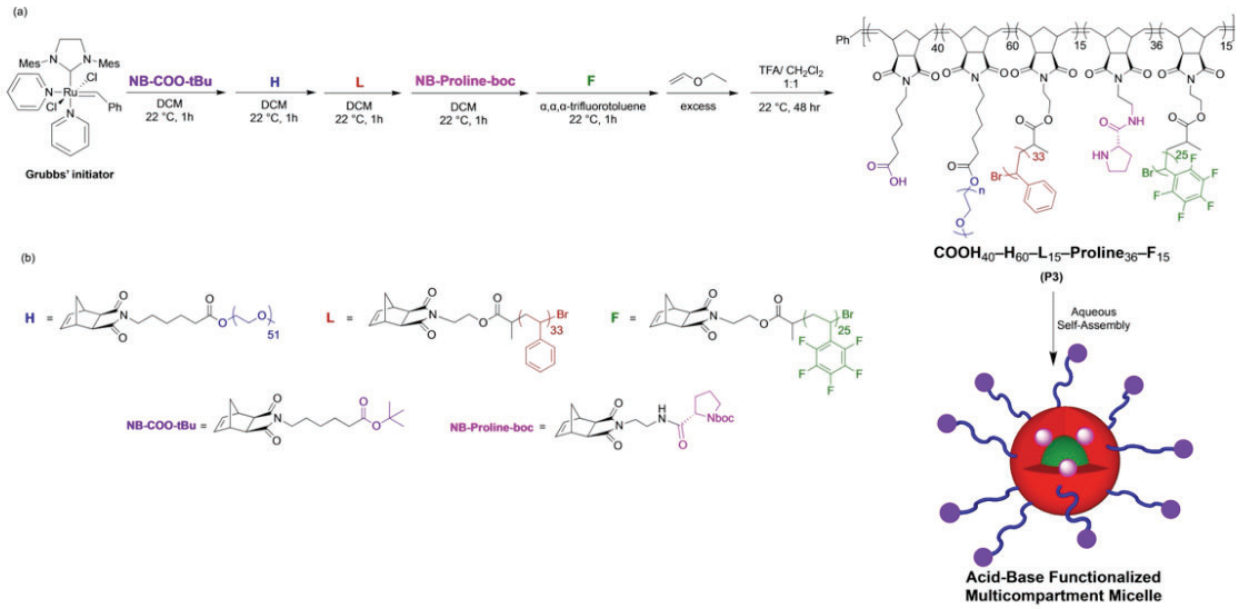

Figure 1. (a) Schematic representation of the preparation of acid-base functionalized MCMs synthesized by ROMP; (b) Chemical structures of **H**, **L**, and **F** macromonomers and the protected acid and L-proline containing *exo*-norbornenes.

Thermal and Photoresponsive Shell Cross-linked Micelles

Enzymes can convert certain substrates among many others with high turnover numbers. Diffusion of substrates in enzymes within nanochannels can be controlled using external stimuli. The team has successfully demonstrated substrate diffusion regulated by light in artificial nanoreactors using photoresponsive cross-linking blocks. The current challenge is applying two or more stimuli to control the reaction pathway. Shell cross-linked micelles (SCMs) with a hydrophobic core, a thermoresponsive hydrophilic corona, and a photoresponsive cross-linked shell have been synthesized and investigated for substrate-selective asymmetric transfer hydrogenation (ATH).

We fabricated the thermo and photoresponsive SCMs based on amphiphilic poly(2-oxazoline) triblock copolymers through living cationic ring-opening polymerization. The SCMs incorporate a thermoresponsive poly(2-isopropyl-2-oxazoline) as the hydrophilic corona and are covalently cross-linked with a photoswitchable spiropyran molecule. Chiral rhodium complexes were immobilized at the hydrophobic core of the SCMs through thiol-ene click chemistry to form the nanoreactors. The SCM-based nanoreactors catalyzed substrate-selective ATH for aromatic ketones in aqueous environment. The thermosresponsiveness of the SCMs was confirmed by turbidimetry measurements of UV-Vis spectroscopy (Figure 2A). Cloud point (T_{cp}) of 56 °C was determined at the mid-point of the heating curves. The SCMs with lower critical solution temperature behavior exhibit a hydrophilic-hydrophobic transition in the outer layer upon heating above T_{cp}. Photoresponsiveness was determined by dynamic light scattering (DLS) showing a decrease of 40 nm in micelle hydrodynamic diameter while switching from visible light to UV light (Figure 2B). A hydrophobic-hydrophilic transition occur in the spiropyran cross-linked layer under UV light irradiation. The external stimuli trigger morphology switching, which alter the hydrophobicity in separate layers of the SCMs, resulting in dynamic substrate selectivity of ATH transformations. Upon UV light irradiation, conversion promotes the less hydrophobic substrates. Temperature elevation, however, has an opposite effect, which allows conversion promotes the

more hydrophobic substrates (Figure 3). Light and temperature switches allow for tunable reaction pathway control and dynamically modulate the substrate selectivity of the ATH, resulting in higher conversion increase for more hydrophobic substrates at higher temperature (60 °C), and higher conversion increase of less hydrophobic substrates under UV light.

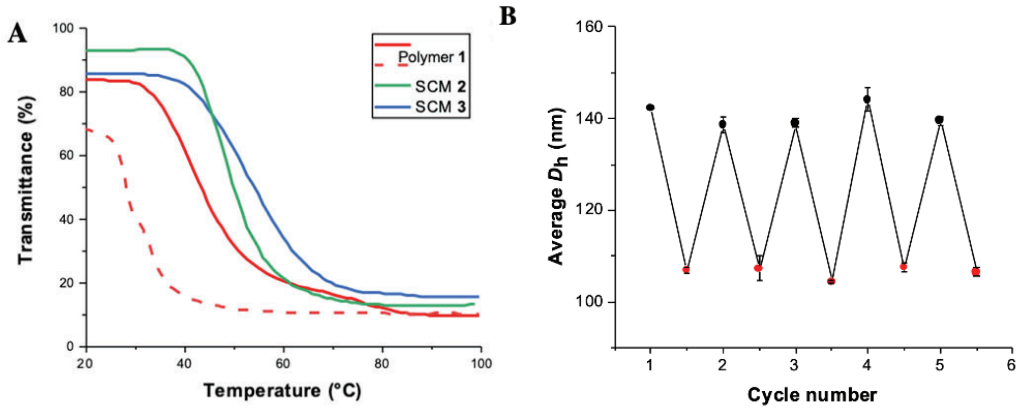

Figure 2. (A) Thermal UV-Vis spectra of SCMs. The solid curves are heating curves and the dash curve is cooling curve. (B) D_h of five consecutive UV-Vis cycles determined by DLS. Black dots represent D_h under visible light, and red dots are D_h under UV light irradiation.

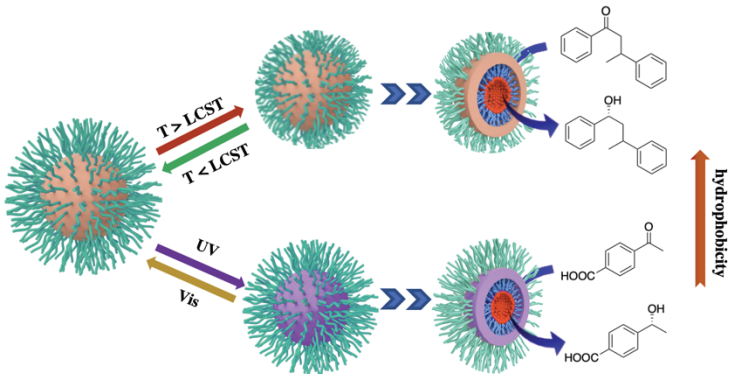

Figure 3. Schematic representation of the thermos- and photo-responsive SCM-based nanoreactors for substrate-selective ATH: Gated behavior induced by the thermo-responsive outer layer for the more hydrophobic substrates; Gated behavior induced by the photo-responsive cross-linked layer for the less hydrophobic substrates.

Multiscale Modeling for MCM and Proline-Catalyzed Aldol Reaction

We also developed a systematic multiscale modeling and simulation approach to predict polymer-polymer (or solvent) miscibility using the Flory-Huggins χ parameter, obtained via density functional theory (DFT), molecular mechanics (MM), and statistical mechanics calculations. A set of χ-parameters were calculated on the **H-L-Proline-F** sequenced amphiphilic bottlebrush copolymers, which are comprised of an ethylene glycol-based hydrophilic block (**H**), styrene-based lipophilic block (**L**), L-proline attached block (**P**), and pentafluorostyrene-based fluorophilic block (**F**), as listed in **Table 1**. We found that pentafluorostyrene-water (**F-W**) pair exhibits the highest χ-parameter value (χ_{F-W}=0.963), followed by the styrene-water (**L-W**) pair (χ_{L-W}=0.756), the L-proline-water (**P-W**) pair (χ_{P-W}=0.459), and the ethylene oxide-water (**H-W**) pair (χ_{H-W}=0.197), implying that blocks **F** and **H** are expected to be the most hydrophobic and hydrophilic, respectively. We then used the calculated χ-parameters to investigate the

morphologies of the multicompartment micelles (MCM) through dissipative particle dynamics (DPD) simulations, as shown in **Figure 4**. From the internal structure of MCM, the effective dielectric constant was estimated using a linear combination of the dielectric constants for individual components, which was considered for the implicit solvent media in our DFT calculations. Through this study, we demonstrated that the L-proline catalyzed asymmetric aldol addition reaction of acetone and 4-nitrobenzaldehyde is energetically more favorable within the MCM environment with the lowest energy barrier for the rate-determining step in comparison to other environments such as DMSO, water and vacuum (**Figure 5**). The kinetic and activation energy results confirm that MCMs provide an optimal hydrophobic microenvironment, effectively reducing water concentration around the reactant species and catalyst, thereby enabling the most efficient and selective aldol addition reaction.

Table 1. Calculated Flory-Huggins χ-Parameters for molecular pairs

χ_{A-B}	L	H	F	P	W
L	0	1.462	0.945	1.075	0.756
H	1.462	0	0.735	0.531	0.197
F	0.945	0.735	0	1.220	0.963
P	1.075	0.531	1.220	0	0.459
W	0.756	0.197	0.963	0.459	0

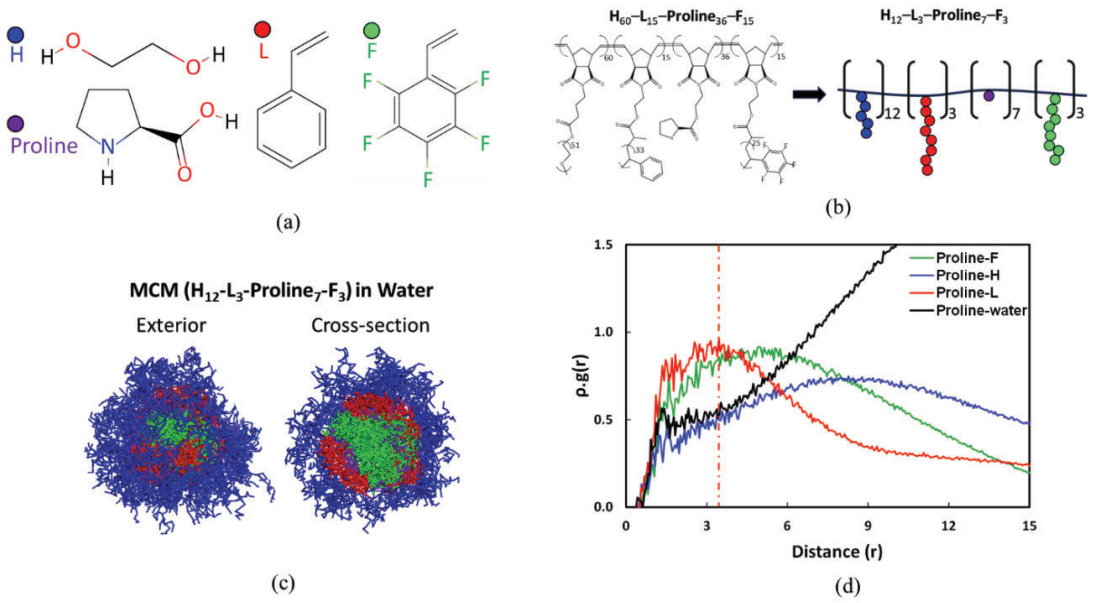

Figure 4. (a) Colored beads used as a visual representation of chemical structures (**H**, **L**, **F** blocks, and L-proline catalyst are represented by blue, red, green, and purple colors, respectively.); (b) coarse grained model of bottlebrush copolymer; (c) DPD simulation results for MCM; (d) pair correlation function analysis for the pairs of block Proline with blocks H, L, F, and water represented in blue, red, green, and grey lines, respectively.

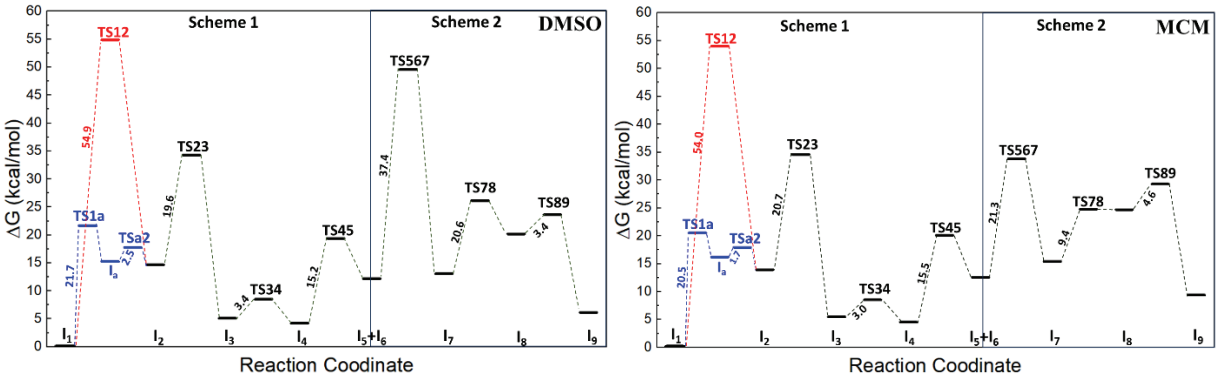

Figure 5. Free energy profiles with activation energies as a function of the reaction coordinates for the L-proline-catalyzed aldol reaction between acetone and 4-nitrobenzaldehyde under (left) DMSO and (right) MCM environment.

Polymer–Silica Nanocomposite for Acid–Base Reactions

The research team is developing a type of polymer–silica nanocomposite tailored with incompatible catalytic active sites for acid–base reactions. Mesoporous silica, known for its diverse functionalization methods and efficiency as a catalyst support, is used as a platform to achieve easy recovery of the catalyst, as well as providing acid active sites. Concurrently, polyoxazoline, a subcategory of pseudopeptide, with its potential to adopt varied polymer conformations, serves as the support for base active sites.

To achieve catalyst compartmentalization, the team performs a stepwise functionalization approach of mesoporous silica where its external and internal surfaces are modified separately with incompatible catalytic sites. This process necessitates attaching polymer onto the external surface of mesoporous silica followed by the surfactant extraction, ensuring no disturbance to the grafted polymers. Dispersed mesoporous silica nanoparticles of SBA-15, MCM-41 and MCM-48 with different pore structures and morphologies have been prepared. Their surfaces have been modified by –SH groups, allowing uniform polymer grafting for achieving well-defined composite structures. Furthermore, –SH will be converted to $–SO_3H$ after polymer grafting to obtain acidic catalyst sites. In the meantime, the team has synthesized various block copolymers of polyoxazoline with $–NH_2$ modified sidechains designed for base catalysis. Study of the polymer–silica interactions is underway, and the team is searching for the optimized conditions of polymer grafting in order to achieve the compartmentalization of the acid and base sites.

Publications Acknowledging this Grant in 2019-2023

(I) Intellectually led by this grant

1) "Nonorthogonal Cascade Catalysis in Multicompartment Micelles" Eman Ahmed, Jinwon Cho, Seung Soon Jang,* and Marcus Weck* *Chem. Eur. J*. **2023**, *29*, e202301231.

2) "Catalytically Active Multicompartment Micelles" Eman Ahmed, Jinwon Cho, Lulu Friedmann, Seung Soon Jang,* and Marcus Weck* *JACS Au* **2022**, *2*, 2316–2326.

3) "Photoresponsive Azobenzene-Functionalized Shell Cross-Linked Micelles for Selective Asymmetric Transfer Hydrogenation" Fangbei Liu, Peiyuan Qu, and Marcus Weck* *Org. Lett.* **2022**, *24*, 4099-4103.

4) "Compartmentalisation of Molecular Catalysts for Nonorthogonal Tandem Catalysis" Peiyuan Qu, Jacob W. Cleveland, Eman Ahmed, Fangbei Liu, Sage Dubrawski, Christopher W. Jones*, and Marcus Weck* *Chem. Soc. Rev*. **2022**, *51*, 57-70.

5) "Structural Transformation of Multicompartment Micelle Induced by Photo-switchable Spiropyran-Merocyanine Transition: Dissipative Particle Dynamics Simulation Approach." Jinwon Cho, Ji Il Choi, and Seung Soon Jang* *J. Phys. Chem. B,* **2022**, 126, 4401-4410.

6) "Cooperativity in the Aldol Condensation using Bifunctional Mesoporous Silica - Poly(styrene) MCM-41 Organic/Inorganic Hybrid Catalysts." Jacob W. Cleveland, Ji Il Choi, Ryoh-Suke Sekiya, Jinwon Cho, Hyun June Moon, Seung Soon Jang,* and Christopher W. Jones* *ACS Appl. Mater. Interfaces* **2022**, 14, 11235-11247.

7) "Design of a bifunctional TEMPO-tertiary amine mesoporous silica catalyst for the three-step cascade synthesis of a chromene derivative" Jacob W. Cleveland, Nima Ronaghi, Christopher W. Jones* *Mol. Catal.* **2022**, *517*, 112021.

8) "Cross-Linked Polymeric Micelles as Catalytic Nanoreactors" Peiyuan Qu, Michael Kuepfert, Eman Ahmed, Fangbei Liu, and Marcus Weck* *Eur. J. Inorg. Chem.* **2021**, 1420-1427.

9) "Self-Assembled Thermoresponsive Molecular Brushes as Nanoreactors for Asymmetric Aldol Addition in Water" Michael Kuepfert, Eman Ahmed, and Marcus Weck* *Macromolecules* **2021**, *54*, 3845-3853.

10) "Creation of discrete active site domains via mesoporous silica poly(styrene) composite materials for incompatible acid–base cascade reactions" Jacob W. Cleveland, Dharam Raj Kumar, Jinwon Cho, Seung Soon Jang, and Christopher W. Jones* *Catal. Sci. Technol.* **2021**, *11*, 1311-1322.

11) "Compartmentalization and Photo-Regulating Pathways for Incompatible Tandem Catalysis" Peiyuan Qu, Michael Kuepfert, Maryam Hashmi, and Marcus Weck* *J. Am. Chem. Soc.* **2021**, *143*, 4705-4713.

12) "One-Pot Synthesis of Linear Triblock Terpolymers and their Aqueous Self-Assembly" Eman Ahmed, C. Tyler Womble, Jinwon Cho, Kristen Dancel-Manning, Dr. William J. Rice, Seung Soon Jang,* and Marcus Weck* *Polym. Chem.* **2021**, *12*, 1967-1974.

13) "Synthesis and Aqueous Self-assembly of ABCD Bottlebrush Block-Copolymers" Eman Ahmed, C. Tyler Womble, and Marcus Weck* *Macromolecules* **2020**, *53*, 9018-9025.

14) "Reversible Photoswitching in Poly(2-oxazoline) Nanoreactors" Michael Kuepfert, Peiyuan Qu, Aaron E. Cohen, Caroline B. Hoyt, Christopher W. Jones,* and Marcus Weck* *Chem. Eur. J.* **2020**, *26*, 11776-11781.

15) "Compartmentalized Nanoreactors for One-pot Redox-driven Transformations" Peiyuan Qu, Michael Kuepfert, Steffen Jockusch, and Marcus Weck* *ACS Catal.* **2019***, 9,* 2701-2706.

16) "Multi-compartment Polymeric Nanoreactors for Non-orthogonal Cascade Catalysis" C. Tyler Womble, Michael Kuepfert, Aaron E. Cohen, and Marcus Weck* *Macromol. Rapid Commun.* **2019**, *40,* 1800580.

(II) Jointly funded by this grant and other grants with intellectual leadership by other funding sources

None.

Ross A. Widenhoefer, Stephen L. Craig

Multi-State Mechanocatalysis

Ross A. Widenhoefer, Stephen L. Craig, Xujun Zheng, Daniel Duan, Jack Malek, Yichen Yu, Rosemary Buhrman
Department of Chemistry, Duke University

Presentation Abstract

Here we report the macroscopic, mechanical regulation of single-site catalytic selectivity, in which an achiral (symmetric) strain improves the chiral selectivity of the reaction. The magnitude of the chiral enhancement increases with increasing strain, and the chiral selectivity returns to its nascent values once the strain is relaxed; we use the term "multi-state mechanocatalysis" (MMC) to reflect these attributes and differentiate the behavior demonstrated here from the use of mechanical force to activate latent catalysts in an off/on fashion. Specifically, the enantioselectivity of the hydrogenation of a methyl 2-amidoacrylate via a fixed rhodium bisphosphine catalyst is improved by embedding the catalyst into a heterogenous elastomeric support and transducing the mechanical deformation of the elastomer to the catalyst. The enantioselectivity of hydrogenation is strain-dependent and reversible upon relaxing the support. Stretching the support by 50% in a single dimension increases the R:S ratio of the product by up to 32%. Combined with computations, the results suggest that hundred-fold improvements in selectivity should be possible as appropriate material and device platforms are developed. Further advances in MMC will be fueled by insights into (a) how tension coupled at the molecular scale influences various catalytic process, and (b) establishing new molecular mechanisms of tunable force delivery. We have shown that force applied to the ligand scaffold of an intact transition metal complex biases the rate of reductive elimination from nickel diaryl complexes and biases the selectivity of rhodium-catalyzed hydroformylation. In addition, we have demonstrated a molecular scaffold in which fast binding of a metal ion to a remote receptor site increases the rate of thermal E-to-Z isomerization of an alkene increases by a factor of as much as 10^4. A quantitative model of the mechanochemistry reproduces the observed acceleration. The work validates the mechanochemical kinetic framework to compressive loads and offers a productive framework for the quantitative analysis of the molecular basis of allosteric control of reaction kinetics. These results provide a foundation for new opportunities in MMC that complement our ongoing efforts.

DE-SC0022146: Multi-state Catalysts Modulated by Mechanical Force

PIs: Ross A. Widenhoefer, Stephen L. Craig
Postdoc: Xujun Zheng
Students: Yichen Yu, Daniel Duan, Jack Malek, Rosemary Buhrman

RECENT PROGRESS

The overarching objective of this project is to further develop and extend the foundation for what we term multi-state mechanocatalysis (MMCs), a new class of

polymer-embedded catalysts that funnel mechanical forces to the molecular level and use them to bias catalysis. Key questions include: how does an applied force of tension to a ligand affect reactivity in the various elementary steps and catalytic processes? What types of ligands, metals, and reactions are most susceptible to mechanical perturbation? And ultimately, what materials are the most promising supports for bulk multi-state mechanocatalysis? Our current activities are directed toward (1) establishing and quantifying key principles of ligand/active site design using macrocyclic bisphosphine force probe ligands (FPL) in homogeneous, single-site catalysts and in isolated transition metal complexes; and (2) establishing quantitative relationships between the mechanically modulated reactivity of individual complexes characterized with the FPLs and the ensemble reactivity of polymer-supported MMCs.

Quantitative force-activity relationships for transition metal reactivity

Our approach to evaluate the effect of force on transition metal reactivity employs macrocyclic force probe ligands (FPLs) E(m,n) and Z(m,n) comprising a 1,1'-biindane photoswitch tethered to the 6,6' positions of an (*R*)-Biphep moiety (Figure 1). The Z and E isomers of the 1,1'-biindane apply a compressive or stretching force, respectively, to the oxygen atoms of the bisphosphine moiety. Force has been calculated to vary from –65 pN to 228 pN for the macrocyclic ligands. Because force applied intramolecularly by the biindane is functionally equivalent to force applied externally, these FPLs provide a convenient method to apply a well-defined force to a single-site metal complex which can be interrogated in solution employing conventional spectroscopy.

Figure 1. Macrocycle bisphosphine FPLs.

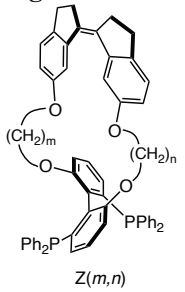

ligand	force (pN)
Z(2,2)	–65
Z(3,3)	–3
MeOBiphep	0
E(3,3)	130
E(2,3)	228

Force-Modulated Reductive Elimination. We have quantified the effect of force on the rate of C(sp^2)–C(sp^2) reductive elimination from nickel(II) bis(2,4,6-trifluorophenyl) complexes **1** in C_6D_6 at 68 °C employing FPLs. Whereas compressive forces up to –65 pN have no significant effect on the rate of reductive elimination, extension forces applied to the diaryl backbone increase the rate of reductive elimination by a factor of three over a ~230 pN range of restoring forces relative to the strain-free MeOBiphep complex. The rate response of reductive elimination from complexes **1** to extension forces is similar to the

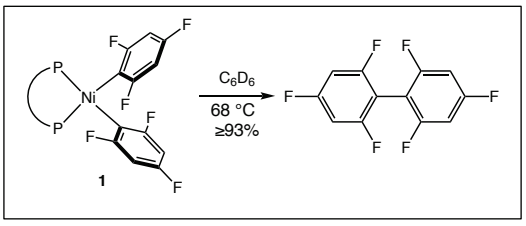

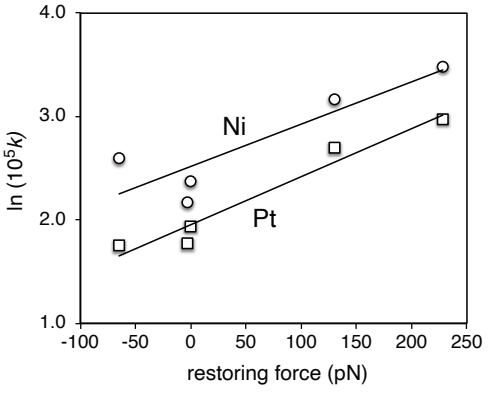

Figure 2. Plots of ln*k* versus restoring force for the reductive elimination from complexes **1** (○) and from (P–P)Pt(4-$C_6H_4NMe_2$)$_2$ (□).

previously observed for the reductive elimination from platinum diaryl complexes (P–P)Pt(4-$C_6H_4NMe_2$)$_2$ over the same range of forces (Figure 2). In both cases, the force/rate dependence of the reductive elimination is attributed to the force-coupled elongation of the (biphep)O···O(biphep) distance in the transition state relative to the ground state. The similar force/rate response suggests that the molecular motions within the first coordination sphere associated with reductive elimination are similar for both metals.

Force-Modulated Selectivity of the Rhodium-Catalyzed Hydroformylation. We have quantified the regio- chemo-, and enantioselectivity of the hydroformylation of 1-alkenes catalyzed by Rh(I) bis(phosphine) complexes as a function of mechanical force applied to the biaryl backbone of these ligands. Extension forces increase the regioselectivity of the hydroformylation of 1-octene from *l*:*b* = 1.2 to 1.9 and decrease the chemoselectivity for C_9 aldehyde relative to 2-octene from 96% to 20% across a ~230 pN change in applied force (Scheme 1). We attribute the latter effect to the decrease in the binding affinity of the ligand with increasing tensile force coupled with the facile isomerization of 1-octene catalyzed by an unligated rhodium carbonyl complex. Variable temperature NMR analysis of the five-coordinate rhodium complexes (P–P)Rh(CO)$_2$H established the exclusive formation of eq-ap isomers (P–P = 90 °) even for the most extended E(m,n) ligands. We posit that rigidity and steric crowding of the binding pocket of the bound bisphosphine ligand precludes formation of seemingly more geometrically suitable eq-eq isomers (P–P = 120 °). As a result, the strain generated by constraining the more extended E(m,n) ligands in an eq-ap orientation leads to global destabilization of the resultant complexes and diminished binding affinity of the ligand.

Scheme 1

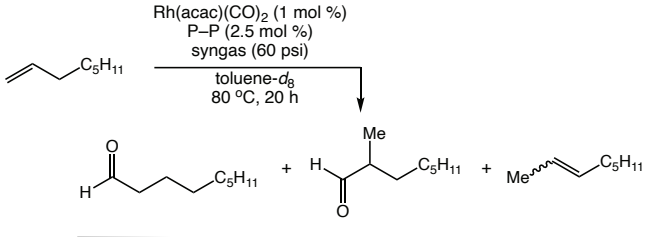

P–P	force (pN)	RHO:2-octene	conv. (%)	*l*:*b*
Z(3,3)	–3	>95:5	84	1.2
MeOBiphep	0	73:27	>95	1.5
E(3,3)	130	36:64	89	1.7
E(2,3)	228	20:80	92	1.9

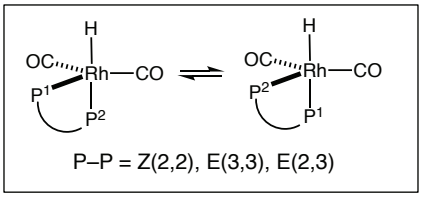

Force-modulated enantioselective hydrogenation. We have quantified the effect of force on the enantioselectivity of the hydrogenation of methyl 2-amidoacrylate (**2**) to form **3** catalyzed by a mixture of [Rh(COD)$_2$][BF$_4$] and P–P in MeOH under H_2 (1 atm) at 25 °C (Table 1). The enantioselectivity of hydrogenation increased dramatically with increasing tensile force ranging from 2% ee to 84% ee across a ~280 pN range of forces (Table 1). Computational analysis of the Rh-catalyzed hydrogenation of **2**

Table 1. Force-dependent enantioselectivity of the rhodium-catalyzed hydrogenation of **2.**

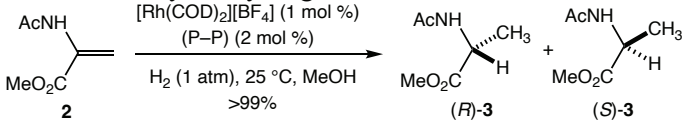

P–P	Restoring force (pN)	ee (%)
Z(2,2)	–65	2
Z(3,3)	–3	28
E(2,3)	130	54
E(3,3)	228	84

supports a mechanism involving stereochemical-determining insertion of hydrogen in to the coordinated C=C bond of (P–P)Rh(**1**)H_2 across the range of forces employed here. The calculated force-coupled enantioselectivity also aligns with the experimental dependence. Importantly, the high force sensitivity, high TON and TOF, and compatibility with non-swelling solvents (MeOH) made catalytic hydrogenation particularly attractive transformation for application to MMC employing catalytically active elastomers (see below).

Allosteric control of olefin isomerization kinetics. Our most extended FPL E(2,2), which is stable indefinitely in solution at room temperature ($t_{1/2} \approx 80$ days), underwent rapid E to Z isomerization of the stiff stilbene C=C bond ($t_{1/2} \approx 1$ min) upon complexation of $PtCl_2$. This behavior represents a rare example of abiological allosteric control amenable to kinetic analysis and we have interrogated this allosteric isomerization both experimentally and computationally. To this end, we first determined the activation barriers of thermal E to Z isomerization for a family of FPLs and their metallated (FPL)$PtCl_2$ counterparts (Table 2). In each case, platinum coordination lowered the $\Delta G^{\ddagger}$ of isomerization commensurate with the strain of the free FPL, which ranged from $\Delta\Delta G^{\ddagger}$ = – 6.7 ± 2.0 kcal/mol in the most strained E(2,2) macrocycle to $\Delta G^{\ddagger}$ = –1.4 ± 0.1 kcal/mol in the least strained E(3,3) macrocycle.

Table 2. The measured and calculated $\Delta G^{\ddagger}$ of E → Z isomerization in E(*m,n*) and [E(*m,n*)]$PtCl_2$ in kcal/mol.

macrocycle	T (°C)	$\Delta G^{\ddagger}_{expt}$	$\Delta G^{\ddagger}_{calc}$
E(2,2)	69 - 84	27.0 ± 2.0	26.1
E(2,2)]$PtCl_2$	–10 - 6	20.3 ± 2.0	18.7
E(2,3)	120 - 135	31.0 ± 2.0	29.6
E(2,3)]$PtCl_2$	64 - 80	26.7 ± 1.9	26.4
E(3,3)	131	31.4 ± 0.1	33.8
E(3,3)]$PtCl_2$	125	30.0 ± 0.1	29.7

To understand the structural and energetic origin of the accelerated isomerization of stiff stilbene by metal coordination and to test the utility of a force-based approach to broader analysis of allosterically controlled reaction kinetics, we optimized conformational ensembles of Z and E isomers of both metal-free and Pt-coordinated macrocycles by DFT. A mechanochemical model of the alkene coupled to a compressive harmonic spring reproduced the observed acceleration of E to Z isomerization upon metal binding to the FPL quantitatively (Table 2). These calculations reveal that the exceptionally large allosteric kinetic effect of Pt binding to the FPLs (up to 10^4-fold acceleration at 300 K) (i) arises from only a small (30-80 pN) increase in the strain of the macrocycle, and (ii) results from the effector binding increasing the strain energy of the reactant without a concomitant increase in the strain energy of the corresponding transition state. This work validates experimentally the generalization of mechanochemical kinetics to compressive loads and demonstrates that the formalism of force-coupled reactivity offers a productive framework for the quantitative analysis of the molecular basis of allosteric control of reaction kinetics.

Multi-state mechanocatalysis (MMC). We have recently shown that extrinsic mechanical force used to stretch a rubbery polymer matrix is delivered to a ligand-coordinated, single-site rhodium catalyst embedded within the matrix increases the enantioselectivity of the hydrogenation of methyl 2-amidoacrylate (**2**). Enantioselectivity increases with increasing strain and returns to its nascent value once the strain is relaxed; these attributes differentiate this behavior from the use of mechanical force to activate

latent catalysts in an off/on fashion. We employed double network (DN) poly(methyl acrylate) gels as elastomeric supports that comprise (i) a first network containing the mechanically active bisphosphine crosslinker $\mathbf{P_{act}}$ (2.5 mol %) and (ii) an interpenetrating second, soft and elastic network containing 1,4-butanediol diacrylate crosslinkers. Because the first network is pre-stretched and brittle due to swelling, force is concentrated in the first network containing $\mathbf{P_{act}}$ when the DN gel is stretched. The resulting elastomer was loaded with rhodium(I) to form the catalytically active, force-coupled matrix **N1**•Rh. Employing similar methods, we synthesized the double network rhodium catalyst $\mathbf{N1_{con}}$•Rh, in which a bisphosphine control ligand ($\mathbf{P_{con}}$) is covalently linked within the first network through a single site and therefore mechanically decoupled from tension in the polymer support.

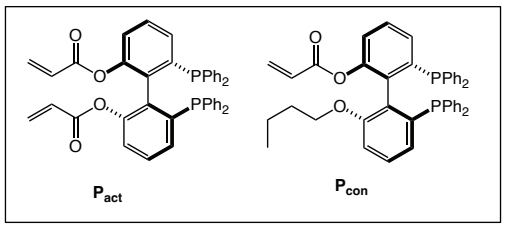

Samples of mechanically active **N1**•Rh stretched manually to different strains in a homemade mold were employed as catalysts for the hydrogenation (1 atm) of **2** in MeOH at 25 °C. The enantioselectivity of hydrogenation increases from 50% ee to 62% ee as the strain is increased from 0 to 50% and it returns to its initial value (50% ee) when the support is returned to its initial, unstretched state (Table 3). Under the same reaction conditions and comparable range of applied strain, we found a negligible change in the enantioselectivity of hydrogenation of **2** as a function of strain employing mechanically decoupled support $\mathbf{N1_{con}}$•Rh (Table 3), supporting a mechanical origin to the improved selectivity observed in **N1**•Rh. The relationship between stretch and enantioselectivity was confirmed across the multiple batches of **N1**•Rh and similar strain-dependent and reversible modulation of enantioselectivity was also observed under uniaxial compression. Combined with computations, the results suggest that hundred-fold improvements in selectivity should be possible as appropriate material and device platforms are developed.

Table 3. Enantioselectivity of the Hydrogenation of **2** as a Function of Strain in **N1**•Rh and $\mathbf{N1_{con}}$•Rh supports under uniaxial stretching.

N1•Rh			$\mathbf{N1_{con}}$•Rh		
strain (%)	yield (%)	ee (%)	strain (%)	yield (%)	ee (%)
0	77	50	0	42	27
22	34	53	32	28	28
40	21	59	62	17	28
50	44	62	0	13	27
0	31	50			

Publications Acknowledging this Grant in 2020-2023

(I) Intellectually led by this grant

1) "Allosteric control of olefin isomerization kinetics via remote metal binding and its mechanochemical analysis. Yu, Y.; O'Neill, R. T.; Boulatov, R.; Widenhoefer, R. A.; Craig, S. L. *Nat. Comm*. in press, DOI:10.1038/s41467-023-40842-5.

2) "Force-Modulated C–C Reductive Elimination from Nickel Bis(polyfluorophenyl) Complexes," Duan, C.; Zheng X.; Craig, S. L.; Widenhoefer, R. A. *Organometallics* **2023**, *42*, 1918–1926.

3) "Force-Modulated Selectivity of the Rhodium-Catalyzed Hydroformylation of 1-Alkenes," Yu, Y.; Widenhoefer, R. A.; Craig, S. L. *ACS Catal.* **2022**, *12*, 13941–13950.

Infusing Theory into Deep Learning for Advancing Catalysis Science

Hongliang Xin
Virginia Tech

Presentation Abstract

Finding catalytic materials with optimal properties for sustainable chemical and energy transformations is one of the pressing challenges faced by our society today. Traditionally, the discovery of catalysts or the philosopher's stone of alchemists relies on a trial-and-error approach with physicochemical intuition. Decades-long advances in science and engineering, particularly in quantum chemistry and computing infrastructures, popularize a paradigm of computational science for materials discovery. However, the brute-force search through a vast chemical space is hampered by its formidable cost. In recent years, machine learning (ML) has emerged as a promising approach to streamline the design of active sites by learning from data. In this poster, we present an interpretable ML framework for accelerating catalytic materials design, particularly in driving sustainable carbon, nitrogen, and oxygen cycles. We will discuss existing challenges and opportunities of ML in predicting catalytic materials, and more importantly, on advancing catalysis theory beyond conventional wisdom. We envision future directions in developing highly accurate, easily explainable, and trustworthy ML strategies, facilitating the maturation of the data science paradigm for sustainability through catalysis.

Grant or FWP Number:
Interpretable Deep Learning of Interfacial Electrokinetics (DE-SC0023323)

PI: Lead PI(s) Name(s) (*include only if different from above*)
Postdoc(s): Name(s)
Student(s): Yang Huang, Shih-Han Wang
Affiliations(s): (*include only if different from above*)

RECENT PROGRESS

Interpretable Deep Learning for Predicting Electronic Descriptors of Metal Surfaces upon Perturbation

Predicting the electronic structure of materials is crucial for understanding their physicochemical properties. We developed an interpretable deep learning approach to accurately predicting the *d*-band characteristics of transition and noble metal surfaces as well as capturing the quantum-mechanical effects governing its modification based on a graph neural network and the semi-empirical tight-binding theory. Integrating the tight-binding theory into graph neural networks within the framework of interpretable deep learning creates predictive models of the *d*-band characteristics of transition and noble metal alloys, and provides a unified framework of interpreting the underlying physical factors governing its variation. Compared to purely data-driven graph neural networks, the TinNet model attains similar accuracy while being intrinsically interpretable in terms of underlying factors of the electronic structure. Application of the TinNet models for a broad range of alloy systems provides deeper insights of commonly referred strain and ligand effects. Several surface alloy systems are utilized for a quantitative demonstration of the

new understanding via SHAP attribution analysis. The framework provides a systematic way of enriching theory by learning from data.

Publications Acknowledging this Grant in 2019-2022

Please classify your publications into two categories according to the source of support for the work published:

(I) Intellectually led by this grant

1. *Mou, T.; Pillai, H. S.; Wang, S.; Wan, M.; Han, X.; Schweitzer, N. M.; Che, F.; Xin, H. Bridging the Complexity Gap in Computational Heterogeneous Catalysis with Machine Learning. Nature Catalysis* ***2023****, 6 (2), 122–136. https://doi.org/10.1038/s41929-023-00911-w.*
2. Huang, Y; Wang, S.-H.; Achenie, L. E. K.; Xin, H. *Resonance effect of electronic descriptors in d-metal catalysis revealed by interpretable deep learning,* ***2023****, Under Review.*

(II) Jointly funded by this grant and other grants with intellectual leadership by other funding sources

(*use ACS Style: http://library.williams.edu/citing/styles/acs.php; for example:*)

1. Deno, N. C.; Richey, H. G.; Liu, J. S.; Lincoln, D. N.; Turner, J. O. Total Synthesis of Sucrose. *J. Amer. Chem. Soc.* **1965**, *87*, 4533-4538.

(*The length of the extended abstract, excluding the Publications list, is limited to 4 pages for university grants and 6 pages for laboratory FWPs. If multiple Presentations refer to the same Grant or FWP, include the Grant/FWP section in only one extended abstract.*)

Zhenzhen Yang

Engineering nanostructured interfaces of hexagonal boron nitride-based materials towards enhanced catalysis

Zhenzhen Yang,[1] Meijia Li,[1] Zili Wu,[1] Miaofang Chi,[1] De-en Jiang,[2] Sheng Dai[1]
[1]Chemical Sciences Division, Oak Ridge National Laboratory, Oak Ridge, TN, 37831, USA; Email: yangz3@ornl.gov; [2]Department of Chemical and Biomolecular Engineering, Vanderbilt University, Nashville, TN 37235, USA.

The catalysis procedures involving small gas molecules (e.g., H_2 and CO_2) promoted by earth-abundant metal-free catalysts is an attractive and challenging subject. Recent advances in utilizing hexagonal boron nitride (h-BN) as a metal-free catalyst in oxidative dehydrogenation of propane have triggered broad interests in exploring h-BN in catalysis.[1] However, h-BN-based materials as robust nanocatalysts in heterogeneous catalysis are still underexplored because of the limited methodologies capable of affording h-BN with controllable crystallinity, abundant porosity, high purity, and defects engineering, which played important roles in tuning their catalytic performance. Herein, our recent progress to address the above issues will be highlighted, including the synthesis of high-quality h-BN-based nanomaterials via both bottom-up and top-down pathways, and their catalytic utilization as metal-free catalysts or as supports to tune the interfacial electronic properties on the metal nanoparticles (NPs). First, we will focus on the fabrication of h-BN nanosheets (h-BNNS) in large-scale with high crystallinity, improved surface area, satisfactory purity, and tunable defects. h-BN derived from the traditional approaches using boron trioxide and urea as the starting materials generally contains carbon/oxygen impurities and shows low crystallinity. Several new strategies were developed to address the issues. Amorphous h-BN precursors could be converted to h-BN nanosheets with high crystallinity assisted by a magnesium metallic flux via a successive dissolution/precipitation/crystallization procedure.[2] The as-fabricated h-BNNS were featured by high crystallinity and purity, as well as abundant porosity. An ionothermal metathesis procedure was developed using inorganic molten salts ($NaNH_2$ and $NaBH_4$) as the precursors.[3-4] The h-BN scaffolds could be produced in large-scale with high yield, and the as-afforded materials possessed high purity and crystallinity. Second, utilization of the as-prepared h-BN library as metal-free catalysts in dehydrogenation and hydrogenation reactions will be summarized, in which they exhibited enhanced catalytic activity over the counterparts from the previous synthesis method.[3, 5] Third, the interface modulation between metal NPs with the as-prepared defects abundant h-BN support will be highlighted.[6] Across all these examples, unique insights into structure-performance relationship and the structure engineering towards activity and selectivity control will be highlighted.

Research supported by the U.S. Department of Energy, Office of Science, Basic Energy Sciences, Chemical Sciences, Geosciences, and Biosciences Division, Catalysis Science Program. This research is part of FWP ERKCC96: Fundamentals of Catalysis and Chemical Transformations. For a full description of recent progress see Extended Abstract for ERKCC96.

References

[1] H. Chen, D. E. Jiang, Z. Yang, S. Dai, *Acc. Chem. Res.* **2023**, *56*, 52-65.
[2] H. Chen, Z. Yang, Z. Zhang, Z. Chen, M. Chi, S. Wang, J. Fu, S. Dai, *Angew. Chem. Int. Ed.* **2019**, *58*, 10626-10630.
[3] H. Chen, C. Xiong, J. Moon, A. S. Ivanov, W. Lin, T. Wang, J. Fu, D. E. Jiang, Z. Wu, Z. Yang, S. Dai, *J. Am. Chem. Soc.* **2022**, *144*, 10688-10693.
[4] H. Chen, Z. Yang, W. Guo, J. R. Dunlap, J. Liang, Y. Sun, K. Jie, S. Wang, J. Fu, S. Dai, *Adv. Funct. Mater.* **2019**, *29*, 1906284.
[5] M. Li, L. Qiu, I. Popovs, W. Yang, A. S. Ivanov, T. Kobayashi, B. P. Thapaliya, D. Moitra, X. Yu, Z. Wu, Z. Yang, S. Dai, *Angew. Chem. Int. Ed.* **2023**, *62*, e202302684.
[6] H. Chen, S. Z. Yang, Z. Yang, W. Lin, H. Xu, Q. Wan, X. Suo, T. Wang, D. E. Jiang, J. Fu, S. Dai, *ACS Cent. Sci.* **2020**, *6*, 1617-1627.

Selective Oxidation of Oxygenates with Well-Defined Gold-Based Surface Catalytic Sites

Francisco Zaera
Department of Chemistry and UCR Center for Catalysis, University of California, Riverside CA 92521.

Presentation Abstract

The long-term objective of our project is to address the issue of selectivity in oxidation reactions of organic oxygenates by using well-defined gold-based catalysts. Gold, in nanoparticle (NP) form and in contact with reducible oxides, have been shown to be quite active as a catalyst and to promote oxidations under mild conditions and using O_2 as the oxidizing agent. Given the central roles that the size of the Au NPs and the details of the metal-oxide interface play in defining catalytic performance, here we focus on controlling those by using a combination of self-assembly synthetic methods to deposit Au NPs and atomic layer deposition (ALD) to grow oxide films of well-defined thicknesses. In this first year of the project we have made great progress on the ALD of titania films on a silica mesoporous material (SBA-15), the thickness of which could be controlled down to the submonolayer level. The uniformity of the films was assessed using absorption-desorption isothermal measurements, the mechanism of the film growth inferred from ^{29}Si solid-state NMR data, and their reducibility evaluated by EPR. Separatetly, initial experiments have been performed on the deposition of Au NPs with narrow size distributions in the 2 - 5 nm diameter range. The performance of these catalysts has been tested for the oxidation of carbon monoxide. It was determined that the addition of titania indeed enhances the Au oxidation activity, and that the order in which the two phases are deposited on the SBA-15 support, Au or TiO_2 first, also affect catalytic performance. The reasons for this are been explored at the present time.

DE-SC0023119: Selective Oxidation of Oxygenates with Well-Defined Gold-Based Surface Catalytic Sites

PI: Francisco Zaera
Graduate Student(s): Wang Ke, Yihan Zhou
Undergraduate Student(s): Colin Smith, Eugene Kwon

RECENT PROGRESS

Overall Objectives

The long-term objective of our project is to address the issue of selectivity in oxidation reactions with oxygenates by using well-defined gold-based catalysts. Our central hypothesis is that the self-assembly synthesis of metal nanoparticles (NPs) and the atomic layer deposition (ALD) of metal oxide thin films can be combined to design novel multicomponent metal/oxide surface sites on solid materials to target specific oxidation catalysis. We follow a three-prong approach to:

- Synthesize novel Au-based catalysts for the selective oxidation of oxygenates,
- Characterize their catalytic sites at a molecular level, and
- Evaluate their catalytic performance.

We aim to:

- Use self-assembly plus ALD synthetic approaches to create unique interfaces, to exert control on the size of the metal NPs and on the thickness and composition of the oxide films;
- Use a combination of characterization techniques (IR, XPS, NMR, EPR, electron microscopy, adsorption-desorption isotherms) to evaluate the nature of the sites made by our synthetic approach; and
- Test the performance of our newly created catalysts for the partial oxidation of alcohols and multifunctional oxygenates, focusing on biomass feedstocks.

Recent Results

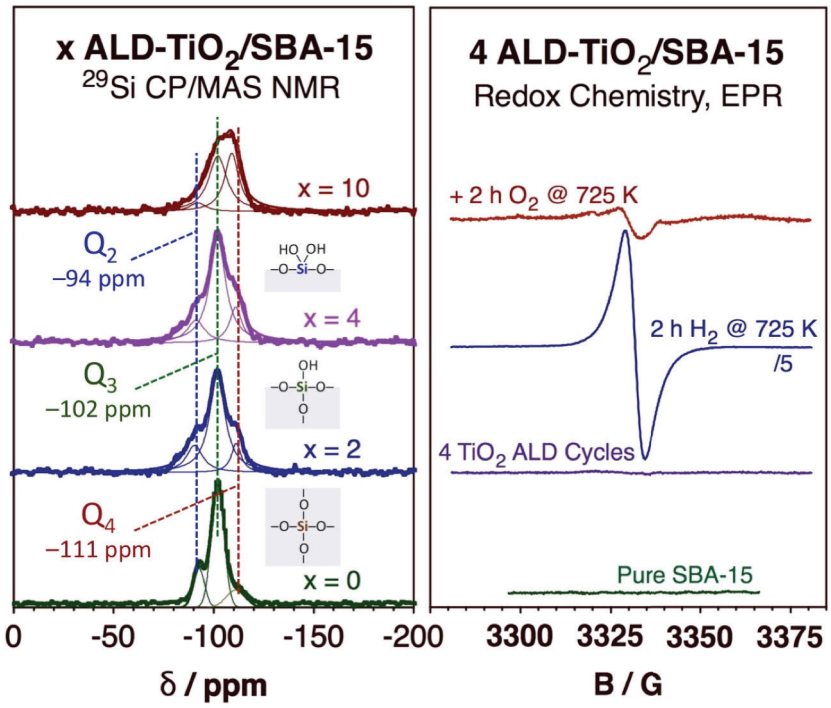

Fig. 1. Characterization of titania films grown on SBA-15 by atomic layer deposition (ALD). Left: ^{29}Si CP/MAS NMR versus number of TiO_2 ALD cycles. Right: EPR spectra for the 4-ALD-cycles sample after reducing and oxidizing treatments.

In our initial work, the redox properties of titania films grown by ALD on SBA-15, a silica-based mesoporous material with one-dimensional pores of approximately 6-7 nm in diameter, were characterized as a function of thickness (the number of ALD cycles used). ^{29}Si CP/MAS NMR (Figure 1-left) helped identify the nature of the surface species that form in the initial stages of deposition, and infrared absorption spectroscopy was used to follow the transition from silica to titania surfaces. The reducibility of the titania sites by CO and H_2 was studied *ex situ* using EPR (Figure 1-right) and *in situ* with ambient-pressure XPS. It was determined that the titania ALD films are amorphous and easier to reduce than crystalline titania, and that the reduction is reversible. A transition in the nature of the surface was also observed, with unique mixed Si–O–Ti sites forming during the first few ALD cycles and a more typical titania surface progressively developing as the film grows in thickness. This research was published in *The Journal of Physical Chemistry Letters*.[1]

We have also been looking into ways to deposit gold nanoparticles on oxide supports with small average diameters and sharp size distributions. The initial work has been carried out on SBA-15. The most promising synthetic approach so far has been one that relies on a previous derivatization of the silica surface with amine groups using the well-established grafting of 3-aminopropyl triethoxysilane (APTES). Gold is then added using $HAuCl_4$ and reduced with $NaBH_4$, after which a final calcination is carried out. We have found that the latter two steps, the reduction and the calcination of the catalyst, are the most influential in determining the size and dispersion of the Au NPs. We have had some initial successes, having been able to synthesize catalysts with Au NPs as small as 2.4 nm in diameter (Figure 2), but we still need to control size in a more systematic way and extend the synthetic procedure to other surfaces, in particular to titania.

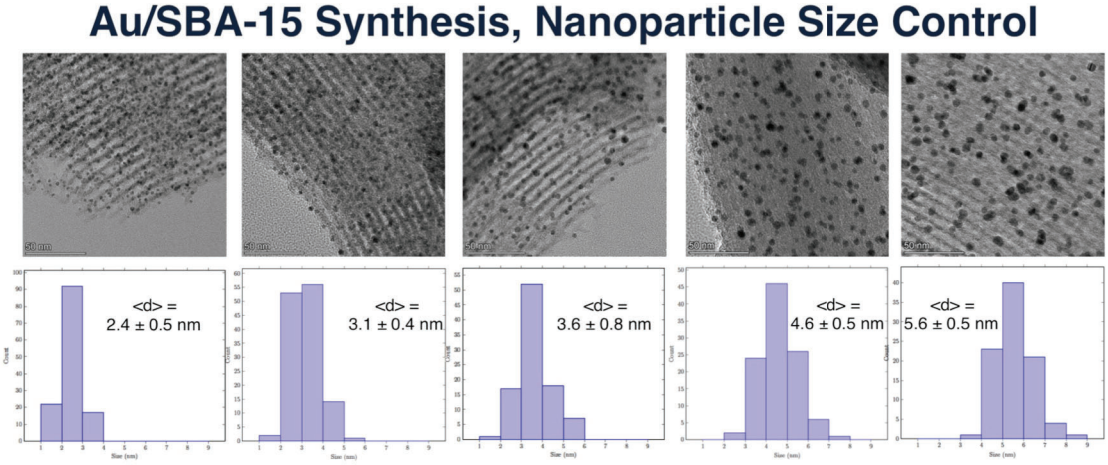

Fig. 2. Synthesized Au/SBA-15 catalysts with varying NP sizes.

In terms of reactivity, we have initiated our evaluation of the catalysts by measuring the kinetics of the catalytic oxidation of carbon monoxide. Both orders of deposition, with TiO_2 added either before or after Au dispersion, were tested for two titania film thicknesses amounting to about half and full TiO_2 monolayers. The resulting catalysts were characterized using various techniques, mainly electron microscopy and N_2 adsorption-desorption isotherms, and the kinetics of the oxidation of CO with O_2 were followed using infrared absorption spectroscopy. Typical kinetic results are shown in Figure 3. A synergy between the Au and TiO_2 phases as it relates to the bonding and conversion of CO was identified, the tuning of which could be controlled by varying the synthetic parameters. The ALD of TiO_2 films proved to be an effective way to maximize the Au-TiO_2 interface sites, and with that help with the activation of molecular oxygen. This work has been published as an invited feature in the journal *Catalysts*.[2]

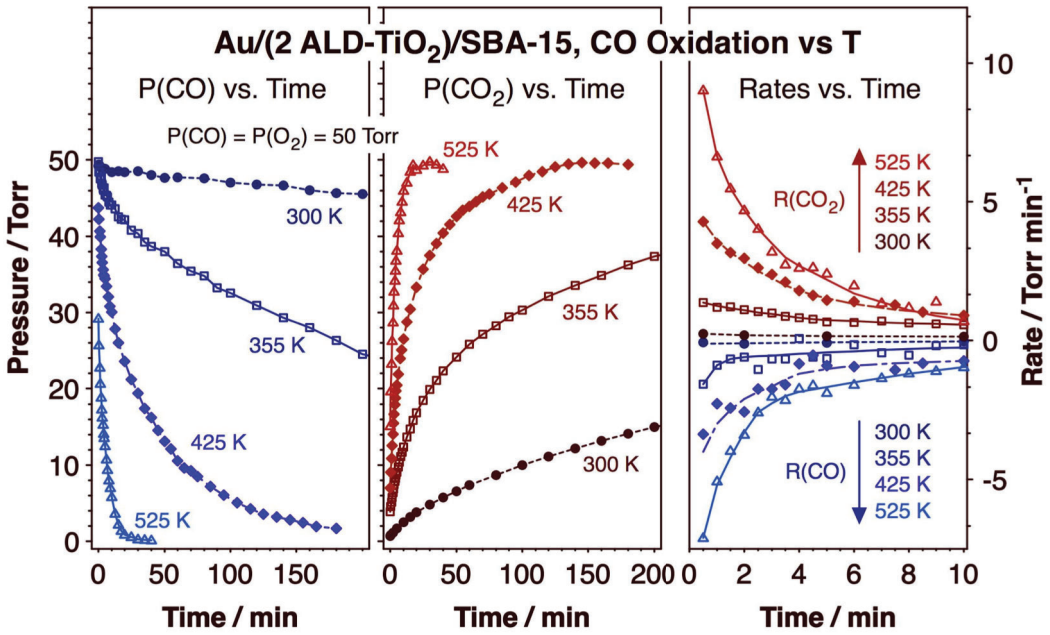

Fig. 3. Kinetics of CO oxidation promoted by a (2 ALD-TiO_2)/Au/SBA-15 catalyst as a function of temperature. Left: CO pressure versus time. Center: CO_2 pressure versus time. Right: CO (blue symbols, negative values) and CO_2 (red symbols, positive values) pressure change rates versus time. Initial CO and O_2 pressures: 50 Torr each.

Publications Acknowledging this Grant in 2020-2023

(I) Intellectually led by this grant

(1) Ke, W.; Qin, X.; Palomino, R. M.; Simonovis, J. P.; Senanayake, S. D.; Rodriguez, J. A.; Zaera, F. Redox Properties of TiO_2 Thin Films Grown on Mesoporous Silica by Atomic Layer Deposition. *J. Phys. Chem. Lett.* **2023**, *14*, 4696-4703.

(2) Qin, X.; Ke, W.; Vazquez, Y.; Lee, I.; Zaera, F. CO Oxidation Catalyzed by Au Dispersed on SBA-15 Modified with TiO_2 Films Grown via Atomic Layer Deposition (ALD). *Catalysts*, **2023**; Vol. 13; pp 1106.

Heterostructure Interfaces for Electrocatalytic Oxygen and Hydrogen Evolution Reactions

Sen Zhang
Department of Chemistry, University of Virginia

Presentation Abstract

Deep decarbonization of the energy sector needs green hydrogen (H_2) from water electrolysis to complement renewable electricity. Nanocrystals with well-defined surfaces and interfaces allow us to bridge the knowledge gap between conventional single-crystal bulk materials and powder catalysts to achieve in-depth understanding of structure-catalytic property relationships. This presentation highlights how heterostructure interfaces of nanocrystals affect catalytic properties for the oxygen evolution reaction (OER) and the hydrogen evolution reaction (HER) for hydroxide exchange membrane water electrolysis (HEMWE). In the first example, Pt nanoparticles are coupled with ultra-thin Ce_2O_3 nanosheets to modulate the electronic state of Pt for the HER. Upon the formation of Pt-Ce_2O_3 interface, Pt become electron-deficient due to electron transfer to the Ce_2O_3 nanosheets, thereby decreasing the hydrogen adsorption energy and improving the HER activity. In the second example, NiFeOOH-TiO_2 heterostructured nanocrystals are synthesized, and the unique NiFeOOH-TiO_2 heterostructure makes NiFeOOH stabilized in the surface of TiO_2 nanorods in a form of well-defined nanoclusters (~1 nm) for the OER. The integration of controlled synthesis of nanocrystals, *in situ* structural characterization, and advanced theoretical calculation enables to understand the reaction mechanism as well as the interfacial effects on the OER and HER catalysis.

Grant or FWP Number: DE‐SC0023443: Fundamental Studies of Catalytic Sites and Catalyst/Membrane Integrations for Advanced Hydroxide Exchange Membrane Electrolyzers

PIs: Sen Zhang, Brent T. Gunnoe, Charles Machan, Huiyuan Zhu, Jingguang G. Chen, William A. Goddard III, Yushan Yan
Postdocs: Macarena Alférez, Yizhen Chen, Qiang Gao, Soonho Kwon, Sameeta Sahoo, Wenjuan Shi, Zhenhua Xie
Students: Elizabeth Johnson, Mollie Morrow, Charles Musgrave, Nathaniel Nichols, Alexandra Oliveira, Chris Webber, Yuanqi Liu, Shen-Wei Yu
Affiliations: University of Virginia, Columbia University, California Institute of Technology, University of Delaware

RECENT PROGRESS

Heterostructured nanocrystal OER catalysts

PGM-free OER electrocatalyst is critical to the development of advanced HEMELs. The NiFeOOH-TiO_2 heterostructured nanocrystals were synthesized via wet-chemical colloidal synthesis. As shown in **Fig. 1a and b**, the unique NiFeOOH-TiO_2 heterostructure makes NiFeOOH, an active catalytic component for the OER, stabilized in the surface of TiO_2 nanorods in a form of small nanoclusters (~1 nm) to maximize their active surface area. The NiFeOOH-TiO_2 exhibited encouraging OER activity and durability in rotating disk electrode (RDE) testing condition, superior to pure NiFeOOH. To understand the atomic structure of NiFeOOH-TiO_2 under the OER condition, *in situ* X-ray absorption spectroscopy (XAS) measurements were conducted at the Ni and Fe K-edges on NiFeOOH-TiO_2 (Ni_xFe_y, x/y ratio tunable) catalysts, as well as monometallic FeO_x-TiO_2 and NiO_x-TiO_2 catalysts. The catalysts were tested at various conditions: open circuit potential (OCP), and at 1.3, 1.52, 1.55, 1.6, and 1.7 V vs. RHE. The Fe and Ni oxidation states under OER potentials were found to be sensitive to Ni/Fe ratio. The NiFeOOH-TiO_2 catalyst was found to show enhanced Ni-Ti and Fe-Ti interaction when the potential becomes more positive. The NiFeOOH/TiO_2 OER catalyst was implemented at the anode of a single-cell HEMEL. The NiFeOOH-TiO_2 was air-sprayed onto commercial Ni foam, and the assembled HEMEL delivered a low cell voltage (~1.7 V) at 500 mA cm^{-2} in 1 M KOH electrolyte at 60 °C with a low decay rate of 0.17 mV h^{-1}, as shown in **Fig. 1c and d**.

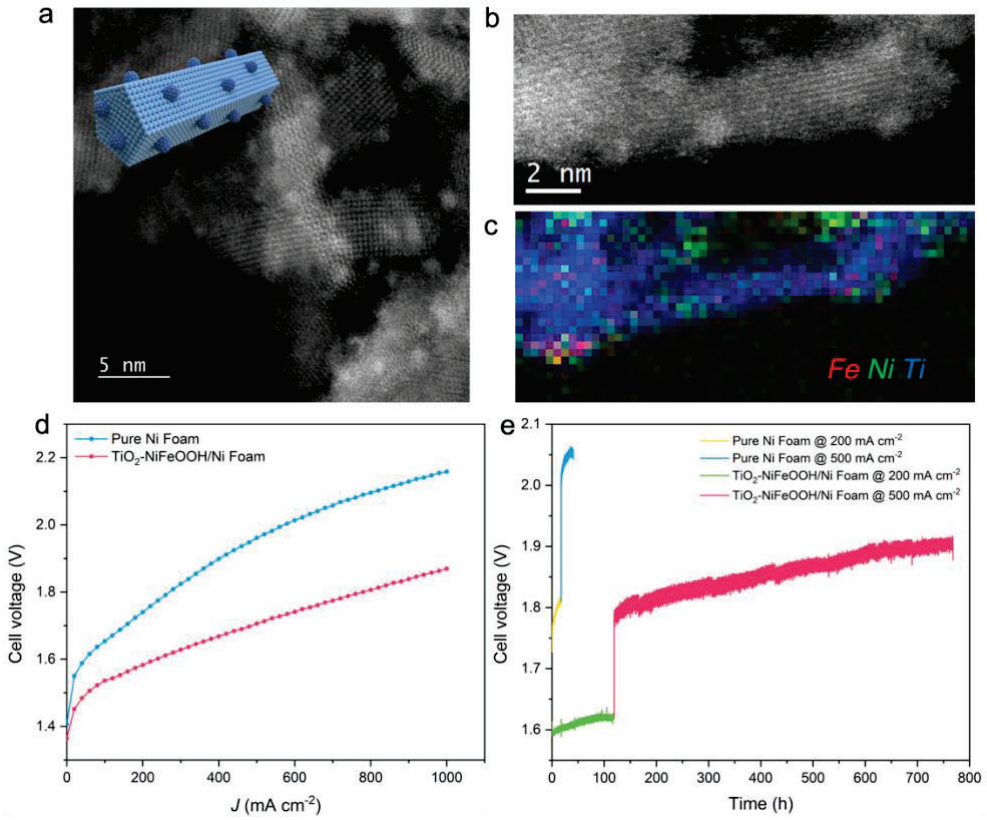

Figure 1. a-c. Scanning transmission electron microscopy (STEM) images (a) and electron energy loss spectroscopy (EELS) elemental mapping of NiFeOOH-TiO_2 nanorods (b, c). Model in a indicates the heterostructure. **d-e**. AEM single cell (5 cm^2) assembled with NiFeOOH-TiO_2 anode (loaded on Ni foam), PtRu cathode, and PAP-TP-85 membrane (1 M KOH, 60 °C), and its comparison with the one with Ni foam anode. Stability test in e

was conducted at 200 mA cm^{-2} first for 120 hours and then 500 mA cm^{-2} for 640 hours for the cell with NiFeOOH-TiO_2 anode.

Monolayer Pt and Au HER catalysts

Mono-layer Pt and Au on transition metal nitrides (TMNs) supports have been developed for the HER catalysis. TMNs are a class of electrocatalyst support materials similar to transition metal carbides (TMCs) with the advantage of avoiding the issues arising from surface deposits of graphitic carbon during synthesis. We explored the feasibility of using TMN-supported Pt and Au as alkaline HER electrocatalysts. TMN of Ti, V, Ta, Mo and W were synthesized by reacting the corresponding films in the flow of ammonia gas at 850 °C for 10 hours. Monolayer coverage of Pt or Au was deposited onto the TMN films using physical vapor deposition in a UHV system equipped with XPS to verify surface compositions. We established a volcano-like trend between the electrochemical HER activity and hydrogen binding energy (HBE) calculated from DFT for well-characterized thin films of TMNs and TMN-supported catalysts.

Pt-Ce_2O_3 HER catalyst

Using non-carbon support with strong metal-metal oxide support electronic interaction is a promising strategy to improve Pt HER efficiency. However, the relative low conductivity of metal oxides is a significant barrier for their application in electrocatalysis. 2D Ce_2O_3 nanosheets with a thickness of 1-2 atomic layers and well-defined (100) basal plane were developed. Such a 2D Ce_2O_3 was used to uniformly coat commercial Vulcan carbon to form a new supporting material. Due to the ultrathin structure of Ce_2O_3, the electrical conductivity of Ce_2O_3-coated Vulcan carbon is comparable to uncoated carbon, and it offers a functional surface to tune Pt energetics and catalytic properties. In alkaline condition, Pt supported on Ce_2O_3-carbon presented a substantially enhanced activity for the HER. Based on the well-defined interfacial structure, DFT calculation was used to understand HER kinetics and compare it with unmodified Pt.

Co and Ni corroles HER catalysts

Corroles are a ring-truncated version of porphyrin and as a result are trianionic supports, rather than dianionic. We have synthesized and isolated 5,10,15-tris(pentafluorophenyl)corrole (tfpc), as well as the corresponding Co(III) complex with a triphenylphosphine ligand. Currently, we are testing deposition conditions with this compound for the HER, as well as using nucleophilic aromatic substitution with primary amines (n-butylamine) to functionalize the fluorophenyl rings. This will allow us to test the conditions required for covalent attachment strategies, as well as model the effect of covalent attachment on catalytic activity. As a point of comparison, we have also synthesized and isolated a series of metal phthalocyanines (Mn-Cu), which are a dianionic ligand framework. For heterogenized molecular catalysts, we are developing strategies to immobilize these complexes onto carbon through covalent binding to make heterogeneous materials for the HER.

Aleksandr V. Zhukhovitskiy

C-H Amination/Aza-Cope Depolymerization of Diene Polymers

Aleksandr V. Zhukhovitskiy, Maxim Ratushnyy, and Sydney E. Towell
Department of Chemistry, University of North Carolina at Chapel Hill

Presentation Abstract

Accumulation of rubber materials has been unsustainable on a global scale. To address this major challenge, we are developing approaches to depolymerize rubber into value-added nitrogen-containing small molecules. Our central strategy hinges on two chemical transformations: allylic C-H amination of unsaturated polymer backbones and subsequent aza-Cope rearrangement, which leads to conversion of an all-carbon polymer backbone into a polyiminium chain that readily undergoes hydrolysis. With respect to the first transformation, I will discuss our advances in accelerating catalytic C-H amination using selenium catalysis, as well as development of highly efficient and chemically simple stoichiometric sulfur-based aminations. With respect to the second transformation, I will present our most recent results on the depolymerization of aminated polybutadiene. I will end on most recent work which is focused on translating the amination/aza-Cope reactivity to vulcanized rubber.

DE-SC0022898: Upcycling of all-carbon polymer backbones into value-added amines via skeletal rearrangement
Postdoc(s): Maxim Ratushnyy
Student(s): Sydney E. Towell

RECENT PROGRESS

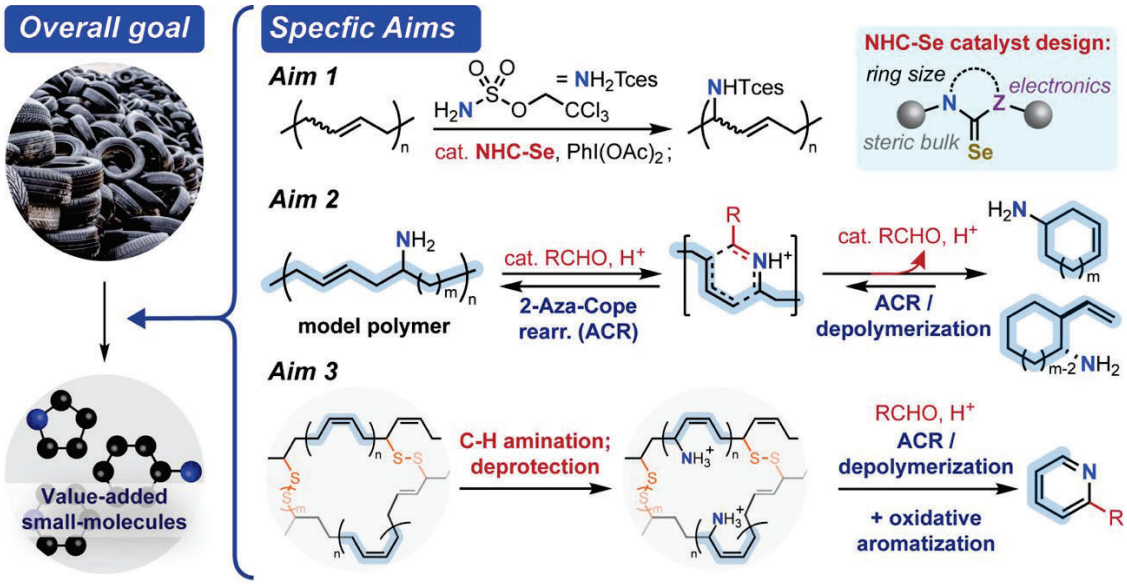

Figure 1. Summary of the proposal aims.

The major goals of the project are to (1) develop allylic C-H amination of diene polymers via selenium catalysis, (2) develop 2-aza-Cope rearrangement (ACR) of model substrates, and (3) adapt the developed C-H amination and ACR to convert diene polymers and rubber into value-added nitrogen-containing small molecules.

Aim 1:

We discovered that 1,3-dimethylimidazolidine-2-selenone is ~20 times more active as a catalyst for allylic C-H amination compared to established amination reported by Michael and coworkers (*J. Am. Chem. Soc.***2020**, *142* (39), 16716–16722). Catalyst loading could be reduced by a factor of 3 compared to the methodology utilized by Michael and coworkers (which was 15 mol%), and the reaction rate is still ~10 times higher. We plan to explore the substrate scope and regioselectivity of this amination and apply it to polybutadiene. Furthermore, we attribute the difference in reactivity to the more pi-acidic saturated 1,3-dimethylimidazolidine N-heterocyclic carbene (NHC) ligand compared to the unsaturated 1,3-dimethylimidazoline NHC ligand utilized by Michael. This insight points the way to more active yet C-H amination catalysis. We have also begun to study the mechanism of the selenium catalyzed amination and isolated and crystallographically characterized the first examples of an NHC-selenodiimide and NHC-selenoimide adducts; we are currently exploring whether these species are on- or off-cycle intermediates.

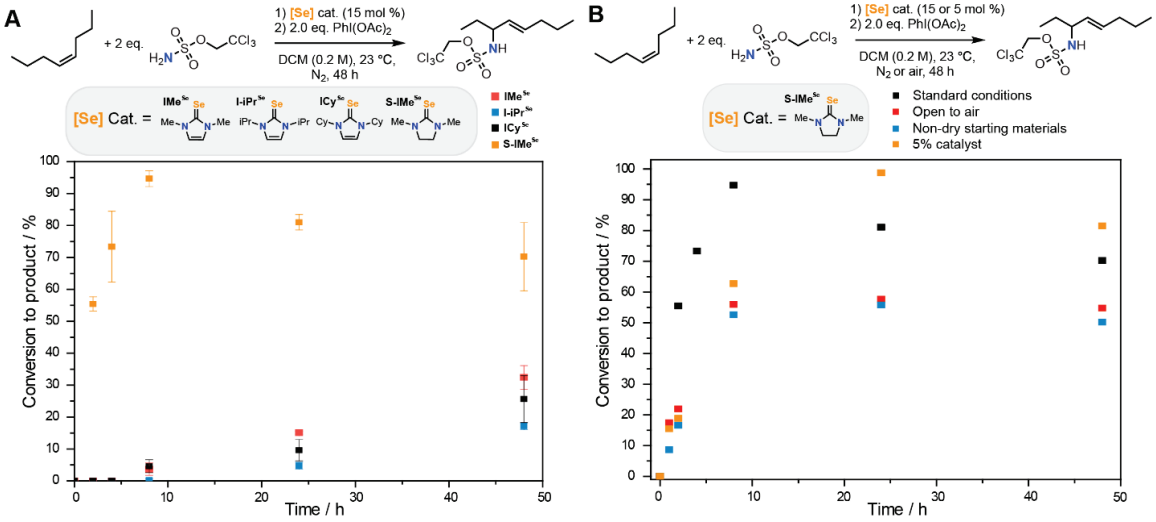

Figure 2. A. Amination kinetics monitored via ^{1}H NMR against an internal standard. B. Testing the sensitivity of the catalysis to air, moisture, and catalyst loading (unless indicated otherwise, all experiments were carried out using 15 mol% catalyst).

Aim 2:

This aim has been nearly completed. We have now optimized the aza-Cope rearrangement/alcoholysis of a small molecule model homoallylic amine substrate, which leads to quantitative conversion and 96% NMR yield of target products (Figure 3). This chemistry has been translated to a 12-mer prepared by acyclic diene metathesis (ADMET), and aminated polycyclooctadiene (which is equivalent to partially aminated polybutadiene, Figure 4). Based on nuclear magnetic resonance (NMR) and gel permeation chromato graphy (GPC) analysis with universal calibration, the latter (M_n = 31 kg/mol) depolymerize

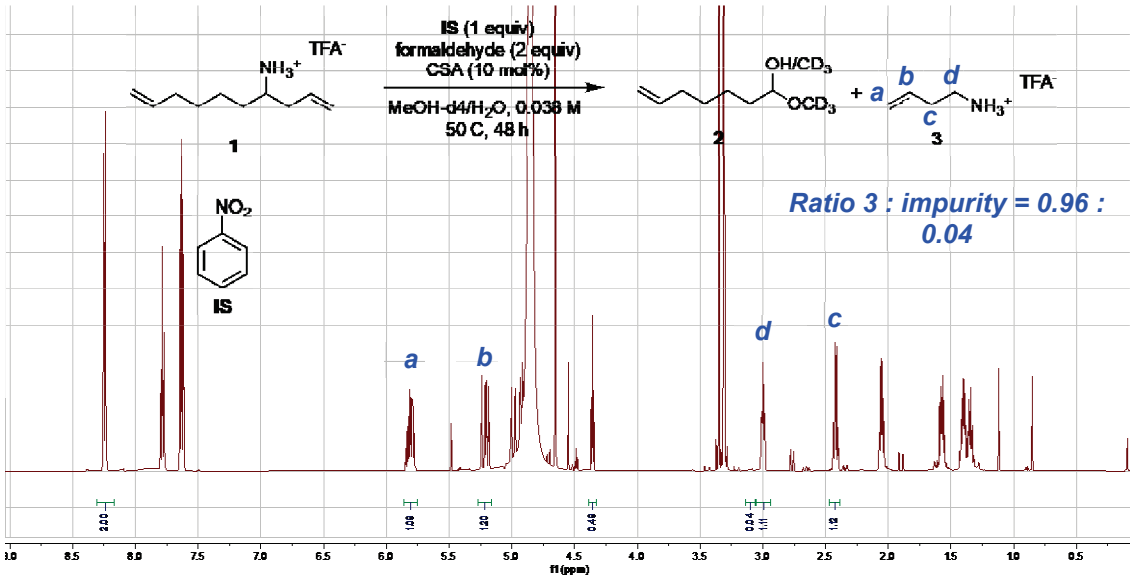

Figure 3. [1]H NMR spectrum of the crude product of the optimized small molecule model ACR.

cleanly within 48 hours to oligomers (85% conversion, M_n = 0.3 kg/mol) with amine and enal end-groups (Figure 4).

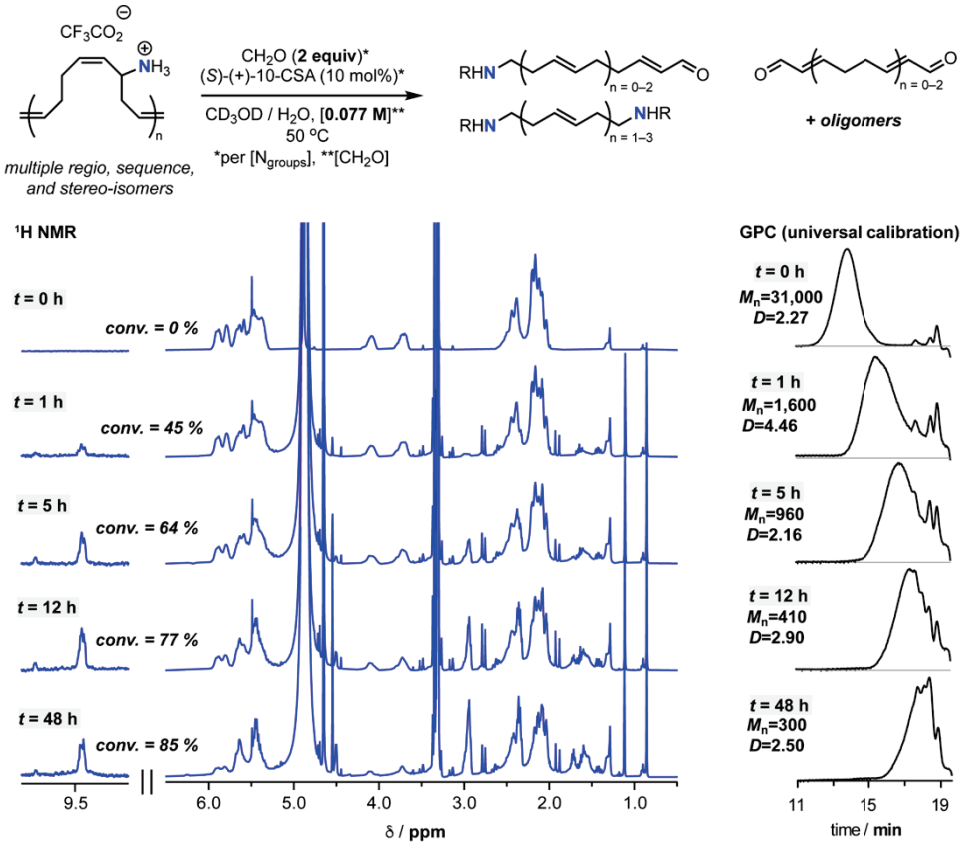

Figure 4. Optimized ACR of the aminated polycyclooctadiene model substrate, monitored by [1]H NMR and GPC with universal calibration.

Aim 3:

Golder and Michael recently reported the use of the original Michael catalytic system to aminate polybutadiene (*Angew. Chem. Int. Ed.* **2023**, e202303115); at the same time, Boydston and Michael reported analogous amination of polynorbornene (*Angew. Chem. Int. Ed.***2023**, e202303174). Although our preliminary polybutadiene amination experiments reported in the proposal are virtually identical to what has now been reported in *Angew. Chem. Int. Ed.* **2023**, e202303115, our more recent developments in aim (1) advance substantially over that chemistry. Furthermore, we found that traditional deprotection of the sulfonamides—critical for us to carry out aza-Cope rearrangements—leads to an insoluble polymer, which we believe to be cross-linked through an as-of-yet unknown mechanism. To get around this issue, we are currently pursuing amination to install carbamate-protected amines, which could be cleaved without inducing undesired cross-linking. One approach we are using to install these carbamate-protected amines is using *N,N′*-bis(methoxycarbonyl) sulfur dimiide (DMSD), which we have already successfully tested on a model small molecule substrate, polybutadiene, and crushed vulcanized polyisoprene rubber (Figure 5). We are now beginning to test this chemistry on vulcanized polybutadiene.

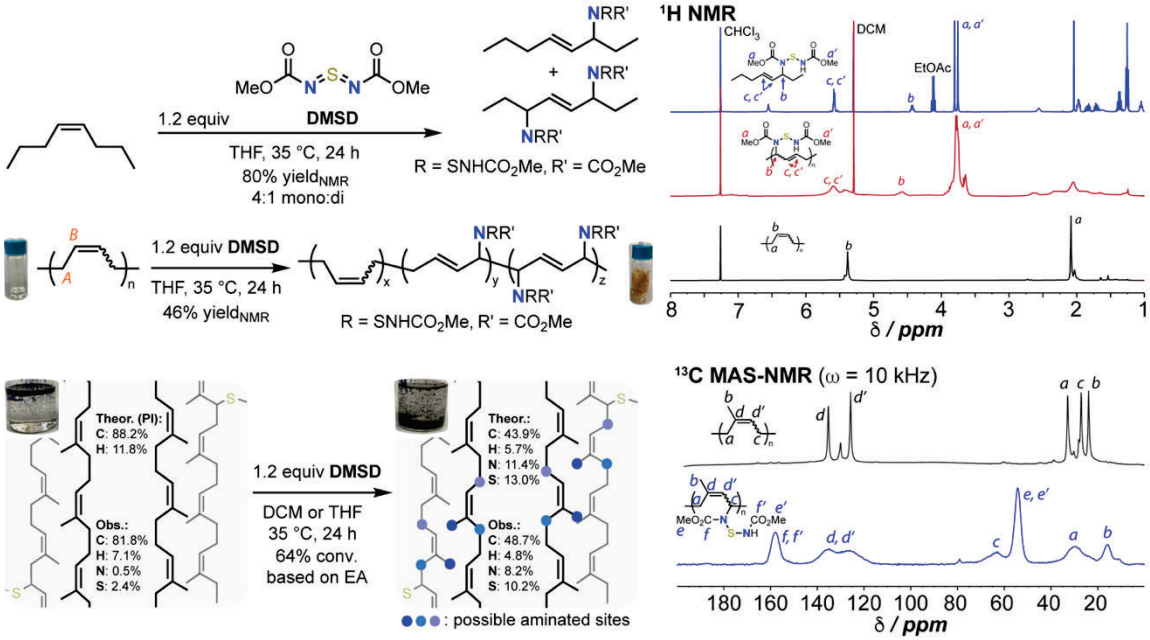

Figure 5. Amination of *cis*-4-octene, *cis*-1,3-polybutadiene, and crushed polyisoprene rubber with DMSD, with corresponding NMR spectra provided on the right. Elemental analysis data for the rubber is provided in the illustration of the rubber structure; inset in the left-hand corner of these illustrations are pictures of the rubber in dichloromethane before and after amination.

Publications Acknowledging this Grant in 2020-2023

n/a

VIRTUAL ATTENDEES ABSTRACTS

Guy Bertrand

Mesoionic Carbenes as Catalytic Reducing Agents

Guy Bertrand, Adam Vianna, Mehdi Abdellaoui, Mohand Melaimi
UCSD–CNRS Joint Research Laboratory (IRL 3555), Department of Chemistry and Biochemistry, University of California San Diego, La Jolla, California, USA.

Carbene-catalysis via single electron transfer (SET) pathways is in its infancy and limited to the involvement of Breslow intermediates as the reducing species. Consequently, only acylation reactions can be performed. We have developed catalytic processes via SET pathways using carbenes by themselves as catalytic reductants, which considerably broadens the scope of the chemical transformations that can be achieved. We have successfully achieved the carbene-catalyzed hydrogenation of anthraquinones using the solvent as a hydrogen donor. Currently, this transformation is carried out by hydrogenation with H_2 using a palladium catalyst, and this is the most expensive step for the large-scale production of hydrogen peroxide (> 3 million tons annually). Our preliminary results show that mesoionic carbenes (MICs) are among the most potent organic ground state reducing agents known today.

DESC0009376: Stable carbenes as transition metal catalyst surrogates

RECENT PROGRESS

Cyclic (Alkyl)(amino)carbenes: Synthesis of Iminium Precursors and Structural Properties.

Since their discovery in 2005, five-membered cyclic (alkyl)(amino)carbenes (CAACs) have found numerous applications in homogeneous catalysis. Better σ-donors and π-acceptors than the well-known N-heterocyclic carbenes (NHCs), these stable singlet carbenes own their growing popularity to the strong bonds they form with transition metals. To encourage further discoveries for CAACs in catalysis, we have reported a divergent, and easily scalable route to iminium precursors of CAACs, using readily available pre-allylated aldehydes. Using crystallographic data and steric maps, we further elaborated on the distinct steric properties of CAACs with respect to popular ligand families, thus providing guidelines when considering CAACs as ligands for transition metals. Our methodology allows for accessing CAAC precursors which were not available with the previously described routes 1 and 2. We expect that these results will foster new designs of CAAC ligands, including a range of chiral CAACs variants providing the use of pre-allylated enantiopure aldehydes.

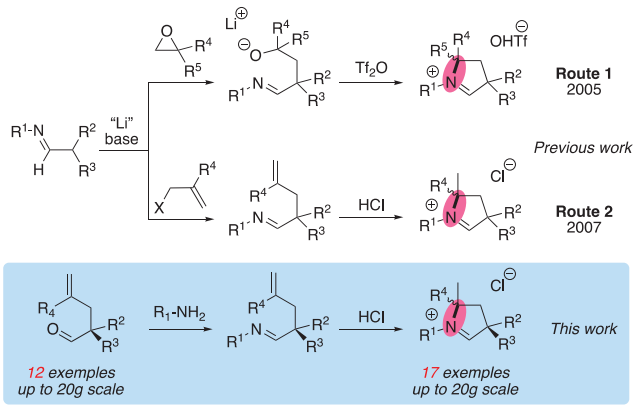

A Simple Access to Cyclic (Alkyl)(amino)carbenes Copper (I) Complexes.

Thanks to the strong bond they form with metal centers, CAACs can stabilize both low and high oxidation states making (CAAC)Cu(I) complexes particularly attractive for catalysis and material science alike. In catalysis, we have demonstrated that these ligands trigger remarkable Markovnikov regioselectivity for the carboboration and silylation of terminal alkynes. In material science, we reported record photoluminescent properties, akin to that of heavy metals, with a CAAC copper carbazole complex. We also took advantage of CAAC's to stabilize a reactive $Cu^0_2Cu^1$ metal cluster, which allowed for demonstrating absolute templating of M(111) cluster surrogates by galvanic exchange. Importantly, CAAC copper complexes are effective carbene transfer reagents through transmetallation, allowing for the preparation of a broad variety of metal complexes (e.g; Au, Ag, Pd and Ir). Traditionally (CAAC)Cu(I) complexes were prepared under inert atmosphere in a two-step sequence beginning by the deprotonation of the corresponding conjugate acid with a strong base (*i.e.* KHMDS) followed by the addition of a copper salt (e.g. CuCl). Continuing our ambition to make CAAC chemistry widely accessible, we have published a practical and green methodology for the preparation of (CAAC)Cu(I) chloride complexes. Indeed, these

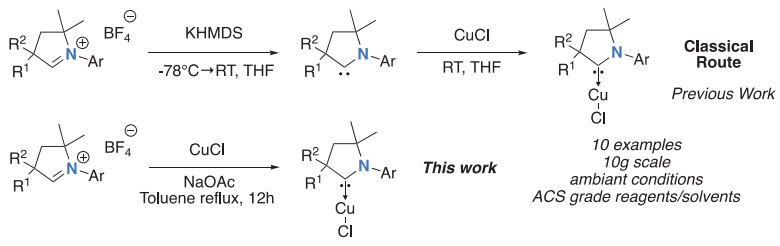

complexes are readily available in good yields by simply refluxing $CAAC^{H}.BF_4$ with copper chloride and sodium acetate in toluene. This methodology extends to other members of the CAAC family such as bicyclic (alkyl)(amino)carbenes (BiCAACs) and cyclic (amino)(barrelene)carbenes (CABC). The later was previously inaccessible by the free carbene route demonstrating the advantage of the weak base approach. Lastly, to showcase this methodology, we performed a multigram synthesis of a catalytically relevant CAAC ligand in air using ACS grade solvents and reagents.

(CAAC)Copper Catalysis Enables Regioselective Three-Component Carboboration of Terminal Alkynes.

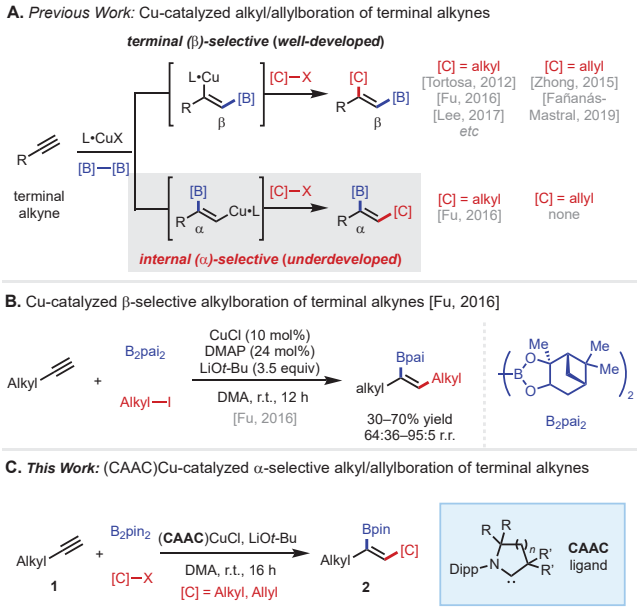

Organoboron compounds play a unique role in the chemical sciences. Carbon–boron bonds can readily be converted into a diverse array of carbon–carbon and carbon–heteroatom linkages via an ever-expanding battery of methods, and organoboron molecules themselves possess myriad of functions in the context of biology and materials science. Copper-catalyzed borylative 1,2-difunctionalization of alkynes is an established means of preparing tri- and tetrasubstitued alkenylboron targets via a mechanism involving migratory insertion of an alkyne into a L_n•Cu^{I}–boryl intermediate followed by coupling of the resulting L_n•Cu^{I}(alkenyl) species with an electrophile. Controlling the regioselectivity of these processes in a way that grants access to either regioisomer in a predictable manner remains challenging. With terminal alkynes, the vast majority of catalytic systems deliver the boryl group to the terminal (β) position, restricting access to the opposite alkenylboron regioisomers.

We have extended our investigations of (CAAC)Cu–boryl catalysis to the three-component carboboration of terminal alkynes and have found that high levels of α-selectivity are maintained across different carbon electrophiles, including allyl electrophiles, which have not been previously employed in an α-selective reaction system. The generality of the method across different alkyne substrates offers a convenient means of preparing tri-substituted alkenylboron compounds with established utility in organic synthesis.

Highly Robust and Efficient Blechert-type Cyclic(alkyl)(amino)carbene Ruthenium Complexes for Olefin Metathesis

Olefin metathesis represents an eco-friendly and highly versatile synthetic tool to build plethora of valuable building blocks. Thanks to the development of bench stable well-defined ruthenium-arylidene complexes, this catalytic reaction is intensively used in polymer chemistry and fine chemistry but has also found applications in the valorisation of the biomass and the depolymerisation of polyethylene. Despite these remarkable

achievements, the quest for more efficient Ru-complexes remains a very active research topic across academia and industry.

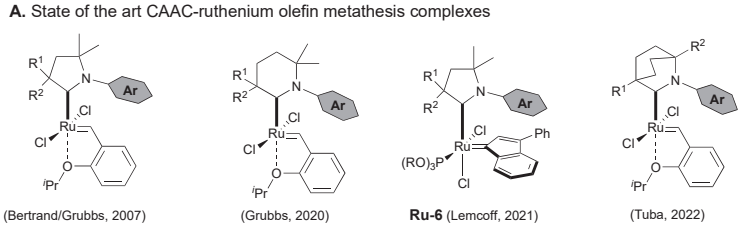

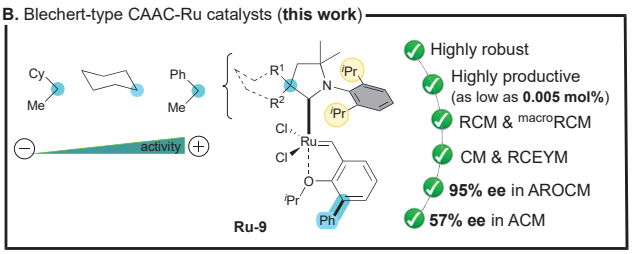

This year, we reported the first Blechert-type ruthenium complexes containing cyclic(alkyl)(amino)carbene (CAAC) ligands. These catalysts demonstrate remarkable thermal stability in solution and excellent catalytic performances at low catalytic loading (up to 0.005 mol%) in ring-closing metathesis (RCM), macro-RCM, ring-closing enyne metathesis (RCEYM), cross-metathesis (CM) and ring-opening cross metathesis (ROCM). Moreover, up to 95% ee was obtained in asymmetric olefin metathesis.

Publications Acknowledging this Grant in 2020-2023

(I) Intellectually led by this grant

1. Yazdani, S.; Junor, G. P.; Peltier, J. L.; Gembicky, M.; Jazzar, R.; Grotjahn, D. B.; Bertrand, G. Influence of Carbene and Phosphine Ligands on the Catalytic Activity of Gold Complexes in the Hydroamination and Hydrohydrazination of Alkynes**.** *ACS Catal.* **2020,** *10*, 5190-5201.
2. Sau, S. C.; Hota, P. K.; Mandal, S. K.; Soleilhavoup, M.; Bertrand, G. Stable Abnormal N-Heterocyclic Carbenes and their Applications. *Chem. Soc. Rev.* **2020**, *49*, 1233-1252.
3. Jazzar, R.; Soleilhavoup, M.; Bertrand, G. Cyclic (Alkyl)- and (Aryl)(amino)carbene Coinage Metal Complexes and Their Applications. *Chem. Rev.* **2020**, *120*, 4141-4168.
4. Junor, G. P.; Lorkowski, J.; Weinstein, C. M.; Jazzar, R.; Pietraszuk, C.; Bertrand, G. The influence of C(sp^3)H-Selenium Isnteractions on the ^{77}Se NMR Quantification of the □-Accepting Properties of Carbenes. *Angew. Chem. Int. Ed.* **2020,** *59*, 22028-22033.
5. Peltier, J. L.; Soleilhavoup, M.; Martin, D.; Jazzar, R.; Bertrand, G. Absolute Templating of M(111) Cluster Surrogates by Galvanic Exchange. *J. Am. Chem. Soc.* **2020,** *142*, 16479-16485.
6. Peltier, J. L.; Tomas-Mendivil, E.; Tolentino, D. R.; Hansmann, M. M.; Jazzar, R.; Bertrand, G. Realizing Metal-Free Carbene-Catalyzed Carbonylation Reactions with CO. *J. Am. Chem. Soc.* **2020,** *142*, 18336-18340.
7. Morvan, J.; Vermersch, F.; Zhang, Z.; Falivene, L.; Vives, T.; Dorcet, V.; Roisnel, T.; Crévisy, C.; Cavallo, L.; Vanthuyne, N.; Bertrand, G.; Jazzar, R.; Mauduit, M. Optically Pure C_1-Symmetric Cyclic(alkyl)(amino)carbene Ruthenium-Complexes for Asymmetric Olefin Metathesis. *J. Am. Chem. Soc.* **2020,** *142*, 19895-19901.
8. Morvan, J.; Mauduit, M.; Bertrand, G.; Jazzar. R. Cyclic (Alkyl)(amino)carbenes (CAACs) in Ruthenium Olefin Metathesis. *ACS Catal.* **2021**, *11*, 1714-1748.

9. Liu, W.; Vianna, A.; Zhang, Z.; Huang, S.; Huang, L.; Melaimi, M.; Bertrand, G.; Yan. X. Mesoionic Carbene-Breslow Intermediates as Super Electron Donors: Application to the Metal-Free Arylacylation of Alkenes. *Chem. Catalysis* **2021,** *1*, 196-206.
10. Gao, Y.; Yazdani, S.; Kendric, A.; Junor, G. P.; Kang, T. Grotjahn, D. B.; Bertrand, G.; Jazzar, R.; Engle, K. M. Cyclic(Alkyl)(Amino)Carbene Ligands Enable Cu-Catalyzed Markovnikov Protoboration and Protosilylation of Terminal Alkynes: A Versatile Portal to Functionalized Alkenes. *Angew. Chem. Int. Ed.* **2021,** *60*, 19871-19878.
11. Vermersch, F.; Oliveira, L.; Hunter, J.; Soleilhavoup, M.; Jazzar, R.; Bertrand, G. Cyclic (Alkyl)(amino)carbenes: Synthesis of Iminium Precursors and Structural Properties. *J. Org. Chem.* **2022,** *87*, 3511-3518.
12. Gao, Y.; Kim, N.; Mendoza, S. D.; Yazdani, S.; Faria-Vieira, A.; Liu, M.; Kendrick, A.; Grotjahn, D. B.; Bertrand, G.; Jazzar, R.; Engle, K. M. (CAAC)Copper Catalysis Enables Regioselective Three-Component Carboboration of Terminal Alkynes**.** *ACS Catal.* **2022,** *12*, 7243-7247.
13. Morvan, J.; Vermersch, F.; Lorkowski, J.; Talcik, J.; Vives, T.; Roisnel, T.; Crévisy, C.; Vanthuyne, N.; Bertrand, G.; Jazzar, R.; Mauduit, M. Cyclic(alkyl)(amino)carbene Ruthenium Complexes for *Z*-Stereoselective (Asymmetric) Olefin Metathesis. *Catal. Sci. Technol.* **2023**, *13*, 381-388.
14. Morvan, J.; Vermersch, F.; Zhang, Z.; Vives, T.; Roisnel, T.; Crévisy, C.; Falivene, L.; Cavallo, L.; Vanthuyne, N.; Bertrand, G.; Jazzar, R.; Mauduit, M. The Ambivalent Role of Rotamers in Cyclic(alkyl)(amino)carbene Ruthenium Complexes for Enantioselective Ring-Opening Cross-Metathesis. *Organometallics* **2023**, 42, 495-504.
15. Lorkowski, J.; Serrato, M.; Gembicki, M.; Mauduit, M.; Bertrand, G.; Jazzar, R. A Straightforward Access to Cyclic (Alkyl)(amino)carbenes Copper (I) Complexes. *Eur. J. Inorg. Chem.* **2023**, e202300074.
16. Haimerl, M.; Schwarzmaier, C.; Timoshkin, A. Y.; Melaimi, M.; Bertrand, G.; Scheer, M. Reactivity of Yellow Arsenic towards Cyclic Alkyl Amino Carbenes (CAACs). *Chem. Eur. J.* **2023**, e202300280
17. Del Vecchio, A.; Talcik, J.; Colombel-Rouen, S.; Lorkowski, J.; Serrato, M. R.; Roisnel, T.; Vanthuyne, N.; Bertrand, G.; Jazzar, R.; Mauduit, M. Highly Robust and Efficient Blechert-type Cyclic(alkyl)(amino)carbene Ruthenium Complexes for Olefin Metathesis. *ACS catal.* **2023**, 13, 6195-6202.

(II) Jointly funded by this grant and other grants with intellectual leadership by other funding sources

1. Soleilhavoup, M.; Bertrand, G. Stable Carbenes, Nitrenes, Phosphinidenes, and Borylenes: Past and Future. *Chem.* **2020**, *6*, 1275-1282.
2. Hu, L.; Meng, G.; Chen, X.; Yoon, J. S; Chan, J. R.; Chekshin, N.; Strassfeld, D. A.; Sheng, T.; Zhuang, Z.; Jazzar, R.; Bertrand, G.; Houk, K. N.; Yu, J.-Q. Enhancing Substrate-Metal Catalyst Affinity via Hydrogen Bonding: Pd(II)-Catalyzed *β*-C(sp^3)−H Halogenation of Free Carboxylic Acids *J. Am. Chem. Soc.* **2023,** in press.

Polymerization Insights through Chemical Imaging

Suzanne A. Blum
University of California, Irvine, Chemistry Department

Presentation Abstract

The majority of catalytic behaviors or polymer properties can arise from minor components—for example, <<1% of catalytically active materials, or bulk properties arising from the differential solvation behaviors of minor components of heteropolymers. Yet, most analytical techniques provide information about only the major compoenents in mixtures. Here, chemical imaging, with an emphasis on fluorescence microscopy, including fluorescence lifetime imaging microscopy, is developed to bridge these gaps. The resulting data inform on catalytic polymerization progress, provide methods to monitor reactions, and underpin the development of more efficient catalytic reactions.

DE-SC0016467

Postdoc(s): Or Eivgi
Student(s): Antonio Garcia, IV; Pía López; Vy Pham, Alexis Ravenscroft

RECENT PROGRESS

A General Autofluorescence Method to Characterize Polymerization Progress

An autofluorescence technique to characterize polymerization progress in real time/in line was developed, which functioned in the absence of typical fluorogenic groups on the monomer or polymer. The monomer dicyclopentadiene and polymer polydicyclopentadiene are hydrocarbons that lack traditional functional groups for fluorescence spectroscopy. Here, the autofluorescence of formulations containing this monomer and polymer during ruthenium-catalyzed ring-opening metathesis polymerization (ROMP) was harnessed for reaction monitoring. The methods fluorescence recovery after photobleaching (FRAP) and here-developed fluorescence *lifetime* recovery after photobleaching (FLRAP) characterized polymerization progress in these native systems—without requiring exogenous fluorophore. (Auto)fluorescence lifetime recovery changes during polymerization correlated linearly to degree of cure, providing a quantitative link with reaction progress. These changing signals also provided relative rates of background polymerization, enabling comparison of 10 different catalyst–inhibitor-stabilized formulations. Multiple-well analysis demonstrated suitability for future high-throughput evaluation of formulations for thermosets. The central concept of the combined autofluorescence and FLRAP/FRAP method may be extendable to monitoring other polymerization reactions previously overlooked for lack of an obvious fluorescence handle.

Polymer Molecular Weight Determination via Fluorescence Lifetime

Control of polymer molecular weight is critical for tailoring structure–function properties; however, traditional molecular weight characterization techniques have limited ability to determine the molecular weight of polymers in real-time, without sample removal from the reaction mixture, with spatial resolution, and of insoluble polymers. Herein, a fluorescence lifetime imaging microscopy (FLIM) method is developed that overcomes these limitations. The method is demonstrated with polynorbornene and polydicyclopentadiene, polymers derived from ruthenium-catalyzed ring-opening metathesis polymerization (ROMP). Polymer M_w, ranging from 35–570 kg/mol as determined by GPC, was quantitatively correlated with fluorescence lifetime. The revealed correlation then enabled time-resolved measurement of M_w during an ongoing ROMP reaction, requiring only 1 s per measurement (of a 45 x 45 mm^2 polymer sample area), and provided spatial resolution, resulting in simultaneous characterization of polymer morphology. To provide fluorescence signal, initial reaction solutions contained a very low doping of a reactive norbornene monomer labeled with fluorescent boron dipyromethene (BODIPY), such that 1 in every 10^7 monomers contained a fluorophore. The resulting FLIM visualization method enables the rapid determination of the molecular weights of growing polymers without removal from the reaction mixture and regardless of polymer solubility.

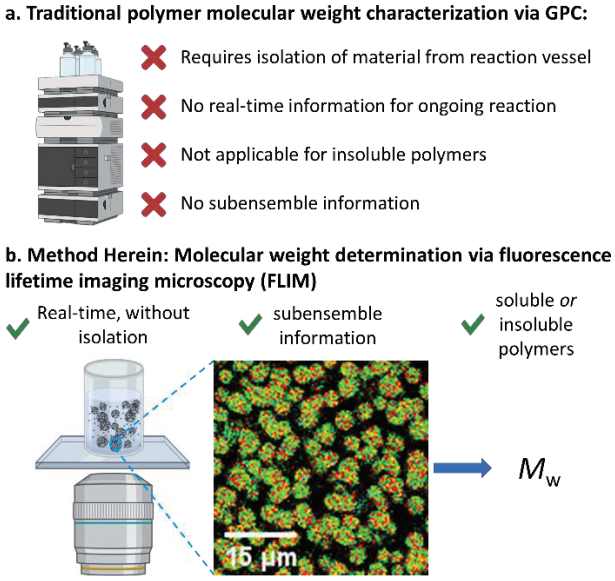

Publications Acknowledging this Grant in 2020-2023

(I) Intellectually led by this grant

(8) "A General Autofluorescence Method to Characterize Polymerization Progress." López, P. A.; Pham, V. H. B.; Blum, S. A. *Angew. Chem. Int. Ed.* **2023**, e202304618. DOI: doi/10.1002/anie.202304618

(7) "Imaging Block-Selective Copolymer Solvation," Eivgi, O.; Ravenscroft, A.; Blum, S. A. *J. Am. Chem. Soc.* **2023**, *145*, 2058–2063. https://doi.org/10.1021/jacs.2c12576

(6) "Polymer Molecular Weight Determination via Fluorescence Lifetime," Garcia IV, A.; Blum, S. A. *J. Am. Chem. Soc.* **2022**, *144*, 22416–22420. https://doi.org/10.1021/jacs.2c10036

(5) "Growth Kinetics of Single Polymer Particles in Solution via Active-Feedback 3D Tracking**,**" Yu, Donggen; Garcia IV, A.; Blum, S. A.*; Welsher, K. D.* *J. Am. Chem. Soc.* **2022**, *144*, 13574–13585. (*denotes equal contribution and co-corresponding authorship) DOI: doi.org/10.1021/jacs.2c04990

(4) "Real-Time Polymer Viscosity–Catalytic Activity Relationships on the Microscale," Eivgi, O.; Blum, S. A. *J. Am. Chem. Soc.* **2022**, *144*, 13574–13585. DOI: doi.org/10.1021/jacs.2c03711

(3) "Superresolved Motions of Single Molecular Catalysts during Polymerization Show Wide Distributions," Saluga, S. J.; Dibble, D. J.; Blum, S. A. *J. Am. Chem. Soc.* **2022**, *144*, 10591–10598. DOI: 10.1021/jacs.2c03566

(2) "Exploring Chemistry with Single-Molecule and -Particle Fluorescence Microscopy," Eivgi, O.; Blum, S. A. *Trends Chem.* **2021***, 4*, 5–14. *(Invited opinion.)* doi.org/10.1016/j.trechm.2021.10.006

(1) "Does Selectivity of Molecular Catalysts Change with Time? Polymerization Imaged by Single-Molecule Spectroscopy," Garcia IV, A.; Saluga, S. J.; Dibble, D. J.; López, P. A.; Saito, N.; Blum, S. A. *Angew. Chem. Int. Ed.* **2021**, *60*, 1550–1555.

Cundari, Thomas R.

Strong Bond Activation by Earth-Abundant Metal Complexes

Presentation Abstract

The activation of strong bonds by Earth-abundant is critical to the efficient utilization of existing hydrocarbon resources as well as the development of carbon-free fuel sources. To these ends, individually and in collaboration with other DOE-BES Catalysis Program PIs, the activation of other strong bonds by Earth-abundant catalysts has been studied via the synergism of theory (our group) and experiment. A promising mechanism of methane activation is via the concerted metalation-deprotonation (CMD) pathway, which has been largely limited to heavy metals and functionalized substrates. In DFT studies, CMD activation of methane is modeled employing Earth-abundant 3d transition metals, to assess the effects of metal identity, formal oxidation state, supporting ligands, *etc*. to understand how such factors impact the kinetics and thermodynamics of methane C—H activation via CMD mechanisms. A comparison of computational methods has also been performed to accomplish a wider scan of potential catalyst candidates.

DE-FG02-03ER15387: Development of Novel Approaches to Earth-abundant Methane Catalysis

Student(s): Cooper Kimbrough (PhD), Ignacio Migliaro (PhD), Dr. William Grumbles (past PhD).

RECENT PROGRESS

Methane activation and functionalization still poses a challenge to make this abundant alkane, the primary component of natural gas, into a more useful and economic resource. One possible method of methane activation is via the concerted metalation-deprotonation (CMD) pathway, which has been largely limited to heavy metals and functionalized substrates. In this DFT study, a CMD activation of methane is assessed employing more Earth-abundant 3d transition metals, to assess the effects of metal, ligands, etc. to understand how such factors impact the kinetics and thermodynamics of methane C—H activation via CMD mechanisms. A comparison of computational methods has also been performed to accomplish a wider scan of potential catalyst candidates. Finally, in collaboration with other DOE-BES Catalysis Program PIs, the activation of other strong bonds by Earth-abundant catalysts has been studied via the synergism of theory (our group) and experiment.

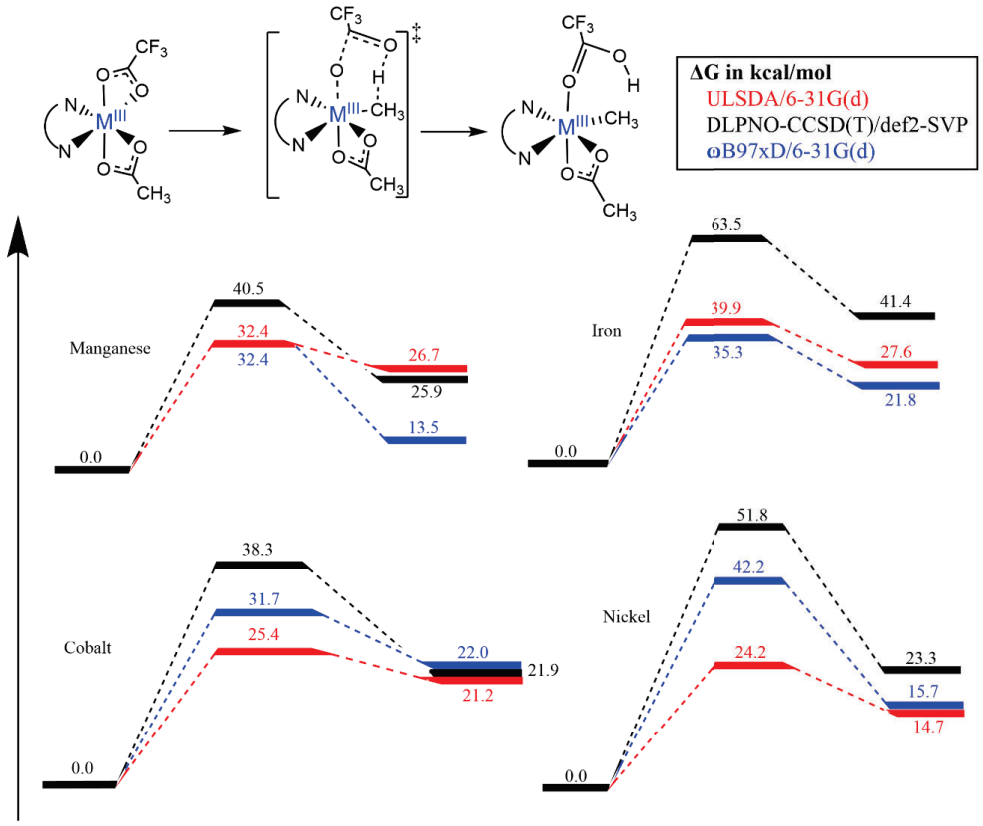

A series of Earth-abundant 3d transition metals were utilized in a concerted metalation deprotonation (CMD) reaction to activate methane. The ligand environments remained the same, but the metal, multiplicities, and computational methods changed to assess the results vis-à-vis the calculated thermodynamics and kinetics of the activation reaction, **see figure above**. The multi-state reactivity of the metals proved to be a very important factor as several metals had significantly higher or lower activation energy barriers as a result of being in low, intermediate, or high spin states, particularly in the cases of manganese and nickel. For some other metals, CMD-mediated methane activation free energy barriers were less affected, *e.g.,* cobalt. Comparing the different levels of theory, some discrepancies were noted, as a result additional comparisons were warranted for each metal to find an acceptable balance of accuracy and computational cost. In the end it was found that a more modern DFT functional with suitable basis sets could replicate much more expensive coupled-cluster methods for methane CMD, albeit with a few caveats. For example, high spin states were much more sensitive to the level of theory as compared to intermediate and low spin states. As expected, more rudimentary DFT functionals such LSDA, which were tested to see if they might be viable for a quick scan of the many possible CMD candidates, gave unreliable energy predictions in relation to DLPNO-CCSD(T). However, optimized geometries were reliable. Thus, such methods could be used to quickly obtain starting points for calculations with higher-order DFT functionals, or to provide an initial scan of metal and ligand dependent trends within a larger catalyst search space.

For future studies, a deeper analysis of supporting ligand effects may have substantial impact on lowering the activation energy barriers for the methane activation as

currently they are very high for all accurate calculations, $\Delta G^{\ddagger}$ >30 kcal/mol. More metals could be trialed, but cobalt has proved to be most promising then manganese emerging as the best options for further research, yielding methane activation barriers commensurate with those seen for precious metal systems that activate via the CMD mechanism.

Publications Acknowledging this Grant in 2022-2023

Intellectually led by this grant

- "Copper(III) Metallacyclopentadienes via Zirconocene-Transfer and Reductive Elimination to an Isolable Phenanthrocyclobutadiene;" Bergman, H.; Beattie, D.; Handford, R.; Suslick, B.; Cundari, T. R.; Liu, Y.; Tilley, T. D. J. Am. Chem. Soc. **2022**, 144, 9853 – 9858.
- "NO Coupling at Copper to cis-Hyponitrite: N_2O Formation via Protonation and H-atom Transfer;" P. Ghosh, M. Stauffer, V. Hosseininasab, S. Kundu, J. Bertke, T. R. Cundari, T. H. Warren J. Am. Chem. Soc. **2022**, 144, 15093 – 15099.
- "On the Mechanism of Intermolecular Nitrogen-Atom Transfer from a Lattice-Isolated Diruthenium Nitride Intermediate;" M. Cosio, W. S. Alharbi, A. Sur, C-H. Wang, A. Ezazi, A. Najafian, T. R. Cundari, D. C. Powers Faraday Trans. **2023**, 244, 154 – 168.
- "Oxidative Addition of Pentafluoropyridine to Tertiary Phosphines;" Y. Gao, I. Migliaro, L. K. Bennet, N. Nolan-Dillard, N. Carter, C. E. Moore, T. R. Cundari, K. M. Clark Chem. Comm. – submitted (7/27/23).
- "Non-Oxidative Methane Activation by a Zinc-Based Frustrated Lewis Pair;" K. Bledsoe, S. D. Illesinghe, Y. Gao, L. K. Bennett, J. A. Byrd, S. Hall, C. E. Moore, T. R. Cundari, K. M. Clark J. Am. Chem. Soc. – submitted (11/27/22).
- Boroujeni, M. R.; Greene, C.; Bertke, J. A.; Cundari, T. R.; Warren, T.H. Chemical and Electrocatalytic Ammonia Oxidation by Ferrocenium, *ChemRxiv* **2023**, doi: 10.26434/chemrxiv-2023-l1dtg-v2
- Okoromoba, O.; Jang, E. S.; McMullin, C.; Cundari, T. R.; Warren, T.H. Copper Catalyzed sp^3 C-H α-Acetylation, *ChemRxiv* **2019**
  doi: 10.26434/chemrxiv.11407116.v1

Jointly funded by this grant and other grants with intellectual leadership by other funding sources

- *NA*

Adam Holewinski

Electrochemically-Assisted Dehydrogenation Reactions for Dual-Electrode Hydrogen Evolution

Adam Holewinski
Department of Chemical & Biological Engineering, University of Colorado Boulder

Presentation Abstract

This project aims to understand and develop electrochemical reactions that produce hydrogen via net-oxidative processes. This contrasts direct electrochemical hydrogen evolution (a reduction reaction) and can in principle be used in electrolysis cells that produce hydrogen in both half-cell reactions (**Figure 1A**). Even though electrolyzer anodes operate at potentials that could (thermodynamically) oxidize the hydrogen molecule, "anodic H_2" can be generated if the reactant at the anode possesses hydrogen moieties with higher chemical potential than H_2. This is the case for a number of renewable organic molecules, including biomass-derived aldehydes. These compounds can improve the economics of hydrogen-producing electrolyzers by co-generation of high-volume chemicals such as monomers for the synthesis of greener materials.

Critical to the electrochemical oxidative dehydrogenation (EOD) process is control over chemical (pure thermally driven) vs. electrochemical steps allowing for adsorbed hydrogen (H*) formed in the process to preferentially desorb from the electrode by recombination ($H^*+H^* \rightarrow H_2$) rather than by discharge ($H^* \rightarrow H^+ + e^-$), which occurs during conventional electrolysis (**Figure 1B**). Work in this project centers around three scientific aims. The first is to understand, at a fundamental level, the surface reactivity requirements for the known process of alkaline EOD for aldehydes. The composition of alloy catalyst structures is being systematically varied to establish how the electronic structure of surfaces can be altered to accelerate this process. We later aim to expand the scope of substrates—in particular, achieving EOD of alcohol functional groups—and to investigate material constraints for achieving EOD under conditions of elevated H_2 pressure and low pH. Detailed understanding is being developed by *operando* spectroscopic tools coupled to rigorous kinetic measurements and computational modeling.

Grant or FWP Number: DE-SC0023424
Electrochemically-Assisted Dehydrogenation Reactions for Dual-Electrode Hydrogen Evolution

Postdoc(s): Rupali Mittal
Student(s): Joe Hasse, Nathanael Ramos, Emma Hollis

RECENT PROGRESS

During these initial project months, research progress was made in characterizing the EOD reaction by cyclic voltammetry and using *operando* infrared spectroscopy to characterize the nature of adsorbate populations on active surfaces. For reference the reaction scheme is depicted in **Figure 1**. A key open question for EOD is whether the favorability of the reaction at high pH is truly a result of the shift in equilibrium toward the geminal diol form of the molecule (**Figure 2**). A further open question is whether organic species moieties actually adsorb after hydrogen abstraction, since the transformation could potentially also be achieved with an outer-sphere electron transfer or if the transferred hydrogen is simply hydridic (H^-) in nature.

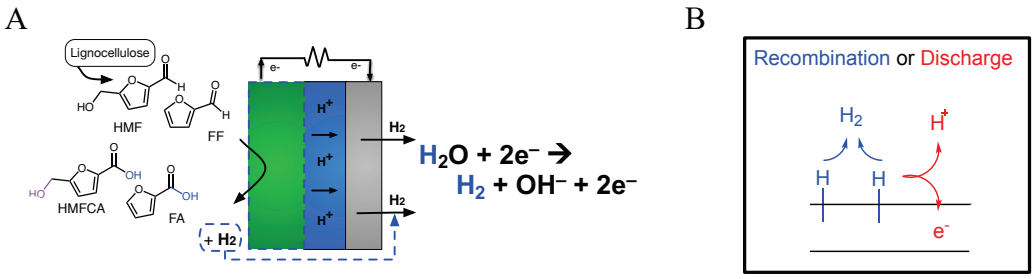

Figure 1: (A) Electrochemical oxidative dehydrogenation concept. (B) Competing mechanisms of hydrogen recombination vs. discharge.

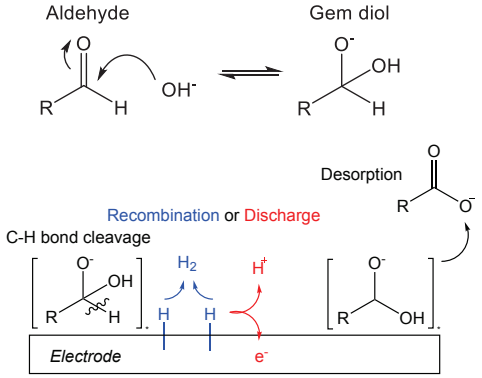

Figure 2: Prevailing proposed reaction pathway involving geminal diol intermediate

Operando studies

We have found using ATR-SEIRAS to probe EOD with furfural, that carbonyl-form furfural is adsorbed in high coverages on Cu surfaces (the most active monometallic for EOD). This is seen by contrasting with Au electrodes, which do not show furfural adsorption and are not active for EOD (**Figure 3**). This leads to one of two key conclusions: either the adsorbed furfural is a spectator and EOD occurs on minority (e.g. defect) sites, OR, the gem-diol species is actually not the precursor to product, and alkaline pH facilitates

a different reaction pathway through an adsorbed intermediate. That intermediate may proceed through a transition state that is stabilized in base, and this would also mean it may be feasible to lower the transition state energy with an appropriately-designed catalytic site. Cu alloys are an initial target toward this end.

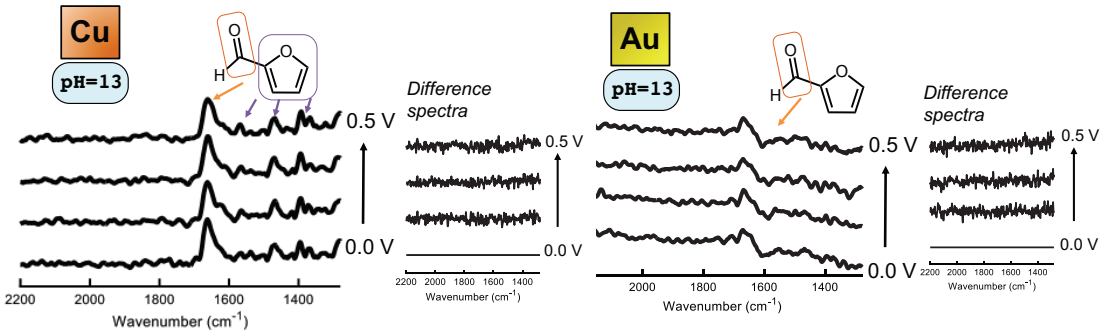

Figure 3: Potential-dependent ATR-SEIRA spectra of furfural over Cu (left) and Au (right) electrodes. Characteristic vibrations associated with adsorbed furfural are seen on Cu, while only solution phase furfural is evident with Au. Also notably, the bands on Cu do not vary in intensity with variation of potential, suggesting the adsorbate is not active or is rapidly restored by equilibrium.

Initial studies of CuNi-alloys are being pursued to compare reactivity. We are attempting to characterize the role of Ni sites as electronic modifiers to Cu, both as isolated sites, and as Ni-ensembles in the surface of the alloy. As an initial step, we are characterizing the top-atomic layer surface structure of these materials using quasi-in-situ low energy ion scattering (LEIS) after different synthesis and post-synthesis electrochemical conditions (**Figure 4**). We have demonstrated that Cu and Ni can be resolved with the method, despite being periodic neighbors and the measurement principle being based on mass differences.

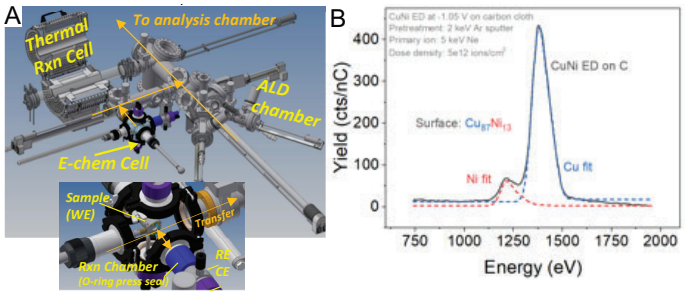

Figure 4: (A) HS-LEIS electrochemical transfer system developed with IonTOF Gmbh. (B) Resolution of Cu and Ni (periodic neighbors, main isotopes Δ5 amu) in an alloy film electrode.

Publications Acknowledging this Grant in 2019-2022

Publications from this grant are currently in preparation.

Adam Holewinski

Electro-oxidative valorization of biomass: design strategies for selective and stable catalysis

Adam Holewinski[1] Michael J. Janik,[2]
1 - Department of Chemical & Biological Engineering, University of Colorado Boulder
2 - Department of Chemical Engineering, Pennsylvania State University

Presentation Abstract

This project aims to develop a fundamental understanding of the factors that dictate activity and selectivity during electrochemical partial oxidation of multi-carbon organic molecules derived from biomass. Value-adding selective conversions of alcohols to aldehydes, and aldehydes to carboxylic acids are considered, with the ultimate goal to establish general principles for controlling selectivity in organic oxidations. Specifically, furfural (FF) and 5-hydoxymethyfurfural (HMF) are used as model systems, where we seek to control the selective conversions between oxygenate functional groups with prevention or control of C-C cleavage steps. Another goal of the work is in achieving these transformations in acidic conditions, which contrasts most existing work (done in base), but is crucial toward compatibility with common pretreatments used to generate small molecules from lignocellulose (e.g. acid hydrolysis or pyrolysis). The constraint of acidic pH prompts a focus on noble metal alloys as a primary platform for tuning reactivity.

Toward these goals, the project investigates three possible mechanisms that may break scaling relations between the adsorption energies of key intermediates and rate determining transition states. These include (i) formation of alloy catalysts that violate common correlations between adsorption energies and the *d*-electron energy center of the constituent metals; (ii) formation of catalyst heterostructures that interface metals and metal-oxides that obey different scaling relations; and (iii) modification of electrolyte composition with anions that can adsorb to catalysts and selectively influence particular adsorbate interactions. Work involves well-defined catalyst material synthesis, comparative kinetics, and *operando* spectroscopies (PI Holewinski), supported by quantum chemical simulations (PI Janik).

Grant or FWP Number: DE-SC0023322
Electro-oxidative valorization of biomass: design strategies for selective and stable catalysis

Student(s): Joseph Hasse, Marc Manyé Ibáñez, Andrew Wong

RECENT PROGRESS

Mechanistic Electrolysis Studies

In this first project year, survey electrolysis studies and operando spectroscopy studies were undertaken. We are performing these studies to understand the requirements for controlling the oxidative progression of oxygenate functional groups (e.g. alcohol to aldehyde, aldehyde to acid) while avoiding undesired pathways that lead to poisoning species—for example, C-C cleavage steps that lead to CO* or overoxidation of acids to bound carboxylate (R-COO*) species (**Figure 1**).

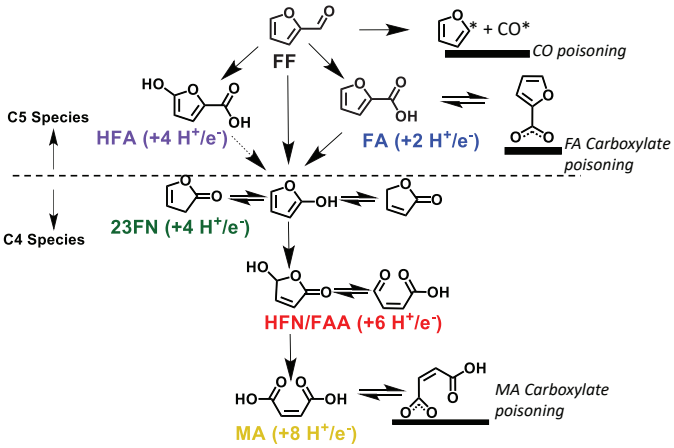

Figure 1: Electro-oxidation pathways of furfural, illustrating CO-poisoning and carboxylate poisoning paths

First, a series of furfural electrolysis studies were run using Pt benchmark catalysts. These were explored at high conversion, in contrast to our prior work that has focused on differential conditions. We observed only weak shifts in product selectivity over time (**Figure 2**), suggesting that most products are in fact terminal. On the other hand, we observed that the accumulation of furoic acid as a product still does lead to a shift in selectivity at later times toward more furoic acid. We have attributed this to readsorption of furoic acid product, with an aromatic adsorbate-adsorbate interaction promoting the formation of more furoic acid as time progresses, albeit with deceleration of the rate.

Coupled to our previous work, we can summarize that (i) Pt is too capable of aldehyde C-C cleavage, necessitating high operating potentials to "outrun" this thermal degradation path and opening up a variety of reactions, but (ii) elevated potentials also fail to yield dramatic rate increases due to accumulation of carboxylate species or formation of less active oxide phases. Ideally, an active structure would allow the relative reactivities toward C-H breaking dehydrogenation steps and C-OH forming oxidation steps to be independently tuned, while also optimizing these respective traits against unwanted C-C cleavage and/or RCOOH overoxidation to carboxylates. Satisfying all these constraints simultaneously presents challenging tradeoffs due to well-known correlations between surfaces' affinities toward various adsorbates.

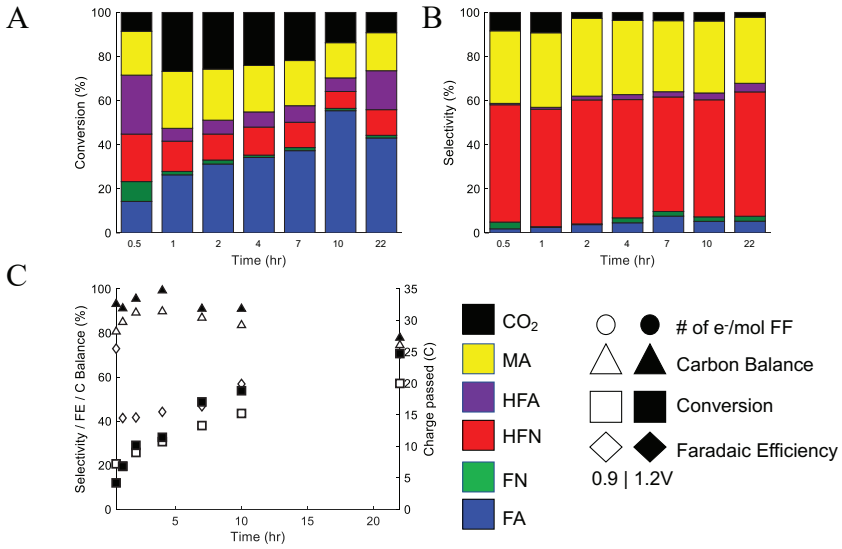

Figure 2: Selectivities to FA (blue), FN (orange), HFN (red), HFA (purple), MA (yellow) and CO_2 (black) given for 0.9 V and 1.2 V (A/B respectively) over 22 hours of electrolysis for 10 mM FF. In panel C, total faradic efficiency (diamonds), furfural conversion (squares), carbon balance (triangles) and # of electrons passed per mol of furfural (circles) are also given.

Computational Insights

To understand where scaling relations might be broken, we have performed quantum chemical screening studies of alloy surfaces and determined their affinities, relative to Pt, for various moieties involved in furfural oxidation, as well as their potential-dependent activation barriers toward C-C cleavage. We have identified AgPt as a particular candidate of interest. AgPt shows deviations from most materials in that it has a higher tendency toward C-H dehydrogenation than Pt while also having a larger barrier to C-C cleavage (**Figure 3**). We are working on synthetic procedures for a series of Ag_xPt_{1-x} alloys at the moment.

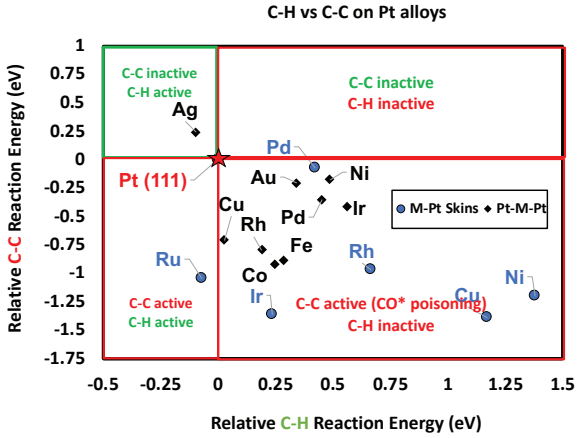

Figure 3: Correlations between DFT-calculated C-H bond cleavage energies and C-C cleavage activation energies. Energy values on axes are relative to Pt.

Initial Studies on Alloy Composition and Electrolyte Tuning

While working on synthesis of AgPt, we first explored the reactivity of PtRu alloys, which are widely commercially available and well-known for their electro-oxidation activity. Although the calculations nominally indicate PtRu should be very active toward C-C cleavage, we found low C_4 product yields. More C_5 products are formed, and less CO_2 is produced (**Figure 4A-B**). We hypothesize that this relates to Ru sites becoming poisoned by carbonaceous species due to their high affinity for carbon. This is followed by most turnovers occurring on Pt sites that are electronically modified by Ru to exhibit less C-C cleavage activity. We are planning to build on the calculations with microkinetic models to capture such emergent behaviors.

We have additionally performed electrolysis screening with different electrolyte ions that can specifically adsorb to electrode surfaces (e.g. sulfate, phosphate) to assess their ability to modify adsorbate-adsorbate interactions as mentioned above. We have only found subtle shifts in product distributions. This effect has led us toward exploration of electrolyte ions with long tail groups, which can more dramatically disrupt solvation in the double layer due to their significant hydrophobicity. Initial results using sodium dodecyl sulfate (SDS) in the electrolyte show that the surface crowding and hydrophobicity induced at the surface do lower C-C cleavage rates, leading to high (>70%) selectivity toward furoic acid, albeit only at lower operating potential (**Figure 4C-D**). At higher potentials, more C_4 products are formed, although oxygen-addition is apparently suppressed, leading to more hydroxyfuranone and less maleic acid.

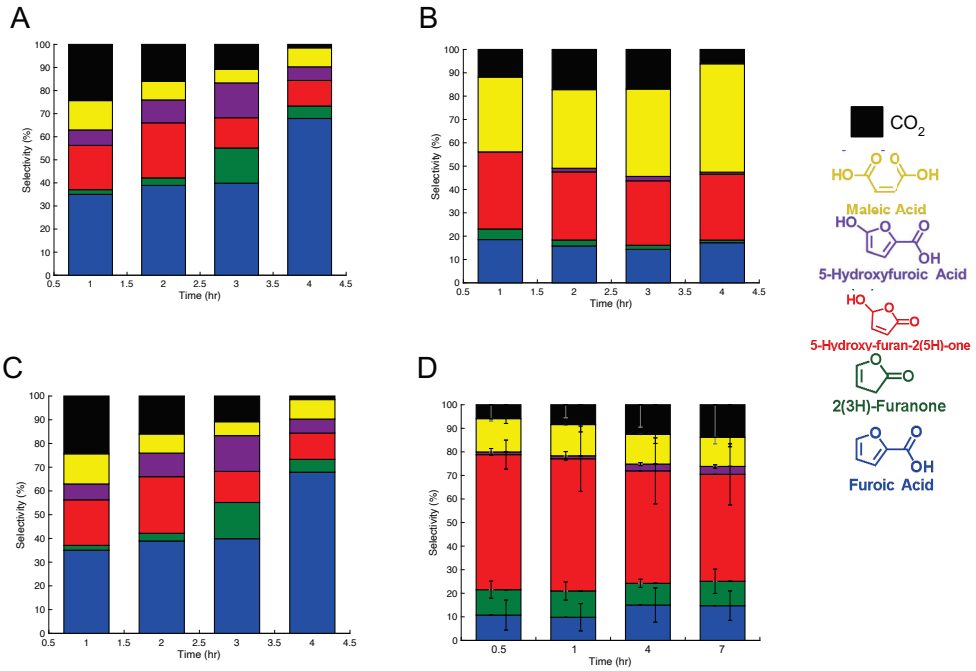

Figure 4: A/B: Selectivities of $Pt_{50}Ru_{50}$ to FA (blue), FN (orange), HFN (red), HFA (purple), MA (yellow) and CO_2 (black) given for 0.9 V (A) and 1.2 V (B) over 4 hours of electrolysis with 10 mM FF. C/D: Selectivities of Pt in the presences of 5mM SDS to FA (blue), FN (orange), HFN (red), HFA (purple), MA (yellow) and CO_2 (black) given for 0.9 V (A) and 1.2 V (B) over 4 hours of electrolysis with 10 mM FF

Publications Acknowledging this Grant in 2019-2022

Intellectually led by this grant

1. Hasse, J. C.; Manyé Ibáñez, M.; Holewinski, A.; "Impact of electrolyte composition on bulk electrolysis of furfural over platinum electrodes." *In revision.*

Jointly funded by this grant and other grants with intellectual leadership by other funding sources

2. Ramos, N.; Manyé Ibáñez, M.; Mittal, R.; Janik, M. J.; Holewinski, A.; "Combining renewable electricity and renewable carbon: Understanding reaction mechanisms of biomass-derived furanic compounds for design of catalytic nanomaterials." *Revision submitted.*

Kozinsky, Boris

Machine learning for accelerated understanding of dynamic catalysis

Presentation Abstract

Detailed mechanistic understanding and ability to control the atomistic dynamics and interfacial reactions between the gas-phase and solid surfaces are crucial for improving catalytic systems. Industrially important examples include H_2 exchange and CO oxidation on nanoparticles (NPs), which lead to markedly different particle behaviors, and mesoscopic surface reconstructions. To gain atomistic insights into adsorbate-induced structural transformation phenomena, we employ a combination of MD based on first-principles machine-learned force fields (MLFFs) with extended X-ray absorption fine structure (EXAFS) measurements. Bayesian machine learned force fields (MLFFs) with quantum-mechanical accuracy are used to perform MD simulations for freestanding metal nanoparticle systems (e.g., Pt and PdAu), as well as to study the effects of gas exposure (e.g., H_2 and CO) on NP dynamics and structure at the length- and timescales relevant for realistic catalytic systems. Experimental EXAFS is used to inform and validate the MLFF models that are used in long time-scale MD simulations. EXAFS is calculated and averaged over the MD trajectories to produce MD-EXAFS. The MD-EXAFS is then compared to experimental EXAFS of well-defined systems collected over various temperatures and reactive conditions.

DE-SC0022199: Machine learning for accelerated understanding of dynamic catalysis

John Francis Kuper Limtiaco

Advancing towards energy self-sufficiency in Guam and Micronesia

John Francis Kuper Limtiaco
University of Guam, College of Natural and Applied Sciences

Presentation Abstract

Seawater is a major reservoir of hydrogen (H_2), considered to be the critical clean energy carrier necessary for achieving sustainable social development. However, the high salt content and presence of organic matter in seawater and their interference in the electrolysis reaction makes the direct utilization of seawater difficult. This challenge is particularly relevant for Guam, an island in the Western Pacific, where its remote location makes the delocalized electrochemical production of H_2 and other potential energy carriers a promising strategy for energy self-sufficiency. Through our engagement with Pacific Northwest National Laboratory (PNNL), University of Guam (UOG) students and early-stage investigators participate in fundamental research aimed at understanding the complexity of the electrode/liquid interfaces and controlling reaction pathways for the electrochemical evolution of H_2 and oxygen, and prevalent side reactions, under the conditions of seawater electrolysis.

In the summer of 2023, two undergraduate students from UOG were recruited to participate in a 10-week internship at PNNL with the goal of developing a fundamental understanding of the cathodic transformations, focusing primarily on the routes for the H_2 evolution reaction as well as competing electrochemical reduction reactions. Students and faculty were trained by PNNL scientists on the use of equipment to measure and evaluate electrochemical performance using model solutions. Through planned activities designed to teach the fundamentals of heterogenous catalysis and electrochemistry, students gained an understanding of the complexity of the electrode/liquid interface via experiments performed to investigate changes in electrochemical performance at the cathode surface, resulting from electrolyte concentration, electrochemical cell geometry, and solution pH.

DE-SC0023652: Controlling reaction pathways under the non-ideal conditions of seawater electrolysis.

Student(s): Anna Lhyn Mallari and Merry Jubilaine Remetira
Affiliations(s): University of Guam, College of Engineering

James R. McKone

Catalytic PCET on Transition Metal Oxides: From Molecules to Materials

James R. McKone, University of Pittsburgh
Giannis Mpourmpakis, University of Pittsburgh
Ellen Matson, University of Rochester
Veronica Augustyn, North Carolina State University
Ethan Crumlin, Lawrence Berkeley National Laboratory

Presentation Abstract

Our research consortium is pursuing fundamental science to support the development of carbon-neutral hydrogen technologies, with a focus on critically comparing the ways in which molecular and extended catalysts activate and transfer reactive hydrogen via proton-coupled electron transfer (PCET). Our work is specifically directed at understanding hydrogen activation and oxygen reduction on tungsten oxides, including molecular polyoxotungstates and extended tungsten-oxide nanomaterials. Several studies are in progress as of the end of the first of three project years. The first comprises multimodal characterization and quantum chemical simulations of hydrogen activation in $WO_3 \cdot nH_2O$ (where n = 0, 1, and 2) via hydrogen insertion and hydrogen spillover. Results to date suggest significant differences between redox reactions at surface and bulk sites with distinct implications for catalytic reactivity via hydrogen and/or oxygen transfer. A second set of studies comprise comparative investigations of structural transformations and thermochemistry of PCET to/from molecular clusters and extended WO_x nanomaterials. Finally, significant ongoing work is directed at studying catalytic hydrogen transfer on WO_x molecules and materials under a variety of reaction conditions using both model compounds (e.g., TEMPO) and oxygen as molecular hydrogen acceptors.

DE-SC0023465: From Molecules to Materials: Understanding Hydrogen Activation and Transfer in Metal Oxides

PI(s)
(as listed on cover page)

Postdoc(s)
Payman Sharifi Abdar, University of Pittsburgh
Haoyi Li, Lawrence Berkeley National Laboratory
Hyunguk Kwon, University of Pittsburgh
Kyung-Eun You, University of Pittsburgh
Noah Holzapfel, North Carolina State University
Zhou Lu, University of Rochester

Student(s)
Shreya Thakkar, University of Pittsburgh
Evan Miu, University of Pittsburgh
Andreas Towarnicky, University of Pittsburgh
Mona Abdelgaid, University of Pittsburgh
Michael Spencer, North Carolina State University
Saeed Saeed, North Carolina State University
Eric Schreiber, University of Rochester
Kathryn Proe, University of Rochester

Observing Surface Reactions on WO_3 Undergoing Hydrogen Spillover

In work led by Crumlin, our team has undertaken a detailed investigation of the dynamics of hydrogen spillover reactions on the surface chemistry of $WO_3 \cdot nH_2O$ (n = 0, 1, 2) using ambient pressure photoelectron spectroscopy (APXPS). Highlights are depicted in Figure 1. Results to date show clear evidence for primary and secondary spillover events involving H-transfer at the Pt/WO_3 interface and between WO_3 units, respectively. APXPS data also show evidence for sequential reduction events as a function of temperature, as well as evidence for direct redox reactions between surface W sites in WO_3 and ambient water vapor.

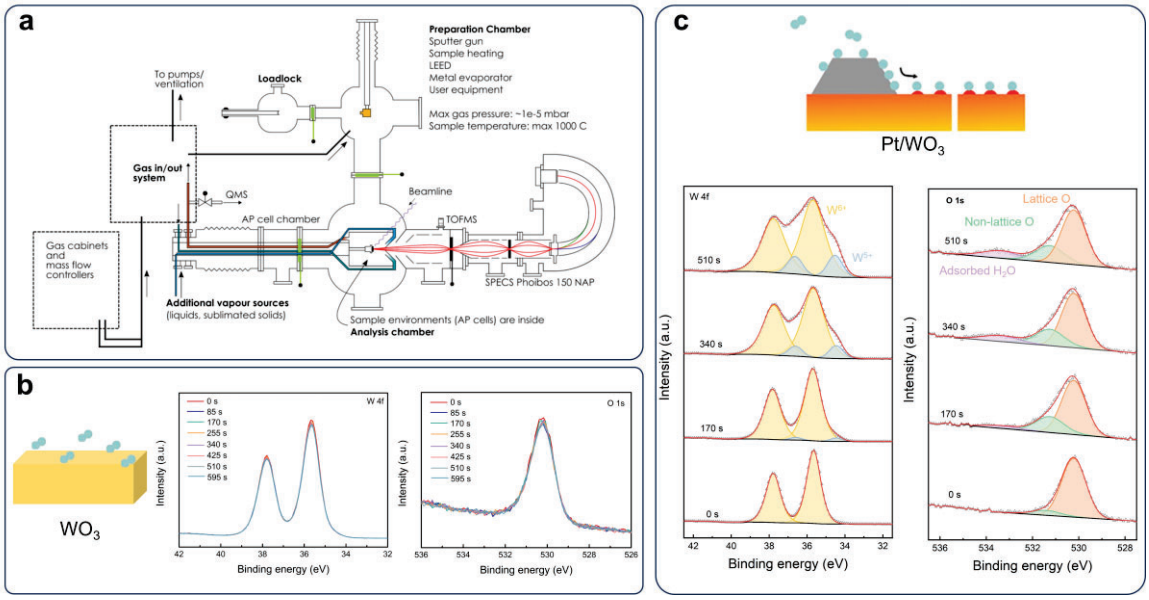

Figure 1. Summary of ongoing work on APXPS measurements: (a) depiction of experimental configuration at LBNL; (b) control data demonstrating negligible H-spillover for WO_3 films exposed to H_2 in the absence of Pt co-catalyst; (c) APXPS data collected in the W 4f and O 1s regions under H-spillover conditions.

Using Data Science to Predict Oxide Bronze Thermochemistry

In a recent study led by PI Mpourmpakis, we have proposed and benchmarked a new type of structural descriptor we call *global connectivity* that emerges from graph-based representations of the bonding network in oxide solids. We further showed that this descriptor, which encodes information about the overall "connectedness" of a periodic structure, can be combined with descriptors of local coordination to build statistical models that correlate well with experimentally observed formal potentials for hydrogen insertion (Figure 2). Notably, these models can be formulated using training data derived entirely from readily available crystallographic data. Hence, this approach supports predictions of key thermodynamic properties of oxide bronzes (and we speculate it to be extensible to numerous other material classes) without the need for quantum chemical calculations.

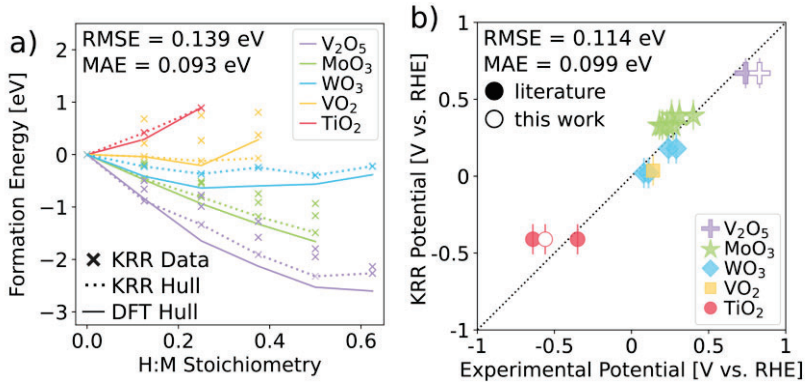

Figure 2. Results from data science models of H-insertion in several model oxide hydrogen bronze formers: (a) convex hull representations of H-insertion energetics comparing DFT calculations with regression models trained on graph descriptors incorporating global and local connectivity; (b) comparisons between H-insertion formal potentials predicted from graph models and empirical measurements. Figure from Miu et al. *Phys Rev. Lett.* **2023** (in Press).

Structure and Thermochemistry of Oxide-Mediated Hydrogen Activation

Matson and Mpourmpakis undertook a series of investigations designed to on-board their research teams to thermodynamic and kinetic analysis of H-atom uptake focused on polyoxovanadate clusters historically investigated by the Matson Laboratory. These systems feature nucleophillic, bridging oxide moieties at the surface of the assembly that interact with H-atom equivalents. Coordination of H-atoms to the surface of the assemblies occurs selectively, with bond dissociation free energies of the resultant hydroxide moieties ranging from 60-70 kcal/mol. These BDFE(O-H) values are sensitive to structural modifications at the surface of the POV-alkoxide cluster and the electronic properties of each cluster. Representative highlights are depicted in Figure 3.

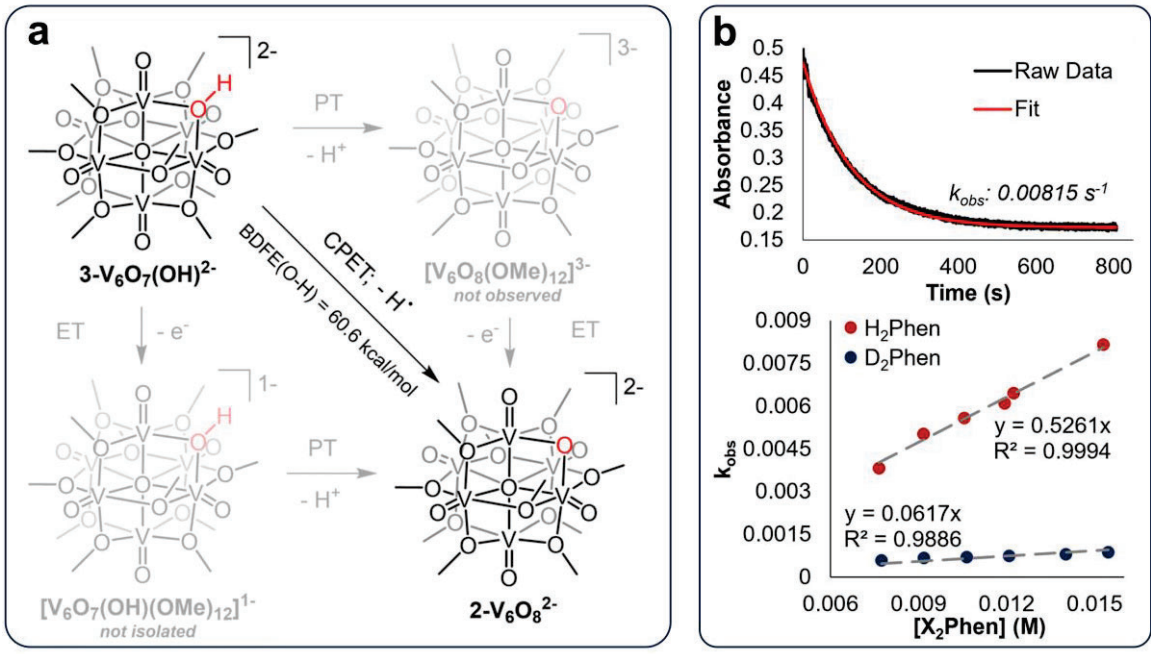

Figure 3. Schematic depiction (a) and empirical evidence (b) for concerted PCET in a molecular polyoxovanadate cluster. From Schrieber et al., *Chem. Sci.* ***2023.*** DOI:10.1039/D2SC05928B.

In closely related work, Augustyn, Matson, and Mpourmpakis have begun characterizing electrochemical hydrogen adsorption/insertion of extended tungsten oxides under aqueous and nonaqueous conditions, in the interest of developing detailed energy landscapes and extracting bond-dissociation free energy (BDFE) values that are directly comparable to BDFEs obtained in molecular clusters. For this study, Augustyn is using particle-based electrodes and electrodeposited nanostructured electrodes, while Matson is carrying out analogous measurements on polyoxotungstate clusters in the solution phase. We are performing electrochemistry in aqueous acidic electrolytes and non-aqueous electrolytes containing organic acids. DFT calculations are being deployed to probe the effect of electronic structure on the hydrogen BDFE between polyoxotungstate and polyoxovanadate clusters as well extended tungsten oxide bronzes. Figure 4 compiles representative results from Augustyn comprising rigorous structural characterization of sequential H-insertion events in anhydrous WO_3.

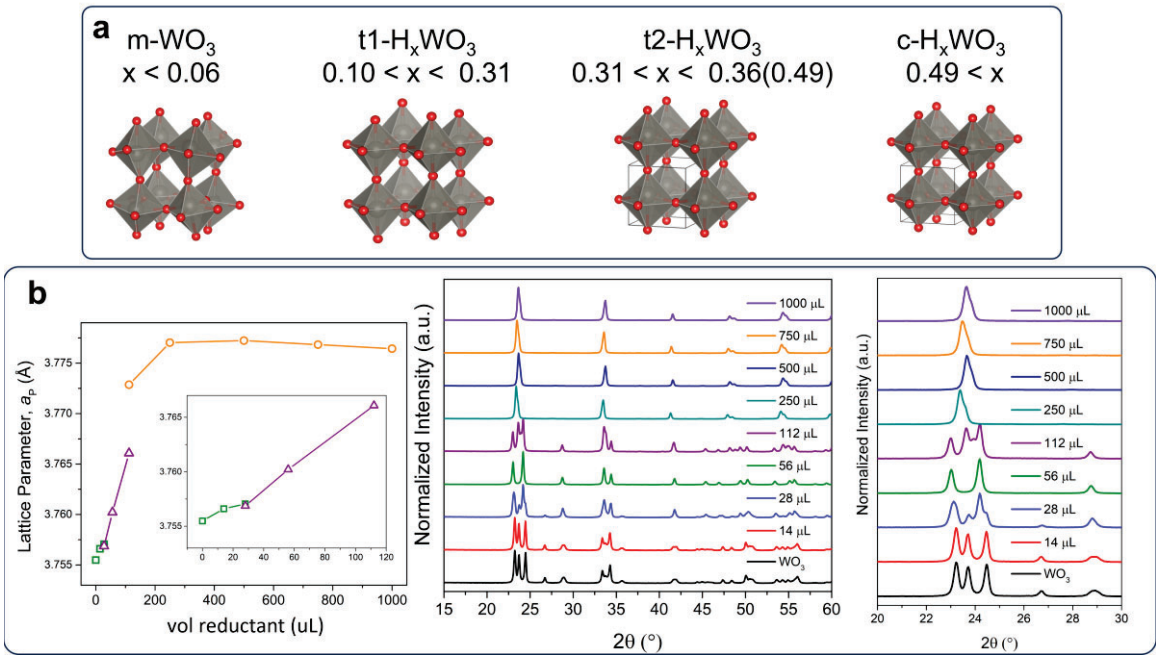

Figure 4. Structural characterization of crystallographic transformations associated with hydrogen uptake in anhydrous WO_3: (a) cartoon depiction of the parent monoclinic structure and 3 sequential phase changes associated with H-uptake; (b) compiled XRD data demonstrating the sequential transformations in (a).

Catalytic PCET On WO_3 Nanomaterials

Studies on catalytic PCET, led by McKone, are focused on measuring reaction rates for electrocatalytic hydrogen transfer to molecular substrates using WO_3 nanomaterials as the hydrogen transfer mediator. One line of inquiry involves sequential hydrogen activation and hydrogenation of a molecular model acceptor 2,2,6,6-Tetramethylpiperidinyloxy (TEMPO) using WO_3 as a transient store of H-equivalents. We term this process *electrochemical looping hydrogenation*, by analogy to well-established work on chemical looping schemes for, e.g., fuel combustion. Figure 5 compiles representative results. Experimental measurements to date have shown the rate of hydrogen transfer to TEMPO is more sensitive to the extent of hydrogen insertion in the oxide than the availability of free protons, which we take as preliminary evidence for a mechanism involving neutral hydrogen atom transfer (HAT). Quantum chemical calculations are being used to further

probe mechanistic pathways and to better understand the optical properties and speciation of the TEMPO molecule in aqueous solution.

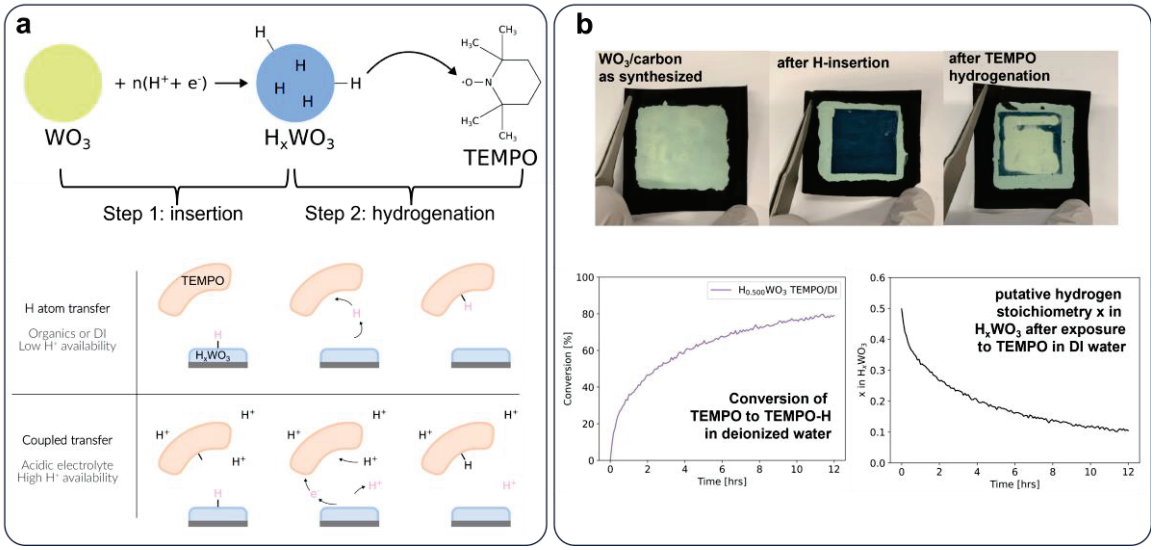

Figure 5. Compiled results depicting catalytic hydrogenation of TEMPO via electrochemical looping hydrogenation: (a) schemes depicting overall reaction and two distinct pathways for concerted PCET; (b) empirical data demonstrating sequential uptake of H-equivalents in $HxWO_3$ via electrochemical insertion followed by TEMPO hydrogenation via H-deinsertion.

Publications Acknowledging this Grant in 2020-2023

(I) Intellectually led by this grant

Miu, E.V.; McKone, J.R.; Mpourmpakis, G.; Global and Local Connectivities Describe Hydrogen Intercalation in Metal Oxides*; Phys. Rev. Lett.* ***2023***, (in press).

Proe, K. R.; Schreiber, E.; Matson, E. M.; Proton-coupled electron transfer at the surface of polyoxovanadate-alkoxide clusters*; Acc. Chem. Res.* **2023**, *12,* 1602–1612.

Schreiber, E.; Brennessel, W. W.; Matson, E. M.; Regioselectivity of H-atom uptake at the surface of reduced polyoxovanadate clusters; *Chem. Sci.* **2023**, *14*, 1386-1396.

(II) Jointly funded by this grant and other grants with intellectual leadership by other funding sources

(none)

LIST OF PARTICIPANTS

First Name	Last Name	E-mail Address
Frank	Abild-Pedersen	abild@slac.stanford.edu
Anastassia	Alexandrova	ana@chem.ucla.edu
Líney	Árnadóttir	liney.arnadottir@oregonstate.edu
Polly	Arnold	pla@lbl.gov
Jason	Azoulay	jdazoulay@gatech.edu
Michal	Bajdich	BAJDICH@slac.stanford.edu
Simon	Bare	srbare@slac.stanford.edu
Bart	Bartlett	bartmb@umich.edu
Desiree	Bernabeo	desiree.bernabeo@orau.org
Guy	Bertrand	gbertrand@ucsd.edu
Aditya	Bhan	abhan@umn.edu
Elizabeth	Biddinger	ebiddinger@ccny.cuny.edu
Suzanne	Blum	blums@uci.edu
Jesse	Bond	jqbond@syr.edu
Chris	Bradley	chris.bradley@science.doe.gov
Katherine	Brown	katherine.brown@science.doe.gov
Matteo	Cargnello	mcargnello@stanford.edu
Bert	Chandler	bert.chandler@psu.edu
Fanglin	Che	fanglin_che@uml.edu
Donna	Chen	dachen@sc.edu
Eugene	Chen	eugene.chen@colostate.edu
Jingguang	Chen	jgchen@columbia.edu
Peng	Chen	pc252@cornell.edu
Zhongfang	Chen	zhongfangchen@gmail.com
Paul	Chirik	pchirik@princeton.edu
Kyoung-Shin	Choi	kschoi@chem.wisc.edu
Cooper	Citek	citek@lbl.gov
Kensha	Clark	kmclark8@olemiss.edu
Geoff	Coates	gc39@cornell.edu
Jorge	Colón	jorge.colon10@upr.edu
Matthew	Conley	mconley@ucr.edu
Stephen	Craig	stephen.craig@duke.edu
Steven	Crossley	stevencrossley@ou.edu
Lisandro	Cunci	lisandro.cunci@upr.edu
Thomas	Cundari	t@unt.edu
Paul	Dauenhauer	hauer@umn.edu
Max	Delferro	delferro@anl.gov
Tianning	Diao	diao@nyu.edu

David	Dixon	dadixon@ua.edu
James	Dorman	james.dorman@science.doe.gov
Keary	Engle	keary@scripps.edu
Carrie	Farberow	carrie.farberow@science.doe.gov
Chris	Fecko	christopher.fecko@science.doe.gov
Gregory	Fiechtner	gregory.fiechtner@science.doe.gov
David	Flaherty	dflaherty3@gatech.edu
Alison	Fout	fout@tamu.edu
Anatoly	Frenkel	anatoly.frenkel@stonybrook.edu
Lymari	Fuentes-Claudio	lfuentes@uagm.edu
Francois	Gabbai	francois@tamu.edu
Rachel	Getman	getman.11@osu.edu
Karen	Goldberg	kig@sas.upenn.edu
Alan	Goldman	alan.goldman@rutgers.edu
John	Gordon	jgordon1@bnl.gov
Jeffrey	Greeley	jgreeley@purdue.edu
T. Brent	Gunnoe	tbg7h@virginia.edu
Javier	Guzman	javier.x.guzman@exxonmobil.com
Thomas	Hamann	hamann@msu.edu
John	Hartwig	jhartwig@berkeley.edu
Tony	Heinz	tony.heinz@stanford.edu
Gregory	Herman	gherman@anl.gov
Adam	Hoffman	ashoff@slac.stanford.edu
Adam	Holewinski	adam.holewinski@colorado.edu
Patrick	Holland	patrick.holland@yale.edu
Jiyun	Hong	jiyun.hong@slac.stanford.edu
Simon	Humphrey	smh@cm.utexas.edu
Seung Soon	Jang	seungsoon.jang@mse.gatech.edu
Michael	Janik	mjanik@psu.edu
Thomas	Jaramillo	jaramillo@stanford.edu
Christopher	Jones	christopher.jones@chbe.gatech.edu
Ayman	Karim	amkarim@vt.edu
Sheima	Khatib	sheimajk@vt.edu
Boris	Kozinsky	bkoz@seas.harvard.edu
Clemens	Krempner	clemens.krempner@ttu.edu
Coleman	Kronawitter	ckrona@ucdavis.edu
Jeremy	Kropf	kropf@anl.gov
Ambarish	Kulkarni	arkulkarni@ucdavis.edu
Johannes	Lercher	johanneslercher@hotmail.com
John Francis	Limtiaco	limtiacoj6850@triton.uog.edu
Charles	Machan	machan@virginia.edu

Karthish	Manthiram	karthish@caltech.edu
Smaranda	Marinescu	smarines@usc.edu
Jean-Sabin	McEwen	js.mcewen@wsu.edu
James	McKone	jmckone@pitt.edu
Gail	McLean	gail.mclean@science.doe.gov
Will	Medlin	medlin@colorado.edu
Raul	Miranda	raul.miranda@science.doe.gov
Liviu	Mirica	mirica@illinois.edu
Karl	Mueller	karl.mueller@pnnl.gov
Leslie	Murray	murray@chem.ufl.edu
Eranda	Nikolla	erandan@umich.edu
Oleg	Ozerov	ozerov@tamu.edu
Umit	Ozkan	ozkan.1@osu.edu
Gerard	Parkin	parkin@columbia.edu
Frederic	Perras	fperras@ameslab.gov
Jonas	Peters	jpetesr@caltech.edu
Craig	Plaisance	plaisance@lsu.edu
Felipe	Polo-Garzon	pologarzonf@ornl.gov
Long	Qi	lqi@ameslab.gov
Srinivas	Rangarajan	srr516@lehigh.edu
Jeffrey	Rimer	jrimer@central.uh.edu
Robert	Rioux	rmr189@psu.edu
Jose	Rodriguez	rodrigez@bnl.gov
Jennifer	Roizen	jennifer.roizen@science.doe.gov
Yuriy	Roman	yroman@mit.edu
Roger	Rousseau	rousseaur@ornl.gov
Aaron	Sadow	sadow@iastate.edu
Caroline	Saouma	caroline.saouma@utah.edu
Philippe	Sautet	sautet@ucla.edu
J.R.	Schmidt	schmidt@chem.wisc.edu
Daniel	Schwartz	daniel.schwartz@colorado.edu
Viviane	Schwartz	viviane.schwartz@science.doe.gov
Susannah	Scott	sscott@ucsb.edu
Sanjaya	Senanayake	ssenanay@bnl.gov
Carsten	Sievers	carsten.sievers@chbe.gatech.edu
Jeremy	Smith	smith962@indiana.edu
Erin	Stache	estache@princeton.edu
Kelsey	Stoerzinger	zinger@umn.edu
Brian	Tackett	bmtacket@purdue.edu
Sara	Thoi	sarathoi@jhu.edu
Christine	Thomas	thomas.3877@osu.edu

T. Don	Tilley	tdtilley@berkeley.edu
Francesca	Toma	francesca.toma@hereon.de
YuYe J.	Tong	yyt@georgetown.edu
Ian	Tonks	itonks@umn.edu
Ba	Tran	ba.tran@pnnl.gov
Josh	Vura-Weis	vuraweis@illinois.edu
Israel	Wachs	iew0@lehigh.edu
Huamin	Wang	huamin.wang@pnnl.gov
Yong	Wang	wang42@wsu.edu
Timothy	Warren	warre155@msu.edu
Jason	Weaver	weaver@che.ufl.edu
Marcus	Weck	mw125@nyu.edu
Michael	White	mgwhite@bnl.gov
Ross	Widenhoefer	rwidenho@chem.duke.edu
Eric	Wiedner	eric.wiedner@pnnl.gov
Philip	Wilk	philip.wilk@science.doe.gov
Kirsten	Winther	winther@slac.stanford.edu
Zili	Wu	wuz1@ornl.gov
Hongliang	Xin	hxin@vt.edu
Peidong	Yang	p_yang@berkeley.edu
Zhenzhen	Yang	yangz3@ornl.gov
Francisco	Zaera	zaera@ucr.edu
Sen	Zhang	sz3t@virginia.edu
Xiaolin	Zheng	xlzheng@stanford.edu
Aleksandr	Zhukhovitskiy	alexzhuk@email.unc.edu

Cover images courtesy of: José Rodriguez (BNL), Patrick Holland (Yale University), Max Delferro (ANL), Polly Arnold (LBNL and University of California Berkeley), Donna Chen (University of South Carolina), Bert Chandler (Penn State)